NASA Conference Publication 3076

Low-Temperature CO-Oxidation Catalysts for Long-Life CO$_2$ Lasers

Edited by
David R. Schryer
Langley Research Center
Hampton, Virginia

Gar B. Hoflund
University of Florida
Gainesville, Florida

NASA

National Aeronautics and
Space Administration

Office of Management

Scientific and Technical
Information Division

1990

PREFACE

Electrical discharge-excited, pulsed CO_2 lasers inevitably undergo some decomposition of CO_2 to CO and O_2. If such lasers are to be operated for extended periods of time in a sealed or closed-cycle mode without severe performance degradation, a suitable catalyst must be used to recombine the CO and O_2 to regenerate CO_2. For many applications--including space-based and portable lasers -- weight, volume, and/or energy constraints require that the catalysts used must have high activity at ambient laser temperatures, which are generally less than 75° C. Furthermore, candidate catalysts must function efficiently at low oxygen partial-pressures since the only oxygen present in the laser gas is that which is due to CO_2 decomposition, and this must be kept low to maintain laser power.

Traditional CO-oxidation catalysts -- noble metals and various base-metal oxides -- do not have sufficient activity at low temperatures and low O_2 concentrations for use in demanding laser application. However, in the past decade or so, several catalysts which do meet these criteria have been developed. It is interesting that these new catalysts represent a combination of the two classes of traditional CO-oxidation catalysts; that is, they generally consist of one or more noble-metals combined with the oxide of a multivalent base-metal. We have suggested the name, "noble-metal/reducible-oxide," and the acronym "NMRO" for this new family of catalysts. Of course, these catalysts have other applications, including air purification, in addition to use in CO_2 lasers.

Because of the importance of low-temperature CO-oxidation catalysts, and recent progress in their development and characterization, an international conference entitled *CO-Oxidation Catalysts for Long-Life CO_2 Lasers* was held October 17-19, 1989, at the Langley Research Center of the National Aeronautics and Space Administration (NASA) in Hampton, Virginia, United States. The conference was jointly sponsored by

PRECEDING PAGE BLANK NOT FILMED

NASA and the Royal Signals and Radar Establishment (RSRE) of the United Kingdom. Most of the papers presented at this conference are included in this volume. Several papers have been modified somewhat for various reasons, including incorporation of recent research results. Unfortunately, a few papers were not received in time for inclusion in this volume.

Readers desiring an introduction to CO_2 lasers or CO-oxidation catalysts are directed to the first two papers in the *Fundamentals* section, which present excellent reviews of these topics. The third paper in this section presents a review of Pt/SnO_2-based catalysts - - perhaps the most thoroughly investigated NMRO catalysts to date - - including a proposed mechanism for the catalysis of CO oxidation by platinized tin-oxide, which may have applicability to other NMRO catalysts as well. The paper on alternative catalysts in the section *Catalyst Development* presents experimental evidence that gold on manganese-dioxide is superior to platinized tin-oxide with respect to both high activity and low decay. It is hoped that these and other papers presented herein will be useful to readers whatever their interest in low-temperature CO-oxidation catalysts may be.

The use of trademarks or manufacturers' names in this publication does not constitute endorsement, either expressed or implied, by the National Aeronautics and Space Administration.

David R. Schryer
NASA Langley Research Center

Gar B. Hoflund
University of Florida

INTRODUCTION

Welcome, ladies and gentlemen. It's a real pleasure for me to welcome you all to Langley Research Center, one of NASA's finest centers. Langley has a unique history which makes it particularly appropriate that we should host this conference dealing with basic technology and practical applications. Langley is the oldest of the NASA centers. We were founded in 1917 and began life as the Langley Aeronautical Laboratory, the first aeronautical research laboratory in the United States. When space exploration became a possibility in the 50's, the Space Task Group was formed here at Langley several years before the official birth of NASA. The Mercury project was developed here at Langley, the first astronauts came here to train, and eventually the Space Task Group was transferred to Houston in 1962. Langley is still the only NASA center with a division, the Instrument Research Division, which is devoted specifically to measurement science.

Proud as we are of Langley's history and accomplishments, we must recognize that in this modern era of technological complexity, research is often most efficiently accomplished by involving people from more than one laboratory. Thus, the Langley catalyst research effort involves researchers from two Langley divisions, plus three universities, and a private corporation. In this conference we will be sharing information with researchers from several other universities, companies, and agencies, as well as from other countries. We are very pleased to co-sponsor this conference with the Royal Signals and Radar Establishment of the United Kingdom and very pleased to have a broad international participation.

I'm particularly interested in the topic of this conference because the Langley catalyst effort began life as a small project under the Director's discretionary fund. The Director's discretionary fund is a small but very important fund available for my decision to provide seed money for innovative high risk research. It is used for special high risk projects that would not be funded through our ordinary procedures for funding research tasks. Of course, because of its high risk nature, not all this research bears fruit as fully as originally hoped, but much of it does produce results--and those projects that do--become incorporated into NASA's regular research program with funding through conventional channels. The Langley catalyst program is one of the many successful and important projects that have grown from that discretionary fund.

I am very pleased that this important international conference is being held here at Langley. I want to welcome you and wish you every success in your joint meetings.

Thank you.

Richard H. Petersen
Director

CONTENTS

SECTION I - FUNDAMENTALS

SECTION II - CATALYST DEVELOPMENT

PRECEDING PAGE BLANK NOT FILMED

SECTION III - LABORATORY STUDIES

SECTION IV - LASER STUDIES AND OTHER APPLICATIONS

INTERNATIONAL CONFERENCE ON
CO-OXIDATION CATALYSTS FOR LONG-LIFE CO$_2$ LASERS

LIST OF ATTENDEES

Mr. Edward Barsack
Raytheon Research
131 Spring Street
Lexington, MA 02173
617/860-3034

Mrs. Carmen E. Batten
NASA Langley Research Center
Mail Stop 234
Hampton, VA 23665-5225
804/864-4151

Mr. L. V. Benningfield
Phillips Petroleum Company
Bartlesville, OK 74004
918/661-1244

Dr. Geoffrey C. Bond
Brunel University
Dept of Chemistry
Uxbridge
Middlesex, UB8 3PH
UNITED KINGDOM
0895/74000

Mr. Thomas Brocki
California Laboratory Inc.
5964 La Place Court
Carlsbad, CA 92008
619/931-1299

Mr. Phillip Brockman
NASA Langley Research Center
Mail Stop 468
Hampton, VA 23665-5225
804/864-1554

Dr. Kenneth G. Brown
NASA Langley Research Center
Mail Stop 234
Hampton, VA 23665-5225

Mr. David R. Brown (now Erik J. Kielin)
ODU Research Foundation
Norfolk, VA 23508
804/864-4753

Ms. Karen Burns
ODU Research Foundation
Norfolk, VA 23508
804/864-4723

Dr. Mark R. Davidson
University of Florida
Chemical Engineering Dept
Gainesville, FL 32611
904/392-9105

Ms. Patricia P. Davis
NASA Langley Research Center
GRIB-IRD
Hampton, VA 23665
804/864-4724

Dr. Adarsh Deepak
Science and Technology Corp
101 Research Drive
Hampton, VA 23666-1340
804/856-1894

Dr. David J. Elliott
Phillips Petroleum Co
342 PL
Bartlesville, OK 74004
918/661-0443

Dr. Gerald D. Ferguson
Naval Air Development Ctr
Code 5011
Warminister, PA 18974-5000
215/441-3284

Dr. Jay Fox
CNVEO Laser Division
ATTN: AMSEL-NV-L
Ft. Belvoir, VA 22060
703/664-4287

Dr. Charles Freed
MIT Lincoln Lab
Room 201
244 Wood Street
P.O. Box 73
Lexington, MA 02173-0073
617/981-3639

Dr. Theresa B. Fryberger
National Bureau of Standards
Chemical Process Metrology Div. 585.04
Bldg 221, Rm B-312
Gaithersburg, MD 20899
301/975-2607

PRECEDING PAGE BLANK NOT FILMED

Dr. David F. Cox
Virginia Tech
Dept of Chemical Eng'r
Blacksburg, VA 24061
703/231-6829

Mr. Steven D. Gardner
University of Florida
Chemical Engineering Dept
Gainesville, FL 32611
904/392-9105

Ms. Cynthia Gautier
CNVEO Laser Division
AMSEL-RD-NV-L
Fort Belvoir, VA 22060
703/664-4287

Mr. Hans-Peter Grieneisen
Laser Systems
FEDERAL REPUBLIC OF GERMANY

Prof. Erdogan Gulari
University of Michigan
Chemical Engineering Dept
3168 Dow Building
Ann Arbor, MI 48109
313/963-5464

Prof. Gary L. Haller
Yale University
Dept of Chemical Engineering
P.O. Box 2159, Yale Station
New Haven, CT 06520-2159
203/432-4378

Mr. Tim Harrell
GEC Avionics, Inc.
2975 Northwoods Parkway
Norcross, GA 30071
404/448-1947

Dr. Michael R. Harris
R.S.R.E.
St. Andrews Road
Malvern
Worchestershire, WR14 3PS
UNITED KINGDOM
0684/894099

Mr. Hartmuth Hecht
Coherent General
FEDERAL REPUBLIC OF GERMANY

Mr. Akira Fujita
JGC Gaithersburg Project Office
910 Clopper Road
P.O. Box 6032
Gaithersburg, MD 20877-0962
301/258-1700

Prof. Richard K. Herz
U. of California, San Diego
Chemical Engineering
Mail Code B/010
San Diego, CA 92093
619/534-6540

Dr. Robert V. Hess
NASA Langley Research Center
Mail Stop 468
Hampton, VA 23665-5225

Dr. Gar B. Hoflund
University of Florida
Chemical Engineering Dept
Gainesville, FL 32611
904/392-9104

Mr. James D. Jensen
CRDEC
APG, MD 21010-5423
301/671-3518

Dr. Kyu-man Jeong
AVCO Research Lab, TEXTRON
2385 Revere Beach Parkway
Everett, MA 02149
617/381-4872

Mr. Patrick L. Jones
Spectra Technology, Inc.
2755 Northup Way
Bellevue, WA 98004-1495
206/827-0460

Dr. Norman Jorgensen
Atomic Energy Authority
Catalyst Unit
Materials Development Division
BF29, Harwell Laboratory
Oxfordshire, OX11 0RA
UNITED KINGDOM
0235-432896

Mr. G. M. Jurscaga
NASA Langley Research Center
FAB
Hampton, VA 23665
804/864-4112

Mr. Charles W. Hench
GR-88, Inc.
12 Fox Chase Circle
Ridgely, MD 21660
301/261-2030

Mr. C. William Hench II
GR-88, Inc.
12 Fox Chase Circle
Ridgely, MD 21660
301/634-1186

Dr. John H. Kolts
Phillips Petroleum Company
370 PL, R & D
Bartlesville, OK 74004
918/661-1802

Dr. Norman A. Kurnit
Los Alamos National Lab
Group CLS-6
MS J564
Los Alamos, NM 87545
505/667-6002

CDR Frederick C. Marcell
Department of the Navy
Space & Naval Warfare Systems Cmd
Room 3320
National Center One
Washington, DC 20363-5100
202/692-5824

Mrs. Krystyna Marcinkowska
Atomic Energy of Canada Ltd
Chalk River Nuclear Laboratories
Chalk River
Ontario, KOJ 1JO
CANADA
613/584-3311

Mr. James McKay
Texas Instruments
MS 3119
P.O. 660246
Dallas, TX 75266
214/480-1931

Mr. Orlando Melendez
University of Florida
Chemical Engineering Dept
Gainesville, FL 32611
904/392-9105

Mr. Irvin M. Miller
Science and Technology Corp
c/o NASA LaRC
Mail Stop 234
Hampton, VA 23665-5225
804/864-4738

Dr. Joseph T. Keiser
Virginia Commonwealth University
Department of Chemistry
Richmond, VA 23173

Mr. David Knapp
Coherent Inc.
3210 Porter Drive
Palo Alto, CA 94304
415/858-7669

Dr. Ehsan Noordally
UOP Limited
Jeffreys Road
Brimsdown, Enfield
Middlesex, EN3 7PN
UNITED KINGDOM
01804/8232

Mr. Rolf Nowack
DLR Inst of Techn Physik
Pfaffenwaldring 38-40
D-7000
Strutgart 80
FEDERAL REPUBLIC OF GERMANY
0711/6862226

Mr. Richard H. Petersen
Director, NASA Langley Research Center
Hampton, VA 23665

Mr. John C. Petheram
GE Astro Space Division
MS 100A
P.O. Box 800
Princeton, NJ 08540
UNITED KINGDOM

Mr. Kirkman Phelps
CRDEC
SMCC R-DDT
APG, MD 21010-5423
301/671-5561

Mr. Richard Powell
Texas Instruments
MS 3119
P.O. 660246
Dallas, TX 75266
214/480-1767

Dr. Edward J. Poziomek
Artech Associates
80-4 Corsey Beach Avenue
East Haven, CT 06512
203/469-6089

Mr. J. R. Morris
B. Quantum Technologies Inc.
3100 W. Alabama
Houston, TX 77098
713/524-7384

Dr. Thomas P. Moser
Hughes Aircraft Company
P. O. Box 902
Mail Station EO/E1/F150
El Segundo, CA 90245
213/616-6185

Mr. Harry T. Price
GEC Avionics, Ltd.
Elstree Way
Borehamwood
Hertfordshire, WD1 6RX
UNITED KINGDOM
01-906-6158

Dr. John R. Richmond
UOP Limited
Jeffreys Road
Brimsdown, Enfield
Middlesex, EN3 7PN
UNITED KINGDOM
01804/8232

Dr. Brian W. Riley
UOP Limited
Jeffreys Road
Brimsdown, Enfield
Middlesex, EN3 7PN
UNITED KINGDOM
01804/8232

Mr. Glen Sachse
NASA Langley Research Center
LTAB FED
Hampton, VA 23665
804/864-1566

Dr. Christopher F. Sampson
Atomic Energy Authority
Materials Dev Divs
Bldg 42g
Harwell Laboratory
Oxfordshire, OX11 0RA
UNITED KINGDOM

Dr. David R. Schryer
NASA Langley Research Center
MS 468
Hampton, VA 23665
804/864-1576

Ms. Jacqueline Schryer
Old Dominion University
Norfolk, VA 23508

Dr. P. M. Schwarzenberger
GEC Avionics Limited
Applied Physics Division
Elstree Way
Borehamwood
Hertfordshire, WD6 1RX
UNITED KINGDOM
441/906/6140

Prof. Paul A. Sermon
Brunel University
Dept of Chemistry
Uxbridge
Middlesex, UB8 3PH
UNITED KINGDOM
0895/74000

Dr. Barry D. Sidney
Science and Technology Corp.
c/o NASA LaRC
MS 234
Hampton, VA 23665
804/864-1547

Dr. Anthony L.S. Smith
Melles Griot Lasers
2251 Rutherford Road
Carlsbad, CA 92008
619/438-2131

Dr. E. Allan Symons
Atomic Energy of Canada Ltd
Chalk River
Ontario, KOJ 1JO
CANADA
613/584-3311

Dr. John Twyman
Atomic Energy of Canada
Chalk River, Ontario, KOJ 1JO
CANADA

Dr. Billy T. Upchurch
NASA Langley Research Center
MS 234
Hampton, VA 23665
804/864-4752

Dr. John D. Van Norman
Old Dominion University
Department of Chemical Sciences
Norfolk, VA 23508
804/683-4078

Dr. Liang-guo Wang
College of William and Mary
NASA LaRC
MS 468
Hampton, VA 23665
804/864-1565

Dr. Francis C. Wang
Lockheed Missile & Space Company
4800 Bradford Blvd, N.W.
Huntsville, AL 35807
205/722-4019

Dr. David V. Willetts
R.S.R.E.
St. Andrews Road
Malvern
Worchestershire, WR14 3PS
UNITED KINGDOM
0684/895414

Dr. George M. Wood
NASA Langley Research Center
Mail Stop 234
Hampton, VA 23665-5225
804/864-4750

SECTION I

FUNDAMENTALS

PULSED-DISCHARGE CARBON DIOXIDE LASERS

David V. Willetts
Royal Signals and Radar Establishment
Great Malvern, Worcs, UK

INTRODUCTION

The purpose of this review is to attempt a general introduction to pulsed carbon dioxide lasers of the kind used or proposed for laser radar applications. There is a strong bias towards understanding those features of operation which impact strongly on gas lifetime issues, and so a decision has been made to omit mention of the theory of laser beams and resonators and the diffraction optics used to describe them. Nevertheless, laser physics is an excellent example of a cross-disciplinary topic, and the molecular spectroscopy, energy transfer, and plasma kinetics of the devices will be explored.

The review is structured to begin by introducing the concept of stimulated emission and population inversions, leading on to the molecular spectroscopy of the CO_2 molecule. This is followed by a consideration of electron-impact pumping, and the pertinent energy transfer and relaxation processes which go on. Since the devices are plasma pumped it is necessary to introduce a complex subject, but this is restricted to appropriate physics of glow discharges. Examples of representative devices are shown, and the review concludes with the implications of the foregoing to plasma chemistry and gas life.

STIMULATED EMISSION (Ref. 1)

Consider the two-level system shown in figure 1. Radiation of frequency E/h causes upward transitions from level 1 to level 2 at a rate $B_{12}IN_1$ where I is the intensity of illumination. Spontaneous emission or collisions cause a dissipative loss from level 2 at a rate $A_{21}N_2$. The nett effect of these processes is the well-known phenomenon of absorption of the incident radiation. However, there is a further process of stimulated emission, akin to (stimulated) absorption, which proceeds at a rate $B_{21}N_2I$. This is not observed with light of low intensity in thermal equilibrium, because the upper state population $(B_{12}/A_{21})N_1I$ is exceedingly low under such conditions. However if we can depart dramatically from thermal equilibrium and set up a condition where $N_2 > N_1$ (a so-called population inversion), the emissive rate $B_{21}IN_2$ exceeds absorption and the latter is replaced by gain, a condition of negative absorption. This arises because it is possible to show by quantum theory that $B_{12} = B_{21} = B$, so that

$$\frac{dI}{dt} = c\frac{dI}{dx} \quad \alpha\left[N_2 - N_1\right]BI \tag{1}$$

(which reduces to the familiar Beer's Law expression for absorption when $N_2 << N_1$). Since the phase, frequency, and direction of the emitted photons are, within uncertainty principle limits, identical to those of the stimulating radiation, coherent addition results with amplification of the incident radiation. With suitable feedback provided by mirrors, oscillation will result, and a coherent output beam will be emitted if one of the feedback mirrors is made partially transmitting.

The arguments may be extended to multilevel systems by invoking the principle of detailed balance (but note however that inversions, or departures from thermal equilibrium, are only possible on

3

limited pairs of transitions). Then at thermal equilibrium the processes in figure 1 may be compared with the Planck radiation law to give $B_{12} = B_{21}$ as before, but also to show that

$$\frac{A_{21}}{B} = \frac{8\pi h^3}{c^3} \nu^3 \qquad (2)$$

independent of the oscillator strength which governs both A_{21} and B in the same way. We see from equation (2) that spontaneous emission competes more and more successfully with stimulated emission as the transition wavelength is reduced. It is for this reason that the first stimulated emissive devices (Masers) were demonstrated in the microwave region and explains why there has been a trend to shorter wavelengths with improving technology; X-ray laser operation is still problematic.

MOLECULAR SPECTROSCOPY OF CARBON DIOXIDE (Ref. 2)

Normal Modes of Vibration

A system of coupled oscillators, typified on the microscopic scale by a simple molecule, can in general carry out a very complex Lissajous motion. It may be shown that all such motions arise from the addition of excitations of 'normal modes' in the correct phase. Carbon dioxide is a linear symmetric triatomic molecule and thus possesses three normal modes, illustrated schematically in figure 2. The bending mode is doubly degenerate. The modes are named and numbered as shown and some insight into their frequencies ω_i may be obtained by assumption of a simple valence force field model. This model joins the point masses with springs which do not interact and which possess force constants k_b and k_s for bending and linear extension respectively. Preserving linear momentum and assuming simple harmonic motion leads to the relations

$$\omega_1^2 = k_s/m_o ; \quad \omega_2^2 = k_b \frac{1 + \frac{2m_o}{m_c}}{m_o} ; \quad \omega_3^2 = k_s \frac{1 + 2\frac{m_o}{m_c}}{m_o} \qquad (3)$$

Despite the simplistic approximation ($\omega_3/\omega_1 = 1.76$; calc. = 1.91) these relations turn out to be very useful for calculating isotopic shifts. The 'springs' have force constant k_s of about 1000 dyne/cm, like typical small man-made springs. The masses are of course very small, about 10^{-26}g. Consequently the vibration frequencies are over 10^{13} Hz.

Vibrational Energies

Solution of the Schrödinger equation for the parabolic potential of a harmonic oscillator yields eigenvalues E_i of $(v_i + d_i/2) \hbar\omega_i$, a ladder of equally spaced rungs. v_i is the vibrational quantum number and d_i is the degeneracy of the level. Anharmonicity causes the ascending rungs to get closer together. The energy level diagram of the low-lying vibrational states of CO_2 appears in figure 3. States are labelled as $(v_1 v_2^l v_3)$ where l is the number of quanta of vibrational angular momentum in the bend. The (100) and (02^{0}0) states interact by Fermi resonance and so the resulting states are mixed and shifted in energy, but this is normally ignored in labelling transitions. Subsequently it will

4

be shown that it is fairly easy to selectively excite ("pump") $v_3 = 1$ to give inversions over $v_1 = 1$ or $v_2 = 2$. The resulting oscillation occurs in bands at about 9 and 10 microns wavelength. Isotopic substitution by ^{13}C and/or ^{18}O shifts the vibrational levels by amounts computable from the valence force field results with a consequent small change in oscillation frequency. There is no longer an automatic coincidence with the 626 'normal' isotopic CO_2 present in the atmosphere, with less resultant atmospheric absorption. This can be of special benefit for long-range remote-sensing systems. 'Sequence band' operation has been obtained on transitions such as $(011) \rightarrow (110)$, in which an extra bending quantum is present in both lower and upper laser levels; these are shifted to longer wavelength than the $(001) \rightarrow (100)$ transitions by anharmonic effects.

Rotational Structure

The solution of Schrödinger's equation for a rigid rotor yields a set of energy levels which are not equally spaced. To first order

$$E_J = BJ(J+1) \qquad\qquad (4)$$

where $B = \dfrac{h}{8\pi^2 I c}$ and J is the rotational quantum number.

Since molecules can vibrate and rotate their total energy is to a good approximation given by the sum of the vibrational and rotational contributions. Since from the above formula rotational quanta are rather small – B is 0.39 cm^{-1} for CO_2 – the resultant energy level diagram is as shown in figure 4. Here some strong laser transitions in the molecule are included. Several features are immediately apparent. The selection rule $\Delta J = \pm 1$ is seen to govern the changes in J; the transition $J \rightarrow J+1$ is termed the R(J) line, while $J \rightarrow J-1$ is called P(J). Alternate levels are missing due to nuclear spin statistics: the nuclear spins of ^{16}O and ^{18}O are zero. The rotational dependence of the matrix elements governing the oscillator strength is roughly the same as the rotational degeneracy, so the distribution of gain among the rotational levels closely follows the thermal distribution, peaking at about $J = 20$. Because rotational relaxation and rotational – translational energy transfer is exceedingly rapid, the rotational levels tend to thermalise at the ambient gas temperature. The vibrational levels are inverted, however, and this leads to an enhanced gain on the P branch transitions. Maximum gain occurs around P(20), which dominates the output unless a dispersive element is placed within the laser cavity to select other transitions.

POPULATION INVERSION MECHANISMS (Ref. 3)

Electron Impact

Although CO_2 lasers can be pumped by a variety of means, the most important is electrical, and is the only method to be considered here. Electrons present in the 'glow discharge' type of plasma, which will be discussed in more detail later, impact molecules and in so doing lose some of their kinetic energy to excitation of the molecule. In the Born approximation for electric-dipole transitions, the cross sections for electron impact excitation are proportional to the optical cross sections, and thus it would be expected that the upper laser level could be populated by this means. On the other hand, neither of the lower states (100) and (020) would be populated; in the first case because the vibration

5

induces no dipole, and in the second because the selection rule $\Delta v = 1$ would be broken. Thus it should be possible to set up a population inversion by this selective excitation technique. Although the Born approximation is not expected to be accurate for electrons of such low energy as encountered in practice in glow discharges, the very first CO_2 laser to be operated did in fact depend on this pumping scheme.

Resonance Transfer

It was soon discovered that a great enhancement in laser power output and efficiency could be obtained by including nitrogen in the laser gas mixture. Energy transfer occurs from vibrationally excited nitrogen ($v = 1$) to the CO_2 ($v_3 = 1$) level at a very high rate, 1.9×10^4 torr^{-1}sec^{-1}, because of the extremely close coincidence in energy of these two states; the energy difference is only 18 cm^{-1}. The $v = 1$ level of nitrogen has a very long radiative lifetime since there is no dipole, and the cross–section for electron impact excitation, shown in fig.5, extends over a broad electron energy range due, not to the forbidden dipole process, but to the existence of an unstable N_2^- state. $N_2(v = 1)$ is thus a near–ideal energy transfer agent.

Relaxation Processes

The optical inactivity of the transition from ground state to lower laser levels has already been mentioned. Thus the radiative lifetimes of these levels is very long, and some other process must be found to empty these levels during laser action, otherwise the population inversion cannot be maintained. Collisional relaxation is the key process; for instance, there is only a 50 cm^{-1} energy mismatch in the processes

$$CO_2(100, 02^\circ 0) + CO_2 (000) \rightarrow 2CO_2 (010) \tag{5}$$
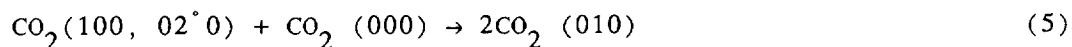
However it remains to find a rapid means of collisionally removing $CO_2(010)$ or even better the lower laser levels directly. At the same time collisional relaxation of the upper laser level, $CO_2(001)$, is highly undesirable since it competes with the pumping process. Fortunately it is found that helium fulfills these criteria admirably, and at the same time is chemically inert and provides an excellent 'buffer gas' in which to run the electric discharge.

Hence, CO_2 lasers are almost invariably operated in a gas mixture containing helium and nitrogen as well as carbon dioxide; the former relaxes the lower laser level and the latter pumps the upper laser level by resonant energy transfer.

PULSED GLOW DISCHARGES (Ref. 4)

Introduction

Numerous definitions of plasma exist; none are entirely satisfactory. For our purposes the following will suffice: an ionised gas maintained in a steady state by an electric field driving a current through it to balance the energy losses. The reader is probably familiar with several types of plasmas such as arcs and glow discharges. Certain properties of the plasma required have already emerged

from previous sections. The gas temperature must be kept fairly low to avoid thermal population of the lower laser level; the exact value depends on a number of parameters such as pumping rate but certainly 100°C should be looked on as rather high. On the other hand, the electron energy required to excite the vibrational states of nitrogen is 2-3 electron volts (see fig. 5), which corresponds to an electron temperature of order 30,000K. In fact the enormous mass ratio between electrons and molecules leads to restricted energy exchange and it is indeed possible to produce a plasma which departs from thermal equilibrium with an electron temperature of about 1eV and a gas temperature around ambient; it belongs to a class known as glow discharges. The gas mixture must contain CO_2 and nitrogen in roughly equal amounts, generally with an excess of helium. It has been experimentally established that extraction of reasonable energy from a fairly compact device requires quite a high molecular density, approaching or roughly equal to one atmosphere.

Steady-State Operation

A number of processes operate which ultimately lead to the mutual neutralisation of the separated charges in a plasma, and the plasma can only exist in a steady state if the rate of production of ions and free electrons balances these loss processes. The carbon dioxide laser can be operated using continuously working or pulsed discharges; while all of the foregoing sections apply equally well to both types, the discharge stability conditions are quite different and lead to quite different engineering designs. In cw lasers, the loss process is predominantly ambipolar diffusion to the wall; in pulsed devices there is insufficient time for this to happen and the plasma adjusts to a condition where gas-phase recombination or electron attachment to neutral species dominate losses. We will now investigate how the rates of these processes can be quantified in order to gain some insight into the conditions within the plasma.

The ionisation rate by impact of plasma electrons may be obtained as follows. For a monoenergetic stream of electrons of velocity v_e and density n_e passing through a gas of molecular density N_0 and ionisation cross section per molecule $Q_i(v)$, simple kinetic theory gives an ionization rate per unit volume $Z_i(v)$ of

$$Z_i(v) = n_e N_0 v_e Q_i(v) \qquad (6)$$

Generalising to electrons distributed in energy such that $f(\epsilon)d\epsilon$ is the fraction of n_e in the range ϵ to $\epsilon + d\epsilon$, we find

$$dZ_i = N_0 v_e Q_i dn_e \qquad (7)$$

$$\left[\frac{2\epsilon}{m}\right]^{\frac{1}{2}} \qquad n_e f(\epsilon)d\epsilon$$

so that

$$Z_e = n_e N_0 \int_{\epsilon_i}^{\infty} \left[\frac{2\epsilon}{m}\right]^{\frac{1}{2}} Q_i(\epsilon) f(\epsilon)d\epsilon \qquad (8)$$

or $\quad Z_i = n_e N_0 S_i \qquad (9)$

where ϵ_i is the ionisation threshold energy.

If further the electron distribution is Maxwellian with a temperature T_e, then

$$f(\epsilon) \;=\; 2 \left[\frac{\epsilon}{\pi} \right]^{\frac{1}{2}} \left[kT_e \right]^{-3/2} \exp - \left[\epsilon / kT_e \right] \tag{10}$$

Figure 6 shows a typical shape of an ionisation cross-section and Maxwellian electron energy distribution. We are concerned with the integral of the product of $Q_i(\epsilon)$ and $f(\epsilon)$, and it is clear from the diagram that under normal circumstances only the high energy tail of the distribution overlaps the cross-section above threshold. Thus the Maxwellian provides the high energy cutoff to the integral, which is not very sensitive to the shape of the ionisation cross-section $Q_i(\epsilon)$. The latter may be approximated by any sensible function such as a step or linear ramp and it is always found that

$$S_i \;=\; \left[\frac{8}{\pi m} \right]^{\frac{1}{2}} Q_i (\max) \, \epsilon_i^{\frac{1}{2}} \; \varphi \left[\frac{\epsilon_i}{kT_e} \right] \exp - \left[\epsilon_i / kT_e \right] \tag{11}$$

where φ is a very slowly varying function of T_e of order unity. Clearly ionisation of the species having the lowest IP is strongly favoured in mixtures of gases and in the CO_2 laser mixture the dominant ionisation will be of CO_2 itself. Of course just as many electrons will be formed as positive ions in the process

$$e + CO_2 \rightarrow CO_2^+ + 2e \tag{12}$$

so the ionisation rate is identical to the electron production rate. However, a series of complex ion-molecule reactions ensure that CO_2^+ is by no means necessarily the dominant positive ion in the plasma. Equation 11 reveals that the ionisation rate rises dramatically with electron temperature, and this is shown schematically in figure 7. Here typical attachment and recombination plots for CO_2 laser gas mixtures are included. The attachment process

$$e + M \rightarrow M^- \tag{13}$$

suffers from the usual conservation restrictions, and processes such as dissociative attachment which are not so impeded tend to predominate; e.g

$$e + CO_2 \rightarrow CO + O^- \tag{14}$$

These attachment processes have a threshold at lower energy than ionisation, so their T_e dependence is as shown in figure 7. Electron-ion recombination coefficients actually fall slowly with T_e because recombination is facilitated by the smaller the relative velocity and hence the longer the 'contact time' between electron and ion. On the other hand the negative ion produced by electron attachment can rapidly recombine with positive ions and be removed.

Self-Sustained Operation

With these arguments and by referring to figure 7 we are in a position to understand the determinants of electron temperature in real devices. Provided that some 'preionisation' (to be discussed later) is present, the discharge will settle down after application of sufficient voltage to run at point a, where ionisation balances attachment. Certain substances such as hydrogen cause electron 'detachment' from negative ions thus reducing the apparent attachment coefficient and operating electron temperature. Under conditions of strong detachment the loss processes become dominated by recombination and the self-sustained discharge operates at point c. Since $kT_e \approx$ energy gained by electron/mean free path = $eE\lambda$, where E is the electric field present in the plasma and the m.f.p $\lambda \propto N_o^{-1}$, we see that there must be a one-to-one correspondence between T_e and E/N_o, the so-called 'reduced' electric field. Consequently, the field at which the discharge runs is not freely variable in the self-sustained regime, but is set by the electron temperature at which ionisation balances attachment or recombination. In typical CO_2 laser mixtures, E/N assumes a value of 10-15 kV/cm atmosphere (3.7 – 5.6 x 10^{-16}Vcm^2). Note that the actual steady-state value of n_e, and thus discharge current, has not entered the discussion, and indeed the current is here determined only by external circuit restraints and can be varied widely at fixed voltage; values of order 200A/cm^2 are not unusual in self-sustained devices.

Electron-Beam-Sustained Operation

Calculations of the type described for ionisation by electron impact are trivially extendable to other impact processes. If instead of the ionisation cross-section we use the vibrational excitation cross-section for nitrogen shown in figure 5, we obtain the excitation rate essentially of the upper laser level. Varying the electron temperature reveals that this process occurs with maximum efficiency at a reduced field of near 4kV/cm atm (1.5 x 10^{-16}Vcm^2), much lower than typical self-sustained laser operating points. If we could ionise the gas by some means other than electron impact by plasma electrons of energy $\sim kT_e$, it may be possible to choose the reduced field, and thus operate at a more optimal value. This can indeed be done by firing high energy electrons (E $\approx$ 100 keV) through a thin foil 'window' into the gas which is ionised by impact with these externally supplied projectiles. The electron temperature may then be set by appropriate choice of an applied electric field which drifts the 'secondary' electrons and positive ions produced by the high-energy electrons towards the electrodes. If the electron temperature is set below T_c in figure 7, it is seen that recombination is the dominant loss process. In the absence of detaching species, attachment dominates losses from T_c to approaching T_a, the point near which self-sustained operation takes over. As detaching species are added recombination dominates the loss processes for increasing T_e.

The steady-state operating current in externally-sustained discharges is not set by the external circuit. For a primary electron transmitted at a current density of J_p, the ionisation and secondary electron production rate is

$$\frac{dn_e}{dt} = J_p \frac{\sigma}{e} N_o \qquad (15)$$

where σ is the collisional ionisation cross-section by high energy electrons. In the attachment-dominated regime, the loss rate is

$$-\frac{dn_e}{dt} = \beta N_o n_e \qquad (16)$$

where β is the attachment coefficient. Thus the equilibrium secondary electron density is

$$n_e = \frac{J_p \sigma}{e\beta} \qquad (17)$$

and consequently the secondary current density J_s amounts to

$$J_s = n_e e\bar{v} = \frac{J_p \sigma}{\beta}\bar{v} \qquad (18)$$

where $\bar{v}$ is the drift velocity under the action of the applied field. We see that the secondary current can be substantially greater than the primary, and the 'magnification ratio' M is

$$M = \frac{J_s}{J_p} = \frac{\sigma}{\beta}\bar{v} \qquad (19)$$

M is typically of order one thousand. The discharge in this regime is <u>ohmic</u>, with an impedance Z of

$$Z = \frac{Ed}{J_s A} = \frac{d}{A}\left[\frac{\beta}{J_p \sigma \mu}\right] \qquad (20)$$

where d and A are the discharge gap and area, respectively, and μ is the electron mobility $\bar{v}/E$. The discharge has conductivity $(J_p \sigma \mu / \beta)$, and its impedance is normally of order 10 ohms.

Stability Conditions

Self-sustained discharges are inherently unstable. Suppose a region of increased electron density forms near one electrode. This will have an enhanced conductivity relative to the rest of the plasma and will tend to 'short-out' some of the field in the gap. Consequently the field in the remainder of the gap will be increased and so too will the ionization rate, which will exceed the loss rate and lead to an uncontrolled growth of n_e-- an 'avalanche'. Thus the region of increased n_e grows until the gap is bridged by a highly conducting streamer-- an arc. Since the arc column is so highly conducting it can sustain current densities many orders greater than glow discharges and so is normally constricted in cross-section. Once established, the conductivity is so high that the electric field, and thus electron temperature, are rather low, insufficient for electron-impact ionisation to exceed losses. On the other hand n_e is so high that collisions with neutral species are so frequent that thermalisation occurs, with the gas temperature being greatly raised above ambient. Under these circumstances the ionisation is maintained thermally ('Saha process').

Arcs are quite unsuitable for pumping carbon dioxide lasers due to the approximate equality of their gas and electron temperatures; true thermal equilibrium is reached so a vibrational inversion cannot be produced. The glow-to-arc transition described above is therefore highly undesirable, and several techniques are used to avoid it. Firstly, the arc takes a small but finite time to develop (~ 1 μs), so that it can be avoided if steps are taken to ensure that the glow discharge is of short duration; low inductance and resistance capacitor-discharge circuits are required. Secondly, the electrode surfaces

10

must be as smooth as possible to avoid local field enhancements due to surface irregularities. Thirdly, it is necessary to 'preionise' the gas before application of the electric field with about 10^7 electron cm^{-3} to avoid the effects of statistical fluctuations on the initial starting avalanche processes. This is generally ensured by UV or X-ray photoionisation of the gas in the gap, or by photoelectric emission from the electrodes. Conversely, species which readily attach electrons increase the likelihood of the glow-to-arc transition and should be avoided. Oxygen is a good example with an upper limit for stable operation of less than 1%, and since it is produced by dissociation of the carbon dioxide, this process needs to be minimised; it will be discussed at more length in the section on plasma chemistry.

Electron-beam sustained discharges are very stable. Fluctuations in n_e do not alter the ionization rate since this depends on the injected flux of primary electrons; ionisation by secondary electron impact is negligible since the electron temperature is chosen, by the appropriate impressed field, to be low, and optimal for pumping N_2 (v = 1). Consequently these discharges are much more tolerant of attaching species such as oxygen, and the limit is set by considerations of impedance mismatch of discharge to pulse forming network or even of carbon dioxide loss. A typical value of several percents of oxygen can be tolerated with graceful performance fall-off rather than catastrophic arcing.

REPRESENTATIVE DEVICES

With the scientific principles discussed, it is possible to examine engineering designs of pulsed CO_2 lasers. Of course very large numbers of designs have evolved for specific applications; here we consider a typical 'single shot' mini-TEA (transversely-excited atmospheric pressure configuration) laser and an electron-beam sustained device, and then examine the consequences of operation at significant repetition rates.

Mini-TEA Laser

Because operating fields increase with pressure, at one atmosphere the field in a self-sustained laser is measured in tens of kilovolts per centimetre. In order to keep operating voltages at reasonable levels, the discharge length along the field direction must be very short. This led to the development of the transversely-excited atmospheric pressure configuration (TEA) with the field orthogonal to the optical axis. A good example is the miniature TEA laser shown in figure 8, of the kind used for tactical rangefinding. A typical discharge section is 1 x 1 x 10 cm and output energy 100 mJ. Profiled electrodes ensure that the field nowhere exceeds that in the discharge. Preionisation is produced here by a row of UV – emitting arcs running parallel to the profiled electrodes. A CO oxidation catalyst to maintain gas life is placed somewhere within the structure which is filled to 1 atmosphere with the typical laser mixture, and the field is applied from a low inductance capacitor through a triggered spark-gap switch (not shown). The resulting current pulse lasts only a few hundred nanoseconds, insufficient time for the glow-arc transition to take place. The optical output consists of a short spike of duration about 50ns in which most of the population inversion is destroyed, followed by a 'tail' of duration about $1\mu s$ in which energy continues to transfer gradually from vibrationally excited nitrogen. The energy loading of the discharge is limited to a few hundred Joules per litre by thermal population of the lower laser level. The high operating electron temperature gives a multimode efficiency of somewhat less than 10%, and a single mode efficiency rather lower still. Such a device offers very simple construction, and can be operated at up to a few pulses per second without gas flow, when convection and thermal diffusion occur fast enough to adequately cool the laser gas mixture.

11

Figure 9 shows the cross-section through an electron-beam sustained device. This can be operated at the optimum 4kV/cm atmosphere and give multimode efficiencies in excess of 20%. The construction is much more complex than self-sustained devices, however, and lends itself best to large volume discharges which can operate stably in this mode. An electron gun is needed to produce the high energy primary beam. This may operate by field emission, thermionic emission, or ion bombardment, and at least some designs can run for tens of microseconds. Thus the facility exists for 'long pulse' operation of the laser, with roughly rectangular output pulses of duration several microseconds or more. The high voltage pulse to the gun is often produced using a pulse transformer and pulse-forming network. Since the gun is a vacuum or very low pressure device the foil separating it from the main discharge (at about an atmosphere) must be well supported. Many of the electrons are stopped by the foil (transmission about 70%) so at appreciable repetition rates the foil support structure must be cooled. Finish and profile of the electrodes are much less critical than for self-sustained devices since the applied field is such that avalanching is insignificant.

Repetition-Rate Operation

Above a pulse repetition frequency (prf) of a few Hz, diffusion and convection are inadequate to cool the gas, which will become hotter with each successive pulse and laser action will cease. Fluctuations in gas density will cause fluctuation in E/N, and thus also lead to discharge instability. It is necessary to deliberately force gas around the system in a flow loop to renew the mixture between pulses. Figure 10 shows a schematic cross-section through such a device. The flow is usually transverse; ie. flow direction, optical axis, and electric field are all orthogonal. The ductwork incorporates a heat exchanger to maintain the gas at the required temperature and a catalyst artifact to oxidise CO to CO_2. The latter is normally fitted close to the discharge on the downstream side to enhance the catalytic activity by use of the unwanted gas heating. Some kind of fan or impeller is built into the ductwork to circulate the gas at the required rate, and to expedite this process it is important, especially at high prf, to minimise the flow impedance of the heat exchanger and catalyst.

PLASMA CHEMISTRY (Ref. 5)

Introduction

We have already seen that carbon dioxide lasers are normally filled with a mixture of nitrogen, carbon dioxide, and helium. In addition it is often difficult to entirely eliminate water vapour from the laser envelope since it is difficult to completely clean many constructional materials. Although these appear a rather unpromising set of reactants, they are subjected in the plasma to a number of energetic processes such as electron impact which can excite and dissociate molecules. Further neutral and ion-molecular reactions then ensue to give rise to interesting and important chemical effects. Obviously the loss of carbon dioxide by dissociation to carbon monoxide and oxygen is directly relevant, but the subsequent oxidation of oxygen and nitrogen to ozone and NO_x can give rise to an oxygen deficit for any catalysis of the CO/O_2 recombination reaction. These and other processes will be explored next.

Carbon Dioxide Dissociation

There are known to be two channels for the dissociation of carbon dioxide by electron impact:

$$e + CO_2 \rightarrow CO + O + e \qquad (21a)$$

$$e + CO_2 \rightarrow CO + O^- \qquad (21b)$$

The former (21b) has a much larger cross-section but higher threshold than the dissociative attachment process (21b), as shown in figure 11. The dissociation rate for any particular electron temperature may be found using the formalism of equation 11. For self-sustained discharges reasonable agreement is found between the measured dissociation rate, of order 10^{21} molecules/coulomb passed (dependent on gas composition, device size, etc), and calculation assuming the process occurs in the bulk of the gas. In this case the relatively high value of T_e leads to the process (21a) being dominant. Electron-beam sustained discharges are normally operated at a much lower electron temperature and the exponential in equation 11 gives rise to very low calculated values of the bulk dissociation by either process. Experimental measurements reported elsewhere in these proceedings, while much lower than comparable self-sustained devices, are higher than the bulk calculations. The same experiments indicate that the dissociation is occurring in the high T_e region of the sheath associated with electron emission from the cathode.

Knowledge of the dissociation rates, coupled with tolerance to dissociation products – namely oxygen, since carbon monoxide does not attach – allows specification of the CO oxidation catalyst. However there are other reactions which can occur with which the catalyst may have to deal.

Oxygen Loss

In experiments on both self-sustained and e-beam sustained CO_2 lasers, it has been observed that, at least initially, carbon monoxide and oxygen are not formed in their correct stoichiometric ratio of 2:1, but in a ratio greater than 2.0. This implies that oxygen is being lost to form other compounds and is therefore unavailable for CO oxidation (although significant CO_2 loss has not been observed in small TEA lasers up to 2×10^7 pulses). These processes therefore merit closer examination, although at the time of writing limited experimental or theoretical progress has been made, largely due to the complexities of the possible reactions. Once carbon dioxide dissociation has taken place, two new species have been added to the gas, one of which, atomic oxygen, is particularly reactive. The reverse reaction

$$O + CO \ (+M) \rightarrow CO_2 \ (+M) \qquad (22)$$

is spin forbidden and proceeds at a negligible rate. The rate constant for the three-body association of oxygen atoms is high, reflecting the spin conservation of the process

$$O + O \ (+M) \rightarrow O_2 \ (+M) \qquad (23)$$

Once molecular oxygen has been formed, it can undergo further reaction with atomic oxygen to form ozone

$$O + O_2 \ (+M) \to O_3 \ (+M) \tag{24}$$

by a fast allowed process. Reaction of oxygen atoms with nitrogen to give nitrous oxide is spin forbidden and to give nitric oxide and nitrogen atoms is highly endothermic; oxygen atoms do not react with nitrogen. Nitrogen oxides are probably formed by several routes. The associative detachment reaction

$$O^- + N_2 \to N_2O + e \tag{25}$$

can produce nitrous oxide from the small amounts of O^- present in the plasma; the product is probably immune to further oxidation. Nitrogen atoms formed by dissociative electron–ion recombination of N_2^+ undergo reactions of the kind

$$N + O + M \to NO + M \tag{26}$$

followed by

$$NO + O + M \to NO_2 + M \tag{27}$$

However once some ozone and nitrogen oxides are formed they are subject to destruction by such processes as

$$NO + O_3 \to NO_2 + O_2 \tag{28}$$

$$O + NO_2 \to NO + O_2 \tag{29}$$

so they do not reach high concentrations. Undoubtedly the complete reaction set is much more complex, with three-body ion-molecule reactions probably playing an important part; unfortunately the rate constants of the latter are not well known, only four being included out of 167 possible reactions in one computer simulation! Nevertheless it would be useful to catalyse exothermic destruction reactions such as

$$2NO + 2CO \to N_2 + 2CO_2 \tag{30}$$

and $N_2O + CO \to N_2 + CO_2 \tag{31}$

Designers of CO oxidation catalysts need therefore to allow for oxidation not just by oxygen, but also the oxides of nitrogen and ozone.

14

While the direct association of CO and oxygen atoms takes place at a negligible rate, the reaction

$$OH + CO \rightarrow CO_2 + H \qquad (32)$$

goes very quickly. Hydroxyl radicals can be formed readily from oxygen atoms in the presence of water vapour by the process

$$O + H_2O \rightarrow 2OH \qquad (33)$$

while the dissociative attachment and ionisation reactions

$$e + H_2O \rightarrow OH + H^- \qquad (34)$$

$$e + H_2O \rightarrow OH + H^+ + 2e \qquad (35)$$

also yield hydroxyl. Thus, carbon monoxide readily reacts with oxygen in the presence of water vapour via reaction (32); the hydrogen atoms complete the chain via

$$H + O_2 \rightarrow OH + O \qquad (36)$$

to regenerate hydroxyl, with the net reaction

$$CO + O_2 \rightarrow CO_2 + O \qquad (37)$$

There is a plethora of further radical and atom loss processes analogous to those described in the previous section, but the overall conclusion is that water vapour behaves as a very effective homogeneous catalyst for carbon monoxide oxidation. It is to be expected that the plasma is the initial source of hydroxyl radicals, both directly from processes (34) and (35) and via the formation of oxygen atoms followed by (33). Thus the effectiveness of water vapour (or hydrogen, which readily reaches equilibrium with water in the plasma) as a catalyst should depend on the plasma electron temperature. Limited experimental work has been undertaken on homogeneous catalysis in CO_2 lasers, but it appears that hydrogen and CO are effective discharge stabilisers in helium-rich mixtures but not in mixtures containing little or no helium. This could be due to the difference in electron temperature, but it must also be pointed out that these molecules are effective electron detachers from negative ions, and thus tend to stabilise the discharge by this means also.

REFERENCES

1　Eyring, H., Walter, J., and Kimball, G. E.:　Quantum Chemistry (Wiley, 1967), Chapter 8.

2　Herzberg, G.:　Molecular Spectra and Molecular Structure II Infrared and Raman Spectra of Polyatomic Molecules (Van Nostrand, 1945).

3　Cheo, P. K.:　'CO_2 lasers' in Levine, A. K., and DeMaria, A. J.:　Lasers Volume 3 (Dekker, 1971).

4　Webb, C. E.: 'The fundamental discharge physics of atomic gas lasers' and
Judd, O. D.: 'Fundamental kinetic processes in the CO_2 laser'; both in Pike, E. R.: High power gas lasers, 1975 (Inst. Phys. Conf., Ser. No 29, 1976).

5　Von Engel, A.:　Electric plasmas, their nature and uses (Taylor & Francis, 1983), Chapter 10.
Smith, I. W. M.: 'Reactive and Inelastic Collisions involving molecules' in Gas Kinetics and Energy Transfer, Vol 2.　(The Chemical Society, 1977).
Hokazono, H. and Fujimoto, H.: Theoretical analysis of the CO_2 molecule decomposition and contaminants yield in a TEA CO_2 laser discharge, J. Appl. Phys. 62 (5), 1585 (September 1987).
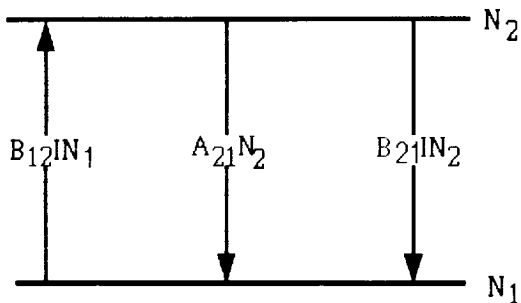
Figure 1. Radiative processes in a
two-level system.
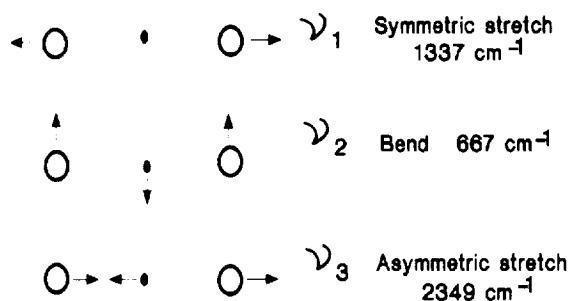
Figure 2. Normal modes of the CO_2 molecule.
Frequencies are for the 626 isotope.
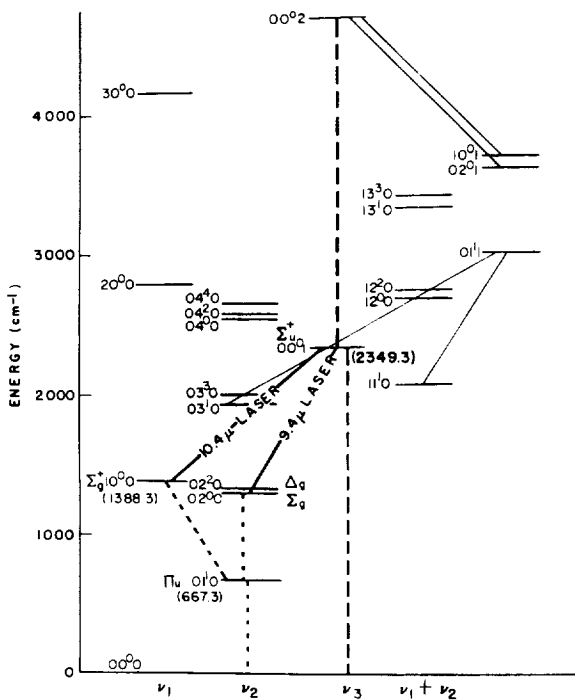
Figure 3. Energy level diagram of low-lying
vibrational levels of the carbon
dioxide molecule.

Permission to reproduce figure
granted by American Physical
Society/American Institute of Physics
(Physical Review, vol. 125, p. 229, 1962).
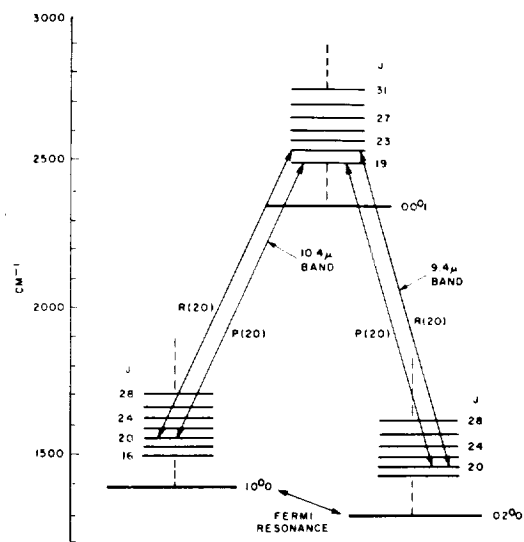
Figure 4. Total effective cross section for
vibrational excitation of N_2 (V = 1 - 8)
by electron impact.
(After Schulz)
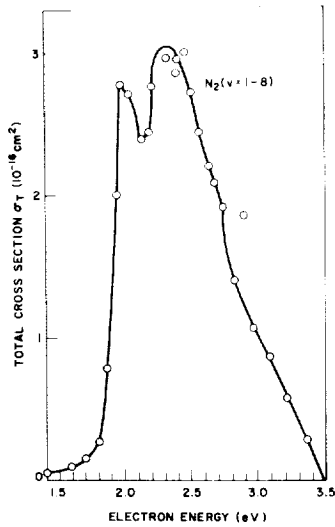
Figure 5. A detailed laser transition diagram for the $00^0 1 - 10^0 0$ and $00^0 1 - 02^0 0$ bands, including rotational levels.
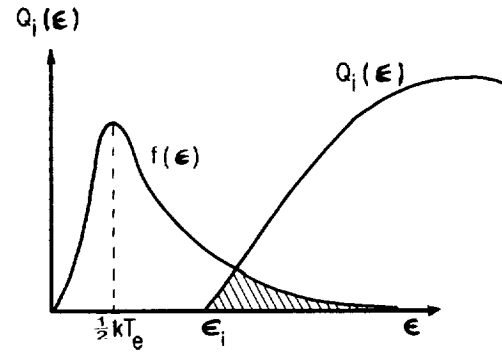
Figure 6. Ionisation cross section and Maxwellian energy distribution.
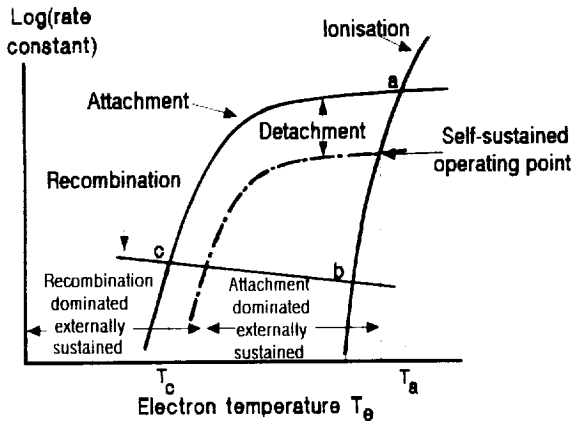
Figure 7. Ionisation and loss processes in pulsed-CO_2 laser discharges.
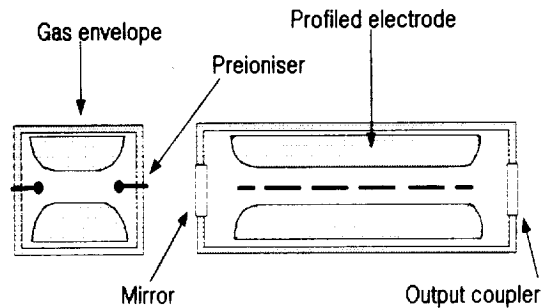
Figure 8. Schematic section through mini-TEA laser.
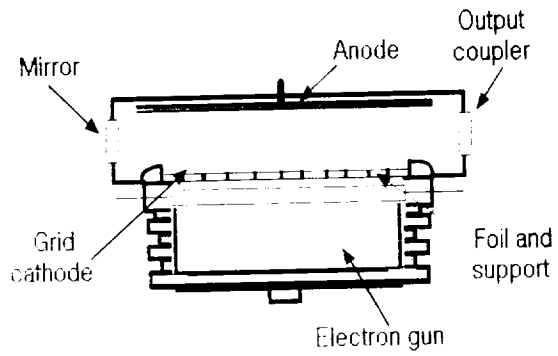
Figure 9. Schematic section through e-beam-sustained carbon dioxide laser.
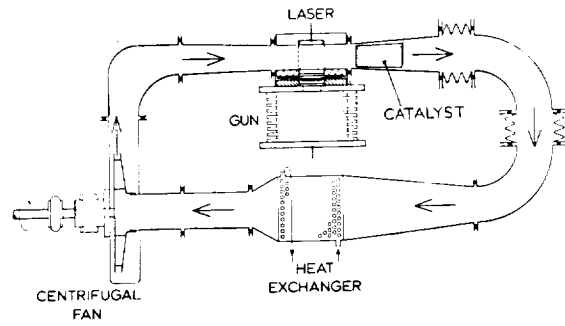
Figure 10. Schematic diagram of a high repetition rate pulsed-CO_2 laser.
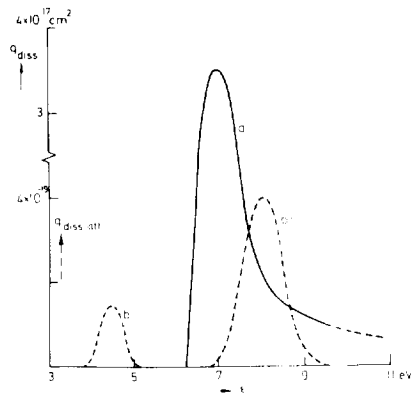
Figure 11. Dissociation $q_{diss} \cdot f(\epsilon)$ (curve a) and dissociative attachment $q_{diss\ att} \cdot f(\epsilon)$ (curves b) of CO_2.

CO-Oxidation Catalysts:
Low-Temperature CO Oxidation Over
Noble-Metal Reducible-Oxide (NMRO) Catalysts

Richard K. Herz
Chemical Engineering Group, Mail Code B-010
Department of Applied Mechanics and Engineering Sciences
University of California, San Diego, California

INTRODUCTION

Oxidation of CO to CO_2 is an important reaction technologically and environmentally and a complex and interesting reaction scientifically. In most cases, the reaction is carried out in order to remove CO as an environmental hazard. A major application of heterogeneous catalysts is catalytic oxidation of CO in the exhaust of combustion devices. The reaction over catalysts in exhaust gas is fast and often mass-transfer-limited since exhaust gases are hot and O_2/CO ratios are high. The main challenges to catalyst designers are to control thermal sintering and chemical poisoning of the active materials.

In the application discussed in these proceedings, sealed CO_2 lasers, CO oxidation is carried out in order to recombine CO and O_2 formed by dissociation of CO_2 in the laser discharge zone. This application differs from exhaust clean-up in ways that present completely different challenges to designers of CO oxidation catalysts. Gas temperatures in lasers must be held low, in the range $0°C \pm 40°C$, in order to minimize power consumption and to keep the gas cool in the laser discharge volume. O_2/CO ratios are stoichiometric or less since these species are formed by CO_2 dissociation and some oxygen may be consumed in other reactions. Additional O_2 cannot be added to facilitate CO oxidation because the laser discharge is degraded by O_2.

Conventional catalysts are not active at low temperatures and low O_2/CO ratios. Over conventional noble-metal catalysts, CO and O_2 compete for the same adsorption sites on the metal surface. At low temperatures and low O_2/CO ratios, adsorbed CO blankets the active surface of the noble metal and prevents O_2 adsorption and reaction. Over conventional base-metal-oxide catalysts, oxygen is held too strongly for it to be removed by CO at low temperatures.

Currently, Pt/SnO_2 and related materials are the most promising catalysts for use in sealed CO_2 lasers. Stark and Harris [1] reported significant reaction rates over Pt/SnO_2 and Pd/SnO_2 at temperatures as low as $-27°C$, conditions under which conventional catalysts are inactive. This report reviews work in the literature on Pt/SnO_2 and related materials. Contained in this report are citations to references 1 through 161.

When Pt and Pd are used in conventional noble-metal CO oxidation catalysts, they are usually dispersed over Al_2O_3. Al_2O_3 does not participate in CO oxidation and serves as an inert support that maintains high noble-metal dispersions. CO adsorbed on the noble metal strongly inhibits O_2 adsorption and, thus, the reaction. In contrast, Bond and coworkers [2,3] demonstrated that SnO_2 interacts synergistically with the noble metal to produce a catalytic activity that is substantially higher than either component separately. Since CO and O_2 have to compete for the same surface sites over noble metals, it is likely that the mixture of the two components in the composite NMRO material provides separate sites for CO and O_2 adsorption: CO adsorbed on the metal can react with oxygen held by the SnO_2. While this hypothesis is probably part of the full explanation, experimental evidence for Pt-Sn metal alloy formation [4] and the sensitivity of the

catalysts to H_2O [5,76], suggest that much remains to be learned about low temperature CO oxidation over Pt/SnO_2 and related materials. How Pt/SnO_2 works and how more active and stable materials can be synthesized remain open questions.

David Schryer at NASA's Langley Research Center coined the phrase "noble-metal reducible-oxide" and acronym "NMRO" to refer to Pt/SnO_2 and related materials. The terms highlight the ease with which SnO_2 can be reduced by CO and H_2 relative to refractory oxides such as Al_2O_3. As intended by this author, Schryer, and coworkers, the class of NMRO materials includes a wide range of materials in applications beyond sealed CO_2 lasers. The class typically consists of a zero-valent metal dispersed over or inter-mixed with a metal oxide that can be reduced to some extent under reaction or pretreatment conditions. Depending on conditions, any of the Group VIIIA and IB elements may serve as the "noble metal." The class also includes materials in which the noble metal is oxidized under some conditions, materials in which some of the metal oxide may become completely reduced to the parent metal under some conditions, and complex materials composed of more than a single metal and a single oxide.

NMRO materials often exhibit "strong metal-support interactions," or "SMSI" behavior, using terminology introduced in the late 1970's by Tauster and coworkers [6, 7]. They applied the term SMSI to refer to behavior exhibited by Pt-group metals dispersed over TiO_2 following high temperature reduction in H_2. Subsequent work, which was reviewed by Vannice at the NASA/RSRE CO_2 Laser Conference in 1986 [8], has shown that SMSI behavior is due to interaction of partially reduced titania ("TiO_x") species interacting with the noble metal. Thus, TiO_2 is a "reducible oxide" and Pt/TiO_2 and Rh/TiO_2 are NMRO materials. Relative to SMSI, the acronym NMRO is more specific in the sense that it refers to interactions only between zero-valent metals and reducible oxides and not between metals and other types of supports. Relative to SMSI, the acronym NMRO is more general in the sense that it refers to a material itself rather than a particular behavior of the material. The term NMRO is also more general in the sense that it includes systems where the reducible oxide does not "support" the metal, for example, materials with high metal-oxide ratios in bulk form or dispersed over an inert support.

NMRO materials have many important applications, as the examples in Tables 1 through 11 demonstrate. Many of the applications involve oxidation or reduction reactions which involve transfer of oxygen atoms. In a noncatalytic application, Pt/SnO_2 and other materials serve as gas detectors (Table 1). Reducing gases such as CO chemisorb on the metal, reduce the oxide in a stoichiometric reaction, and change the electrical characteristics of the oxide, providing the sensor signal. NMRO materials catalyze CO oxidation in many types of applications (Table 2), and CO, H_2 and hydrocarbon oxidation and NO reduction in automotive "three-way" catalysts (Table 3). Hydrocarbons can be completely oxidized in catalytic heaters (Table 4) or partially oxidized over NMRO materials (Table 5). CO_2 and CO can be hydrogenated over NMRO catalysts to form methane and higher hydrocarbons in Fischer-Tropsch processes (Tables 6 and 7). Methanol and other oxygenated products can also be formed during CO hydrogenation (Table 8). In reactions not involving oxygen transfer, NMRO materials catalyze reforming reactions of hydrocarbons (Table 9). NMRO materials also serve as catalytic electrodes in electrochemical processes and catalyze photochemical processes (Table 10). Miscellaneous applications are listed in Table 11.

An essential aspect of NMRO materials of interest here is that the combination of noble metal and reducible oxide has a synergistic effect: these composite materials show unique catalytic activity which is not a simple addition of the characteristics of the separate materials. Synergistic effects have been demonstrated over Pt/SnO_2 CO oxidation catalysts [2,3], Ag/MnO_2 CO oxidation catalysts [9], Pt/TiO_2 [10] and Rh/TiO_2 [11] CO hydrogenation catalysts, and for NO reduction [12] and ethylene hydrogenation [3] catalysts, for example.

There are three general ways in which the two types of components in NMRO composite materials can interact synergistically:

(a) one component may alter the properties of the other component,

(b) the two components may each provide independent catalytic functions in a complex reaction mechanism,

(c) unique catalytic sites may be formed through combination of the two components at the atomic level.

All three of these interactions may be important in low temperature CO oxidation over NMRO catalysts.

In order to organize the material in this review, the effect of the noble metal on the oxide will be discussed first, followed by the effect of the oxide on the noble metal, the interaction of the noble metal and oxide to form unique catalytic sites, and the possible ways in which the CO oxidation reaction is catalyzed by the NMRO materials.

METAL EFFECT ON OXIDE

Metals dispersed over metal oxides have been shown to catalyze the reduction of the oxide by CO and H_2: Ru catalyzed reduction of Fe oxide [13], reduction of SnO_2 catalyzed by various metals [2,14], Pt catalyzed reduction of various metal oxides [15-17], Pd catalyzed reduction of various oxides [16], and Rh catalyzed reduction of TiO_2 [18]. In some cases, interaction with the noble metal can stabilize reduced oxide species against reoxidation [17]. In other cases, the reoxidation of the reducible oxide can be catalyzed, for example, Pd catalyzed oxidation of SnO_2 [2]. For H_2 and O_2, at least one function of the metal in catalyzing oxide reduction involves catalyzing dissociation of the diatomic molecules during their dissociative adsorption. For adsorbed CO, H, and O on the metal, the oxidation and reduction reactions may occur at the interface between the metal and the oxide. Defect sites in the oxide located at the metal-oxide interface may participate in the reaction, for example, oxygen vacancies at the interface between Pt and ceria [19]. Alternatively, adsorbed CO, H and O may "spillover" from the metal and move out over the surface of the reducible oxide. Bond, et al. [3,2] proposed that the synergistic enhancement of CO oxidation over Pd/SnO_2 is due to spillover of both CO and O from the Pd onto the SnO_2, with reoxidation of the support being the slow step in the reaction. Studies of H spillover include: Pt/SnO_2 [20], Pt/TiO_2 [21,22], $Pt/ReO_x/Al_2O_3$ [23], and Rh/Al_2O_3 [24].

OXIDE EFFECT ON METAL

The effects of the oxide on the metal are more varied. Choice of the metal oxide affects the dispersion of the reduced metal that can be achieved, for example, for Pd/SnO_2 [2] and Ru [25]. The dispersion and distribution of metals between metal particles in bimetallic catalysts can also be affected by the support, for example, for Rh/Au catalysts [26]. These effects indicate that there can be significant interactions between the metal and the oxide support.

Except for gold, all of the "noble" metals can be oxidized to some extent under some conditions - pretreatment conditions if not reaction conditions - even supported Pt [27]. Oxide supports tend to stabilize the oxidized form of supported noble and base metals against reduction treatments, for example, for Cu in Cu/ZnO [28-29], Pt on Al_2O_3 [30], Pt on SnO_2 [31], Pd on SnO_2 [32], Ni on MgO/SiO_2 [33]. Oxidation of large supported metal particles to form an oxide that "wets" the supporting oxide, followed by re-reduction of the noble metal, can lead to redistribution of the supported metal, [30]. Under severe oxidizing conditions, compound

formation can occur between the oxide form of the supported metal and the oxide support, deactivating the metal [34].

For small, oxide-supported metal particles, the electronic structure of the metal atoms may be affected by the oxide, affecting the metal's catalytic activity. Doi and coworkers [25,35] found the electronic structure of Ru atoms in CO hydrogenation to be markedly affected by metal oxide supports: Ru atoms on basic oxides like MgO and TiO_2 were electron rich but those on acidic oxides such as silica-alumina and titania-alumina were electron deficient, affecting the yield of hydrocarbons. In some cases, different phases of the reducible oxide interact with the noble metal differently. Wolf and coworkers [36] compared Pt on the rutile and anatase phases of TiO_2 and found that CO adsorbed linearly on Pt on anatase and in the bridged mode on Pt on rutile, with the Pt/rutile being more active for CO oxidation. SnO_2 was determined to not be a direct catalyst but to modify supported Pt and Pd in studies of electrochemical oxidation of methanol [37-39].

A major complication in analyzing such evidence of synergistic behavior over NMRO materials is that the structure and composition of these composite materials can be quite heterogeneous at the atomic level. This heterogeneity can be caused by a number of mechanisms, and experimental determination of surface structure and composition at the atomic level is extraordinarily difficult. Until this stage in the review, one may have inferred that the materials are composed of metal particles in contact with a reducible oxide support, each component modifying the other to some extent. This picture is accurate for some materials under some conditions. However, direct intermixing of various forms of the two components can occur at the atomic level, especially under reducing conditions. Under reducing conditions, the reducible oxide may be reduced to the extent that suboxide species can diffuse into the metal or reduced completely such that the parent metal of the oxide forms a metal alloy with the noble metal. This complexity is a focus of the rest of this section and the next section.

Oxide or suboxide species can partially or completely cover the surfaces of supported metal particles, as has been shown for Pt/TiO_2 [62]. There are several possible mechanisms for this "decoration" of supported metal particles by oxide species. One mechanism can be a gradual growth of the oxide over the surface on the metal particle, or "encapsulation," that is driven by interfacial energies [40,41]. Another mechanism involves dissolution of suboxide species in the metal under reducing conditions, followed by segregation to the surface of the metal under oxidizing conditions, as Gorte [42] showed for Pt/TiO_2 and Pt/Nb_2O_5 and Tang et al. [43] showed for Pt/TiO_2. Under severe reducing conditions, the oxide may be reduced to the metal and form an alloy with the supported noble metal [4]. Under subsequent oxidizing conditions, segregation may occur to produce oxide species on the surface of the noble metal or redistribute the noble metal over the surface of the oxide.

Once decoration of the metal with oxide species occurs, the oxide species can affect catalytic activity by serving as an inert agent that blocks and deactivates sites on the metal or by modifying the electronic structure and catalytic properties of neighboring noble metal atoms. White and coworkers [44,45] found that TiO_x on Rh both blocks CO adsorption by covering some Rh sites and modifies CO adsorption on other Rh sites. In a calorimetric study of CO and H adsorption over Pt on the anatase phase of TiO_2, Herrmann, et al. [46] found that the reduced support modifies the chemical properties of the surface Pt atoms. Sadeghi and Henrich [47] found evidence for charge transfer from reduced Ti cations to Rh atoms in Rh/TiO_2.

FORMATION OF UNIQUE SITES

Alloy formation between the noble metal and the parent metal of the reducible oxide can form unique catalytic sites, either through modification of the alloyed noble metal atoms or formation of sites involving both types of metal atoms. In previous work [4] and at this meeting [159],

Hoflund and coworkers provided evidence for Pt-Sn alloy formation in Pt/SnO$_2$ catalysts. Pt-Sn alloys as well as Sn-aluminates and SnO have been found in Pt/Sn/Al$_2$O$_3$ hydrocarbon reforming catalysts [48]. McCabe and Mitchell [66,67] demonstrated synergistic CO oxidation activity with Pt-Ag alloys, and Oh and Carpenter [68] did so for Pt-Rh alloys.

Unique catalytic sites may also form at the interface between the noble metal and its oxide support and between the metal and partial overlayers of oxide or suboxide on the metal. TiO$_x$ overlayers have been proposed to catalyze the dissociation of CO during CO hydrogenation to methane and higher hydrocarbons for Pt [42,43, 45,47,49-52] and Rh [45,50,53,54]. One model is that the oxygen end of CO is attracted to the oxide, weakening the bond between the oxygen end and the carbon end bonded to the metal [8]. The interaction between TiO$_x$ overlayers and Pd catalyzes the formation of methanol during CO hydrogenation [55].

FUNDAMENTAL STUDIES OF NMRO MATERIALS

Because of the complex interactions possible in NMRO materials, interactions which give them their unique synergistic properties, a wide variety of experimental techniques are required to analyze the materials and their properties. Surface sensitive techniques, such as those used in references [31,47,56-58] that can be used to probe the surface composition and structure of the materials are necessary, in addition to kinetic measurements. Although porous, high-surface-area catalysts are desired in applications, "model" systems composed of one component distributed over the flat surface plane of a large single crystal of the other component are often preferable for fundamental studies [10,42,59-61].

CO OXIDATION AND NMRO CATALYSTS

During oxidation of CO by O$_2$, whether in the gas-phase or over a catalyst surface, two basic steps must occur: dissociation of the O$_2$ molecule and formation of an O-CO bond. These two steps usually occur in separate events. Over the surface of a catalyst, then, O$_2$ must adsorb and dissociate and CO must adsorb next to and react with an O atom [63].

Over zero-valent noble metals (on inert, nonreducible-oxide supports), CO and O$_2$ compete for the same sites on the surface. Low temperature activity is minimal because CO covers the metal surface and inhibits O$_2$ adsorption. CO dominates the surface because O$_2$ adsorption has more stringent open site requirements since it must dissociate and because O$_2$ adsorption probabilities or "sticking coefficients" on bare metal surfaces are at least an order of magnitude lower than CO sticking coefficients [64,65].

Over metal oxide surfaces the picture is more complex. However, low temperature CO oxidation activity is also minimal over simple oxide surfaces, primarily because of the strong bonding of oxygen to the surface [63].

NMRO materials such as Pt/SnO$_2$ are synergistic composite materials with significant low temperature CO oxidation activity. The limiting steps with conventional catalysts involve oxygen: competition between O$_2$ and CO adsorption over metal catalysts and removal of oxygen bound to oxide catalysts. Thus, we can postulate that one or both of these processes are facilitated over NMRO catalysts: O$_2$ adsorption and dissociation is enhanced relative to CO adsorption and/or oxygen can be removed from the oxide surface relatively easily. Evidence that competition between CO and O$_2$ is reduced over NMRO materials comes from kinetic studies that show that CO doesn't inhibit the reaction significantly, as it does over noble metals supported on non-reducible, inert supports [71,77,78].

An obvious way that the first process, O_2 adsorption and dissociation, can be enhanced relative to CO adsorption is provision of separate but neighboring sites for the two molecules. Hoflund and coworkers [4, 159] showed that a Pt-Sn metal alloy can form in Pt/SnO_2 during reducing pretreatments, and NASA Langley researchers [76] showed that a reducing pretreatment is required to obtain high activity over Pt/SnO_2. If a Pt-Sn alloy were stable during low temperature CO oxidation, competition between CO and O_2 could be reduced if CO adsorbed on Pt atoms and O_2 adsorbed on Sn atoms or a site consisting of a Pt and an Sn atom. Such a scenario is similar to the explanations proposed by McCabe and Mitchell [66,67] to explain enhanced CO oxidation activity over $Pt/Ag/Al_2O_3$ and by Oh and Carpenter [68] for enhanced CO oxidation activity over $Pt/Rh/Al_2O_3$.

The second process mentioned above is that CO adsorbs on noble metal atoms and then removes oxygen from neighboring regions of reducible oxide. Wolf [36,72] and coworkers proposed that O transfer from the rutile form of TiO_2 participates in CO oxidation over Pt/TiO_2 as well as the usual Langmuir-Hinshelwood mechanism over Pt. Jun, et al. [73] found that O chemisorbed on Ag/SnO_2 participated in the complete oxidation of ethylene and lowered the selectivity for ethylene oxide.

Both of the processes just discussed involve reaction at atomic interfaces between the two components of the composite materials. In either case, the preparation and pretreatment of the catalyst to obtain intimate contact between the noble metal and the reducible oxide becomes critical. Further work is required to determine the importance, in determining this atomic or interfacial contact, of alloy formation between the noble metal and the parent metal of the reducible oxide (e.g., Pt-Sn alloy formation) and the importance of suboxide species on noble metal surfaces. In addition to catalyst preparation and activity testing, fundamental studies of the solid state thermodynamics and kinetics of NMRO materials are required.

A third possibility is that one of the components serves as a reservoir, or "port hole" in the terminology of Boudart and H. S. Taylor [160], which supplies one of the reactants to the other component. Bond and coworkers [2,3] proposed that spillover of both CO and O from noble metal to the oxide is important in low temperature SnO_2-based NMRO catalysts. A different scenario was proposed by Imamura, et al. [9] to explain low temperature CO oxidation over Ag/MnO_2. They proposed that the role of MnO_2 is to serve as a readily re-oxidizable reservoir of O that keeps Ag supplied with O and in an oxidized state. They further proposed that CO was oxidized by reaction with the Ag oxide. One might call this proposal "reverse" spillover from the oxide support to the metal.

In addition to eliminating competition between CO and O_2 by the presence of separate adsorption sites, O_2 dissociation may be facilitated over NMRO catalysts. Booker and Keiser [70] showed that surface hydroxyl groups on Rh/Al_2O_3 can oxidize adsorbed CO to CO_2. Croft and Fuller [5] showed that the presence of gas-phase H_2O can enhance the activity of Pd/SnO_2. Studies by Schryer and coworkers at NASA Langley [76] have shown that the presence of H_2O can affect the behavior of Pt/SnO_2 catalysts. The way in which H_2O might participate is suggested by the mechanism of homogeneous CO oxidation in the gas phase [63,69]. In the gas phase, traces of H_2 or H_2O serve as a catalyst of the CO oxidation reaction. O_2 is dissociated by collision with H to form OH and O radicals. CO is oxidized by collision with OH radicals to form CO_2 and H, not by collision with O atoms. Oxide surfaces are usually found in a hydroxylated and protonated state, even when H_2O has not been added to a reactant stream deliberately [32,74,75, 161]. Hoflund and coworkers obtained evidence for the presence of hydroxyl groups on Pt/SnO_2 [159]. Hydroxyl groups and protons on the reducible-oxide surface might participate by catalyzing the dissociation of O_2. Finally, the possibility that CO is oxidized over NMRO catalysts by surface hydroxyl groups, as in the homogeneous reaction mechanism, must also be considered [76].

Determining which of the processes proposed above - or an entirely unexpected process - oxidizes CO at low temperatures over NMRO materials will take further careful work. Some of the recent work involving Au catalysts keeps the work stimulating. Over Au co-precipitated with a variety of base metal oxides, Haruta, et al. [79] obtained complete oxidation of 1% CO in air at $-70^{\circ}C$ (66 cm^3/min over 0.2 g). Huber, et al. [80] observed reaction between CO and O_2 in a matrix with Au at 4 K.

ACKNOWLEDGEMENT

Table 1. Gas Sensor Applications

Application	Material	Reference
CO sensor	Pt/SnO_2	[81-83]
"	Pt/TiO_2	[84]
"	Ag/SnO_2	[85]
"	$Au/MgO/SnO_2$	[86]
H_2 sensor	$Pt/Pd/TiO_2$	[87]
"	Ag/SnO_2, Pd/SnO_2	[88]
Combustible gas sensor	$Pd/In_2O_3/SnO_2$	[89]
"	Pd/Sb-doped-SnO_2	[90]
"	Pd/SnO_2	[91]
"	$Pd/ZnO/SnO_2$	[92]
"	$Pd/(SnO_2, In_2O_3, Fe_2O_3, MnO_2,$ or $ZnO)$	[93]
Reducing gas sensor	Pt/ZnO	[94,95]
Reducing and oxidizing gas sensor	Pt/SnO_2	[96]
O_2 sensor	Pt/ZrO_2	[97]

Table 2. CO Oxidation Applications

Application	Catalyst	Reference
$CO + O_2$ for CO_2 laser	Pt/SnO_2	[1,77,98, 99]
"	Pd/SnO_2	[1,2,100]
"	(Pt or Pd)/Cr/(preferably Mn)/SnO_2	[101]
"	(Pt and/or Pd)/(optionally Fe, Ru, Cu, or Re)/(Al_2O_3, TiO_2, or MgO)	[102]
"	(Pt, Pd, Rh, or Ir)/(Al_2O_3 or SnO_2)	[103]
"	Cu/CuO	[99]
$CO + O_2$	$Pt/CeO_2/SnO_2$	[104]
"	Pt/CeO_2	[19]
"	Pt/TiO_2	[36,72]
"	Au/(oxide of Fe, Co, or Ni)	[79]
"	Ag/MnO_2	[9]

Table 3. NO Reduction and Three-Way Automotive Applications

Application	Catalyst	Reference
CO + NO	Pd/SnO_2	[12]
CO + NO	$Pt/V_2O_5/TiO_2$	[105]
CO + NO & CO + O_2	(Pt, Pd, Rh, or Ru)/(Mo, W, or V oxide)/TiO_2	[106]
Three-way automobile catalysts	Pt/Pd/Rh/(various reducible oxides)/Al_2O_3	[107-110]

Table 4. Hydrocarbon Complete Oxidation Applications

Application	Catalyst	Reference
Catalytic heater	Pt/(Sn, Y, or rare-earth)	[111]
"	Pd/Pt/(Ca-aluminate)/SiO_2/TiO_2	[112]

Table 5. Hydrocarbon Partial Oxidation Applications

Application	Catalyst	Reference
Ethylene oxidation	Ag/SnO_2	[73]
Propylene oxidation	Pd/TiO_2, Cu/TiO_2	[113]
"	$Pt/Ba(Sn_{0.6}In_{0.4})O_3$	[114]

Table 6. CO$_2$ Hydrogenation Applications

Application	Catalyst	Reference
$CO_2 + H_2$, methane formation	$Rh/(Al_2O_3, MgO, C, ZrO_2, TiO_2, ZnO,Al_2O_3)$	[121]
$CO_2 + H_2$, unspecified products	Rh/TiO_2	[122]

Table 7. CO Hydrogenation Applications

Application	Catalyst	Reference
$CO + H_2$, unspecified products	(Rh, Pd, or Ru)/TiO_2	[74, 123]
"	Rh/TiO_2	[122,124]
"	$Ru/Fe/TiO_2$	[125,126]
"	$Ru/(MgO, TiO_2,$ or $Al_2O_3/TiO_2)$	[35]
"	Rh/TiO_2	[53,54]
"	Pt/TiO_2	[127]
$CO + H_2$, methane formation,	$Pt/(TiO_2$ or $Nb_2O_5)$	[42]
"	Pt/TiO_2	[10,43]
"	(Rh, Ir, Ru)/TiO_2	[128]
$CO + H_2$, olefin synthesis	Ru/TiO_2	[129]
$CO + H_2$, Fischer-Tropsch synthesis	$Ru/Fe/TiO_2$, Fe/TiO_2	[13]
"	$Co/Re/TiO_2$	[130]
"	$Co/Ru/TiO_2$	[131]
"	$Ru/(Nb, Ta,$ or V oxide)/TiO_2	[132]
$CO + H_2$, liquid-phase reaction	$Ru/(TiO_2$ or $Nb_2O_5)$	[133]

Table 8. Alcohol Synthesis, Methanol Decomposition Applications

Application	Catalyst	Reference
CO + H₂, methanol synthesis	Cu/ZrO₂	[134,135]
"	Cu/ZnO	[28,29,136, 137,158]
"	(Pt, Rh, or Ir)/(MgO or ZnO)	[11]
"	Pd/(TiO₂ or Nd₂O₃)	[138]
CO + H₂, CH₄ and methanol synthesis	Pd/(TiO₂ or SiO₂)	[55]
CO + H₂, alcohol (ethanol) synthesis	La₂O₃-promoted-(Rh or Rh/Pt)/TiO₂	[139]
Methanol decomposition to CO + H₂	Ni/SiO₂/MgO	[33]

Table 9. Hydrocarbon Reforming and Related Applications

Application	Catalyst	Reference
Reforming	Pt/Sn/Al₂O₃	[48,140]
"	Pt/Ni-sulfide/SnO₂	[141]
Hydrogenolysis of alkanes	Ru/(various metal oxides)	[25]
Isomerization	Pt/S-containing-halide/ZrO₂	[142,143]
Paraffin isomerization	Pt/Rh/halide/SnO₂	[144]
Dehydrogenation	Pt/ZnO/SnO₂	[145]
"	Pt/Li/GeOx/SnO₂	[146]
Dehydrocyclization	Pt/Co/SnO₂/Al₂O₃	[147]
Hydroprocessing of aromatics to cyclo-paraffins	Pt/Co/Cl/SnO₂	[148]

Table 10. Electrochemical and Photochemical Applications

Application	Catalyst	Reference
Methanol electro-oxidation	(Pt or Pd)/SnO$_2$	[37,38,39]
Fuel cell (air electrode)	Pt/SnO$_2$	[39,149,150,151]
"	Pt/Sb-promoted-SnO$_2$	[56,152]
O$_2$ & Cl$_2$ evolution	(Pt, Pd, or Ru)/SnO$_2$	[153]
Photocatalytic lignin oxidation	(Pt, Ag, or Au)/TiO$_2$	[154]
Electrosynthesis of peroxides	Pt/Sb$_2$O$_5$/SnO$_2$	[155]
Photoassisted H$_2$ production	CdS/SiO$_2$ plus Pt/(TiO$_2$, ZnO, SnO$_2$, or WO$_3$)	[156]
Photography	Ag/Pd/TiO$_2$	[157]

Table 11. Miscellaneous Applications

Application	Catalyst	Reference
Vinyl acetate production	Pd/Au/SnO$_2$	[115]
Alcohol oxycarbonylation	Pd/V$_2$O$_5$/TiO$_2$	[116]
CO + H$_2$O, light olefin synthesis	Rh/Nb$_2$O$_5$	[117]
CO + H$_2$O, water gas shift	Cu/ZnO	[118]
Electroless deposition of Pd/SnO$_x$ for electroplating	Pd/SnO$_x$	[119]
CO chemisorption	Os/TiO$_2$	[120]
Unknown reaction	Rh/Au/(SiO$_2$, TiO$_2$, or Al$_2$O$_3$)	[26]

REFERENCES

1. Stark, D. S.; Harris, M. R., "Catalyzed recombination of carbon monoxide and oxygen in sealed carbon dioxide TEA laser gases at temperatures down to -27 degree," J. Phys. E, 16(6), 492-6 (1983)

2. Bond, G. C.; Fuller, M. J.; Molloy, L. R., "Oxidation of carbon monoxide catalyzed by palladium on tin(IV) oxide: an example of spillover catalysis," Proc. Int. Congr. Catal., 6th, Meeting Date 1976, Volume 1, 356-64. Edited by: Bond, G. C.; Wells, P. B.; Tompkins, F. C. Chem. Soc.: Letchworth, Engl. (1977)

3. Bond, G. C.; Molloy, L. R.; Fuller, M. J., "Oxidation of carbon monoxide over palladium-tin(IV) oxide catalysts. Example of spillover catalysis," J. Chem. Soc., Chem. Commun., (19), 796-7 (1975)

4. Gardner, S. D.; Hoflund, G. B.; Davidson, M. R.; Schryer, D. R., "Evidence of alloy formation during reduction of platinized tin oxide surfaces," J. Catal., 115(1), 132-7 (1989)

5. Croft, G.; Fuller, M. J., "Water-promoted oxidation of carbon monoxide over tin(IV) oxide-supported palladium," Nature (London), 269(5629), 585-6 (1977)

6. Tauster, S. J.; Fung, S. C.; Garten, R. L., J. Am. Chem. Soc. 100, 170 (1978)

7. Tauster, S. J.; Fung, S. C., J. Catal. 55, 29 (1978)

8. Vannice, M. A., "Strong metal-support interactions," NASA Conf. Publ., 2456 (Closed-Cycle, Freq.-Stable CO_2 Laser Technol.), 121-140 (1987)

9. Imamura, S.; Sawada, H.; Uemura, K.; Ishida, S., "Oxidation of carbon monoxide catalyzed by manganese-silver composite oxides," J. Catal. 109, 198-205 (1988)

10. Demmin, R. A.; Gorte, R. J., "Study of methanation kinetics on a clean and a titania-covered platinum foil," J. Catal., 105(2), 373-85 (1987)

11. Ichikawa, M., "Catalysis by supported metal crystallites from carbonyl clusters. I. Catalytic methanol synthesis under mild conditions over supported rhodium, platinum, and iridium crystallites prepared from rhodium, platinum, and iridium carbonyl cluster compounds deposited on zinc oxide and magnesium oxide," Bull. Chem. Soc. Jpn., 51(8), 2268-72 (1978)

12. Fuller, M. J.; Warwick, M. E., "Catalysis of the nitric oxide-carbon monoxide reaction: a further example of synergism in the palladium-stannic oxide system," Chem. Ind. (London), (18), 787-8 (1976)

13. Van der Kraan, A. M.; Nonnekens, R. C. H.; Stoop, F.; Niemantsverdriet, J. W., "Characterization of iron-ruthenium/titanium dioxide and iron/titanium dioxide catalysts after reduction and Fischer-Tropsch synthesis by Moessbauer spectroscopy," Appl. Catal., 27(2), 285-98 (1986)

14. Frety, R.; Charcosset, H.; Trambouze, Y., "Tin dioxide reduction by hydrogen. Influence of the deposition of certain active species on the reaction kinetics," Ind. Chim. Belge, 38(5), 501-5 (1973)

15. Frety, R.; Bolivar, C.; Charcosset, H.; Tournayan, L.; Trambouze, Y., "Catalytic effect of platinum (or of platinum group metals) on the hydrogen reduction of various metal oxides," React. Kinet. Heterogeneous Chem. Syst., Proc. Int. Meet. Soc. Chim. Phys., 25th, Meeting Date 1974, 681-90. Edited by: Barret, Pierre. Elsevier: Amsterdam, Neth. (1975)

16. Verhoeven, W.; Delmon, B., "Heterogeneous reactions. Reduction of metal oxides by hydrogen. I. Initiation of the reduction by the incorporation of a metal phase," Bull. Soc. Chim. Fr., (10), 3065-73 (1966)

17. Tang, S.; Xiong, G.; Wang, H., "Metal-support interaction on the model platinum-titanium oxide $Pt-TiO_2$, $Pt-Ti_2O_3$ and $Pt-TiO$ cosputtering film-type catalysts. II. AES and XPS studies," Cuihua Xuebao, 8(3), 234-41 (1987)

18. Levin, M. E.; Salmeron, M.; Bell, A. T.; Somorjai, G. A., "The characterization of titanium and aluminum oxide overlayers on rhodium and gold by XPS," Surf. Sci., 195(3), 429-42 (1988)

19. Jin, T.; Mains, G. J.; White, J. M., J. Phys. Chem., 91, 3311-3315 (1987)
20. Rao, L.; Chen, Y.; Li, W., "Study of metal-semiconductor catalyst: hydrogen spillover on platinum/tin dioxide at room temperature," Wuli Huaxue Xuebao, 3(6), 626-31 (1987)
21. Beck, D. D.; Bawagan, A. O.; White, J. M., "Spillover of Deuterium on Pt/TiO$_2$. 2. Sequential H$_2$-D$_2$ exposure and effects of oxygen," J. Phys. Chem. 88, 2771 (1984)
22. Beck, D. D.; White, J. M., "Spillover of Deuterium on Pt/TiO$_2$. 1. Dependence on Temperature, Pressure, and Exposure," J. Phys. Chem. 88, 2764 (1984)
23. Augustine S. M.; Sachtler, W. M. H., "On the mechanism for the platinum-catalyzed reduction of rhenium in Pt-Re/gamma-Al$_2$O$_3$," J. Catal. 116, 184-194 (1989)
24. Crucq, A., Lienard, G., Degols, L., and Frennet, A., "Hydrogen adsorption on Rh," Appl. Surf. Sci. 17, 79 (1983).
25. Miyake, H.; Doi, Y.; Soga, K., "Electronic effects in ruthenium/metal oxide catalysts on several hydrogenations," Shokubai, 29(6), 450-3 (1987)
26. Nunez, G. M.; Rouco, A. J., "Support effects on metal-metal interaction in rhodium-gold bimetallic catalysts," J. Catal., 111(1), 41-9 (1988)
27. Herz, R. K.; Shinouskis, E. J., "Transient oxidation and reduction of alumina-supported platinum," Applic. Surf. Sci. 19, 373-397 (1984)
28. Parris, G. E.; Klier, K., "The specific copper surface areas in copper/zinc oxide methanol synthesis catalysts by oxygen and carbon monoxide chemisorption: evidence for irreversible carbon monoxide chemisorption induced by the interaction of the catalyst components," J. Catal., 97(2), 374-84 (1986)
29. Campbell, C. T.; Daube, K. A.; White, J. M., "Copper/zinc oxide(0001) and zinc oxide/copper(111): model catalysts for methanol synthesis," Surf. Sci., 182(3), 458-76 (1987)
30. Yao, H. C.; M. Sieg, H. K. Plummer, J. Catal. 59, 365-374 (1979)
31. Cox, David F.; Hoflund, Gar B.; Laitinen, Herbert A., "XPS investigation of tin oxide supported platinum," Langmuir, 1(3), 269-73 (1985)
32. Harrison, P. G.; Maunders, B. M., "Tin oxide surfaces. Part 12. A comparison of the nature of tin(IV) oxide, tin(IV) oxide-silica, and tin(IV) oxide-palladium oxide: surface hydroxyl groups and ammonia adsorption," J. Chem. Soc., Faraday Trans. 1, 80(6), 1341-56 (1984)
33. Akiyoshi, M.; Hattori, H.; Tanabe, K., "Catalytic activities of supported transition metals for decomposition of methanol to carbon monoxide and hydrogen," Sekiyu Gakkaishi, 30(3), 156-60 (1987)
34. Yao, H. C.; S. Japar, M. Shelef, J. Catal. 50, 407-418 (1977)
35. Doi, Y.; Miyake, H.; Soga, K., "Electronic effects of carbon monoxide hydrogenation over ruthenium-metal oxide catalysts," J. Chem. Soc., Chem. Commun., (5), 347-8 (1987)
36. Lane, G. S.; Wolf, E. E., "Characterization and Fourier transform infrared studies of the effects of titania crystal phases during carbon monoxide oxidation on platinum/titania catalysts," J. Catal., 105(2), 386-404 (1987)
37. Hughes, V. B.; McNicol, B. D., "Evaluation of semiconducting tin oxide as an electrocatalyst support," J. Chem. Soc., Faraday Trans. 1, 75(9), 2165-76 (1979)
38. Katayama-Aramata, A.; Toyoshima, I., "Palladium + tin oxide catalyst for electrooxidation of methanol and its chemical characterization by x-ray photoelectron spectroscopy," J. Electroanal. Chem. Interfacial Electrochem., 135(1), 111-19 (1982)
39. Katayama, A., "Electrooxidation of methanol on a platinum-tin oxide catalyst," J. Phys. Chem., 84(4), 376-81 (1980)
40. Spencer, M. S., "Equilibrium and kinetic aspects of strong metal-support interactions (SMSI) in platinum/titanium dioxide and other catalysts," Prepr. - Am. Chem. Soc., Div. Pet. Chem., 30(1), 157-61 (1985)
41. Vishwanathan, V.; Narayanan, S.; Viswanathan, B., "Effect of reduction on strong metal support interaction (SMSI) behavior of rhodium-titanium dioxide system," Indian J. Chem., Sect. A, 26A(8), 686-8 (1987)

42. Gorte, R. J., "Support-metal interaction studies on model supported catalysts," Report, DOE/MC/19204-1769; Order No. DE86009187, 57 pp. Avail. NTIS From: Energy Res. Abstr. 1986, 11(12), Abstr. No. 26824 (1985)

43. Tang, S.; Xiong, G.; Wang, H., "The nature of the strong metal-support interaction state of the platinum/titania system," J. Catal., 111(1), 136-45 (1988)

44. Belton, D. N.; Sun, Y. M.; White, J. M., "Chemisorption of carbon monoxide, nitrous oxide, and hydrogen on transition metal-titania thin film model catalysts," Report, Order No. AD-A172728/8/GAR, 27 pp. Avail. NTIS From: Gov. Rep. Announce. Index (U. S.) 1987, 87(2), Abstr. No. 702,147 (1986)

45. Belton, D. N.; Sun, Y. M.; White, J. M., "Chemisorption of carbon monoxide, nitric oxide, and hydrogen on transition metal-titania thin film model catalysts," J. Catal., 102(2), 338-47 (1986)

46. Herrmann, J. M.; Gravelle-Rumeau-Maillot, M.; Gravelle, P. C., "A microcalorimetric study of metal-support interaction in the platinum/titania system," J. Catal., 104(1), 136-46 (1987)

47. Sadeghi, H. R.; Henrich, V. E., "Electronic interactions in the rhodium/titania system," J. Catal., 109(1), 1-11 (1988)

48. Li, Y.; Xia, Y., "A study of the valence state of tin in platinum-tin/eta-alumina reforming catalysts," Shandong Haiyang Xueyuan Xuebao, 1, 77-86 (1982)

49. Woo, S. I., "Interactions of rhodium carbonyl compounds supported on inorganic oxides with carbon monoxide, hydrogen, and propylene," Korean J. Chem. Eng., 4(2), 170-81 (1987)

50. Belton, D. N.; Sun, Y. M.; White, J. M., "Chemisorption of carbon monoxide, nitrous oxide, and hydrogen on transition metal-titania thin film model catalysts," Report, Order No. AD-A172728/8/GAR, 27 pp. Avail. NTIS From: Gov. Rep. Announce. Index (U. S.) 1987, 87(2), Abstr. No. 702,147 (1986)

51. Ocal, C.; Ferrer, S., "A new carbon monoxide adsorption state on thermally treated platinum/titania model catalysts," Surf. Sci., 178(1-3), 850-5 (1986)

52. Anderson, A. B.; Dowd, D. Q., "Carbon monoxide adsorption on platinum(111) doped with titanium oxide (TiO), iron oxide (FeO), zinc oxide, and iron and platinum ad-atoms. Molecular orbital study of carbon monoxide-dopant interactions," J. Phys. Chem., 91(4), 869-73 (1987)

53. Levin, M. E.; Salmeron, Mi.; Bell, A. T.; Somorjai, G. A., "The effects of titania and alumina overlayers on the hydrogenation of carbon monoxide over rhodium," J. Chem. Soc., Faraday Trans. 1, 83(7), 2061-9 (1987)

54. Levin, M. E.; Salmeron, M.; Bell, A. T.; Somorjai, G. A., "The enhancement of carbon monoxide hydrogenation on rhodium by titanium oxide (TiOx) overlayers," J. Catal., 106(2), 401-9 (1987)

55. Rucker, T. G., "The effect of additives on the reactivity of palladium surfaces for the chemisorption and hydrogenation of carbon monoxide: a surface science and catalytic study," Report, LBL-23804; Order No. DE87014685, 195 pp. Avail. NTIS From: Energy Res. Abstr. 1987, 12(23), Abstr. No. 47990 (1987)

56. Hoflund, G. B., "Preparation and properties of platinum crystallites supported on polycrystalline tin oxide, "Stud. Surf. Sci. Catal., 16(Prep. Catal. 3), 91-100 (1983)

57. Hoflund, G. B., "A review of tin oxide-based catalytic systems: preparation, characterization and catalytic behavior," NASA Conf. Publ., 2456 (Closed-Cycle, Freq.-Stable CO_2 Laser Technol.), 179-92 (1987)

58. Asbury, D. A.; G. B. Hoflund, "A surface study of the oxidation of polycrystalline tin," J. Vac. Sci. and Technol. A 5, 1132 (1987)

59. Jacobs, H.; Mokwa, W.; Kohl, D.; Heiland, G., "Characterization of the growth mechanisms of thin palladium layers in dioxide: structure and reactivity of a supported palladium catalyst," Fresenius' Z. Anal. Chem., 319(6-7), 634 (1984)

60. Cox, D. F., et al., "Surface properties of clean and gas-dosed $SnO_2(110)$," J. Vac. Sci. and Technol. A 5, 1170 (1987)

34

61. Badyal, J. P. S.; Gellman, A. J.; Judd, R. W.; Lambert, R. M., "Single crystal modeling of the SMSI phenomenon: structure, composition, electronic effects, and carbon monoxide chemisorption at the ruthenium(0001)/titanium oxide (TiO$_x$) interface," Catal. Lett., 1(1-3), 41-50 (1988)

62. Hoflund, G. B.; Grogan, A. L., Jr.; Asbury, D. A., "An ISS, AES, and ESCA study of the oxidative and reductive properties of platinized titania," J. Catal. 109, 226-31 (1988)

63. Herz, R. K., "Chemical engineering design of CO oxidation catalysts," NASA Conf. Publ., 2456(Closed-Cycle, Freq.-Stable CO$_2$ Laser Technol.), 103-12 (1987)

64. Herz R. K.; Marin, S. P., "Surface chemistry models of carbon monoxide oxidation on supported platinum catalysts," J. Catal. 65, 281-296 (1980)

65. Boecker, D.; Gonzalez, R. D., "CO oxidation studies over supported noble metal catalysts and single crystals: a review," NASA Conf. Publ., 2456(Closed-Cycle, Freq.-Stable CO$_2$ Laser Technol.), 85-102 (1987)

66. McCabe, R. W., "Alumina-supported Pd-Ag catalysts for low-temperature CO and methanol oxidation," NASA Conf. Publ., 2456(Closed-Cycle, Freq.-Stable CO$_2$ Laser Technol.), 165-78 (1987)

67. McCabe, R. W.; Mitchell, P. J., "Exhaust-catalyst development for methanol-fueled vehicles. 2. Synergism between palladium and silver in methanol and carbon monoxide oxidation over an alumina-supported palladium-silver catalyst," J. Catal., 103(2), 419-25 (1987)

68. Oh, S. H.; Carpenter, J. E., "Platinum-rhodium synergism in three-way automotive catalysts," J. Catal. 98, 178-190 (1986)

69. Mulcahy, M. F. R., "Gas Kinetics," John Wiley and Sons, New York (1973)

70. C. P. Booker and J. T. Keiser, "The reduction of Rh^{+3} on supported rhodium surfaces by CO," J. Phys. Chem, in press (1989)

71. Oh, S. H.; Eickel, C. C., "Effects of cerium addition on carbon monoxide oxidation kinetics over alumina-supported rhodium catalysts," J. Catal., 112(2), 543-55 (1988)

72. Lane, G. S.; Wolf, E. E.; "Characterization and Fourier Transform Infrared studies of the effects of TiO$_2$ crystal phases during CO oxidation on Pt/TiO$_2$ catalysts," J. Catal. 105, 386 (1987)

73. Jun, K. W.; Han, C. S.; Chon, H., "Oxidation of ethylene over silver/alpha-aluminum oxide and silver/stannic oxide," Taehan Hwahakhoe Chi, 28(2), 109-13 (1984)

74. Munoz, A.; Gonzalez-Elipe, A. R.; Munuera, G.; Espinos, J. P.; Rives-Arnau, V., "IR and XPS studies of the reactivity of carbon monoxide with titanium-hydrogen species at the support on rhodium/titanium dioxide catalysts," Spectrochem. Acta, Part A, 43A(12), 1599-605 (1987)

75. Chinchen, G. C.; Spencer, M. S.; Waugh, K.C.; Whan, D. A., "Promotion of methanol synthesis and the water-gas shift reactions by adsorbed oxygen on supported copper catalysts," J. Chem. Soc., Faraday Trans. 1, 83(7), 2193-212 (1987)

76. Schryer, D. R., B. T. Upchurch, R. V. Hess, G. M. Wood (NASA Langley Research Center), B. D. Sidney, I. M. Miller (Science and Technology Corporation), K. G. Brown, J. D. Van Norman, J. Schryer, D. R. Brown (Old Dominion Univ.), G. B. Hoflund (Univ. Florida), and R. K. Herz (Univ. California, San Diego), "Pt/SnO$_2$-Based CO-Oxidation Catalysts for Long-Life Closed-Cycle CO$_2$ Lasers," This volume (1990).

77. Miller, I. M.; Wood, G. M.; Schryer, D. R.; Hess, R. V.; Upchurch, B. T.; Brown, K. G., "Optimization of the catalytic oxidation of carbon monoxide for closed-cycle carbon dioxide laser applications," NASA Tech. Memo., NASA-TM-86421, NAS1.15:86421, 12 pp. Avail. NTIS From: Sci. Tech. Aerosp. Rep. 1985, 23(15), Abstr. No. N85-25445 (1985)

78. Choo, K. Y.; Kim, H.; Boo, B., "Catalytic oxidation of carbon monoxide on platinum and tin(IV) oxide," Taehan Hwahakhoe Chi, 24(3), 183-92 (1980)

79. Haruta, M.; T. Kobayashi, H. Sano, N. Yamada, Chem. Lett. (Japan) 1987, pp. 405-408 (1987)

80. Huber, H.; D. McIntosh; G. A. Ozin, Inorg. Chem. 16, 975 (1977).

81. Lee, D. D.; Sohn, B. K.; Ma, D. S., "Low power thick film carbon monoxide gas sensors," Sens. Actuators, 12(4), 441-7 (1987)

82. Matsushima, S.; Miura, N.; Yamazoe, N., "Carbon monoxide sensitive platinum/tin dioxide diode type gas sensor," Chem. Lett., (10), 2001-4 (1987)

83. Senda, T.; Okayama, Y., "Apparatus for the detection of carbon monoxide," Ger. Offen. DE 2437352, 13 Feb 1975, 19 pp. (1975)

84. Fujioka, T., "Gas sensors," Jpn. Kokai Tokkyo Koho JP 63/81255 A2 [88/81255], 12 Apr 1988, 7 pp. (1988)

85. Otsuki, H.; Kobayashi, M.; Usami, Y., "Carbon monoxide detector," Jpn. Kokai Tokkyo Koho JP 62/47547 A2 [87/47547], 2 Mar 1987, 4 pp. (1987)

86. Kobayashi, T.; Haruta, M.; Sano, H., "Gold-supporting tin oxide for selective carbon monoxide sensing," Chem. Express, 4(4), 217-20 (1989)

87. Matsumoto, Y.; Hombo, J.; Yoshikawa, T.; Sato, E., "Hydrogen sensitivity of platinum-palladium/p-calcium ferrite diode," Mater. Res. Bull., 24(3), 331-42 (1989)

88. Yamazoe, N.; Kurokawa, Y.; Seiyama, T., "Catalytic sensitization of tin dioxide sensor," Anal. Chem. Symp. Ser., 17(Chem. Sens.), 35-40 (1983)

89. Yoo, K. S.; Jung, H. J., "Gas-sensing characteristics of semiconducting materials based on indium sesquioxide depending on composition changes," Sens. Actuators, 12(3), 285-90 (1987)

90. Yannopoulos, L. N., "Antimony-doped stannic oxide-based thick-film gas sensors," Sens. Actuators, 12(1), 77-89 (1987)

91. Wada, K.; Yamazoe, N.; Seiyama, T., "Effects of palladium addition in tin(IV) oxide gas sensor," Nippon Kagaku Kaishi, (10), 1597-602 (1980)

92. Matsumoto, T.; Nishioka, K., "Sensitivity characteristics of a gas sensor using zinc oxide and tin(IV) oxide," A&R, 17(3), 97-104 (1979)

93. Sato, T.; Shiota, T., "Metal oxide gas sensor elements," Japan. Kokai JP 51/137494 [76/137494], 27 Nov 1976, 6 pp. (1976)

94. Saito, S.; Miyayama, M.; Koumoto, K.; Yanagida, H., "Gas sensing characteristics of porous zinc oxide and platinium/zinc oxide ceramics," J. Am. Ceram. Soc., 68(1), 40-3 (1985)

95. Yanagida, H.; Koumoto, K.; Miyayama, M.; Saito, S., "Gas sensing characteristics of porous zinc oxide ceramics with and without platinum catalyst," Anal. Chem. Symp. Ser., 17(Chem. Sens.), 95-100 (1983)

96. Micheli, A. L.; Chang, S. C.; Hicks, D. B., "Tin oxide gas-sensing microsensors from metalloorganic deposited (MOD) thin films," Ceram. Eng. Sci. Proc., 8(9-10), 1095-105 (1987)

97. Badwal, S. P. S.; Ciacchi, F. T.; Haylock, J. W., "Nernstian behavior of zirconia oxygen sensors incorporating composite electrodes," J. Appl. Electrochem., 18(2), 232-9 (1988)

98. Sidney, B. D., "Studies of long-life pulsed carbon dioxide laser with platinum/tin dioxide catalyst," NASA Conf. Publ., 2456(Closed-Cycle, Freq.-Stable CO_2 Laser Technol.), 211-18 (1987)

99. Rogowski, R. S.; Miller, I. M.; Wood, G.; Schryer, D. R.; Hess, R. V.; Upchurch, B. T., "Evaluation of catalyst for closed cycle operation of high energy pulsed carbon dioxide lasers," Proc. SPIE-Int. Soc. Opt. Eng., 415(Coherent Infrared Radar Syst. Appl. 2), 112-17 (1983)

100. Stark, D. S.; Crocker, A.; Steward, G. J., "A sealed 100-Hz carbon dioxide TEA laser using high carbon dioxide concentrations and ambient-temperature catalysts," J. Phys. E, 16(2), 158-61 (1983)

101. Kolts, J. H., Phillips Petroleum Co., "Catalyst for oxidation of carbon monoxide particularly in lasers," Eur. Pat. Appl. EP 311084 A1, 12 Apr 1989, 11 pp. Designated States: AT, BE, CH, DE, ES, FR, GB, GR, IT, LI, LU, NL, SE (1989)

102. Phillips Petroleum Co., "Carbon Monoxide Oxidation Catalysts," U. S. Patent 4,808,394, European Appls. 306,944-45A (1989)

103. Hughes Aircraft Co., "Catalysts for Carbon Dioxide Regeneration in Lasers," World Patent Appl. 103 (1989)

104. Wang, D.; Wang, S.; Ma, L., Activity of tin dioxide-supported rare earth oxide catalysts for carbon monoxide oxidation," Beijing Gongye Daxue Xuebao, 14(3), 33-9 (1988)

105. Wei, Z.; Li, W., "Catalytic behavior of platinum-vanadium pentoxide/titanium dioxide catalyst in carbon monoxide + nitric oxide reaction," Huanjing Kexue, 9(2), 7-11 (1988)

106. Kato, A.; Yamashita, H.; Kawagoe, H.; Tate, T.; Watanabe, N.; Matsuda, S., "Method for simultaneous removal of nitrogen oxides and carbon monoxide," Jpn. Kokai Tokkyo Koho JP 61/291026 A2 [86/291026], 20 Dec 1986, 6 pp. (1986)

107. Gandhi, H. S.; Shelef, M., "The role of research in the development of new generation automotive catalysts," in "Catalysis and automotive pollution control," A. Frucq and A. Frennet (Eds.), Studies in Surf. Sci. Catal. 30, pp. 199-214 Elsevier (1987)

108. Taylor, K. C., "Automobile catalytic converters," Springer-Verlag, Berlin (1984)

109. Cooper, B. J.; Evans, W. D. J.; Harrison, B., "Aspects of automotive catalyst preparation, performance and durability," in "Catalysis and automotive pollution control," A. Frucq and A. Frennet (Eds.), Studies in Surf. Sci. Catal. 30, pp. 117-141 Elsevier (1987)

110. Herz, R. K.; Shinouskis, E. J., "Dynamic Behavior of automotive catalysts. 4. Impact of air/fuel ratio excursions during driving," Ind. Eng. Chem. Res. Devel. 24, 385-390 (1985)

111. Anon., "Catalyst bed for flameless heaters," Res. Discl., 153, 15-16 (1977)

112. Nishino, A.; Ono, Y.; Numoto, H.; Takeuchi, Y., "Studies on carbon monoxide oxidizing performance of molded catalyst composed of calcium aluminate-metal oxides. III. Carbon monoxide oxidation on platinum-palladium catalysts supported on calcium aluminate-silicon dioxide-titanium dioxide molds," Nippon Kagaku Kaishi, (4), 645-53 (1987)

113. Kaji, T.; Oono, H.; Nakahara, T.; Yamazoe, N.; Seiyama, T., "Fixation of palladium(II) and copper(II) complexes on the surface of tin(IV) oxide powders and their catalytic activity for propene oxidation," Nippon Kagaku Kaishi, (7), 1088-93 (1980)

114. Herrmann, J. M.; Foujols, D.; Forissier, M.; Rosa-Nunes, M.,"Catalytic activity in propene oxidation of pure and platinum-doped tin-indium mixed perovskites," Actas Simp. Iberoam. Catal., 9th, Volume 2, 1573-4. Soc. Iberoam. Catal.: Lisbon, Port. (1984)

115. Capp, C. W., "Vinyl acetate," Fr. FR 1566124, 2 May 1969, 5 pp. (1969)

116. Gaffney, A. M.; Leonard, J. J.; Sofranko, J. A.; Sun, H. N., "Heterogeneous catalyst for alcohol oxycarbonylation to dialkyl oxalates," Prepr. - Am. Chem. Soc., Div. Pet. Chem., 32(1), 247-51 (1987)

117. Iizuka, T.; Inoue, T.; Tanabe, K., "Synthesis of light olefins from carbon monoxide and water over supported rhodium catalysts," React. Kinet. Catal. Lett., 33(2), 249-52 (1987)

118. Bybell, D. G.; Deutsch, P. P.; Herman, R. G.; Himelfarb, P. B.; Nunan, J. G.; Young, C. W.; Bogdan, C. E.; Simmons, G. W.; Klier, K., "Promotion by cesium(I) and poisoning by thallium(I) of the copper/zinc oxide catalysts for methanol synthesis and the water-gas shift reaction," Prepr. - Am. Chem. Soc., Div. Pet. Chem., 31(1), 282-90 (1986)

119. Sharp, D. J., "Photoselective metal deposition," Plating, 58(8), 786-90 (1971)

120. O'Young, Chi Lin; Katzer, James R., "Infrared studies of carbon monoxide chemisorption on a highly dispersed supported osmium catalyst," J. Phys. Chem., 91(23), 6013-16 (1987)

121. Jozwiak, W. K., "Effect of a support on the adsorptive-catalytic properties of deposited rhodium," Zesz. Nauk. - Politech. Lodz., Chem., (No. 41), 104-19 (1987)

122. Worley, S. D.; Dai, C. H., "Effect of potassium on the hydrogenation of carbon monoxide and carbon dioxide over supported rhodium catalysts," Report, AU-TR-9; Order No. AD-A171553/1/GAR, 24 pp. Avail. NTIS From: Gov. Rep. Announce. Index (U. S.) 1986, 86(26), Abstr. No. 656,411 (1986)

123. Mochida, I.; Ikeyama, N.; Fujitsu, H., "Catalytic activities for carbon monoxide-hydrogen reaction and CO activation over noble metal catalysts supported on titanium dioxide," Nippon Kagaku Kaishi, (12), 2248-54 (1987)

124. Dai, C. H.; Worley, S. D., "Effects of potassium on carbon monoxide methanation over supported rhodium films, "Report, AU-TR-8; Order No. AD-A171535/8/GAR, 17 pp. Avail. NTIS From: Gov. Rep. Announce. Index (U. S.) 1986, 86(26), Abstr. No. 656,409 (1986)

125. Berry, F. J.; Lin, Liwu; Du, H.; Liang, D.; Tang, R.; Wang, C.; Zhang, S., "An in situ Moessbauer spectroscopic investigation of titania-supported iron-ruthenium catalysts," J. Chem. Soc., Faraday Trans. 1, 83(8), 2573-83 (1987)

126. Lin, L.; Berry, F. J.; Du, H.; Liang, D.; Tang, R.; Wang, C.; Zhang, S., "Titania supported iron-ruthenium catalysts for Fischer-Tropsch synthesis," Stud. Surf. Sci. Catal., 31(Prep. Catal. 4), 467-77 (1987)

127. Demmin, R. A., "The methanation kinetics of model platinum catalysts," 179 pp. Avail. Univ. Microfilms Int., Order No. DA8703195 From: Diss. Abstr. Int. B 1987, 47(10), 4233 (1986)

128. Mori, T.; Taniguchi, S.; Mori, Y.; Hattori, T.; Murakami, Y., "Absence of high methanation activity of titania-supported rhodium, ruthenium and iridium catalysts in their strong metal-support interaction state," J. Chem. Soc., Chem. Commun., (18), 1401-2 (1987)

129. Tkachenko, O. P.; Shpiro, E. S.; Gruenert, W.; Beilin, L. A.; Minachev, Kh. M., "Selective synthesis of lower olefins from carbon monoxide and hydrogen over a ruthenium-titanium dioxide-catalyst," Izv. Akad. Nauk SSSR, Ser. Khim., (10), 2390 (1987)

130. Behrmann, W. C.; Mauldin, C. H.; Arcuri, K. B.; Herskowitz, M., "Surface-supported particulate metal compound catalysts, their preparation and their use in hydrocarbon synthesis reactions," Eur. Pat. Appl. EP 266898 A2, 11 May 1988, 26 pp. Designated States: DE, FR, GB, IT, NL, SE (1988)

131. Iglesia, E.; Soled, S. L.; Fiato, R. A., "Cobalt-ruthenium catalysts for Fischer-Tropsch synthesis and process for their preparation," U.S. US 4738948 A, 19 Apr 1988, 10 pp. (1988)

132. Wachs, I. E.; Yang, D. B., "Catalysts comprising ruthenium on titania surface modified with group VA oxide of vanadium, niobium or tantalum," U.S. US 4711871 A, 8 Dec 1987, 6 pp. Cont.-in-part of U.S. Ser. No. 626,457, abandoned. (1987)

133. Fujimoto, K.; Kajioka, M., "Hydrogenation of carbon monoxide over solid catalysts dispersed in liquid medium. I. Slurry-phase Fischer-Tropsch synthesis with supported ruthenium catalysts," Bull. Chem. Soc. Jpn., 60(6), 2237-43 (1987)

134. Denise, B.; Sneeden, R. P. A., "Oxide-supported copper catalysts prepared from copper formate: differences in behavior in methanol synthesis from carbon monoxide/hydrogen and carbon dioxide/hydrogen mixtures," Appl. Catal., 28(1-2), 235-9 (1986)

135. Amenomiya, Y., "Methanol synthesis from carbon dioxide + hydrogen. II. Copper-based binary and ternary catalysts," Appl. Catal., 30(1), 57-68 (1987)

136. Vedage, G. A.; Pitchai, R.; Herman, R. G.; Klier, K., "Water promotion and identification of intermediates in methanol synthesis," Int. Congr. Catal., [Proc.], 8th, Meeting Date 1984, Volume 2, II47-II58. Verlag Chemie: Weinheim, Fed. Rep. Ger. (1985)

137. Nunan, J.; Klier, K.; Young, C.-W.; Himelfarb, P. B.; Herman, R. G., "Promotion of methanol synthesis over copper/zinc oxide catalysts by doping with cesium," J. Chem. Soc., Chem. Commun., (3), 193-5 (1986)

138. Berube, M. N.; Sung, B.; Vannice, M. A., "Sulfur poisoning of supported palladium methanol synthesis catalysts," Appl. Catal., 31(1), 133-57 (1987)

139. Bond, G. C.; Richards, D. G., "Lanthanum oxide promoted rhodium/titania and rhodium-platinum/titania catalysts for alcohol formation from synthesis gas," Appl. Catal., 28(1-2), 303-19 (1986)

140. V. I. Kuznetsov, et al., "Mossbauer spectroscopic and chemical analysis of the composition of Sn-containing components of Pt-Sn/Al$_2$O$_3$(Cl) reforming catalyst," J. Catalysis 99, 159-170 (1986)

141. Adams, F. H.; Knapik, H. P. G., "Hydrocarbon conversion with a selectively sulfided acidic multimetallic catalytic composite," U.S. US 4107083, 15 Aug 1978, 12 pp. (1978)

142. Baba, S.; Kawamura, T.; Takaoka, H.; Kimura, T.; Minato, Y.; Iida, K.; Imai, T., "Isomerization of hydrocarbons," Jpn. Kokai Tokkyo Koho JP 61/280440 A2 [86/280440], 11 Dec 1986, 10 pp. (1986)

143. Baba, S.; Kawamura, T.; Takaoka, H.; Kimura, T.; Minato, Y.; Iida, K.; Imai, T., "Isomerization of hydrocarbons Jpn. Kokai Tokkyo Koho JP 61/280440 A2 [86/280440], 11 Dec 1986, 10 pp. (1986)

144. Rausch, R. E., "Paraffin isomerization with a catalytic composite of platinum or palladium metal, rhodium metal, tin oxide, halogen, and alumina carrier," U.S. US 3992476, 16 Nov 1976, 10 pp. Continuation of U.S. 3,898,154. (1976)

145. Box, E. O., Jr., "Dehydrogenation catalysts comprising Group VIII metals on tin-containing supports," Phillips Petroleum Co., U.S. US 3692701, 19 Sep 1972, 4 pp. (1972)

146. Hayes, J. C., "Multicomponent composite dehydrogenation catalyst," Japan. JP 53/22560 [78/22560], 10 Jul 1978, 4 pp. (1978)

147. Pollitzer, E. L.; Hayes, J. C., "Dehydrocyclization with an acidic multimetallic catalytic composite," U.S. US 4046828, 6 Sep 1977, 12 pp. Cont.-in-part of U.S. 3,960,710. (1977)

148. Pollitzer, E. L.; Hayes, J. C., "Hydroprocessing aromatics to make cycloparaffins," U.S. US 3992464, 16 Nov 1976, 15 pp. Continuation of U.S. 3,960,710. (1976)

149. Takei, Tatsuko; Laitinen, H. A., "Mechanistic aspects of cathodic oxygen reduction in alkaline solution on platinum-coated tin(IV) oxide/silicon electrode," Surf. Technol., 15(3), 239-54 (1982)

150. Watanabe, M.; Venkatesan, S.; Laitinen, H. A., "Preparation of dispersed platinum on conductive tin oxide and its catalytic acivity for oxygen reduction," J. Electrochem. Soc., 130(1), 59-64 (1983)

151. Laitinen, H. A., "Catalyzed air electrodes," Report, UCRL-15320, 22 pp. Avail. NTIS From: Energy Res. Abstr. 1981, 6(8), Abstr. No. 11346 (1980)

152. Tseung, A. C. C., "Inhibition of sintering in supported fuel cell catalysis," Spec. Rep. EPRI SR - Electr. Power Res. Inst. (Palo Alto, Calif.), EPRI SR-13, Conf. Proc.: Fuel Cell Catal. Workshop, 23-5 (1975)

153. Iwakura, C.; Inai, M.; Tamura, H., "Foreign metal-doped tin(IV) oxide film anodes for oxygen and chlorine evolution," Chem. Lett., (3), 225-8 (1979)

154. Ohnishi, H.; Matsumura, M.; Tsubomura, H.; Iwasaki, M., "Bleaching of lignin solution by a photocatalyzed reaction on semiconductor photocatalysts," Ind. Eng. Chem. Res., 28(6), 719-24 (1989)

155. Kiselev, E. Yu.; Kondrikov, N. B.; Shub, D. M.; Reznik, M. F.; Eliseenko, L. G., "Electrode for electrochemical processes and method of producing it," U.S.S.R. SU 1333717 A1, 30 Aug 1987 From: Otkrytiya, Izobret. 1987, (32), 97 (1987)

156. Sobczynski, A.; Bard, A. J.; Campion, A.; Fox, M. A.; Mallouk, T.; Webber, S. E.; White, J. M., "Photoassisted hydrogen generation: platinum and cadmium sulfide supported on separate particles," J. Phys. Chem., 91(12), 3316-20 (1987)

157. Ragoisha, G. A.; Kisel, L. F.; Sokolov, V. G.; Sviridov, V. V., "Bistability effect of a titanium dioxide/silver^{1+}/palladium^{2+} system in the presence of hypophosphite ions," Dokl. Akad. Nauk BSSR, 30(7), 635-7 (1986)

158. Bart, J. C. J.; Sneeden, R. P. A.., "Copper-zinc oxide-alumina methanol catalysts revisited," Catal. Today, 2(1), 1-124 (1987)

159. Drawdy, G. E.; Hoflund, G. B.; Gardner, S. D.; Yngvadottir, E.; Schryer, D. R., "Effect of Pretreatment on a Platinized Tin Oxide Catalyst Used for Low-Temperature CO Oxidation," This volume (1990).

160. Boudart, M., paper presented to the North American Meeting of the Catalysis Society, San Diego, California, May 18-22, 1987

161. Cox, D. F.; Hoflund, G. B.; Laitinen, H. A., "A study of the dehydration of tin oxide surface layers," Applic. Surf. Sci. 20, 30-38 (1984)

Pt/SnO₂-BASED CO-OXIDATION CATALYSTS FOR LONG-LIFE CLOSED-CYCLE CO₂ LASERS

David R. Schryer, Billy T. Upchurch, Robert V. Hess, and George M. Wood
NASA Langley Research Center
Hampton, VA

Barry D. Sidney and Irvin M. Miller
Science and Technology Corporation
Hampton, VA

Kenneth G. Brown, John D. Van Norman, Jacqueline Schryer,
and David R. Brown*
Old Dominion University
Norfolk, VA

Gar B. Hoflund
University of Florida
Gainesville, FL

Richard K. Herz
University of California, San Diego
La Jolla, CA

ABSTRACT

Noble-metal/tin-oxide based catalysts such as Pt/SnO₂ have been shown to be good catalysts for the efficient oxidation of CO at or near room temperature. These catalysts require a reductive pretreatment and traces of hydrogen or water to exhibit their full activity. Addition of Palladium enhances the activity of these catalysts with about 15 to 20 percent Pt, 5 percent Pd, and the balance SnO₂ being an optimum composition. Unfortunately, these catalysts presently exhibit significant decay due in part to CO₂ retention, probably as a bicarbonate. Research on minimizing the decay in activity of these catalysts is currently in progress. A proposed mechanism of CO oxidation on Pt/SnO₂-based catalysts has been developed and is discussed in this paper.

INTRODUCTION

Pulsed CO₂ lasers have several potential remote-sensing applications, both military and non-military, which require long-life operation with high conversion-efficiency and good power-stability. However, two problems are potentially associated with such applications.

One problem is that the electrical discharge normally used to excite pulsed CO₂ lasers generally decomposes some of the CO₂:

$$CO_2 \xrightarrow{\text{Elec. Disch.}} CO + 1/2\ O_2$$

---
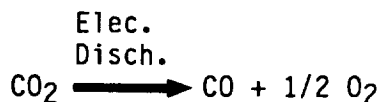
*Now Erik J. Kielin

This decomposition is harmful to long-life laser operation both because of the loss of CO_2 and because of the buildup of O_2. The loss of CO_2 results in a corresponding gradual loss of laser power. The buildup of even relatively small concentrations of O_2 molecules can cause rapid power loss and even complete laser failure. Although CO_2 lasers differ somewhat in their tolerance of O_2, it is generally desirable to keep the O_2 concentration below a few tenths of 1 mole-percent. CO has no significant deleterious effect on laser performance at moderate concentrations.

The second problem is that the atmosphere contains a significant concentration, about 300 ppm, of common-isotope CO_2 ($^{12}C^{16}O_2$). If common-isotope CO_2 is used in a CO_2 laser intended for atmospheric transmission, the emission frequencies available to the laser will correspond to the absorption frequencies of the atmospheric CO_2 and poor transmission will result.

The solutions to these two problems are superficially quite simple: (1) continuously remove O_2 as it is formed and replenish CO_2 and (2) use some form of rare-isotope CO_2 (such as $^{12}C^{18}O_2$, $^{13}C^{16}O_2$, or $^{13}C^{18}O_2$) in lasers intended for applications involving atmospheric transmission so that the emission frequencies of such lasers will differ from the absorption frequencies of atmospheric $^{12}C^{16}O_2$. Actual implementation of these two solutions, however, is far from simple.

Removal of O_2 and replenishment of CO_2 can be achieved in certain applications simply by operating the laser open-cycle with a continuous flow-through of fresh laser-gas and the consequent removal of dissociation products. However, for space-based applications or other applications involving weight and/or volume constraints, the amount of gas required for open-cycle operation would be unacceptable and, instead, closed-cycle laser operation with recycling of the laser gases would be imperative. Closed-cycle operation would also be highly desirable for any applications where rare-isotope CO_2 is used for enhanced atmospheric transmission because of the expense of the large volumes of rare-isotope gas which would be required for flow-through operation.

Achievement of closed-cycle operation of pulsed CO_2 lasers requires catalytic recombination of the decomposition products, CO and O_2, to regenerate CO_2.

$$CO + 1/2\ O_2 \xrightarrow{\text{Cat.}} CO_2$$
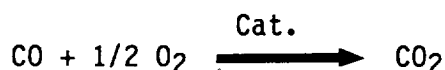
Candidate catalysts must have high efficiency at steady-state laser conditions which are, generally, 25°C to 100°C and about one atmosphere of total pressure with low partial-pressures of CO and O_2. Some excess CO may be added to the laser-gas mixture but generally it is not. It is desirable that little or no heating of the catalyst be required in order to minimize power consumption.

The catalytic oxidation of CO to CO_2 has been extensively studied at various conditions for a number of catalysts. These include the noble metals and various metal oxides (refs. 1 and 2) and the commercial catalyst, Hopcalite (ref. 3), which is a mixture of CuO and MnO_2 plus small quantities of other oxides. However, few catalysts have sufficiently high activity to allow operation at the low steady-state temperatures and low oxygen partial pressures characteristic of typical pulsed CO_2 lasers.

The most promising catalysts studied to date, whose performance has been verified by actual closed-cycle laser operation, consist of Pt and/or Pd on tin (IV) oxide (refs. 4 and 5). A systemmatic study of (Pt, Pd)/SnO_2 catalysts for use with closed-cycle pulsed CO_2 lasers, including the preparation and testing of improved catalyst formations, has been in progress at the Langley Research Center of NASA (LaRC) for the past several years (refs. 5-16). This study has been expanded by joint research with investigators at Old Dominion University, the University of Florida, the University of California, San Diego, and Science and Technology Corporation (refs. 1, 5-11, 13, 15-21).

TEST FACILITIES

Catalyst research at LaRC is carried out both in laboratory reactors and in a commercial CO_2 TEA laser.

Laboratory Reactors

Laboratory reactors are used for catalyst study under controlled conditions. Several laboratory reactors are presently operational, most of which are flow-through (plug-flow) reactors. In these reactors a test-gas mixture flows through a reactor tube containing a catalyst sample which is situated in a temperature-controlled oven. The gas which enters and exits the reactor tube is quantitatively analyzed with either a gas chromatograph (GC) or mass spectrometer (MS) and from this analysis the amount of CO and O_2 converted to CO_2 by the catalyst sample is determined. For many tests the test-gas mixtures used are purchased premixed in a high-purity He carrier, typically 1.00 percent CO and 0.50 percent O_2 plus 2.00 percent Ne (as an internal calibration standard for gas analysis). For some tests the gas mixtures are blended in the laboratory using high-purity component gases and calibrated flow controllers.

All except one of the reactors are used with common-isotope gases and use GC's for gas analysis. These GC's are fully automated so that tests with common-isotope gases can be conducted in the flow-through reactors continuously around-the-clock. One flow-through reactor is used with rare-isotope gases and uses an MS for gas analysis.

Studies performed in the flow-through reactors are (1) parametric studies to determine the effect of such parameters as catalyst mass, temperature, reactor residence-time, pretreatment conditions, etc., on the performance of a given catalyst material, (2) comparison of different catalyst compositions (such as Pt/SnO_2, Pd/SnO_2, and Pt + Pd/SnO_2) and concentrations to determine the optimum catalyst formulation, (3) long-term performance tests (using an automated-GC reactor) to determine how a catalyst performs with long-term exposure to the test gases, and (4) isotopic studies (using the MS reactor) to determine the interaction of a given catalyst with rare-isotope gases.

A recirculating and a pulsed reactor are also available. In the recirculating reactor a gas mixture is continuously recirculated through a temperature-controlled reactor tube containing a sample of catalyst, and the conversion of CO and O_2 to CO_2 is monitored as a function of time. Gas analysis is performed with a GC. This reactor is used to study the kinetics and mechanism of catalysis for selected catalyst compositions.

With the pulsed reactor, the single-gas or gas-mixture to be studied (in a He carrier) is exposed to the catalyst sample in a series of discrete pulses. The pulses are spaced in time such that the gas exiting the reactor after each pulse can be analyzed by GC. The cumulative gain or loss of each species as a function of time can thus be more finely resolved than with the continuous flow-through and recirculating reactors. The pulsed reactor is used for both reaction and chemisorption studies.

Laser Reactor

A Lumonics model TEA-820 pulsed CO_2 laser (7 Watt, 1-50 pulses/second) is available for catalyst testing under actual laser operating conditions. The laser is operated closed-cycle with an external catalyst bed (in a temperature-controlled oven) and the results are compared with the open-cycle performance of the laser at the same flow rate. It is intended that ultimately the laser will be operated with no heating of the catalyst other than by the laser gas. Gas analysis is performed with a GC in current common-isotope tests. An MS will be used when the laser is operated with rare-isotope CO_2.

RESULTS

The following results have been obtained in studies performed to date.

Common-Isotope Laboratory Studies

(1) Pt on SnO_2 (Pt/SnO_2) has significantly higher catalytic activity for CO oxidation than either Pt or SnO_2 alone (ref. 5). The effect is clearly synergistic and apparently involves separate but complementary roles for the Pt and SnO_2 phases.

(2) The efficiency of Pt/SnO_2-catalyzed oxidation of CO to CO_2 is approximately proportional to catalyst mass until complete conversion is achieved (ref. 5).

(3) The catalyst mass required to achieve complete oxidation of a given concentration of CO is roughly proportional to the flow rate of the gas through the catalyst (ref. 7). This makes possible the extrapolation of results obtained with laboratory reactors to CO_2 lasers.

(4) A technique for achieving much higher Pt loadings than are commercially available has been developed (ref. 16). Platinum loadings as high as 46 percent have been achieved. All metal loadings given in this paper are percentages by weight.

(5) The activity for CO oxidation of Pt/SnO_2 catalysts increases with Pt loading until a maximum activity is reached at about 17 percent Pt (Ref. 14). Since Pt loadings between 11 percent and 17 percent and between 17 percent and 24 percent were not tested, the precise optimum loading is somewhat uncertain but it is believed to lie in the range of 15 to 20 percent.

(6) Addition of a small quantity of Pd to a Pt/SnO_2 catalyst can enhance its activity. For example, a catalyst consisting of 1 percent Pt and 1 percent Pd (with the balance SnO_2) has been found to be more active than a catalyst with 2 percent Pt and no Pd. For a catalyst with 15 to 20 percent Pt, the optimum Pd loading is about 5 percent.

(7) A reductive pretreatment enhances the activity of Pt/SnO_2 catalyts relative to no pretreatment or to pretreatment with O_2 or an inert gas (Ref. 15). Pretreatment consists of a flow of the pretreatment gas (in a helium carrier, for safety and convenience) over the catalyst sample at an elevated temperature prior to exposure of the catalyst to the reaction gas mixture at the selected reaction temperature. Both CO and H_2 are suitable gases for reductive pretreatment (Ref. 15); in this study they were used at a concentration of 5 percent in He.

(8) The temperature at which a Pt/SnO_2 catalyst is pretreated can affect its subsequent activity (Ref. 15). Pretreatment temperatures of 125°C, 175°C, and 225°C resulted in equal catalytic activity, for the catalyst tested, but pretreatment at 100°C yielded somewhat lower activity.

(9) Duration of the pretreatment also affects subsequent catalyst activity (Ref. 15). Catalyst activity after a 20-hour CO pretreatment was found to be lower than after a 1-hour pretreatment. Too short a pretreatment also diminishes catalyst activity. For optimum results the effluent gases from the pretreatment should be analyzed and the pretreatment terminated when no significant yield of oxidation product (CO_2 or H_2O) is detected.

(10) Pretreatment of a Pt/SnO_2 catalyst sample at elevated temperatures--above about 125°C--results in an initial dip in catalyst activity before the steady-state activity is achieved for studies in the flow-through reactors (Ref. 15). No dip occurs if the catalyst is pretreated at lower temperatures. If the catalyst is exposed to moisture following pretreatment but prior to exposure to the reaction gas mixture, or if the reaction gas mixture is humidified, no dip occurs (Ref. 15).

(11) In many cases moisture not only eliminates the initial dip in catalyst activity, it also enhances the activity of the catalyst (Ref. 15). In fact, addition of moisture has been shown to increase the activity even of an unpretreated catalyst. As discussed in the following section, this is believed to be due to conversion of surface oxides to more-active surface hydroxyls.

(12) No initial dip in catalyst activity has been observed in flow-through reactor studies when the Pt loading exceeded 24 percent even at pretreatment temperatures of 225°C. No dip has been observed in studies in the recirculating reactor at any Pt loading or pretreatment temperature.

(13) The activities of Pt/SnO_2 catalysts exhibit some decay with time. Initial activity can be readily restored by outgassing the catalyst either by heating it or by exposing it to an inert gas for about 2 hours. In either case, restoration of activity has been found to be associated with outgassing of CO_2 from the catalyst but decay in activity occurs again when CO oxidation is resumed. An additional long-term decay which is not associated with CO_2 retention has also been observed. This decay is reversible by reduction of the catalyst.

(14) The yield of CO_2 for a given catalyst sample and set of reaction conditions is increased by addition of O_2 to a stoichiometric mixture of CO and O_2 and decreased by addition of CO to such a mixture (Ref. 22). The reaction has been found to be approximately first order with respect to O_2 concentration. Determination of the reaction order with respect to CO concentration is currently in progress. The true rate equation appears to be somewhat complex.

45

Rare-Isotope Catalyst Studies

(1) Reaction of $C^{18}O$ and $^{18}O_2$ on a common-isotope $Pt/Sn^{16}O_2$ catalyst yields about 85 percent $C^{18}O_2$ and 15 percent $C^{18}O^{16}O$ (Ref. 10). This concentration of the mixed-isotope species $C^{18}O^{16}O$ is unacceptable.

(2) A technique has been developed for modifying the surface of common-isotope Pt/SnO_2 so that all reactive surface oxygens are ^{18}O (ref. 10). Reaction of $C^{18}O$ and $^{18}O_2$ over this modified catalyst yielded only $C^{18}O_2$, within experimental error, in a test of 17 days (Ref. 23).

(3) Rare-isotope studies have indicated that some sort of carbonate or biocarbonate species is formed when CO is oxidized on Pt/SnO_2 catalysts (ref. 10).

Surface Characterization Studies

Extensive surface characterization studies have been performed by Hoflund and coworkers at the University of Florida. These studies utilized an ultrahigh vacuum system containing multiple surface techniques including ion scattering spectroscopy (ISS), electron spectroscopy for chemical analysis (ESCA), Auger electron spectroscopy (AES), and electron stimulated desorption (ESD) with pretreatment capabilities at elevated pressures and temperatures. The following results have been obtained:

(1) The surface hydrogen present at a polycrystalline tin oxide film has been studied using ESD before and after annealing the film at 500°C (Ref. 17). Annealing reduces the concentration of surface hydrogen by a factor of 8, and energy analysis of the desorbing ions indicates that at least 3 chemical bonding states of H are present at the surface. Further research is necessary to elucidate the nature of these states.

(2) The reduction by vacuum annealing from 200 to 350°C of a platinized tin oxide film has been examined using ISS, ESCA and AES (Ref. 18). The data show that tin is reduced to metallic form which alloys with the supported platinum.

(3) Since Pt/Sn alloys form in reduced Pt/Sn systems, it is important to characterize the behavior of Pt/Sn alloys. As part of a continuing study of Pt/Sn alloy surfaces, the reduction in H_2 of an air-exposed Pt/Sn alloy surface has been examined using ISS, ESCA and angle-resolved AES (Ref. 19). Initially, a tin-depleted Pt-rich region is covered by a 30Å thick uniform layer of tin oxide. During reduction, oxygen is removed from the surface forming metallic tin and platinum migrates to the surface through vacancies left by the oxygen to alloy with the metallic tin.

(4) An unsupported commercial 2 percent Pt/SnO_2 catalyst has been examined using ISS, AES, and ESCA as a function of pretreatment temperature (air exposed, 75, 100, 125, and 175°C) at 4 and 40 Torr of CO (Ref. 24). During the reduction the O/Sn ratio is decreased, the Pt is reduced from platinum oxides to $Pt(OH)_2$, the surface hydroxyl group concentration is reduced, and a Pt/Sn alloy forms. This is the same catalyst whose activity as a function of reductive-pretreatment temperature is discussed in item (8) of the section on common-isotope studies.

(5) A silica-supported Pt/Sn catalyst developed at NASA has been characterized before and after pretreatment at 125 and 225°C in CO (Ref. 20). The 125°C reduction, which yields a highly catalytically active surface, converts the Pt oxides primarily to $Pt(OH)_2$. Reduction at 225°C produces a surface which is much less active catalytically. The surface studies show that this is due to coverage of the surface Pt by contaminant species, including silica, and reduction of the $Pt(OH)_2$ to metallic Pt.

Laser Studies

(1) The Lumonics Model TEA-820 laser has been operated closed-cycle with a catalyst bed of 150 g of 2 percent Pt/SnO_2 at 100°C (Refs. 5 and 8). The laser achieved 96.5 percent (± 3.5 percent) of steady-state open-cycle power for 28 hours (1 x 10^6 pulses at 10 pulses/second). Both the laser and catalyst were fully operational at the conclusion of the test. Additional laser tests are in progress.

(2) Herz and coworkers at the University of California, San Diego, (ref. 21) have developed a computer program which can be used to design catalyst monoliths for specific laser applications. The critical information a user needs to supply is the first-order-overall rate constant and activation energy for the catalyst formulation of interest. After the user supplies other information such as gas composition, gas flow rate and monolith dimensions, the program computes the conversion of oxygen and pressure drop as a function of monolith length. By varying input parameters, the user can investigate various design alternatives. One conclusion of a design study performed with the program is that standard off-the-shelf monoliths are not optimal for use in CO_2 laser applications. This is because standard monoliths have been designed for combustion or emission control applications where reactions occur very fast at high temperature and high gas flow-rates. Gas flow-rates in lasers are relatively low and reactions occur at low temperatures and thus, are relatively slow. Monoliths optimized for laser applications to provide for minimum monolith size will have thicker layers of active catalyst material than monoliths used for combustion and emission control. The computer program is available through NASA's COSMIC office.

PROPOSED MECHANISM

One result of the study described in the foregoing sections of this paper is that several features of the mechanism of Pt/SnO_2-catalyzed CO oxidation have begun to emerge. Primary among these is the role of surface hydroxyl groups in the oxidation of CO chemisorbed on Pt sites. Although much is still, at best, uncertain or ambiguous and much else is simply unknown, it is now possible to put forth, in some detail, a tentative mechanism which is consistent with a broad range of experimental observations. This proposed mechanism, including detailed reaction equations is presented in this section.

The experimental observations reported in the previous section suggest the postulate that surface OH groups participate in the oxidation of CO chemisorbed on Pt sites. Hoflund and coworkers have observed OH groups on both tin-oxide and platinized tin-oxide surfaces (refs. 17 and 24). Reductive pretreatment of

the catalyst enhances its activity but pretreatment at elevated temperatures also dehydrates the catalyst surface and thereby depletes the surface concentration of OH. The initial reaction which occurs when the catalyst is exposed to the test-gas mixture further depletes the surface concentration of OH and partially re-oxidizes the surface. This results in the observed decline in catalyst activity. Rehydroxylation of the surface, probably by migration of H (or H^+) from the catalyst bulk, eventually restores the catalyst activity. The sequential decline and increase in catalyst activity results in the observed dip. If the OH concentration at the catalyst surface is restored by humidification of either the catalyst or the reaction gas no dip is observed. Humidification of the catalyst surface may increase the OH concentration above the initial value and the activity of the catalyst may then be enhanced as reported in Reference 15.

Most of the CO_2 formed immediately desorbs from the Pt phase, but a fraction of the CO_2 molecules interact with surface OH sites and are retained, probably as bicarbonate. This bicarbonate eventually undergoes decomposition, but until such decomposition occurs, the chemisorbed-CO_2/bicarbonate species ties up OH sites and, thus, contributes to the observed decay in catalyst activity. Outgassing of the chemisorbed CO_2 restores the catalyst activity, as observed.

An equation set which represents the foregoing proposed mechanism is

Pretreatment

(1) $HOSnO_x$ + Reduction → Sn + HOSn

(2) $HOPtO_y$ + Reduction → Pt + HOPt

The surface of the "tin-oxide" and "platinum" phases of platinized tin-oxide consists of complex hydroxy oxides which are represented here as $HOSnO_x$ and $HOPtO_y$, respectively; following reduction some Pt and Sn are formed which are present predominantly as a PtSn alloy with some surface hydroxyl groups (refs. 18-20).

Chemisorption

(3) $O_2(g)$ + PtSn → O_2•PtSn　　　　　　　　　　Rate Determining Step

(4) CO(g) + Pt → CO•Pt　　　　　　　　　　　　　　　　　　Fast

CO chemisorbs readily on Pt but does not chemisorb significantly on Sn, whereas O_2 chemisorbs on both Pt and Sn (ref. 25). It is assumed herein that these chemisorption properties hold for the Pt and Sn atoms of the PtSn alloy as well as for the individual metals. Although O_2 can chemisorb on Pt, it is not normally significantly present on room-temperature Pt surfaces when CO is also present; this is because of the relatively low sticking coefficient of O_2 on Pt as well as the fact that each O_2 molecule requires a pair of adjacent vacant surface sites whereas CO molecules require only individual vacant sites (ref. 1). We suggest that the presence of Sn atoms in the PtSn alloy component of prereduced platinized tin-oxide significantly alters this situation. Because each Pt atom of

the PtSn alloy is surrounded by Sn atoms which can chemisorb O_2 but not CO, O_2 molecules can compete with CO molecules for chemisorption on vacant Pt atoms with adjacent Sn atoms providing the necessary second sites. However, because of the higher sticking coefficient of CO on Pt, surface coverage by CO will still exceed that by O_2 for $CO:O_2$ ratios anywhere near stoichiometry. In fact, chemisorption of O_2 probably is the rate limiting step of this reaction set.

CO Oxidation

(5) $CO \bullet Pt + HOSn + Bulk \rightarrow CO_2(g) + Sn + H \bullet Bulk$
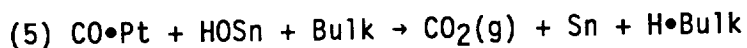
We propose that chemisorbed CO is oxidized predominately by surface hydroxyls rather than by oxygen atoms. This is analogous to the situation in the gas-phase oxidation of CO (ref. 1) and is consistent with the results presented in the previous section.

Hydrogen Exchange

(6) $Pt + H \bullet Bulk \rightarrow H \bullet Pt + Bulk$

It is assumed that hydrogen (possibly as H^+) is relatively plentiful in the prereduced catalyst and that it exchanges readily between the bulk and the surface, preferentially at Pt sites.

Surface Rehydroxylation

(7) $O_2 \bullet PtSn + H \bullet Pt \rightarrow HOSn + OPt + Pt$
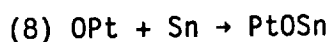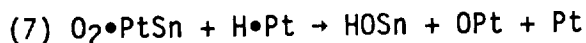
(8) $OPt + Sn \rightarrow PtOSn$ Fast

Although the oxidizing species, HOSn, is regenerated by equation (6), the surface is also reoxidized--and, thus, deactivated--by this step. This is probably the cause of the downward portion of the initial dip in activity when the catalyst has been dehydrated during pretreatment. It is possible that surface reoxidation can be partially undone by

(9) $H \bullet Pt + PtOSn \rightarrow 2Pt + HOSn$
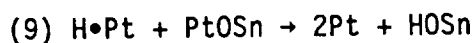
However, the experimental data suggest that conversion of surface oxide to surface hydroxyl is most readily accomplished by reaction with water:

(10a) $PtOSn + H_2O \bullet Surface \rightarrow HOPt + HOSn + Surface$ Fast

or
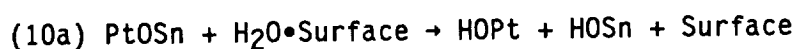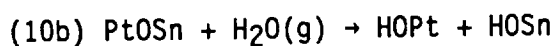
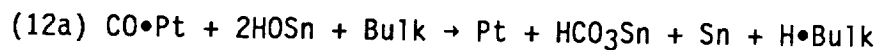(10b) $PtOSn + H_2O(g) \rightarrow HOPt + HOSn$ Fast

Although water may conceivably migrate from the catalyst bulk to the surface to allow the catalyst to come out of the initial dip in activity via equation (10a), it is more likely that the migrating species is H (or H^+) yielding surface H_2O via

(11) $HO \bullet Surface + H \bullet Bulk \rightarrow H_2O \bullet Surface + Bulk$

Of course, if water is supplied continuously by humidifying the reaction gas mixture, OH groups are continuously regenerated by equation (10b) and no dip in activity occurs; in fact the activity may be enhanced somewhat, as observed (Ref. 15).
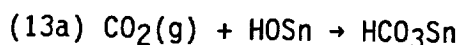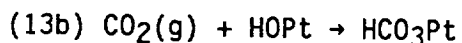
Bicarbonate Formation and Decomposition

(12a) $CO \cdot Pt + 2HOSn + Bulk \rightarrow Pt + HCO_3Sn + Sn + H \cdot Bulk$

or

(12b) $CO \cdot Pt + 2HOSn + Bulk \rightarrow HCO_3Pt + 2Sn + H \cdot Bulk$

Although the oxidation of chemisorbed CO normally proceeds with the immediate release of $CO_2(g)$, as in equation (5), bicarbonate formation can occur as in equation (12a) or (12b) when two HOSn groups are adjacent to a chemisorbed CO. It is not known whether the bicarbonate group is on a Pt on an Sn site; either would effectively deactivate the catalyst. It is possible that bicarbonate formation can occur by reaction of surface hydroxyl with gas phase CO_2:

(13a) $CO_2(g) + HOSn \rightarrow HCO_3Sn$

or

(13b) $CO_2(g) + HOPt \rightarrow HCO_3Pt$

However, experimental data indicate that CO_2 retention by the catalyst is relatively insensitive to the gas phase concentration of CO_2 in most cases. It is not yet known whether bicarbonate decomposition is thermal or caused by reaction with surface hydrogen. Nevertheless, it is clear that a steady-state eventually is attained in which bicarbonate is formed at the same rate at which it is decomposed. This steady-state then limits the effective activity of the catalyst to a value about half of its activity if no bicarbonate buildup occurred. In addition to the fairly rapid loss of activity due to bicarbonate buildup, some sort of slow morphological change further deactivates the catalyst with a half-life of several months.

The foregoing mechanism admittedly is speculative in many ways. It is likely that it will require modification in some (perhaps many) details. Nevertheless, it is consistent with all experimental data currently available and it offers a point of departure for future studies of Pt/SnO_2-based catalysts. It is presented for consideration in this context.

CONCLUDING REMARKS

Noble-metal/tin-oxide based catalysts such as Pt/SnO_2 have been shown to be good catalysts for the efficient oxidation of CO at or near room temperature. They are the most promising catalysts for use in closed-cycle pulsed CO_2 lasers whose performance has actually been verified by tests in such lasers. The catalysts require a reductive pretreatment and traces of hydrogen or water to exhibit their full activity. Addition of

Palladium enhances the activity of these catalysts with about 15 to 20 percent Pt, 5 percent Pd, and the balance SnO_2 being an optimum composition. Unfortunately, these catalysts presently exhibit significant decay due in part to CO_2 retention, probably as a bicarbonate. Research on minimizing the decay in activity of these catalysts is currently in progress. A proposed mechanism of CO oxidation on Pt/SnO_2-based catalysts has been developed and is discussed in this paper. The mechanism, although somewhat speculative, is consistent with experimental results obtained to date.

REFERENCES

1. Herz, Richard D.: Chemical Engineering Design for CO Oxidation Catalysts. Closed-Cycle Frequency-Stable CO_2 Laser Technology, Carmen E. Batten, Irvin M. Miller, George M. Wood, Jr., and David V. Willetts, Eds., NASA CP-2456, pp. 103-112, 1987.

2. Engel, T., and Ertl, G.: Oxidation of Carbon Monoxide. The Chemical Physics of Solid Surfaces and Heterogeneous Catalysis, P. A. King and D. P. Woodruff, Eds., pp. 73-93, Elsevier, New York, 1982.

3. Kiang, San: Transient Isotopic Tracing Technique for the Resolution of the Room Temperature Oxidation of Carbon Monoxide Catalyzed by Commercial Hopcalite Catalyst. Pd.D. Thesis, Columbia University, 1978.

4. Stark, D. S.; Crocker, A.; and Steward, G. J.: A Sealed 100 Hz CO_2 TEA Laser Using High CO_2 Concentrations and Ambient-Temperature Catalysts. J. Phys. E. Sci. Instrum., vol. 16, pp. 158-161, 1983.

5. Brown, Kenneth G.; Sidney, B. D.; Schryer, D. R.; Upchurch, B. T.; Miller, I. M.; Wood, G. M.; Hess, R. V.; Batten, C.; Burney, L. G.; Paulin, P. A.; Hoyt, R.; and Schryer, J.: Catalytic Recombination of Dissociation Products with Pt/SnO_2 for Rare and Common Isotope Long-Life, Closed-Cycle CO_2 Lasers. SPIE Proc., vol. 663, pp. 136-144, 1986.

6. Rogowski, R. S.,; Miller, I. M..; Wood, G. M.; Schryer, D. R.; Hess, R. V.; and Upchurch, B.T.: Evaluation of Catalyst for Closed-Cycle Operation of High Energy Pulsed CO_2 Lasers. SPIE Proc., vol. 415, pp. 112-117, 1983.

7. Miller, I. M.; Wood, G. M. Jr.; Schryer, D. R.; Hess, R. V.; Upchurch, B. T., and Brown, K. G.: Optimization of the Catalytic Oxidation of CO for Closed-Cycle CO_2 Laser Applications. NASA TM-86421, 1985.

8. Sidney, Barry D.; Schryer, David R.; Upchurch, Billy T.; Hess, Robert V.; Wood, George M.; Miller, Irvin M.; Burney, L. Garland; Brown, Kenneth G.; Van Norman, John D.; and Schryer, Jacqueline: Research on Catalysts for Long-Life Closed-Cycle CO_2 Laser Operation. SPIE Proc., vol. 783, pp. 162-168, 1987.

9. Schryer, David R.; Sidney, Barry D.; Miller, Irwin M.; Hess, Robert V.; Wood, George M.; Batten, Carmen E.; Burney, L. Garland; Hoyt, Ronald F.; Paulin, Patricia A.; Brown, Kenneth G.; Schryer, Jacqueline; and Upchurch, Billy T.: NASA-LaRC Research on Catalysts for Long-Life Closed-Cycle CO_2 Lasers. Closed-Cycle Frequency-Stable CO_2 Laser Technology, Carmen E. Batten, Irvin M. Miller, George M. Wood, Jr., and David V. Willetts, Eds., NASA CP-2456, pp. 113-120, 1987.

10. Upchurch, Billy T.; Wood, George M. Jr.; Hess, Robert V.; and Hoyt, Ronald F.: Rare Isotope Studies Involving Catalytic Oxidation of CO Over Platinum-Tin Oxide. Closed-Cycle, Frequency-Stable CO_2 Laser Technology, Carmen E. Batten, Irvin M. Miller, George M. Wood, Jr., and David V. Willetts, Eds., NASA CP-2456, pp. 193-198, 1987.

11. Batten, Carmen E.; Miller, Irvin M.; Paulin, Patricia A.; and Schryer, Jacqueline: Studies of CO Oxidation on Pt/SnO_2 Catalyst in Surrogate CO_2 Laser Facility. Closed-Cycle, Frequency-Stable CO_2 Laser Technology, Carmen E. Batten, Irvin M. Miller, George M. Wood, Jr., and David V. Willetts, Eds, NASA CP-2456, pp. 193-198, 1987.

12. Sidney, Barry D.: Studies of Long-Life Pulsed CO_2 Laser with Pt/SnO_2 Catalyst. Closed-Cycle, Frequency-Stable CO_2 Laser Technology, Carmen E. Batten, Irvin M. Miller, George M. Wood, Jr., and David V. Willetts, Eds., NASA CP-2456, pp. 211-218, 1987.

13. Brown, K. G.; Schryer, J.; Schryer, D. R.; Upchurch, B. T.; Wood, G. M.; Miller, I. M.; Sidney, B. D.; Batten, C. E.; and Paulin, P. A.: Characterization of Pt/SnO_2 Catalysts for CO Oxidation. Closed-Cycle, Frequency-Stable CO_2 Laser Technology, Carmen E. Batten, Irvin M. Miller, George M. Wood, Jr., and David V. Willetts, Eds., NASA CP-2456, pp. 219-226, 1987.

14. Hess, R. V.; Buoncristiani, A. M.; Brockman, P.; Bair, C. H.; Schryer, D. R.; Upchurch, B. T.; and Wood, G. M.: Recent Advances in Efficient Long-Life, Eye-Safe Solid-State and CO_2 Lasers for Laser Radar Applications. SPIE Proc., vol. 999, pp. 2-18, 1989.

15. Van Norman, John D.; Brown, Kenneth G.; Schryer, Jacqueline; Schryer, David R.; Upchurch, Billy T.; and Sidney, Barry D.: The Effect of Pretreatment and H_2O on the Activity of a Pt/SnO_2 Catalyst. NASA CP-3076.

16. Upchurch, Billy T.; Schryer, David R.; Wood, George M.; and Hess, Robert V.: Development of CO Oxidation Catalysts for the Laser Atmospheric Wind Sounder (LAWS). SPIE Proc., Vol. 1062, 1989.

17. Hoflund, Gar B.; Grogan, Austin L., Jr.; Asbury, Douglas A.; and Schryer, David R.: A Characterization Study of a Hydroxylated Polycrystalline Tin Oxide Surface. Thin Solid Films, vol. 169, pp. 69-77, 1989.

18. Gardner, Steven D.; Hoflund Gar B.; Davidson, Mark R.; and Schryer, David R.: Evidence of Alloy Formation During Reduction of Platinized Tin Oxide Surfaces. J. Catalysis, vol. 115, pp. 132-137, 1989.

19. Gardner, Steven D.; Hoflund, Gar B.; and Schryer, David R.: Surface Characterization Study of the Reduction of an Air-Exposed Pt_3Sn Alloy: Part IV. J. Catalysis, 1990.

20. Gardner, Steven D.; Hoflund, Gar B.; Schryer, David R.; and Upchurch, Billy T.: Platinized Tin Oxide Catalysts for CO_2 Lasers: Effects of Pretreatment. SPIE Proc., vol. 1062, pp. 21-28, 1989.

21. Herz, R. K.; Guinn, K.; Goldblum, S.; and Noskowski, E.: Design of Catalytic Monoliths for Closed-Cycle Carbon Dioxide Lasers. Final Report for NASA Contract NAG-1-823, Univ. of Califiornia, San Diego, 1989.

22. Upchurch, Billy T.; Brown, David R.; Miller, Irvin M., and Schryer, David R.: LaRC-Developed Catalysts for CO_2 Lasers. NASA CP-3076.

23. Upchurch, Billy T.; Miller, Irvin M.; Brown, David R.; Wood, George M., Jr.; Schryer, David R.; and Hess, Robert V.: Rare-Isotope and Kinetic Studies of Pt/SnO_2 Catalysts. NASA CP-3076.

24. Drawdy, Jean E.; Hoflund, Gar B.; Gardner, Steven D.; Yngvadottir, Eva; and Schryer, David R.: Characterization Studies of a Commercial Pt/SnO_2 Catalyst. NASA CP-3076.

25. Bond, G. C.: Heterogeneous Catalysis: Principles and Applications, Second Edition, p. 29, Clarendon Press, Oxford, 1987.

SECTION II

CATALYST DEVELOPMENT

THE OXIDATION OF CARBON MONOXIDE USING TIN OXIDE BASED CATALYSTS

Christopher F Sampson and Norman Jorgensen
United Kingdom Atomic Energy Authority
Harwell Laboratory, Oxfordshire, OX11 0RA
United Kingdom

SUMMARY

The preparation conditions for precious metal/tin oxide catalysts were optimised for maximum carbon monoxide/oxygen recombination efficiency. This was achieved by controlling the tin digestion, the peptisation to form the sol, the calcination process and the method of adding the precious metals. Extensive studies of the tin oxide structure were carried out over the temperature range 20 to 500°C in air or hydrogen environments using Raman scattering and X-ray diffraction. Adsorbed species on tin oxide, generated in an environment containing carbon monoxide, gave rise to a Raman band at about 1600 cm^{-1} which was assigned to carbonaceous groups, possibly carbonate.

INTRODUCTION

Closed cycle CO_2 gas lasers are used in several applications. These applications can range from highly technical observation systems to heavy duty steel cutting tools. During the operation of these lasers dissociation of carbon dioxide occurs as shown in equation 1.

$$2CO_2 \rightleftharpoons 2CO + O_2 \qquad (1)$$
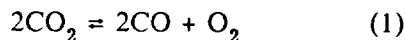
Molecular oxygen reduces the stability and operational efficiency of the laser; therefore, it is essential that the level is kept to a minimum. It is known that the recombination of CO and O_2 to form CO_2 can be achieved using a suitable catalyst (ref 1). The catalyst used in this application must meet the following requirements:-

1. The recombination of CO and O_2 at a rate at least equal to the generation rate.
2. It must be stable over a long time.
3. Under operational conditions it must maintain adequate efficiency.
4. The device must be mechanically stable during transportation, operation and non-working periods.

We have shown that high surface area tin oxide may be coated with various precious metals forming a catalyst with high activity for CO oxidation. However, the stability and efficiency of the final catalyst is crucially dependent on both the preparation conditions and the subsequent heat treatments.

57

The aims of the work reported here were to prepare a catalyst that would be effective under carbon dioxide laser conditions and to examine the effect of the preparation parameters on the structure and activity of these materials.

EXPERIMENTAL

Tin Oxide Sol Preparation

Tin (IV) oxide may be prepared directly from tin metal by controlled reaction with nitric acid. The dispersed oxide particles have a size which is dependent on the concentration of the acid, generally being larger for higher concentrations. The dried metastannic acid is non-crystalline, but crystallinity develops on calcining at 350°C.

The physical and chemical properties of commercial metastannic acid can be quite variable, perhaps due to differences in the preparation conditions. The tin oxide used in this work was therefore freshly prepared using Analar grade chemicals.

To form a tin oxide sol which can be used for coating substrates metastannic acid is peptised using an organic base. To do this the precipitated metastannic acid is thoroughly washed, removing ions, until the supernatant liquid has a conductivity of 4.5 mS or less. It will then peptise in the organic base, forming a sol with an oxide content typically $300gl^{-1}$, with particles of average size 210 nm (measured using a Malvern Zetasizer). The tin oxide catalyst support is then obtained by drying and then calcining at 350°C.

Precious Metal Catalyst Preparation

Tin oxide prepared by the method described above was impregnated with precious metal by one of the two routes listed below:

(a)   Co-precipitation achieved by mixing the components at the sol stage, followed by drying and calcination.

(b)   Wet impregnation of the dried and calcined tin oxide, followed by drying and calcination (incipient wetness technique).

The precious metals Pt and Pd were added such that the content after calcination at 350°C was in the range O to 3% of the tin oxide mass.

Activity Testing

All the samples discussed in this paper were pretreated and activity tested under identical conditions. After the calcination treatment the sample was mounted in the test reactor, reduced in a H_2/He gas stream and finally stabilised in oxygen. The activity testing was carried out in a flowing gas mix of 0.5% O_2, 1.0% CO and 98.5% N_2 at a space velocity of 36000 h^{-1}, and the unreacted CO and O_2 monitored to determine the recombination rate for the catalyst.

Raman Spectroscopy

The Raman Scattering experiments were carried out using a Spex Triplematic monochromator fitted with an intensified 1024 photo-diode detector. The laser beam sources were capable of being adjusted over a wavelength range 441 nm (He/Cd) to 514 nm (Ar ion). The power of the source beam was 100 m watts but was reduced to 10 m watts at the sample. To obtain comparable results all the high temperature oxidising and reducing atmosphere experiments were carried out using a Stanton Redcroft HSM 5 Hot Stage.

X-Ray Diffraction

The room temperature X-ray diffraction experiments were carried out using a Siemens fully automated D500 X-ray Diffractometer with copper K_α radiation and analysed using a secondary monochromator through a scintillation counter.

The high temperature experiments were carried out using a Harwell designed precision apex goniometer with a G.T.P Engineering high temperature attachment. The specimen hot stage assembly is controlled by a Eurotherm micro processor system. The primary beam was Cu K_α radiation and the diffracted beam passed through a curved graphite crystal secondary monochromator. Data collection was carried out using a Hewlett-Packard series 200, 9816 micro-computer.

RESULTS AND DISCUSSION

Activity Testing

Powdered catalysts prepared by the incipient wetness technique were more active than those containing the same quantity of precious metals prepared by the co-precipitation route. This is possibly due to a proportion of the precious metals being locked inside the tin oxide particles and hence unavailable for reaction. All subsequent experiments were conducted using catalysts prepared by the incipient wetness technique.

Mixtures containing 0, 1, 2 or 3% Pt and Pd were prepared as indicated in Table 1. Each of these powdered mixtures was tested for oxygen removal activity at room temperature over a period of about 40 min. The activity measurements, shown in figures 1, 2 and 3, suggest that the Pt/Pd samples fall into three categories. The first group contained the 2% Pd, 2% Pt, 1% Pt/1% Pd, and 1% Pt/2% Pd samples. Each of these activated to some extent, especially the 2% Pt sample, but then deactivated later in the test (figure 1). Despite this deactivation, the 2% Pt sample was more active at the end of the test than those in the second group.

This second group, containing the 3% Pt/1% Pd, 2% Pt/1% Pd and 1% Pt/3% Pd samples sustained activity at a reasonable level for the duration of the test (figure 2). The third group containing the 2% Pt/2% Pd, 2% Pt/3% Pd, 3% Pt/2% Pd and 3% Pt/3% Pd samples continued activating during the test period (figure 3).

The final level of activity of the Pt/Pd samples containing 2 or 3% Pt was similar in each case, except for the 2% Pt/2% Pd and was in excess of 90%. It was therefore difficult to further analyse these results, but for the samples with lower precious metal concentrations this was possible. The sample containing 2% Pt was more than twice as active as that containing 2% Pd. Also from the activity profiles for 1% Pt/Pd samples it can be seen that 3% Pd (ie. 1% Pt/3% Pd) gives activity similar to, but still less, than for the 2% Pt sample.

Catalytic activity was increased by adding more Pt or Pd, but was more critically dependent on the Pt content. Because the catalysts were operating in excess of 90% conversion in many cases the apparent effect of increasing precious metal loading was to sustain the high level of activity for a longer period of time. This has also been observed for powdered or coated monolith catalysts tested at 60°C, where activity is sustained for longer periods of time.

Effect of Calcination on Tin Oxide Structure

The X- ray diffraction profile for metastannic acid calcined at 350°C has very broad peaks indicating poor crystallinity, which was only marginally improved on calcining at 600°C. On calcining at 1000°C the peaks sharpen considerably. It was only possible to obtain a Raman spectrum with well defined peaks for the 1000°C calcined sample.

A sample of un-peptised tin oxide was then enclosed in a cell and heated at intervals of 100°C from room temperature to 500°C. The sample was heated for 30 min at each set temperature prior to the Raman spectrum being recorded. It can be seen from the spectra in figure 4 that the A_{1g} band moved from 635 cm^{-1} at 20°C to 626 cm^{-1} at 500°C, and that the B_{2g} band originally at 776 cm^{-1} moved similarly. The temperature dependence of the wavenumber shift is displayed in figure 5. The spectra observed are very similar in appearance to those recorded previously for single crystals (ref 2) and textured samples (ref 3), and the wavenumber shift mimics that observed for single crystals (ref 4).

On expanding the spectra in figure 4 it was noted that the E_g band at 477 cm^{-1} decreased in intensity with increasing temperature while the band at 502 cm^{-1} increased. Several other bands, notably those around 240 and 540 cm^{-1}, became more resolved as the temperature increased. This could be due to orientation effects of small crystallites occuring in the random powder sample. These changes have been observed for many samples and appear characteristic of the tin oxide.

An identical series of experiments was carried out for base peptised tin oxide, with very similar results to those for the un-peptised material.

The lattice parameters were calculated from X-ray spectra collected at each temperature. From these results the coefficient of expansion has been calculated to be a = 6.10 x 10^{-6} per °C and c = 6.28 x 10^{-6} per °C.

Tin Oxide Reduction

It has been observed that tin oxide/precious metal catalysts have enhanced activity if treated in a reducing atmosphere prior to use. In this series of experiments tin oxide was subjected to hydrogen/helium atmospheres over the temperature range 20 to 500°C. Using Raman and X-ray techniques it was hoped that any changes in the oxidation state of the tin would be observed.

The cell was well flushed with H_2/He prior to heating the sample in exactly the same fashion as for the calcinations. The spectrum recorded at 20°C had a much higher background than that in air, but the A_{1g} and B_{2g} bands were clearly visible (figure 6). As the temperature increased so did the background intensity. This may be due to changes either in the hydroxyl groups or the electronic nature of surface lattice sites. Local electronic changes can cause band fluorescence producing a rise in the background intensity. A study was made in the region about 3600 cm^{-1} for surface hydroxyl groups, but none were detected.

Since the Raman spectra revealed no reduced tin it was decided to repeat the experiments using X-ray diffraction instead. The representative sample of the resulting X-ray profiles displayed in figure 7 shows there was no phase transition or partial reduction from Sn^{4+} to Sn^{2+}, but there was a change in the lattice spacing of the tin oxide. After cooling the sample to 20°C in the H_2/He gas flow, spectra indicated that a small quantity of β-tin was present in the dominant SnO_2 phase. It is surprising that heterogeneous oxide phases were not observed when the sample was being heated to 500°C.

Geurts et al (ref 3) observed a partial phase change when heating SnO in air below 450°C with both SnO_2 and β-tin present. On continuing heating to 650°C the SnO and β-tin were completely transformed to SnO_2.

Peptised Tin Oxide in a CO Environment

Experiments were conducted in the high temperature Raman cell in order to determine the influence of carbon monoxide, present at 5% of an otherwise helium flow, on the reduction of the tin oxide. Just below 200°C a band developed at approximately 1600 cm^{-1}. On heating further towards 500°C the band intensified (figure 8), and persisted on cooling to 20°C.

This band can be attributed to the CO stretch in, for example, a carbonate formed on the surface of tin oxide. Such bands have also been observed for silica and alumina samples in similar environments and conditions (ref 5).

Precious Metal/Tin Oxide Catalysts

A precious metal coated tin oxide sample was calcined at 1000°C for 1h in air. On cooling to 20°C the Raman spectrum contained the A_{1g} and B_{2g} bands with a high background. This high background is a common feature of precious metal coated oxides, eg. alumina, and is due to the limited penetration of the laser system.

On heating the sample in a CO/He environment a small band appeared at about 1600 cm^{-1} at 100°C, a considerably lower temperature than for the tin oxide. As for the tin oxide sample, this band grew with increasing temperature up to 500°C. However, the species disappeared on cooling to 20°C, probably due to desorption or catalytic decomposition under the influence of the precious metal.

This influence of precious metals, or indeed transition metals, on the presence of adsorbed species on support oxide surfaces is commonly observed. An example is the formation of species such as NCO from CO and NO on the metal, followed by migration onto the support. The catalytic reaction forming NCO can occur directly on the oxide surface, but at a significantly higher temperature.

CONCLUSIONS

To achieve optimum catalyst performance the preparation of the metastannic acid and peptisation to form the tin sol must be carefully controlled. If the tin oxide is calcined at 350°C a stable, high surface area support is obtained. Greater crystallinity can be induced by heating to 1000°C, but this is accompanied by a decrease in surface area. The precious metals were then best added subsequently by the incipient wetness technique. It was noted that 2% Pt on tin oxide had an activity several times that for a 2% Pd catalyst, and that the higher Pt/Pd loaded catalysts had extended lifetimes.

Some temperature dependent structural changes were observed using Raman and X-ray techniques for tin oxide when heated in air or hydrogen environments, however no reduction of Sn^{4+} was observed. On cooling from 500°C to 20°C in H$_2$/He some β-tin was produced. Data collected in this environment suggested that the quantity of surface hydroxyl groups was very low.

Species formed on tin oxide in He/5% CO above 200°C gave rise to a band at about 1600 cm^{-1}. The band persisted on cooling to 20°C, and is assigned to the CO stretch, possibly in a carbonate. In the presence of precious metal the band appeared at about 100°C, but disappeared on cooling from 500 to 20°C. This was attributed to the catalytic effect of the precious metal.

REFERENCES

1. G C Bond, M J Fuller, L R Molloy; Proc. 6th Int. Congr. Cat. 1, 356 (1977).

2. R S Katigar, P Dawson, M I Hargreave, G R Wilkinson; Phys. C : Solid Phys., Vol 4 (1971).

3. J Geurts, S Rau, W Richter, and F J Schmitte; Thin Solid Films, 121, 217-225 (1984).

4. P S Peercy and B Morosi; Phys. Rev. B, Vol 7, No.6, (March 1973).

5. C Johnston; "Infrared Studies of Adsorption on Oxide Supported Iron Catalysts"; PhD Thesis.

Table 1. Precious metal tin oxide catalysts

Pd (w/o)	Pt loading 0 w/o	Pt loading 1 w/o	Pt loading 2 w/o	Pt loading 3 w/o
0			X	
1		X	X	X
2	X	X	X	X
3		X	X	X
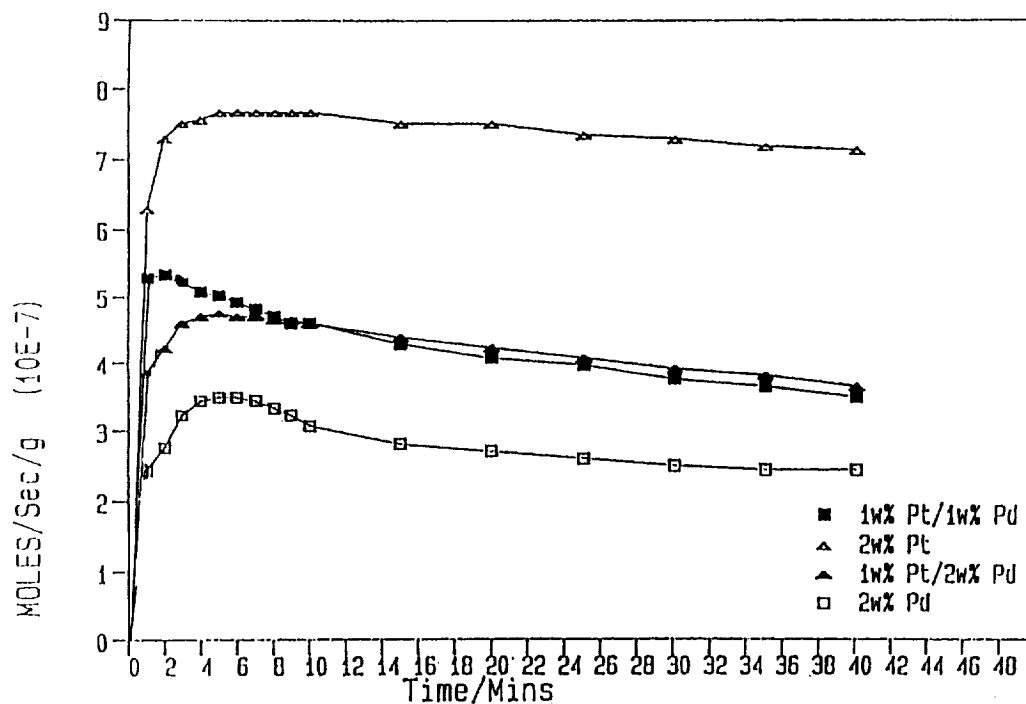
Figure 1. Activity tests of group 1 catalysts.
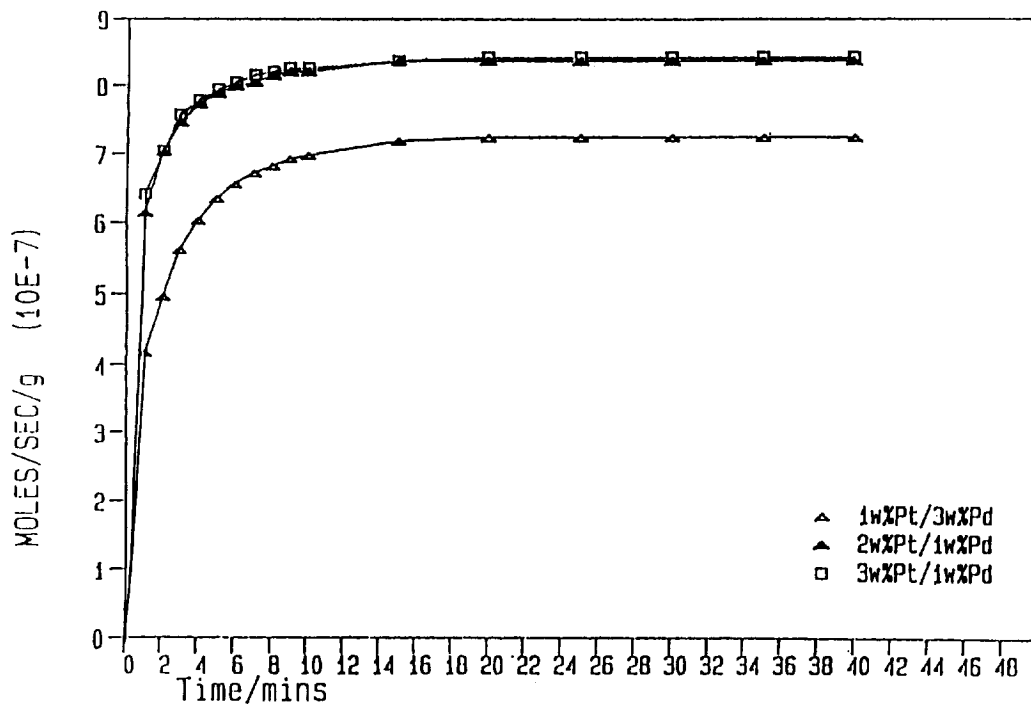
Figure 2. Activity tests of group 2 catalysts.
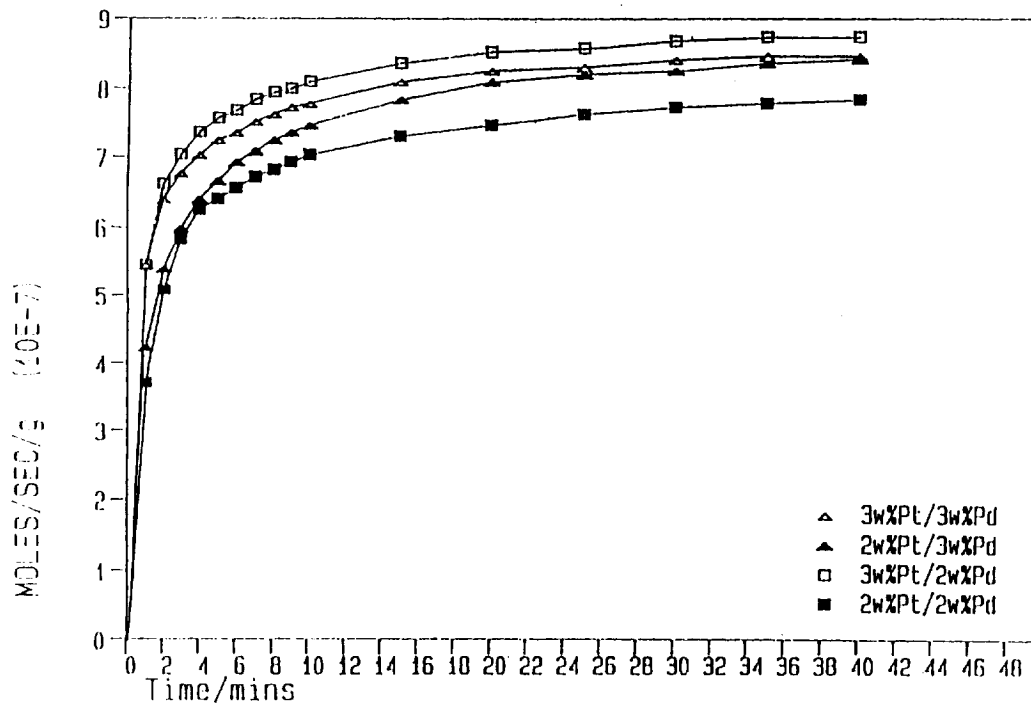
Figure 3. Activity tests of group 3 catalysts.
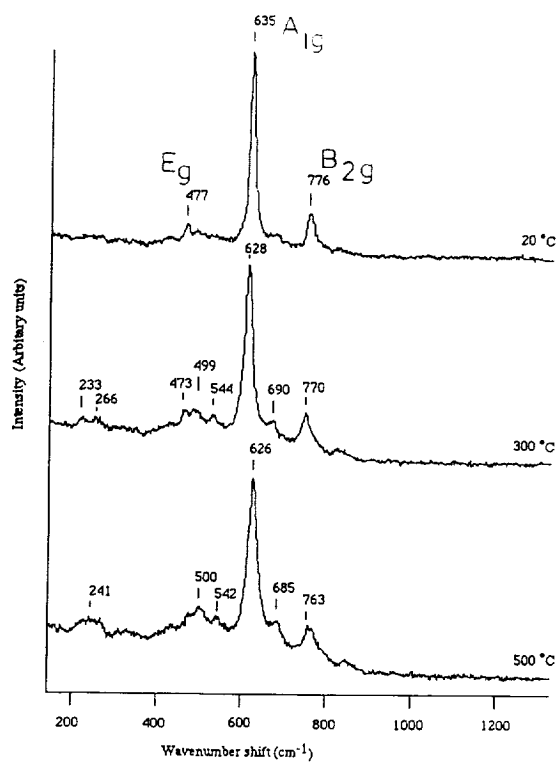
Figure 4. High-temperature Raman spectra of
SnO$_2$ in air.
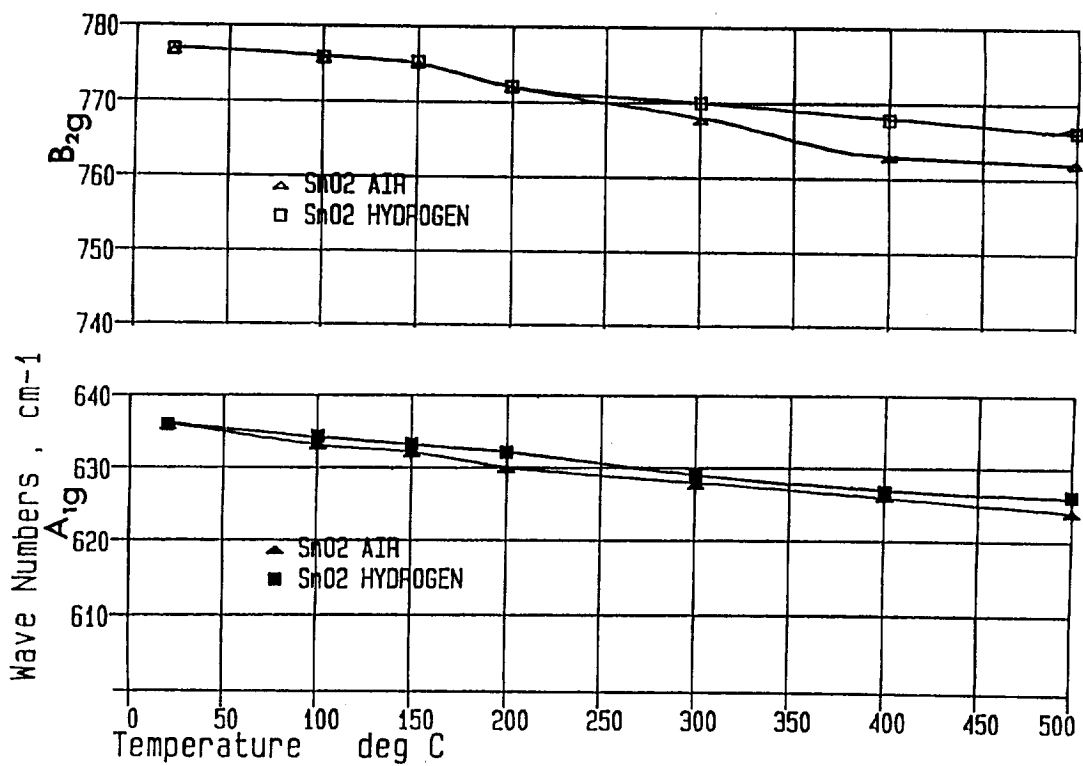
Figure 5. Temperature dependence of frequencies of
Raman-active modes in SnO$_2$.
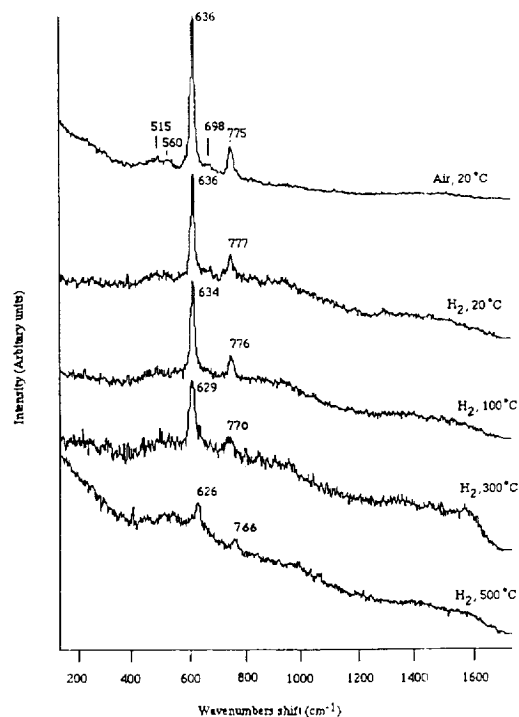
Figure 6. High-temperature Raman spectra of peptised
SnO$_2$ in hydrogen.
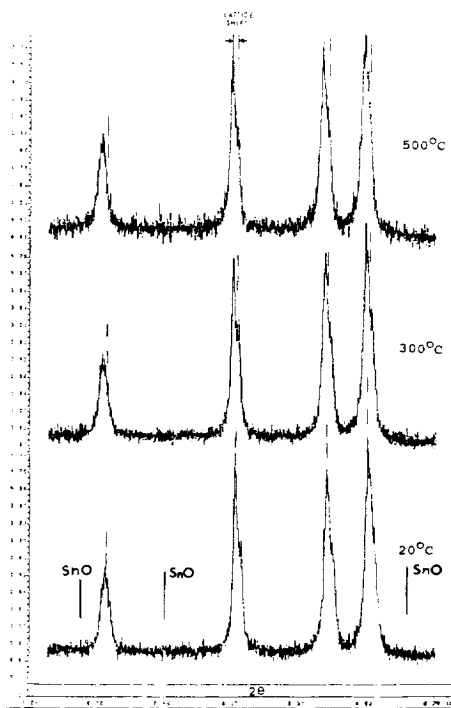
Figure 7. High-temperature X-ray diffraction pattern
for SnO$_2$ in hydrogen gas mix.
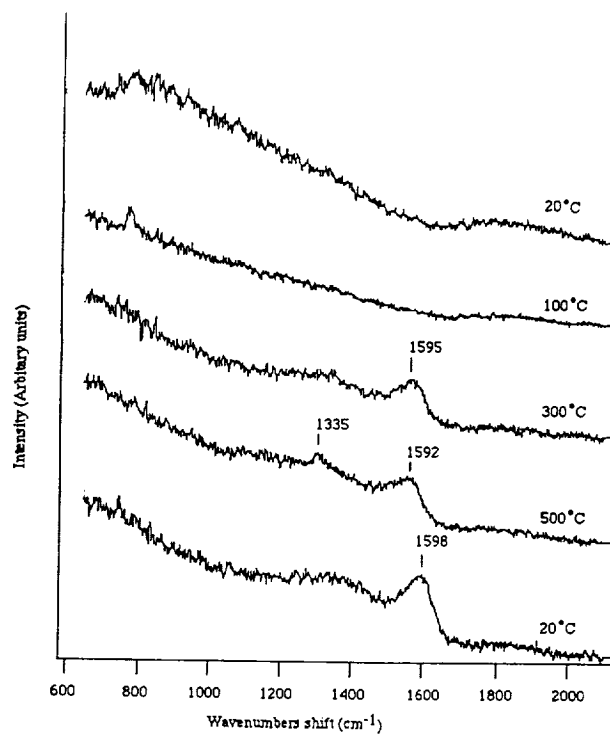
Figure 8. High-temperature Raman spectra
of SnO₂ in CO.

LaRC-DEVELOPED CATALYSTS FOR CO_2 LASERS

Billy T. Upchurch
NASA Langley Research Center
Hampton, Virginia 23665

Erik J. Kielin*
Old Dominion University
Norfolk, Virginia 23508

Irvin M. Miller
Science and Technology Corporation
Hampton, Virginia 23666

ABSTRACT

Pulsed CO_2 lasers have many remote sensing applications from space, airborne, and ground platforms. The NASA Laser Atmospheric Wind Sounder (LAWS) system will be designed to measure wind velocities from polar earth orbit for a period of up to three years. Accordingly, this and other applications require a closed-cycle pulsed CO_2 laser which necessitates the use of an efficient $CO-O_2$ recombination catalyst for these dissociation products which otherwise would degrade the laser operation. The required catalyst must not only operate at low temperatures but also must operate efficiently for long time periods.

The research effort at NASA LaRC has centered around development and testing of CO oxidation catalysts for closed-cycle, pulsed, common and rare-isotope CO_2 lasers. We have examined available commercial catalysts both in a laser and under simulated closed-cycle laser conditions with our efforts aimed toward a thorough understanding of the fundamental catalytic reaction and utilized these data to design and synthesize new catalyst compositions to better meet the catalyst requirements for closed-cycle pulsed CO_2 lasers. In this paper we report syntheses and test results for catalysts developed at Langley Research Center which have significantly better long-term decay characteristics than previously available catalysts and at the same time operate quite well under lower temperature conditions.

*Formerly David R. Brown

INTRODUCTION

This report will outline the progress made at NASA Langley Research Center on the production, characterization, and testing of catalysts for the recombination of CO and O_2, the dissociation products of pulsed-discharge CO_2 lasers. The objective is to develop a catalyst with adequate activity and stability which would enable closed-cycle laser operation for periods of up to three years as required by the Laser Atmospheric Wind Sounder (LAWS) system.

Catalyst Requirements

Adequate activity implies that the catalyst have a high enough conversion efficiency to recombine CO and O_2 at a rate equal to or greater than its dissociation rate. For a pulsed-discharge CO_2 laser operating at 10 joules per pulse, dissociation rates have been estimated to be 10^{18} molecules per pulse. At 10 pulses per second (pps) the catalyst must have a recombination rate of 10^{19} molecules per second. Additionally, candidate catalysts must retain high conversion efficiency over a temperature range from ambient to 100°C and in low partial pressures of CO and O_2 without interference from other laser gas components--CO_2 in particular.

Adequate stability implies that the catalyst retain its recombination efficiency during the lifetime of operation as well as retain its structural integrity (i.e. must not crumble or dust). The LAWS system requires a lifetime of 10^9 pulses. At 10 pps, this period is about 10^8 seconds or three years. Consequently, the catalyst must show minimal decay in order to minimize the weight of catalyst required to provide the necessary recombination over the entire period of operation. To preserve the catalyst's structural integrity, it is necessary to develop a method of incorporating thin coatings of catalyst materials onto inert supports such as monoliths.

Because the laser signal is generated by CO_2, a gas present in the atmosphere, transmission of the laser signal can be diminished. In order to improve atmospheric transmission, the

LAWS system will use rare isotope CO_2 ($C^{18}O_2$). As a result, a candidate catalyst must operate with $C^{18}O_2$ without isotopic scrambling.

Catalysts Investigated

It has been shown that a combination of Pt and SnO_2 synthesized under the appropriate conditions is more active toward CO oxidation than either component alone.[1] It has also been shown that increased Pt loading increases catalyst activity for unsupported Pt/SnO_2. Addition of Pd further increases activity (Figure 1). The $CO-O_2$ recombination catalysts reported here are those available commercially and those produced at Langley Research Center (LaRC). These catalysts are mainly Pt/SnO_2 or $(Pt+Pd)/SnO_2$, either supported or unsupported, with various promoters and dopants.

In the continued improvement of the catalyst, studies to optimize the Pt/SnO_2 and Pt/Pd ratios for those yielding the highest activity are presented. A unique method of preparation whereby the Pt loading can be varied from 1% to 46% by weight of the Pt/SnO_2 is used. In addition to the optimization studies, an investigation of the effect of various dopants and promoters on the activity of Pt/SnO_2 is also presented.

In making the catalyst mechanically stable, as required by the LAWS system, methods of depositing the catalyst on inert supports such as silica spheres, silica gel, and monoliths are being developed. Although the support material is generally inert, support constituents such as water can affect the activity of Pt/SnO_2. As a result, the effect of water on catalyst activity will be discussed.

PROCEDURES

Catalyst Preparation

Preparation of the LaRC catalysts has been explained in detail earlier.[2] Briefly, tin is oxidized to metastannic acid via slow, nitric acid oxidation of 30-mesh tin granules.

$$Sn + 2HNO_3 \longrightarrow H_2SnO_3 + NO + NO_2$$
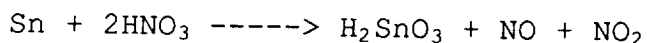
To ensure removal of excess nitric acid and water, the slurry is heated to dryness using a hotplate temperature of about 150°C. This heating converts metastannic acid to tin(II)oxide via dehydration.

$$H_2SnO_3 + heat \longrightarrow H_2O + SnO_2$$
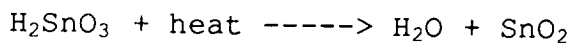
For coating silica spheres or high surface-area silica gel with metastannic acid, tin is oxidized in the presence of the deaerated support.

Before deposition of platinum or palladium, the supported or unsupported substrate is deaerated in the presence of a solution of either tetraaminoplatinum(II)hydroxide or tetraaminopalladium-(II)nitrate. Platinum and palladium are then deposited via formic acid reduction.

$$Pt(NH_3)_4(OH)_2 + H \cdot CO_2H + heat \longrightarrow Pt + 4NH_3 + CO_2 + 2H_2O$$
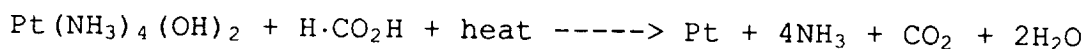
Again the slurry is heated to dryness to remove excess water, formic acid, and the volatile byproducts. The preparation is completed by drying the catalyst in a convection oven in air at 150°C.

The above preparation has the unique characteristic of using volatile, chlorine-free reagents. The advantages of this are that the catalyst-poisoning chlorides are eliminated and that the excess reagents as well as their byproducts are volatile.

Catalyst Characterization

Catalysts are tested for their general activity, surface area, and water content. The general activity of catalyst samples is determined in plug flow reactors. Selected samples are tested in a system incorporating a pulsed-discharge CO_2 laser. For samples used in kinetic studies, a recycle reactor is used. All systems have been described in previous papers.[3,4]

Activity screening. Each catalyst sample was screened in a plug flow reactor for its ability to recombine a stoichiometric test-gas mixture containing 1% CO and 0.5% O_2 in He with a 2% Ne internal standard. Gas mixtures were analyzed with an inline Shimadzu GC using a concentric column; the external column contains Activated Molecular Sieve for separating CO, Ne, O_2 and N_2, and the internal column contains a Porapak mixture for separating CO_2 from the other components. The peak areas of CO_2, Ne, O_2, N_2, and CO are determined via electronic integration using a Shimadzu CR3-A integrator. These areas are converted to concentrations by comparison to the 2% Ne internal standard.

Unless otherwise noted, a 150-mg sample of catalyst was used for screening. Each sample was reductively pretreated in situ at 125°C using a gas containing 5% CO in He with a 2% Ne internal standard flowing at 10 sccm. During pretreatment CO is oxidized to CO_2. When the CO_2 concentration was below 0.02% of the total analyzed sample, the catalyst sample was considered pretreated; this generally required 1 to 3 hours.

A general screening proceeds as follows. At preset times (ten consecutive then every four hours) 1-mL samples of test gas were analyzed for CO_2, O_2, and CO concentration. Next, the percent yield of CO_2, and the percent losses of O_2 and CO were calculated.

Surface area determination. The surface area of a catalyst sample is determined via the method of Brunauer, Emmett, and Teller (BET) using a Quantachrome Quantasorb instrument. The amount of sample used in determining the surface area ranges from 30 mg to 150 mg depending on the assumed surface area of the sample being tested.

Ignitions. A known weight of catalyst, about 100-mg, is heated in a porcelain crucible at 1000°C to constant weight. The first heating runs 60 minutes followed by at least two 30-minute heatings. The weight loss is assumed to be equal to the amount of water present in the catalyst.

RESULTS AND DISCUSSION

Because the purpose of this research is to improve upon the catalytic activity of previously produced catalysts, the discussion will focus on the relative changes in catalytic activity due to the addition of (1) other noble metals, (2) water, and (3) dopants.

Comparative Catalyst Study

Some of the earliest produced LaRC, $CO-O_2$ recombination catalysts were compared with those commercially available. The Pt loading of the LaRC-prepared catalysts is shown below.

	LaRC 1 and 1A	LaRC 2	LaRC 3	LaRC 6
Wt % Pt in Pt/SnO_2	46.0	1.03	3.01	5.84
Wt % Pt in $Pt/SnO_2/SiO_2$	15.5	0.206	0.622	1.237
% Area coverage by Pt	33.3	0.367	1.121	2.23

Figure 2 shows the activity--under stoichiometric test gas flow-- of the above catalysts as well as those prepared by Engelhard (Eng), General Motors (GM), and Teledyne (TD). Activity is defined as sccm of CO_2 produced per minute per gram of catalyst. The GM and TD catalysts have the lowest activity. At elevated temperatures and in air, where excess oxygen is available, however, these have higher activities. These catalysts then are unsuited for a closed-cycle laser application.

The Engelhard catalyst (2% Pt/SnO_2) shows similar activity to LaRC 2 yet the latter uses a lower Pt loading making it more economical. LaRC 1 and 1A show higher activity than the others tested, but the excessive weight of Pt used makes it less cost effective. It may be necessary, however, to use such high loadings to achieve the activity per unit weight of catalyst required by the LAWS system.

Catalyst Optimization Study

Optimization of Pt/SnO₂. In order to determine the best Pt/SnO₂ ratio, compositions of Pt/SnO₂ supported on SiO₂ spheres and varying from 1% to 46% Pt by weight were prepared by the method discussed earlier. Their Pt loading on a weight percentage basis is shown in Table I; surface areas are indicated where available.

The catalysts were tested for activity in a plug-flow reactor under stoichiometric test gas conditions. The results of the tests are shown in Figure 3 as sccm of CO_2 produced per minute per gram of catalyst. The bimodal distribution indicates that peaks in activity exist for catalysts containing approximately 17% or 39% Pt by weight, the higher of these two peaks being for the 17% Pt/SnO₂. These results indicate that a Pt loading around 17% by weight provides the best activity under these conditions.

Figure 4 show the slope (% CO_2 yield/time) for the Engelhard and LaRC catalysts containing 24%, 32%, 39%, and 46% Pt by weight. Smaller negative slopes indicates better decay characteristics zero slope indicating no decay. Accordingly, sample 32-B, 39-B, and 46-B show less than half the decay rate of the Engelhard, and sample 24-B shows about 1/10th the decay rate of the Engelhard. Because the lower loadings (3%, 11%, and 17%) had nonlinear slopes between 5,000 and 10,000 minutes, they were not considered here.

Optimization of Pt/Pd. In order to determine the optimum Pt/Pd ratio, silica gel supported (Pt+Pd)/SnO₂ samples with Pd loadings from 1% to 19.5% by weight were prepared and tested in a plug flow reactor. To minimize differences due to sample preparation, samples were prepared from the same lot of silica gel-supported Pt/SnO₂ . The Pd was added in a separate step. As a result, the atom ratio of Pt/SnO₂ is constant for all samples at 19.5%, and only the Pt/Pd ratio varies. Note that one sample contains no Pd.

Figure 5 shows the percent yield of CO_2 as a function of time for the aforementioned samples. The general shape of the curves is nearly the same indicating that the decay rate is approximately equal for each catalyst. The activities vary only slightly, but

significantly nonetheless. The lower loadings of Pd (1% and 2% by weight) decreased catalyst activity relative to the activity of the standard catalyst, Pt/SnO_2, whereas higher loadings (10% and 19.5% by weight) had little effect. A significant increase in activity, however, was observed for a Pd loading of 5% by weight; this is equal to 1/2 the amount of Pt on an atomic basis.

Figure 6 shows the sccm of CO_2 per gram of catalyst formed at 20000 minutes for various Pd compositions. Again, the graph shows an approximate 30% decrease in activity for the lower loadings of Pd, while showing little change in activity for the higher loadings. Notably, the 5% loading of Pd showed about 33% greater activity than the standard suggesting that approximately 5% Pd is the best loading for $(Pt+Pd)/SnO_2$ catalyst with high Pt loading.

Catalyst-Support Interaction

The effect of water on the recombination efficiency of Pt/SnO_2 catalysts has been extensively investigated at NASA Langley Research Center.[5,6] Thermogravimetric analysis (TGA) of the Engelhard sample shows a weight loss of 3.73% when heated to 850°C. It is likely that the weight loss is due mostly to water. It has been shown that the initial dip in activity of the 2% Pt/SnO_2 (Engelhard) catalyst is alleviated if small amounts of water vapor are added to the pretreatment gas (Figure 7).

Silica gel support. Because of the importance of water to the activity of Pt/SnO_2 catalysts, high surface area silica gel was used to support some of the LaRC formulations. Silica gel, aside from its inert support properties, is a desiccant. The vapor pressure of water over silica gel is dependent on both the temperature and the concentration of water in the silica gel (Table II). Consequently, the amount of water reaching the catalyst can be controlled. The desiccant effect of silica gel might also be of practical utility in the laser where it could control the water vapor level so as not to reduce laser power.

The first silica gel-supported Pt/SnO_2 catalyst contained 7% Pt, 42% SnO_2, and 51% SiO_2. Figure 8 shows the percent yield of CO_2 for this catalyst for 35,000 minutes. At 85°C the catalyst

gave 100% yield indicating a potentially higher activity. The temperature was lowered in order to observe a measurable activity. After stabilization at 50°C, the percent yield remained around 90%.

A long-term test of this catalyst--106 days--near ambient temperature is shown in Figure 9. The graph shows that the catalyst's activity is susceptible to temperature fluctuations. Notably, the catalyst efficiency ranged from 90% to 65% loss of CO over the 106 days. This results in an extrapolated half-life of 228 days (Figure 10).

Effect of water on silica gel-supported Pt/SnO$_2$. To determine how this catalyst's activity varies under different concentrations of water, a known weight of deionized water was added to a known weight of catalyst. The quantity of water was incremented from sample to sample until saturation was reached. Two samples were prepared by dehydrating the catalyst in air in a convection oven either with or without a desiccant of magnesium perchlorate. The same amount of catalyst on a dry basis was tested. Two samples were tested simultaneously against the standard catalyst, no water added or removed. Figure 11 shows the reproducibility of activity for the standard catalyst.

Figure 12 shows the percent yield of CO$_2$ as a function of water content at 12,000 minutes of exposure to test gas. Neither the decay rate nor the catalyst activity was significantly affected by dehydrating or hydrating the catalyst. The activity remains relatively constant over the range of water compositions until saturation is reached at which point a 35% decrease in activity was observed. This result demonstrates that using silica gel as a support minimizes changes in activity due to water which could be advantageous for closed-cycle CO$_2$ lasers where an excess of water can significantly reduce the laser's power.

Monolithic supports. Supporting the catalyst formulations on a rugged, high surface-area, monolithic structure is currently under investigation at LaRC. One candidate monolith being investigated is a Cordierite monolith made by Dow Corning (Figure 13). It measures 3 inches in diameter and 0.5 inches thick, has

400 cells per square inch, and has a BET surface area of less than 1 m^2/g. A method of increasing the surface area to over 200 m^2/g and leaving a silica gel-like framework has been developed. The method involves leaching the monolith in dilute nitric acid to remove the Mg and Al. Sufficient structural integrity is retained during the process.

Effect of Promoters on Catalyst Activity

Chromium as a promoter. Figure 14 shows the percent yield of CO_2 over a 14,000 minute period for a Pt/SnO$_2$ catalyst both with and without Cr. The added Cr did not affect the decay characteristics and decreased the activity slightly.

Acidic oxide promoters. It is generally known that acidic oxides have little affinity for CO_2, the degree of affinity being inversely related to the oxide's acidity. In order to increase the rate of release of CO_2 and minimize CO_2 retention on the catalyst, a series of samples of Pt/SnO$_2$ with acidic oxide promoters were made and tested for catalytic activity. Oxides of antimony, arsenic, and phosphorus were chosen. Figure 15 shows the percent yield of CO_2 for 15,000 to 20,000 minutes. Relative to the catalyst containing no promoters three observations can be made: (1) the antimony oxide severely reduced the conversion efficiency; (2) the phosphorus oxide reduced the conversion efficiency by about 17% but did not affect the decay rate; and (3) the arsenic oxides increased the decay rate of the catalyst. For the amounts used, these oxides are not promising promoters.

Another oxide promoter whose identity is presently proprietary has been shown to enhance catalyst activity in quantities as low as 1% by weight, but decrease activity in higher amounts, 5% by weight (Figure 16).

SUMMARY

During the course of research at LaRC, catalysts exhibiting higher activity and lower decay rates than catalysts made previously have been prepared. An inherently clean method of preparing catalysts has been developed. Some noble-metal reducible oxide catalysts--Pt/SnO_2 in particular--have a demonstrated high activity at ambient temperatures. Traces of water appear to be necessary. Optimum loadings for Pt and Pd for Pt/SnO_2 and $(Pt+Pd)/SnO_2$ catalysts have been determined.

A method of supporting some of the LaRC catalyst formulations on silica spheres and high surface area silica gel has been developed. Investigation of monolithic structures for catalyst support is underway. A method of increasing the surface area of Cordierite monoliths from less than 1 m^2/g to greater than 200 m^2/g and leaving a silica gel-like structure has been developed.

Future efforts will focus on (1) adapting the catalyst for use with rugged high-porosity monolithic supports; (2) further reducing the long-term decay in the catalyst; (3) testing and modeling long-term behavior for reliable performance prediction for missions of interest; and (4) investigating alternative catalysts for higher conversion efficiency.

REFERENCES

1. Brown, Kenneth G.; Sidney, Barry D.; Schryer, David R.; Upchurch, Billy T.; Miller, Irvin M.; Wood, George M.; Hess, Robert V.; Batten, Carmen E.; Burney, Garland L.; Paulin, Patricia A.; Hoyt, Ronald F.; Schryer, Jacqueline: Catalytic Recombination of Dissociation Products with Pt/SnO_2 for Rare and Common Isotope Long-Life, Closed-Cycle CO_2 Lasers. SPIE Proc., vol. 663, 1986.

2. Upchurch, Billy T.; Miller, Irvin M.; Brown, David R.; Davis, Patricia P.; Schryer, David R.; Brown, Kenneth G.; Van Norman, John D.: Catalyst for Carbon Monoxide Oxidation, U.S. Patent No. 4,912,082.

3. Batten, Carmen E.; Miller, Irvin M.; Paulin, Patti A.; Schryer, Jacqueline: Studies of CO Oxidation on Pt/SnO_2 Catalyst in a Surrogate CO_2 Laser Facility, NASA CP-2456, pp. 199-210.

4. Schryer, David R.; Sidney, Barry D.; Miller, Irvin M.; Hess, Robert V.; Wood, George M.; Batten, Carmen E.; Burney, Lewis G.; Hoyt, Ronald F.; Paulin, Patricia A.; Brown, Kenneth G.; Schryer, Jacqueline; Upchurch, Billy T.: NASA-LaRC Research on Catalysts for Long-Life Closed-Cycle CO_2 Lasers, NASA CP-2456, 1987.

5. Schryer, David R.; Upchurch, Billy T.; Van Norman, John D; Brown, Kenneth G.; Schryer, Jacqueline: The Effects of Pretreatment Conditions on a Pt/SnO_2 Catalyst for the Oxidation of CO in CO_2 Lasers. J. Catalysis, **122**, 193-7, 1990.

6. Upchurch, Billy T.; Schryer, David R.; Wood, George M.; Hess, Robert V.: Development of CO Oxidation Catalysts for the Laser Atmospheric Wind Sounder (LAWS), SPIE Proc., vol. 1062, 287-293, 1989.

80

Table I. LaRC Catalysts on 10 Micron Sphere Support

Catalyst Sample	Pt as percent of:		BET Area m²/gram
	Total Mass	Coating Only	
1 B	0.21	1.01	
3 B	0.63	3.03	
6 B	1.24	5.90	
11 B	2.45	11.0	143
17 B	4.02	17.1	157
24 B	5.92	23.7	134
32 B	8.73	32.1	131
39 B	11.4	38.9	
46 B	14.7	46.0	

Table II. Vapor Pressures of Silica Gel at 40°C

% Water	Vapor Pressure, mm Hg
0.75	0.0076
1.0	0.013
1.2	0.050
3.0	0.175
6.0	0.505
12.0	1.500
20.0	2.500

Source: W. R. Grace Co.; Davidson Silica Gel
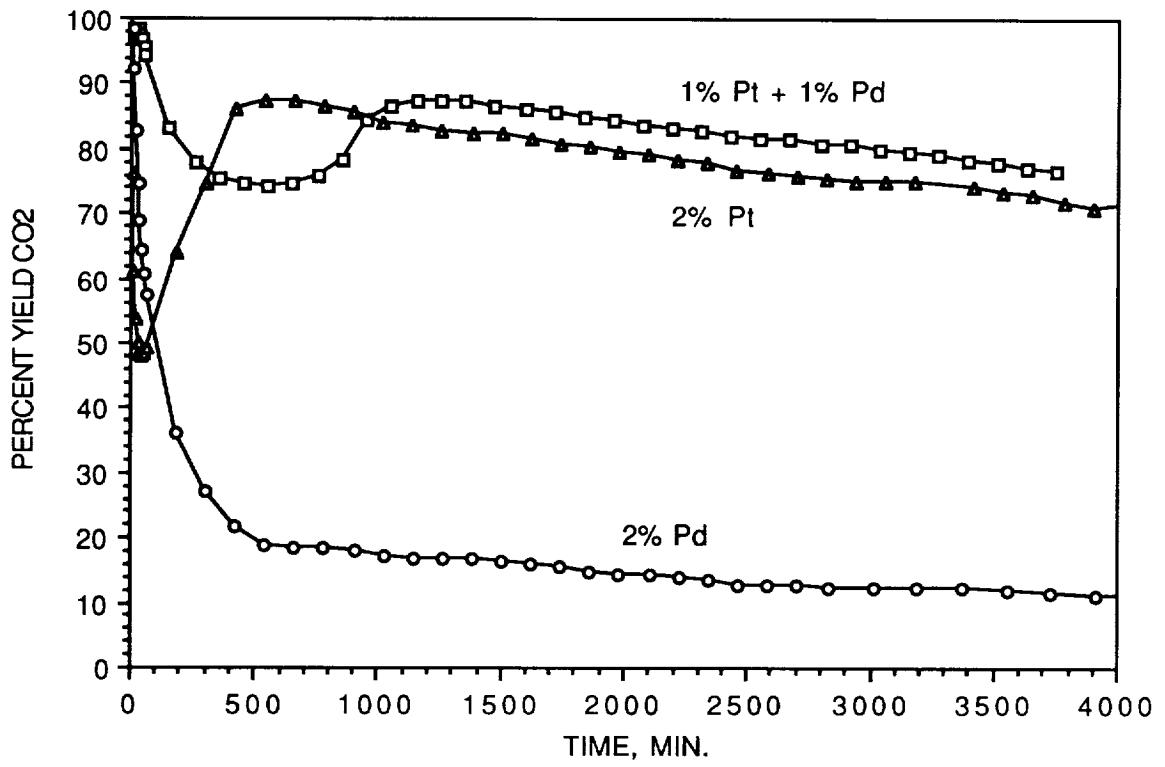
Figure 1. Comparison of Pt/SnO2, Pd/SnO2, and (Pt+Pd)/SnO2 catalysts
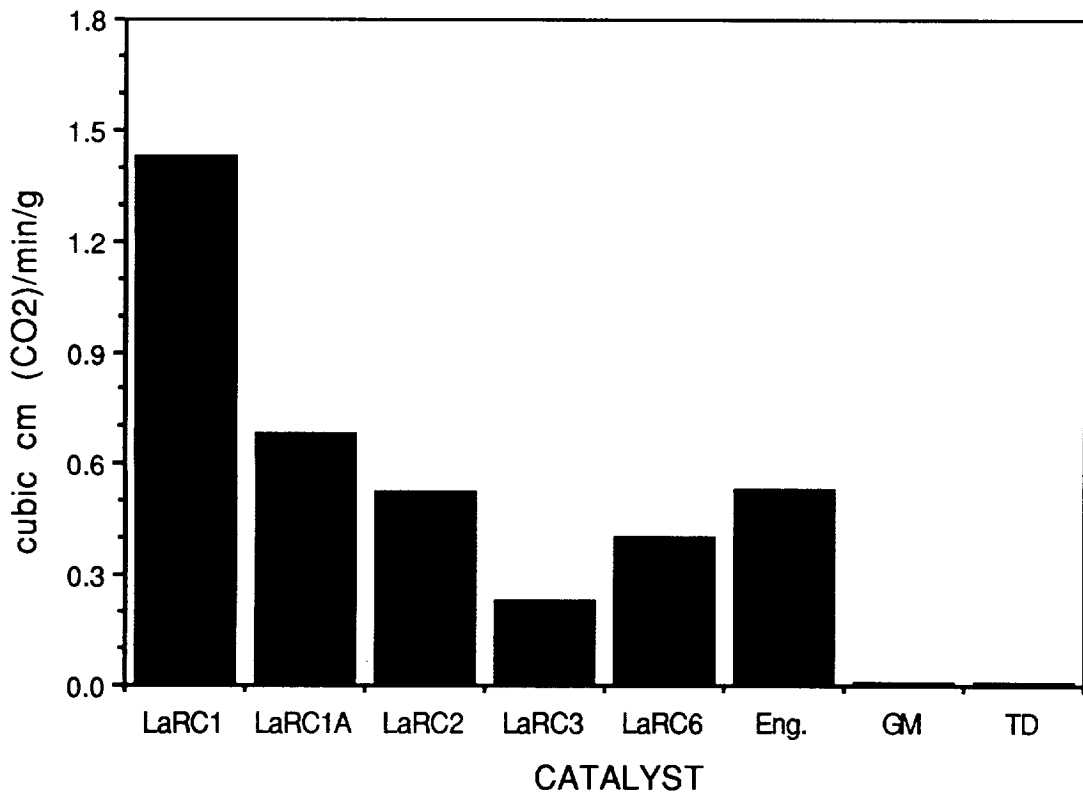
Figure 2. Comparison of commercial and LaRC catalysts
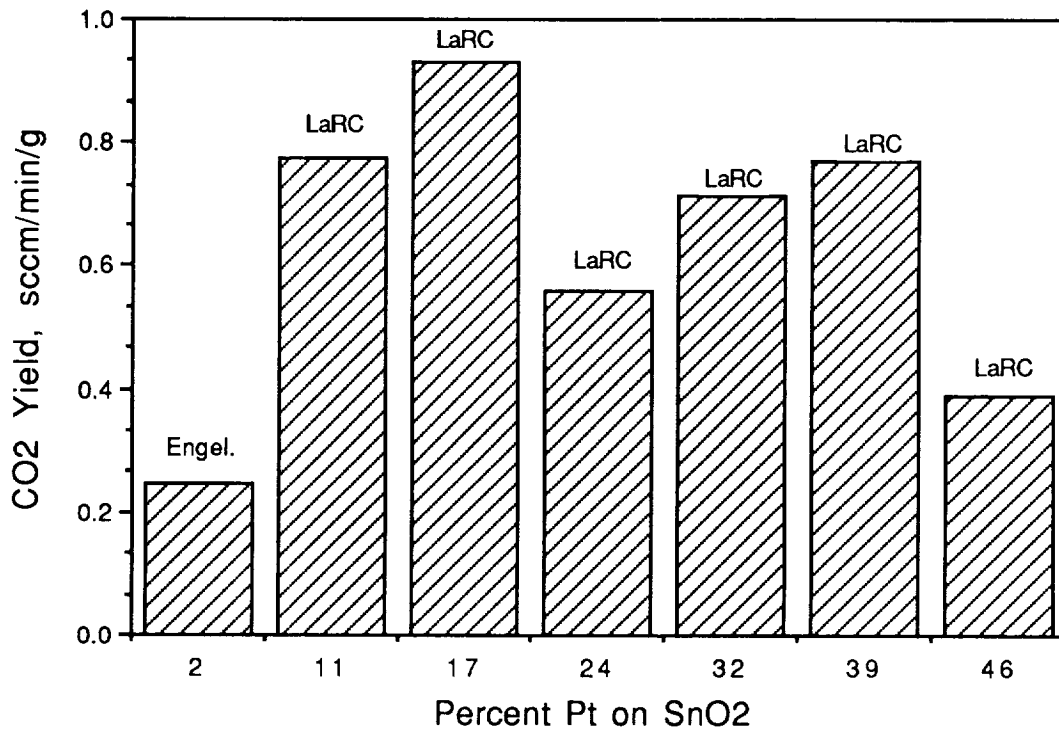
Figure 3. Effect of Pt loading on the activity
of Pt/SnO2 catalysts
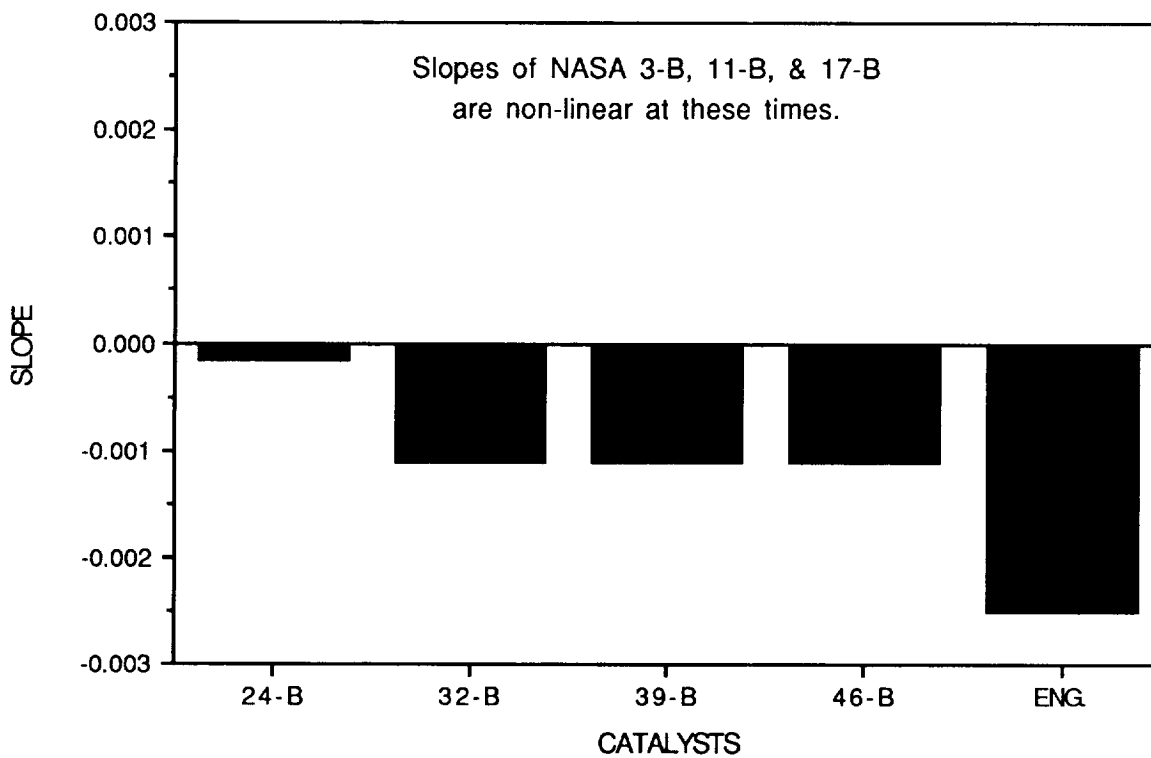
Figure 4. Slope of the activity curve between 5,000
and 10,000 minutes for some Pt/SnO2 catalysts
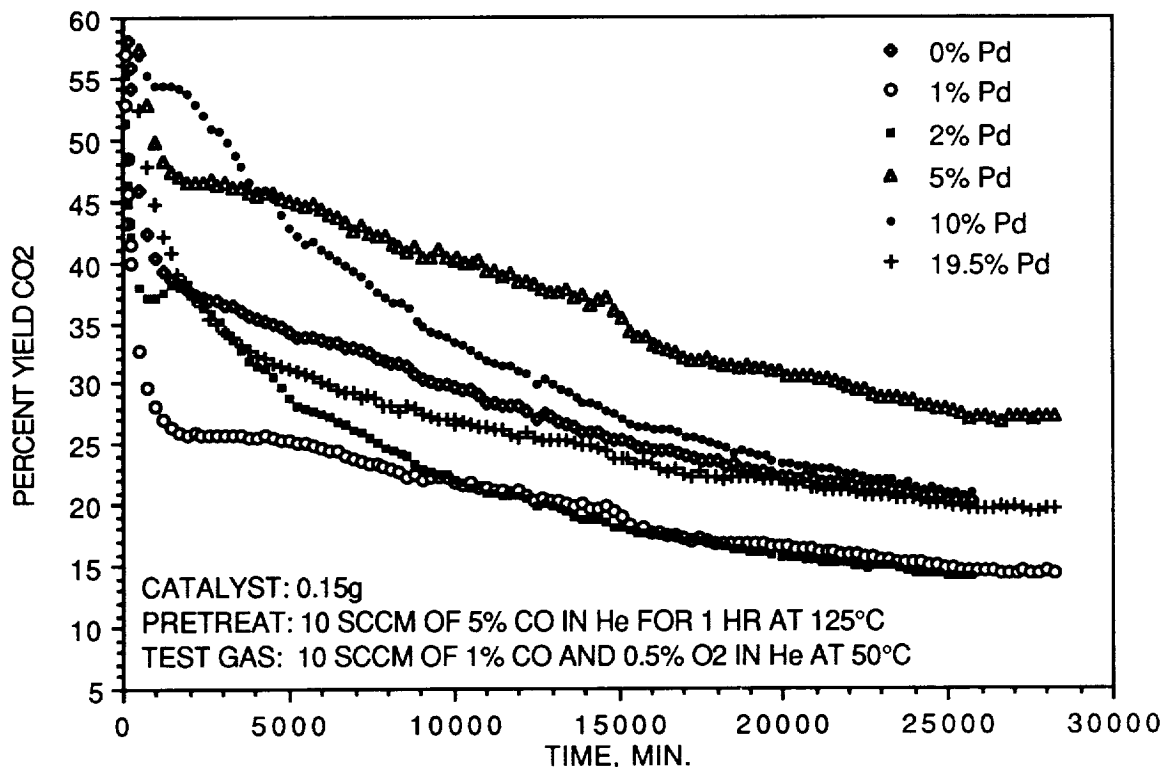
Figure 5. Effect of Pd loading on the activity of silica gel-supported (Pt+Pd)/SnO2 catalysts
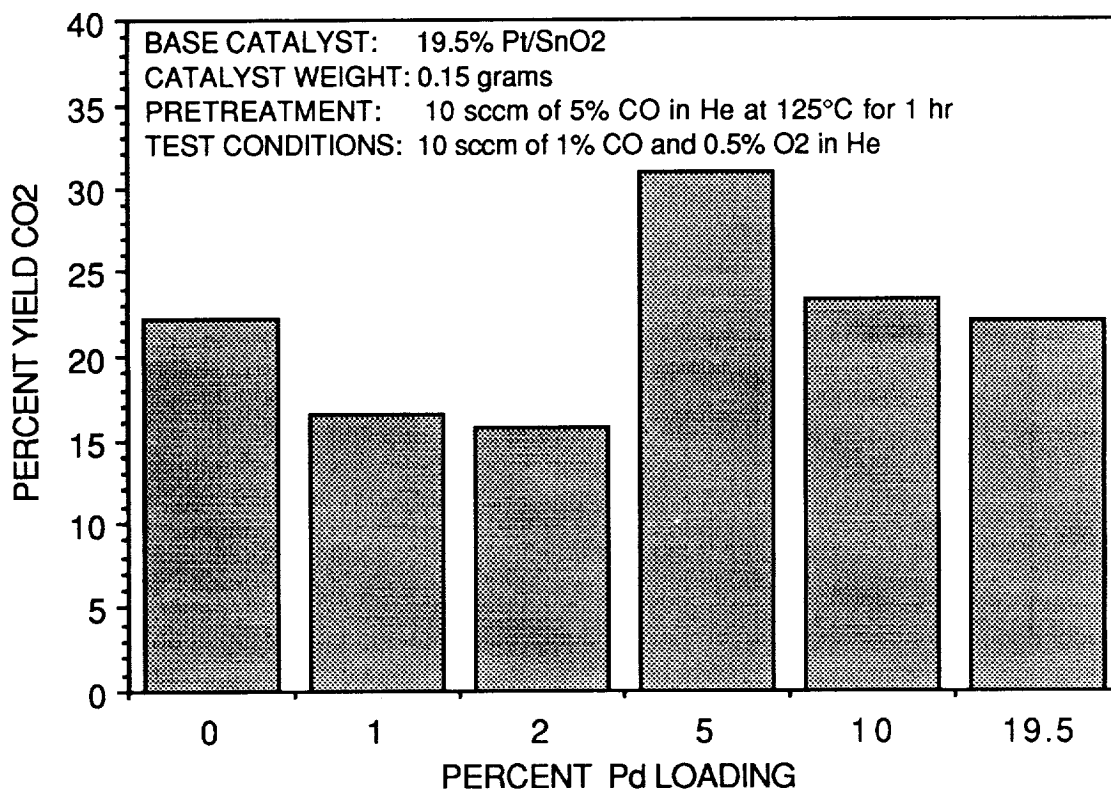
Figure 6. Activity at 20,000 minutes of some (Pt+Pd)/SnO2 catalysts

84

C-2
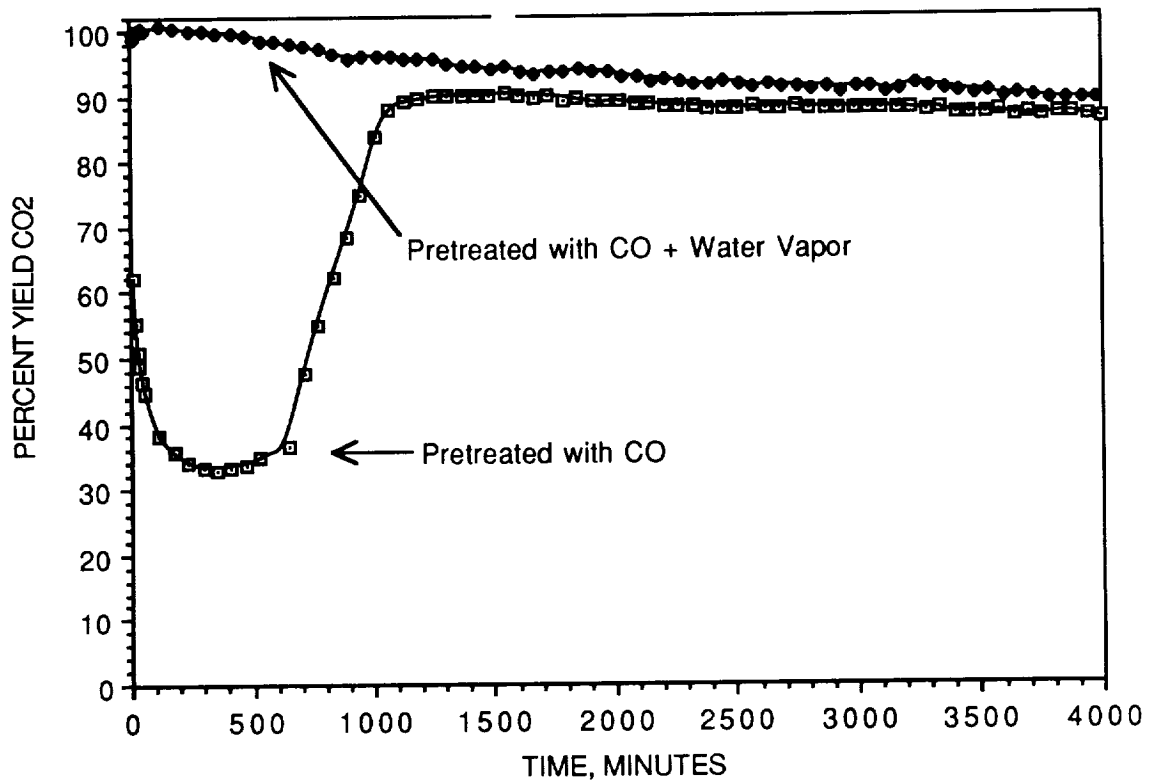
Figure 7. Effect of water vapor during pretreatment
on the activity of 2% Pt/SnO2
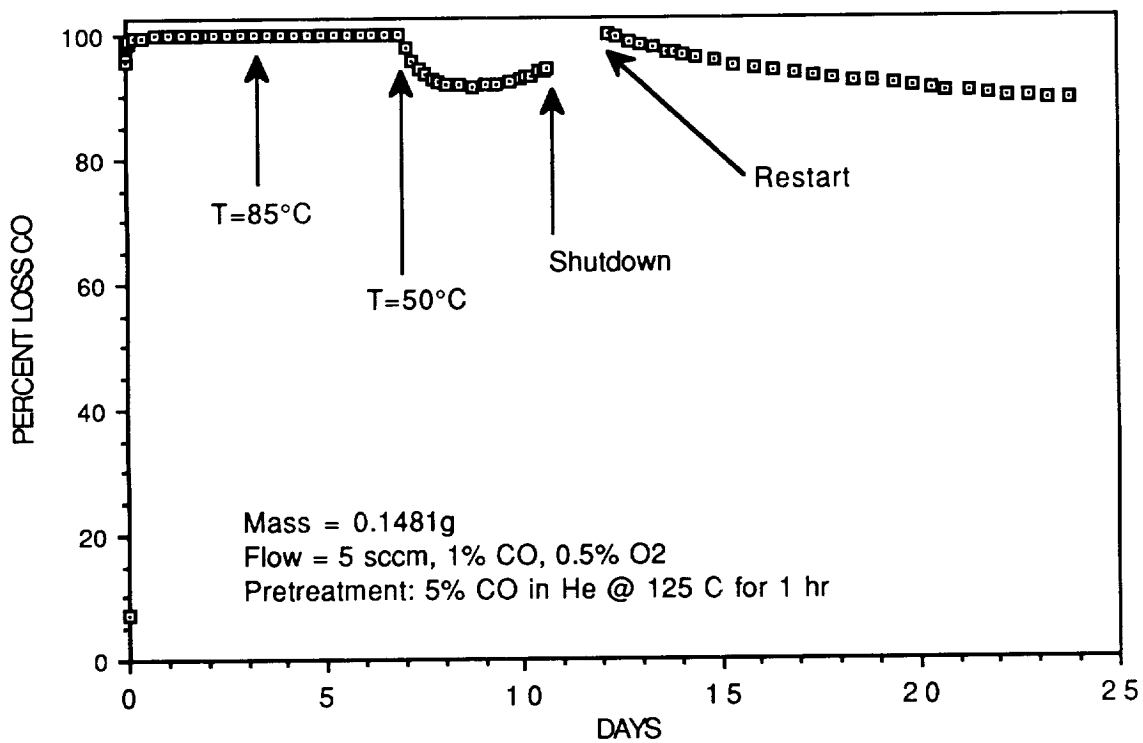
Figure 8. Activity of LaRC 1C, a silica gel-supported
Pt/SnO2 catalyst
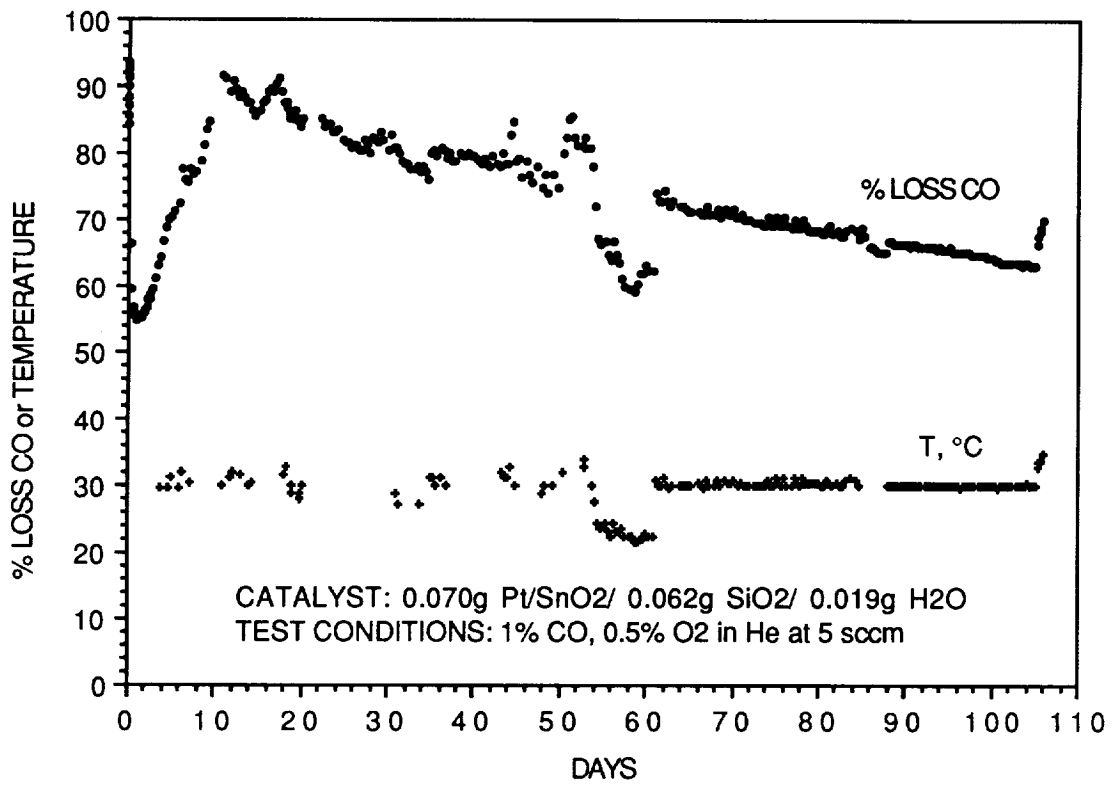
Figure 9. Long-term activity of LaRC 1C at near
ambient temperature
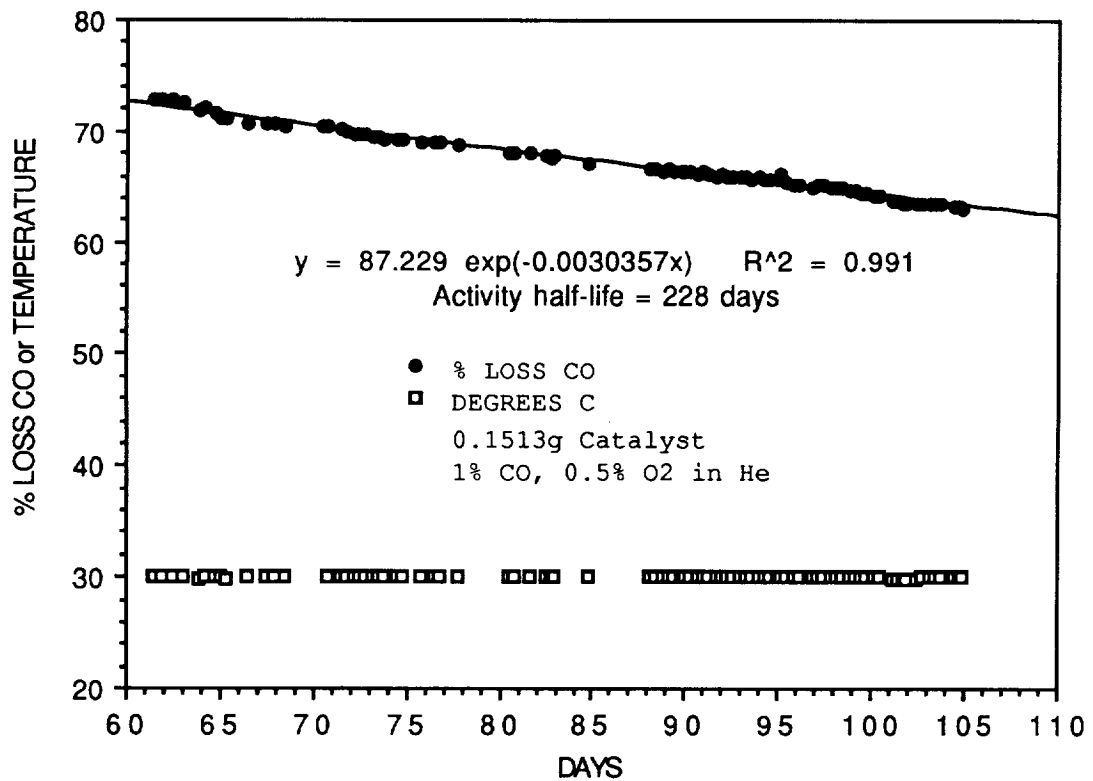
Figure 10. Extrapolated halflife of LaRC 1C
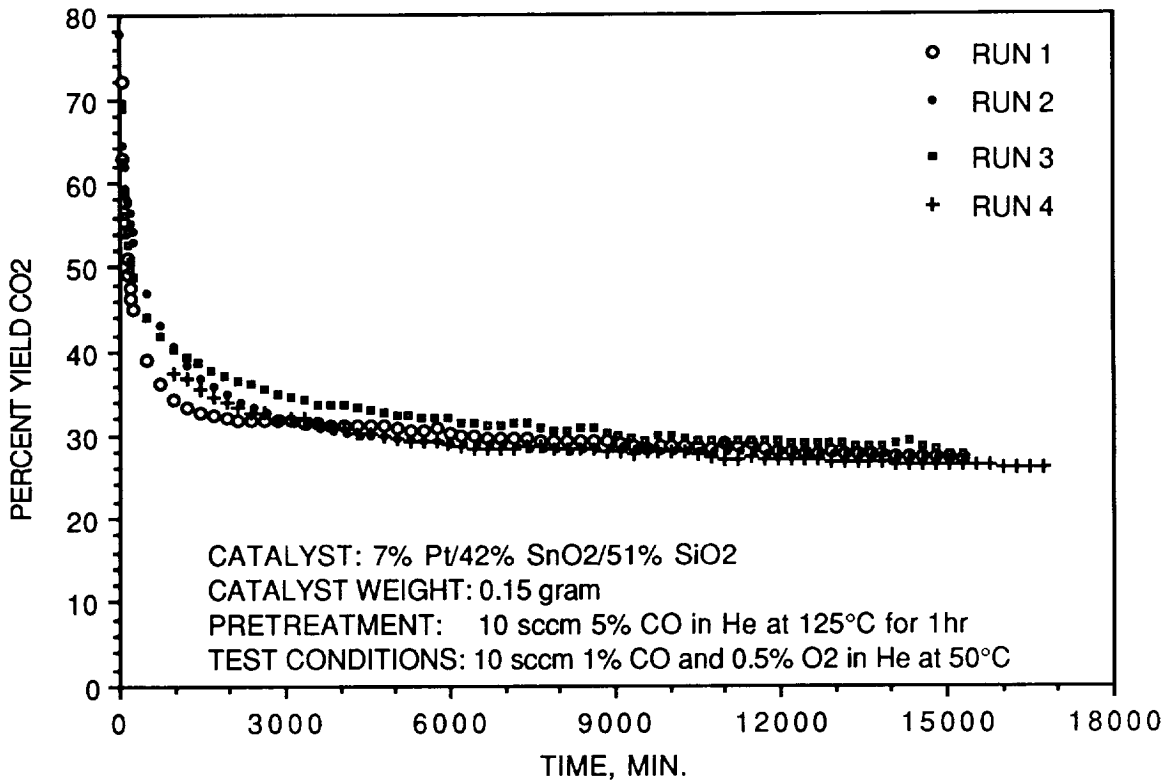
Figure 11. Reproducibility in activity for repeated
screening tests of LaRC 1C,3
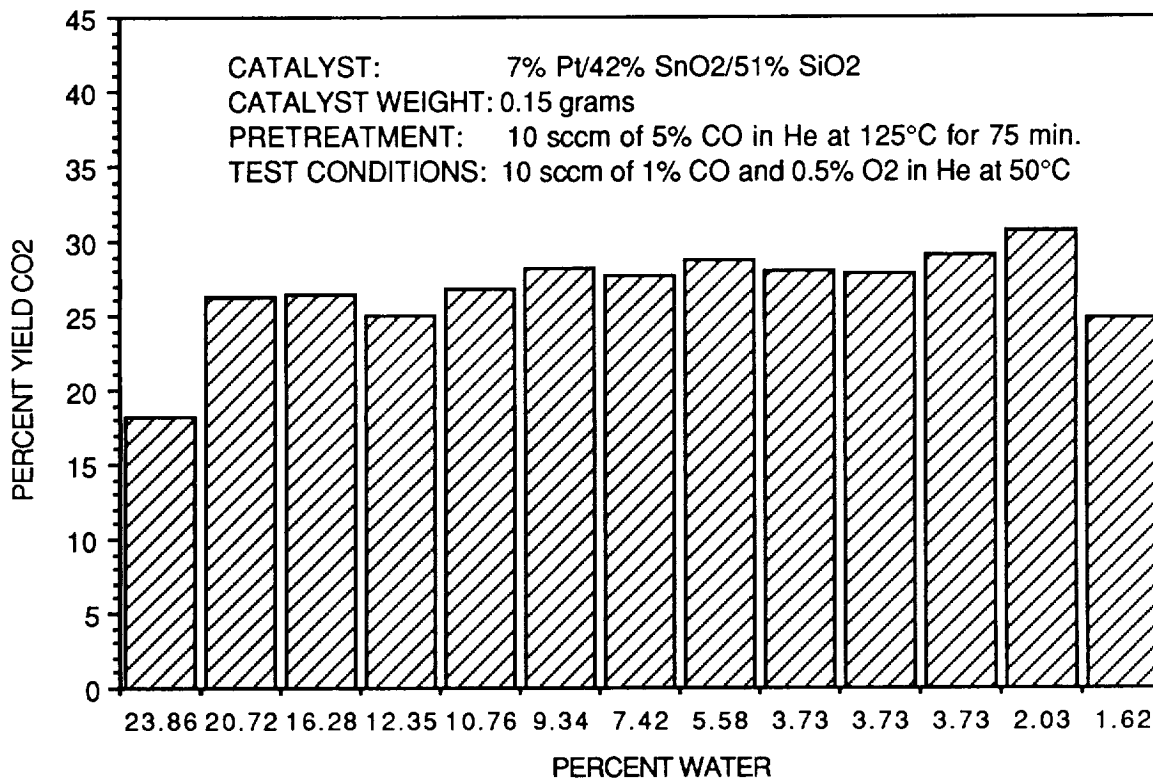
Figure 12. Effect of water on the activity of LaRC 1C, a
silica gel-supported Pt/SnO2 catalyst
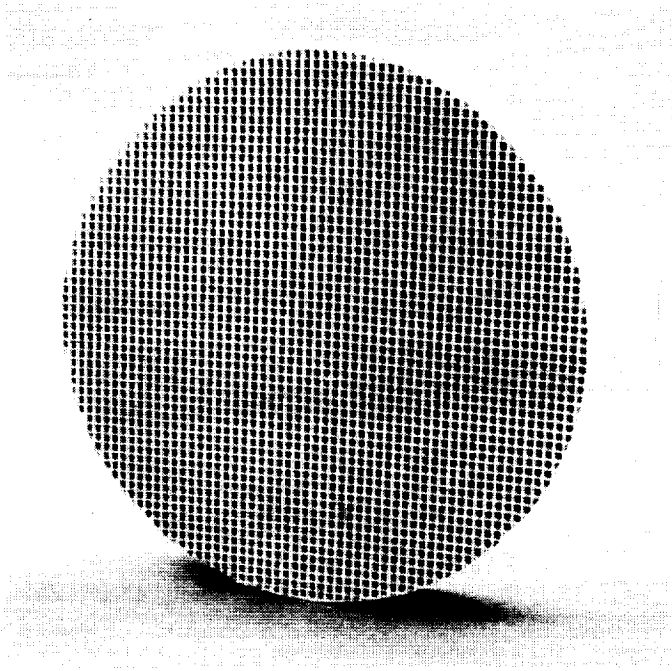
Figure 13. Cordierite honeycomb monolith; 3 inches in diameter
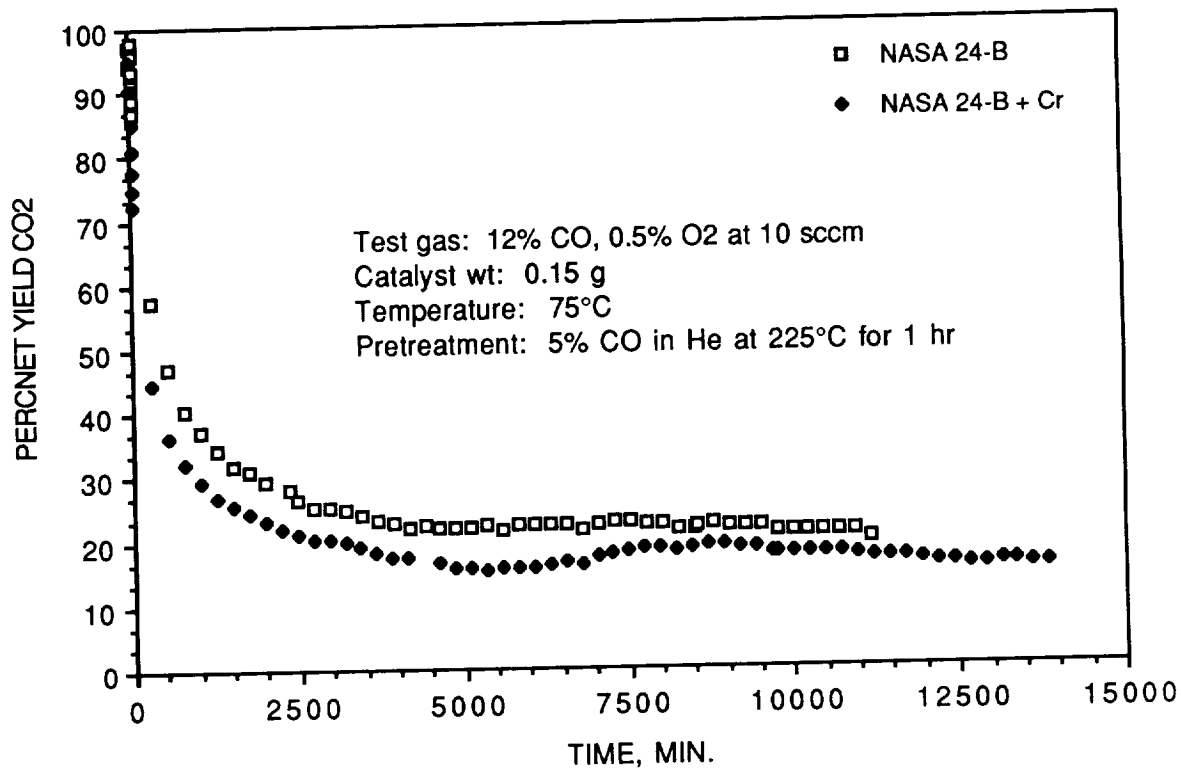by 1/2 inch thick, 400 cells per square inch

Figure 14. Comparison of LaRC 24B with and
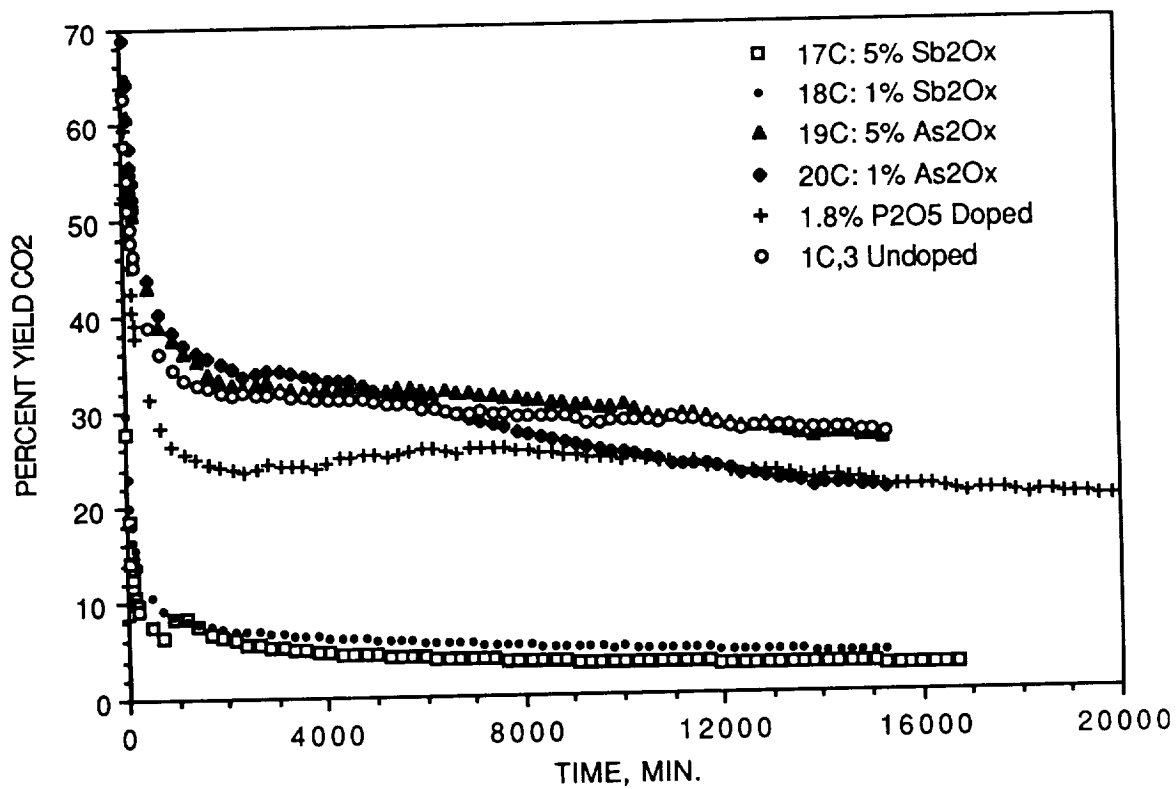without Cr as a promoter

Figure 15. Comparison of activities for silica gel-supported
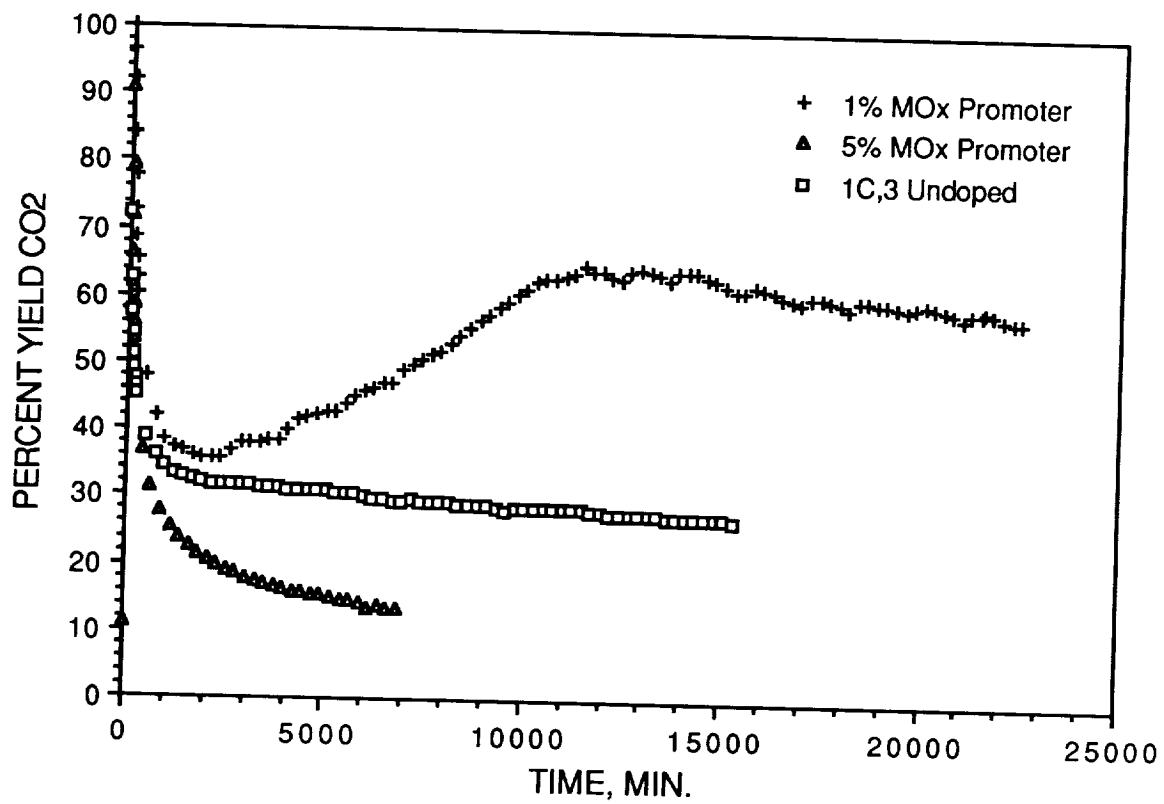Pt/SnO2 doped with various acidic oxides

Figure 16. Comparison of activities for silica gel-supported
Pt/SnO2 with those doped with an acidic oxide promoters

Phillips CO-Oxidation Catalysts for Long-Lived CO$_2$ Lasers: Activity and Initial Characterization Studies

J. H. Kolts, D. J. Elliott and F. Pennella
Research and Development, Phillips Petroleum Company
Bartlesville, Oklahoma

Summary

Four different catalysts have been developed specifically for use in sealed carbon dioxide lasers. The catalysts have been designed to be low dusting, stable to shock and vibration, have high activity at low temperatures and have long active lifetimes. Measured global CO oxidation rates range from 1.4 to 2.2 cc CO converted per minute per gram of catalyst at ambient temperature. The catalysts also retain substantial activity at temperatures as low as -35 C. The Phillips laser catalysts are prepared in a variety of different shapes to meet the different pressure drop and gas flow profiles present in the many different styles of lasers. Each catalyst has been tested in sealed TEA* lasers and has been shown to substantially increase the sealed life of the laser. Activity measurements made on the precious metal catalysts which were prepared with and without activity promoters showed that the promoter materials increase catalyst CO oxidation activity at least an order of magnitude at ambient temperature. Initial studies using H$_2$ and CO chemisorption, X-ray diffraction (XRD) and X-ray photoelectron spectroscopy (XPS) have shown that the activity promoters do not significantly affect the precious metal crystallite size or the electronic structure around the precious metal. In addition, the formation or lack of formation of solid solutions between the precious metal and promoters has also been shown not to affect the activity of the promoted catalyst.

Introduction

The operation of pulsed CO$_2$ lasers over long periods of time in a sealed-off condition requires that a technique be developed to control the build-up of oxygen that occurs during the normal operation of the laser. The presence of oxygen has been thought to be one of the most important factors which cause discharge instability (1-4). The use of gas phase additives in sealed CO$_2$ lasers has had some success in extending the useful sealed life of the laser. However, when the laser must operate over several million pulses or at high repetition rates it becomes necessary to use a catalyst which recombines carbon monoxide and oxygen to carbon dioxide at a rate which is at least equal to or greater than that at which they are being formed during operation of the laser. Many of the CO oxidation catalysts which have been tested in pulsed CO$_2$ lasers have been based upon Pt or other precious metals supported on SnO$_2$ which may contain other metal promoters to enhance catalytic activity (5-9). Laser testing of the tin catalysts has clearly shown that catalytic recombination of CO and O$_2$ can extend the sealed usable life of pulsed CO$_2$ laser systems.

During the past several years Phillips Petroleum has developed a series of four proprietary catalysts (designated LC-0100, LC-0200, LC-0300 and LC-0400) which have

*transversely excited atmospheric pressure configuration

been shown, on several occasions, to be effective at substantially extending the sealed-off lifetime of pulsed CO_2 lasers at temperatures as low as -35 C. Each of the different catalysts have been designed to have minimal dust formation, be stable to shock and vibration, have high activity at low temperatures, and have long active lifetimes.

Experimental

Catalytic activity measurements were made using a continuous flow system schematically shown in Figure 1. Carbon monoxide was continuously monitored using an Anarad infrared analyzer. Oxygen and carbon dioxide were spot checked using gas chromatography. The catalyst reactor consisted of a 7 mm i.d. quartz tube fitted with thermocouple well, which was in contact with either the upstream or downstream edge of the catalyst bed. The LC-0100 and LC-0400 catalysts were loaded as full size particles (1 or 2 grams); the LC-0300 catalyst was broken to approximately 3/16 inch particles. Void spaces between catalyst particles were packed with 16/30 mesh quartz chips to enhance flow characteristics and transfer heat away from the catalyst particles during the highly exothermic CO oxidation reaction. By using this packing method the increase in gas temperature across the catalyst bed was kept to less than 10 C. The LC-0200 catalyst, which is a monolith supported material, was tested as a 1 inch diameter by 1 inch deep cylinder in a quartz reactor just slightly larger than the monolith or as material which had been crushed to approximately 1/8 inch particles.

Unless otherwise specified, all of the catalysts were reduced in flowing hydrogen at 300 C for two hours prior to each experiment. After reduction, the catalyst was cooled under a helium purge. The standard experiment consisted of passing 400 sccm of simulated laser blend containing 1.20% CO, 0.60% O_2, 32% CO_2, and 32% He with the balance being nitrogen. Reactor and inlet gas temperatures were controlled by placing the reactor and inlet gas lines in a Thermotron environmental chamber. Global rates are expressed as ml of CO at STP converted per minute per gram of catalyst. Although this method of activity measurement introduces sometimes severe limitations due to external and internal heat and mass transfer effects, the authors have found the global rates calculated in this manner to be very useful in determining how much catalyst would be needed in various laser applications, using the known carbon monoxide or oxygen production rates of each laser and the gas recirculation rates within the laser.

Results

Each of the Phillips catalysts are based on precious metals, activity promoters, and support materials which not only provide needed structural and flow characteristics but also enhance the activity of the catalytic components. Each one of the four catalysts to be discussed here use a chemically distinct support.

LC-0100 Series. This series of catalysts are prepared on activated cylindrical tablets that are nominally 4.7 mm in diameter and 4.7 mm in height. The average bulk density of the finished catalyst is 1 gram per cc, with nitrogen BET* surface areas in the 50 to 60 m^2/gram range. Figure 2 shows a lifetime test for the catalyst at two different activation temperatures. No improvement in catalyst activity is obtained when hydrogen activation is carried out at temperatures above 300 C. As shown in the figure the catalyst has initially high CO conversion

*Brunauer, Emmett, and Teller

activity which declines to a steady state value after approximately 100 hours of testing. After the steady state activity has been reached, (1.4 cc CO/min/gram), no degradation of activity was observed in tests which lasted as long as 35 days. Soaking of the catalyst in a CO_2, N_2 and He blend which contained no CO or O_2 had no detrimental effect on activity. Exposure of the catalyst to atmospheric oxygen for several hours reduced CO oxidation activity by about 90%; however, when the catalyst was reactivated in hydrogen or carbon monoxide at 300 C, its activity returned to that of the fresh catalyst. To illustrate the strong effects of heat and mass transfer, where full size particles had an activity of 1.4 cc CO/min/gram, a one gram sample of the same catalyst crushed to 30/40 mesh and mixed with an equal volume of quartz chips gave 100% CO conversion at virtually any feed rate. In high flow cases the catalyst temperature easily exceeded 150 C.

Figure 3 shows catalyst activity as a function of inlet gas temperature. The three different curves are for catalysts prepared using the same method over a 14 month interval to check synthesis repeatability. Figure 4 shows low temperature data over a several hour test period. Catalysts used in both Figures 3 and 4 were brought to their steady state activity level at ambient temperature before temperature testing was begun.

LC-0200 Series. This series of catalysts are prepared by supporting the active catalyst components on a standard cordierite monolith. Activity testing of the crushed monolith catalyst (1/8 inch particles) gave a steady state rate of CO conversion of approximately 2 cc CO/min per gram of supported catalyst material (does not include weight of cordierite monolith). Testing of a 1 by 1 inch monolithic cylinder having 100 cells/inch gave 100% conversion under our test conditions. Figure 5 is a photograph of a Phillips monolith catalyst that was used successfully in high pulse rate TEA laser tests.

LC-0300 Series. The LC-300 series of catalysts have been designed specifically for applications where large volumes of gas must be passed over the catalyst with low pressure drop. This catalyst is also the hardest and most durable of any of the Phillips laser catalysts. The catalyst is supplied as 15.9 mm diameter by 9.5 mm thick tablets with seven 3.2 mm holes to improve diffusion and pressure drop characteristics (see Figure 6). Average bulk density of the finished catalyst is 0.8 grams/cc with an N_2 BET surface area of 50 m^2/g. As shown in Figure 7 the catalyst has a steady state activity of 1.5 cc CO/min per gram of catalyst. This catalyst is not as susceptible to reversible poisoning by atmospheric oxygen as the LC-0100 catalyst.

LC-0400 Series. The LC-0400 series of catalysts have been designed specifically to reduce the reversible poisoning of the catalyst by atmospheric oxygen during shipment and loading into the CO_2 laser. The catalyst is normally supplied as 3.2 mm diameter spheres. Catalysts having diameters of 4.8, 7.9 or 12.7 mm can also be prepared. The average bulk density of the finished catalyst is 0.72 grams/cc with an N_2 BET surface area in the 250 to 300 m^2/gram range. As shown in Figure 8 the catalyst is quite tolerant to exposure to oxygen and moisture. The data were taken after the catalyst had been stored in the shipping container for thirty days then exposed to laboratory atmosphere for 6 hours before pretreatment and testing.

Characterization Studies

As mentioned earlier, each of the Phillips catalysts contains precious metals, support material and activity promoters. Comparative tests of pairs of catalysts prepared by identical

procedures, one with and the other without the activity promoters, showed that the activity promoters increased the rate of CO oxidation at ambient temperature by at least one order of magnitude. Catalysts that contained only the supported promoters were totally inactive for CO oxidation.

We are now engaged in a series of studies aimed at understanding the specific role played by the promoters in increasing so dramatically the low temperature activity of these catalysts. We report here preliminary results of X-ray diffraction studies, H_2 and CO chemisorption studies, and XPS analysis for catalysts in the LC-0100 series.

XRD studies. The purpose of the XRD studies was, on the one hand, to determine the influence of the promoters on the crystallinity and the sintering characteristics of the precious metals and, on the other hand, to establish whether solid solutions of the precious metals and of the promoters are formed and whether their formation is responsible for the increased catalytic activity.

For this work, in order to obtain XRD patterns of sufficient intensity for peak shape analysis, it was necessary to use catalysts with significantly higher contents of precious metals and promoters than the catalysts used in the activity tests. Three catalysts were investigated: one contained only the support and a precious metal (Catalyst 1), the other two also contained promoters (Catalysts 2 and 3). The latter two catalysts had identical composition, but were prepared by different procedures referred to here as A and B.

After reduction of these catalysts in hydrogen at 300 C, the precious metal XRD pattern of the catalyst prepared by procedure A (Catalyst 2) was very similar to that of the catalyst without promoters (Catalyst 1). In contrast, both the breadth and the shape of the precious metal peaks were affected by the promoters in the catalyst prepared by procedure B (Catalyst 3). This difference is illustrated in Figure 9 for the metal [111] peak. The asymmetry of the metal peaks in Catalyst 3 reflects alterations of the metal lattice constant and consequent shifts in the XRD peak arising from the formation of solid solutions of the precious metal and the promoters with a broad range of stoichiometries. Despite these differences in the XRD patterns, there was little difference in activity between catalysts prepared by procedure A and by procedure B.

In the absence of promoters, the average crystallite size of the precious metals, as measured from the breadth of the [111] peak using Scherrer's equation, was a function of the temperature at which the catalyst was reduced in hydrogen, increasing with increasing temperature. The same trend was observed in the presence of the promoters, but, because of the peak broadening described above, only a qualitative comparison of Catalyst 1 with Catalyst 3 was possible.

These results indicate that the promoters do not influence significantly the crystallinity of the precious metal or its sintering as a function of temperature. They also show that bulk solid solutions of the precious metals and the promoters may be formed, but that their formation is not necessary for promoting the activity of the precious metals.

Chemisorption measurements. H_2 and CO chemisorption measurements were made on catalysts containing the same amounts of precious metal and promoters as in the activity tests. Three catalysts were studied containing the same amount of precious metal: one without

promoters (Catalyst 4), and the other two with the same amounts of promoters; of these, one (Catalyst 5) was prepared by procedure A, and the other (Catalyst 6) by procedure B. The catalysts were reduced at 200 or 300 C in hydrogen, and were evacuated overnight at 250 C, before the chemisorption measurements. Isotherms were measured at ambient temperature (22-25 C). As shown in Table 1, there was no significant difference in the total volumes of gas absorbed by the unpromoted and the promoted catalysts. These results are in accord with the results of the XRD experiments and indicate that the promoters do not affect the dispersion of the precious metals.

XPS studies. Two of the catalysts used in the chemisorption measurements, catalysts 4 and 5, were also subjected to XPS analysis. The XPS spectrometer is equipped with a chamber for the pretreatment of the samples at high temperatures, so that the samples could be oxidized and reduced in the chamber and moved directly into the instrument. Only data for the reduced samples are reported here.

As anticipated from the results of the XRD studies and of the chemisorption studies, the relative surface coverage of the precious metal was essentially identical in the two samples. More significantly, the binding energies of the representative precious metal lines were the same, within experimental error, for the two samples. This indicates that the promoter produces no significant changes in the electron density around the precious metal.

Altogether, the results reported here lead to the conclusion that the observed changes in catalytic activity produced by the addition of the promoters are not related to the formation of bulk alloys, nor can they be attributed to changes in the dispersion of the precious metal, to changes in the electronic density around the precious metal atoms, or to changes in the CO chemisorption capacity of the catalyst. It is likely that more subtle electronic phenomena are responsible for the effects of the promoters on the catalytic activity.

Conclusions

The preceding discussion has described four different catalysts that have been developed by Phillips Petroleum for use in carbon dioxide lasers. Each of the catalysts has been proven to be effective in numerous pulsed CO_2 TEA laser tests. Using simulated laser test conditions, the full size catalyst particles have global CO conversion rates between 1.4 and 2.2 cc CO converted per minute per gram of catalyst. The different particle shapes available allow optimization of pressure drop and gas flow profiles. Initial chemisorption studies, XRD and XPS studies have been conducted in an attempt to explain the role of activity promoters and how they increase CO conversion rates by over an order of magnitude. These studies have shown that the promoters do not significantly affect the precious metal dispersion or the electronic structure around the precious metal; in addition, the formation of solid solutions between the precious metals and promoters also do not seem to affect catalyst activity. Characterization studies are continuing which may allow us to elucidate what the exact role of the activity promoters are.

Acknowledgments

References

1. P. Bletzinger, D. A. LaBorde, W. F. Bailey, W. H. Long, P. D. Tannen, and A. Garscadden, IEEE J. Quantum Electronics, QE-11, 317, (1975).

2. D. S. Stark and M. R. Harris, J. Phys. E: Sci. Instrum., 21, 715, (1988).

3. W. J. Wiegand and W. L. Nighan, Appl. Phys. Lett., 22, 583, (1973).

4. H. Hokazono and H. Fujimoto, J. Appl. Phys., 62, 1585, (1987).

5. C. F. Sampson and N. J. Gudde, NASA CP, 2456, 65, (1986).

6. A. Holt, M. G. Cheek, and E. N. Clegg, US Patent 4639432, (1987).

7. C. J. Wright and C. F. Sampson, US Patent 4524051, (1985).

8. H. T. Price and S. R. Shaw, NASA CP, 2456, 77, (1986).

9. D. S. Stark and M. R. Harris, J. Phys. E., 16, 492, (1983).

Table 1. Relative volumes of H_2 and CO chemisorbed at 100 torr by unpromoted and promoted catalysts.

A. Reduction temp=200 C. Promoted catalyst prepared by procedure A.

	Promoted	Unpromoted
H_2	1.0	0.9
CO	1.0	1.0

B. Reduction temp=300 C. Promoted catalyst prepared by procedure B.

	Promoted	Unpromoted
H_2	1.0	1.0
CO	1.0	1.1
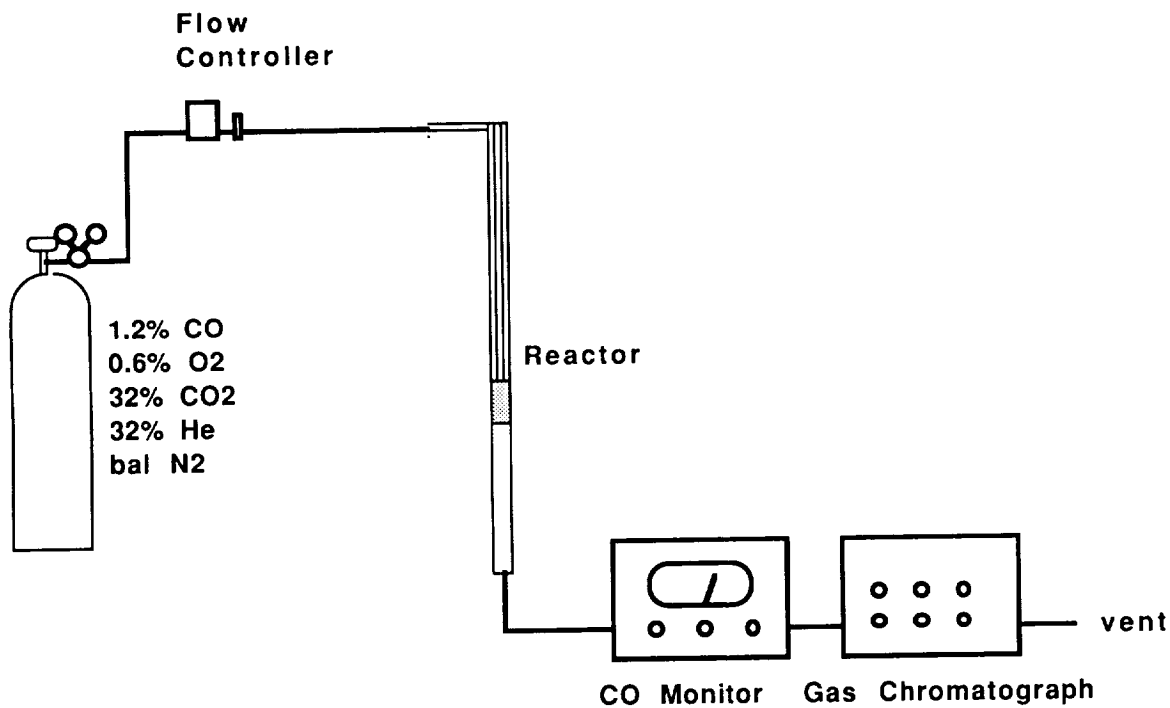
Figure 1. Apparatus used to measure CO oxidation rates.
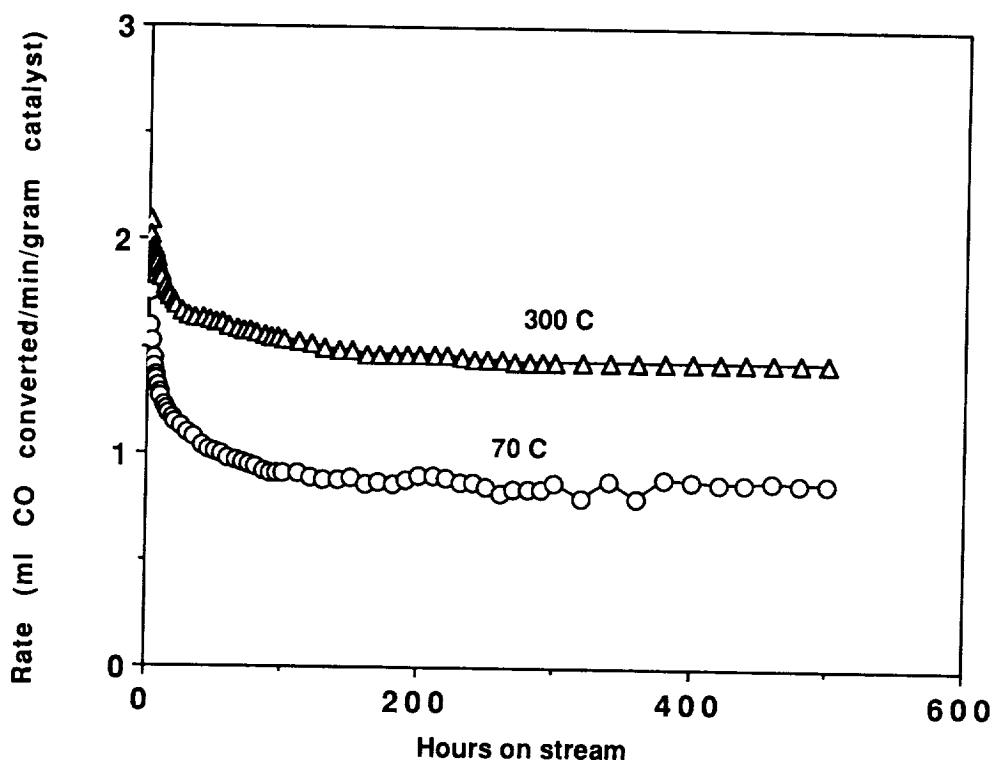
Figure 2. Activity of LC-0100 catalyst at ambient temperature after two hour activation in hydrogen at 70 C and 300 C.
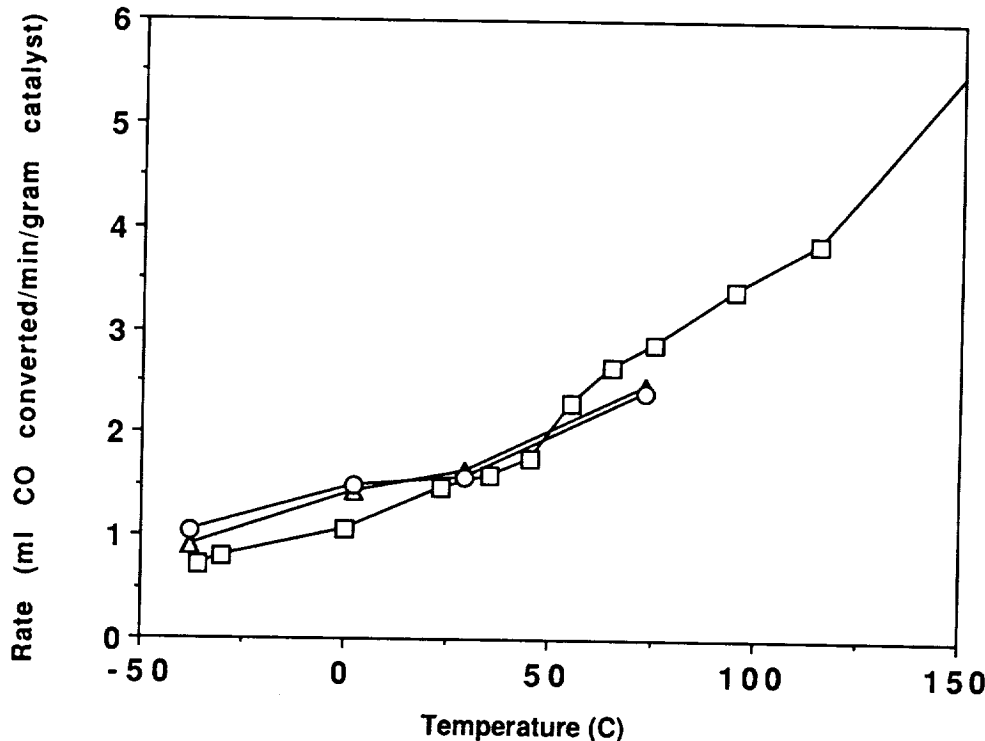
Figure 3. Activity of LC-0100 catalyst as a function of temperature for three samples of catalyst prepared over a 14 month interval.
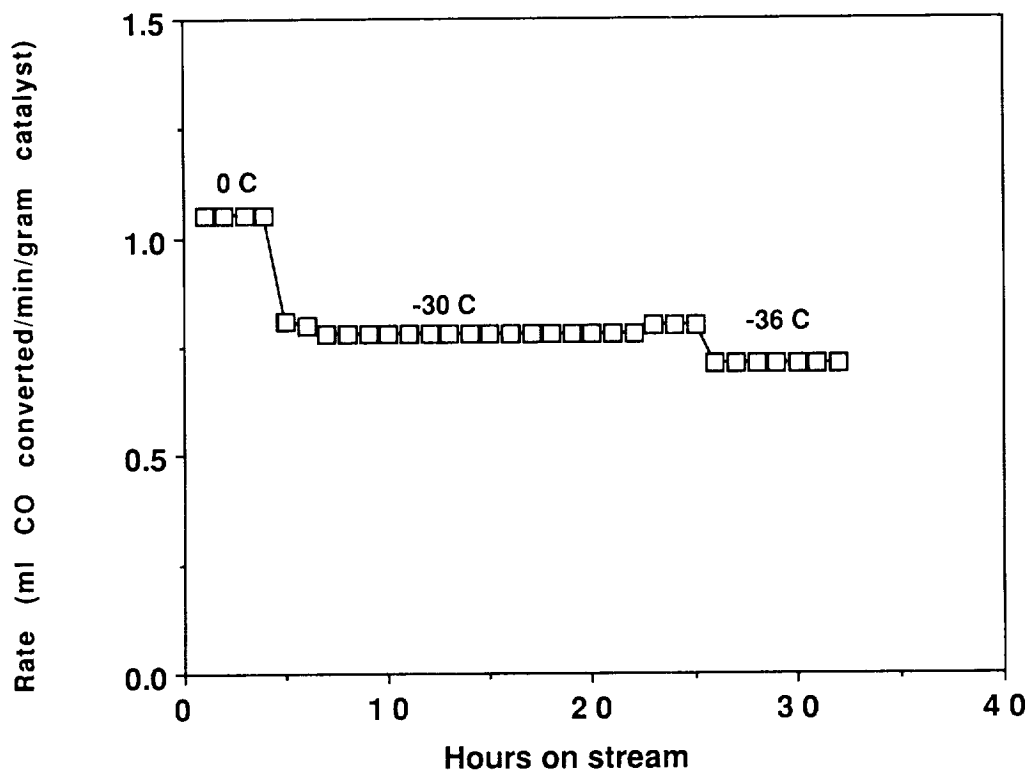
Figure 4. Low temperature data for the LC-0100 catalyst as a function of hours on stream after reaching steady-state activity.
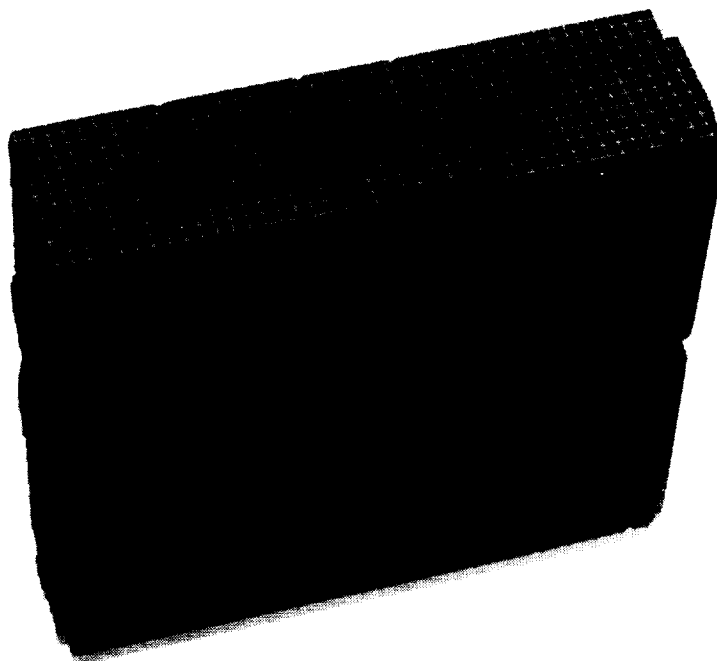
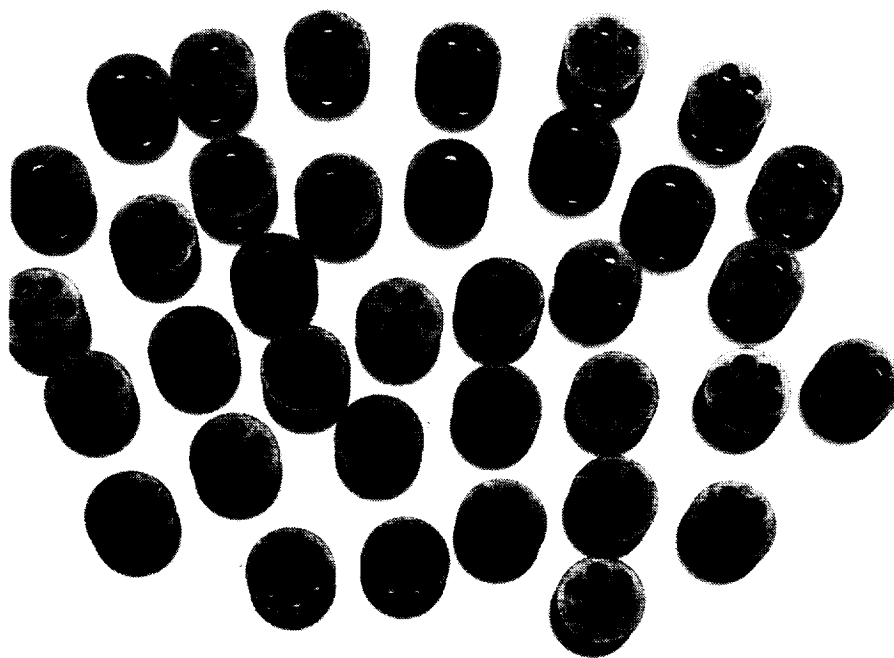**Figure 5.** Phillips LC-0200 cordierite monolith CO oxidation catalyst.

Figure 6. Phillips LC-0300 CO oxidation catalyst.
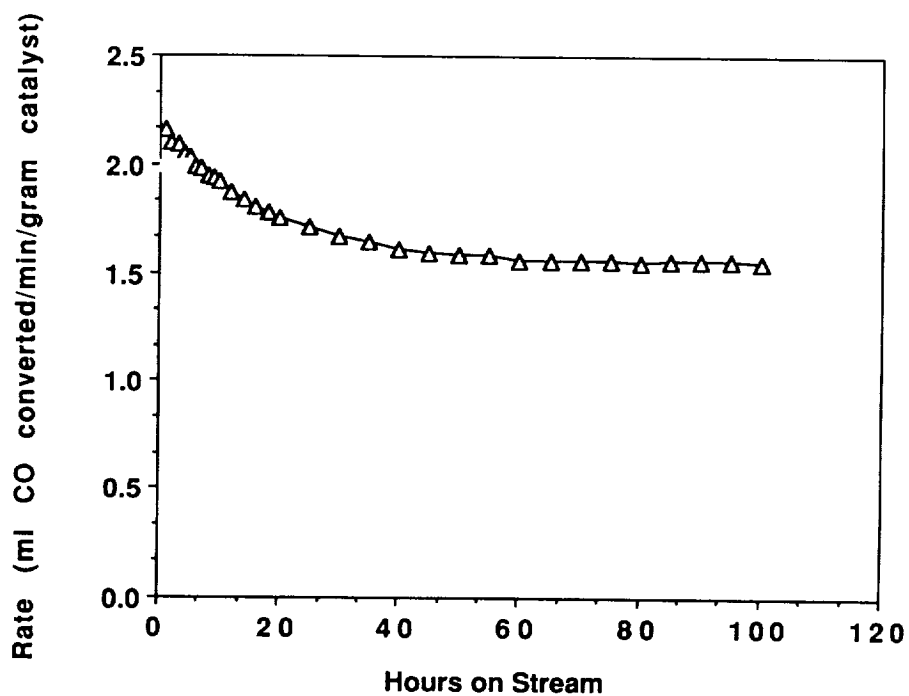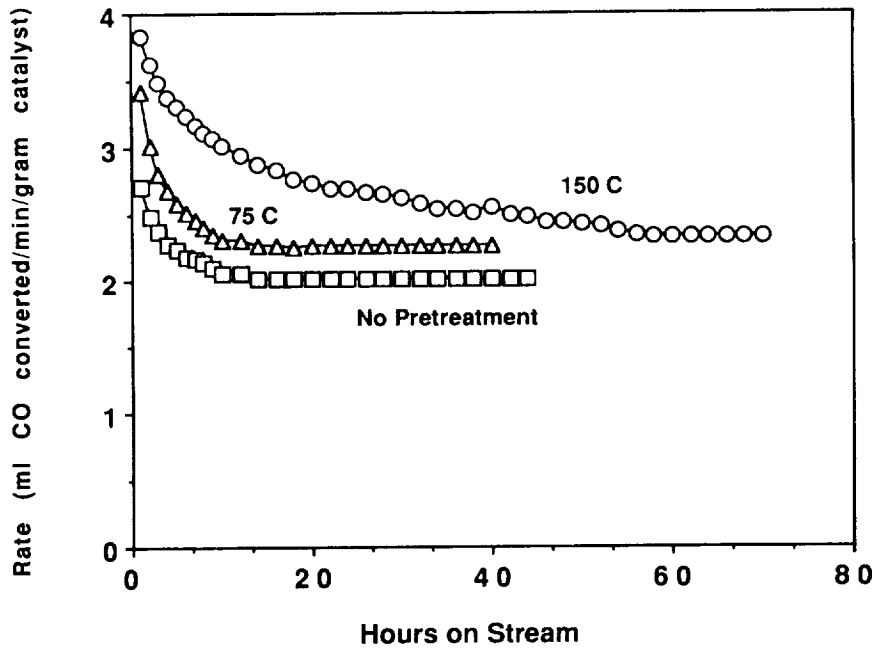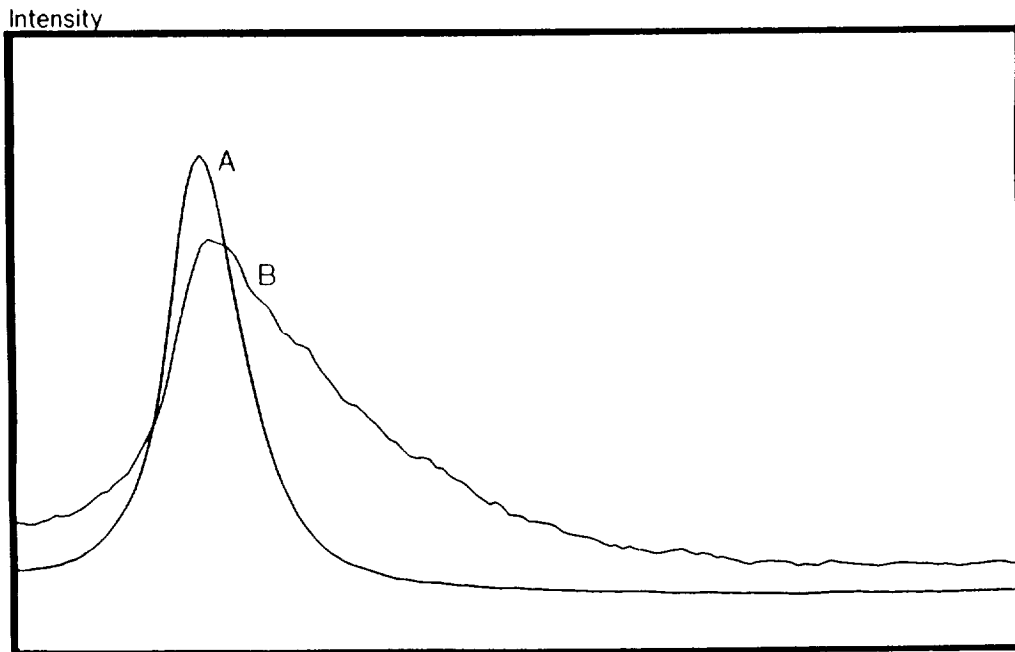

Figure 7. Activity of LC-0300 catalyst at ambient temperature after activation at 100 C in hydrogen prior to testing.

Figure 8. Activity of LC-0400 catalyst at ambient temperature under simulated shipping conditions including air exposure followed by activation in H_2 at temperature shown.

Figure 9. [111] Peak for (A) unpromoted catalyst and (B) promoted catalyst prepared by procedure B.

SYNTHESIS, CHARACTERIZATION AND EVALUATION OF CO-OXIDATION
CATALYSTS FOR HIGH REPETITION RATE CO_2 TEA LASERS

Thomas P. Moser
Hughes Aircraft Company
Electro-Optical and Data Systems Group
El Segundo, California

ABSTRACT

An extremely active class of noble metal catalysts supported on titania was developed and fabricated at Hughes for the recombination of oxygen (O_2) and carbon monoxide (CO) in closed-cycle CO_2 TEA lasers. The incipient wetness technique was used to impregnate titania and alumina pellets with precious metals including platinum and palladium. In particular, the addition of cerium (used as an "oxygen storage" promoter) produced an extremely active $Pt/Ce/TiO_2$ catalyst. By comparison, the complementary $Pt/Ce/\gamma-Al_2O_3$ catalyst was considerably less active. In general, chloride-free catalyst precursors proved critical in obtaining an active catalyst while also providing uniform metal distributions throughout the support structure. Detailed characterization of the $Pt/Ce/TiO_2$ catalyst by both SEM and EDX analyses demonstrated uniform dendritic crystal growth of the metals throughout the support, while ESCA analysis was used to characterized the oxidation states of Pt, Ce and Ti. The performance of the catalysts was evaluated with an integral flow reactor system incorporating real time analysis of O_2 and CO. With this system, the transient and steady-state behavior of the catalysts were evaluated. The kinetic evaluation was complemented by tests in a compact, closed-cycle Hughes CO_2 TEA laser operating at a pulse repetition rate of 100 Hz with a catalyst temperature of 75 to 95°C. The $Pt/Ce/TiO_2$ catalyst was compatible with a $^{13}C^{16}O_2$ gas fill.

INTRODUCTION

Long lifetime, high repetition rate CO_2 TEA lasers are required for a number of important applications including advanced rangefinding and chemical detection. The primary life-limiting process of such lasers is the generation of oxygen or some unknown coincidentally formed species in the glow discharge. If such a

103

species accumulates to a sufficient concentration, the discharge can rapidly degenerate into an arcing process. To prevent arcing, a catalyst can be used to maintain oxygen levels and other deleterious species below consequential levels.

With the increasing demand for high energy, rapidly pulsed CO_2 lasers, considerable attention has been given to the application of CO oxidation catalysts in sealed lasers (1-16). For the most part, however, these investigations have been concerned with the testing of commercial CO oxidation catalysts not necessarily designed for laser applications.

The first extended operation of a sealed TEA laser was reported by Stark et al (1). Operating with high CO_2 levels (eg. 60% CO_2, 40% N_2, 0% He), they demonstrated the continuous operation of a 1 Hz laser aided by a hot (1100°C) platinum wire catalyst. Quantitative details regarding the performance of the platinum wire catalyst were provided by Stark and Harris (2). The hot wire approach was significantly limited in application, however. For high repetition rate devices, both rapid recirculation and cooling of the internal gases are required. Correspondingly, increased catalytic activity would be required to compensate for the increased oxygen production. Under such conditions, a hot platinum wire would consume a prohibitive amount of energy, while introducing an enormous heat removal problem.

With ever stringent engineering constraints posed by laser designs, the practical catalytic solution will likely include a "low temperature" (20 to 100°C) CO oxidation catalyst, preferably in either a monolithic or pellet form. Although highly active at low temperature, Hopcalite (60% MnO_2, 40% CuO) has demonstrated only limited success (3), primarily because of its propensity to form dust and to deactivate by CO_2 adsorption and water contamination. Other catalytic systems include both alumina (Al_2O_3) (4, 5) and tin oxide (SnO_2) (6-15) supported precious metals. In particular, the catalysts which utilize an SnO_2 support have received much attention, primarily because of their reported low temperature capabilities and compatibility with isotopic $^{12}C^{18}O_2$ lasers.

The present investigation involves the fabrication, characterization and evaluation of a new class of precious-metal laser catalysts supported on titania (TiO_2) which use cerium as an "oxygen storage promoter" for improved low temperature activity. As an example, the detailed synthesis, characterization and evaluation of a robust (pellet) $Pt/Ce/TiO_2$ catalyst are presented. Results with a TEA laser using both $^{12}C^{16}O_2$ and $^{13}C^{16}O_2$ are also summarized.

104

EXPERIMENTAL

Support Material

Titania

The titania support was supplied as 1/8 inch extrudates from Norton Company as a 90/10 mixture of the anatase and rutile phases, respectively. Surface area analysis by the BET method yielded 34 m^2/gram with an average pore diameter of 73 angstroms.

Alumina

The alumina support was supplied as 3.2 mm diameter spheres (Grace LBD) consisting primarily of gamma phase alumina. The BET surface area was 110 m^2/gram.

Catalyst Preparation

The incipient wetness technique was used to impregnate blank titania (TiO_2) and alumina (γ-Al_2O_3) pellets with platinum, palladium, and cerium. Chloride-free catalyst precursors including tetraammineplatinum (II) nitrate, $[Pt(NH_3)_4](NO_3)_2$, tetraammine-palladium (II) nitrate, $[Pd(NH_3)_4](NO_3)_2$, and cerium nitrate, $Ce(NO_3)_3 \cdot 6H_2O$ were used as the source of platinum, palladium, and cerium, respectively. The specific pore volume of the support material was determined by measuring the saturation volume (pore volume as measured for a specific solvent) volumetrically with water. Once this saturation volume was known, a volumetric solution composed of the appropriate metal salts was prepared with a prescribed concentration level. This quantitative solution was then mixed with the appropriate mass of blank support, resulting in the physical adsorption of the solution onto the surface and into the interior of the pellet. A slight excess (ca. 5%) of solution was used in the impregnation procedure to allow uniform and complete saturation. The residual solution was retained for recovery and analysis. The catalyst preparation was completed by slowly drying the "wetted" catalyst pellets in a flowing air hood followed by activation in flowing helium (200°C; 2h), calcination in flowing oxygen (400°C; 4h), and reduction in flowing hydrogen (300°C; 4h). The metal loadings were determined by a material balance, taking into account the concentration of metal in the solution and the saturation volume of the support material.

Catalyst Characterization

BET Surface Area

A Quantasorb Jr. (Quantachrome Corporation) was used to measure surface areas by employing the single point BET method with nitrogen as the adsorbate.

Scanning Electron Microscopy (SEM)

Scanning electron micrographs were obtained with a Cambridge Stereoscan 250 Mk 3 Scanning Electron Microscope equipped with an EDAX PV9100 Energy Dispersive X-ray (EDX) analysis system. Micrographs were obtained with a backscattering detector, while a windowless detector was employed for EDX elemental detection down to the atomic weight of carbon.

Electron Spectroscopy for Chemical Analysis (ESCA)

Information concerning the oxidation states of Pt, Ce, and Ti were obtained by ESCA analysis. A Perkin Elmer 5500 ESCA/SAM with MgK_α X-rays was used with a chamber pressure of approximately 10^{-9} torr. Spectra were referenced to the C 1s covalent peak at 284.6 eV.

Catalyst Evaluation

Figure 1 shows the flow scheme for the low flow catalyst test station. A certified gas mixture having a composition of 0.5% oxygen, 1.0% CO, 17% nitrogen, 17% CO_2 and the balance helium was used for routine catalyst evaluation. Other gases including hydrogen, carbon monoxide, oxygen and helium were also deliverable for special processes, such as catalyst conditioning. The combination of high precision rotameters (Fisher Porter Model 10A3555) and individually calibrated mass flow controllers (Tylan Model FC-280) allowed for accurate and reproducible gas flow rates and the synthesis of special gas blends. The system pressure was monitored by an absolute pressure transducer/indicator. For real time gas analysis, a specifically tuned Beckman Industrial nondispersive infrared analyzer (Model 868) was used for CO analysis, while a Beckman oxygen analyzer (Model 755A) monitored oxygen levels.

The reactor was fabricated from standard wall Pyrex tubing having an inner diameter of nominally 0.5 inches and a length of 15 inches (Figure 2). The catalyst pellets were charged to the reactor

together with Pyrex spheres (1/8 inch in diameter) which served to minimize radial temperature gradients. The catalyst zone was held in place by "plugs" of Pyrex wool. The catalyst bed temperature was monitored with a sub-miniature type K sheathed thermocouple. The reactor was oriented vertically.

The catalytic activity for both CO and oxygen disappearance was calculated as:

$$\text{Activity} = \frac{Q \ (X_i^{\text{inlet}} - X_i^{\text{outlet}})}{V_c} \tag{1}$$

where
Q = flow rate across catalyst bed (standard cm^3/min)
X_i = mole fraction (i = O_2, CO)
V_c = volume of catalyst bed including void volume (cm^3)

Laser Testbed

A sealed modular TE laser was used to investigate catalytic performance. The transmitter used a corona discharge for preionization with transverse gas flow. The modular approach was chosen to allow for both a compact 1 to 3 Hz source or as a 100 Hz device with the straightforward addition of a flow module. The fully integrated, closed-cycle modular laser assembly shown in Figure 3 consisted of, from top to bottom, a potted PFN, discharge module and optical bench, a side mounted catalyst/heat exchanger section, and a tangential fan. A more detailed description of the device was given previously (17).

RESULTS AND DISCUSSION

Role of Catalytic Precursors

The selection of an appropriate chemical complex type for Pt, Pd and Ce proved extremely critical for synthesizing an active catalyst. In particular, catalyst samples prepared with chloride-free metal salts such as tetraammineplatinum (II) nitrate, tetraamminepalladium (II) nitrate and cerium nitrate resulted in deep penetration of the metals into the interior of the titania pellet. By contrast, catalysts prepared with chloride-based metals, including

hexachloroplatinic acid-6-hydrate, resulted in "eggshell" metal distributions in the support structure. In all cases, the chloride-free preparations resulted in superior catalytic performance. The relatively lower catalytic activity associated with the chloride-based preparations resulted from poor metal dispersion coupled with the inactive nature of metal sites complexed with chloride ions.

Catalyst Supports and Promoters

Figures 4 and 5 show respectively the O_2 and CO disappearance activity for a series of Pt, Pd, Pt/Ce, and Pd/Ce catalysts supported on titania. The 2.0 wt% Pt/2.0 wt% Ce (Pt/Ce/TiO$_2$) catalyst clearly demonstrated the highest activity throughout the 25 to 200°C temperature range. The analogous 2.0 wt% Pd/2.0 wt% Ce (Pd/Ce/TiO$_2$) catalyst was not only less active than the Pt/Ce/TiO$_2$ variety, but also less active than the 4.4 wt% Pd (Pd/TiO$_2$) catalyst and the 3.8 wt% Pt (Pt/TiO$_2$) catalyst. Furthermore, the Pd/Ce/TiO$_2$ catalyst was the least active of the series. These results suggest a distinct synergistic effect between Pt and Ce which was not apparent between Pd and Ce. Moreover, the simple impregnation of Ce onto TiO$_2$ yielded an inactive material.

Inasmuch as alumina is one of the most common support materials, it provided a basis for comparison with other supported catalyst systems, particularly for metals supported on titania as in the present study. Figures 6 and 7 make a direct comparison between the 2.0 wt% Pt/2.0 wt% Ce on titania (Pt/Ce/TiO$_2$) catalyst and the 2.0 wt% Pt/2.0 wt% Ce on gamma alumina (Pt/Ce/Al$_2$O$_3$) catalyst. Since the titania and alumina pellets had different particle densities, the activities were normalized on both a volume and mass basis (Figures 6 and 7, respectively). Despite having a much lower surface area (34 versus 110 m^2/gram), the Pt/Ce/TiO$_2$ catalyst was considerably more active than the Pt/Ce/Al$_2$O$_3$ variety. Whereas the Pt/Ce/TiO$_2$ catalyst demonstrated considerable activity between 25 to 100°C, the Pt/Ce/Al$_2$O$_3$ catalyst was inactive in the same temperature range.

As with automotive catalysts (18), the addition of cerium apparently helps to balance the relatively weak adsorption of oxygen with the strong adsorption of carbon monoxide. Furthermore, as suggested by the above results, this "oxygen storage" property appears to be directly linked to a chemical interaction between Pt, Ce, and TiO$_2$.

In-Laser Testing

The modular CO_2 TE laser was tested for extended periods at a 100 Hz repetition rate in a completely sealed condition using the Hughes Pt/Ce/TiO$_2$ catalyst. Typically, the laser was operated for several hours at a time, turned off overnight, and restarted the next day. The test results are as follows:

- -100 Hz repetition rate
- -80 mJ/pulse, no fall off over time
- -1 MW peak power
- -5×10^6 total shots
- -75 to 95°C catalyst temperature
- -Operation with $^{12}C^{16}O_2$ or $^{13}C^{16}O_2$

The Pt/Ce/TiO$_2$ catalyst is currently being tested in a higher energy (250 mJ) device at 200 Hz.

Characterization of Hughes Pt/Ce/TiO$_2$ Catalyst

Scanning Electron Microscopy (SEM)

Figure 8 shows both a longitudinal and a transverse view of a sectioned catalyst pellet using a conventional high power microscope. The longitudinal cross section clearly shows a random distribution of Pt and Ce within the pores of the pellet. In addition, the extent of titania reduction or perhaps the density variation throughout the pellet is indicated qualitatively by the dark "band" about the pellet.

Using a backscattering SEM image technique, a mapping of the Pt/Ce distribution was obtained. Figure 9a clearly shows the dendritic crystal growth of both Pt and Ce in the TiO$_2$ matrix. Figure 9b shows a close-up view of Figure 9a point A. EDX analysis of the exterior of the pellet (side surface point B, Figure 9a) indicated considerable amounts of Pt and Ce. By contrast, the dark portion of the catalyst pellet as viewed in Figure 8 was void of both Pt and Ce as indicated by the EDX spectrum.

Electron Spectroscopy for Chemical Analysis (ESCA)

Information concerning the oxidation states of Pt, Ce and Ti were obtained by ESCA analysis. This information lends insight into the redox (reduction/oxidation) mechanism functioning at the catalytic surface.

Figure 10 shows the Pt 4f ESCA spectrum for the $Pt/Ce/TiO_2$ catalyst, including both the raw data and fitted curves reflecting the different chemical states of platinum. The Pt $4f_{7/2}$ peak at 70.6 eV and the Pt $4f_{5/2}$ peak at 73.9 eV correspond to metallic platinum (19, 20). The curve fitting analysis indicated the presence of both PtO (oxidation state of Pt^{+2}) and PtO_2 (oxidation state of Pt^{+4}). Likewise, the Ce 3d ESCA spectrum (Figure 11) also indicated multiple oxidation states. The Ce 3d peaks at both 885.3 and 903.6 eV correspond to metallic cerium (21). The fitted Ce 3d peak at 881.2 eV is associated with Ce_2O_3 (oxidation state of Ce^{+3}), whereas the fitted peak at 899.5 eV is associated with CeO_2 (oxidation state of Ce^{+4}). Since it is generally assumed that lattice oxygen is responsible for the catalytic oxidation of carbon monoxide (22), the presence of multiple oxidation states for both Pt and Ce suggests these metals may participate in a redox mechanism.

The corresponding 2p ESCA spectrum for Ti is given in Figure 12. In contrast with the Pt and Ce spectra, the Ti spectrum indicated only a single oxidation state. The Ti $2p_{3/2}$ peak at 458.4 eV and the Ti $2p_{1/2}$ peak at 464.1 eV are associated with the Ti^{+4} oxidation state of TiO_2 (20, 23).

CONCLUSIONS

The development of laser catalysts at Hughes has led to significant improvements in the performance of long-life repetitively pulsed closed-cycle CO_2 TEA lasers. Laser demonstrations in excess of 10^6 continuous shots at 100 Hz were facilitated by a Hughes $Pt/Ce/TiO_2$ catalyst functioning between 75 to 95°C. In addition, the compatibility of this catalyst was confirmed with an isotopic $^{13}C^{16}O_2$ TEA laser.

ACRONYMS

BET	Brunauer, Emmett, and Teller
EDX	Energy dispersive X-ray
ESCA	Electron Spectroscopy for Chemical Analysis
PFN	Pulsed frequency network
SEM	Scanning electron microscopy
TE	Transversely excited
TEA	Transversely-excited atmospheric pressure configuration

REFERENCES

1. D. S. Stark, P. H. Cross and M. R. Harris: A Sealed, UV-Preionisation CO_2 TEA Laser with High Peak Power Output. J. Phys. E: Sci. Instrum., **11**, 1978, pp. 311-315.

2. D. S. Stark and M. R. Harris: Platinum-Catalysed Recombination of CO and O_2 in Sealed CO_2 TEA Laser Gases. J. Phys. E: Sci. Instrum., **11**, 1978, pp. 316-319.

3. R. B. Gibson, A. Javan, K. Boyer: Sealed Multiatmosphere CO_2 TEA Laser: Seed-gas compatible System Using Unheated Oxide Catalyst. Appl. Phys. Lett., **32**(11), 1978, pp. 726, 727.

4. C. Willis and J.G. Purdon: Catalytic Control of the Gas Chemistry of Sealed TEA CO_2 Lasers. J. Appl. Phys., **50**(4), 1979, pp. 2539- 2543.

5. M. S. Sorem and G. Faulkner: Catalytic Converters for Closed-Cycle Operation of Isotopic CO_2 TEA Laser. Rev. Sci. Instrum., **52**(8), 1981, p. 1193.

6. G. C. Bond, L. R. Molloy, and M. J. Fuller: Oxidation of Carbon Monoxide over Palladium-Tin (IV) Oxide Catalysts: An Example of Spillover Catalysis. J. Chem. Soc. Chem. Comm., 1975, pp. 796-797.

7. D. S. Stark and M. R. Harris: Catalysed Recombination of CO and O_2 in Sealed CO_2 TEA Laser Gases at Temperatures Down to -27°C. J. Phys. E: Sci. Instrum., **16**, 1983, pp. 492-496.

8. D. S. Stark, Z. Crocker, and G. J. Steward: A Sealed 100 Hz CO_2 TEA Laser using High CO_2 Concentrations and Ambient Temperature Catalysts. J. Phys. E: Sci. Instrum. **16**, 1983, pp. 158-161.

9. C. F. Sampson and N. J. Gudde: The Oxidation of Carbon Monoxide using a Tin Oxide Catalyst. Closed-Cycle, Frequency-Stable CO_2 Laser Technology, NASA CP-2456, 1987.

10. H. T. Price and S. R. Shaw: High Repetition Rate Sealed CO_2 TEA Lasers using Heterogeneous Catalysts. Closed-Cycle, Frequency-Stable CO_2 Laser Technology, NASA CP-2456, 1987.

11. D. R. Schryer, B. D. Sidney, I. M. Miller, R. V. Hess, G. M. Wood, C. E. Batten, L. G. Burney, R. F. Hoyt, P. A. Paulin, K. G. Brown, J. Schryer, and B. T. Upchurch: NASA-LaRC Research on Catalysts for Long-Life Closed-Cycle CO_2 Laser. Closed-Cycle, Frequency-Stable CO_2 Laser Technology, NASA CP-2456, 1987.

12. B. T. Upchurch, G. M. Wood, R. V. Hess, and R. F. Hoyt: Rare Isotope Studies involving Catalytic Oxidation of CO over Platinum-Tin Oxide. Closed-Cycle, Frequency-Stable CO_2 Laser Technology, NASA CP-2456, 1987.

13. C. E. Batten, I. M. Miller, P. A. Paulin: Studies of CO Oxidation on Pt/SnO_2 Catalyst in a Surrogate CO_2 Laser Facility. Closed-Cycle, Frequency-Stable CO_2 Laser Technology, NASA CP-2456, 1987.

14. K. G. Brown and J. Schryer: Characterization of Pt/SnO_2 Catalysts for CO Oxidation. Closed-Cycle, Frequency-Stable CO_2 Laser Technology, NASA CP-2456, 1987.

15. B. D. Sidney: Studies of Long-Life Pulsed CO_2 Laser with Pt/SnO_2 Catalyst. Closed-Cycle, Frequency-Stable CO_2 Laser Technology, NASA CP-2456, 1987.

16. P. G. Browne and A. L. S. Smith: Long-Lived CO_2 Lasers with Distributed Heterogeneous Catalysis. J. Phys D: Appl. Phys., **7**, 1974, pp. 2464-2470.

17. D. B. Cohn, M. P. Hasselbeck, W. H. Affleck, R. E. Eldridge, T. P. Moser, G. R. Sasaki, T. A. Watson, and P. J. Bailey: Compact High Repetition Rate CO_2 TEA Lasers. SPIE, **1042**, CO_2 Lasers and Applications, 1989, pp. 63-69.

18. S. E. Oh and C. C. Eickel: Effects of Cerium Addition on CO Oxidation Kinetics over Alumina-Supported Rhodium Catalysts. J. Catal., **112**, 1988, pp. 543-555.

19. T. Sheng, X. Guoxing, and W. Hongli: The Nature of the SMSI State of the Pt/TiO_2 System. J. Catal., **111**, 1988, pp. 136-145.

20. G. B. Hoflund, A. L. Grogan, and D. A. Asbury: An ISS, AES, and ESCA Study of the Oxidative Reductive Properties of Platinized Titania. J. Catal., **109**, 1988, pp. 226-231.

21. J. Z. Shyu, W. H. Weber, and H. S. Gandhi: Surface Characterization of Alumina-Supported Ceria. J. Phys. Chem., **92**, 1988, pp. 4964-4970.

22. P. Mars and D. W. van Krevelen: Oxidation carried out by means of Vanadium-Oxide Catalysts. Chem. Eng. Sci., **3**, Spec. Suppl., 1954, pp. 41-59.

23. M. K. Bahl, S. C. Tsai, and Y. W. Chung: Auger and Photoemission Investigations of the $Pt-SrTiO_3$ (100) Interface: Relaxation and Chemical Shift Effects. Phys. Rev. B., **21**(4), 1980, pp. 1344-1348.
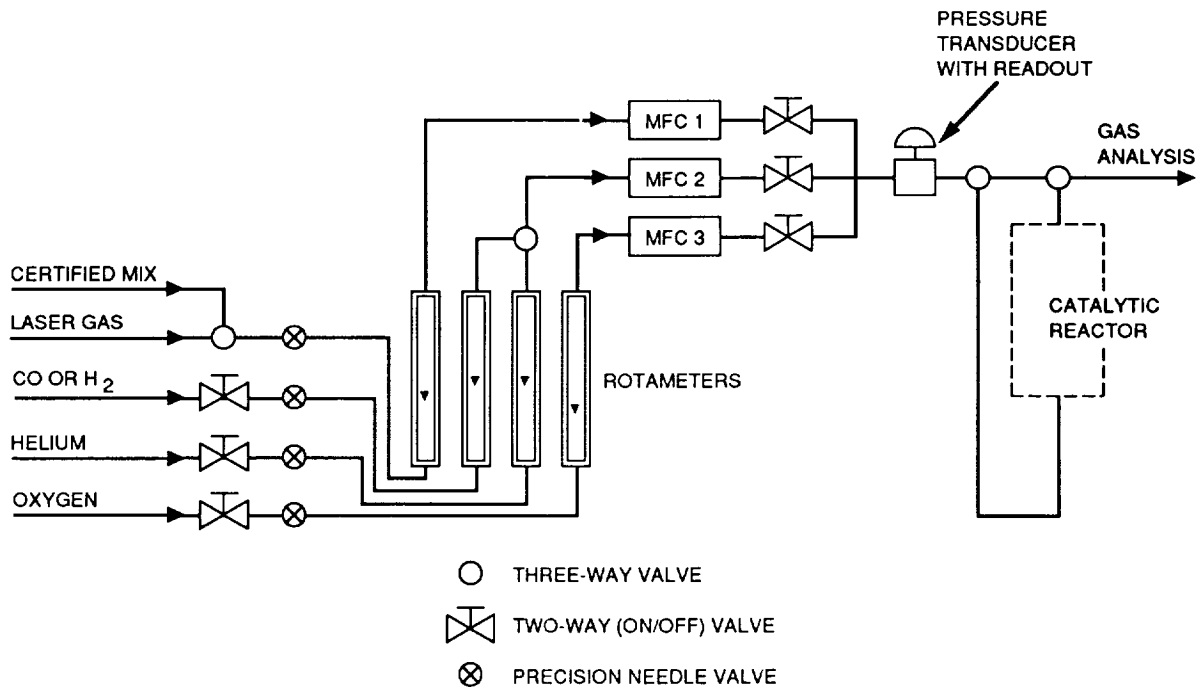
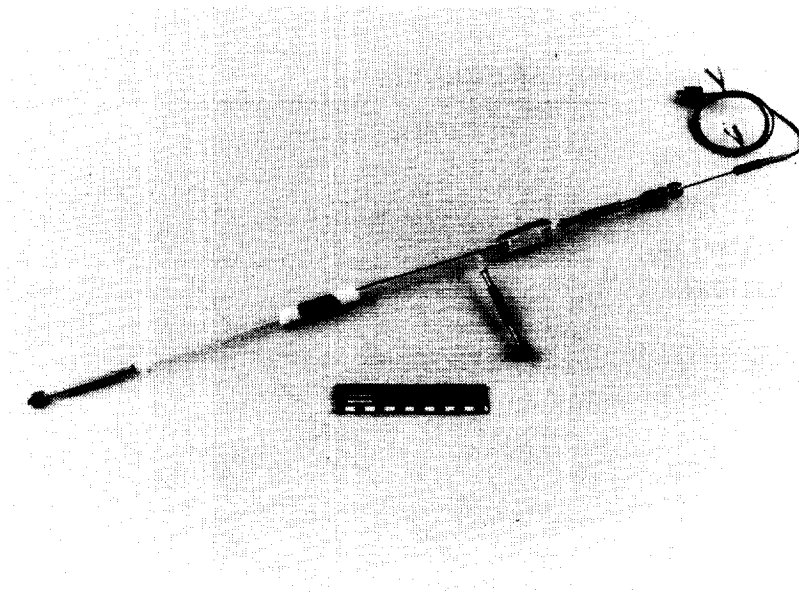Figure 1. Flow scheme for low flow catalyst test station.
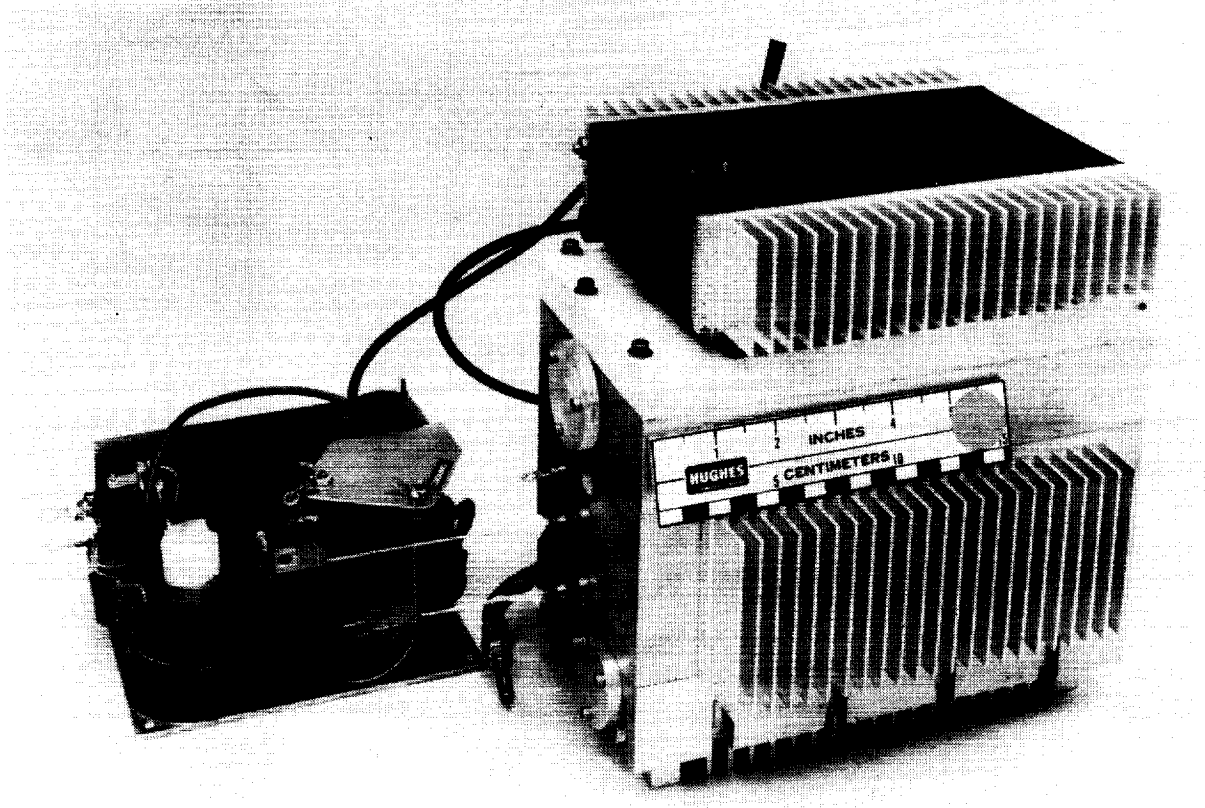

Figure 2. Catalytic reactor.

Figure 3. Modular TE laser.

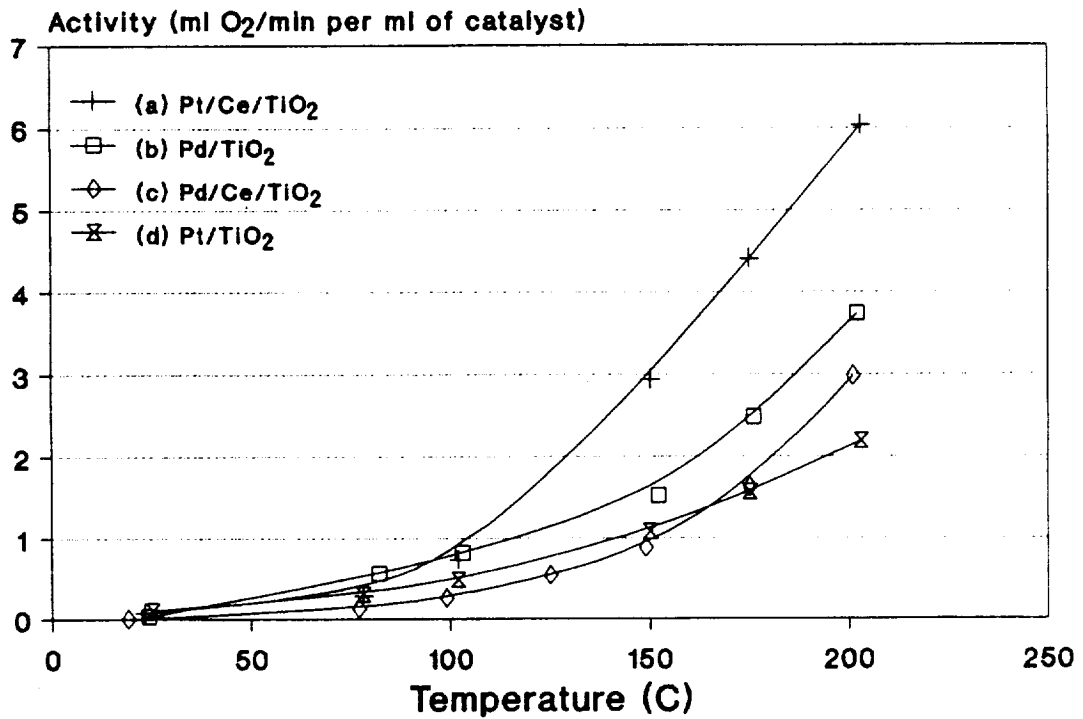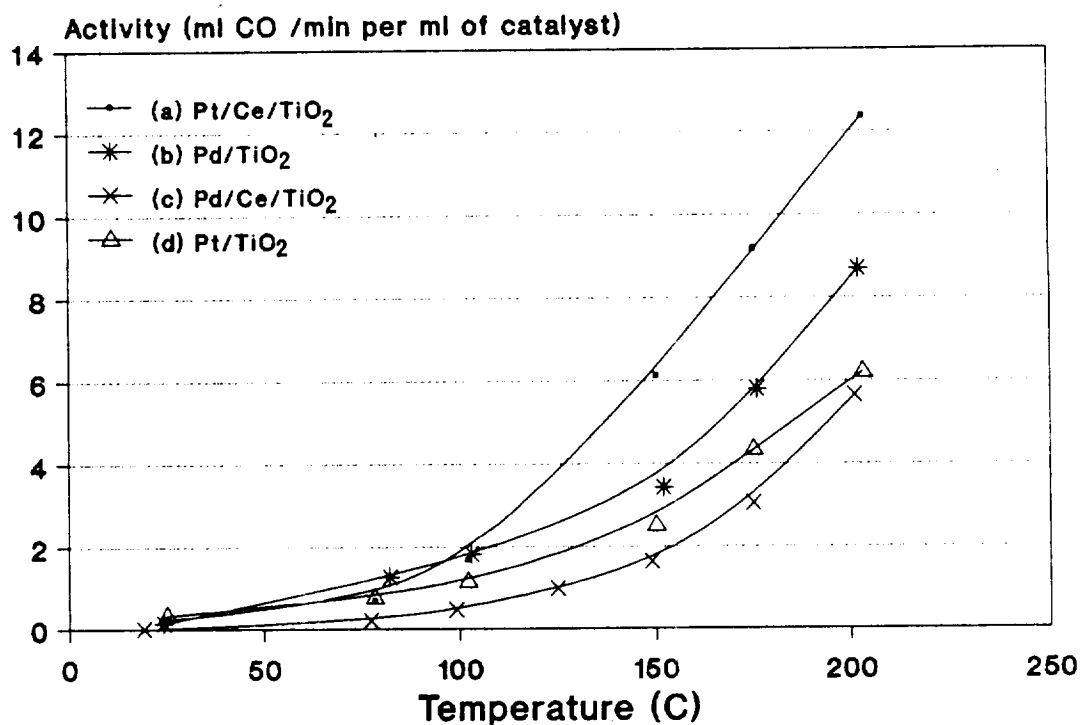Figure 4. Oxygen disappearance activity for titania-supported Hughes catalysts.

Activity (ml CO /min per ml of catalyst)

Figure 5. Carbon monoxide disappearance activity for titania supported Hughes catalysts.

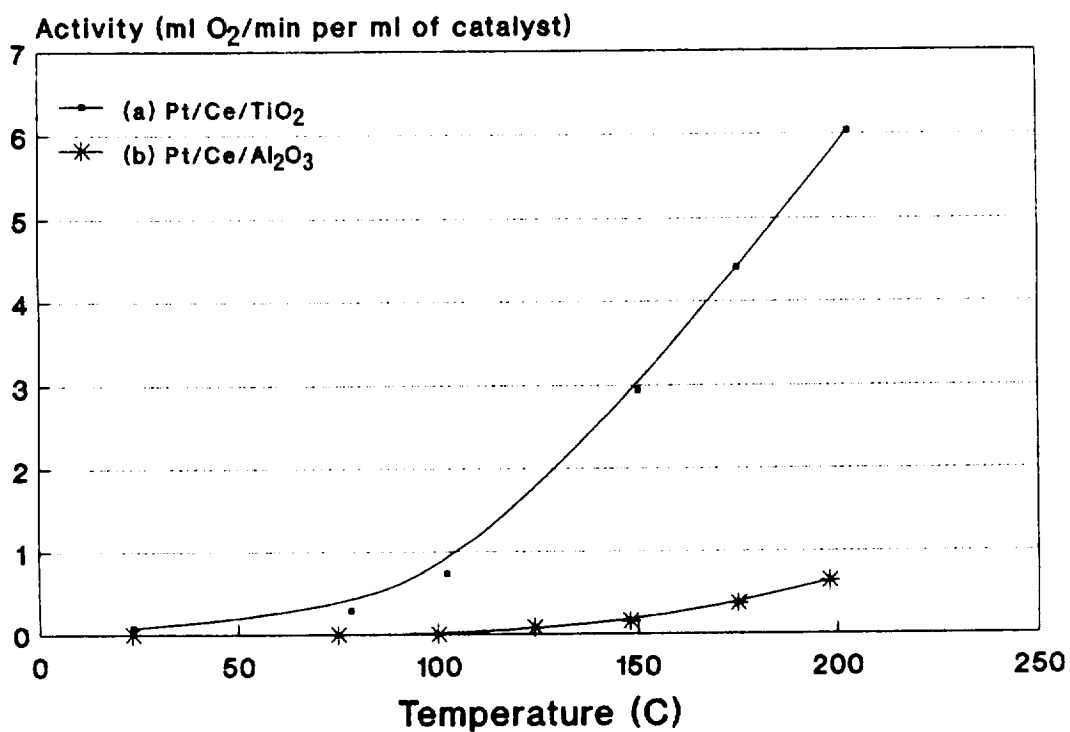**Activity (ml O$_2$/min per ml of catalyst)**

Figure 6. Comparison of alumina- and titania-supported Hughes Pt/Ce catalysts: Activity normalized on a volume basis.
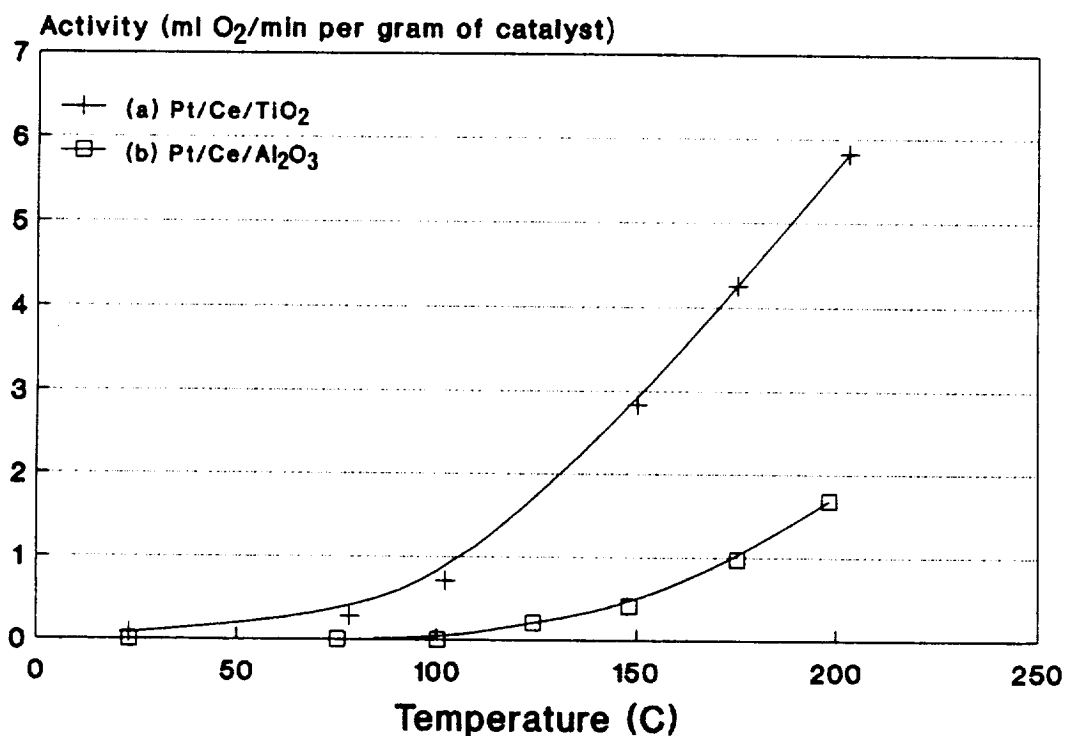
117

Figure 7. Comparison of alumina- and titania-supported Hughes Pt/Ce
catalysts: Activity normalized on a mass basis.
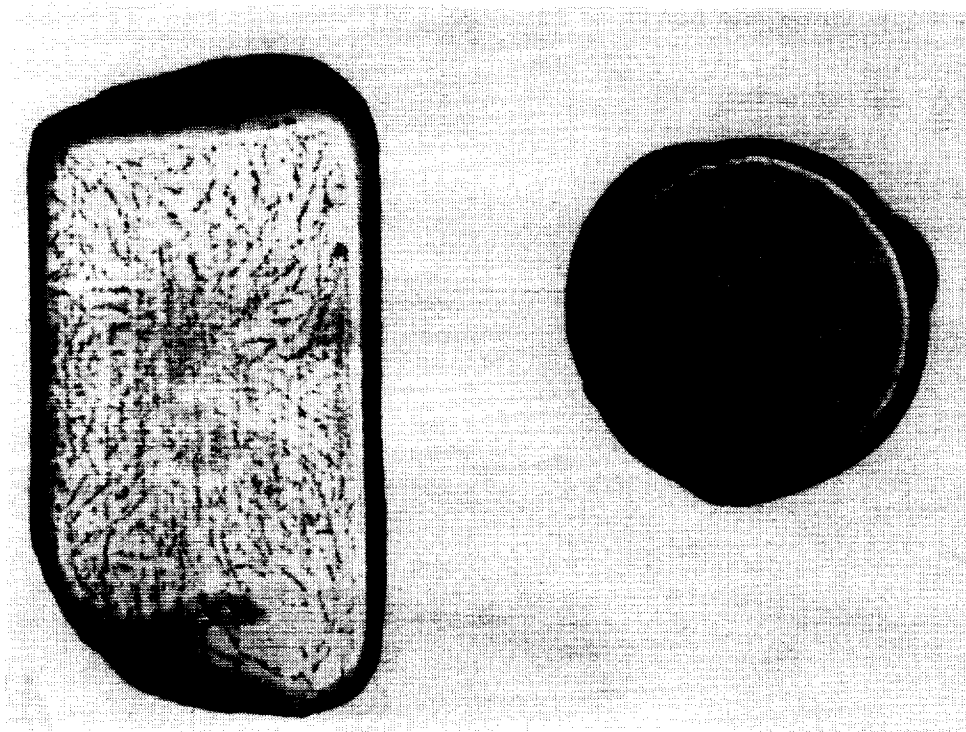

Figure 8. Longitudinal and transverse views of a sectioned Hughes
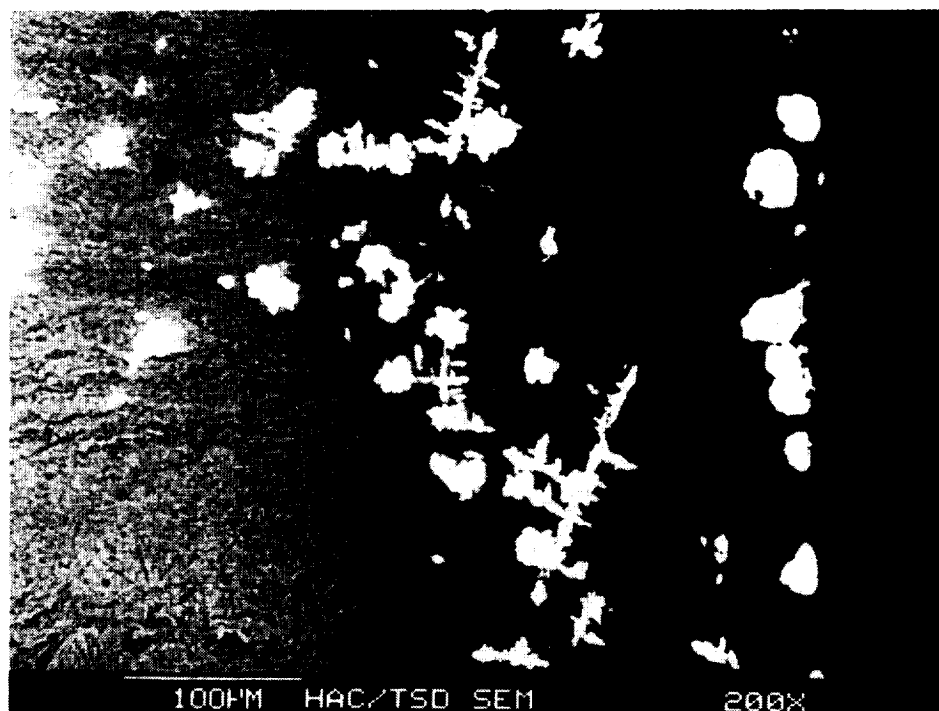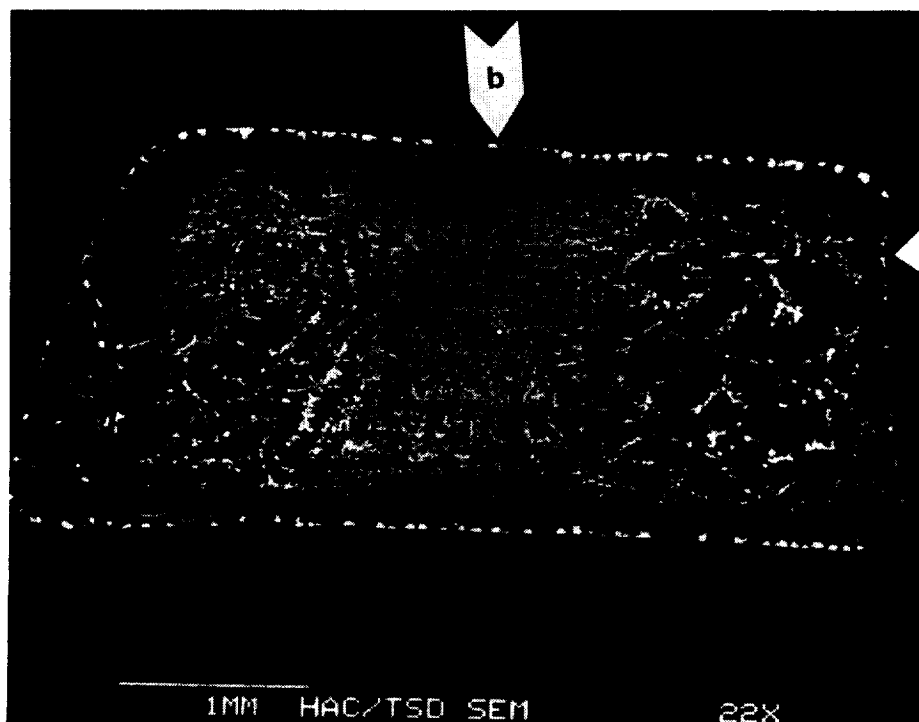Pt/Ce/TiO$_2$ catalyst pellet.

Figure 9. SEM backscattering image of a Hughes $Pt/Ce/TiO_2$ catalyst: (a) longitudinal view, (b) longitudinal close-up, point A.
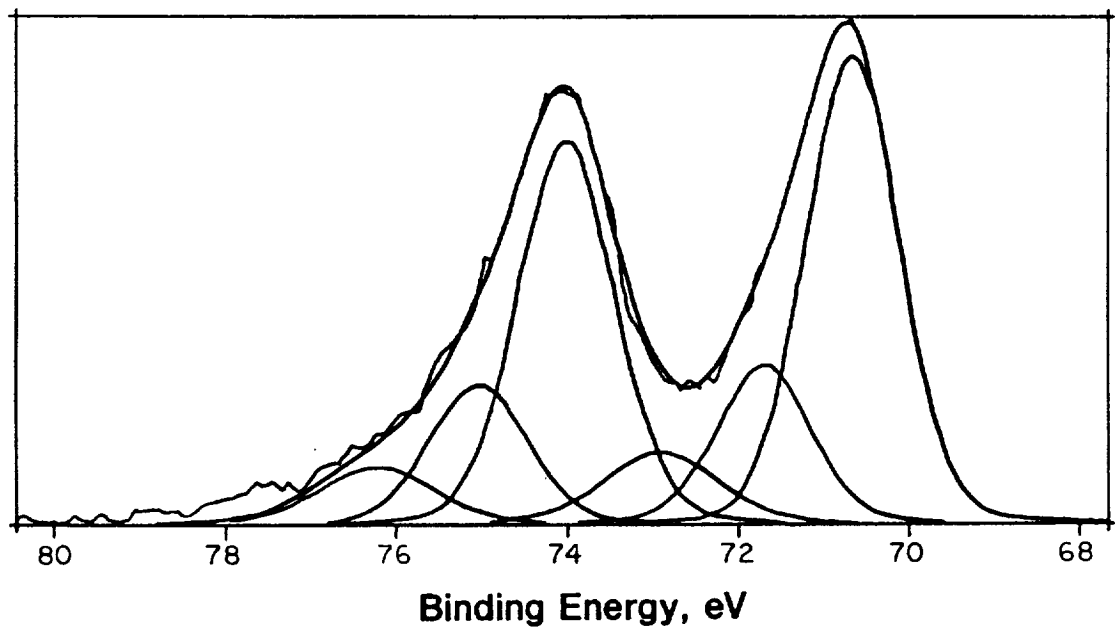
119

Figure 10. Platinum 4f ESCA spectrum of the Hughes Pt/Ce/TiO$_2$ catalyst.
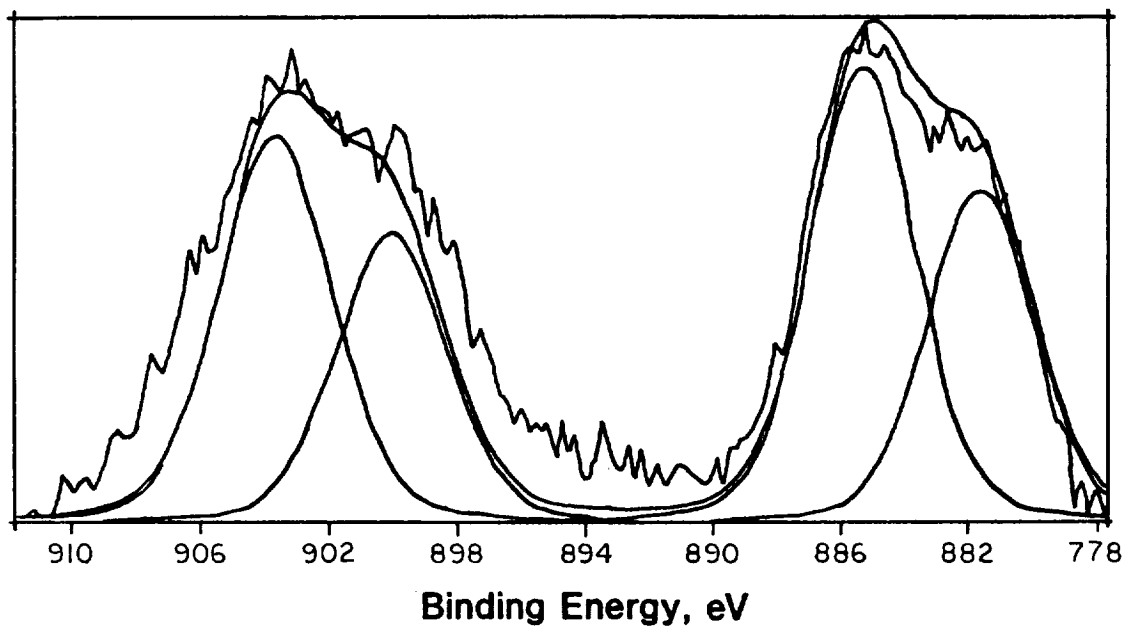

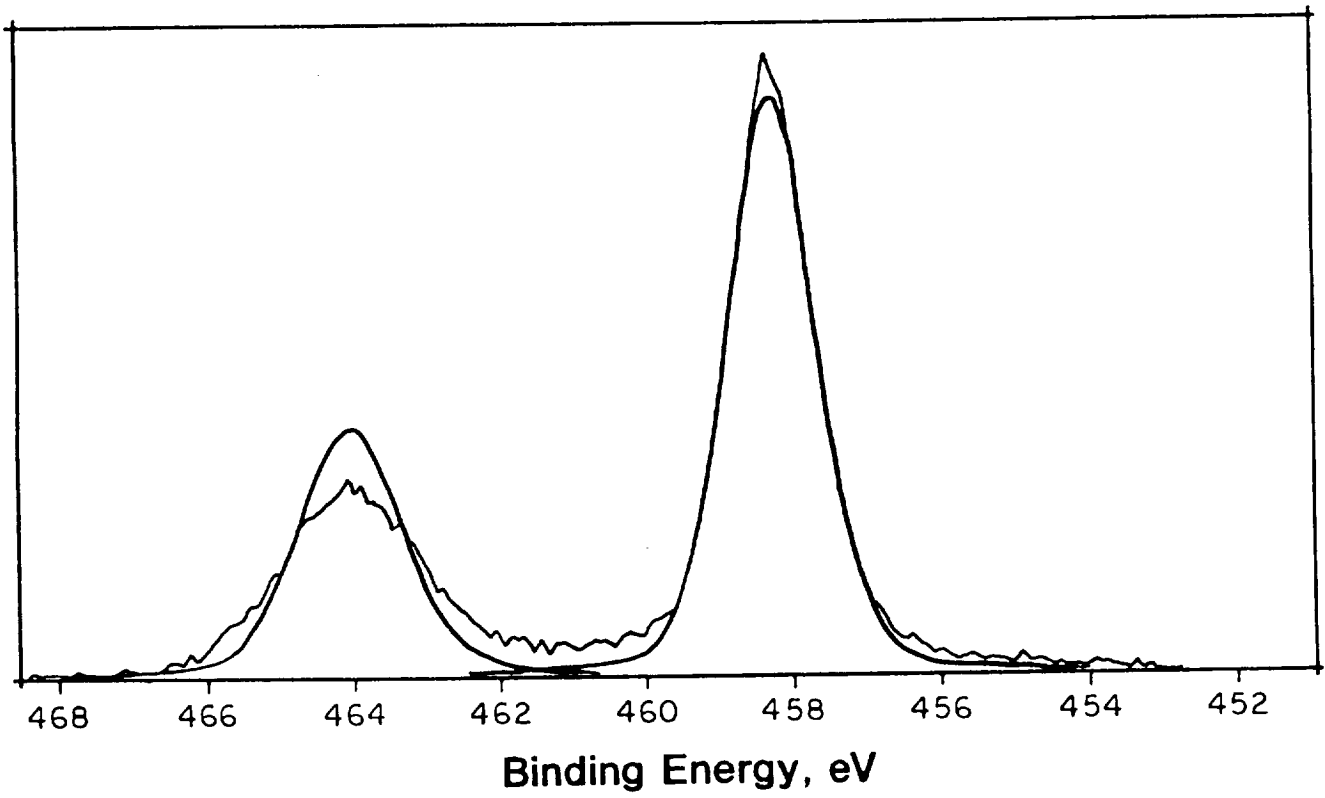Figure 11. Cerium 3d ESCA spectrum of the Hughes Pt/Ce/TiO$_2$ catalyst.

Figure 12. Titanium 2p ESCA spectrum of the Hughes Pt/Ce/TiO$_2$ catalyst.

ALTERNATIVE CATALYSTS FOR LOW-TEMPERATURE CO OXIDATION

Steven D. Gardner and Gar B. Hoflund
Department of Chemical Engineering
University of Florida
Gainesville, FL

David R. Schryer, Jacqueline Schryer, Billy T. Upchurch and David R. Brown*
NASA Langley Research Center
Hampton, VA

ABSTRACT

MnO_x, Ag/MnO_x, Au/MnO_x, Cu/MnO_x, Pd/MnO_x, Pt/MnO_x, Ru/MnO_x, Au/CeO_x and Au/Fe_2O_3 were synthesized and tested for CO oxidation activity in low concentrations of stoichiometric CO and O_2 at 30-75°C. Catalytic activity was measured for periods as long as 18000 minutes. At 75° Au/MnO_x is most active sustaining nearly 100% CO conversion for 10000 minutes. It also retains high activity at 50 and 30°C with negligible decay in activity. A direct comparison between an unpretreated 10% Au/MnO_x catalyst and an optimized 19.5% Pt/SnO_2 (pretreated) catalyst shows that the Au/MnO_x catalyst exhibits much higher catalytic activity and far superior decay characteristics. Other catalysts including Au/CeO_x and Au/Fe_2O_3 also perform well. The Cu/MnO_x exhibits a high initial activity which decays rapidly. After the decay period the activity remains very stable making Cu/MnO_x a potential candidate for long-term applications such as CO_2 lasers in space.

INTRODUCTION

The catalytic oxidation of carbon monoxide near ambient temperatures has important applications. Closed-cycle CO_2 lasers produce CO and O_2 in the laser discharge resulting in a rapid loss of output power. This problem can be overcome by incorporating a low-temperature CO oxidation catalyst into the laser system which converts the dissociated products back into CO_2 (1-3). Also, air filtration devices often contain catalysts to oxidize dangerous levels of toxic CO. Such devices are utilized in fire safety equipment and in underground mines as respiratory aids.

Consequently, the development of low-temperature CO oxidation catalysts has received considerable attention (1-19). Although significant progress has been made with regard to understanding the reaction mechanism (6,7,10,13), there remains a need for development of catalysts which exhibit higher activities for prolonged periods at low temperatures (typically less than 100°C) and in the diverse range of oxidation environments which are encountered. Factors which determine oxygen availability and gaseous impurities often have a pronounced effect on catalyst performance. CO oxidation in ambient air has the advantages of excess O_2 and low CO_2 concentrations which facilitate the reaction considerably. Consequently, numerous materials are known to oxidize CO in excess O_2 at low temperatures (4,5,14-17), but complications due to presence of humidity and/or air pollutants are often detrimental to their activity. In CO_2 lasers, CO and O_2 are present in small stoichiometric quantities in a large amount of CO_2. Although the catalytic reaction benefits from the fact that the lasers usually operate at temperatures somewhat above ambient (25-100°C), catalytic CO oxidation is difficult under these conditions.

*Now Erik J. Kielin

123

Recently, Haruta and coworkers prepared supported-gold catalysts on various base-metal oxides including MnO_x, Fe_2O_3, CO_3O_4, NiO and CuO and determined their catalytic activities toward the oxidation of H_2 and/or CO (18,19). Most of the CO oxidation runs were carried out using 1 volume % CO in dry air. At $0°C$ Au/Fe_2O_3 and Au/NiO maintain essentially 100% CO conversion under the flow conditions used over a 7-day test period. Similar performance was also observed for Au/Fe_2O_3 and Au/CO_3O_4 at $30°C$ in 76% relative humidity. Therefore, these catalysts appear to be quite useful in air purification devices, but activities in the presence of air contaminants were not determined. These catalysts may be useful in CO_2 lasers even though the reaction conditions are quite different as described above. It is interesting to note that Haruta and coworkers apparently did not examine the behavior of Au/MnO_x toward CO oxidation.

Catalysts consisting of Pt and/or Pd supported on tin oxide have been researched extensively for use in CO_2 lasers (1-13). Although these materials can exhibit considerable CO oxidation activity in this application, there are complications which must be overcome. Acceptable activity is observed only after the catalyst undergoes a reductive pretreatment. Unfortunately, such pretreatments often lead to considerable induction periods often lasting several days during which the observed activity declines before reaching a maximum (7). Even after acceptable activity is recovered these materials exhibit a steady decay in performance over time. Efforts to understand and correct these problems continue (6-10).

The purpose of the present study is to explore the behavior of materials other than platinized tin oxide as catalysts for low-temperature CO oxidation particularly with regard to CO_2 laser applications. Several materials were synthesized and screened for CO oxidation activity using small concentrations of stoichiometric CO and O_2 in He and temperatures between 30 and $75°C$. The tests were run for periods as long as 18000 minutes in order to observe the induction and decay characteristics of the catalysts.

CATALYSTS PREPARATION

A review of the literature provided a basis for selection of support materials examined in this study which include iron oxide (Fe_2O_3), nonstoichiometric manganese oxides (MnO_x), and ceria (CeO_x) where x is between 1.5 and 2. The materials investigated were synthesized using established impregnation and coprecipitation techniques (20). The samples prepared include MnO_x, Pt/MnO_x, Ag/MnO_x, Pd/MnO_x, CuO/MnO_x, Au/MnO_x, Au/CeO_x and Au/Fe_2O_3.

The MnO_x was used as received from the Kerr-McGee Company, U.S.A. It was prepared by the electrolytic oxidation of manganous sulfate and has a B.E.T. surface area of 74 m^2/g. The MnO_x served as a sample itself as well as an impregnation support for other materials.

Two Pt/MnO_x samples (0.2 wt% Pt) were prepared by impregnation of MnO_x using an aqueous solution of $Na_2Pt(OH)_6$. Sample #1 was dried in air at $280°C$ for 4.5 hours while sample #2 was dried in air at $75°C$ for 3 hours. Pd/MnO_x (0.2 wt% Pd) was prepared by impregnating MnO_x with an aqueous solution of $PdCl_2$. The product was dried in air at $280°C$ for 4.5 hours.

A sample which contained admixtures of CuO and MnO_x was prepared from the products of several procedures. Procedure A involved coprecipitation from aqueous solutions of $CuSO_4$ + sucrose and $KMnO_4$. The precipitate was washed with water and dried in air at 105°C for 15 hours. The Cu:Mn molar ratio was approximately 1.4. In procedure B the former product was dried in air at 280°C for 2 hours. In procedure C MnO_x was precipitated from aqueous solutions of sucrose and $KMnO_4$. The precipitate was washed and dried as outlined in procedure A. The final product consisted of an admixture of 0.4 grams from procedure A, 0.7 grams from procedure B, 0.3 grams from procedure C and 0.2 grams of commercial CuO powder.

A technique in which $Mn(OH)_2$ was precipitated in the presence of ultrafine Ru powder was utilized to prepare a 2 wt% Ru/MnO_x sample. A solution of $Mn(NO_3)_2$ was added dropwise to a stirred mixture of Ru powder in NH_4OH. The resulting product was dried and calcined at 400°C for 2 hours.

Four supported Au samples were synthesized via coprecipitation from aqueous $HAuCl_4$ and the nitrate of the corresponding support metal. The composition of the materials is approximately 5 at% Au/MnO_x, 10 at% Au/MnO_x, 20 at% Au/CeO_x and 5 at% Au/Fe_2O_3 on a Au/metal basis. In each case the appropriate precursor solutions were added dropwise to a stirred solution of sodium carbonate at room temperature. After washing and drying the precipitates were calcined in air at 400°C for 4 hours. Two Au/Fe_2O_3 samples were prepared which differed only in the temperature of the wash water utilized (25°C and 80°C).

EXPERIMENTAL

The reactor used to test the CO oxidation activity of the catalysts has been described previously (11). Screening of catalysts for CO oxidation has typically been carried out using a test gas consisting of a few percent CO in air (excess oxygen), but the catalytic behavior under stoichiometric CO and O_2 and in the presence of CO_2 has not been determined. Since the catalytic behavior can vary considerably under different environments as described above, it is necessary to perform such experiments. Except for the data shown in figure 9, all tests were conducted using 0.15 grams of catalyst and a reaction gas mixture of 1% CO, 0.5% O_2 and 2% Ne in helium at a pressure of 1 atm. flowing at 10 sccm. The reaction temperatures investigated were 75, 50 and 30°C as noted. The conversions are quite high under these conditions which correspond to operating the reactor in an integral mode.

In most cases the catalysts were tested as prepared without additional pretreatments. Unless noted otherwise, each catalyst was loaded in the reactor and exposed to flowing helium for about one hour as the reaction temperature stabilized. Then the helium flow was changed to the reaction gas mixture and product sampling was begun. At predetermined time intervals, an automated sampling valve directed a small fraction of the reaction products to a gas chromatograph for analysis of %CO_2 yield, %CO loss and %O_2 loss, and the results were plotted versus time.

RESULTS AND DISCUSSION

During these initial activity screening experiments, emphasis is placed upon characteristics of the overall CO oxidation activity curves with respect

to temperature and time. An appropriate catalyst for use in CO_2 lasers must not only exhibit high activity at low temperatures (25-100°C) but also maintain acceptable activity over a lifetime of up to 3 years. Since a catalyst cannot be practically tested for a 3-year lifetime, its activity profile must be extrapolated with reasonable confidence. Nevertheless, it is necessary to exercise caution when evaluating potential catalysts for CO_2 lasers because a catalyst which exhibits the best activity initially might succumb to decay mechanisms which render it inferior after extended use. Consequently, a catalyst exhibiting only marginal activity intially may become the optimal choice if the corresponding activity decay remains negligible.

CO oxidation activity curves for several MnO_x-based catalysts appear in figure 1. Initially, MnO_x and Cu/MnO_x exhibit the highest CO oxidation activities although their performance rapidly deteriorates. However, after about 2000 minutes the reaction curve for Cu/MnO_x appears to approach a steady-state conversion with negligible activity decay. MnO_x may approach a more active steady-state conversion but more extensive testing is required to be certain. Even though the Pt/MnO_x #1 and Ag/MnO_x samples display superior activity throughout most of the test period, extrapolation of the data in figure 1 indicate that Cu/MnO_x may be the optimal catalyst in a long-term run.

Figure 1 also depicts an interesting comparison between the catalytic activities of Pt/MnO_x #1 (dried for 4.5 hours at 280°C) and Pt/MnO_x #2 (dried for 3 hours at 75°C). The poor activity exhibited by Pt/MnO_x #2 may be the result of incomplete removal of surface impurities (such as Na, Cl or OH) associated with the impregnation step. However, as found in previous studies of MnO_2 and MnO_2-CuO catalysts (21-23), the inactivity is most likely the result of incomplete surface activation. MnO_x-based catalysts usually require heating between 100-200°C in air or oxygen to produce an active surface. The heat treatments apparently activate the surface through the creation of reactive sites via partial surface reduction depletion of adsorbed water or surface hydroxyl groups, and/or concurrent micropore generation.

An interesting observation is that the reaction profiles of Pt/MnO_x #1 and Ag/MnO_x are remarkably similar. This is unexpected based on the different catalytic properties of Pt and Ag. It is possible that this behavior results primarily from exposure of MnO_x to similar basic solutions followed by drying in air at 280°C for 4.5 hours. The activity curve for pure MnO_x (as-received and common to both samples) is quite different in character, which is consistent with this hypothesis. Nevertheless, both materials performed well during the 10000-minute test period oxidizing 70-80% of available CO at 75°C.

As mentioned above Pt/SnO_2 catalysts have received considerable attention for use in CO_2 lasers. Figure 2 shows a comparison of CO oxidation performance between the Pt/MnO_x #1 sample (see figure 1) and a commercial Pt/SnO_2 catalyst manufactured by Engelhard Industries. At 75°C the Pt/MnO_x #1 sample exhibits superior activity after approximately 2500 minutes of reaction. Due to the limited reaction data for Pt/SnO_2, further comparisons require data extrapolation. Pt/MnO_x #1 represents the optimal catalyst over an extended time period assuming that the indicated trends continue. This also is true for Ag/MnO_x which behaves identically to Pt/MnO_x #1.

Figure 2 represents a valid comparison because the sample size and experimental parameters used were identical in both tests. It should be noted,

126

however, that the Pt/SnO_2 was pretreated in a 5% CO/He stream at 225°C for 1 hour prior to activity testing. Such reductive pretreatments significantly enhance the performance of Pt/SnO_2 catalysts (7). A surface characterization study of the changes induced during pretreatment of the Engelhard catalyst has been carried out by Drawdy et al. (10). The fact that no pretreatments were used for the MnO_x-based catalysts is an advantage. Furthermore, since the precious metal loading for the Pt/MnO_x #1 and Ag/MnO_x samples is only 0.2 wt% (compared with 2 wt% for the Pt/SnO_2 catalyst), there also appears to be an economic advantage over the Engelhard catalyst. Of course, the Ag/MnO_x catalyst is the least costly.

The fact that reductive pretreatments activate Pt/SnO_2 catalysts provided motivation to investigate the effects of similar pretreatments on Pt/MnO_x catalysts. Two pretreatment conditions were used in which the Pt/MnO_x #1 sample was exposed to 5% CO/He for 1 hour at 125 and 225°C. The effects on catalytic performance are shown in figure 3. It is clear that the pretreatments are detrimental to the CO oxidation activity of Pt/MnO_x. In fact, the observed activity of Pt/MnO_x decreases with increasing pretreatment temperature; a trend opposite to that which is observed for Pt/SnO_2 catalysts (7). A possible explanation may involve the reducibility of the MnO_x and SnO_2 supports. It appears that catalysts based upon these materials require a certain degree of surface reduction for optimal activity. There is evidence that a completely dehydroxylated or an entirely oxygenated MnO_x surface is not active toward low-temperature CO oxidation (21,22). Similarly, surface hydroxyl groups are believed to be instrumental in the CO oxidation mechanism over Pt/SnO_2 (7-10). Given the relative instability of MnO_x with respect to SnO_2, such an optimum degree of surface reduction most likely results from milder pretreatments than those used to generate the data shown in figure 3. In fact, heat treatments in air or oxygen appear to be more beneficial for MnO_x CO oxidation catalysts (21,22,24-26). Although the CO reductive pretreatments at 125 and 225°C are appropriate for Pt/SnO_2, they apparently are too severe for Pt/MnO_x.

Additional insight on the pretreatment effects may be gained by considering the initial reaction characteristics with regard to CO_2 production, CO loss and O_2 loss (determined by GC analysis). These data are shown in figures 4, 5 and 6 for Pt/MnO_x catalysts which were not pretreated, pretreated at 125°C and pretreated at 255°C respectively. For unpretreated Pt/MnO_x #1, figure 4 shows that a considerable amount of catalyst surface oxygen is utilized in CO_2 formation during the early stages of reaction because the O_2 loss is much lower than the CO_2 production. The participation of catalyst oxygen during CO oxidation has been observed for MnO_x catalysts previously (14,25-27). After a 125°C CO pretreatment, the catalyst activity is decreased, and this decrease is accompanied by a decrease in the utilization of catalyst oxygen as shown in figure 5. Since the curves now nearly coincide, the early stages of CO oxidation on this pretreated surface appears catalytic in nature with only gas-phase oxygen being utilized. The data of figure 6 obtained after pretreating in CO at 225°C indicate essentially opposite behavior to that shown in figure 4. That is, the surface appears to have been reduced to a point where gas-phase oxygen is utilized not only in CO_2 formation but in catalyst regeneration as well. Even though the catalyst surface acquires excess oxygen from the gas phase, this fresh surface oxygen does not appear to participate in the reaction or restore the catalytic activity which was lost during the pretreatment.

A consistent interpretation of the data in figures 4-6 may be realized by invoking a surface REDOX mechanism for CO oxidation. The active surface in figure 4 appears to reach a situation wherein both surface and gas-phase oxygen participate in the reaction. The active surface is partially reduced after the first 30 minutes of reaction, and the extent of reduction depends upon the relative rates of surface reduction by CO and reoxidation by gas-phase O_2. During the CO pretreatments, the surface can be reduced to such an extent that catalyst oxygen is not available for reaction. Therefore, the resulting surfaces are not as active toward CO oxidation. These data suggest that it might be possible to determine optimal pretreatment conditions and that these optimal conditions would be less severe than the ones used in this study. The exact form(s) of the active surface oxygen species remains to be determined.

Figure 7 shows the CO oxidation performance of Au/CeO_x, Au/Fe_2O_3 #1 and Au/Fe_2O_3 #2 at 75, 50 and 30°C. Several important features appear in these activity curves. The Au/CeO_x exhibits very high activity at 75°C oxidizing greater than 80% of the available CO. Also, the reaction profile exhibits negligible decay over 10000 minutes. This represents a significant improvement over the performance of Pt/MnO_x #1 and Ag/MnO_x shown in figure 1. At 50°C Au/CeO_x continues to perform well maintaining a 43% CO_2 yield.

Figure 7 also provides an interesting comparison between Au/Fe_2O_3 #1 (washed with hot water) and Au/Fe_2O_3 #2 (washed with cold water). The activity of Au/Fe_2O_3 #1 is clearly superior although some decay in performance is evident. Surface Cl is generally believed to inhibit low-temperature CO oxidation. Therefore, the difference in activity of the two samples may be attributable to poisoning by surface chlorine (originating from the gold precursor $HAuCl_4$) which is not as effectively removed by washing with cold water compared to hot water. Nevertheless, it is interesting to note that the activity of Au/Fe_2O_3 #2 steadily increases with time (negative or inverse decay). This behavior may be a consequence of some surface process which removes the surface Cl as the reaction proceeds.

It is interesting to compare the performance of Au/Fe_2O_3 #2 with that of a Au/Fe_2O_3 catalyst investigated by Haruta et al. (18,19). They observed that Au/Fe_2O_3 is essentially 100% efficient in oxidizing 1% CO in air even below 0°C. The lower activities found in this study apparently are due to the difficulties involved in oxidizing CO in a stoichiometric mixture as described above.

CO oxidation activity curves for a second set of MnO_x-based materials appear in figure 8. The data indicate that Au/MnO_x is clearly the most active catalyst examined in this study. At 75°C, Au/MnO_x sustains nearly 100% CO_2 yield over a 10000 minute period, and excellent activity is also observed at 50 and 30°C. At all temperatures the activity profiles are exceptional in that they exhibit negligible decay over the entire test period.

Figure 8 also shows the activity curves for two Ag/MnO_x samples (0.2 wt% and 1.0 wt% Ag). As stated above, the two samples were prepared in a similar manner differing only in Ag content. The data indicate that small Ag loadings result in better catalytic behavior. Both reaction profiles are similar up to 1000 minutes of reaction after which the 1 wt% Ag/MnO_x sample exhibits accelerated decay in activity.

Although Pd/MnO_x and Ru/MnO_x are the least active catalysts according to the data in figure 8, significant conversions are nevertheless observed. However, both these two materials and the others used in this study probably would be improved by optimizing preparation and pretreatment techniques. Such optimization studies will be carried out for the more promising catalysts particularly Au/MnO_x.

Most of the effort related to developing a low-temperature CO oxidation catalyst thus far has been expended on platinized tin oxide systems. Therefore, it is important to compare the behavior of the Au/MnO_x and Pt/SnO_2 catalysts. This comparison is shown in figure 9 for an optimized 19.5% Pt/SnO_2 catalyst and a 10% Au/MnO_x catalyst using 0.1 g of each and a flow rate of 10 sccm at about 50°C. The Pt/SnO_2 catalyst was optimally pretreated, and the Au/MnO_x catalyst was not pretreated. The optimized Pt/SnO_2 catalyst is nearly twice as active as the Engelhard Pt/SnO_2 catalyst. As observed in figure 9, the activity of the Pt/SnO_2 catalyst is high initially but rapidly drops to about 42% and then continues to decline slowly. Outgassing results in the catalyst regaining its initial high activity followed by a rapid loss in activity to value of about 35% with continuing decline in activity. The activity of the Au/MnO_x catalyst is initially about 78%. It rises rapidly to almost 90% and then remains constant over the duration of the test. Outgassing has little effect on the activity of the Au/MnO_x catalyst. This direct comparison demonstrates that the Au/MnO_x catalyst is vastly superior to the optimized Pt/SnO_2 catalyst with respect to both catalytic activity and decay characteristics. Furthermore, the Au/MnO_x catalyst is much less costly than the Pt/SnO_2 catalyst because about half the amount of Au is required per unit weight of catalyst, Au costs about three-fourths as much as Pt, and the activity of Au/MnO_x is more than twice that of Pt/SnO_2 so less than half the total weight of the Au/MnO_x catalyst would be required for a given application. The fact that no pretreatment is required for the Au/MnO_x catalyst is also a significant advantage with regard to laser applications. Taking all of these considerations into account, there is no justification for further development of platinized tin oxide systems for low-temperature CO oxidation applications. Efforts are continuing by Hoflund, Gardner, Schryer and Upchurch to support the Au/MnO_x catalysts on monolith supports, test these monolith supported catalysts, and characterize the Au/MnO_x catalysts.

SUMMARY

Selected materials have been prepared and tested as low-temperature CO oxidation catalysts for long-term use in CO_2 lasers. The materials were prepared utilizing impregnation and coprecipitation techniques and include MnO_x, Pt/MnO_x, Ag/MnO_x, Pd/MnO_x, Cu/MnO_x, Ru/MnO_x, Au/MnO_x, Au/CeO_x and Au/Fe_2O_3. Each was tested for CO oxidation activity in low concentrations of stoichiometric CO and O_2 at temperatures between 30 and 75°C. Although most of the materials exhibit significant CO oxidation activity, Au/MnO_x is exceptionally active. At 75°C, Au/MnO_x sustains nearly 100% CO_2 yield for 10000 minutes with no evidence of activity decay under the test conditions used. Exceptional activities are also observed at 50 and 30°C. Many of the catalysts tested perform better than a platinized tin oxide catalyst either with regard to activity, decay characteristics or both. For example, Cu/MnO_x has a lower activity than several of the catalysts tested, but it shows negligible decay making it a potential candidate for long-term performance. Pt/MnO_x #1 and Ag/MnO_x exhibit similar and higher activities but decay more rapidly than

Cu/MnO_x and less rapidly than the commercially available platinized tin oxide. Pretreatment in CO at 125 and 225°C decreases the activity. Optimization studies of preparative and pretreatment variables need to be performed in order to further increase the performance of low-temperature CO oxidation catalysts.

A direct comparison between the catalytic behavior of a Au/MnO_x catalyst and an optimized Pt/SnO_2 catalyst has been carried out. The performance of the Au/MnO_x catalyst is vastly superior to that of the Pt/SnO_2 catalyst with regard to both activity and decay characteristics. Combined with the facts that the Au/MnO_x catalyst requires no pretreatment and is less costly than Pt/SnO_2 catalysts, it appears that the Au/MnO_x catalyst is the appropriate choice for CO_2 laser applications.
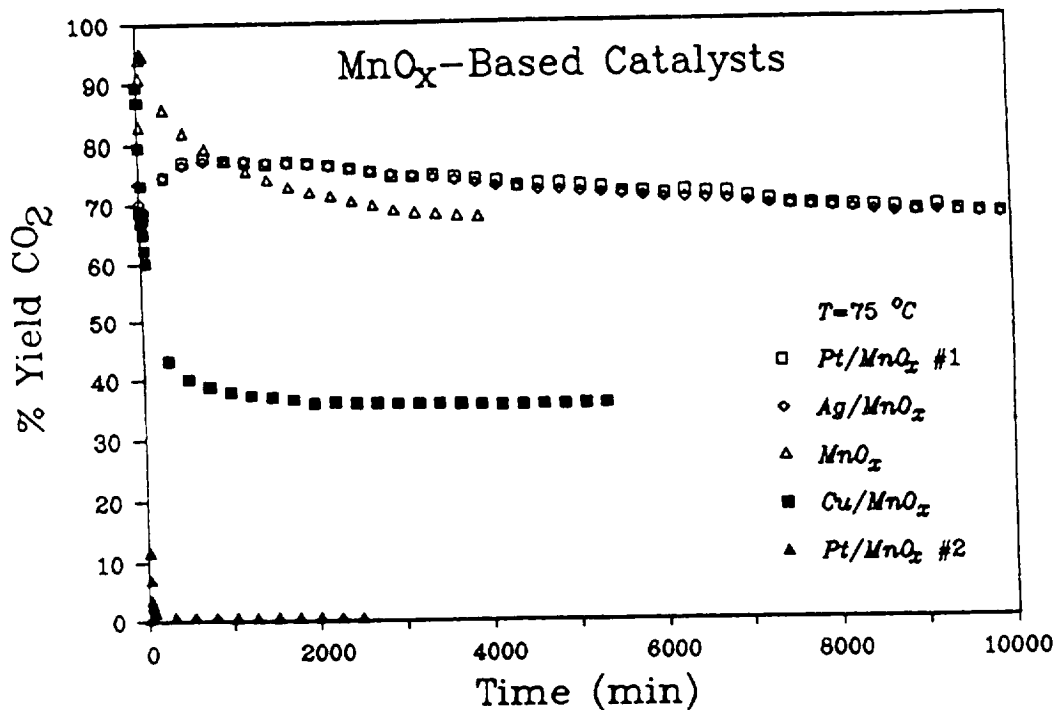
Figure 1. CO oxidation activity of 0.2 wt% Pt/MnO$_x$ #1, 0.2 wt% Ag/MnO$_x$, MnO$_x$, 60 at% Cu/MnO$_x$ and 0.2 wt% Pt/MnO$_x$ #2 at 75°C as a function of time.
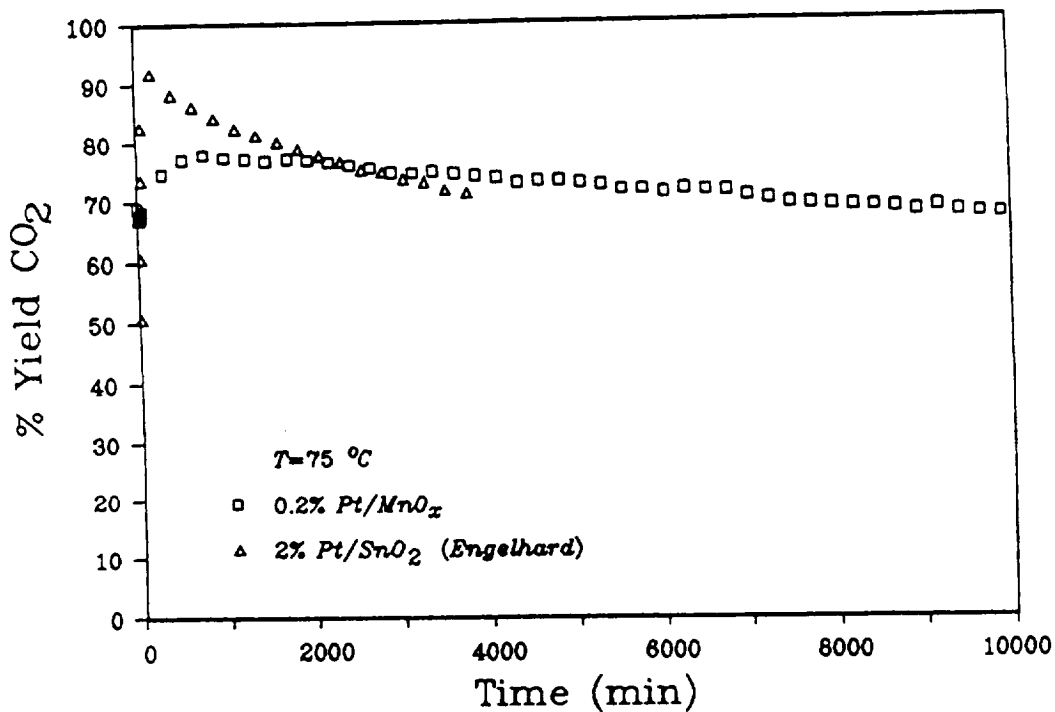
Figure 2. Comparison of CO oxidation activity between 0.2 wt% Pt/MnO$_x$ #1 and a commercial 2 wt% Pt/SnO$_2$ catalyst at 75°C.
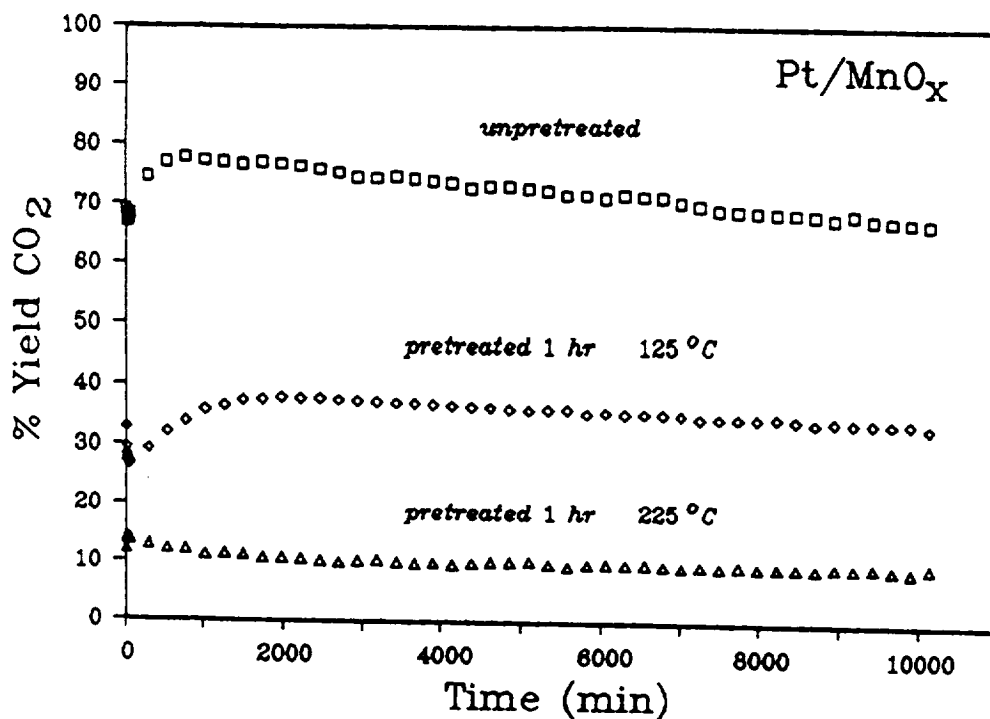
Figure 3. Effect of pretreatment at 125 and 225°C in 5% CO/He for 0.2 wt% Pt/MnO$_x$ #1 on catalytic CO oxidation at 75°C.
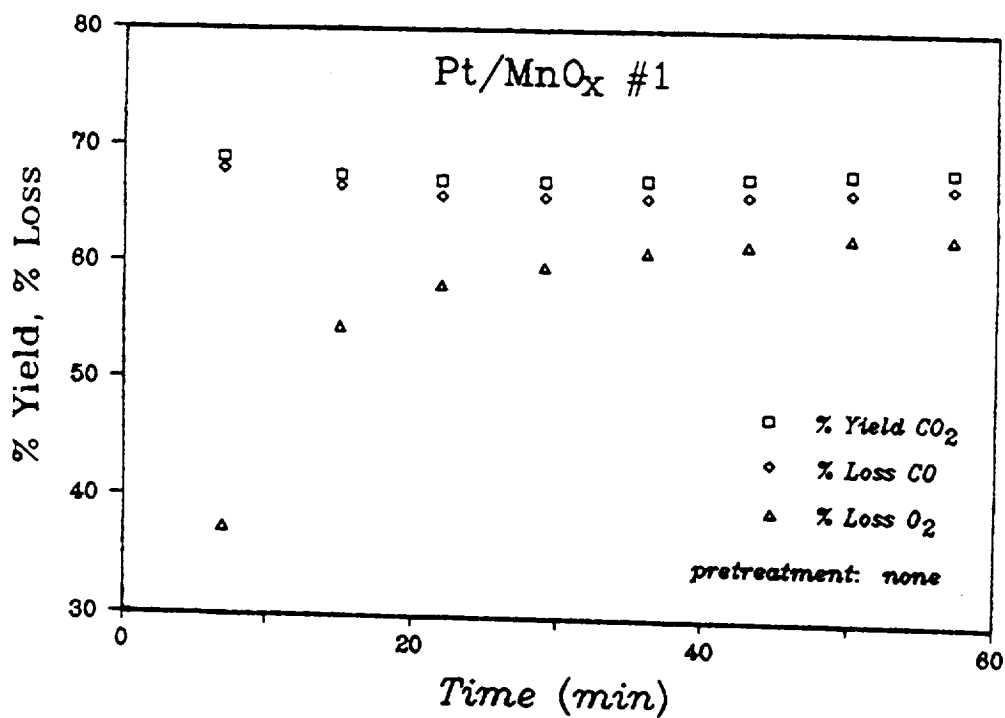
Figure 4. % CO$_2$ yield with corresponding % loss CO and O$_2$ for unpretreated 0.2 wt% Pt/MnO$_x$ #1 (75°C reaction temperature).
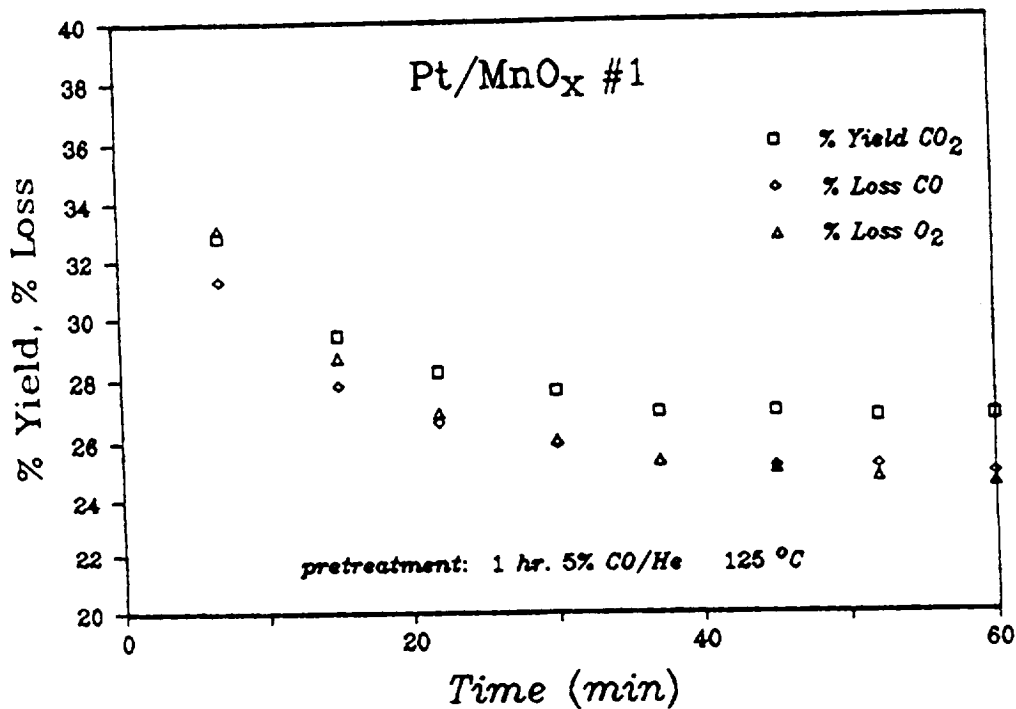
Figure 5. % CO_2 yield with corresponding % loss CO and O_2 for 0.2 wt% Pt/MnO$_x$ #1 pretreated in 5% CO/He for 1 hour at 125°C (75°C reaction temperature).
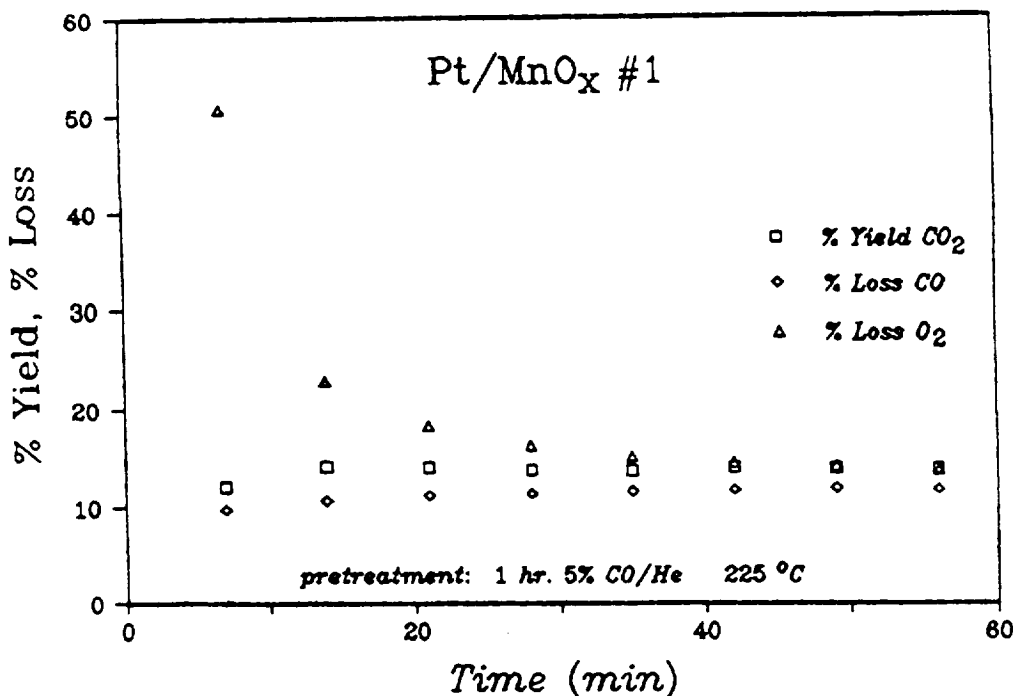
Figure 6. % CO_2 yield with corresponding % loss CO and O_2 for 0.2 wt% Pt/MnO$_x$ #1 pretreated in 5% CO/He for 1 hour at 225°C (75°C reaction temperature).
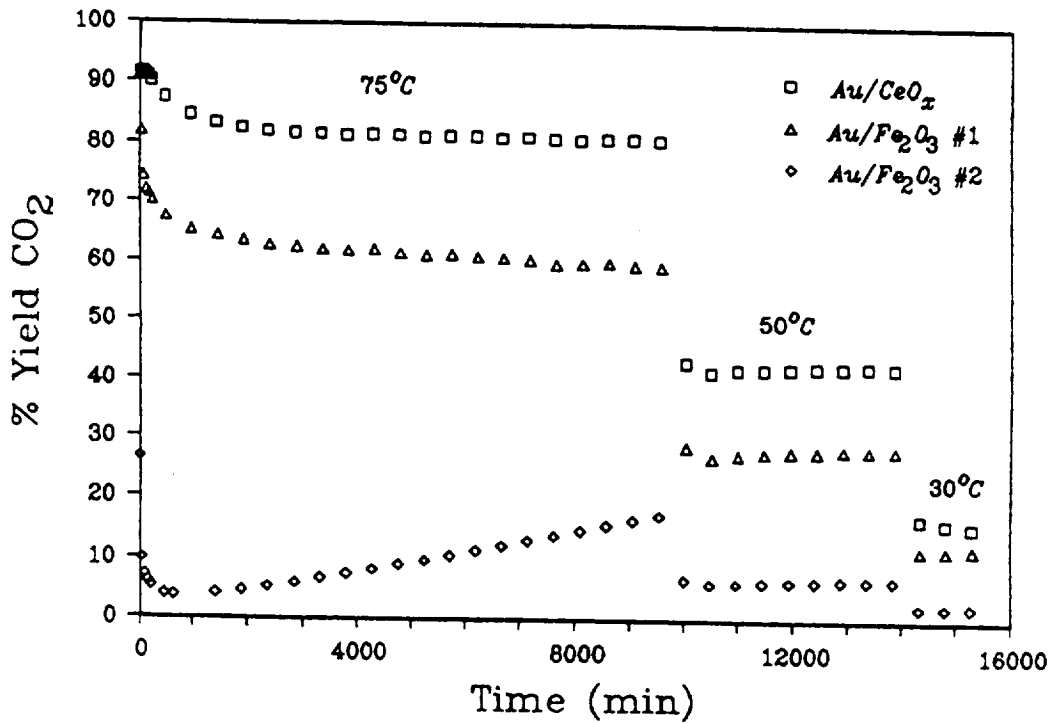
Figure 7. CO oxidation activity of 20 at% Au/CeO$_x$, 5 at% Au/Fe$_2$O$_3$ #1 and 5 at% Au/Fe$_2$O$_3$ #2 at 75, 50 and 30°C as a function of time.
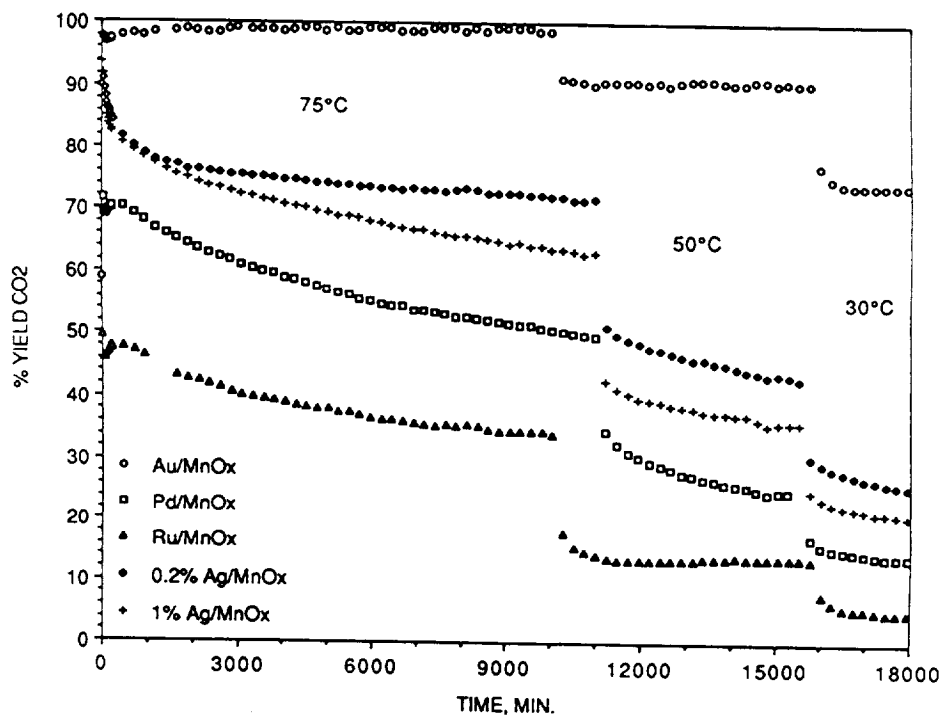
Figure 8. CO oxidation activity of 5 at% Au/MnO$_x$, 0.2 wt% Pd/MnO$_x$, 2 wt% Ru/MnO$_x$, 0.2 wt% Ag/MnO$_x$ and 1.0 wt% Ag/MnO$_x$ at 75, 50 and 30°C as a function of time.

Activity Comparison of Pt/SnO_2 and Au/MnO_x
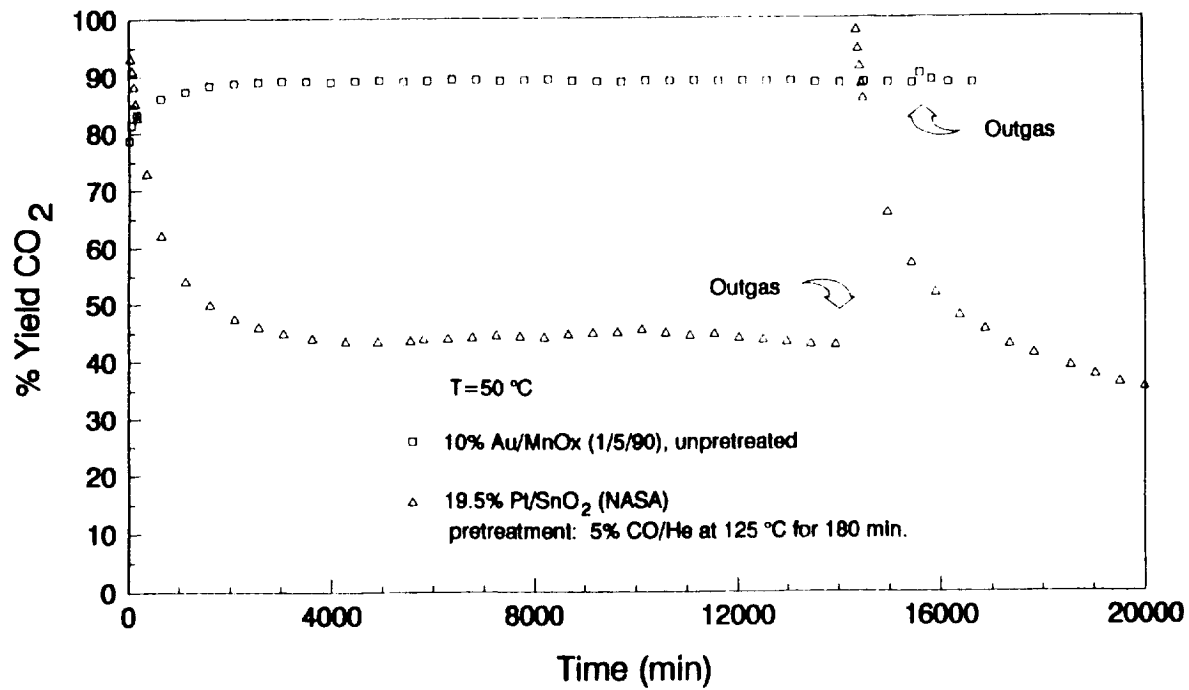
Figure 9.   Activity comparison of Pt/SnO_2 and Au/MnO_x.

REFERENCES

1. "Closed-Cycle, Frequency-Stable CO_2 Laser Technology, Proceedings of a workshop help at NASA Langley Research Center, Hampton, VA, June 10-12, 1986," C.E. Batten, I.M. Miller and G.M. Wood, Jr., eds., NASA Conference Publication #2456.

2. D.S. Stark, A. Crocker and G.J. Steward, "A sealed 100-Hz CO_2 laser using high CO_2 concentrations and ambient temperature catalysis," J. Phys. E: Sci. Instrum. 16, 158-161 (1983).

3. D.S. Stark and M.R. Harris, "Catalysed recombination of CO and O_2 in sealed CO_2 TEA laser gases at temperatures down to -27°C," J. Phys. E: Sci. Instrum. 16, 492-496 (1983).

4. G.C. Bond, L.R. Molloy and M.J. Fuller, "Oxidation of Carbon Monoxide over Palladium-Tin(IV) Oxide Catalysts: An Example of Spillover Catalysis," J.C.S. Chem. Comm. 796-797 (1975).

5. G. Croft and M.J. Fuller, "Water-promoted oxidation of carbon monoxide over tin(IV) oxide-supported palladium," Nature 269, 585-586 (1977).

6. S.D. Gardner, G.B. Hoflund, M.R. Davidson and D.R. Schryer, "Evidence of Alloy Formation during Reduction of Platinized Tin Oxide Surfaces," J. Catal. 115, 132-137 (1989).

7. D.R. Schryer, B.T. Upchurch, J.D. Van Norman, K.G. Brown and J. Schryer, J. Catal. 122(1990)193.

8. B.D. Sidney, D.R. Schryer, B.T. Upchurch, R.V. Hess, G.M. Wood, I.M. Miller, L.G. Burney, K.G. Brown, J.D. Van Norman and J. Schryer, "Research on catalysts for long-life closed-cycle CO_2 laser operation," SPIE Proceedings, Vol. 783, p. 162, 1987.

9. S.D. Gardner, G.B. Hoflund, D.R. Schryer and B.T. Upchurch, "Platinized tin oxide catalysts for CO_2 lasers: effects of pretreatment," SPIE Proceedings, Vol. 1062, p. 21, 1989.

10. J.E. Drawdy, G.B. Hoflund, S.D. Gardner, E. Yngvadottir and D.R. Schryer, "Effect of Pretreatment on a Platinized Tin Oxide Catalyst used for Low-Temperature CO Oxidation," Surface and Interface Analysis 00, 00 (1990).

11. B.T. Upchurch, D.R. Brown and I.M. Miller: LaRC-Developed Catalysts for CO_2 Lasers. CO Oxidation Catalysts for Long-Life CO_2 Lasers, NASA CP-3076, 1990. (Paper of this compilation)

12. C.F. Sampson and N.J. Gudde: The Oxidation of Carbon Monoxide using a Tin Oxide Catalyst. Closed-Clycle, Frequency-Stable CO_2 Laser Technology, NASA CP-2456, 1987.

13. D.R. Schryer, B.T. Upchurch, R.V. Hess, G.M. Wood, B.D. Sidney, J.D. Van Norman, I.M. Miller, K.G. Brown, J. Schryer, D.R. Brown, G.B. Hoflund and R.K. Herz: CO-Oxidation Catalysts for Long-Life Closed-Cycle CO_2

Lasers. CO Oxidation Catalysts for Long-Life CO_2 Lasers, NASA CP-3076, 1990. (Paper of this compilation)

14. M. Katz, "The Heterogeneous Oxidation of Carbon Dioxide," in Advances in Catalysis and Relation Subjects eds. W.G. Frankenburg, E.K. Rideal and V.I. Komarewsky, Academic Press, New York, 1953, vol. 5, p. 177.

15. S. Imamura, H. Sawada, K. Uemura and S. Ishida, "Oxidation of Carbon Monoxide Catalyzed by Manganese-Silver Composite Oxides," J. Catal. 109, 198-205 (1988).

16. S. Imamura, S. Yoshie and Y. Ono, "Effect of Samarium on the Thermal Stability and Activity of the Mn/Ag Catalyst in the Oxidation of CO," J. Catal. 115, 258-264 (1989).

17. M.J. Fuller and M.E. Warwick, "The Catalytic Oxidation of Carbon Monoxide on SnO_2 -CuO Gels," J. Catal. 34, 445-453 (1974).

18. M. Haruta, T. Kobayashi, H. Sano and N. Yamada, "Novel Gold Catalysts for the Oxidation of Carbon Monoxide at a Temperature far Below 0°C," Chem. Lett. 405-408 (1987).

19. M. Haruta, N. Yamada, T. Kobayashi and S. Iijima, "Gold Catalysts Prepared by Coprecipitation for Low-Temperature Oxidation of Hydrogen and of Carbon Monoxide," J. Catal. 115, 301-309 (1989).

20. F.G. Ciapetta and C.J. Plank, "Catalyst Preparation," in Catalysis, ed. P.H. Emmett, Reinhold Pub. Corp., New York, 1954, vol. I (Part 1), p. 35.

21. V. Dondur, S. Lampa and D. Vucelic, "Thermal Analysis of MnO_x-CuO Catalysts," J. Chem. Soc., Faraday Trans. 1 79, 1633-1638 (1983).

22. S. Kanungo, "Physicochemical Properties of MnO_2 and MnO_2-CuO and Their Relationship with the Catalytic Activity for H_2O_2 Decomposition and CO Oxidation," J. Catal. 58, 419-435 (1979).

23. J.A. Lee, C.E. Newnham, F.S. Stone and F.L. Tye, "Temperature Programmed Desorption Studies on gamma-Phase Manganese Dioxide in Static Water Vapor Environments," J. Colloid Interface Sci. 45(2), 289-294 (1973).

24. M. Kobayashi, H. Matsumoto and H. Kobayashi, "Distribution of Oxidation Power of Surface Oxygen Species on Manganese Dioxide during the Oxidation of Carbon Monoxide," J. Catal. 21, 48-55 (1971).

25. M. Kobayashi and H. Kobayashi, "Application of Transient Response Method to the Study of Heterogeneous Catalysts," J. Catal. 27, 100-107 (1972).

26. E.C. Pitzer and J.C.W. Frazer, "The Physical Chemistry of Hopcalite Catalysts," J. Phys. Chem. 45, 761-776 (1961).

27. M.I. Brittan, H. Bliss and C.A. Walker, "Kinetics of the Hopcalite-Catalyzed Oxidation of Carbon Monoxide," AIChE Journal 16(2), 305-314 (1970).

A Computer Program for the Design of Optimum
Catalytic Monoliths for CO$_2$ Lasers

K. Guinn, S. Goldblum, E. Noskowski, and R. Herz*
Chemical Engineering Group, Mail Code B-010
University of California, San Diego
La Jolla, California

INTRODUCTION

Pulsed CO$_2$ lasers have many applications in aeronautics, space research, weather monitoring and other areas. Full exploitation of the potential of these lasers is hampered by the dissociation of CO$_2$ that occurs during laser operation. The development of closed-cycle CO$_2$ lasers requires active CO-O$_2$ recombination (CO oxidation) catalysts and design methods for implementation of catalysts inside lasers. This paper will discuss the performance criteria and constraints involved in the design of catalyst configurations for use in a closed-cycle laser and will present several design studies performed with a computerized design program that we have written. Trade-offs between catalyst activity and dimensions, flow channel dimensions, pressure drop, O$_2$ conversion and other variables will be discussed.

A pulsed CO$_2$ laser produces useful laser light output when the laser gas volume is exposed to a high electrical potential for a period on the order of milliseconds [1,2]. Low lying vibrational-rotational energy level CO$_2$ molecules are excited to higher energy levels. The relaxation of the excited molecules to low lying energy levels produces infrared radiation ($\approx 10\mu$m). The energy deposited by the electrical discharge alters the composition of the gas mixture by dissociation of CO$_2$ into stoichiometric ratios of CO and O$_2$. In a high pulse repetition rate (PRR) CO$_2$ laser system, without a method of recombining the CO and O$_2$, the laser gas O$_2$ concentration would continue to increase with time. Depending on the particular system used, O$_2$ concentrations above a threshold level, on the order of 1%, severely degrade the laser output quality. The lasing process also raises the temperature of the laser gas volume. The output of the laser is sensitive to the temperature of the operating gas due to the effect of temperature on the distribution of CO$_2$ molecules among the rotational-vibrational energy levels.

An open-cycle laser system requires a continuous supply of fresh gas to maintain O$_2$ concentrations below threshold levels. The higher the PRR, the higher the fresh gas flow rate required to maintain acceptable O$_2$ concentrations. If rare isotope CO$_2$ gases [1,3], such as ^{12}C^{18}O$_2$, were to be used in an open-cycle laser system, the cost of supplying large quantities of CO$_2$ gases would be prohibitive. The safety requirements for handling and for the disposal of CO, O$_2$, and CO$_2$ gases is another concern for open-cycle systems. Clearly, for portable uses, such as in satellites or in the field, open-cycle system operation is not feasible.

*Author to whom correspondence should be addressed.

Closed-cycle systems can be envisioned to require a one time charge of the operating gas and to operate for a given number of pulses ($>10^7$) at a specified PRR and power output [4-7]. Portable closed-cycle systems would necessarily have power consumption constraints and, therefore, be limited in the output power and PRR. In a typical closed-cycle CO_2 laser system (Fig. 1), a gas mixture, comprised of CO_2 and other "inert" gases, is continuously recirculated through the system by a blower. The recombination of CO and O_2 is accomplished by the monolith catalyst section of the system (Fig. 2) and provides the laser section with a fresh supply of operating gas. The heat exchangers allow for the operation of the monolith catalyst section at elevated temperatures while maintaining moderate laser section temperatures. The monolith catalyst material is very porous (high surface area) and has catalytic material dispersed throughout. The performance of the monolith catalyst is measured by the section's ability to recombine CO and O_2, the size and weight of the monolith, and the pressure drop produced as a result of gas flow through the monolith. Monolith catalyst performance is dependent on a number of interrelated factors, such as the catalyst's geometry, convective heat and mass transport rates from the bulk gas to the catalyst, inlet gas properties, inlet molar gas flow rate, and catalytic activity. A monolith support is chosen over other supports, e.g. powders, beads, etc., because of the reduced level of particulate production, and the sturdiness of the monolith under high volumetric gas flow conditions.

MONOLITH CATALYST SECTION MODEL

A flexible model of the monolith catalyst may be developed to determine the bulk-average gas temperature, composition, and pressure along the length of the monolith. The adjustable parameters required to specify the operating condition of the monolith are listed in Table 1. The model assumptions, balance equations, and model results follow.
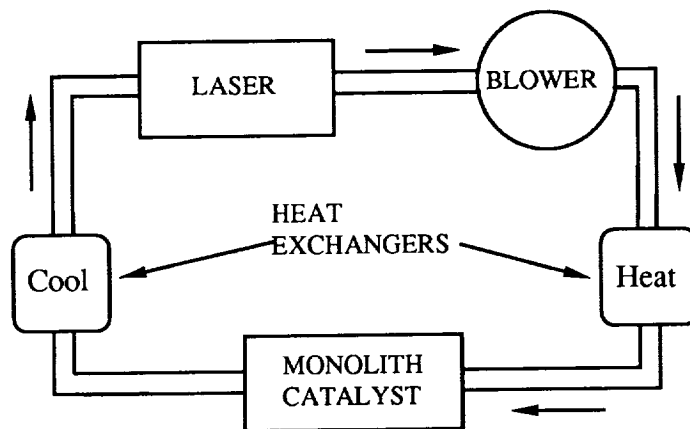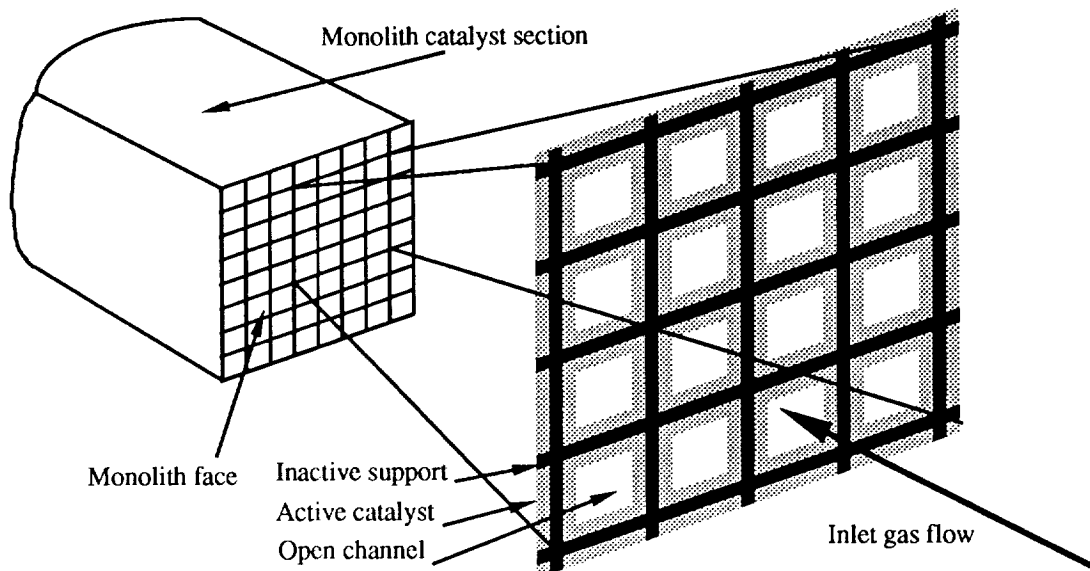

Figure 1. A typical closed-cycle CO_2 laser.

Figure 2. Monolith catalyst section.

Model Assumptions

- Steady state conditions.
- Identical conditions exist in each channel of the monolith.
- Channel gas flow is laminar and fully developed. The neglect of entrance effects for heat and mass transfer calculations provide for a conservative estimate of the amount of catalyst required. Pressure drop due to entrance and exit effects is neglected; therefore, the actual pressure drops will be somewhat greater than calculated.
- The kinetics of the reaction, $^1/_2O_2 + CO \rightarrow CO_2$, is first-order overall. That is, the reaction rate is $\propto [O_2]^a [CO]^b$, where the sum of a and b equals one. O_2 and CO_2 appear in stoichiometric ratios, $2:1 \equiv CO:O_2$. The concentration of O_2 is followed and the remaining species concentrations are calculated. The effect of temperature on the reaction rate is through an Arrhenius dependence of a reaction rate constant.
- Inlet gas composition, temperature and flow rate are known. Gas properties, viscosity, diffusivity, and thermal conductivity, are updated with changes in temperature, pressure, and reactant concentrations.
- Diffusivity in the porous catalytic layer is calculated using size and void fraction of micropores and macropores. Equimolar counterdiffusion in porous catalytic layer is assumed.
- Either adiabatic or isothermal monolith operating conditions can be selected by the operator. These two operating conditions provide the upper and lower bounds for oxygen conversion for a given inlet gas condition.
- Axial heat conduction in the porous catalytic layer and support is assumed to be negligible. For adiabatic monolith operation, transverse heat conduction in the porous catalytic layer and support is assumed to be such that the porous catalytic layer and support temperature are uniform transversely.

141

- Slab geometry is used for calculation of the species concentration in the porous catalytic layer. A characteristic porous catalytic layer thickness is calculated to account for porous catalytic material in the channel corners.
- Heat and mass transport between the flowing gas and the channel walls are described using the limiting Sherwood (Sh_∞) and Nusselt (Nu_∞) numbers for constant wall concentration and temperature boundary conditions in square channels [8].

Model balance equations

The steady state conservation equations for O_2 in the flowing gas and O_2 in the porous catalytic layer are

$$\frac{d\Phi_G}{d\zeta} = -\frac{\gamma}{\Gamma}\left[\Phi_G - \Phi_W\right] \quad , \text{ and } \quad \frac{d^2\Psi}{d\lambda^2} = \varphi^2\Psi \quad , \tag{1,2}$$

with initial and boundary conditions,

$$\Phi_G = 1 \text{ at } \zeta = 0 \quad , \quad \Psi = 1 \text{ at } \lambda = 0 \text{ for all } \zeta \quad , \text{ and } \quad \frac{d\Psi}{d\lambda} = 0 \text{ at } \lambda = 1 \quad . \tag{3,4,5}$$

Φ_G is the dimensionless bulk-average O_2 molar flow rate in the flowing gas. Variables and parameters are defined in detail in the notation list. Φ_W is the O_2 concentration at the channel wall times bulk-average volumetric flow rate divided by the inlet bulk-average O_2 molar flow rate. [$\Phi_G - \Phi_W$] is proportional to the concentration driving force for transport of O_2 from the flowing gas to the channel wall. ζ is the dimensionless distance down the length of the monolith. Ψ is the dimensionless O_2 concentration inside the porous catalytic layer at a dimensionless depth λ into the layer. The solution to Eqn. 2 yields an overall O_2 reaction rate in the porous catalytic layer as a function of Φ_W. At steady state, this reaction rate is equal to the rate of transport of O_2 from the flowing gas to the channel wall, and leads to

$$\Phi_W = \Phi_G\left[\frac{1}{\alpha + 1}\right] \quad . \tag{6}$$

The steady state energy balance on the flowing gas relates the rise in the dimensionless bulk-average temperature of the flowing gas, θ_G, to the heat transferred to the gas from the channel wall and yields

$$\frac{d\theta_G}{d\zeta} = -\left[\frac{d_h S St}{\Gamma}\right]\left[\theta_G - \theta_W\right] \quad , \text{ with initial condition, } \quad \theta_G = 1 \text{ at } \zeta = 0 \quad , \tag{7,8}$$

where θ_G is the dimensionless bulk-average temperature of the flowing gas, and θ_W is the dimensionless temperature at the channel wall. An energy balance on the porous catalytic layer equates the heat generation from the oxygen consumption reaction to the heat transferred from the porous catalytic layer and yields

142

$$- \left[\frac{\omega\,\alpha}{\Gamma}\right]\,\Phi_W = \left[\theta_G - \theta_W\right] \quad . \tag{9}$$

Combining the two energy balance equations, Eqns. 7 and 9, and substituting for Φ_W using Eqn. 6 results in two final differential equations to be integrated,

$$\frac{d\Phi_G}{d\zeta} = - \left[\frac{\Gamma}{\gamma} + \frac{\Gamma}{\alpha\gamma}\right]^{-1}\,\Phi_G \quad,\text{and}\quad \frac{d\theta_G}{d\zeta} = \frac{[d_h\,S\,\alpha\,\omega\,St]}{[\,1 + \alpha]\,\Gamma^2}\,\Phi_G \quad, \tag{10,11}$$

with the same initial conditions for Φ_G and θ_G as above. Pressure drop for the laminar flow is calculated using the Hagen-Poiseuille equation,

$$\frac{d\wp}{d\zeta} = \frac{-32}{Eu\,Re} \quad,\text{with an initial condition of}\quad \wp = 1 \quad\text{at}\quad \zeta = 0 \quad, \tag{12,13}$$

where $\wp$ is the dimensionless pressure. Eqns. 10-12 are coupled to each other through the variable Φ_G and the parameters α, ω, Γ, γ, St, Eu, and Re, each of which is a function of θ_G, Φ_G and $\wp$.

Model results

The adjustable parameters required to specify the monolith catalyst section operating conditions are listed below in Table 1. They are used to compute the dimensionless parameters α, ω, Γ, γ, St, Eu, and Re, and to integrate the dimensionless variables in Eqns. 10-12. A computer program was written to perform integration using the fourth-order Runge-Kutta method. The program allows θ_G, θ_W, Φ_G, Φ_W and $\wp$ to be determined as ζ varies from zero to the desired dimensionless monolith catalyst section length. The computer program requires readily available parameters to calculate parameters such as mass and heat transfer coefficients, bulk-gas and effective diffusion coefficients, and thermal conductivity. Results for a monolith catalyst section operating under conditions specified in Table 1 are shown in Figs. 3, 4 and 5.

Fig. 3 shows the behavior of θ, Φ, and $\wp$ as ζ varies from 0 to 100. $\theta_G \approx \theta_W$ and $\Phi_G \approx \Phi_W$; therefore, θ_G, θ_W, Φ_G, and Φ_W are not shown individually on this small scale plot. The behavior of θ, Φ, and $\wp$ can be explained using Eqns. 1-12, in which all parameters and variables are positive valued. The right side of equation (11) is positive, therefore, $d\theta_G/d\zeta > 0$. The left hand side of Eqn. 9 is negative, therefore, $\theta_W > \theta_G$. Similar examination of Eqns. 6 and 10 results in $d\Phi_G/d\zeta < 0$ and $\Phi_W > \Phi_G$. Eqn. 12 indicates that $d\wp/d\zeta < 0$. The drop in $\wp$ is negligible for the gas flow rate specified in Table 1. Pressure drop can be significant for higher gas flow rates.

Fig. 4 is an expansion of Fig. 3 in the $\zeta = 45$ to 50 region. The separation between θ_G and θ_W is now visible and provides an indication of the thermal driving force between the channel wall and the bulk-gas. Heat produced from the oxidation of CO in the active catalyst layer of the channel wall is transferred from the channel wall to the bulk-gas.
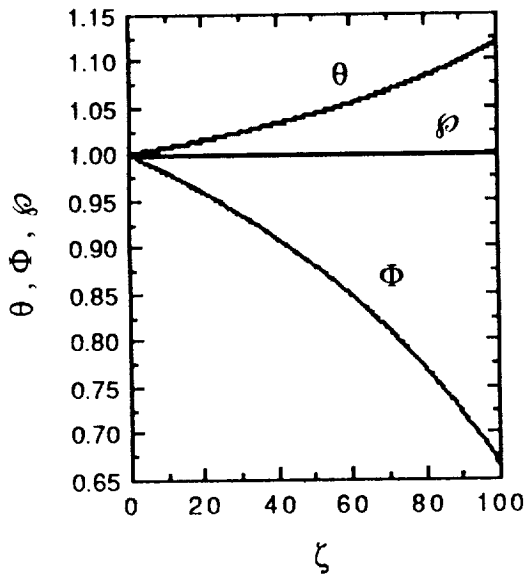
Figure 3. Results for Table 1 case. Dimensionless bulk-gas temp (θ), pressure ($\wp$), and O_2 concentration (Φ) vs distance from mono-inlet (ζ).
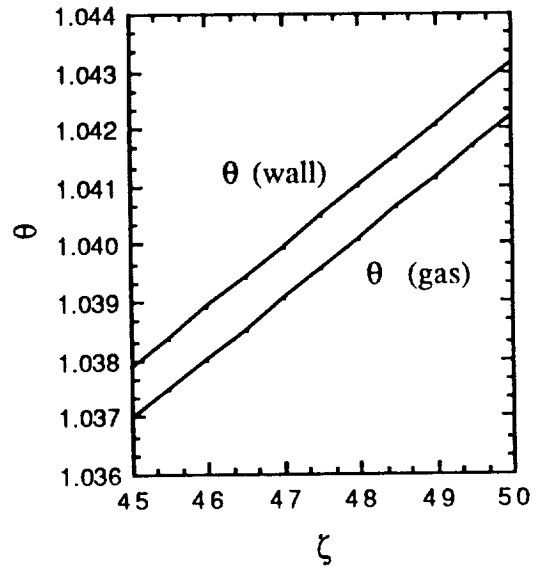
Figure 4. Dimensionless temperatures for Table 1 case.
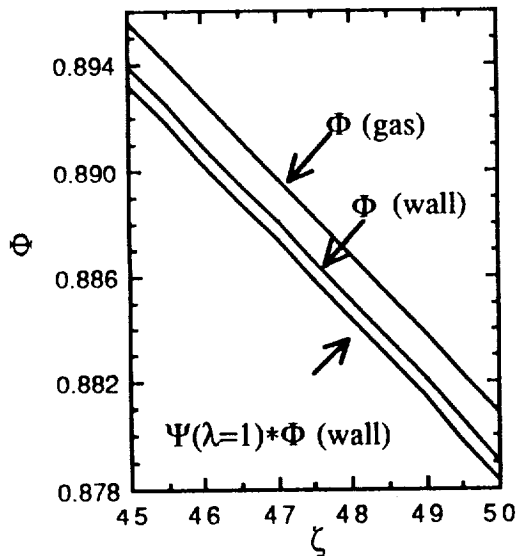
Figure 5. Dimensionless O_2 concentrations for Table 1 case.

0.82 mm opening
1.38 mm wall
14% void

209 mm
($\Delta P = 0.5$ in. H_2O)

10 mm

1.2 mm opening
0.27 mm wall
67% void
(standard size)

502 mm
($\Delta P = 0.22$ in. H_2O)

Figure 6. Optimum design vs. standard commercial size.

144

Fig. 5 is an expansion of Fig. 3 in the ζ = 45 to 50 region. An additional curve, $\Psi(\lambda=1)*\Phi_W$, is the scaled O_2 concentration at the centerline of the monolith channel support wall. O_2 is consumed in the porous catalytic layer as mass transport to the center of the monolith channel support wall occurs, therefore $\Psi(\lambda=1)*\Phi_W$ is less than Φ_W or Φ_G. The separation between the curves indicates the O_2 mass transport driving force. The difference between Φ_G and Φ_W is an indication of the driving force between the bulk gas and the channel wall. The difference between Φ_W and $\Psi(\lambda=1)*\Phi_W$ is an indication of the driving force between the channel wall and the centerline of the monolith channel support wall.

Table 1: Monolith catalyst section operating parameters

Monolith dimension

Facial cross sectional area = 1.0e+4 mm^2
Support + active layer thickness = 1mm
Active layer thickness = 0.25mm

Gas inlet properties
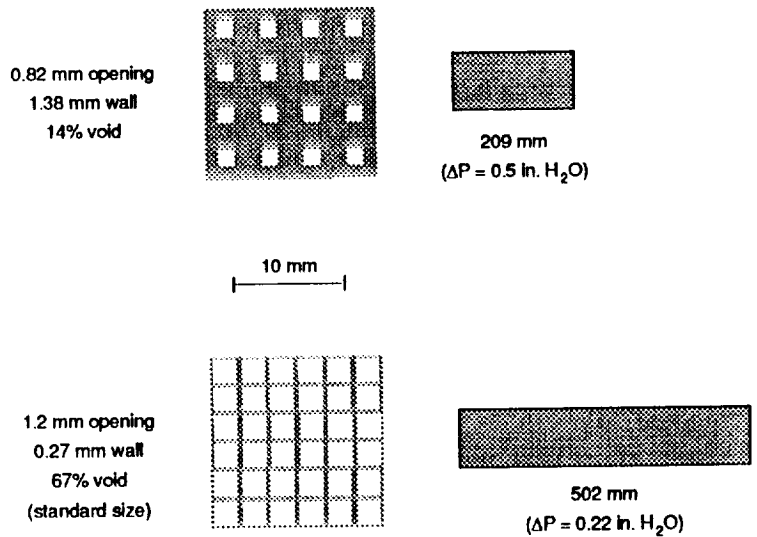
Flowrate = 0.25 liters/s
Temperature = 300 K
Pressure = 101.325 kPa
Composition 37% CO_2, 2% CO, 1% O_2,
 40% N_2, 20% He

Thermal operation is "adiabatic"

Catalyst properties

Void fraction as macropores = 0.25
Void fraction as micropores = 0.48
Macropore radius = 500nm
Micropore radius = 12nm
Active layer density = 0.5 x 10^{-3} g/mm^3
Rate constant (298 K) = 123.4mm^3/g • s
Activation energy = 39,700 J/mol

DESIGN STUDY

Design constraints

A design study for a monolith catalyst section, operating under parameters similar to those listed in Table 1, was performed. For the study, the support wall was assumed to be composed entirely of active catalytic material. Additional constraints, 25% O_2 conversion (Φ_G[exit]=0.75) and a 0.125kPa ($\approx$0.5 in H_2O) pressure drop across the monolith section, were imposed. The monolith facial cross sectional area and inlet gas conditions (composition, temperature, flow, and pressure) were held constant. Active support wall thickness and channel opening dimensions were varied and the minimum monolith length determined under the imposed constraint conditions.

The rationale for minimizing the monolith length follows from the assertion that the smallest monolith leads to the smallest, lightest and least expensive laser system. In portable laser systems size, weight, and cost considerations are critical. The choice of the shortest monolith section reduces the system weight by reducing the required monolith section housing length. The housing material weight per unit length is typically an order of magnitude more than that of the monolith material. The monolith material can be quite expensive; a smaller system requires less materials and is less costly. The 25% conversion requirement ensures a constant gas temperature rise. A constant pressure drop across the monolith section ensures that an identical amount of energy is expended to circulate the gas through the system. Excluding laser pulse energy, system energy

requirements (blower energy and heating and cooling loads) are fixed by the pressure drop and conversion requirements. Constant gas inlet conditions and 25% conversion ensure that a chosen laser PRR can be maintained without exceeding a the maximum allowable laser section inlet O_2 concentration.

Design results

Fig. 6 shows the optimum monolith section design geometry in comparison with a standard monolith design. The optimum monolith length is substantially less than the standard monolith length, whereas the optimum support wall thickness is substantially greater than standard thickness. As the monolith support wall thickness is increased, more catalytic material can be packed into a shorter monolith while conversion and pressure drop constraints are still satisfied. However, a thicker support wall has a larger O_2 mass transport resistance. A point is reached where the benefit of having thicker walls is negated by the large O_2 mass transport resistance and an optimum monolith length is determined.

DISCUSSION

The design study presented above shows that the use of off-the-shelf commercial monolith designs for CO_2 laser applications dramatically increases the overall monolith size required relative to the optimum design presented here. Off-the-shelf monoliths are designed for pollutant emission control and have been optimized for large gas flows and fast reactions at high temperatures. They have relatively thin monolith catalyst section dimensions and high % void volume. The slow reaction rates obtained over laser catalysts allow use of relatively thick monolith wall dimensions. With lower gas flow rates, low % void volume can be used to obtain compact monoliths, thereby reducing the size, weight, and cost of the laser system.

Using a computer program to generate variable and parameter values along the length of the monolith allows for rapid optimization of the monolith section under a set of constraints. Use of a computer program also allows for complex channel geometries, such as cylindrical, hexagonal, triangular, etc., to be incorporated into the monolith design.

MODEL IMPLEMENTATION USING LASCAT

LASCAT, a computer program based on the monolith catalyst section model presented above, provides a means to design a monolith catalyst section that will satisfy a user specified set of design requirements. LASCAT is available from the NASA COSMIC Program Office, and the program's order number is LAR-14190. LASCAT requires the specification of the parameters listed in Table 1 and a few others. Values of key parameters (Re, C_{PG}, ρ_g, D_{AB}, D_{ABeff}, and mole fractions) are provided at the inlet and exit of the monolith section. F_G, T and P are integrated instead of the corresponding nondimensional parameters, Φ_G, θ_G and $\wp$. C, T and P values are provided along the length monolith.

See Appendix 1 of this report for information on the implementation and compatibility of LASCAT and Appendix 2 for a short tutorial and an example of the LASCAT output. The documentation supplied with the full program contains an extended tutorial, a detailed explanation of each menu, and a documented program listing.

ACKNOWLEDGEMENT

Variables and parameters

A = CO oxidation reaction rate constant (mm^3 / g-cat s) layer

C = concentration of oxygen (mol / mm^3)

C_{PG} = bulk-average gas heat capacity (J / g K)

D_{AB} = diffusion constant for O_2 in bulk gas mixture (mm^2 / s)

D_{ABeff} = effective diffusion constant for oxygen in porous catalytic layer (mm^2 / s)

d_h = hydraulic diameter of monolith channel, 4(cross sectional area)/(wetted perimeter) (mm)

Eu = Euler number, Eu = $P_0 d_h^4$ / $\upsilon^2 \rho_g$

F_G = bulk-average gas molar flow rate of oxygen, $F_G = C_G \upsilon$ (mol / s)

h = average heat transfer coefficient (W / mm^2 K)

ΔH_{rxn} = heat of CO oxidation reaction (J / mol O_2 converted)

k = bulk-average gas thermal conductivity (J / m K)

k_m = average mass transfer coefficient (mm / s)

Nu_∞ = limiting Nusselt number, $Nu_\infty = h\, d_h$ / k

P = pressure in the channel at a position ζ (kPa)

$\wp$ = dimensionless pressure at position ζ, $\wp = P$ / P_0

Re = Reynolds number , Re = $d_h \upsilon \rho_g$ / $\mu_g d_h^2$

S = Surface area of the channel wall per unit open volume of monolith channel (mm^2/ mm^3)

Sh_∞ = limiting Sherwood number, $Sh_\infty = k_m\, d_h$ / D_{AB}

St = Stanton number , St = h d_h^2 / $\upsilon_0 \rho_g C_{PG}$

t_c = characteristic thickness of porous catalytic layer (mm)

T = temperature (K)

x = distance along the length of the monolith channel (mm)

z = depth into the porous catalytic layer (mm)

Subscripts

C,c   in porous catalytic

G,g   in flowing gas

O,o   at inlet conditions

W,w   in gas at channel wall

Greek

α = dimensionless rate constant, $\alpha = t_c \rho_c \eta A$ / k_m

γ = dimensionless mass transfer coefficient, $\gamma = d_h S k_m d_h^2$ / υ_0

Γ = dimensionless volumetric flow rate, $\Gamma = \upsilon$ / υ_0

ω = dimensionless heat of reaction, $\omega = -\Delta H_{rxn} k_m F_{G0}$ / $h\, T_{G0} \upsilon_0$

ζ = dimensionless distance along the length of the monolith channel, $\zeta = x$ / d_h

η = effectiveness factor of the reaction in the monolith porous catalytic layer , $\eta = \tanh (\varphi)$ / φ

θ = dimensionless bulk gas temperature, $\theta_G = T_G$ / T_{G0}, $\theta_w = T_w$ / T_{G0}

λ = dimensionless depth into the porous catalytic layer, $\lambda = z$ / t_c

μ_g = viscosity of gas in channel (Pa-s)

ρ_c = density of porous catalytic layer material (g-cat / mm^3)

ρ_g = density of flowing gas (g / mm^3)

υ = volumetric flow rate of flowing gas (mm^3 / s)

Φ_G = dimensionless bulk-average oxygen concentration in flowing gas, $\Phi_G = F_G$ / F_{G0}

Φ_W = dimensionless channel wall surface oxygen concentration, $\Phi_W = [C_W(\zeta)\, \upsilon(\zeta)]$ / F_{G0}

φ = Thiele modulus, $\varphi^2 = [t_c^2 \rho_c \eta A]$ / D_{ABeff}

Ψ = dimensionless O_2 concentration in the porous catalytic layer. $\Psi(\lambda) = [C_C(\lambda) / C_W(\zeta)]$

REFERENCES

1. Witteman, W. J., The CO_2 Laser, pp. 1-3,22-52,Springer-Verlag, New York (1987).
2. Dudley, W.W., CO_2 Laser, Effects and Applications, pp. 1-12, 36-51, Academic Press, New York, (1976).
3. Upchurch, B.T., G.M. Wood, R.V. Hess, and R.F. Hoyt, "Rare isotope studies involving catalytic oxidation of CO over platinum-tin oxide", in NASA Conference Publication-No.2456, pp.193-197(1987).
4. Stark, D.S., and M.R. Harris, "Catalysed recombination of CO and O_2 in sealed CO_2 TEA laser gases at temperatures down to -27°C", J. Phys. E: Sci. Instrum., (16) 492-496 (1983).
5. Stark, D.S., A. Crocker., and G.J. Steward, "A sealed 100-Hz CO_2 TEA laser using high CO_2 concentrations and ambient-temperature catalysts",J. Phys. E: Sci.Instrum., (16) 158-161 (1983).
6. NASA, Langley Research Center,"Catalytic Oxidation of CO for Closed-Cycle CO_2 Lasers", NASA Tech Briefs, p. 36, June (1987).
7. Price, H.T., and S.R. Shaw, "High repetition rate sealed CO_2 TEA lasers using heterogeneous catalysts", in NASA Conference Publication 2456, pp. 77-84(1987).
8. Burmeister, L.C., Convective Heat Transfer, pp. 240-241, John Wiley and Sons, New York (1983).

The LASCAT program is written in the FORTRAN programming language and is compatible with FORTRAN 77 standards. Detailed implementation instructions are provided below for Apple Macintosh and Digital Equipment Corporation VAX computers. Familiarity with the particular operating system is assumed.

<u>Computer: Apple Macintosh SE or II.</u>
Operating System: Apple System Version 6.0
Application Program: Absoft's MacFortran/020 Version 2.3
Compilation Options (Macintosh SE):
-Use compilation options   B (Compile Using Long Addresses)
                              E (Generate Errors List), and
                              U (* = Unit 9).
Compilation Options (Macintosh II):
-Use compilation options   B (Compile Using Long Addresses),
                              E (Generate Errors List),
                              M (68020/68030 instructions),
                              P (68881/68882 instructions), and
                              U (* = Unit 9).
Compilation and Execution:
-Place the LASCAT program in the <u>same folder</u> as the MacFortran/020 application and supporting files.
-Double click on MacFortran/020 application to launch the MacFortran/020 application.
-From the File Menu choose the "Select File" option. Select File LASCAT.
-From the Compile Menu choose the "Options" option and verify the compilation options selected are identical to the compilation options described above. If the options selected need to be changed, remember to save the new set of compilation options by clicking on the "Save" box. Exit the compilation options section by clicking on the "OK" box.
-From the Compile Menu choose the "Compile and Execute" option. The program will be compiled and executed. The output file, LDATA, and any selectable parameter files will be placed in the same folder as the LASCAT and MacFortran/020 files.

<u>Computer: Digital Equipment Corporation VAX</u>
Operating System: VAX/VMS Version 4.6
Application Program: VAX FORTRAN V4.8-276
Compilation and Execution :
-Rename the LASCAT program *LASCAT.for*
-To compile LASCAT.for, type *for LASCAT.for*
-To link LASCAT.for type *link LASCAT*
-To execute LASCAT.for *type run LASCAT*
-The output file, LDATA.DAT, and any selectable parameter files will be placed in the your directory. Use an editing program to examine files.

NOTE: The FORTRAN program LASCAT is available from the NASA COSMIC Program Office. The program order number is LAR-14190 (1,907 lines)

The LASCAT Tutorial provides a step by step example of the use of the program LASCAT. Required user input and comments are detailed on the left margin and the corresponding screen outputs are indented. Input(s) required by the operater are boldfaced. The example shown below was run on a Macintosh II using Absoft's MacFortran/020 Version 2.3. (Review the Program Implementation and Compatibility section for program complilation and execution details.) This tutorial will be of the greatest benefit if used while actually executing the program.

Compile and execute LASCAT application program.

******   PROGRAM LASCAT   *******

The purpose of this program is to calculate the gas concentration and
temperature profiles of a monolith catalyst section of a CO2 laser. The
CO2 decomposes when the laser is pulsed. The CO and O2 produced as a result
of pulsing are detrimental to the efficient operation of the laser. The
recombination reaction is CO + 1/2 O2 -> CO. This program provides the
means to model the performance of a monolith catalyst section under various
gas compositions, temperatures, catalyst activities, gas flowrates, oxygen
conversion, monolith face and length dimensions. Results can indicate if
constraints such as conversion, maximum gas temperature, and monolith weight
are satisfied and how the system parameters may be altered to meet these
constraints. Parameters and options may be altered to tailor the monolith
design. Default values can also be used as a starting point for the design
process. A review of the parameters and options chosen may be made prior
to execution of the computational portion of the program.

(HIT RETURN KEY TO CONTINUE)

A program introductory statement is presented. **Hit RETURN key** after reading.

LASCAT Main Menu

1) Read in new operating parameters
2) Show current operating parameters
3) Change operating parameters
4) Run program
5) Exit program

Enter the number corresponding to choice above.

The LASCAT Main Menu is presented. The main menu provides different options (1-5). Specific details for each option are provided in the Menu Description section. To choose one of these options, simply enter the desired number, then RETURN. For this example, **hit the 2 key and hit RETURN key**.

SELECTABLE PARAMETER SUMMARY

Monolith Dimensions(mm):
Support wall thickness: 1.00   Face dimension: 100.00 x 100.00
Channel inner dimension: 4.00   No.Face channels: 20.00 x 20.00
Active layer thickness: .25   % monol.volume open : 64.0

Monolith inlet parameters:
Gas Composition (mole fraction):   CO2: .3700 CO: .0200 O2: .0100
                                    N2: .4000 He: .2000 Ar: 0.0000
Gas Flow rate(liters/s):   .250   Gas Temperature(K): 300.00
Inlet Gas Pressure (kPa):   101.325

Catalyst Properties:
Catalyst Density (g/mm^3): 0.500E-03
Reaction rate constant at 298K(mm^3 /gcat-s):   123.40
Activation energy(J/mol):   39700.00
Void-fraction as micropores: .24   Void-fraction as macropores: .48
Avg. micropore radius (nm): .12E+02 Avg. macropore radius (nm): .50E+03
Thermal Operation (adiabatic/isothermal): Adiabatic

Computational loop parameters:
Output file (Full Profile/Summary): Full Profile
Termination on (O2 conversion/Length): O2 conversion. %:   2.500
Computation loop step size(mm): .5556   Display every 5.00 mm

==> Hit Return when finished viewing <==

The selectable parameter summary lists the parameter values that will be used in the computation portion of the program. When the program is initially run, default parameter values are assigned. As we'll see later, the values of the parameters can be changed. Hopefully, a review of the parameter summary above will hint to the meaning of each parameter. The use of each parameter is detailed in the Menu Description section. Let's assume the present values are satisfactory and proceed. **Hlit RETURN key.**

LASCAT Main Menu

1) Read in new operating parameters
2) Show current operating parameters
3) Change operating parameters
4) Run program
5) Exit program

Enter the number corresponding to choice above.

We have returned to the main menu. To save space, the main menu will listing will be abbreviated as "LASCAT Main Menu....". To run the computational portion of the program using the current parameter set listed in the selectable parameter summary, **hit 4 key and RETURN key.** Note: the program will alert you that it has completed computations by beeping three times.

Initial values
Reynolds number =   9.880
Gas Heat Capacity (J/K-g) =   1.797
Gas Density (g/cm^3) =   .0011817
Gas Velocity (mm/s) =   39.063
Effectiveness factor =   .99969
 Bulk Gas Diffusivity(cm^2/s)=   .22540
 Effective Diffusivity(cm^2/s)=   .053407
Step size(mm) =   .555556

Distance mm	%Conver	O2gas mmol/L	O2wall mmol/L	O2center mmol/L	Tgas K	Twall K	DPress kPa
0.000	0.0000	0.4065	0.4060	0.4058	300.000	300.179	-0.0
5.000	0.2239	0.4052	0.4048	0.4046	300.236	300.416	-0.730 E-05
10.000	0.4574	0.4040	0.4035	0.4033	300.474	300.656	-0.146 E-04
15.000	0.6933	0.4027	0.4022	0.4020	300.714	300.897	-0.219 E-04
20.000	0.9314	0.4014	0.4009	0.4008	300.956	301.141	-0.293 E-04
25.000	1.1718	0.4001	0.3996	0.3994	301.201	301.388	-0.366 E-04
30.000	1.4146	0.3988	0.3983	0.3981	301.448	301.637	-0.440 E-04
35.000	1.6598	0.3975	0.3970	0.3968	301.697	301.888	-0.513 E-04
40.000	1.9075	0.3961	0.3957	0.3955	301.949	302.141	-0.587 E-04
45.000	2.1577	0.3948	0.3943	0.3941	302.204	302.398	-0.661 E-04
50.000	2.4104	0.3934	0.3930	0.3928	302.461	302.656	-0.735 E-04
52.778	2.5519	0.3927	0.3922	0.3920	302.605	302.801	-0.776 E-04

Final values
 Mole fractions:
  He = .2001 Ar = 0.0000 CO2 = .3706
  CO = .0195 O2 = .0098 N2 = .4001
Gas Pressure (kPa):   101.325
Reynolds number =   9.817
Gas Heat Capacity (J/K-g) =   1.799
Gas Density (g/cm^3) =   .0011720
Gas Velocity (mm/s) =   39.378
Effectivness factor =   .99965
 Bulk Gas Diffusivity(cm^2/s)=   .22832
 Effective Diffusivity(cm^2/s)= .053988
Step size(mm) =   .555556

==> Hit Return to Return to Main Menu <==

The previous information provides initial and final values of important parameters along with values of key parameters along the length of the monolith. The units for each parameter are specified. A few minutes spent in reviewing the trend of each parameter, either initial vs. final or along the length of the monolith, is well worth the time. For example, the gas heat capacity increases from 1.797 to 1.799 due to the change in gas composition and the change in gas temperature. The gas temperature rises from 300.000 to 302.605 due to the exothermic nature of the reaction $CO + 1/2O_2 \rightarrow CO_2$.

NOTE: The full documentation supplied with LASCAT continues this tutorial.

SECTION III

LABORATORY STUDIES

MECHANISTIC STUDIES OF THE CO-OXIDATION REACTION ON CATALYSTS FOR USE IN LONG-LIFE CO_2 LASERS[1]

Talat Dawood, John R Richmond and Brian W Riley
UOP Limited, Enfield, Middlesex, EN3 7PN, UK.

SUMMARY

The catalytic recombination of carbon monoxide and oxygen has been studied under conditions expected to be present in a sealed E-beam CO_2 laser system. These conditions are typically a gas inlet temperature of $60^{\circ}C$, a substoichiometric CO/O_2 ratio of ca. 2.5/1 with an oxygen feed rate of ca. 5 micromoles/s, a carrier gas comprising He, N_2 and CO_2 in the ratio of 3:2:1, near atmospheric pressure and a gas velocity of 4 m/s. Heterogeneous catalysts, based on precious metal supported on tin oxide, have been coated onto ceramic monoliths and tested for catalytic activity and stability after a reduction/passivation step. Two catalyst systems have been chosen. These are $Pt/Pd/SnO_2$ and $Pt/Ru/SnO_2$.

Under the conditions described above, a characteristic decline in catalytic activity is apparent for both systems, and exit gas temperature has been recognised as a sensitive parameter by which to monitor the activity changes. A semilogarithmic plot of exit temperature as a function of time has revealed two distinct processes connected with the decline in activity: one process is associated with reduction of the oxidised precious metal (at Site A), whilst the other is related to the formation and approach to steady-state of an active site at the metal/support interface (Site B).

Surface species have been identified using on-line Fourier Transform Infrared (FTIR) spectroscopy. Two characteristic absorption bands have been detected. In the case of Pt/Ru, a distinct band at ca. 2055 cm^{-1} has been identified as linearly adsorbed CO, and a broad, rather weak absorption band at ca. 1890 cm^{-1} identified as bridge-bonded CO; for Pt/Pd, the corresponding absorption bands are found at ca. 2070 cm^{-1} and 1870-1890 cm^{-1} respectively. No marked changes in band intensity could be discerned over a three-hour period under reaction conditions.

In contrast, flushing with laser gas mix resulted in significant band shifts as well as an attenuation of the bands, consistent with a lowering of the surface coverage of CO. These effects were more pronounced for Pt/Pd. Moreover, in the presence of oxygen alone, the linearly bound species could be removed from the surface in each case. The FTIR studies indicate that high surface coverages of CO are present on the reduced metal under reaction conditions and that upon exposure to air, the reactive CO species is linearly bonded to the precious metal surface. Related CO/O_2 titration experiments on the Pt/Pd monolith have shown that neither reactant displaces the other from the surface and that both spillover and metal/support effects could be associated with these catalysts.

Finally, various poisons and promoters have been added to the catalysts either during preparation or under reaction conditions. In the case of the Pt/Pd system, potassium and manganese act as catalyst poisons at the 1% w/w level. Conversely, in the presence of water (with a relative humidity of ca. 33% at room temperature), manganese stabilises the catalyst. For the Pt/Ru system, the addition of acetone to the feed results in irreversible deactivation. Microreactor pulse experiments have shown that this acetone chemisorbs on the support and indicate that the poisoning effect of acetone is metal/support related. Conversely, water has been shown to be a promoter and stabiliser under present conditions.

A reaction mechanism consistent with the experimental observations has been proposed. It is suggested that under reaction conditions, CO reacts with a surface oxygen atom at Site A, as well as reacting with the support to induce a strong metal/support interaction (Site B). Dissociated oxygen is transported to the precious metal surface via Site B, and water promotes this process. Poisoning is accounted for by adsorption of the rate-inhibiting species at the metal/support interface.

INTRODUCTION

The recombination of CO and O_2, formed during the operation of a sealed E-beam CO_2 laser system, is essential in maintaining the lifetime and integrity of the laser itself. The deployment of heterogeneous catalysts, based on precious metal supported on tin oxide, has been recognised as an important approach with which this problem may be overcome (1). Factors governing the suitability of the heterogeneous catalytic approach are ones of intrinsic

activity, stability (i.e. catalyst lifetime) and tolerance to poisoning under realistic working conditions. These factors have all been addressed in the present study.

EXPERIMENTAL

Materials

Certified gas bottles containing $He:N_2:CO_2$ in the ratio of 3:2:1 (henceforth termed laser gas mix) and substoichiometric (ca. 2.5:1) CO/O_2 mixtures in laser gas mix (termed reaction gas) were supplied by Air Products Ltd. or Electrochem Ltd. No impurities could be detected by FTIR spectroscopy, and gases were used without further purification. Pure laser gas mix was used to dilute the premixed CO/O_2 in laser gas mix to the required level (typically ca. 5 micromoles O_2/s). Certified bottles containing 1% CO in N_2 and 1% O_2 in N_2 supplied by Air Products Ltd. and cylinders of "white spot" nitrogen (99.99%) and hydrogen (99.998%) supplied by BOC Ltd. were used without further purification.

Ceramic monoliths used in these experiments were manufactured by Corning and had a cell density of 400 per sq. inch. The artifacts were cylindrical in shape with a diameter of ca. 21mm and either 75 mm (Pt/Ru, Pt/Pd/K) or 50 mm (Pt/Pd, Pt/Pd/Mn) in length.

Monolith Preparation and Pretreatment Procedure

Monoliths were coated with metastannic acid and calcined before addition of the active components. These were introduced using standard impregnation techniques. All coated monoliths were then dried and calcined prior to catalyst pretreatment.

The pretreatment routine typically involved an in-situ reduction at ca. $60^{\circ}C$, bringing the hydrogen slowly to 100% using laser gas mix as diluent whilst monitoring the exotherm via a thermocouple situated a few millimetres from the exit of the monolith. Then the system was flushed with laser gas mix and a similar procedure was employed using air instead of hydrogen. This procedure has been termed reduction/passivation.

Test Equipment and Procedures

The test apparatus was a microreactor flow system constructed from 6 mm o.d. stainless steel tubing. The monolith itself was sealed in a glass reactor which was contained within a temperature-controlled incubator. Exit temperatures were monitored by thermocouple, as mentioned above. CO and O_2 levels were detected separately.

The microreactor pulse system consisted of a small section of 6 mm o.d. stainless steel tubing connected to a Perkin-Elmer F11 gas chromatograph with FID detector. 0.5 g samples of catalyst or support (30-80 mesh) were positioned inside the microreactor, and microlitre quantities of acetone were pulsed into the N_2 carrier and over the catalyst bed. The system was calibrated by pulsing acetone through an empty reactor.

FTIR experiments were carried out using a Nicolet 5-DXC Fourier transform infrared spectrometer at $4cm^{-1}$ resolution utilising a liquid nitrogen cooled MCT detector. The spectrometer was operated in diffuse reflectance (DRIFTS) mode, using a controlled environment sample chamber (supplied by Spectra-Tech Inc.). The chamber allowed collection of diffuse reflectance spectra of catalysts and infrared active surface species under in-situ reaction conditions. A stainless steel gas flow system was constructed in order to flow laser gas mix and reaction gas through the reaction chamber. The gases were admitted via Brooks Model 5850 TR mass flow controllers, and reaction rates monitored using a Systech EC90M oxygen analyser connected to the gas exit. This system also allowed in-situ pretreatment of the catalyst sample (see figure 1). Samples of powdered Pt/Ru and Pt/Pd monolith were examined, and a typical sample size of 100 mg was used. All catalysts were reduced and passivated in the manner described above and at the appropriate temperature of reaction.

RESULTS AND DISCUSSION

Deactivation Studies

Figure 2 shows the deactivation curve for a Pt/Ru monolith tested under substoichiometric conditions at 4m/s, ca. $60^{\circ}C$, with an oxygen feed rate of 7.9 micromoles/s. After 30 minutes, the reactant feed was stopped, and the catalyst flushed with laser gas mix for one hour. It can be seen from the figure that upon reintroduction of the reactants, the catalyst has regenerated,

indicative of a reversible deactivation process. The exit temperature was monitored and found to closely follow the deactivation trend. A two-step graph was generated on plotting natural logarithm of exit temperature (in Kelvin) versus time (see figure 3). The sensitivity of the temperature parameter can be appreciated from an estimation of the relative error on the points on this graph (+/- 0.05%).

It was also discovered that the Pt/Ru monolith could be fully regenerated by following the reduction/passivation pretreatment described above, and upon readmission of the reactants under similar conditions, an identical deactivation curve was generated. Further, the deactivation trend was reversed over a 30 minute period on effecting a small temperature increase (ca. 8°C). These observations suggest that the decline in activity is related to changes in surface concentrations of reactive intermediates.

The exit temperature plots for the Pt/Pd and Pt/Pd/Mn monoliths (tested under the same conditions as the Pt/Ru monolith) are shown in figure 4. Again the two regimes can be easily distinguished.

On comparing the CO and O_2 deactivation traces for these catalysts, it was noted that over the initial minutes of reaction, the CO concentration fell sharply below the O_2 concentration, indicative of a surface reduction process. After several minutes the two traces yielded the corresponding deactivation rates expected for stoichiometric reaction.

The activity changes characteristic of Pt/Pd and Pt/Pd/Mn under dry-gas conditions were not repeated under wet-gas conditions. The same monolith samples were tested under identical conditions, except with a relative humidity of ca. 33% at room temperature in this case. The resultant exit temperature plots are shown in figure 5. It is evident that the water has a net promoting and stabilising effect, although of the two catalysts, the manganese-containing one appears to have the better stability.

The effect of potassium on catalyst performance was investigated by testing the activity of the Pt/Pd/K monolith at 4m/s, ca. 60°C, with an oxygen feed rate of 7.9 micromoles/s. With regard to initial activity, gross deactivation was observed relative to the non poisoned Pt/Pd monolith. The characteristic exit temperature plot generated from the exit temperature is shown in figure 6. It should be pointed out here that the rate of deactivation in the second stage (as measured by the gradient on the graph) is very close to that for the non poisoned catalyst. In fact, potassium decreases the initial activity of the catalyst without significantly affecting the Pt/Pd deactivation profile.

That initial decrease could be explained by an increase in the CO self-poisoning effect, based on evidence from the surface science literature where it has been shown that K increases the heat of adsorption of CO on Pt (2). Other evidence reported below would lead to the conclusion that both K and Mn affect the oxidisability of the precious metal, but this could well be via an increase in the strength of CO chemisorption on the metal.

Poisoning Studies

In order to assess the effects of various potential catalyst poisons on the rate of reaction, microlitre quantities of acetone, hexane, water and chloroform were injected into the feed and over the previously reacted Pt/Ru monolith at 2m/s with an oxygen feed rate of 3.8 micromoles/s and a substoichiometric gas ratio. The catalyst had been reduced and passivated at room temperature prior to reaction. The corresponding deactivation curves are shown in figures 7-9 (n.b. the semilogarithmic plot is used merely as a convenient way of representing the data in this case).

Figure 7 shows that the deactivation rate increases with the introduction of acetone into the gas feed. Subsequent injections do not appear to have as significant an effect on the catalytic rate. The deactivation curve for a non poisoned Pt/Ru monolith section, tested under identical conditions and after a similar pretreatment, is shown by the dotted deactivation curve. It may be noted here that although the dotted deactivation curve illustrates the effect of acetone on the initial and overall deactivation, the deactivation rate appears to be greater for the fresh versus reacted monolith section over the initial stages of the reaction.

The same Pt/Ru monolith was given the reduction/passivation pretreatment at room temperature as before and retested under identical reaction conditions. It is evident from figure 8 that the initial activity has dropped by ca. 25% compared with the value observed in figure 7. This correlates well with the net deactivation at steady-state of ca. 20% found in figure 7 and indicates that this deactivation is irreversible under present pretreatment conditions.

In order to further investigate the nature of the poisoning effect of acetone, a parallel series of experiments were performed (with reference to the support) on powdered samples of Pt/Ru/SnO$_2$ and Pt/Pd/SnO$_2$ catalysts using the microreactor pulse system. The samples were subjected to the reduction procedure described earlier, except now at room temperature and using nitrogen as diluent instead of laser gas mix. It was found that the quantity of acetone taken up by the support corresponded

to ca. 5 microlitres (ca. 68 micromoles) and that this quantity of acetone was indistinguishable from that taken up by the catalysts. From the BET surface area of the catalyst support (ca. 130 m^2/g), it was estimated that this value corresponded to approximately one-fifth of a monolayer of acetone. The temperature was ramped up to 90°C, whereupon neither desorption nor dissociation of acetone could be detected by FID.

These experiments can be used to explain the net deactivation observed over the Pt/Ru monolith sample. They strongly support a deactivation mechanism which involves the blocking of active sites on the support which in turn lower the average rate of reaction on the surface of the catalyst. This would explain why a molecule which would not have been expected to chemisorb strongly on the metal under reaction conditions has a significant effect on the deactivation rate. The results could support a spillover type mechanism, such as that proposed by Bond and co-workers (3), but would also be consistent with a system in which the metal was strongly interacting with the support to produce active sites.

Figure 8 also shows the cumulative effect of pulsed injections of hexane and water on the Pt/Ru monolith. In the case of hexane, the results suggest that this compound is a poison, and the poisoning effect appears to be a function of hexane partial pressure. However, it is also evident that the hexane injection induces stability in the catalyst system. Since it is unlikely that hexane molecules would chemisorb on the support at these reaction temperatures, the effects observed may be a function of an impurity such as hexene. In comparison, water acts as a promoter under present conditions. The figure shows a sharp transient increase in activity, indicative, perhaps, of the removal of a surface poison from the catalyst. This transient increase in activity would seem to be practically independent of pulse size. In addition to this behaviour, water appears to have a net promoting effect on overall activity (~15%).

Finally, figure 9 shows the further effect of added chloroform. Now the net effect is that of a poison, with the activity changes mirror images of those observed for water. It is plausible that chloroform induces poisoning via Cl⁻ transfer to the active metal, as chlorides have been associated with the blocking of active Ru sites which chemisorb CO (4). However, other studies have also indicated that Cl⁻ would weaken the CO bond (5), suggesting that Cl⁻ should decrease the effects of self-poisoning (should they be present here). An alternative model for chloride poisoning will be explored below.

The FTIR work was designed to look at concentrations of surface species at the very early stages of reaction, where it was believed that the most significant changes on the surface would occur. Carbonyl absorption band assignments were primarily based upon those outlined in the review of Sheppard and Nguyen (6), and only the frequency range of significance (1300 - 2600 cm^{-1}) has been displayed in the figures.

In order to discover the nature of CO chemisorption on these catalysts, the Pt/Ru catalyst was reduced and then CO introduced to the sample in a stream of laser gas mix. An absorption band at 2052 cm^{-1} was present, and this band shifted downward to 2044 cm^{-1} upon stepwise heating in a flow of helium (see figure 10). This band is assigned to a linearly bound carbonyl group. It is evident from the figure that CO is strongly bound to the surface, since the band intensity does not decrease significantly even at 250°C. However, this species evidently reacts (or is displaced) upon exposure to air, since the carbonyl absorption band is completely removed from the spectrum.

The reduction/passivation process was next investigated at the end of each stage. Spectra were taken after the reduction stage using pure hydrogen and then after flushing with laser gas mix, after admission of pure air and after a final flushing with laser gas mix. The spectra are shown in figure 11. No bands could be distinguished after a hydrogen pretreatment. Upon flushing with laser gas mix, a band at ca. 2035 cm^{-1} and a rather weak absorption band at ca. 1890 cm^{-1} were assigned to linear and bridge-bonded carbonyl species. These two bands have frequencies which fall in the ranges expected or low surface coverages of CO associated with bimetallic particles of an alloy such as ruthenium/platinum. The reason for the CO bands must be dissociative chemisorption of CO_2 on the reduced metal. Upon exposure to air, the linearly bound species was removed and a distinct broad band associated with molecularly adsorbed water appeared at ca. 1650 cm^{-1}. This water is assumed to be a by-product of the reduction/oxidation process. Identical behaviour was observed in the case of Pt/Pd, with the corresponding absorption bands appearing at ca. 2030 cm^{-1} and 1870 cm^{-1}. Carbonyl band frequencies such as these are consistent with those reported for low surface coverages of CO on metals such as platinum or palladium where linear and bridge-bonded carbonyl groups are associated with metal sites of low coordination number.

The FTIR spectra recorded for Pt/Ru and Pt/Pd catalyst under reaction conditions are shown in figures 12-17, and the corresponding absorption bands tabulated in Table 1. These

catalysts were examined at high flow rates (1 l/min) with no detectable conversion , and lower flow rates (100 ml/min) with ca. 20% conversion and no deactivation over a 2-3 hour period. With regard to the spectra, it should first be noted that the small rises observed at ca. 2170 cm^{-1} and 2120 cm^{-1} are due to gas phase CO. In summary, two distinct absorption bands at ca. 2055 cm^{-1} and 1890 cm^{-1} were detected for Pt/Ru (see figures 12-14); the corresponding absorption bands for Pt/Pd were detected at ca. 2070cm^{-1} and 1870/1890 cm^{-1} (see figures 15 and 17). These bands are consistent with those reported for saturated surface coverages of linear and bridge-bonded carbonyl species on supported Ru/Pt and Pd/Pt catalysts in the reduced state. In all cases the bands were of similar intensity throughout the period of reaction, even when the reaction rate was observed to increase significantly (~50% for low flow experiments). It is apparent, then, that these intermediates quickly attain a steady-state concentration on the surface, and their reactivity cannot therefore be assessed from these experiments. Nonetheless, it should be noted that in the case of Pt/Pd, flushing with laser gas mix reduces the intensity of the linearly bound absorption band as does exposure to air (see figure 16). Flushing with laser gas mix does not appear to have as significant an effect in the case of Pt/Ru (cf. top spectra from figures 12-14).

A final piece of information relates to the FTIR spectra for the Pt/Pd sample tested at low flow rate (figure 17). The asymmetry of the linearly bound carbonyl band was more pronounced here, and a shoulder could be distinguished at ca. 2100 cm^{-1} because of lack of interference from bands due to gas phase carbon monoxide. The position and appearance of this shoulder is indicative of CO bound linearly to partially oxidised metal particles of platinum/palladium. From these observations it has been concluded that the platinum/palladium component is heterogeneous in nature.

CO/O_2 Titration Experiments

To assess the oxidation/reduction behaviour of these catalysts, the regenerated Pt/Pd monolith was reduced in H_2 or CO and then oxidised at ca. $62^{o}C$ (using nitrogen as a diluent) and the CO/O_2 uptakes measured using the flow system described earlier.

It was immediately noted that neither CO nor O_2 displaced each other from the surface. Further, the O_2 uptake corresponded to ca. 30 ml, independent of reducing agent used.

In contrast, the amount of CO used to reduce the monolith was ca. 58 ml; in other words, within experimental error, the reaction of CO with O_2 on the surface was found to be stoichiometric. Significantly, if the catalyst had been completely oxidised beforehand, as is suggested above, this CO must have reacted (at least in part) directly from the gas phase. Further, assuming approximately 1:1 metal to CO stoichiometry, these results would suggest that after a CO reduction, the net CO uptake on the metal would be ca. 30 ml.

Next, the oxidised monolith catalyst was reduced with H_2 and the CO uptake recorded at ca. $62^{\circ}C$. The amount of CO adsorbed on the catalyst was ca. 12 ml. This value is much lower than that expected on the basis of corresponding CO and O_2 uptakes and indicates either that the reduced metal is strongly interacting with the support (thus suppressing CO chemisorption), or perhaps O_2/CO spillover, or indeed a combination of these effects.

This last experiment was repeated using wet gas (saturated water vapour at room temperature) with ca. 100 ppm O_2 impurity in the gas feed. An identical CO uptake was recorded, indicating that water does not significantly suppress this behaviour.

Finally, in order to relate this data to the reaction itself, the uptake of CO was determined during the initial stages of reaction from an integration of the CO and O_2 analyser traces for the Pt/Pd monolith (as reported above). After 6 minutes, the CO and O_2 uptakes were 94 ml and 36 ml respectively (i.e. a net CO uptake of ca. 22 ml); the values over a further 4 minutes were found to be 46 ml and 23 ml respectively (i.e. stoichiometric reaction). Thus, it would appear that the surface of the catalyst is up to 38% "reduced" under substoichiometric conditions (n.b. the relative amounts of reacted and adsorbed CO cannot be determined here). The corollary to this conclusion is that the catalyst is not less than 62% "oxidised". If this oxygen was solely associated with the metal (i.e. surface oxygen atoms), the reaction would be predicted to be close to zero-order in oxygen. However, this is not consistent with the literature, where it has been reported (under similar conditions) that the reaction is zero-order in CO and first-order in O_2 (1). Thus, it is more likely that most of the oxygen is associated with the support, possibly in an associatively bound state at the metal/support interface.

If this model is correct, then the passivation step introduces oxygen into the support, and this oxygen can be removed by reaction with CO or H_2, probably via a spillover mechanism. Such a model is supported by isotopic labelling studies (7).

Proposed Reaction Mechanism

Any reaction mechanism which explains the experimental results has to account for the abrupt change highlighted by the exit temperature (after ca. 20 minutes) and also the poisoning phenomenon encountered with added gas components.

It is suggested that the overall decline in activity is accounted for by two distinct catalytic sites and that one of these (Site A) is associated solely with the precious metal (PM) (refer to figure 18). Upon a reduction/passivation pretreatment, carbon monoxide reacts from the gas phase with a reservoir of surface oxygen to form carbon dioxide at site A (STEP 1). CO quickly attains a saturation level on the reduced part of the metal surface (as suggested by FTIR) and probably reacts in the linearly bound form with oxygen at an adjacent Site A. (STEP 1 (a)). Further, gas phase CO continually reacts with the support to induce a precious metal (PM)/Sn interaction (Site B) (STEP 2). This site is produced under net reducing conditions and does not chemisorb CO readily. Site B reacts by dissociating O_2 across the PM/Sn interface to produce Site A plus non interacting SnO_2 (STEPS 3-4). The slow decline in activity is regarded as simply an approach to steady-state (STEP 5).

In summary, catalytic reaction is proposed to involve gas phase and linearly adsorbed CO molecules which can reduce the metal oxide (Site A) to metal as well as reducing the support (probably via spillover). This latter reduction induces a metal/support interaction, producing a second catalytic site (Site B) that can dissociate O_2 to regenerate Site A. On doing so the metal/support interaction (i.e. Site B) is destroyed. The overall process is therefore oscillatory.

This mechanism accounts for the stepped change mentioned above, with Site A depleting rapidly as Site B builds up in concentration. Site B reaches a maximum concentration and then decays to a steady-state concentration. The activity pattern outlined in figure 6 could be evidence for the buildup and decline in concentration of Site B if water was maintaining the concentration of Site A. Here the rate-determining step would shift from being that of oxygen transfer to the metal (via Site B) to that of CO oxidation at the surface itself. From a comparison of the initial exit temperatures shown in figures 5 and the corresponding steady-state exit temperatures shown in figure 6, it is evident that the water-promoted catalysts do indeed approach the initial exit temperatures found in the corresponding dry-gas reaction. These observations are consequently in line with the above suggestion.

167

The promotional effect of water can therefore be explained in terms of an increase in the rate of transfer of dissociated oxygen to the precious metal. The sharp increase in activity shown in figure 9 is caused by a transient increase in the concentration of Site A, and the net stabilising effect of water is accounted for by a change in the rate-determining step of the reaction.

Poisoning is accounted for by chemisorption of molecules at Site B. Compounds that can form a stable transition state are potential poisons which either block Site B or produce an inactive Site A (e.g. Cl⁻ transfer in the case of chloroform). Acetone and chloroform are particularly suitable for bonding to Site B via the oxygen and chloride atoms respectively.

The regeneration of the monolith upon heating or flushing with laser gas mix can be regarded as a reoxidation of the metal, with Site A being formed from Site B via a kinetically slow step. This process has also been reported elsewhere (8).

There is strong experimental evidence for PtSn alloying in the literature. Temperature programmed reduction studies on alumina-supported Pt/Sn systems have shown that PtSn alloys are indeed feasible in the presence of hydrogen, albeit at elevated temperatures (9). More recently the NASA group, utilising ion-scattering spectroscopy, have reported PtSn alloy formation upon CO reduction (10). Unfortunately, the FTIR spectra produced in this study cannot be used to directly determine the existence of a metal/support interaction, since even the alloying effect produces a negligible shift in the absorption frequency of CO on the precious metal (11).

An alternative mechanism for CO oxidation over Pt/SnO_2 has been recently proposed (12). Reaction and deactivation are proposed to occur via the formation of surface hydroxl and carbonate/bicarbonate species. No evidence has been found in the FTIR spectra to indicate that these intermediates exist under the experimental conditions used in this study. If such species were present, absorption bands would be expected at ca. 3600 cm^{-1}, 1530 cm^{-1} and 1390 cm^{-1} respectively.

It should be concluded here that reaction on these catalysts is complex and that further study is needed to understand the elementary steps involved in the CO oxidation process. Of particular relevance would be kinetic and isotopic work.

GENERAL CONCLUSIONS

From the present work a number of general conclusions may be made regarding the CO oxidation reaction under possible laser operating conditions:

1. For Pt/Ru and Pt/Pd systems supported on tin oxide and prepared in the manner described above, an inherent two-stage reaction process is observed, the extent of which can be conveniently monitored by a change in the reaction exotherm.

2. The initial process is believed to be a decrease in the level of oxidised metal, which can be partially recovered by heating or by flowing inert laser gas mix over the catalyst.

3. Potassium and manganese act as poisons when added to the Pt/Pd catalyst at the 1% w/w level. Both are thought to be associated with lowering of the oxidisability of the precious metals.

4. Addition of acetone to the gas feed has been shown to be detrimental to the activity of a Pt/Ru catalyst, resulting in irreversible deactivation. This is believed to be due to irreversible chemisorption of acetone on the support, and suggests a probable metal/support interaction, the extent of which is a function of chemisorption on the support. Water, on the other hand, has been shown to enhance the activity as well as stability of these catalysts. This is thought to be due to water promoting the rate of oxidation of the metal via the metal/support interface.

5. FTIR results have shown that under reaction conditions two modes of CO chemisorption co-exist on the reduced precious metal surface: these are linearly bonded and bridge-bonded CO. A high surface coverage of CO is probable, and in the presence of oxygen alone, the reactive species is not bridge-bonded but linearly bonded CO. However, under reaction conditions these species quickly attain a steady-state concentration, and their surface concentrations do not change significantly with time even when the reaction rate is changing considerably.

6. The cumulative evidence supports a reaction scheme in which two, interdependent, active sites are involved in CO oxidation under pseudo-operating conditions. One site is mainly associated with the metal function of the catalyst whilst the other is intrinsically dependent upon the metal/support interface.

REFERENCES

(1) "Closed-Cycle, Frequency-Stable CO_2 Laser Technology, Proceedings of a workshop held at Langley Research Centre, Hampton, VA, June 10-12, 1986," Batten, C. E.; Miller, I. M.; and Wood, G. M., Jr.: eds., NASA Conference Publication 2456.

(2) Crowell, J. E.; Garfunkel, E. L.; and Somorjai, G. A.: Surf.Sci., vol. 121, 1982, pp. 303-320.

(3) Bond, G. C.; Fuller, M. J.; and Molloy, L. R.: Proc. 6th Int. Congr. Catal., vol 1, 1977, pp. 356-364.

(4) Narita, T.; Miura, H.; Sugiyama, K.; Matsuda, T.; and Gonzalez, R. D.: J.Catal., vol. 103, 1987, pp. 492-495.

(5) Chen, H. W.; Zhong, Z.; and White, J. M.: J.Catal., vol. 90, 1984, pp. 119-126.

(6) Sheppard, N.; and Nguyen, T. T.: Adv. Infrared Raman Spectroscopy, vol. 5, 1978, pp. 67-148.

(7) Upchurch, B. T.; Wood, G. M., Jr.; Hess, R. V.; and Hoyt, R. F.: in reference (1), pp. 193-197.

(8) Brown, K. G.; Schreyer, J.; Schreyer, D. R.; Upchurch, B. T.; Wood, G. M.; Miller, I. M.; Sydney, B. D.; Batten, C. E.; and Paulin, P. A.: in reference (1), pp. 219-225.

(9) Lieske, H.; and Volter, J.: J.Catal., vol. 90, 1984, pp. 96-105.

(10) Gardner, S. D.; Hoflund, G. B.; Schryer D. R.; and Upchurch, B. T.: SPIE Vol. 1062, "Laser Applications in Meteorology and Earth and Atmospheric Remote Sensing," 1989, pp. 21-28.

(11) Bastein, A. G. T. M.; Toolenaar, F. J. C. M.; and Ponec, V.: J. Catal., vol. 90, 1984, pp. 88-95.

(12) Upchurch, B. T.; Schryer, D. R.; Wood, G. M.; and Hess, R. V.: SPIE Vol. 1062, "Laser Applications in Meteorology and Earth and Atmospheric Remote Sensing," 1989, pp. 287-293.

Acknowledgments

TABLE I. ABSORPTION BAND POSITIONS AND ASSIGNMENTS FOR CATALYSTS UNDER REACTION CONDITIONS

FIG.NO.	CONDITIONS	M-CO (cm^{-1})	M_2-CO (cm^{-1})	H_2O SURFACE (cm^{-1})
10	CO ADS. IN LM AT RT REDUCED IN H_2 ONLY	2052	- - - - -	- - - - -
12	REACTION AT RT 1 l/min RX (PRETREAT. AT RT)	2059	c.1890(w)	- - - - -
	1 l/min LM	2052*	c.1890(w)	- - - - -
13	REACTION AT 50°C 1 l/min RX (PRETREAT AT 50 C)	2059	c.1890(w)	- - - - -
	1 l/min LM	2049*	c.1890(w)	- - - - -
14	REACTION AT RT 0.1 l/min RX (PRETREAT. AT RT)	2054	- - - - -	- - - - -
	1 l/min LM	2054*	- - - - -	- - - - -
15	REACTION AT RT 1 l/min RX (PRETREAT AT RT)	2072	c.1870	c.1640
	1 l/min LM	2049** (sh.2100)	c.1850	c.1640
17	REACTION AT RT 0.1 l/min RX (PRETREAT. AT RT)	2071 (sh.)	c.1890	c.1640
	1 l/min LM	2047**	c.1850	c.1640

GLOSSARY

* Slight attenuation of band on exposure to laser mix

** Attenuation of band on exposure to laser mix

w   Weak in intensity

sh.   Shoulder

RX   Reaction mixture

LM   Laser mixture

cm^{-1} Wavenumber

RT   Room temperature

PG

PC | MF | MF | PC

FLOWMETERS

REACTION
VESSEL
IN
SPECTROMETER
SAMPLE
CHAMBER

OXYGEN
ANALYSER

BF

1% CO/
0.4% O₂
IN
LASER
MIX

AIR   H₂

LASER
MIX

PC - PRESSURE CONTROLLER	⋈	ON/OFF VALVE
MF - MASS FLOW CONTROLLER	⋈	NEEDLE/CONTROL VALVE
PG - PRESSURE GAUGE		
BF - BUBBLE FLOWMETER	⋈	3 WAY VALVE
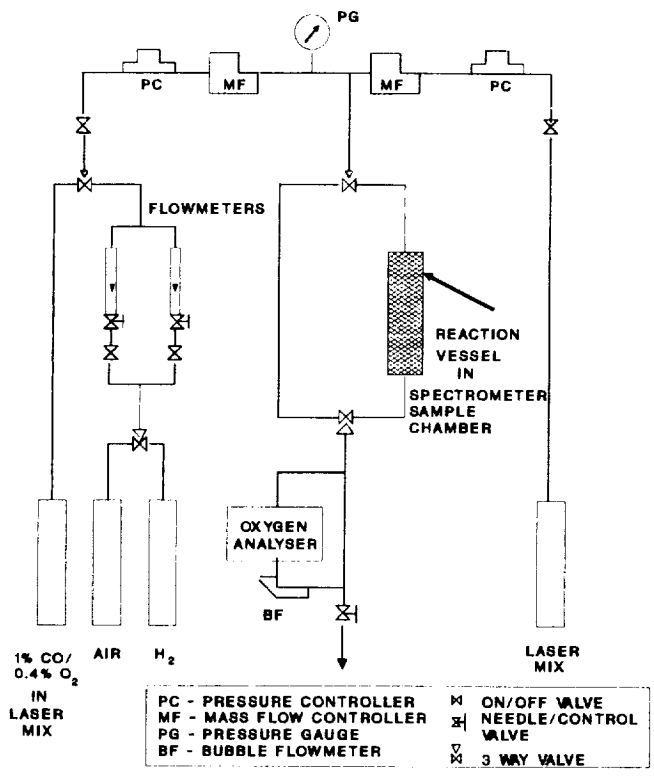
Fig.1 - FTIR REACTION SYSTEM

% Conversion (O_2)

flush with
laser mix

80

60

40

20

0

0   50   100   150   200   250   300   350
Time - minutes
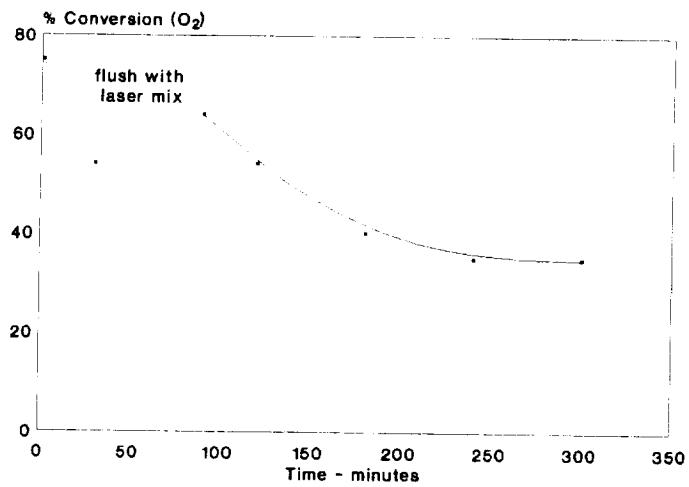
Fig.2 - Deactivation curve for Pt/Ru monolith at 4m/s

172
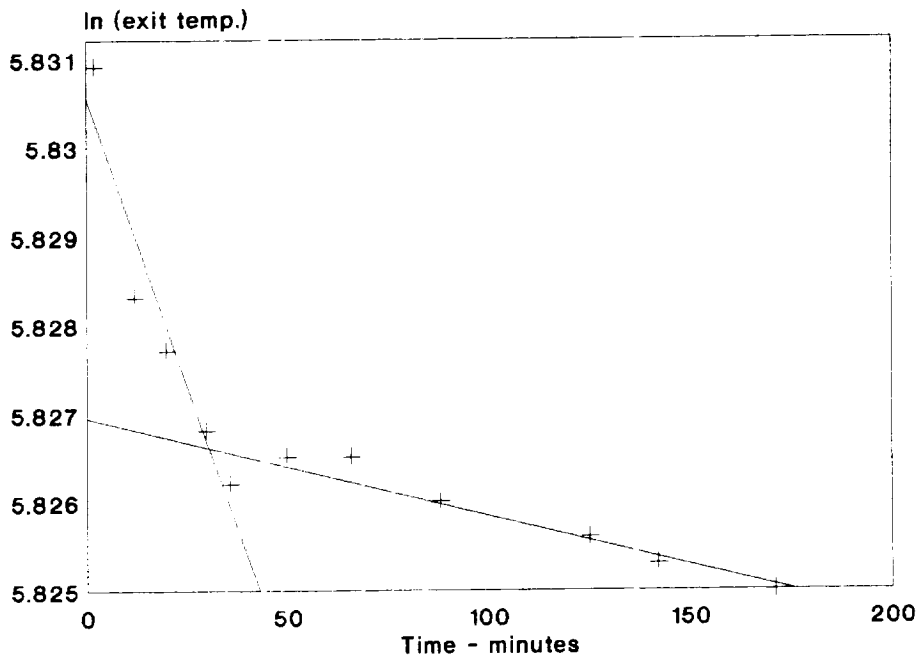
Fig.3 - Pt/Ru Monolith tested at 4 m/s
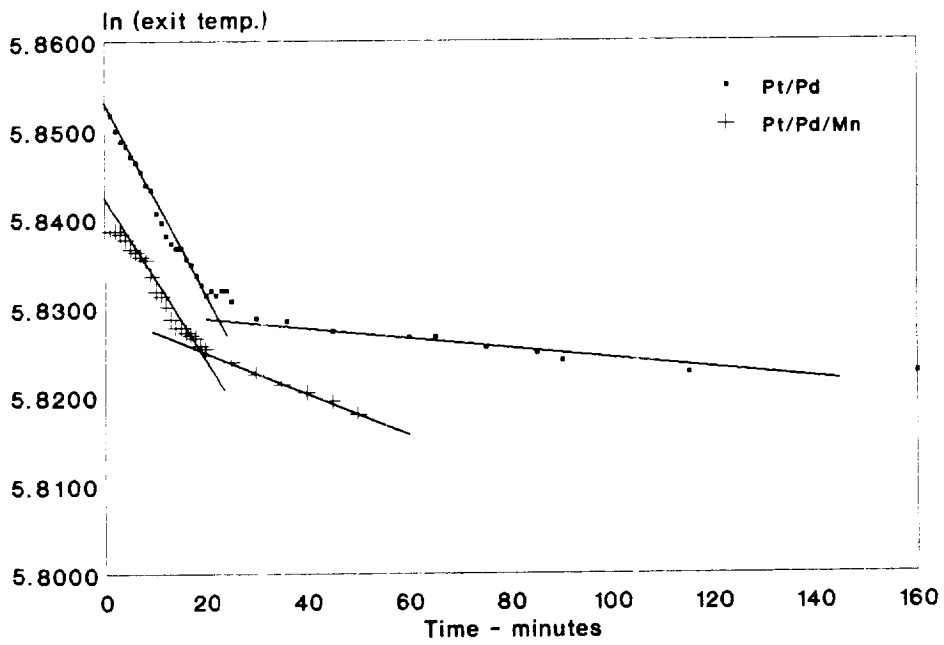
Fig.4 - Pt/Pd Monoliths tested at 4 m/s

173
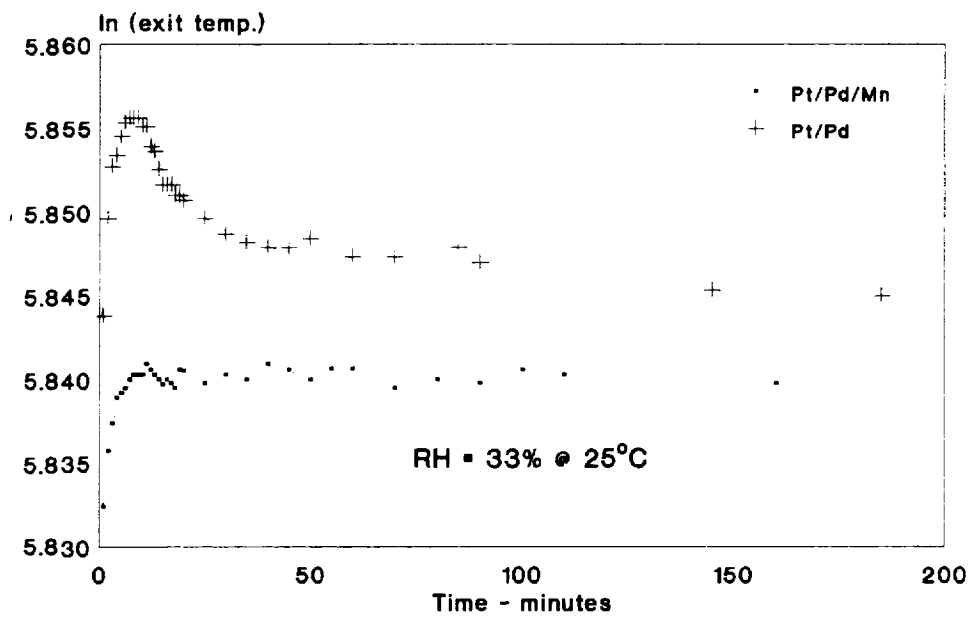
Fig.5 - Pt/Pd monoliths tested at 4 m/s in the presence of water
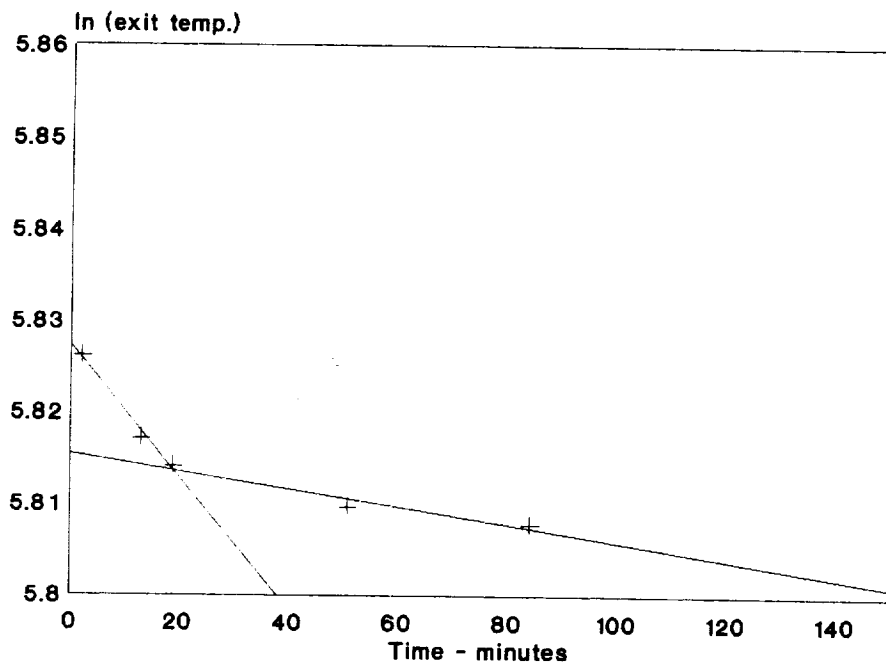

Fig.6 - Pt/Pd/K Monolith tested at 4 m/s

174
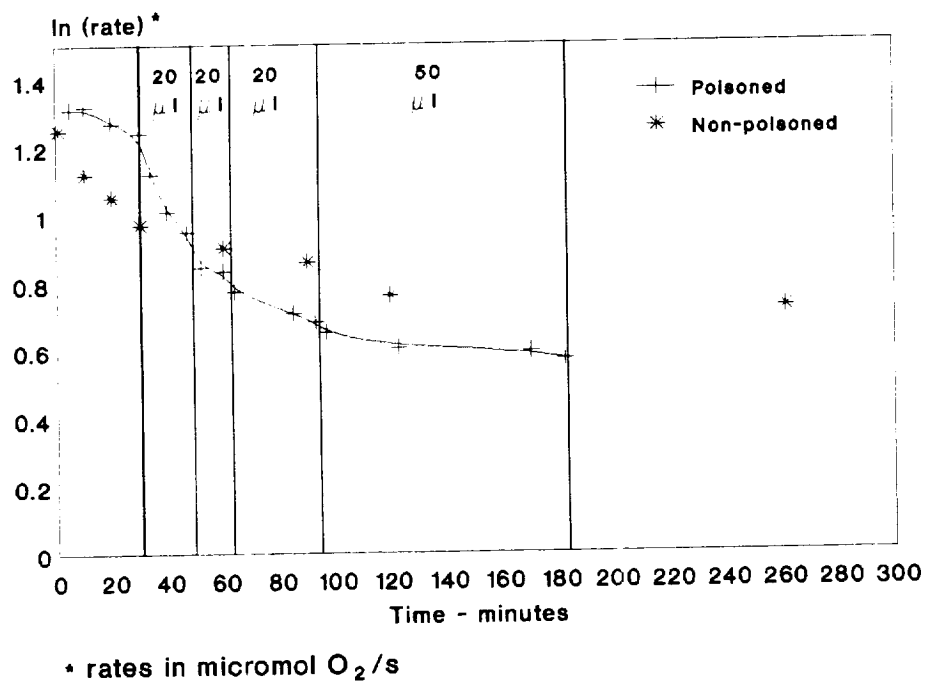
Fig.7 - Deactivation profile for a fresh vs. regenerated Pt/Ru monolith with added acetone
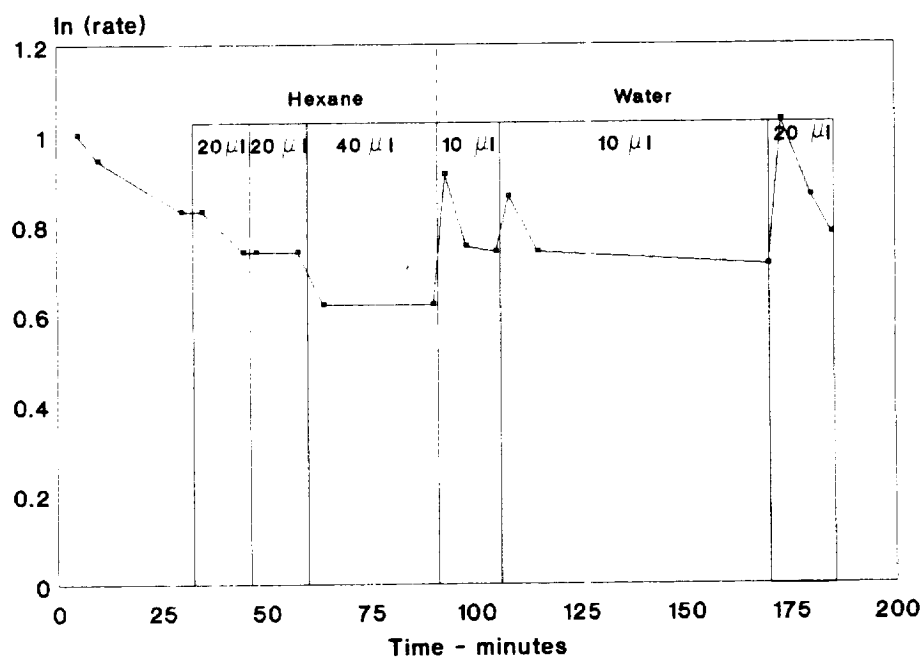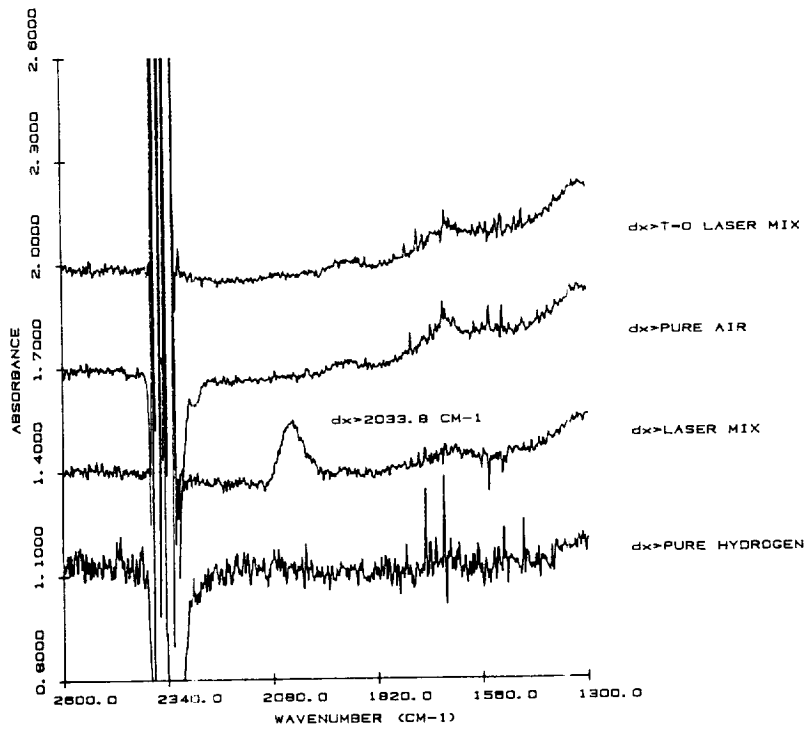

Fig.8 - Cumulative deactivation profile for a deactivated Pt/Ru monolith with added hexane and water

175

In (rate)

10 μl Chloroform	20 μl Chloroform	40 μl Chloroform

Time - minutes
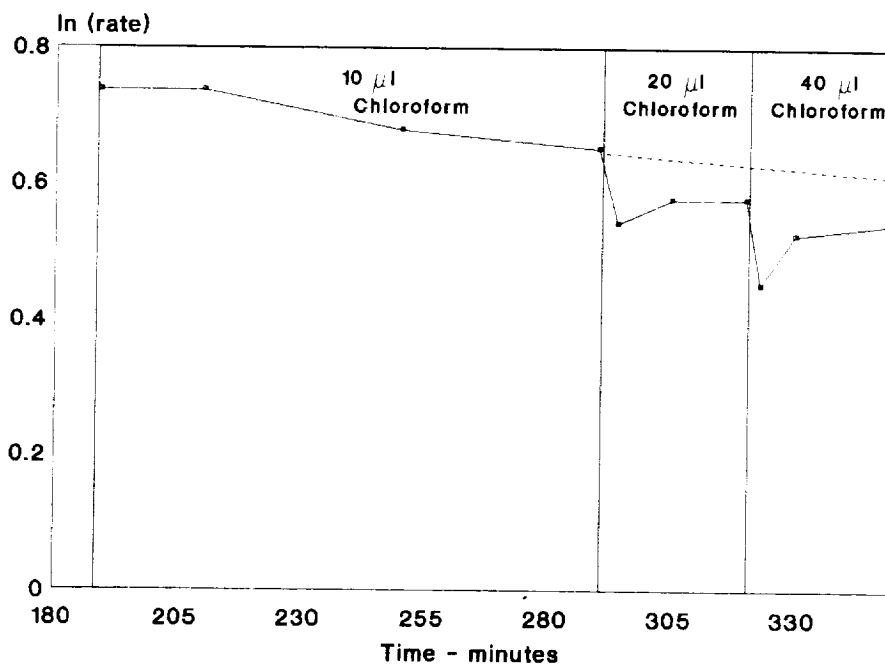
Fig.9 - Cumulative deactivation profile for a deactivated Pt/Ru monolith with added hexane, water and chloroform

dx>T=23C

dx>T=50C

dx>T=92C

dx>T=150C

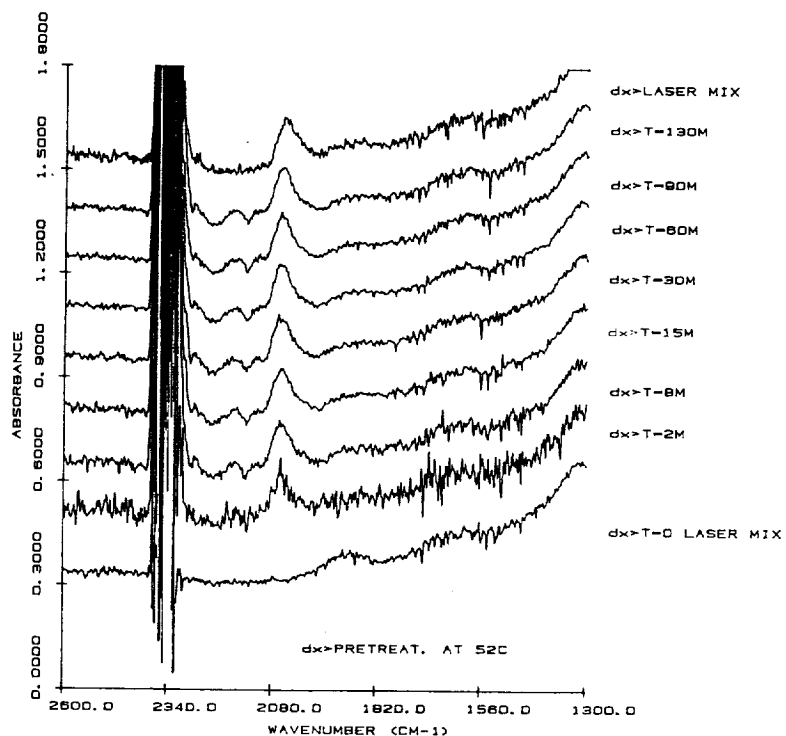dx>T=210C

dx>T=250C

dx>EXPOSED TO AIR, RT

WAVENUMBER (CM-1)
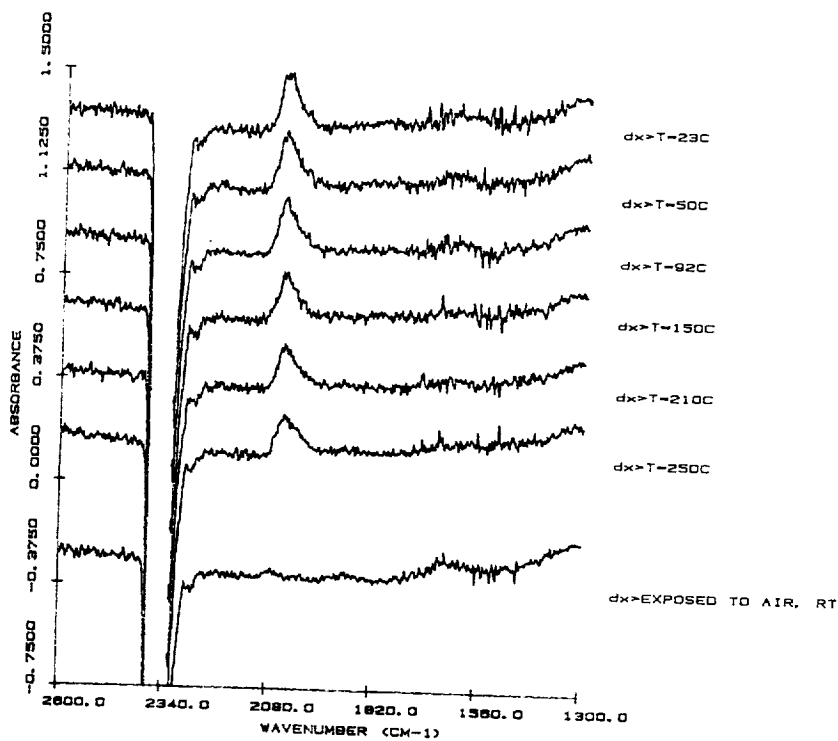
Fig.10 - FTIR Spectra showing CO desorption/reaction on Pt/Ru in Helium/Air
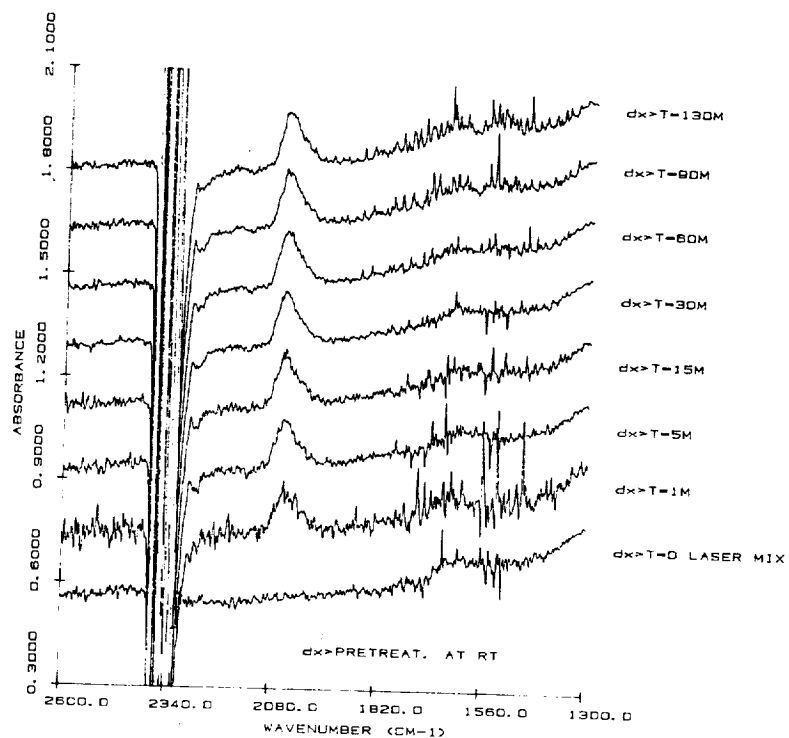
Fig.11 - FTIR Spectra showing CO₂ dissociation/CO reaction
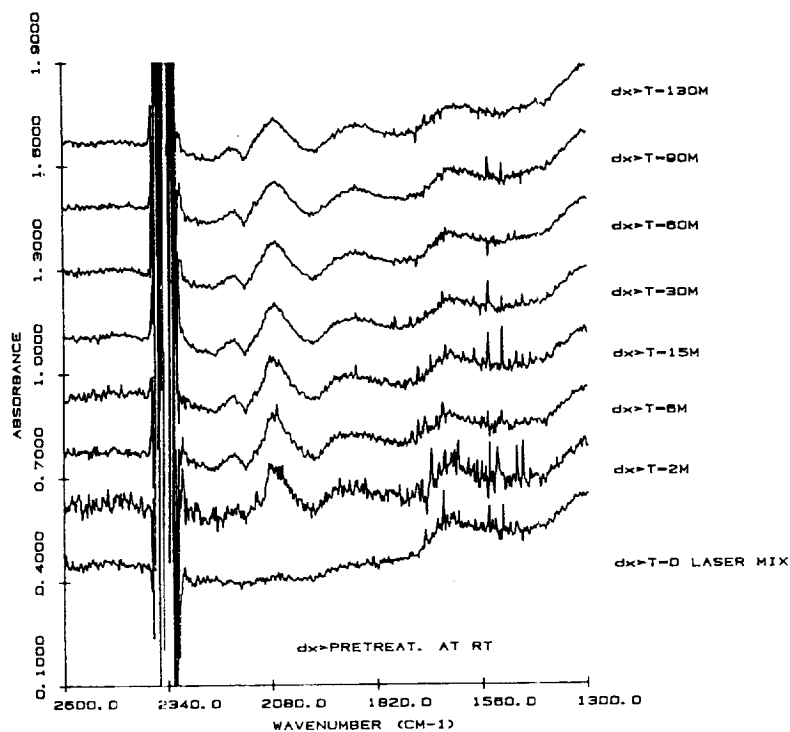on Pt/Ru during pretreatment
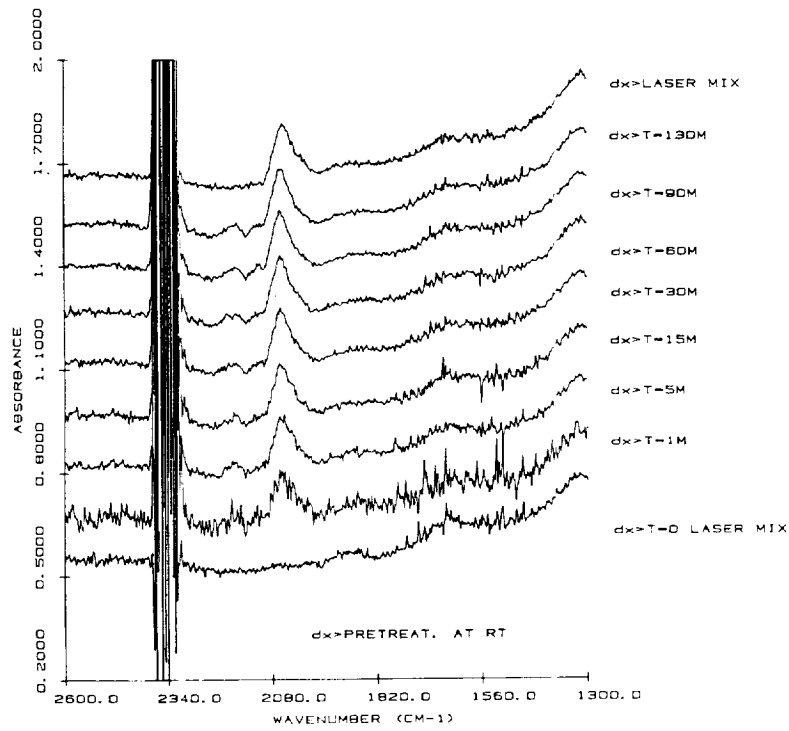
Fig.12 - FTIR Spectra for Pt/Ru with 1 l/min
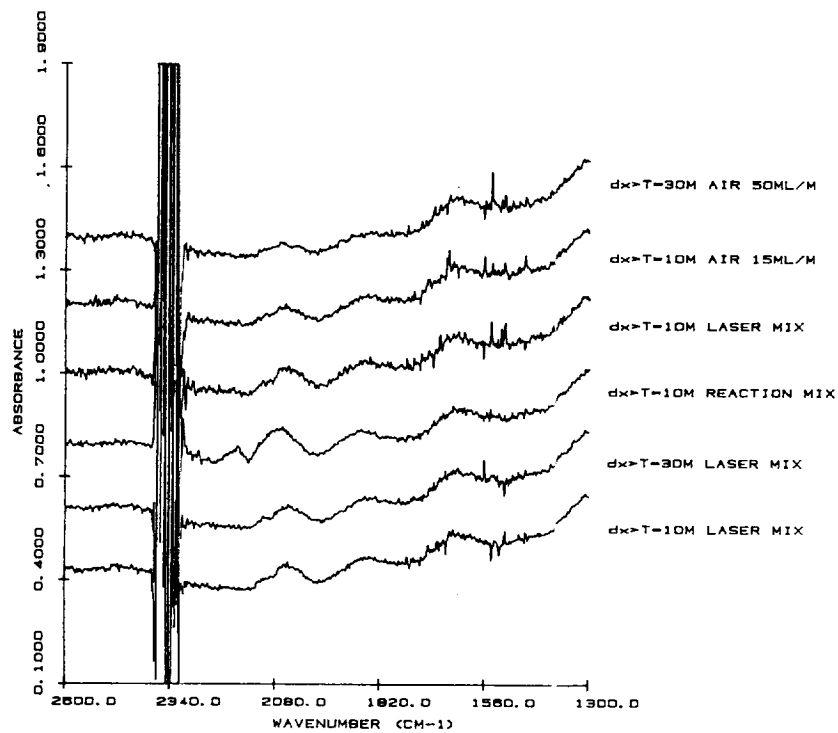reaction gas at room temperature

177

Fig.13 - FTIR Spectra for Pt/Ru with 1 l/min reaction gas at 52°C

Fig.14 - FTIR Spectra for Pt/Ru with 100 ml/min reaction gas at room temperature

178

Fig.15 - FTIR Spectra for Pt/Pd with 1 l/min
reaction gas at room temperature

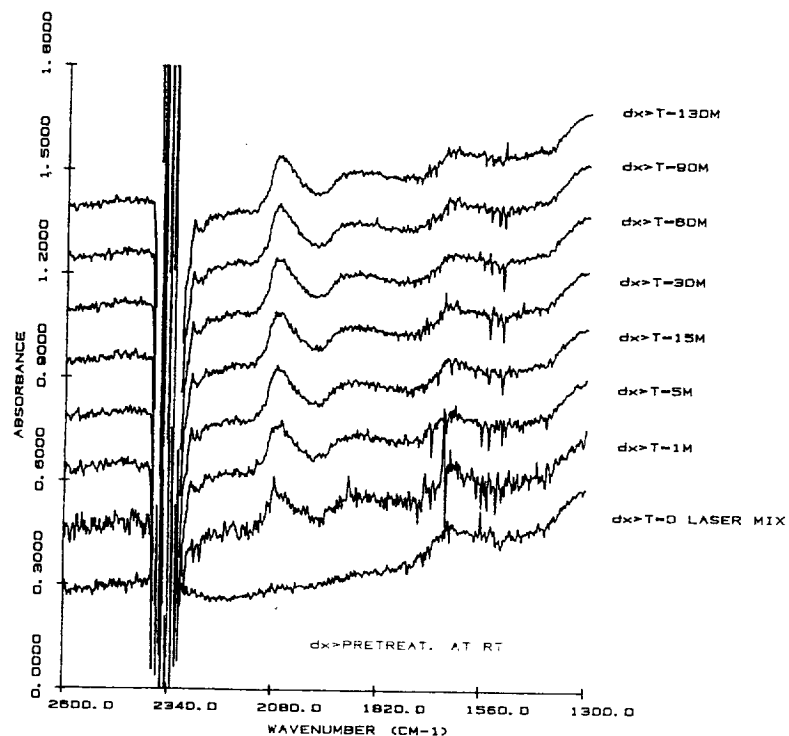Fig.16 - FTIR Spectra for reacted Pt/Pd
on flushing with laser mix and air

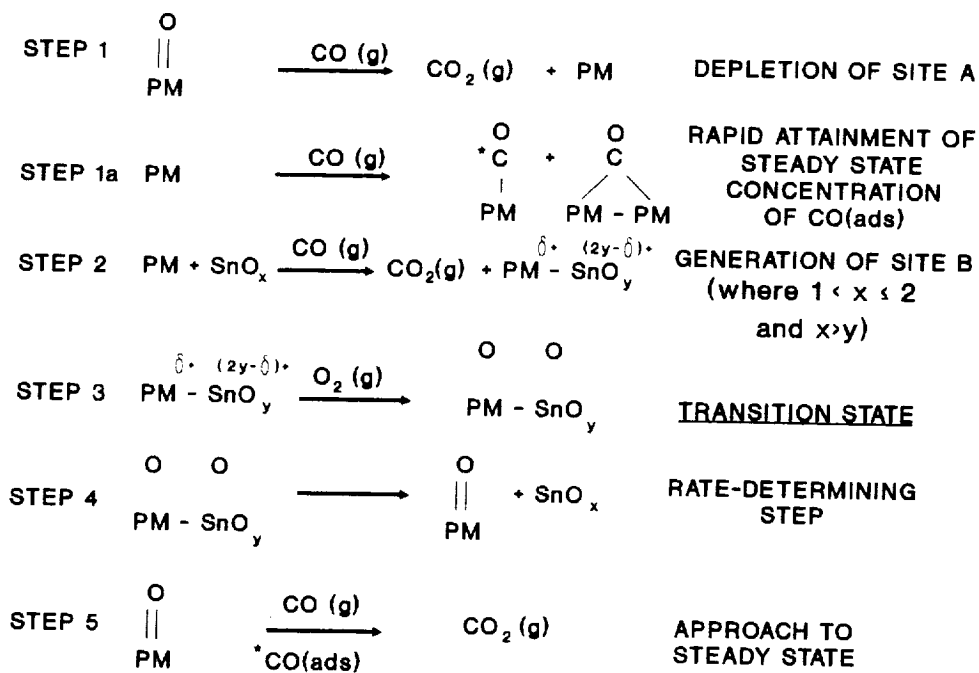Fig.17 - FTIR Spectra for Pt/Pd with 100 ml/min
reaction gas at room temperature

FIG.18 - PROPOSED REACTION MECHANISM FOR LASER CATALYSTS

C-3

THE EFFECT OF H_2O AND PRETREATMENT ON THE ACTIVITY OF A Pt/SnO_2 CATALYST

John D. Van Norman, Kenneth G. Brown, and Jacqueline Schryer
Old Dominion University
Norfolk, VA

David R. Schryer, and Billy T. Upchurch
NASA Langley Research Center
Hampton, VA

Barry D. Sidney
Science and Technology Corporation
Hampton, VA

ABSTRACT

CO oxidation catalysts with high activity at 25°C to 100°C are important for long-life, closed-cycle operation of pulsed CO_2 lasers. A reductive pretreatment with either CO or H_2 has been shown to significantly enhance the activity of a commercially available platinum on tin (IV) oxide (Pt/SnO_2) catalyst relative to an oxidative or inert pretreatment or no pretreatment. Pretreatment at temperatures of 175°C and above causes an initial dip in the observed CO_2 yield before the steady-state yield is attained. This dip has been found to be caused by dehydration of the catalyst during pretreatment and is readily eliminated by humidifying the catalyst or the reaction gas mixture. It is hypothesized that the effect of humidification is to increase the concentration of OH groups on the catalyst surface which play a role in the reaction mechanism.

INTRODUCTION

CO oxidation catalysts are important for long-life closed-cycle operation of CO_2 lasers which are excited by pulsed electrical discharges since such discharges decompose some of the CO_2 to CO and O_2 (Ref. 1). The gradual loss of CO_2 results in a corresponding gradual loss of laser power. However, the buildup of even small concentrations of O_2 molecules can cause discharge instabilities, which result in severe power loss, and even complete laser failure. Although CO_2 lasers differ somewhat in their O_2 tolerance, it is generally desirable to keep the O_2 concentration below a few tenths of 1 mole-percent. CO has no significant deleterious effect on CO_2 laser performance at moderate concentrations.

Many of the potential applications of pulsed CO_2 lasers, including remote sensing from satellites and other space vehicles, require that they operate in a closed-cycle mode with no addition of make-up gas or removal of decomposition products because of volume and weight contraints. To achieve such operation the CO and O_2 produced by the electrical discharge must be recombined continuously to regenerate CO_2. Thus, these lasers represent a new and important application for CO oxidation catalysts. Candidate catalysts must have high efficiency at average laser conditions which are generally 25°C to 100°C and about one atmosphere of total

pressure with low partial-pressures of CO and O_2. Some excess CO may be added to the laser-gas mixture but generally it is not. For space applications no heating of the catalyst is allowed in order to minimize power consumption.

The catalytic oxidation of CO to CO_2 has been extensively studied for a number of catalysts over a wide range of conditions (Refs. 2 and 3). However, few catalysts have the desired efficiency at the low average temperatures and low oxygen partial-pressures characteristic of typical repetitively pulsed CO_2 lasers. The most promising catalysts studied to date whose performance has been verified by actual closed-cycle laser operation consist of Pt and/or Pd on tin (IV) oxide (Refs. 4 and 5). The present paper presents results of studies of various pretreatment techniques on the activity of a commercially available platinum on tin (IV) oxide (Pt/SnO_2) catalyst.

EXPERIMENTAL

The catalyst used in this investigation was 2% (by weight) Pt/SnO_2 powder obtained from Engelhard Industries. This catalyst had an average particle size of 1 ^{e}m and a BET surface area of 6.9 m^2/g. Tests were performed in a plug-flow reactor previously described by Batten et al. (Ref. 6). Gravimetric-grade premixed gas-mixtures which were commercially obtained were used for all experiments. All gas mixtures contained 2.00% Ne as an internal standard in addition to their other constituents. The carrier gas was dry, high-purity He. Gas mixtures were analyzed prior to use in each experiment. All gas analyses were obtained using commercial gas chromatographs (GCs). Sampling and analysis were automated for unattended, continuous operation. The chromatographic column was a coaxial-type with a silica gel/molecular sieve combination to allow concurrent analysis for CO, CO_2, N_2, O_2, and H_2O using a Ne internal standard. The GCs were calibrated frequently with a gravimetric-grade calibration mixture consisting of 1.00% CO, 1.00% CO_2, 1.00% O_2, and 2.00% Ne in dry, high-purity He.

The protocol for all experiments was as follows. A weighed catalyst sample packed between quartz-wool plugs in a reactor tube was inserted into the flow system in the reactor oven and brought to the desired initial temperature. In most cases the catalyst was then exposed for some time to a flow of one of the following pretreatment gases: pure He, 5.00% CO in He, 5.00% H_2 in He, or 5.00% O_2 in He. After pretreatment the gas flow over the sample was temporarily switched to pure He and the reactor-oven temperature was lowered to the desired test temperature. When the test temperature was reached, the gas flow was switched to a stoichiometric mixture of 1.00% CO and 0.50% O_2. The product gases which exited the reactor were then analyzed periodically for CO, CO_2, and O_2 concentrations to determine the conversion efficiency for the particular experimental conditions. The N_2 concentration was also monitored to determine if any air leaks developed in the gas lines or the reactor itself.

In a few cases catalyst samples which served as controls were not pretreated prior to exposure to the reaction-gas mixture. In other experiments the catalyst samples were exposed to H_2O vapor following pretreatment or the reaction gas mixture was humidified.

RESULTS

Figure 1 is a typical plot of percent loss of CO and O_2 relative to their initial concentrations and of percent yield of CO_2 relative to the initial concentration of CO. The pretreatment and test conditions are given on this and subsequent figures. The values of the 3 parameters can be seen to be essentially equal at all times, which indicates that the reaction is stoichiometric. For simplicity, only the percent yield of CO_2 is plotted in subsequent figures even though the percent loss of CO and O_2 were determined and stoichiometry was observed in all cases.

In figure 1 note the initial dip in the percent yield of CO_2 before the steady-state value is attained. Investigation of the cause of this dip yields important insight into the behavior of Pt/SnO_2 catalysts, as discussed below.

Figure 2 presents the percent conversion of CO to CO_2 for four different pretreatment gas compositions: (1) pure He, (2) 5% O_2 in He, (3) 5% CO in He, and (4) 5% H_2 in He. Pretreatment with the reducing gases, CO and H_2, produces approximately equal steady-state CO_2 yields which are significantly higher than those for the other pretreatment gases, although the steady-state yield is more rapidly attained with the H_2 pretreatment. Pretreatment with O_2 in He results in only slightly greater CO_2 yield than pretreatment with He alone. An initial dip in activity is observed in all cases. Clearly, a reductive pretreatment of the catalyst results in significantly greater CO_2 yields than does either oxidative or inert pretreatment. Therefore, CO pretreatment was employed for all subsequent tests.

Figure 3 compares the percent CO_2 yield for an unpretreated catalyst sample with that for an equal-mass sample pretreated with CO for 1 hour and for another sample pretreated for 20 hours. Both pretreatments enhance the CO_2 yield but the 20 hour-pretreatment is less effective than that for 1 hour.

Figure 4 compares the percent yield of CO_2 for an unpretreated catalyst sample to that for equal-mass samples pretreated at various temperatures. All of the pretreated samples exhibited greater CO_2 yields than the unpretreated sample. No difference in CO_2 yield is observed for pretreatment temperatures of 125°C through 225°C, but the 100°C pretreatment results in a somewhat lower yield.

It is apparent from figures 3 and 4 that a fairly mild pre-reduction of these catalysts is sufficient to produce significant activity and that more severe pretreatment (e.g., 20 hours or so) produces less than optimum results. Analysis of the exit gas during each pretreatment showed that conversion of CO to CO_2, and thus reduction of the catalyst surface, was

complete in less than 1 hour for the conditions utilized. It is recommended that such an analysis be performed each time a catalyst sample is pretreated and that pretreatment be terminated when no further reduction of the sample is observed.

DISCUSSION

The initial dip in CO_2 yield which is frequently encountered following catalyst pretreatment is more than an experimental inconvenience. Figure 5 shows the results of a 27-day test of a 1.50 g catalyst sample which was pretreated with pure He for 20 hours at 225°C and 10 SCCM prior to testing at 85°C and 10 SCCM. This test produced a dip that lasted for about 25,000 minutes or 17 days. Clearly such a dip is unacceptable for virtually all practical applications. The long duration of the dip in this case appears to have been caused by the long pretreatment time and relatively large sample mass. Nevertheless, a dip lasting even a day or two is not only inconvenient but can cause erroneous results if its existence is not known and a test is terminated at or near the trough of the dip. Thus, it is important to determine the cause of the dip and to eliminate it if possible. In order to achieve these goals, a review of the conditions under which the dip occurs is in order.

In figures 3 and 4 it can be seen that no dip occurs in the CO_2 yield for the unpretreated catalyst samples. However, a dip is clearly present for the samples in figure 3 which were pretreated for 1 hour and 20 hours at 225°C. In figure 4, no dip is present for the samples which were pretreated at 100°C and 125°C, but a dip occurs for the samples pretreated at 175°C and 225°C, although this is somewhat difficult to see in this figure. Figure 6 is an expansion of the first 800 minutes of figure 4 with only the 125°C and 175°C pretreatment data shown. In figure 6 a dip can clearly be seen for the 175°C pretreatment but not for the 125°C pretreatment.

Figure 7 presents the CO_2 yield for a sample that underwent a vacuum pretreatment for 2 hours at a catalyst temperature of 225°C prior to its exposure to the reaction gas mixture at 85°C and 5 SCCM. A pronounced initial dip can be seen.

It is apparent from the foregoing observations that the initial dip in CO_2 yield occurs only when the catalyst samples have been exposed to an elevated temperature during pretreatment. Based on the data presented in Figure 6, the critical temperature for the onset of the dip lies somwhere between 125°C and 175°C. All samples which were exposed during pretreatment to a temperature of 175°C or higher exhibit the dip, but the dip is not exhibited by any sample that was pretreated at 125°C or less or not pretreated at all.

This observation suggests that the dip may somehow be associated with dehydration of the catalyst during pretreatment at elevated temperatures. This hypothesis is confirmed by the data presented in figure 8. The two equal-mass catalyst samples represented in this figure were both pretreated with CO in He for 2 hours at 225°C and then exposed to the reaction gas mixture at 85°C and 10 SCCM. However, one sample was

humidified following pretreatment and before reaction by exposure for 20 minutes to a 5 SCCM flow of He that had been bubbled through water. The H_2O content of the He was about 2 mole-percent. The unhumidified sample exhibited the initial dip; the humidified sample did not.

Alternatively, humidification of the catalyst can be achieved simply by humidifying the reaction gas mixture. Furthermore, a relatively low H_2O content is sufficient. Figure 9 reproduces the CO_2 yield which was originally presented in figure 2 and which clearly exhibits an initial dip. The other curve is the CO_2 yield from an equal-mass catalyst sample which underwent identical pretreatment but for which the reaction-gas mixture was humidified by passing it through a container of $CaCl_2 \cdot 2H_2O$. The resultant H_2O content of the reactant gas was about 0.2 mole-percent. No dip occurs. Furthermore, a higher yield of CO_2 was attained with the humidified reaction-gas than with the dry reaction-gas. Croft and Fuller (ref. 7) have previously reported an enhancement of CO_2 yield for a Pd/SnO_2 catalyst when the reaction gas was humidified. They did not, however, address the problem of the pretreatment-induced activity dip dealt with in this paper.

A possible explanation of the phenomena reported herein is as follows. It is postulated that OH groups on the surface of the tin-oxide phase serve as oxidants for CO chemisorbed on adjacent Pt sites. Hoflund et al., (ref. 8) have observed OH groups as a significant constituent of tin-oxide surfaces. Reductive pretreatment of the catalyst enhances chemisorption of O_2 on the tin-oxide surface. Chemisorbed O_2 is converted to OH by reaction with surface H_2O or H. Pretreatment of the catalyst at elevated temperatures dehydrates its surface and thereby significantly depletes the surface concentration of OH. The initial reaction which occurs when the catalyst is exposed to the test-gas mixture further depletes the surface OH and partially reoxidizes the surface resulting in the observed decline in catalyst activity. Migration of H_2O (or possibly OH or H) from the catalyst bulk eventually increases the surface concentration of OH and restores the catalyst activity. The sequential decline and increase in catalyst activity results in the observed dip. If, after pretreatment, the OH concentration at the catalyst surface is restored by humidification of the catalyst or the reaction gas, no dip is observed. Also, if the pretreatment temperature is low enough that surface OH and H_2O are substantially retained, no dip is observed. If the OH concentration at the catalyst surface is increased by humidification, the activity of the catalyst is somewhat enhanced as shown in figures 8 and 9 and as observed by Croft and Fuller (ref. 13).

CONCLUSIONS

The pretreatment conditions of Pt/SnO_2 catalysts are important in determining their activity for the oxidation of CO to CO_2. Reductive pretreatment with either CO or H_2 is superior to oxidative or inert pretreatment. The pretreatment conditions can be relatively mild with the temperature as low as 125°C and the duration only long enough to reduce the catalyst surface. Pretreatment at elevated temperatures results in an initial dip in the observed CO_2 yield before the steady-state yield is attained. This dip is associated with dehydration of the catalyst and can

readily be eliminated by humidifying the catalyst or the reaction-gas mixture. Such humidification can result in an enhancement of catalyst activity, possibly by increasing the concentration of OH groups on the catalyst surface.

REFERENCES

1. Schryer, David R.; Sidney, Barry D.; Miller, Irwin M.; Hess, Robert V.; Wood, George M.; Batten, Carmen E.; Burney, L. Garland; Hoyt, Ronald F.; Paulin, Patricia A.; Brown, Kenneth G.; Schryer, Jacqueline; and Upchurch, Billy T.: NASA-LaRC Research on Catalysts for Long-Life Closed-Cycle CO_2 Lasers. Closed-Cycle Frequency-Stable CO_2 Laser Technology, Carmen E. Batten, Irvin M. Miller, George M. Wood, Jr., and David V. Willetts, Eds., NASA CP-2456, pp. 113-120, 1987.

2. Herz, Richard D.: Chemical Engineering Design for CO Oxidation Catalysts. Closed-Cycle Frequency-Stable CO_2 Laser Technology, Carmen E. Batten, Irvin M. Miller, George M. Wood, Jr., and David V. Willetts, Eds., NASA CP-2456, pp. 103-112, 1987.

3. Engel, T., and Ertl, G.: Oxidation of Carbon Monoxide. The Chemical Physics of Solid Surfaces and Heterogeneous Catalysis, P. A. King and D. P. Woodruff, Eds., pp. 73-93, Elsevier, New York, 1982.

4. Stark, D. S.; Crocker, A.; and Steward, G. J.: A Sealed 100 Hz CO_2 TEA Laser Using High CO_2 Concentrations and Ambient-Temperature Catalysts. J. Phys. E. Sci. Instrum., vol. 16, pp. 158-161, 1983.

5. Brown, Kenneth G.; Sidney, B. D.; Schryer, D. R.; Upchurch, B. T.; Miller, I. M.; Wood, G. M.; Hess, R. V.; Batten, C.; Burney, L. G.; Paulin, P. A.; Hoyt, R.; and Schryer, J.: Catalytic Recombination of Dissociation Products with Pt/SnO_2 for Rare and Common Isotope Long-Life, Closed-Cycle CO_2 Lasers. SPIE Proc., vol. 663, pp. 136-144, 1986.

6. Batten, Carmen E.; Miller, Irvin M.; Paulin, Patricia A.; and Schryer, Jacqueline: Studies of CO Oxidation on Pt/SnO_2 Catalyst in Surrogate CO_2 Laser Facility. Closed-Cycle, Frequency-Stable CO_2 Laser Technology, Carmen E. Batten, Irvin M. Miller, George M. Wood, Jr., and David V. Willetts, Eds, NASA CP-2456, pp. 193-198, 1987.

7. Croft, G. and Fuller, M. J.: Water-Promoted Oxidation of Carbon Monoxide Over Tin(IV) Oxide-Supported Palladium. Nature, vol. 269, pp. 585-586, 1977.

8. Hoflund, Gar B.; Grogan, Austin L., Jr.; Asbury, Douglas A.; and Schryer, David R.: A Characterization Study of a Hydroxylated Polycrystalline Tin Oxide Surface. Thin Solid Films, vol. 169, pp. 69-77, 1989.
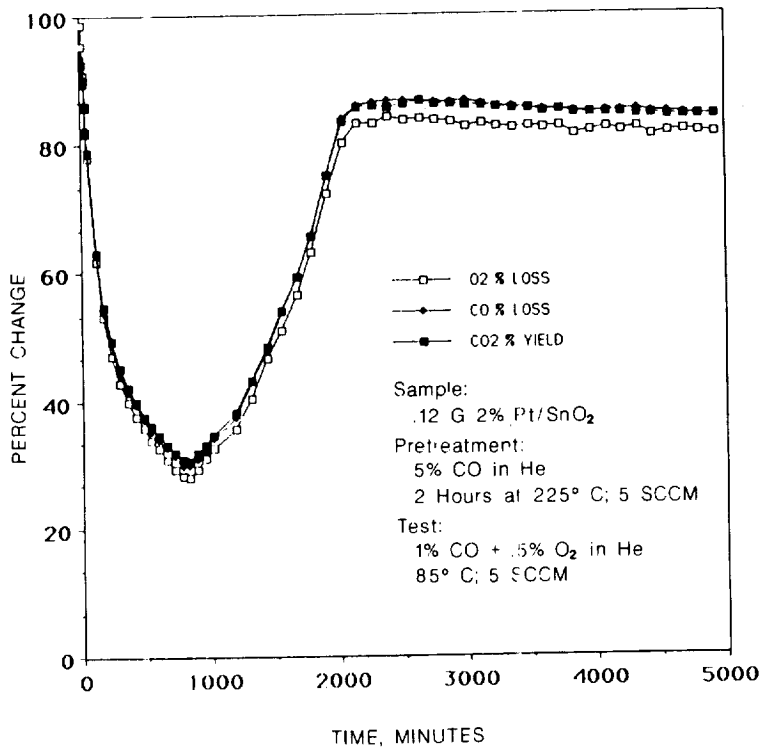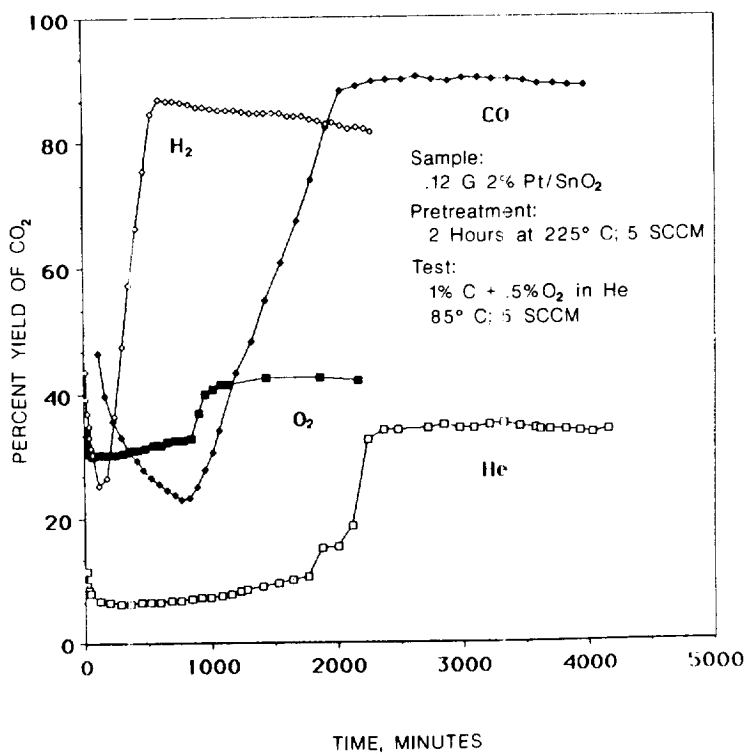
Figure 1. Typical test of Pt/SnO2 catalyst.

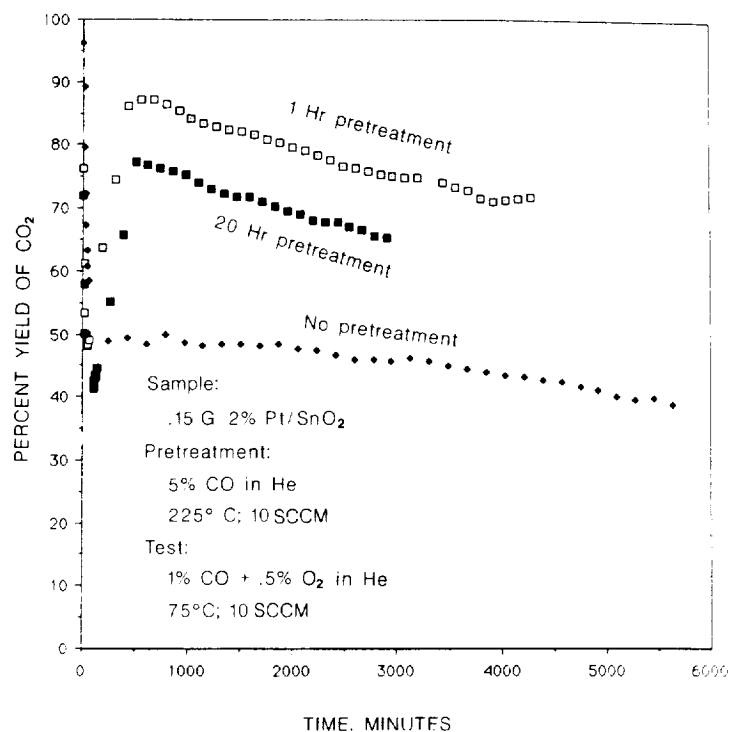Figure 2. Effect of several pretreatment gases on activity of Pt/SnO2 catalyst.

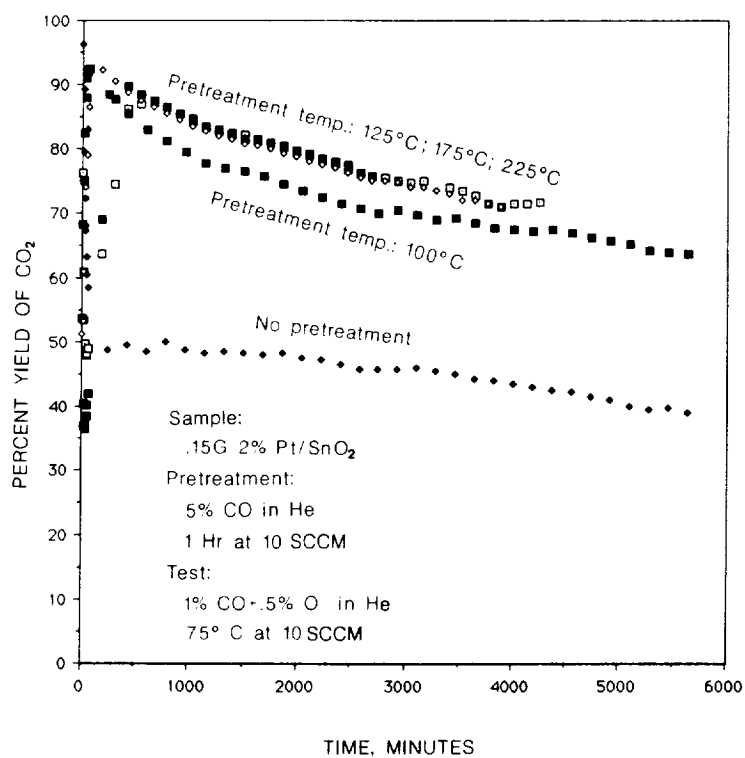Figure 3. Effect of pretreatment duration on activity of Pt/SnO$_2$ catalyst.

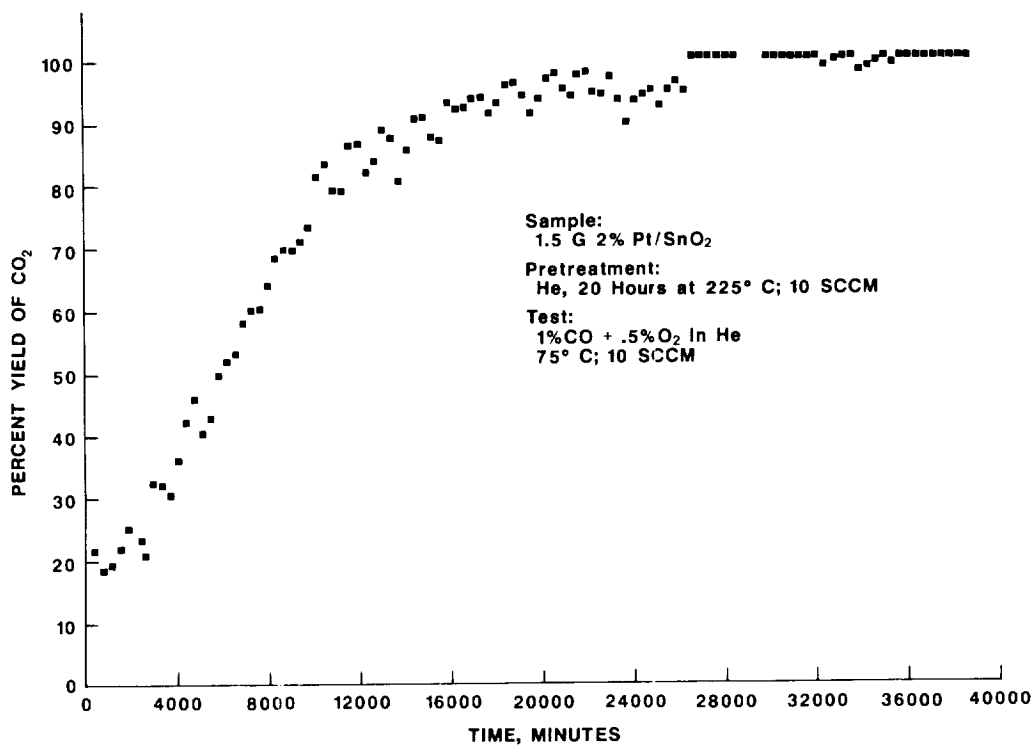Figure 4. Effect of pretreatment temperature on activity of Pt/SnO$_2$ catalyst.

Figure 5. 28-day test of 1.5 grams of Pt/SnO₂ catalyst following extended pretreatment.
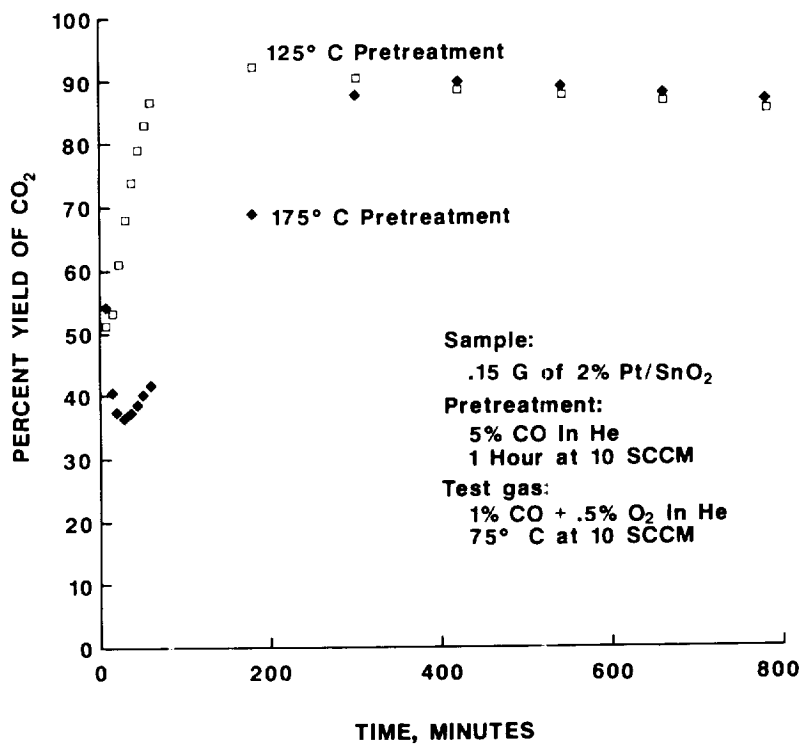

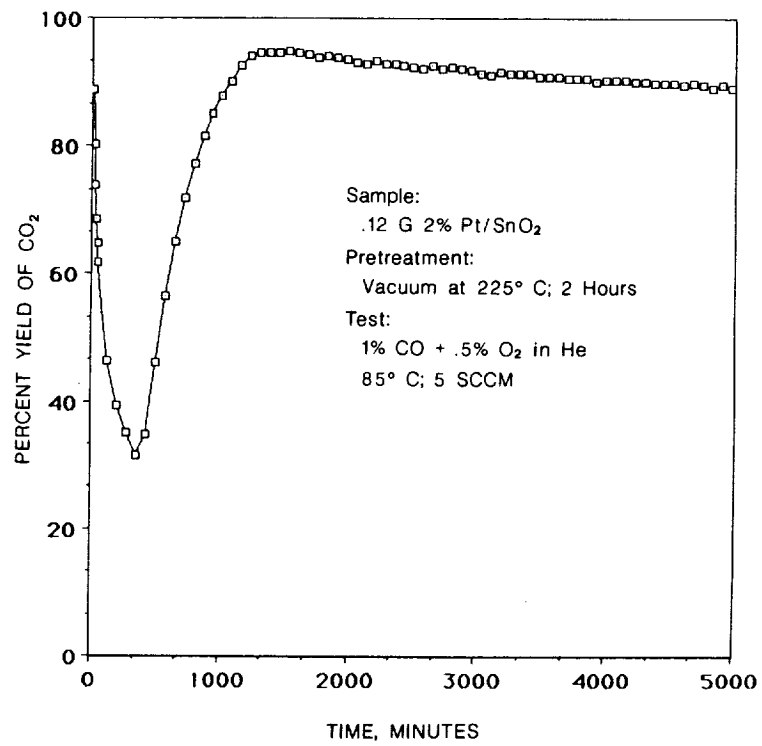Figure 6. Expansion of selected data from Figure 4.

Figure 7. Effect of vacuum pretreatment on behavior of Pt/SnO$_2$ catalyst.
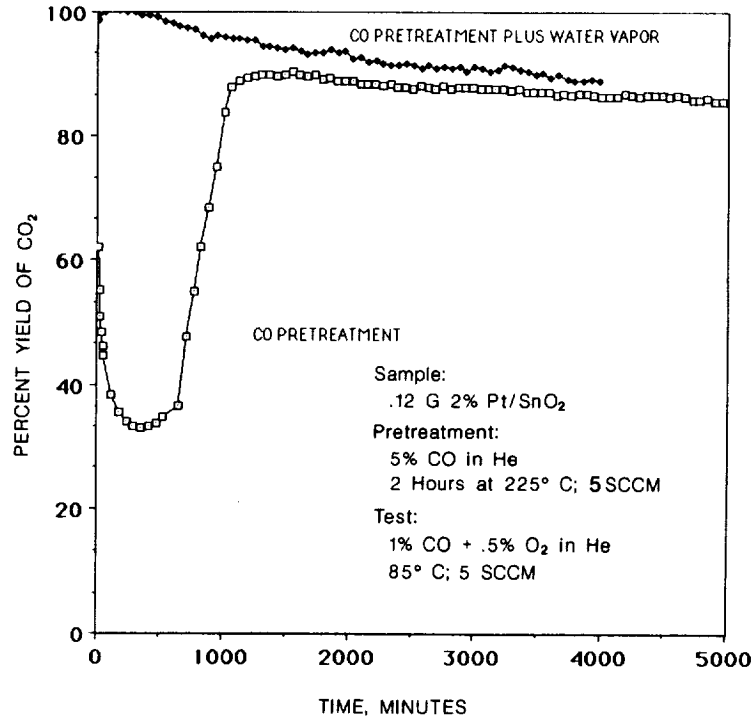

Figure 8. Effect of water addition following pretreatment on behavior of Pt/SnO$_2$ catalyst.
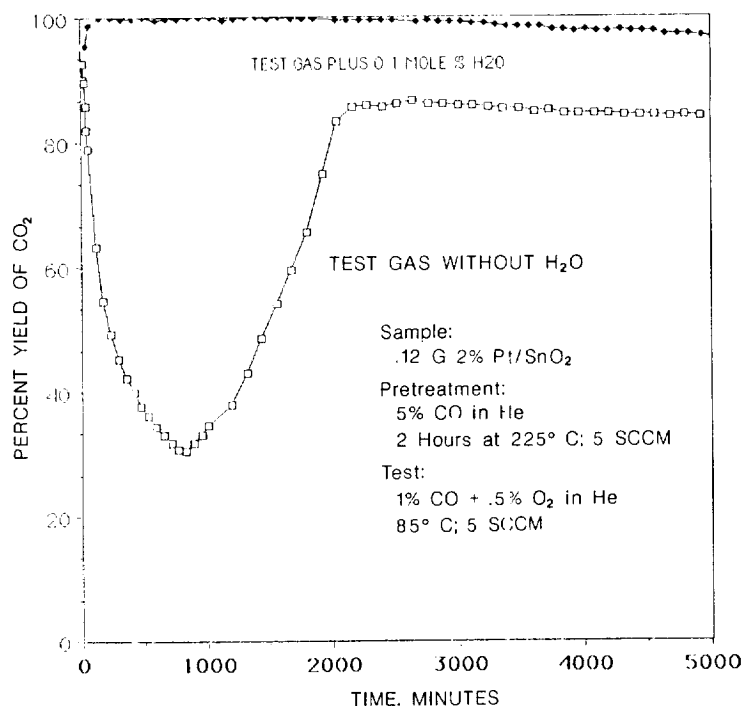
Figure 9. Effect of adding water to test gas on behavior of Pt/SnO_2 catalyst.

RARE-ISOTOPE AND KINETIC STUDIES OF Pt/SnO$_2$ CATALYSTS

Billy T. Upchurch, George M. Wood, David R. Schryer, Robert V. Hess
NASA Langley Research Center
Hampton, VA 23665

Irvin M. Miller
Science and Technology Corporation
Hampton, VA 23666

Erik J. Kielin
Old Dominion University
Norfolk, VA 23529

ABSTRACT

Closed-cycle pulsed CO$_2$ laser operation requires the use of an efficient CO-O$_2$ recombination catalyst for these dissociation products which otherwise would degrade the laser operation. The catalyst must not only operate at low temperatures but also must operate efficiently for long periods. In the case of the Laser Atmospheric Wind Sounder (LAWS) laser, an operational lifetime of 3 years is required. Additionally, in order to minimize atmospheric absorption and enhance aerosol scatter of laser radiation, the LAWS system will operate at 9.1 micrometers with an oxygen-18 isotope CO$_2$ lasing medium. Consequently, the catalyst must not only operate at low temperatures but must also preserve the isotopic integrity of the rare-isotope composition in the recombination mode.

Several years ago an investigation of commercially available and newly synthesized recombination catalysts for use in closed-cycle pulsed common and rare-isotope CO$_2$ lasers was implemented at the NASA Langley Research Center. Since that time, mechanistic efforts utilizing both common and rare oxygen isotopes have been implemented and continue. Rare-isotope studies utilizing commercially available platinum-tin oxide catalyst have demonstrated that the catalyst contributes oxygen-16 to the product carbon dioxide thus rendering it unusable for rare-isotope applications. A technique has been developed for modification of the surface of the common-isotope catalyst to render it usable. In this paper we report on results of kinetic and isotope label studies using plug flow, recycle plug flow, and closed internal recycle plug flow reactor configuration modes.

INTRODUCTION

A problem affecting the use of pulsed CO$_2$ lasers for applications involving atmospheric transmission is the attenuation of the intensity of the laser output due to absorption by atmospheric CO$_2$ which is present at about 330 ppm concentration. As this is predominantly the common isotope, $^{12}C^{16}O_2$, the use of a rare-isotope of CO$_2$ would enable the laser to emit at frequencies which would not be readily absorbed by the atmosphere.

Among the available rare-isotope CO_2 compounds, $^{12}C^{18}O_2$ is the least expensive. Furthermore, in addition to providing enhanced atmospheric transmission, it has the added advantage of enhanced aerosol scattering due to its comparatively short wavelength of 9.1 micrometers which may be further enhanced by surface interactions with some aerosol species (ref. 3). Frequency-envelopes or "windows" which are favorable for atmospheric transmission are presented for various CO_2 isotopes in references 1 and 2.

A second problem associated with the operation of pulsed CO_2 lasers is that the electrical discharge normally used to excite such lasers inevitably decomposes some of the CO_2 to CO and O_2. This decomposition is harmful to long-life laser operation both because of the loss of CO_2 and because of the buildup of O_2. The loss of CO_2 results in a corresponding gradual loss of laser power; the buildup of even small concentrations (about 0.1 percent to 1.0 percent) of O_2 can cause rapid power loss and even complete laser failure. To obviate these problems with no wastage of costly rare-isotope gases the product CO and O_2 must be recombined with a suitable catalyst.

Rare-isotope $^{12}C^{18}O_2$ laser operation has been carried out at 300°C with a common-isotope Pt/Al_2O_3 catalyst at Los Alamos National Laboratory (ref. 4). In these studies, while the alumina was considered an inert substrate and not a participant in the catalytic recombination of $^{12}C^{18}O$ and $^{18}O_2$ to form CO_2, special attention and care were necessary to reduce the exchange or scrambling of the normal-isotope oxygen in $Al_2^{16}O_3$ with the $^{18}O_2$ and the $^{12}C^{18}O$ dissociation products of the laser medium. A platinum-tin oxide catalyst (Pt/SnO_2) has been shown to operate with a respectable recombinative efficiency at considerably lower temperatures than achieved in the Los Alamos study of platinum on alumina (ref. 5), but again the possibility of isotope exchange between a common-isotope catalyst and rare-isotope gases exists.

The primary goals of the present study were to measure isotopic exchange between the rare-isotope laser gases $^{12}C^{18}O_2$, $^{12}C^{18}O$, and $^{18}O_2$ and common-isotope Pt/SnO_2 catalyst material and to develop techniques to maximize isotopic integrity of the rare-isotope laser gases to maintain laser power at the desired frequency. A further goal was to utilize common and rare-isotope gases to determine mechanistic details of CO oxidation on the Pt/SnO_2 catalyst.

Experiments described in this paper demonstrate that, while some oxygen exchange between the gaseous oxygen and carbon monoxide species and the Pt/SnO_2 substrate does indeed occur even at low reaction temperatures, isotopic scrambling may be eliminated by an inexpensive isotope-exchange surface-labeling technique developed at Langley Research Center (ref. 6). Also, evidence is presented for the formation of a carbonate species on the catalyst when the conversion of CO and CO_2 occurs.

EXPERIMENTAL

The experimental apparatus for isotope measurements consisted of a test gas cylinder connected through a gas-drying chamber, flow controller, and a temperature-controlled catalyst reactor-chamber to a mass spectrometer gas-sampling inlet. The drying chamber was charged with anhydrous magnesium perchlorate. A Hastings mass-flow controller was placed upstream from the catalyst chamber. Excess gas flow not passing into the mass spectrometer was diverted through a Hastings mass-flow meter to the outside atmosphere. The mass spectrometer was a DuPont CEC Model 21-104 magnetic-sector unit. The catalyst reactor-chamber was built from components and maintained temperature control within 0.5°C. The catalyst of 1 percent Pt/SnO_2 was obtained from Englehard Industries. All catalyst charges were placed in the chamber enclosed within a 6.35 mm internal diameter by an approximately 40 cm long quartz tube. The catalyst was held in place by quartz wool plugs on each end of the charge. All rare-isotope gas compositions were obtained from Cambridge Isotope Laboratories with stated isotopic purities of better than 98 atomic-percent and were analyzed mass spectrometrically in our laboratory prior to use. All other gases were from Scott Specialty Gases. Chemisorption measurements were carried out using a Shimadzu thermal-conductivity-detector gas-chromatograph. All test-gas flow rates were 5 standard cubic centimeters per minute. All CO concentrations were 2 percent by volume in neon. All O_2 concentrations were 1 percent by volume in neon. All stoichiometric mixtures of CO and O_2 were 2 percent and 1 percent, respectively, with a 2 percent neon spike (as an internal standard) and the balance helium. Hydrogen was 7.5 percent by volume in helium.

For kinetic studies a recycle plug-flow reactor was operated in a recirculating volume of approximately 200 ml with a recirculating flow rate of 200 ml/min. Samples were contained in a temperature-controlled quartz reactor tube as in the isotope measurement experiment. The recycle plug-flow reactor was evacuated and filled with test gas and operated in a closed recycle configuration for all kinetic studies. Internal recycle flow rates were nominally 200 ml/min for all kinetic experiments. Catalyst test specimens were 0.050 g in order to lower conversion rates enough to allow sufficient gas chromatographic analyses to follow the reaction through several half-lives. During tests to determine the kinetic order for oxygen in the catalytic reaction the CO concentration was nominally held constant at 50 percent. Initial oxygen concentrations were nominally 2 percent. Repetitive tests were carried over a temperature range of 0-125°C using a NASA prepared platinum oxide/silica gel catalyst (refs. 7, 8, 9).

RESULTS AND DISCUSSION

During carbon monixide chemisorption studies, it was found that some CO chemisorbed onto the Pt/SnO_2 catalyst at room temperature while other CO was oxidized and immediately evolved as CO_2 with the consequent reduction of the catalyst surface by removal of some oxide. A room-temperature CO chemisorption titration of a 1.0 gram sample of 1 percent Pt/SnO_2 catalyst was found to bind 42 microliters of CO in some form. Thermal desorption yielded 42 microliters of CO_2 as measured mass

spectrometrically. To determine whether or not the CO was converted to CO_2 by the heat involved in the thermal desorption another sample of catalyst with chemisorbed CO was treated with gaseous HCl. It evolved CO_2 at room temperature, which indicated that oxidation of the CO had already occurred, possibly as a carbonate-like species. Subsequently, chemisorption of $^{12}C^{18}O$ upon a normal isotope Pt/SnO_2 catalyst substrate followed by thermal desorption of CO_2 yielded an approximately 4:4:1 ratio of $^{12}C^{16}O^{18}O:^{12}C^{18}O_2:^{12}C^{16}O_2$ as would be expected from a carbonate species, thus lending further support to the existence of such an intermediate species in the recombinative mechanism.

Since the primary goal of this research was to develop a catalytic $CO-O_2$ recombination system for the operation of a rare-isotope closed-cycle pulsed CO_2 laser system, isotope-exchange studies were subsequently carried out to thoroughly investigate the Pt/SnO_2 catalyst system with regard to isotopic interactions with all laser gas species as shown in table I.

As is noted in table I, $^{12}C^{18}O$ was found to readily extract some oxygen-16 from common-isotope Pt/SnO_2 at temperatures from room temperature upwards. Thus, the common-isotope catalyst cannot be used, in unmodified form, for regeneration of the dissociation products which would be encountered in a closed-cycle rare-isotope CO_2 laser. Rows 2, 3, and 4 in table I show that there was no exchange or scrambling reaction observed between $^{18}O_2$ (alone or in combination with $^{16}O_2$) and the $Pt/Sn^{16}O_2$ catalyst substrate until temperatures substantially greater than the expected operating temperatures of the laser catalyst bed were attained.

When a stoichiometric mixture of the oxygen-18 labeled carbon monoxide and oxygen was passed over the common-isotope Pt/SnO_2 catalyst at 100°C, 85 percent $^{12}C^{18}O_2$ and 15 percent $^{12}C^{16}O^{18}O$ were initially formed (row 5, table I). These yields gradually changed to 90 percent and 10 percent, respectively, after 8 hours or more of operation. Evidently, there are two reactive mechanisms occurring. The dominant reaction appears to involve CO and O_2 adsorbed on the catalyst surface, while the lesser reaction involves oxidation of CO by the SnO_2 surface. In addition, the SnO_2 surface then slowly become isotopically labeled with oxygen-18 via the interactive exchange mechanism. Complete surface labeling by this technique would, however, require an inordinately long time even if diffusion from the bulk were inoperative.

With the foregoing data in hand, it was decided to deliberately label the surface of the $Pt/Sn^{16}O_2$ catalyst with oxygen-18 by first removing all readily reactive oxygen-16 by hydrogen reduction followed by reoxidation of the reduced surface to $Sn^{18}O_2$. If all of the active normal-isotope oxygen at the surface could be exchanged in this way, then the catalyst would be suitable for use in a rare-isotope closed-cycle CO_2 laser if diffusion of the bulk matrix oxygen-16 to the surface is negligable.

The chemical reduction of the Pt/SnO_2 catalyst was accomplished by exposing it to a flowing stream of 7.5 percent H_2 in helium at 225°C. The active surface-oxygen removal was judged complete after the mass spectrometrically monitored $H_2^{16}O$ concentration in the stream had dropped to the instrument background level. The reduced substrate surface was

then reoxidized at 225°C with a gas stream containing 1 percent $^{18}O_2$ until the $^{18}O_2$ concentration exiting the catalyst chamber had attained and remained at the 1 percent concentration level for at least 1 hour as measured on the mass spectrometer. The temperature was then reduced to ambient under neon flow. The preceding isotope-exchange labeling of the metal-oxide catalyst was accomplished in about 5 hours and is covered in a patent (ref. 6).

The 1 percent $Pt/1sn^{18}O_2$ surface-labeled catalyst was then evaluated under conditions listed in row 6 of table I and was found to maintain the isotopic integrity of the rare-isotope gas composition in a test of 17 days duration. The subsurface normal oxygen-16 isotope in the bulk of the catalyst material obviously does not diffuse to the surface at or below the test temperature of 100°C during the test duration.

Kinetic studies were undertaken for the Pt/tin oxide/silica gel catalyst using the recycle reactor in the internal recycle mode. The graphical results of these studies were consistent with a rate law showing first order oxygen dependency over the temperature range of 0-125°C. In earlier studies, we and others reported that the overall reaction took place with an overall first order rate law (refs. 10, 11). Activation energies over the above temperature interval are tabulated in table II for the CO oxidation reaction. The activation energy for the reaction was found to be 36 kJ/mol over the 0-75°C interval with an abrupt decrease to 17 kJ/mol over the 75-125°C interval. The former value is somewhat lower than that reported by Stark and Harris for unsupported platinum on tin oxide catalyst (ref. 10). The decrease in the activation energy at 75°C has mechanistic implications which have not thus far been explained. Furthermore, if the overall reaction is first order then the obvious conclusion is that the reaction must be zero order in CO. Preliminary studies indicate that such is indeed the case under excess oxygen conditions. However, under excess CO conditions the reaction seems to be inhibited, thus indicating otherwise. As is noted in table II, the activation energy for the stoichiometric condition does not show a change at 75°C as was observed in the excess CO experimental condition. Kinetic studies are continuing.

CONCLUDING REMARKS

Rare-isotope studies have demonstrated that when CO and O_2 are reacted on a Pt/SnO_2 catalyst the dominant reaction mechanism involves these adsorbed species and only a minor amount of oxidation of the CO by oxygen from the SnO_2 occurs. Furthermore, we have developed a simple, economical surface-labelling technique, validated in a 17-day test, to prevent isotopic scrambling from this minor reaction between rare-isotope CO and common-isotope Pt/SnO_2. Additionally, we have obtained supportive evidence for the formation of some carbonate-like intermediate species when CO is oxidized on Pt/SnO_2.

Results of kinetic studies on NASA prepared Pt/SnO_2/silica gel cataysts have demonstrated a first order dependence of O_2 for the CO oxidation reaction over the temperature range of 0-125°C with an abrupt decrease in activation energy at 75°C. Investigations are continuing with mechanistic and other studies for improving the performance of CO oxidation catalysts and to better predict a successful outcome for their application in long-life closed-cycle CO_2 lasers.

REFERENCES

1. Freed, C.; Ross, C.; and O'Donnell, R. C., _J. Mol. Spec._, 49, 439-453, (1974).

2. Freed, L. E.; Freed, C.; and O'Donnell, R. G., _IEEE J. Quant. Elect._, QE-18, 1229-1239, (1982).

3. Hess, R. V.; Brockman, P.; Schryer, D. R.; Miller, I. M.; Bair, C. H.; Sidney, B. D.; Wood, G. M.; Upchurch, B. T.; and Brown, K. G., NASA TM-86415, (1985).

4. Sorem, M. S. and Faulkner, A., _Rev. Sci. Instrum._, 52, 1193-1196, (1981).

5. Brown, K. G.; Sidney, B. D.; Schryer, D. R.; Upchurch, B. T.; Miller, I. M.; Wood, G. M.; Hess, R. V.; Burney, L. G.; Paulin, P. A.; Hoyt, R. F.; and Schryer, J., _SPIE Proceedings_, 663, 136-144, (1986).

6. Hess, R. V.; Upchurch, B. T.; Brown, K. G.; Miller, I, M.; Schryer, D. R.; Sidney, B. D.; Wood, G. M.; and Hoyt, R. F., Isotope Exchange in Oxide Containing Catalyst. U.S. Patent No. 4,839,330, June 13, 1989.

7. Upchurch, B. T.; Schryer, D. R.; Wood, G. M.; and Hess, R. V., _SPIE Proceedings_, 1062, (1989).

8. Upchurch, B. T.; Miller, I. M.; Brown, D. R.; Davis, P. P.; Schryer, D. R.; Brown, K. G.; and Van Norman, J. D., Catalyst for Carbon Monoxide Oxidation. U.S. Patent No. 4,912,082, March 27, 1990.

9. Upchurch, B. T.; Miller, I. M.; and Davis, P. P., Process for Making a Noble Metal on Tin Oxide Catalyst. U.S. Patent No. 4,855,274, August 8, 1989.

10. Stark, D. S., and Harris, M. R., _J. Phys. E.: Sci. Instrum._, 16, 492-496, (1983).

11. Miller, I. M.; Batten, C. E.; and Wood, G. M., NASA CP 2456, (1987).

TABLE I - OXYGEN ISOTOPE LABEL STUDIES

Reactants	Catalyst	T, °C	Product Yields
$C^{18}O$	$Pt/Sn^{16}O_2$	24-150	$C^{16}O^{18}O$
$^{18}O_2$	$Pt/Sn^{16}O_2$	25-225	No Reaction
$^{18}O_2 + {}^{16}O_2$	$Pt/Sn^{16}O_2$	25-225	No Reaction
$^{18}O_2 + {}^{16}O_2$	$Pt/Sn^{16}O_2$	> 350	$^{16}O^{18}O$
$C^{18}O + 1/2^{18}O_2$	$Pt/Sn^{16}O_2$	100	85-90% $C^{18}O_2$
			15-10% $C^{16}O^{18}O$
$C^{18}O + 1/2^{18}O_2$	$Pt/Sn^{18}O_2$	100	$C^{18}O_2$

TABLE II. O_2 ACTIVATION ENERGY VALUES FOR $Pt/SnO_2/SiO_2/H_2O$ CATALYST (CO EXCESS)

Run Number	E, kJ/mol	Temp Range, °C
184	36.1	0 - 35
185	36.8	0 - 35
174	36.9	33 - 57
175	35.7	35 - 57
176	28.6*	35 - 52
177	34.5	41 - 57
178	44.6*	35 - 62
179	35.2	35 - 73
181	16.5	75 - 100
182	15.7	75 - 125
183	17.8	75 - 126
This Work	E = 35.9 kJ/mol	0 - 73
This Work	E = 16.7 kJ/mol	75 - 125
Stark and Harris	E = 41.4 kJ/mol	21 - 60
This Work	E = 35.0 kJ/mol	35 - 100†

*Excluded Value

† Stoichiometric Gas Mix

EFFECT OF PRETREATMENT ON A PLATINIZED TIN OXIDE CATALYST USED FOR LOW-TEMPERATURE CO OXIDATION

Jean E. Drawdy, Gar B. Hoflund, Steven D. Gardner and Eva Yngvadottir
Department of Chemical Engineering
University of Florida
Gainesville, Florida

David R. Schryer
NASA Langley Research Center
Hampton, Virginia

ABSTRACT

A commercial platinized tin oxide catalyst used for low-temperature CO oxidation has been characterized using ion scattering spectroscopy (ISS), Auger electron spectroscopy (AES) and electron spectroscopy for chemical analysis (ESCA) before and after reduction in 40 Torr of CO for 1 hour at various temperatures from 75 to 175°C. The reduction results in loss of surface oxygen, formation of metallic tin, conversion of platinum oxides to Pt-O-Sn and $Pt(OH)_2$ and a small amount of metallic Pt which alloys with the tin. These results should be useful in understanding how the pretreatment temperature affects the catalytic activity of platinized tin oxide toward CO oxidation.

INTRODUCTION

Low-temperature, CO-oxidation catalysts are important for long-life, closed-cycle operation of CO_2 lasers which are used in remote sensing applications such as weather monitoring from space vehicles. The electrical discharge in CO_2 lasers decomposes relatively small amounts of CO_2 into CO and O_2. While the power output of the laser decreases slowly with loss of CO_2 and buildup of CO, it decreases dramatically with buildup of very low O_2 concentrations. A solution to this problem is to recombine the discharge products back into CO_2 using a heterogeneous catalyst incorporated in some manner into the laser system. In order to meet volume and weight constraints, it is necessary for the catalyst to have a high activity at low temperatures (< 100°C).

Stark et al. (1) have found that platinized tin oxide with or without a Pd modifier is an effective low-temperature CO oxidation catalyst. Based on this finding, numerous studies of platinized tin oxide systems relating to CO oxidation have been carried out (2). A 2 wt. % platinized tin oxide catalyst is now commercially available from Engelhard Industries. Schryer et al. (3) have studied the catalytic behavior of this material toward CO oxidation and found that the activity of the catalyst depends upon the pretreatment conditions used as shown in figure 1. For the pretreatment and reaction conditions used (see figure 1), the unpretreated catalyst exhibits the lowest long-term activity. A 100°C pretreatment in CO greatly enhances the long-term activity, and a further enhancement occurs by carrying out the pretreatment at 125°C. Utilizing higher pretreatment temperatures up to 225°C yields no change in the catalytic activity compared to the 125°C pretreatment. In order to understand

201

how platinized tin oxide catalysts function in converting CO and O_2 to CO_2 at low temperatures, it is necessary to characterize the composition and chemical states of the species present at these surfaces. This has been accomplished in this study using several surface chacterization techniques including ion scattering spectroscopy (ISS), electron spectroscopy for chemical analysis (ESCA) and Auger electron spectroscopy (AES) to examine the surface of the Engelhard catalyst before and after pretreatment in CO as a function of pretreatment temperature. It is anticipated that these studies will lead to a better understanding of this catalytic process and eventually to the development of improved catalysts for this application.

EXPERIMENTAL

The Engelhard platinized tin oxide catalyst has an average particle size of 1 μm and a BET surface area of 6.9 m^2/g. For the characterization studies the powder was pressed into thin disks about 1 cm in diameter. These were inserted directly into the ultrahigh vacuum system for pretreatment and characterization. Pretreatment was carried out by moving the sample into a preparation chamber (base pressure of 10^{-7} Torr), adjusting the pressure to 40 Torr in CO and heating the sample at the prescribed temperature for 1 hour. Then the sample was allowed to cool while the preparation chamber was pumped down to 10^{-7} Torr before moving the sample into the characterization chamber (base pressure of 10^{-11} Torr) for analysis by ISS, ESCA and AES. The samples were heated at 75, 100, 125 and 175°C in the preparation chamber using a sample heater (4) which did not expose the reducing gas to hot spots which would have dissociated the CO. Two different as-prepared samples were analyzed without prereduction, and the results were found to be reproducible. A new sample was prepared and introduced into the analysis chamber for each reduction temperature used.

ISS, ESCA and AES data were taken using a double-pass cylindrical mirror analyzer (CMA) (Perkin-Elmer PHI Model 25-270) as the charged-particle energy analyzer. ISS spectra were collected in the nonretarding mode using a 147° scattering angle and pulse counting detection (5). A 1-keV, 100 nA $^4He^+$ primary ion beam was defocused over a 1-cm-diameter area, and spectra were collected as quickly as possible (typically 90 s) to minimize beam damage. AES was performed in the nonretarding mode using a 3-keV, 10-μA primary electron beam with a 0.2-mm spot diameter. ESCA was performed in the retarding mode using Mg Kα excitation and 50-eV pass energy for collection of survey spectra and 25 eV for obtaining elemental lineshape information.

RESULTS AND DISCUSSION

An ESCA survey spectrum taken from the as-received, Engelhard platinized tin oxide catalyst is shown in figure 2. The peaks present of significant size are due only to O and Sn, and no peaks due to C or other typical contaminants appear. In fact, this spectrum is essentially identical to an ESCA spectrum obtained from a very clean tin oxide surface. It is most interesting that the predominant Pt 4f peaks are so small that they cannot be readily discerned in this spectrum. A corresponding Auger spectrum taken from the same surface is shown in figure 3. Again, the predominant features are due to Sn and O, and this spectrum is similar to one obtained from a clean tin oxide surface. However, a feature due to Pt appears at about 64 eV. It can be described as an edge rather than a typically shaped Auger peak. Similar Pt

features have been observed in a study of the electrochemisorption of Pt on tin oxide (6). This feature is more prominent than the Pt ESCA peaks in figure 1. In agreement with the ESCA data, no contaminant peaks are apparent in this Auger spectrum. As the catalyst is reduced at various temperatures, very small changes are observed in the ESCA and Auger spectra corresponding to figures 1 and 2 but taken from the reduced surfaces. Therefore, these survey spectra are not shown.

ISS is a particularly useful technique for examining catalytic surfaces because it is very highly surface sensitive (outermost one or two atomic layers). ISS spectra taken before (a) and after (b-e) reduction are shown in figure 4. The spectrum shown in (a) consists of peaks due to O, Sn, and Pt, and the high inelastic background is characteristic of ISS spectra taken from nonmetallic surfaces. In such a case inelastically scattered ions are not efficiently neutralized since the electron mobility at a nonmetallic surface is low so these ions contribute to the background signal. A previous study by Asbury and Hoflund (7) showed that O penetrates beneath the surface during a room-temperature, oxygen exposure of polycrystalline Sn. This suggests that the fairly large O peak in (a) is due to O associated with the Pt and/or perhaps with hydroxyl groups attached to Sn (8) which may lie above the surface.

The ISS spectra shown in figure 1 (b) to (e) were obtained from samples reduced in 40 Torr of CO for 1 hour at 75, 100, 125 and 175°C respectively. All four spectra have two characteristics in common. Firstly, the pretreatments have resulted in negligible inelastic backgrounds which is indicative of the formation of surfaces with a metallic nature. Secondly, the O peak is no longer discernable after the reductions which is also consistent with the observation that the surfaces appear to be metallic. The reductive pretreatment results in an increase in the Sn-to-Pt ratio, and the extent of this increase is greater at higher reduction temperatures. An increase in the ISS Sn/Pt ratio during reduction has been found to be indicative of alloy formation as described in a study of platinized tin oxide model catalysts by Gardner et al. (9). All of the ISS spectra shown in figure 4 were taken using the same instrument settings, but the maximum peak heights vary considerably. Although the variation is not understood, it could be due to changes in ion neutralization probability, surface morphological changes or changes in the concentration of surface hydrogen which have been shown to alter the ISS signal strength (10,11).

Sn 3d ESCA spectra and Sn(MNN) AES spectra taken before and after reduction are shown in figures 5 and 6 respectively. Before pretreatment (air-exposed sample) the Sn $3d_{5/2}$ lineshape and peak position (486.4 eV) indicate that the Sn is present in the +2 or +4 oxidation states most likely as SnO, $Sn(OH)_2$, SnO_2 or $Sn(OH)_4$ and that metallic Sn is absent. As discussed by Hoflund et al. (12), it is not possible to distinguish between these species based on the ESCA Sn 3d peaks, but more specific information can be gained about these species using electron energy loss spectroscopy (ELS) (13,14), valence-band ESCA (8, 14), electron stimulated desorption (ESD) (8, 15) or secondary ion mass spectrometry (SIMS) (16-18). The metallic ESCA Sn $3d_{5/2}$ peak appears at an energy of 484.6eV (19). When a small amount of metallic Sn and a relatively large amount of tin oxides or hydroxides are present, a slight broadening appears on the low binding energy sides of the oxidic ESCA Sn 3d features. This is the case for the 175°C-reduced sample as shown in

figure 5. Samples reduced at lower temperatures also yield this metallic shoulder, and the amount of metallic Sn produced generally increases as the annealing temperature increases with the most being produced at 175°C. However, the amounts of metallic Sn produced at 75 and 100°C appear to be similar. Similar observations can be made by considering the AES Sn(MNN) peaks shown in figure 6. The high kinetic energy oxidic peak lies at 430 eV while the high kinetic energy metallic peak lies at 423 eV. The peaks shown in figure 6a are characteristic of oxidic Sn. When metallic Sn is present, the height of the splitting between the two primary peaks decreases. This is observed in spectra (b) to (e) taken from the reduced samples. In agreement with the ESCA Sn 3d spectra, the extent of metallic Sn formation is greater at elevated reduction temperatures with the maximum amount of metallic Sn being produced at 175°C. Further reduction either for prolonged periods or at higher temperatures than used in this study would undoubtedly result in the production of increased amounts of metallic Sn.

The ESCA O 1s peaks are shown in figure 7. These were taken before (a) and after reduction at (b) 175°C. The peak shown in (a) exhibits a distinct asymmetry on the high binding energy side due to the presence of hydroxyl groups which are responsible for a shoulder at about 531.8 eV (8, 20). It is also possible that the very small shoulder at about 533.0 eV is due to adsorbed water. This assignment is consistent with results obtained in the study of hydrated polycrystalline tin oxide films by Tarlov and Evans (20). Pretreatment at 75°C slightly reduces the amounts of adsorbed water and hydroxyl groups present while pretreatment at 100°C or above eliminates the adsorbed water and further reduces the concentration of hydroxyl groups. The 175°C pretreatment results in the lowest surface hydroxyl group concentration. It is interesting to note that these hydroxyl species are strongly bonded to the surface and require annealing at 600°C in vacuum for nearly complete removal (8, 14, 21).

The O content of the near-surface region is decreased by the pretreatment process. The AES and ESCA O/Sn atomic ratios obtained at the various pretreatment temperatures are listed in table I. A decrease in the O/Sn ratio is caused by loss of adsorbed water, a decrease in hydroxyl group concentration, reduction of tin oxides and hydroxides to metallic Sn and reduction of SnO_2 to SnO. However, the relative importance of these factors cannot be completely assessed from the types of data taken in this study. The amount of Pt present on these surfaces is so small that changes in the Pt oxidation state, which are discussed below, would not affect the O/Sn atomic ratios presented in table I. The AES and ESCA results in table I are different both with respect to magnitude and trend. The AES data indicate that the near-surface region loses about 20% of its O regardless of the reduction temperature. The ESCA O/Sn atomic ratios are considerably larger than the AES values and decrease monotonically as the pretreatment increases. Either the ESCA values differ from the AES values due to inaccuracies in the tabulated cross sections or the variation is due to the fact that AES and ESCA probe different volumes of the near-surface region. If the difference were due only to inaccurate cross sections, then the ESCA O/Sn ratios obtained from the reduced samples would not show such a large variation with reduction temperature. Thus, the variation is due to the fact the ESCA probes more deeply than AES, which is consistent with mean-free-path arguments also. The kinetic energies of the ESCA O 1s electrons are 723 eV and the Sn 3d electrons are about 770 eV, while the kinetic energies of the AES O electrons are about 510 eV and the Sn electrons are about 430 eV. The corresponding average mean free paths (λ) are about

6Å for ESCA and 4Å for AES (24). Since most of the ESCA and AES electrons originate within a depth of about 3λ, ESCA probes about 18 Å beneath the surface while AES probes about 12 Å . Then, the data of table I indicate that the near-surface region probed by AES contains less O than the region probed by ESCA for the untreated sample and samples reduced from 75 to 175°C. Reduction at any of the temperatures used causes the AES O/Sn ratio to drop from 1.32 to about 1.06 whereas to ESCA O/Sn ratio decreases monotonically as the reduction temperature increases. The essentially constant AES value probably results from a competing process, i.e., O leaving the surface as CO_2 during the reduction and O migrating to the near-surface region from further beneath the surface. This is consistent with the trend of the ESCA data implying that subsurface reduction takes place to a greater extent at higher temperatures. A similar phenomenon has been observed previously for the reduction of a TiO_2(001) surface (25).

The ESCA Pt 4f peaks obtained from the unpretreated samples are shown in figure 8a, and the peak assignments used in this study are listed in table II. Most of these assignments were taken from a standard reference (19), but the 72.3 eV feature has been assigned as Pt-O-Sn in previous studies of platinized tin oxide surfaces (12, 23). The spectrum shown in figure 8a indicates that very little metallic Pt is present and that the Pt species consist mostly of Pt-O-Sn, $Pt(OH)_2$ and Pt oxides. In fact, a spectrum very similar to this one has been taken from a codeposited platinum/tin oxide film after calcining in air at 725 K for 1.5 hours (12).

ESCA Pt 4f spectra taken after pretreating at 75 and 100°C are shown in figures 8b and c respectively. These two spectra are quite similar in that very little metallic Pt is present and the predominant species consist of Pt-O-Sn and $Pt(OH)_2$. The metallic Pt apparently is in the form of small crystallites. A shoulder due to PtO_2 may also be present in both spectra, but this shoulder is smaller after the 100°C reduction. The relative amounts of Pt-O-Sn and $Pt(OH)_2$ are similar in both spectra. Pretreating at a temperature 25°C higher produces a significant change in the Pt species present as shown in figure 8d. The predominant Pt species after the 125°C reduction are $Pt(OH)_2$ and Pt-O-Sn in approximately equal amounts. Also, a small amount of metallic Pt is present after this treatment, and features due to Pt oxides do not appear.

Reduction at 175°C produces a further and more pronounced shift in Pt chemical state toward $Pt(OH)_2$ as shown in figure 8e. The Pt-O-Sn feature is now a shoulder on the $Pt(OH)_2$ peak, and the amount of metallic Pt present is decreased compared to the lower temperature reductions. The spectrum shown in figure 8a, taken from the untreated sample, exhibits a prominent feature at 79.8 eV. Since the splitting between the Pt $4f_{7/2}$ and Pt $4f_{5/2}$ peaks is about 3.35 eV, this feature does not correspond to the Pt $4f_{5/2}$ peak of any of the species listed in table II. The 75°C pretreatment reduces the size of this feature, and it does not appear after the 100 or 125° pretreatment. Therefore, it behaves like an oxidic feature and reappears in figure 8e.

It is interesting to compare the spectral information contained in figure 8 with the kinetic information contained in figure 1. The unpretreated catalyst exhibits a low activity compared to any reduced catalyst. This correlates with the facts that the Pt is predominantly oxidic on the unpretreated catalyst and that significant changes in the Pt chemical state occur during

the reductive treatments used in these studies. As the pretreatment temperature increases, more of the Pt is converted into $Pt(OH)_2$. This fact suggests that the $Pt(OH)_2$ plays an important role in the conversion of CO and O_2 into CO_2 at low temperatures as has also been found to be the case for a silica-supported platinized tin oxide catalyst (26) for which the catalytic activity increases by addition of water to the reaction mixture after pretreating the catalyst at 225°C (27). The previous characterization study (26) demonstrates that pretreatment of this catalyst at 225°C removes most of the Pt hydroxyl species thereby lowering its catalytic activity. This does not occur with the Engelhard catalyst which yields identical catalytic behavior for pretreatments from 125 to 225°C. The ESCA data are consistent with this fact in that much of the Pt is present as $Pt(OH)_2$ after the 125° reduction, and it becomes the predominant Pt chemical state after the 175°C reduction. In this discussion a relationship is being drawn between the long-term catalytic behavior (past the first 500 minutes of operation) and the chemical state of the Pt after the pretreatment but before the reaction is run (time = 0 on figure 1). The initial catalytic behavior is quite complex (3) and changes may occur in the Pt chemical state during this period. Consequently, characterization studies are in progress in which the state of the catalytic surface is being examined as the reaction is run for various periods of time. These studies should lead to an understanding of the chemical changes responsible for the unusual initial catalytic behavior and the long-term decay in catalytic activity.

A small amount of metallic Pt forms during both the 125 and 175°C pretreatment, and metallic Sn is also present as stated above. Paffett and Windham (28) have deposited layers of Sn on Pt (111) and found that alloy formation during annealing at or above 150°C is strongly suggested by their data. Also Fryberger* has found that Pd deposited on $SnO_2(110)$ alloys with the Sn even at room temperature. It is anticipated that alloy formation occurs in the Engelhard catalyst under the pretreatment conditions used in this study. Since the amount of Pt present on this surface is small, most of the metallic Sn probably is not alloyed while all of the Pt probably is alloyed.

SUMMARY

A platinized tin oxide catalyst commercially available from Engelhard Industries for low-temperature CO oxidation has been examined using surface analytical techniques including ISS, AES and ESCA before and after pretreatment by annealing in 40 Torr of CO for 1 hour at 75, 100, 125 and 175°C, and the results have been correlated with catalytic activity data. The unpretreated sample consists primarily of oxidic Sn (SnO_2, SnO and $Sn(OH)_x$) with a very small amount of Pt present as Pt-O-Sn, $Pt(OH)_2$, PtO and PtO_2 species. Reduction results in loss of both O and OH from the Sn and produces metallic Sn. The extent of these processes increases as the pretreatment temperature increases. The chemical state of the Pt changes with pretreatment temperature. At or below 100°C, the predominant forms are Pt-O-Sn and $Pt(OH)_2$. As the reduction temperature increases, more $Pt(OH)_2$ forms. This fact suggests that $Pt(OH)_2$ plays an important role in the low-temperature catalytic oxidation of CO. The results demonstrate that the application of surface analytical techniques in studies of real catalysts can provide information which is useful in understanding catalytic behavior.

*T. Fryberger, personal communication

ACKNOWLEDGMENT

REFERENCES

1. D.S. Stark, A. Crocker and G.J. Steward, J. Phys. E: Sci. Instrum. 16(1983)158.

2. Closed-Cycle, Frequency-Stable CO_2 Laser Technology, edited by C.E. Batten, J.M. Miller, G.M. Wood, Jr. and D.V. Willetts, NASA Conference Publication 2456, 1987.

3. D.R. Schryer, B.T. Upchurch, J.D. Van Norman, K.G. Brown and J. Schryer, J. Catal. 00(1990)00.

4. G.R. Corallo, "Chemical and Electronics State Characterization of the Surface Region of Metals Following Chemisorption of Simple Gases," PhD Dissertation, University of Florida, 1987.

5. R.E. Gilbert, D.F. Cox and G.B. Hoflund, Rev. Sci. Instrum. 53(1982)1281.

6. H.A. Laitinen, J.R. Waggoner, C.Y. Chan, P. Kirszensztejn, D.A. Asbury and G.B. Hoflund, J. Electrochem. Soc. 133(1986)1568.

7. D.A. Asbury and G.B. Hoflund, J. Vac. Sci. Technol. A 5(1987)1132.

8. G.B. Hoflund, A.L. Grogan, Jr., D.A. Asbury and D.R. Schryer, Thin Solid Films 169(1989)69.

9. S.D. Gardner, G.B. Hoflund, M.R. Davidson and D.R. Schryer, J. Catal. 115(1989)132.

10. E. Taglauer and W. Heiland, Appl. Phys. 9(1976)261.

11. H.H. Brongersma, M.J. Sparnaay and T.M. Buck, Surface Sci. 71(1978)657.

12. G.B. Hoflund, D.A. Asbury and R.E. Gilbert, Thin Solid Films 129(1985)139.

13. D.F. Cox and G.B. Hoflund, Surface Sci. 151(1985)202.

14. D.F. Cox, G.B. Hoflund and H.A. Laitinen, Appl. Surface Sci. 20(1984)30.

15. G.B. Hoflund, Scanning Electron Microscopy IV(1985)1391.

16. D.F. Cox, G.B. Hoflund and W.H. Hocking, Appl. Surface Sci. 26(1986)239.

17. G.B. Hoflund, P.H. Holloway and W.H. Hocking, in Secondary Ion Mass Spectrometry SIMS IV, Proceedings of the Fourth International Conference, Osaka, Japan, edited by A. Benninghoven, J. Okano, R. Shimizu and H.W. Werner, Springer-Verlag, Berlin 36(1984)231.

18. G.B. Hoflund, D.F. Cox, F. Ohuchi, P.H. Holloway and H.A. Laitinen, Appl. Surface Sci. 14(1982-3)281.

19. C.D. Wagner, W.M. Riggs, L.E. Davis, J.F. Moulder and G.E. Muilenberg (editor), Handbook of X-Ray Photoelectron Spectroscopy, Perkin-Elmer Corporation, Eden Prairie, Minnesota, 1979.

20. M.J. Tarlov and J.F. Evans, Chem. Mater. 00(1989)00.

21. E.W. Giesekke, H.S. Gutowsky, P. Kirkov and H.A. Laitinen, Inorg. Chem. 6(1967)1294.

22. L.E. Davis, N.C. MacDonald, P.W. Palmberg, G.E. Riach and R.E. Weber, Handbook of Auger Electron Spectroscopy, Perkin-Elmer Corporation, Eden Prairie, Minnesota, 1972.

23. S.F. Cox, G.B. Hoflund and H.A. Laitinen, Langmuir 1(1985)269.

24. M.P. Seah and W.A. Dench, Surf. Interface Anal. 1(1979)2.

25. G.B. Hoflund, H.-L. Yin, A.L. Grogan, Jr., D.A. Asbury, H. Yoneyama, O. Ikeda and H. Tamura, Langmuir 4(1988)346.

26. S.D. Gardner, G.B. Hoflund, D.R. Schryer and B.T. Upchurch, in Proceedings of SPIE - International Society for Optical Engineering; Laser Applications in Meteorology and Earth and Atmospheric Remote Sensing edited by M.M. Sokoloski, published by SPIE, Bellingham, Washington, 1062(1989)21.

27. B.T. Upchurch, D.R. Schryer, G.M. Wood and R.V. Hess, in Proceedings of SPIE - International Society for Optical Engineering: Laser Applications in Meteorology and Earth and Atmospheric Remote Sensing, edited by M.M. Sokoloski, published by SPIE, Bellingham, Washington, 1062(1989)287.

28. M.T. Paffett and R.G. Windham, Surface Sci. 208(1989)34.

TABLE I

O/Sn Atomic Ratios Versus Pretreatment Temperature

Pretreatment	AES[†]	ESCA[††]
untreated	1.32	1.56
75°C	1.08	1.45
100°C	1.05	1.39
125°C	1.04	1.33
175°C	1.05	1.21

[†]Calculated using methods described in reference 22.

[††]Calculated using methods described in reference 19.

TABLE II

ESCA Pt 4f Peak Assignments

Species	Binding Energy (eV)
Pt°(bulk) [1]	70.9
Pt°(crystallite) [2]	71.3
Pt-O-Sn [2]	72.3
Pt(OH)$_2$ [1]	72.8
PtO [1]	74.2
PtO$_2$ [1]	74.9

1. Assignments taken from reference 19.

2. Assignments taken from references 12 and 23.
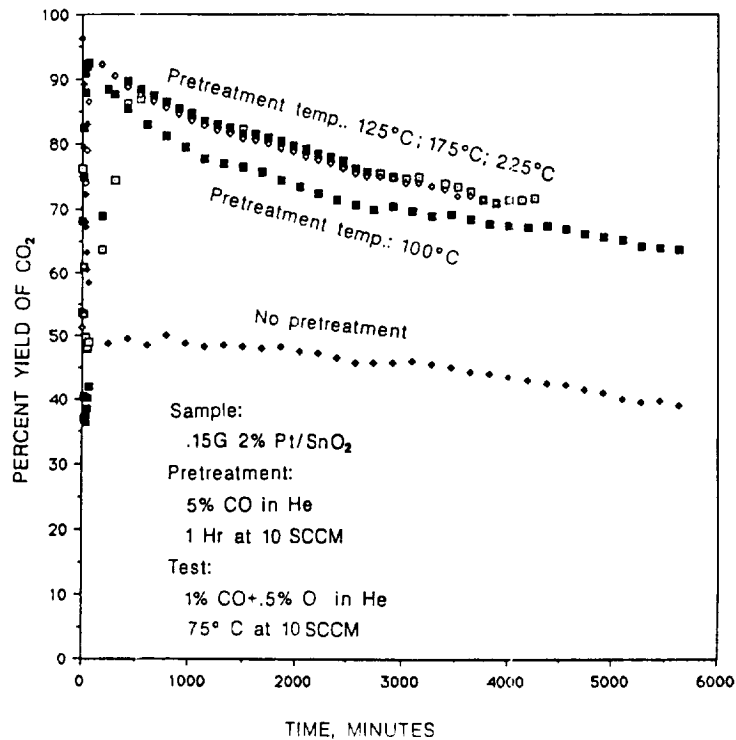
Figure 1. Catalytic activity of the Engelhard platinized tin oxide catalyst for CO oxidation shown as a function of time and pretreatment temperature. The pretreatment and reaction test conditions are given in the figure.
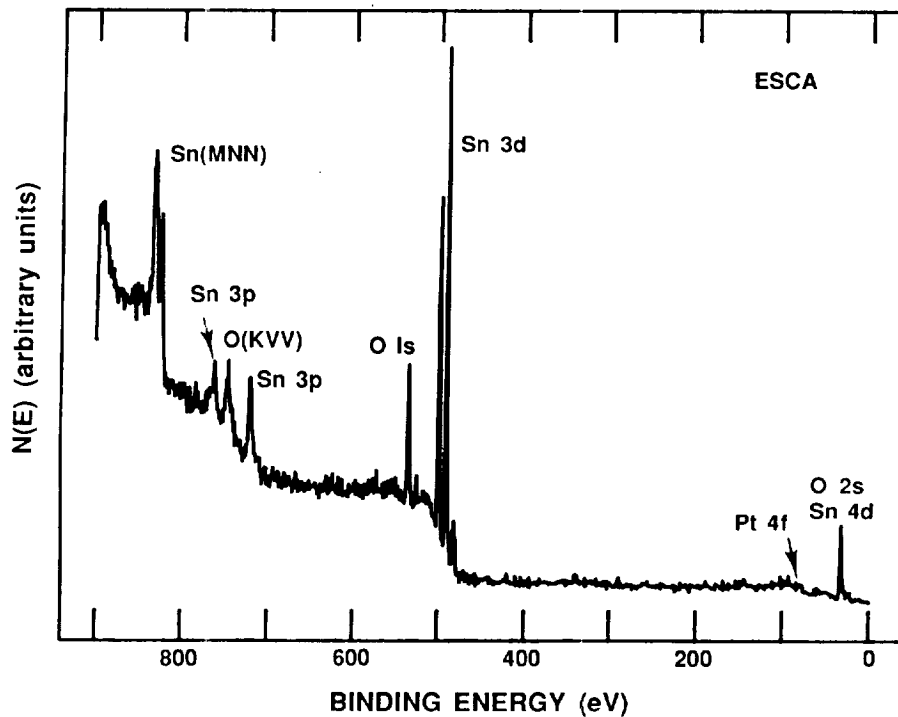
Figure 2. ESCA survey spectrum taken from the as-received Engelhard platinized tin oxide catalyst.
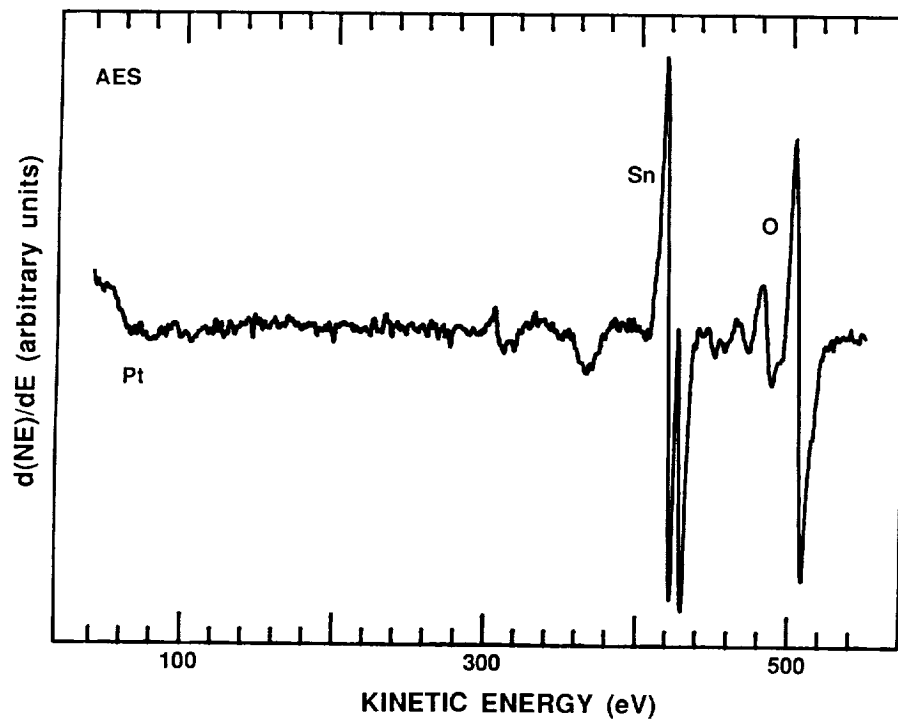
Figure 3.   Auger spectrum taken from the same as-received sample as the ESCA
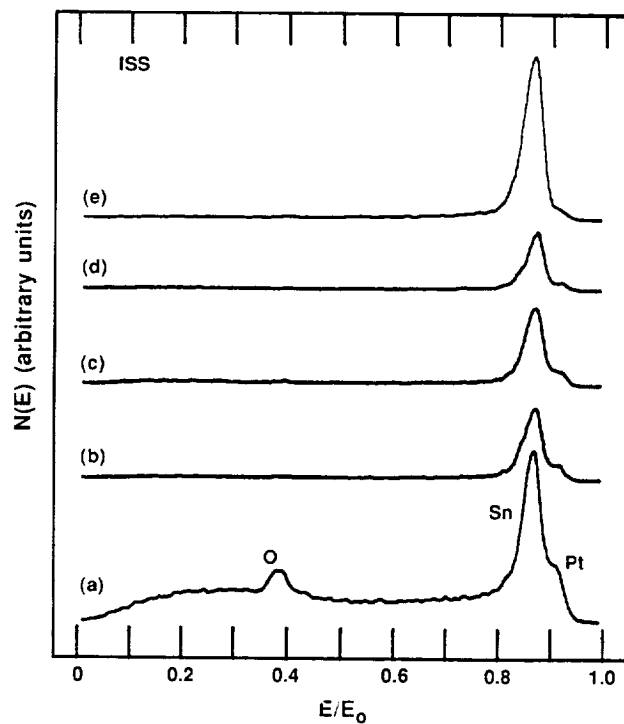spectrum shown in figure 2.

Figure 4.   ISS spectra taken from (a) an unpretreated sample and samples re-
duced at (b) 75, (c) 100, (d) 125 and (e) 175°C in 40 Torr of CO
for 1 hour.
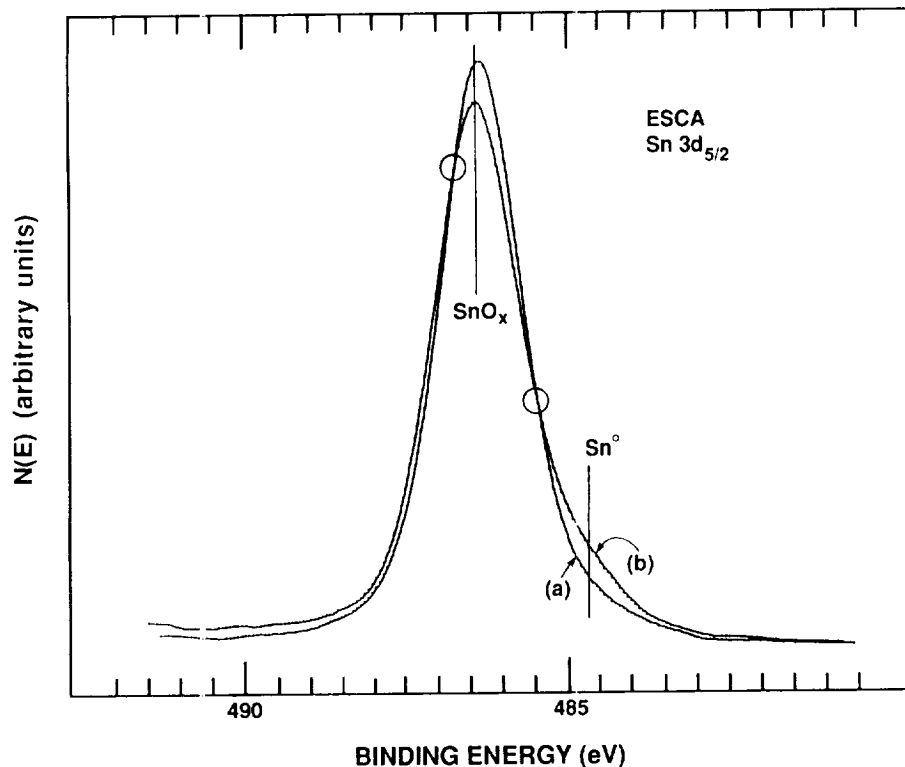
Figure 5. ESCA Sn 3d peaks obtained from (a) an unpretreated sample and (b) a sample reduced at 175°C in 40 Torr of CO for 1 hour. The circled regions indicate crossing points.
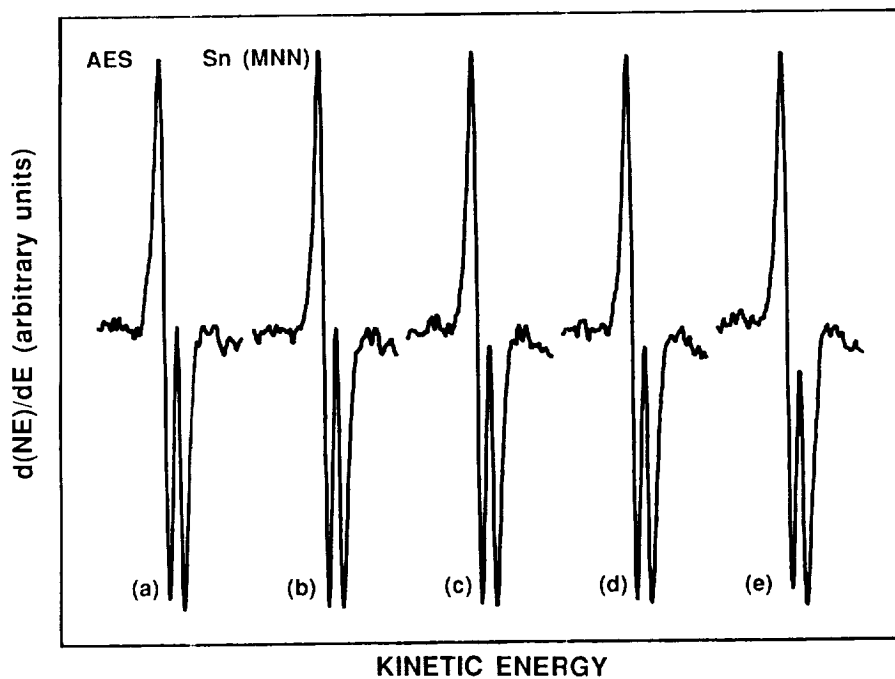

Figure 6. AES Sn (MNN) peaks obtained from (a) an unpretreated sample and samples reduced at (b) 75, (c) 100, (d) 125 and (e) 175°C in 40 Torr of CO for 1 hour.
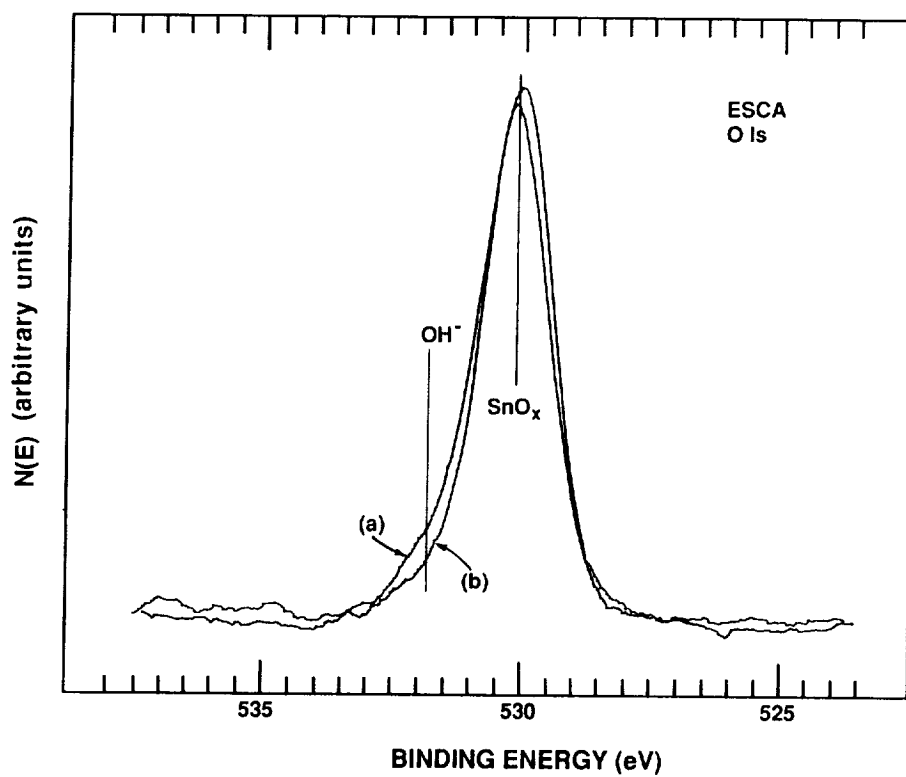
213

Figure 7.   ESCA O 1s peaks obtained from (a) an unpretreated sample and (b) a sample reduced at 175°C in 40 Torr of CO for 1 hour.
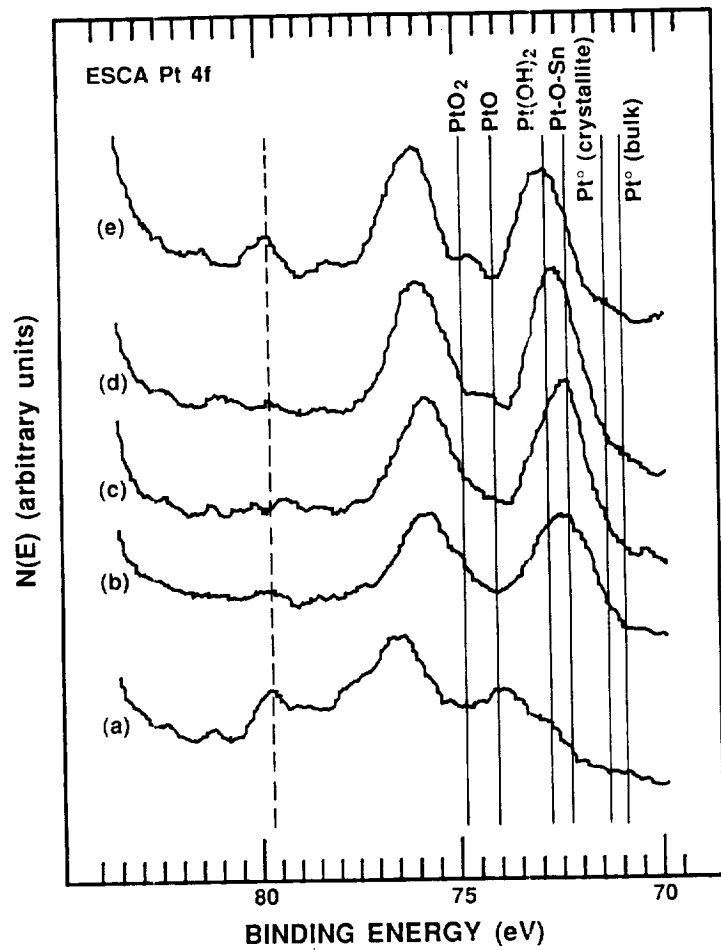
Figure 8.   ESCA Pt 4f peaks obtained from (a) an unpretreated sample and samples reduced at (b) 75, (c) 100, (d) 125 and (e) 175°C in 40 Torr of CO for 1 hour.

PLATINIZED TIN OXIDE CATALYSTS FOR CO_2 LASERS:

EFFECTS OF PRETREATMENT

Steven D. Gardner and Gar B. Hoflund
Department of Chemical Engineering
University of Florida
Gainesville, Florida

David R. Schryer and Billy T. Upchurch
NASA Langley Research Center
Hampton, Virginia

ABSTRACT

$Pt/SnO_2/SiO_2$ surfaces used for low-temperature CO oxidation in CO_2 lasers have been characterized before and after reduction in CO at 125 and 250°C using ion scattering spectroscopy (ISS) and X-ray photoelectron spectroscopy (XPS). XPS indicates that the Pt is present initially as PtO_2. Reduction at 125°C converts the PtO_2 to $Pt(OH)_2$ while reduction at 250°C converts the PtO_2 to metallic Pt. ISS results suggest tht during the 250°C reduction the Pt and Sn in the outermost atomic layer of the catalyst are covered by impurities originating from the silica substrate. The XPS results are consistent with partial SnO_2 reduction to SnO. The surface dehydration, change of Pt chemical state, and migration of substrate impurities over surface Pt and Sn appear to explain why a CO pretreatment at 250°C produces inferior CO oxidation activity compared to a 125°C CO pretreatment.

INTRODUCTION

The catalyzed oxidation of CO has important applications for closed-cycle, pulsed CO_2 lasers (1,2). In order to maintain power during the sealed operation of a CO_2 laser, it is necessary to recombine CO and O_2 which are produced during the laser discharge because the O_2 quenches the lasing action. This reaction may be brought about through the integration of an appropriate CO-oxidation catalyst within the CO_2 laser unit. Such an approach preserves the discharge quality of the laser while the advantages of sealed operation are maintained.

Research has indicated that platinized tin oxide is an efficient CO-oxidation catalyst at conditions which correspond to steady-state CO_2 laser operation (1,3). Although the performance of Pt/SnO_2 has been maximized, efforts to understand the reaction mechanism continue. It has been demonstrated that the activity of Pt/SnO_2 towards CO oxidation is a strong function of pretreatment procedures (4). For example, a reductive pretreatment using CO or H_2 produces superior activity relative to an inert or oxidative pretreatment or no pretreatment at all. The pretreatment temperature influences the catalytic performance as well. Compared with high-temperature reductions, low-temperature reductions near 125°C produce surfaces which are more active. For CO reductions above about 175°C, a sharp, temporary decrease in activity is observed initially. This induction period is believed to be the result of surface dehydration caused by combination and desorption of surface hydroxyl groups (4). No significant induction period results when Pt/SnO_2 is

217

humidified either after CO pretreatment or during the reaction itself. The data obtained thus far also suggest that optimum pretreatment times exist which is consistent with the hypothesis involving surface dehydration. While the exact function of surface hydroxyl groups in the overall reaction remains unknown, it is thought that OH^- groups might serve as oxidants for CO chemisorbed on Pt (4,5). There is also evidence which suggests that OH^- may stabilize a carbonate complex which ultimately decomposes to yield CO_2 (6).

Acknowledging the importance of surface hydroxyl groups, there has been considerable effort directed towards the development of a platinized tin oxide catalyst which is supported on a silica substrate (7). It is hypothesized that the hygroscopic silica may benefit Pt/SnO_2 by preventing extensive surface dehydration and consequent activity loss. Experiments have been conducted wherein the catalyst performance has been optimized with respect to several variables including pretreatment procedures. Superior performance is realized from a reductive pretreatment in 5% CO/He at 125°C for 1 hour. As pretreatment temperatures approach 250°C there is a significant decrease in the observed activity. Although not as active as Au/MnO_x (8), the optimized $Pt/SnO_2/SiO_2$ catalyst represents a significant improvement over commercially available Pt/SnO_2 with respect to low-temperature CO oxidation activity and performance decay (5).

In order to explain these experimental observations, it is necessary to characterize the catalyst surface species which are present before and after a given pretreatment procedure. The present study utilized ion scattering spectroscopy (ISS) and X-ray photoelectron spectroscopy (XPS) to examine the concentrations and chemical states of surface species associated with a $Pt/SnO_2/SiO_2$ catalyst as a function of CO pretreatment temperature.

EXPERIMENTAL

The catalyst prepared for this study consisted of a thin layer of platinum and tin oxide dispersed on a silica gel substrate (7). The silica gel was impregnated with tin oxide via evaporation of a stirred solution of tin metal powder and silica gel in concentrated nitric acid at 150°C. Subsequently, platinum was precipitated from an aqueous solution of platinum tetraamine dihydroxide and formic acid with heating followed by drying at 150°C. The final product was heated in air at 150°C for 4 hours.

Two as-prepared $Pt/SnO_2/SiO_2$ samples were inserted into an ultrahigh vacuum (UHV) system (base pressure of 10^{-11} Torr). After initial surface characterization, the samples were each transferred into a preparation chamber connected to the UHV system and reduced in 10 Torr of CO for two hours at 125 and 250°C. Heating was accomplished via conduction from a platform heating element which was resistively heated (9) in order to avoid dissociating the reducing gas. Sample temperatures were measured using a thermocouple attached to the stainless steel sample support block. After reduction, each sample was returned to the UHV chamber without air exposure for further characterization.

Energy analysis for the ISS and XPS experiments was accomplished using a Perkin-Elmer PHI Model 25-270 double-pass cylindrical mirror analyzer (CMA). The CMA contained an internal, movable aperture which varied the polar acceptance angle for incoming particles. ISS spectra were collected in the nonretarding mode using a 147° scattering angle and pulse counting detection

(10). A 100 nA, 1 keV ^{4}He$^+$ primary beam was defocused over a 1 cm^2 area to minimize sputter damage. Survey and high-resolution XPS spectra were recorded with Mg Ka excitation in the retarding mode using 50 and 25 eV pass energies respectively.

RESULTS AND DISCUSSION

XPS survey spectra taken before and after CO reduction from two Pt/SnO$_2$/SiO$_2$ catalyst samples appear in figures 1 and 2 respectively. The two catalyst samples examined (designated as samples A and B) were similar in that both were randomly dispensed from the same catalyst batch. For the air-exposed surfaces, the spectra in figures 1a and 2a exhibit predominant peaks due to Sn and O while peaks due to Pt are present but less discernible. Differences between figures 1a and 2a with regard to the O/Sn ratio suggest that the as-prepared catalyst samples lack uniformity in average surface composition. Nevertheless, important information may still be obtained with respect to data taken from each catalyst sample before and after reduction. A thick tin oxide surface layer (> 50 angstroms) is indicated by the lack of Si XPS signals arising from the silica substrate. Only trace amounts of carbon and surface contaminants are detected. Reduction in CO results in changes in the Sn and O signals as shown in figures 1b and 2b. The spectra indicate that the surface region of sample A (reduced at 125°C) becomes oxygen-enriched while surface oxygen depletion occurs in sample B (reduced at 250°C). A possible mechanism responsible for this result is discussed below.

ISS spectra taken from sample B before and after reduction appear in figures 3a and 3b respectively. Figure 3a reveals distinct Pt and O features while the Sn peak appears as a shoulder on the Pt peak. After catalyst reduction, figure 3b indicates that the surface composition has changed considerably. The Pt and Sn peaks have decreased in intensity and a new group of peaks has emerged centered near 0.55 E/E$_0$. Although features due to Si would appear in this region, it is most probable that these peaks are due to impurities commonly associated with silica such as sodium. Considering the stability of silica, it seems unlikely that silica species would migrate to any appreciable extent under these pretreatment conditions. Since ISS is essentially sensitive to the outermost layer of surface atoms, the data in figure 3 suggest that the 250°C reduction results in physical coverage (encapsulation) of the majority of surface Pt and Sn. This encapsulation hypothesis is confirmed by an ISS experiment performed after the reduced surface was lightly sputtered. As shown in figure 4, the sputtering process uncovered significant amounts of underlying Pt and Sn. Although surface charging features appear in these ISS spectra, the peaks which correspond to Pt and Sn remain prominent and meaningful.

The data presented thus far suggest that a 250°C CO reduction promotes movement between Pt and Sn at the surface and underlying impurities contained within the silica substrate. The resulting migration of substrate species over surface Pt and Sn is consistent with the more bulk-sensitive XPS results in figures 2a and 2b. As discussed below, oxygen migration from the subsurface region may also be important as the reduction of Pt proceeds. However, changes due to surface desorption mechanisms cannot be ruled out and most likely are important. A consistent observation is that oxygen surface desorption as well as bulk diffusion processes are more prevalent at 250°C than at 125°C which would explain the overall trend that is observed in the XPS survey

spectra. At 125°C surface desorption mechanisms do not appear to be significant, and as a result XPS indicates that migrating oxygen species concentrate near the surface resulting in the increased O-to-Sn peak height ratio. Whether substrate coverage of surface Pt and Sn is extensive at 125°C is uncertain due to the lack of ISS data for sample A.

High resolution XPS spectra of the O 1s features are shown in figures 5 and 6. The fact that two distinct O 1s peaks appear is unusual and suggests that differential charging is occurring. Differential charging is indicative of an insulating surface which tends to acquire a steady-state charge during analysis. A net surface charge may result from an unbalance between photoelectron loss and electron gain from the immediate environment. When such complications arise peak binding energies shift proportionately to the extent of surface charging thus requiring correction. As indicted, these two peaks are obtained from both samples both before and after reduction. However, during catalyst reduction, the peak separations decrease from about 9 eV to 7.3 eV with the smaller peak remaining essentially stationary in binding energy. Therefore differential charging appears less severe on the reduced samples indicating that these surfaces are more metallic in nature (although they remain predominantly insulating). As shown in figure 7, the Pt 4f XPS spectra exhibit broad features suggesting that multiple Pt oxidation states are present even after reduction. Due to charging effects, however, the corresponding binding energies require correction. It is interesting to note the results when the Pt 4f spectra taken before and after reduction are corrected, respectively, by the 9 and 7.3 eV oxygen peak separations noted above. Adjusted for surface charging accordingly, figure 7a indicates that a mixture of PtO_2, PtO and perhaps $Pt(OH)_2$ is present on the air-exposed surfaces. After oxidation, peak positions shift toward lower binding energies as surface Pt is partially reduced. After reduction at 125°C, figure 7b indicates a major peak corresponding to $Pt(OH)_2$, while figure 7c reveals that metallic Pt is dominant after the 250°C reduction. A comparison of figures 7b and 7c suggests that increasing the CO reduction temperature from 125°C to 250°C seems to increase the extent to which Pt is reduced, although in either case multiple Pt states remain.

The Sn 3d XPS spectra taken before and after reduction from both samples appear in figures 8 and 9. After reduction, the spectra in both figures indicate a peak shift which is essentially equal to the 1.7 eV oxygen peak shift noted above. Although metallic and oxidic Sn exhibit approximately this ame peak shift, the overall conservation of peak shape and character which is depicted suggests that the peak shift results from the aforementioned surface charging effects. Therefore, it appears that most of the Sn remains essentially oxidic in nature during CO reduction at both temperatures. However, the Sn 3d peaks become slightly wider along the low-binding energy side as the reduction temperature increases indicating that a very small amount of Sn may have been reduced. Several possibilities exist regarding the form of the reduced Sn. There is evidence that metallic Sn and possibly alloyed Sn form when platinized tin oxide surfaces are annealed in vacuum near 450°C (11). Similar conclusions have been reached when a commercial Pt/SnO_2 catalyst is reduced in CO at temperatures up to 175°C (5). In both cases, however, the metallic or alloyed Sn appeared as a baseline shoulder on the low-binding energy side of the tin oxide Sn 3d XPS peaks. After CO reduction in the present study, the overall character of the tin oxide Sn 3d peaks is somewhat different with the entire low-binding energy side exhibiting a broadened

appearance. Paparazzo and coworkers (12) have noted similar results using XPS to study air-exposed and annealed SnO_2 and SnO surfaces. Their XPS experiments were able to discern SnO_2 from SnO and metallic Sn. The annealed surfaces exhibited metallic features which emerged as distinct peaks or shoulders near the baseline of the respective tin oxide Sn $3d_{5/2}$ peaks. Quite unlike the metallic features, the spectral contrasts observed between SnO_2 and SnO appeared as nominal shifts over the entire Sn $3d_{5/2}$ peaks. The latter observation is more consistent with the results observed in this study. The data in figures 7 and 8 therefore suggest that during the pretreatments a small fraction of SnO_2 may have been reduced to some lower oxide of Sn such as SnO.

The XPS data are consistent with the suggestion that surface hydroxyl groups facilitate CO oxidation on platinized tin oxide catalysts (4). After CO reduction, a greater oxygen surface concentration is indicated for sample A relative to sample B. Hydrogen should also be present at these temperatures (13). The superior performance which results from a 125°C CO pretreatment may therefore be attributed to hydroxyl groups which are not desorbed at these pretreatment conditions. It is also unlikely that encapsulation occurs at the lower temperature. Indeed, assuming that the charge corrections to the Pt 4f XPS features are valid, the spectra indicate that a greater concentration of surface $Pt(OH)_2$ is present after the 125°C CO reduction.

A related study by Drawdy et al. (5) is consistent with much of the data presented above. In that study a 2 wt% Pt/SnO_2 catalyst (Engelhard Corporation) was characterized using ISS, XPS and Auger electron spectroscopy (AES) after CO reductive pretreatments at 75, 100, 125 and 175°C. Coincident with increasing reduction temperature was an increase in the concentration of surface $Pt(OH)_2$ species. XPS indicated that $Pt(OH)_2$ is the predominant Pt specie after reduction at 175°C. It is interesting that pretreatments near 175°C promote superior activity enhancement for the Engelhard Pt/SnO_2 catalyst. In fact nearly identical activity enhancement is observed for pretreatments between 125 and 225°C. Therefore, with respect to both catalysts, these two studies suggest that the pretreatments which favor $Pt(OH)_2$ formation on the catalyst surface are the most beneficial. Apparently, the Pt/SnO_2 catalyst continues to benefit from pretreatments at higher temperatures since it does not undergo interactions with a silica substrate.

It is important to emphasize that the benefits of these reductive pretreatments are realized only after several hours of reaction. During this period the surface may undergo significant changes with respect to the types of surface species present and their chemical states. Further research is in progress which will characterize the surfaces of these pretreated catalysts as a function of reaction time. Additional pretreatment temperatures are also being investigated to further examine the surface alterations described above.

SUMMARY

The effects of two CO pretreatment temperatures on a $Pt/SnO_2/SiO_2$ surface have been examined using ISS and XPS. A CO reduction at 250°C promotes migration of silica substrate impurities over surface Pt and Sn while depleting the surface region of oxygen. At 125°C, CO reduction results in surface oxygen enrichment. Subsequent to both CO reductions, most of the Sn appears to remain oxidic while surface Pt is only partially reduced. Increasing the CO reduction temperature increases the extent to which the Pt is reduced. After

a 125°C reduction, $Pt(OH)_2$ appears dominant while after a 250°C reduction most of the Pt is in metallic form. The data are consistent with a dual mechanism which suggests that surface dehydration and substrate migration over surface Pt and Sn are responsible for the inferior CO oxidation activity produced by a 250°C CO pretreatment. The XPS results are consistent with partial SnO_2 reduction to SnO but more direct evidence would be desirable.

REFERENCES

1. "Closed-Cycle, Frequency-Stable CO_2 Laser Technology, Proceedings of a workshop held at Langley Research Center, Hampton, VA, June 10-12, 1986," C.E. Batten, I.M. Miller and G.M. Wood, Jr., eds., NASA Conference Publication 2456.

2. D.S. Stark, A. Crocker and G.J. Steward, "A sealed 100-Hz CO_2 laser using high CO_2 concentrations and ambient temperature catalysis," J. Phys. E: Sci. Instrum. 16, 158-161 (1983).

3. D.S. Stark and M.R. Harris, "Catalysed recombination of CO and O_2 in sealed CO_2 TEA laser gases at temperatures down to -27°C," J. Phys. E: Sci. Instrum. 16, 492-496 (1983).

4. D.R. Schryer, B.T. Upchurch, J.D. Van Norman, K.G. Brown and J. Schryer, "The effects of pretreatment conditions on a Pt/SnO_2 catalyst for the oxidation of CO in CO_2 lasers," J. Catal. 00, 00 (1990).

5. J.E. Drawdy, G.B. Hoflund, S.D. Gardner, E. Yngvadottir and D.R. Schryer, "Effect of Pretreatment on a Platinized Tin Oxide Catalyst used for Low-Temperature CO Oxidation," Surface and Interface Analysis 00, 00 (1990).

6. C.H.F. Peden and J.E. Houston, "Identification of a Carbonate Species during CO Oxidation on Deactivated Rh(111)," to be published.

7. B.T. Upchurch, D.R. Schryer, G.M. Wood and R.V. Hess, "Development of CO oxidation catalysts for the Laser Atmospheric Wind Sounder (LAWS)," in Proceedings of SPIE - International Society for Optical Engineering: Laser Applications in Meteorology and Earth and Atmospheric Remote Sensing, edited by M.M. Sokoloski, published by SPIE, Bellingham, Washington, 1062, 287 (1989).

8. S.D. Gardner, G.B. Hoflund, D.R. Schryer, J. Schryer, B.T. Upchurch, and D.R. Brown, "The Catalytic Behavior of Noble Metal/Reductible Oxide Materials for Low-Temperature CO Oxidation," submitted to Langmuir.

9. G.B. Hoflund, G.R. Corallo and M.R. Davidson, to be published.

10. R.E. Gilbert, D.F. Cox and G.B. Hoflund, "Computer-interfaced digital pulse counting circuit," Rev. Sci. Instrum. 53(8), 1281 (1982).

11. S.D. Gardner, G.B. Hoflund, M.R. Davidson and D.R. Schryer, "Evidence of Alloy Formation during Reduction of Platinized Tin Oxide Surfaces," J. Catal. 115, 132 (1989).

12. E. Paparazzo, G. Fierro, G.M. Ingo and N. Zacchetti, "XPS Studies on the Surface Thermal Modifications of Tin Oxides," Surface and Interface Analysis 12, 438 (1988).

13. G.B. Hoflund, A.L. Grogan, Jr., D.A. Asbury and D.R. Schryer, "A Characterization Study of a Hydroxylated Polycrystalline Tin Oxide Surface," Thin Solid Films 169, 69 (1989).
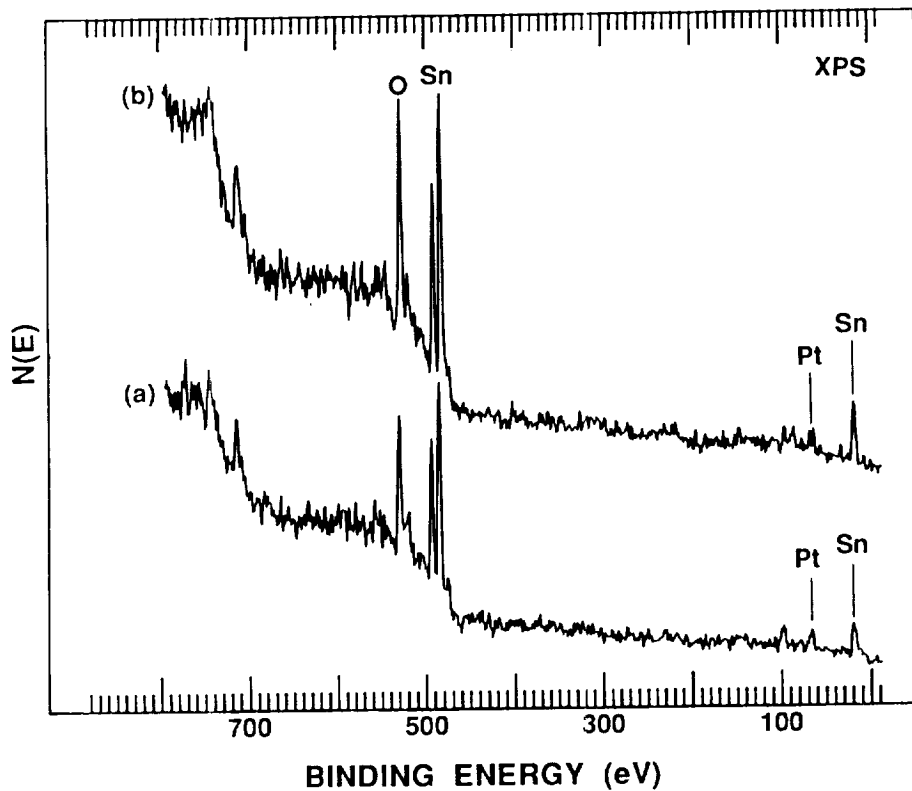
FIGURE CAPTIONS

Figure 1. XPS survey spectra taken from the platinized tin oxide surface of sample A (a) before and (b) after CO reduction at 125°C.
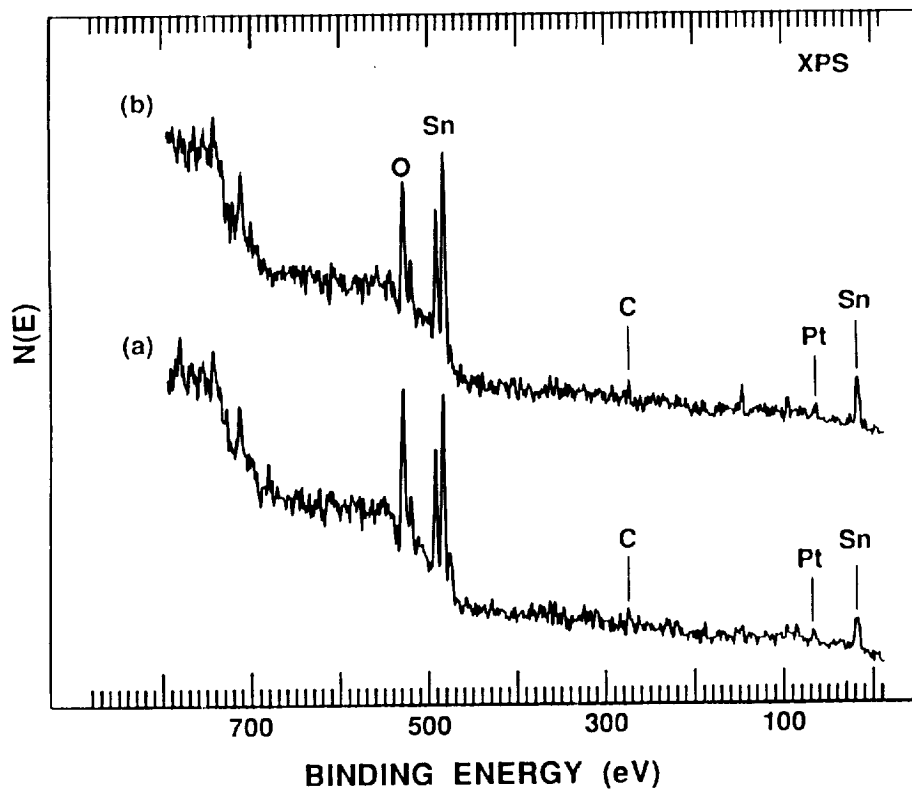
Figure 2. XPS survey spectra taken from the platinized tin oxide surface of sample B (a) before and (b) after CO reduction at 250°C.
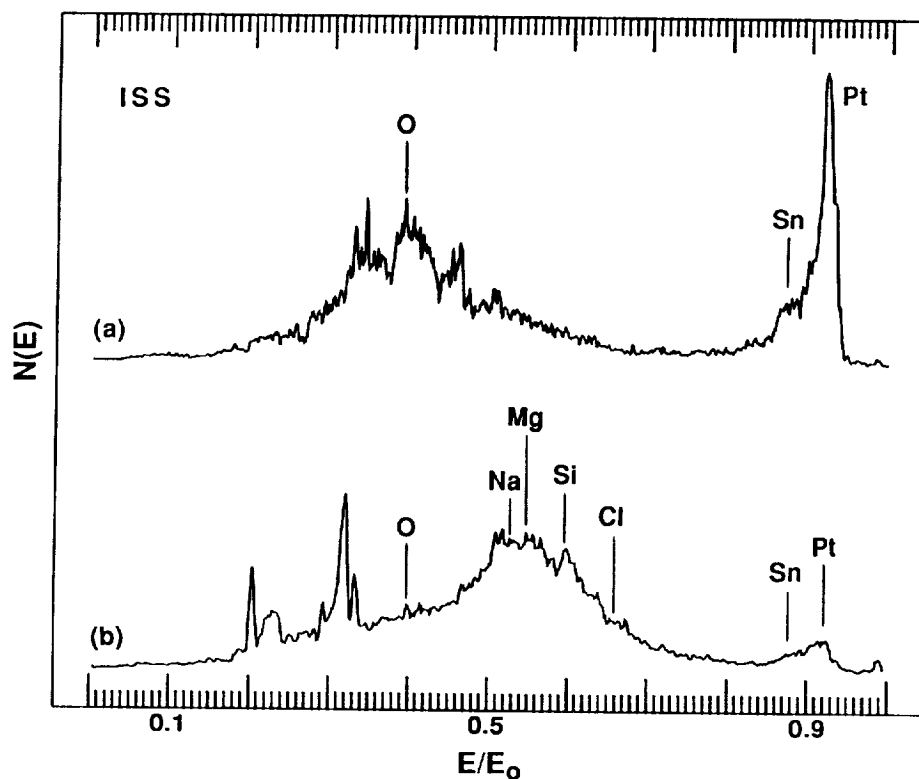
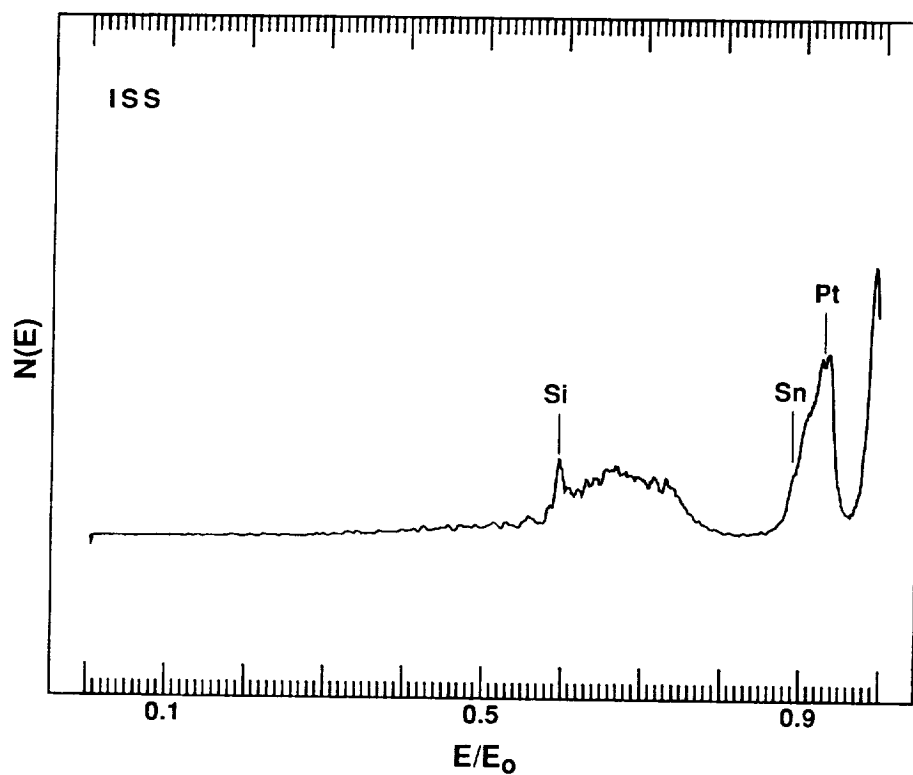Figure 3. ISS spectra taken from sample B (a) before and (b) after CO reduction at 250°C.

Figure 4. ISS spectrum taken from sample B after reduction and subsequent sputtering with 2 keV, 40 mA ^{4}He$^+$ ions for 5 minutes using a beam current of 10 μA over a 1 cm^2 area.
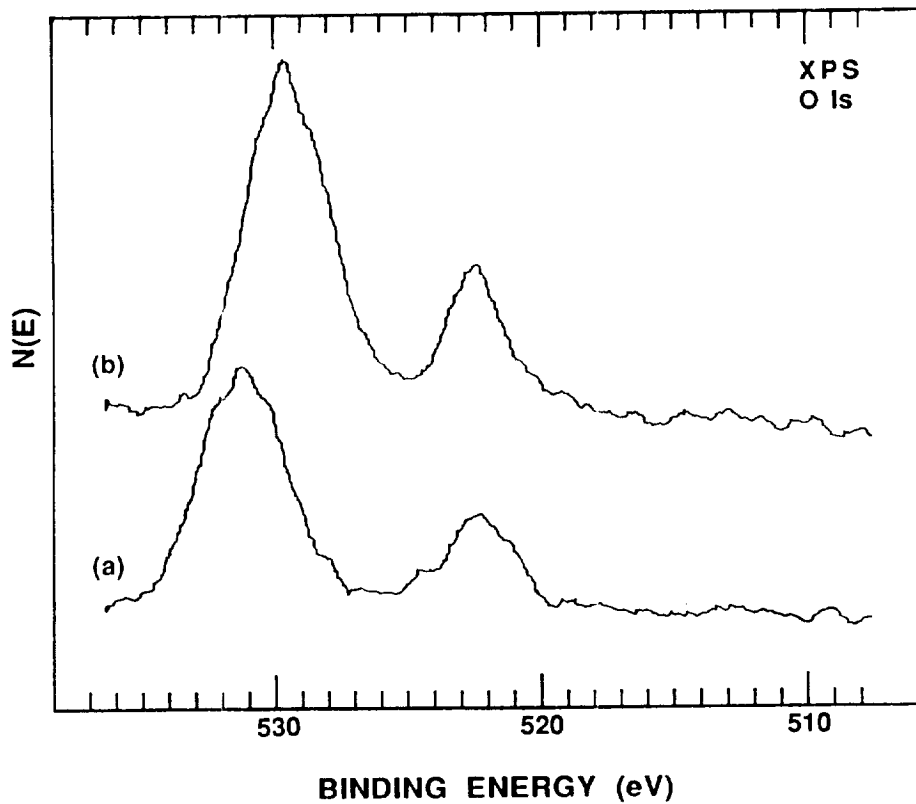
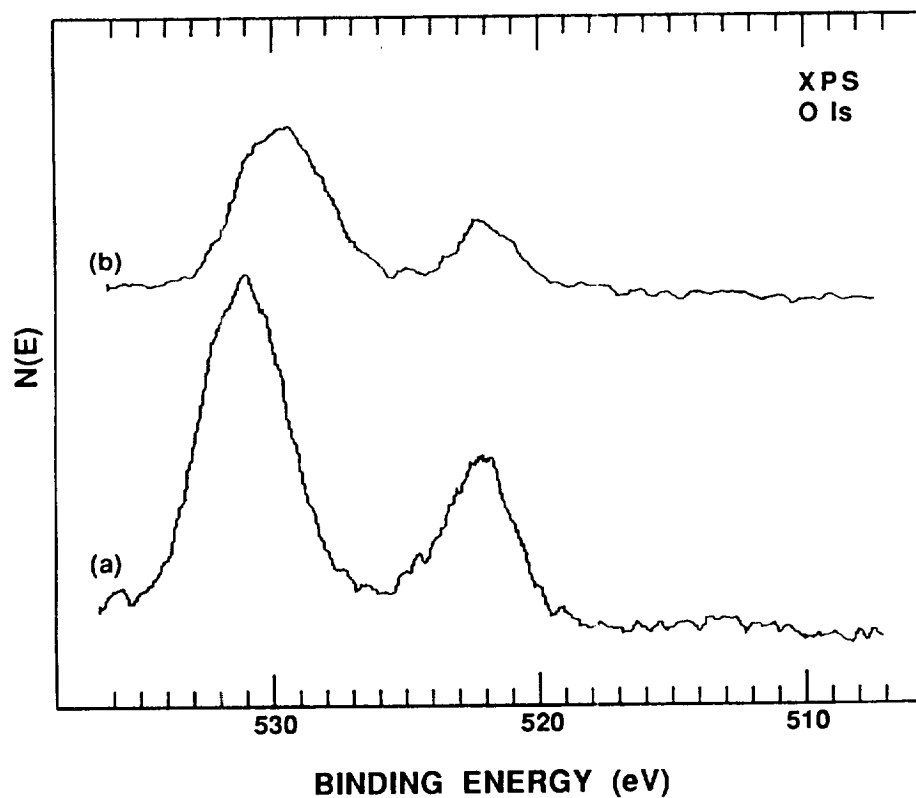Figure 5. O 1s XPS spectra taken from sample A (a) before and (b) after CO reduction at 125°C.

Figure 6. O 1s XPS spectra taken from sample B (a) before and (b) after CO reduction at 250°C.
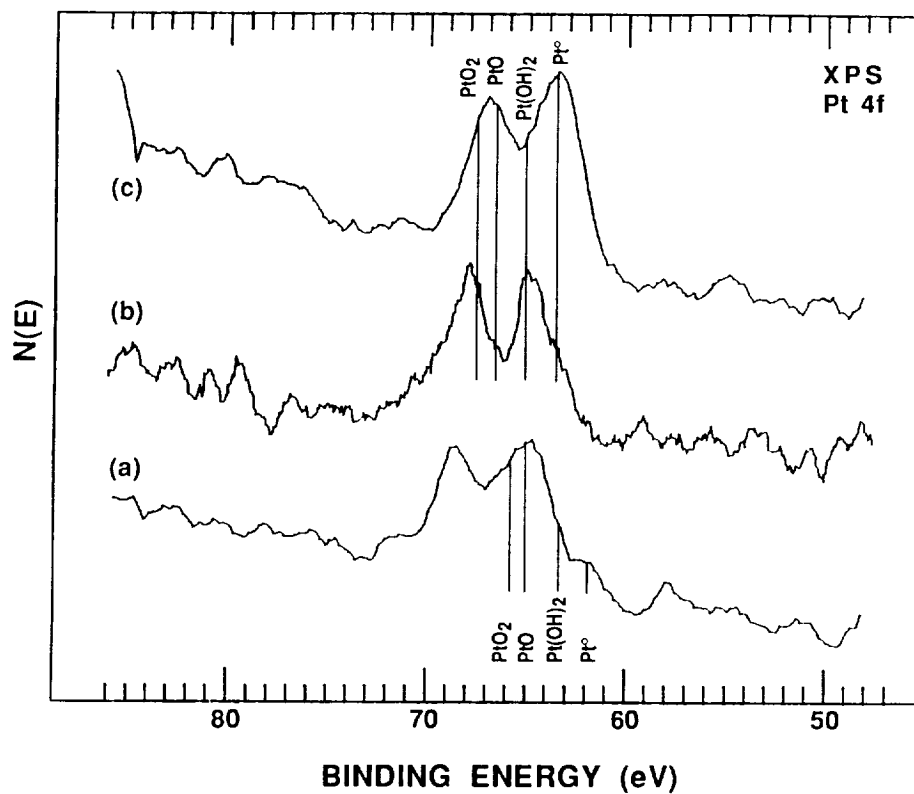
Figure 7. Pt 4f XPS spectra taken from (a) the as-entered platinized tin oxide surface, (b) sample A after CO reduction at 125°C and (c) sample B after CO reduction at 250°C.

Figure 8. Sn 3d XPS spectra taken from sample A (a) before and (b) after CO reduction at 125°C.

Figure 9. Sn 3d XPS spectra taken from sample B (a) before and (b) after CO reduction at 250°C.

#A2, p-1

Figure 1. XPS survey spectra taken from the platinized tin oxide sur-
face of sample A (a) before and (b) after CO reduction at
125 °C.

Figure 2. XPS survey spectra taken from the platinized tin oxide sur-
face of sample B (a) before and (b) after CO reduction at
250 °C.

Figure 3. ISS spectra taken from sample B (a) before and (b) after
CO reduction at 250 °C.

Figure 4. ISS spectrum taken from sample B after reduction and sub-
sequent sputtering with 2 keV, 40 mA ^{4}He$^+$ ions for 5 minutes
using a beam current of 10 μA over a 1 cm^2 area.

Figure 5. O 1s XPS spectra taken from sample A (a) before and (b) after CO reduction at 125 °C.

Figure 6. O 1s XPS spectra taken from sample B (a) before and (b) after CO reduction at 250 °C.

Figure 7. Pt 4f XPS spectra taken from (a) the as-entered platinized tin oxide surface, (b) sample A after CO reduction at 125 °C and (c) sample B after CO reduction at 250 °C.
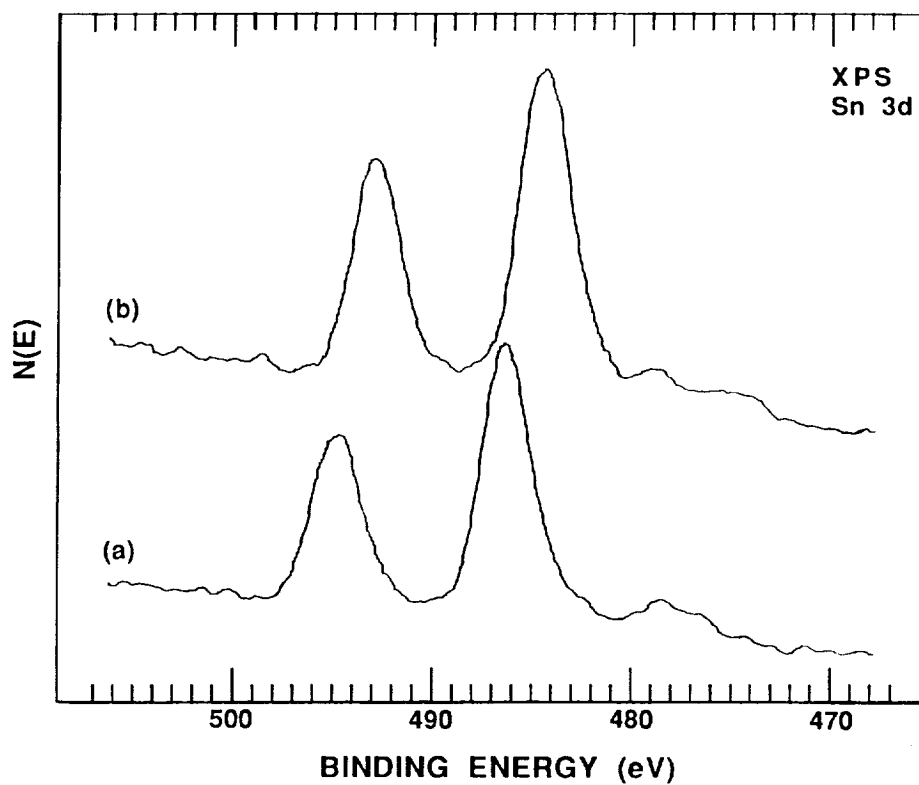

Figure 8. Sn 3d XPS spectra taken from sample A (a) before and (b) after CO reduction at 125 °C.
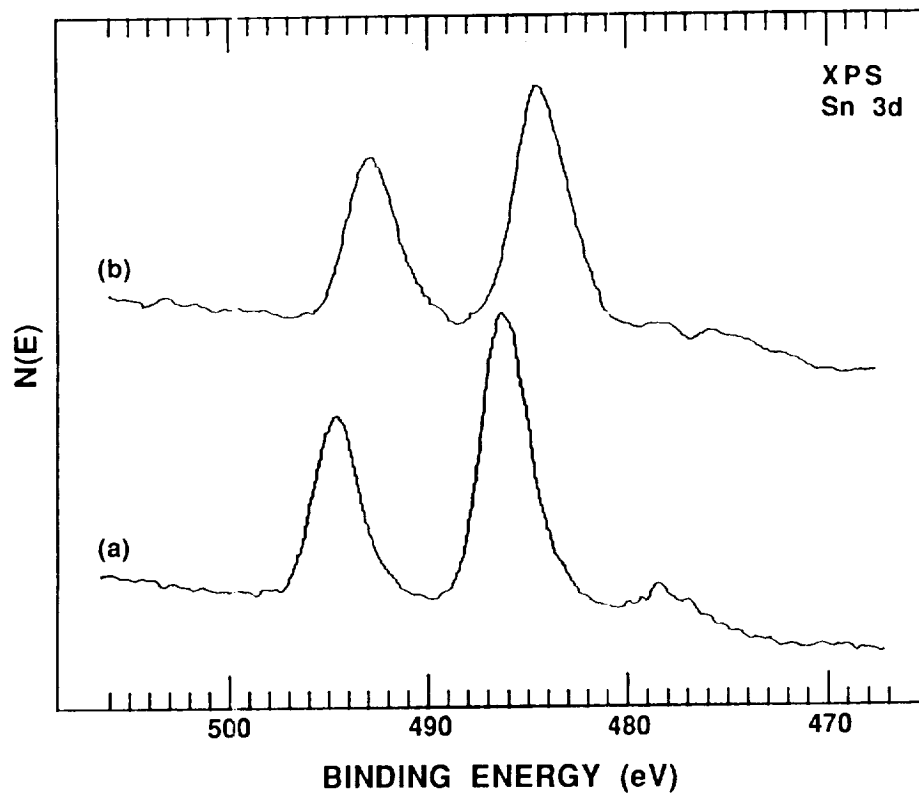
Figure 9. Sn 3d XPS spectra taken from sample B (a) before and (b) after CO reduction at 250 °C.

CHARACTERIZATION STUDY OF POLYCRYSTALLINE TIN OXIDE

SURFACES BEFORE AND AFTER REDUCTION IN CO

Jean E. Drawdy, Gar B. Hoflund and Mark R. Davidson
Department of Chemical Engineering
University of Florida
Gainesville, Florida

David R. Schryer
NASA Langley Research Center
Hampton, Virginia

ABSTRACT

Polycrystalline tin oxide surfaces have been examined before and after reduction in 40 Torr of CO at 100 and 175°C using Auger electron spectroscopy (AES), electron spectroscopy for chemical analysis (ESCA), ion scattering spectroscopy (ISS) and electron stimulated desorption (ESD). The changes in the surface composition and chemical states of the surface species generally are subtle for the reductive conditions used. However, significant changes do occur with regard to the amounts and the chemical forms of the hydrogen-containing species remaining after both the 100 and 175°C reductions.

INTRODUCTION

Tin oxide is an important component in many catalytic systems including Pt/SnO_x for low-temperature CO oxidation (1-4), electrocatalytic methanol oxidation (5-8) and oxygen reduction (9-11); CrO_x/SnO_y (12) and SnO_x/CuO (13) for NOX reduction; SbO_x/SnO_y (14) and CuO_x/SnO_y (15) for selective oxidation of propene to acrolein; and $Pt/Sn/Al_2O_3$ for hydrocarbon reforming (16-20). Most tin oxide-containing catalysts are activated by pretreating in CO or H_2 at elevated temperature prior to use as a catalyst. The conditions used during the reductive pretreatment are very important in optimizing the activity of a given catalyst. This is expected since tin oxide is a hydrated, reducible oxide. During reduction of tin oxide several changes occur including loss of water of hydration, loss of surface hydroxyl groups and loss of lattice oxygen to form SnO, suboxides or tin metal. All of these processes can occur, and the extent of each process depends upon the severity of the reductive treatment. Therefore, a large variety of complex surfaces can be produced by varying the parameters of the reductive process. This has a large effect on the catalytic properties of the surface particularly since the surface hydrogen content and the REDOX behavior of reduced tin oxide are often responsible for its catalytic properties in numerous reactions.

Previous studies (21-25) have shown that hydrogen is a major constituent of tin oxide surfaces. Nevertheless, many commonly used surface techniques are relatively insensitive to surface hydrogen so it often is neglected even though it may be responsible for the chemical behavior of a given tin oxide surface. It is of interest to determine both the chemical forms of the hydrogen present and their concentrations which is quite difficult. Tarlov and Evans (25) have addressed this topic using X-ray photoelectron spectroscopy (XPS or ESCA) and suggest that various complex forms of mixed tin oxides and

hydroxides and adsorbed water exist on tin oxide surfaces depending upon the history of a given surface. Electron stimulated desorption (ESD) (23) is another surface technique which is particularly useful for examining surface hydrogen present at tin oxide surfaces (21). ESD yields information about the relative amounts of hydrogen present at various surfaces and is capable of distinguishing between different chemical forms. Unfortunately, it is difficult to determine the nature of the adsorbed forms of surface hydrogen from the ESD spectral features.

A few studies of the reduction of tin oxide by annealing in vacuum (21,22,24-29) or a reducing gas at low pressure (30), by ion bombardment (26-29,31) or by exposure to a reducing plasma (32) have appeared, but the reduction of tin oxide in a reducing gas at higher pressure and elevated temperature apparently has not been addressed. The purpose of this present study is to examine the changes induced at a polycrystalline tin oxide surface by reduction in 40 Torr of CO at 100 and 175°C for 1 hour. These conditions are similar to those often used to activate tin oxide-containing catalysts. Furthrmore, ESD is used in these studies to examine hydrogen present at these surfaces before and after reduction. The next part of this study describes the effects of reduction on platinized tin oxide films and compares their behavior with that of bare tin oxide films presented in this study.

EXPERIMENTAL

Thin polycrystalline tin oxide films supported on titania foil were prepared using a high temperature spray hydrolysis method described previously (33). These films were analyzed before and after reduction in 40 Torr of CO at 100 and 175°C for 1 hour. The reduction was carried out in a sample pre-treatment chamber attached to the ultrahigh vacuum analysis chambers (base pressure of 10^{-11} Torr) using a sample heater system (34) which does not dissociate the reducing gas.

The tin oxide films were analyzed before and after reduction using several surface characterization techniques including Auger electron spectroscopy (AES), ion scattering spectroscopy (ISS), ESCA and ESD. AES, ISS and ESCA were performed using a double-pass cylindrical mirror analyzer (CMA) (Perkin-Elmer PHI Model 25-270) as the charged-particle energy analyzer. AES was performed using the internal, coaxial electron gun with a primary beam energy of 3 keV, spot size of about 0.5 mm and primary beam current of about 10 uA. The CMA was operated in the nonretarding mode using phase-sensitive detection with a 10 kHz oscillating voltage of 0.5 Vpp applied to the outer cylinder. ISS was also performed in the nonretarding mode using pulse counting detection (35). A 1 keV $^4He^+$ primary ion beam (100 nA defocused over a spot size of about 1 cm in diameter) was used. Exposure to the primary beams in both AES and ISS was minimized in order to reduce beam-induced damage. ESCA was performed using Mg Kα excitation and operating the CMA in the retarding mode with a 50 eV pass energy for collection of survey spectra and a 25 eV pass energy for collection of high-resolution spectra.

ESD was performed using a quadrupole mass spectrometer coupled to an energy prefilter and ion focusing lens (23) as the ion detection system. A 2 keV, 100 nA primary electron beam defocused over a spot of 1.0 mm diameter provided the excitation. Two types of ESD spectra were collected. The first was a mass spectrum obtained by collecting ions of kinetic energy between 2

and 3 eV. The second was an ion energy distribution (ESDIED) at selected masses.

RESULTS AND DISCUSSION

A. ISS, AES and ESCA Results

Three sets of ISS, AES, ESCA and ESD data were taken from an as-prepared tin oxide sample, a sample reduced at 100°C and a sample reduced at 175°C both in 40 Torr of CO for 1 hour. These data are described and compared in this section. An ESCA survey spectrum taken from the tin oxide film reduced at 100°C is shown in figure 1. This spectrum exhibits peaks due to O and Sn but no peak due to C. It is similar to the ESCA survey spectra taken from the as-prepared sample and the sample reduced at 175°C except that the O/Sn ratio varies from sample to sample. Also, the O and Sn peak shapes obtained from the three samples vary as described below.

Auger spectra taken from the as-prepared, 100°C-reduced and 175°C-reduced samples are shown in figures 2, 3 and 4 respectively. Although the spectra appear to be quite similar, there are substantial differences. Peaks due only to Sn and O appear in these spectra except for the spectrum taken from the 100°C-reduced sample which also exhibits a fairly large C peak considering the fact that the C AES sensitivity factor is smaller than that of Sn and O (36). Other differences include the shapes of the predominant Sn and O peaks, the low kinetic-energy structure and the O/Sn peak-height ratios. The as-prepared sample exhibits both Sn and O peaks and low-energy features which differ considerably from the equivalent features in the spectra obtained from the reduced samples. The Sn Auger peak positions of the metal and oxide differ by about 5 eV so a mixture of Sn metal and oxides produce a feature with a reduced splitting between the two peaks compared to either the metallic or oxidic feature as discussed in previous studies (3,37,38). Thus, the shape of the predominant tin peaks in figure 2 indicates that the surface of the as-prepared sample consists of a mixture of metallic tin and tin oxide. Both the O/Sn peak-height ratio and the shape of the low kinetic energy features (50-90 eV) are consistent with this suggestion. Based on UPS data and work function measurements, Powell and Spicer (39) first suggested that the outermost layer of Sn remains metallic during oxidation. This is supported by an ISS, ESCA and AES study by Asbury and Hoflund (37) in which they showed that O penetrates beneath the Sn surface during oxidation leaving a layer of Sn at the surface. An angle-resolved ESCA study by Asbury and Hoflund (40)* showed that the near-surface region of the oxygen-exposed sample is enriched in Sn and that this Sn is metallic. Although much evidence collected in different studies over many years suggests that the outermost layer of a tin oxide surface consists of metallic Sn, this notion is contrary to intuitive thinking. Therefore, continued effort should be devoted to gaining more direct evidence related to this interesting question.

The Auger spectra taken from the samples reduced at 100 and 175°C in CO shown in figures 3 and 4 respectively contain Sn features which have increased splitting compared to that in figure 2, and these peaks are shifted to slightly higher kinetic energies. Also, the low kinetic energy features have decreased considerably. These changes are indicative of oxidation of the metallic component of the as-prepared sample. It seems unusual that a reductive treatment would result in more complete oxidation of the outermost atomic

---
*Unpublished data

233

layer. However, the same phenomenon has been observed in a surface characterization study of $TiO_2(001)$ (41). In this study it was shown that sputtering a $TiO_2(001)$ surface lowers the O concentration in the near-surface region by creating O vacancies. Annealing this surface in 10^{-6} Torr of H_2 at 400°C actually increases the O concentration in the near-surface region by providing a chemical driving potential which results in the migration of bulk O to the surface. It appears that a similar process occurs by annealing an as-prepared tin oxide surface in CO resulting in oxidation of the metallic Sn overlayer and the concommitant changes in the Auger spectral features.

ISS spectra taken from the as-prepared, 100°C-reduced and 175°C-reduced tin oxide surfaces are shown in figure 5a, b and c respectively. ISS is an important surface analytical technique because it is highly surface sensitive yielding compositional information about the outermost atomic layer whereas AES and ESCA probe much more deeply beneath the surface. The ISS spectrum shown in figure 5a exhibits three features; a large Sn peak at an E/E_O of 0.87, a very small O peak at an E/E_O of 0.37 and an even smaller Cl peak at an E/E_O of 0.65. A peak due to C at an E/E_O of 0.28 does not appear in this spectrum. This spectrum is characteristic of those obtained from polycrystalline Sn exposed to O_2 at lower pressure or to air (37). Furthermore, the inelastic background is very low, which is characteristic of ion scattering from a metallic surface (42). This fact lends support to the assertion that the outermost atomic layer of an as-prepared tin oxide surface is metallic Sn.

An ISS spectrum taken from the 100°C-reduced tin oxide surface is shown in figure 5b. The O peak is comparable to that shown in figure 5a obtained from the as-prepared surface. However, a broad and poorly defined peak appears at an E/E_O lower than that of O (about 0.26). This feature is due to C; an assignment which is consistent with the fact that a significant C peak appears in the Auger spectrum obtained from this surface (see figure 3). There are two possible reasons for the presence of this C. The first reason is C contamination, but this probably is not the source since the other tin oxide surfaces do not exhibit any features due to C. The second and more likely possibility is that O vacancies are produced at or just beneath the surface through removal of lattice O to form CO_2 during the reduction. These vacancies may be active sites for adsorption of CO molecules thereby resulting in the presence of C at this surface. Also, the AES O/Sn ratio is greater for this surface than for the as-prepared surface. This fact supports the assertion that adsorbed CO probably is the source of C on the 100°C-reduced surface.

The ISS spectrum taken from the 175°C-reduced tin oxide surface is shown in figure 5c. This spectrum exhibits only two peaks due to Sn and O, and the O peak is smaller than those obtained from the as-prepared and 100°C-reduced surfaces. No peak due to Cl is present. The background is quite low indicating that the surface is conductive. This agrees with the results of electrical conductivity studies (43,44) which show that tin oxide surfaces exhibit much lower resistivity after reduction.

The ESCA Sn $3d_{5/2}$ peaks obtained from the as-prepared and 100°-reduced samples are shown in figure 6. The differences are fairly small so it is difficult to draw conclusions concerning the chemical changes which occur during the reduction from these spectra. The spectrum obtained from the reduced sample has a FWHM which is about 0.2 eV wider than that of the spec-

trum obtained from the as-prepared sample. Paparazzo et al. (45) have ex-
amined SnO and SnO_2 standards and claim that there is a 0.18 eV difference in
Sn 3d binding energy. Therefore, the increase in FWHM during reduction pro-
bably is due to conversion of Sn^{+4} to Sn^{+2}. Although ESCA is fairly insensi-
tive for distinguishing between Sn^{+4} and Sn^{+2}, electron energy loss spectros-
copy (ELS) is capable of making this distinction (31). Studies using ELS are
currently in progress to monitor the Sn chemical state during the reduction of
tin oxide.

The metallic Sn $3d_{5/2}$ ESCA peak lies at about 484.6 eV which is about 1.8
eV lower than the binding energy of the SnO_2 Sn $3d_{5/2}$ ESCA peak. Clearly, a
significant metallic Sn peak is not present before the reduction nor does one
form during reduction. ESCA probes quite deeply beneath the surface (~ 60Å)
compared to AES and particularly compared to ISS. This fact suggests that the
absence of a distinct metallic Sn peak in the ESCA Sn $3d_{5/2}$ spectrum obtained
from the as-prepared sample does not imply that an atomic layer of metallic Sn
is not present at the surface. In fact, preliminary angle-resolved ESCA data
(40) do indicate that the surface layer of air-exposed polycrystalline Sn is
metallic. Although a distinct metallic Sn $3d_{5/2}$ peak does not appear in
figure 6, the increase in the ESCA signal near 484.6 eV may be due to the
formation of a small amount of metallic Sn during the 100°C reduction.

The ESCA O 1s peaks taken from the as-prepared, 100°C-reduced and 175°C-
reduced tin oxide surfaces are shown in figure 7a and b.
There are several forms of O at these surfaces including adsorbed water,
hydroxyl groups bond to both Sn^{+2} and Sn^{+4}, SnO, SnO_2 and possibly multiple
forms of adsorbed oxygen (46). Although numerous ESCA studies of tin oxide
have been published, very little reliable information, e.g., binding energies
and peak shape data, is available due to the difficulty in interpreting the
complex O and Sn ESCA features. Generally, the primary oxidic O 1s ESCA
feature due to SnO or SnO_2 has a binding energy of 530.6 eV, that due to
hydroxyl groups has a binding energy of 531.8 eV and the peak due to adsorbed
water has a binding energy of 532.8 eV (25). Considering the high resolution
data presented in figure 7, it is apparent that changes in the chemical states
of the O species present in about the outermost 50-60 Å do occur during these
reductions and that these changes are both complex and subtle. It is inter-
esting that the O 1s peak shape obtained from the as-prepared sample is simi-
lar to that obtained from the 175°C-reduced surface. One important difference
is that the spectrum taken from the as-prepared surface exhibits more struc-
ture on the high binding energy side which is due to adsorbed water and hy-
droxyl groups. A secondary ion mass spectrometry (SIMS) study (22) has shown
that these species mostly reside in a hydrated layer about 30 Å thick at these
tin oxide surfaces. The concentrations of these species are reduced by the
reduction at 175°C. The 100°C-reduced surface yields O 1s peak with a lower
binding energy of about 530.3 eV and an increased FWHM. The Auger spectrum
obtained from this surface has an O/Sn ratio which is greater than that of the
as-prepared and 175°C-reduced surfaces. This additional O may be due to
adsorbed CO, other O-containing species which do not desorb or decompose at
100°C and subsurface O which migrates to the surface under a chemical driving
potential provided by the reducing environment. These same species also are
probably responsible for the increased FWHM of the O 1s spectrum in figure 7b.

The as-prepared and 175°C-reduced samples do not yield a C 1s ESCA peak,
but the 100°C-reduced surface does as shown in figure 8. This feature appears

to be composed of at least four different peaks with binding energies of 284.5, 285.6, 287.3 and 288.5 eV. Some of these peaks are due to contamination which accumulated during sample preparation or atmospheric exposure, and one or more of these features may be due to CO which adsorbed during the 100°C reduction.

B. ESD Results

Two different types of ESD spectra were taken in this study. The first is mass (m/e) spectra obtained by mass analyzing electron-stimulated desorbing ions at a preselected kinetic energy. The second is ion-energy distribution (ESDIED) spectra obtaining by preselecting mass and scanning some energy range (typically 0-10 or 0-20 eV).

An m/e ESD spectrum obtained from the as-prepared sample is shown in figure 9. Peaks due to H^+(1 amu), H_2^+(2 amu), O^+(16 amu), OH^+(17 amu), H_2O^+(18 amu), H_3O^+(19 amu), CO^+ or N_2^+(28 amu), and Cl^+(35 and 37 amu) are observed in this spectrum. There are considerable variations in the peak heights in this spectrum, but since the ESD cross sections are not known and can vary considerably, it is not currently possible to determine species surface concentrations from these spectra. The H^+ peak is the largest (peaks of higher mass have been expanded by a factor of 3), and the H_3O^+ peak height is about one-third that of the H^+ peak. All other peaks are quite small compared to the H^+ peak. The various peaks containing H and O are expected since these elements are both major constituents of these tin oxide films. The Cl is also a constituent present in small quantities since $SnCl_4$ and HCl are components used to prepare the tin oxide films. The CO or N_2 peak is due to contamination and has been observed in previous ESD studies of tin oxide films (47). ESD is a very sensitive technique both with regard to composition and to depth specificity (23). Comparison of the ESD spectrum in figure 9 with those of previous studies (47) shows that the tin oxide films examined in this study contain very low levels of surface contamination. Both H_3O^+ and F^+ species could comprise the 19 amu ESD peak. Surface studies of F-containing surfaces(48)* indicate that when an F^+ peak is present in ESD spectra, an F peak also appears in the corresponding Auger spectra. Since no F peak is present in the Auger spectra obtained from these tin oxide surfaces, the 19 amu ESD peak is assigned as due to H_3O^+ in this study.

ESDIED spectra for the 1,2,16,17,18 and 19 amu species are shown in figure 10a,b,c,d,e and f respectively. Important information can be gained from these spectra because each surface species desorbs with a characteristic kinetic energy distribution assuming that multiple desorption mechanisms are not operative (23). This method has been used by Corallo and Hoflund (49) to show that multiple states of adsorbed H are present on an annealed Si(100) surface. In that study it is shown that very small features in the ESDIED spectra are reproducible and meaningful. This fact is important with regard to the interpretation of the tin oxide ESDIED spectra presented below. The 1 amu spectrum clearly consists of multiple features with kinetic energies 0.7, 1.2, 2.1, 2.7, 3.1, 4.7, 5.4, 7.5 and 10 eV. Other H binding states may be present, but they do not yield readily distinguishable features. Although ESDIED is usually capable of identifying and distinguishing between different binding states, it does not yield specific bonding information about these states. In this sense ESDIED is similar to temperature programmed desorption (TPD). The H_2^+ ESDIED spectrum consists of a narrow and well-defined ESDIED

---

*Unpublished data

236

peak with a kinetic energy of 1.4 eV and higher lying peaks at about 6 and 17 eV with a gently increasing background indicative of a broad distribution of binding states which desorb with large kinetic energies. Both the 16 and 17 amu ESDIED spectra are similar in shape exhibiting peaks due to four bonding states at 1.2, 2.0, 2.7 and 3.7 eV. This may suggest that they are physically related. Perhaps a desorbing OH^+ splits into a neutral H and O^+ which then has the same ESDIED spectrum as the OH^+. The 16 amu ESDIED spectrum also exhibits peaks at 4.7, 7 and 18 eV. The main feature in the H_2O^+ ESDIED spectrum is fairly broad and may be composed of two peaks with kinetic energies of 1.4 and 2.5 eV. Since the H_2 peak also has a kinetic energy of 1.4 eV, it is possible that the origin of the detected H_2^+ species is through decomposition of a desorbing H_2O^+ into a neutral O and H_2^+. This is more plausible than the existence of molecularly adsorbed H_2 which then desorbs as H_2^+. A shoulder also appears at 3.6 eV on the 18 amu ESDIED spectrum which is a third binding state of adsorbed H_2O, and an increasing background due to binding states which yield higher kinetic energy ions is also present. The H_3O^+ ESDIED spectrum consists of multiple peaks with kinetic energies of 0.7, 1.2, 3.1, 3.6, 4.0, 5.0 and 7.5 eV. The 19 amu peak is quite large. This is reasonable since an adsorbed H_2O probably would readily pick up an H^+ in the H-rich environment of this surface. It is apparent from these complex ESD data that numerous O_xH_y species are present in varying amounts on tin oxide surfaces. Although most previous studies of tin oxide surfaces discuss hydroxyl groups and adsorbed water and make assignments based on the presence of these species, such specific assignments appear to be dubious based on these ESD results.

An m/e and the corresponding ESDIED spectra taken from the 100°C-reduced tin oxide surface are shown in figures 11 and 12 respectively. The ESD signals are all smaller after the reductive treatment indicating the loss of hydrogen-containing species during the reduction. The Cl^+ peaks are no longer present in the m/e spectrum, and small 14 and 28 amu peaks appear. The 14 amu peak is due to N^+ and has been observed previously (47). Also, the H_3O^+/H^+ peak-height ratio is decreased by the reduction.

The 1 amu ESDIED spectrum shown in figure 12 has a considerably different shape than that obtained from the as-prepared sample and also contains many features. However, it is difficult to make a direct comparison with H^+ ESDIED spectrum shown in figure 10 because the spectra obtained from the 100°C-reduced surface are shifted to lower kinetic energies. The magnitude of this shift is about 1.4 eV, but its origin is not understood. The 19 amu spectrum has a similar shape before and after the 100°C reduction, but the 17 amu peak is considerably narrower. This suggests the loss of one or more forms of hydroxyl groups during the reduction.

m/e ESD and ESDIED spectra taken from the 175°C-reduced sample are shown in figures 13 and 14 respectively. Peaks due to H^+, H_2^+, OH^+, H_2O^+, H_3O^+ and CO^+ appear in the m/e spectrum, but the signal strength is low indicating that even more hydrogen-containing species are removed during the 175°C reduction. It is interesting to note that both the 19 and 2 peaks are of significant size and that the size of the H_2^+ peak is nearly as large as the H_3O^+ peak. It is possible that most of the adsorbed water was removed during the 175°C reduction but that the chemical form which remains yields the desorbing H_2^+ species.

It was only possible to obtain ESDIED spectra for the H^+ and H_3O^+ desorbing ions because the signal strengths were too low for the other desorbing ions. The spectra shown in figure 14 also have shifted in kinetic energy but about 1 eV to higher kinetic energy in this case. Again, the spectral shape varies significantly indicating that the types of hydrogen-containing species at the surface are further altered by the 175°C reduction.

REFERENCES

1. Closed-Cycle, Frequency-Stable CO_2 Laser Technology, proceedings of a workshop sponsored by NASA Langley Research Center, Hampton, Virginia, June 10-12, 1986, NASA Conference Publication 2456, 1987.

2. D.S. Stark, A. Crocker and G.J. Steward, J. Phys. E: Sci. Instrum. 16(1983)158.

3. J.E. Drawdy, G.B. Hoflund, S.D. Gardner, E. Yngvadottir and D.R. Schryer, Surface Interface Anal. 00(1990)00.

4. D.R. Schryer, B.T. Upchurch, J.D. Van Norman, K.G. Brown and J. Schryer, J. Catal. 00(1990)00.

5. M.M.P. Janssen and J. Moolhuysen, J. Catal. 46(1977)289.

6. M.M.P. Janssen and J. Moolhuysen, Electrochim. Acta 21(1976)869.

7. M.R. Andrew, J.S. Drury, B.D. McNicol, C. Pinnington and R.T. Short, J. Appl. Electrochem. 6(1976)99.

8. A. Katayama, J. Phys. Chem. 84(1980)376.

9. M. Watanabe, S. Venkatesan and H.A. Laitinen, J. Electrochem. Soc. 130(1983)59.

10. C. Iwakura, M. Inai, T. Uemura and H. Tamura, Electrochim. Acta 26(1981)579.

11. A.C.C. Tseung and S.C. Dhara, Electrochim. Acta 19(1974)845.

12. F. Solymosi and J. Kiss, J. Catal. 54(1978)42.

13. M.J. Fuller and M.E. Warwick, J. Catal. 42(1976)418.

14. Y. Boudeville, F. Figueras, M. Forissier, J.-L. Portefaix and J.C. Vedrine, J. Catal. 58(1979)52.

15. D.E. Self, J.E. Drawdy (Oakes) and M.G. White, AIChE J. 29(1983)625.

16. R. Burch and L.C. Garla, J. Catal. 71(1981)360.

17. F.M. Dautzenberg, J.N. Helle, P. Biloen and W.M.H. Sachtler, J. Catal. 63(1980)119.

18. B. Coq and F. Figueras, J. Mol. Catal. 25(1984)87.

19. J. Volter, G. Lietz, M. Uhlemann and M. Hermann, J. Catal. 68(1981)42.

20. G.B. Hoflund, D.A. Asbury and R.E. Gilbert, Thin Solid Films 129(1985)139.

21.   G.B. Hoflund, A.L. Grogan, Jr., D.A. Asbury and D.R. Schryer, Thin Solid Films 169(1989)69.

22.   D.F. Cox, G.B. Hoflund and W.H. Hocking, Appl. Surface Sci. 26(1986)239.

23.   G.B. Hoflund, Scanning Electron Microscopy IV (1985)1391.

24.   D.F. Cox, G.B. Hoflund and H.A. Laitinen, Appl. Surface Sci. 20(1984)30.

25.   M.J. Tarlov and J.F. Evans, Chem. Mater. 00(1990)00.

26.   D.F. Cox, T.B. Fryberger and S. Semancik, Phys. Rev. B 38(1988)2072.

27.   E. de Fresart, J. Darville and J.M. Gilles, Solid State Commun. 37(1980)13.

28.   E. de Fresart, J. Darville and J.M. Gilles, Appl. Surface Sci. 11/12(1982)637.

29.   E. de Fresart, J. Darville and J.M. Gilles, Surface Sci. 126(1983)518.

30.   T.W. Capehart and S.C. Chang, J. Vac. Sci. Technol. 18(1981)393.

31.   D.F. Cox and G.B. Hoflund, Surface Sci. 151(1985)202.

32.   J.H. Thomas III, Appl. Phys. Lett. 42(1983)794.

33.   G.B. Hoflund, D.F. Cox, G.L. Woodson and H.A. Laitinen, Thin Solid Films 78(1981)357.

34.   G.B. Hoflund, M.R. Davidson and G.R. Corallo, to be published.

35.   R.E. Gilbert, D.F. Cox and G.B. Hoflund, Rev. Sci. Instrum. 53(1982)1281.

36.   L.E. Davis, N.C. MacDonald, P.W. Palmberg, G.E. Riach and R.E. Weber, Handbook of Auger Electron Spectroscopy, Physical Electronics Division, Perkin-Elmer Corporation, Eden Prairie, Minnesota, 1976.

37.   D.A. Asbury and G.B. Hoflund, J. Vac. Sci. Technol. A 5(1987)1132.

38.   D.A. Asbury and G.B. Hoflund, Surface Sci. 199(1988)552.

39.   R.A. Powell and W.E. Spicer, Surface Sci. 55(1976)681.

40.   D.A. Asbury and G.B. Hoflund

41.   G.B. Hoflund, H.-L. Yin, A.L. Grogan, Jr., D.A. Asbury, H. Yoneyama, O. Ikeda and H. Tamura, Langmuir 4(1988)346.

42.   S.D. Gardner, G.B. Hoflund, M.R. Davidson and D.R. Schryer, J. Cata. 115(1989)132.

43.   T.W. Capehart and S.-C. Chang, J. Vac. Sci. Technol. 18(1981)393.

44.   S.-C. Chang, J. Vac. Sci. Technol. A 1(1983)524.

45.   E. Paparazzo, G. Fierro, G.M. Ingo and N. Zacchetti, Surface Inter. Anal. 12(1988)438.

46.   S.-C. Chang, J. Vac. Sci. Technol. 17(1980)366.

47.   G.B. Hoflund, D.F. Cox, F. Ohuchi, P.H. Holloway and H.A. Laitinen, Appl. Surface Sci. 14(1982-83)281.

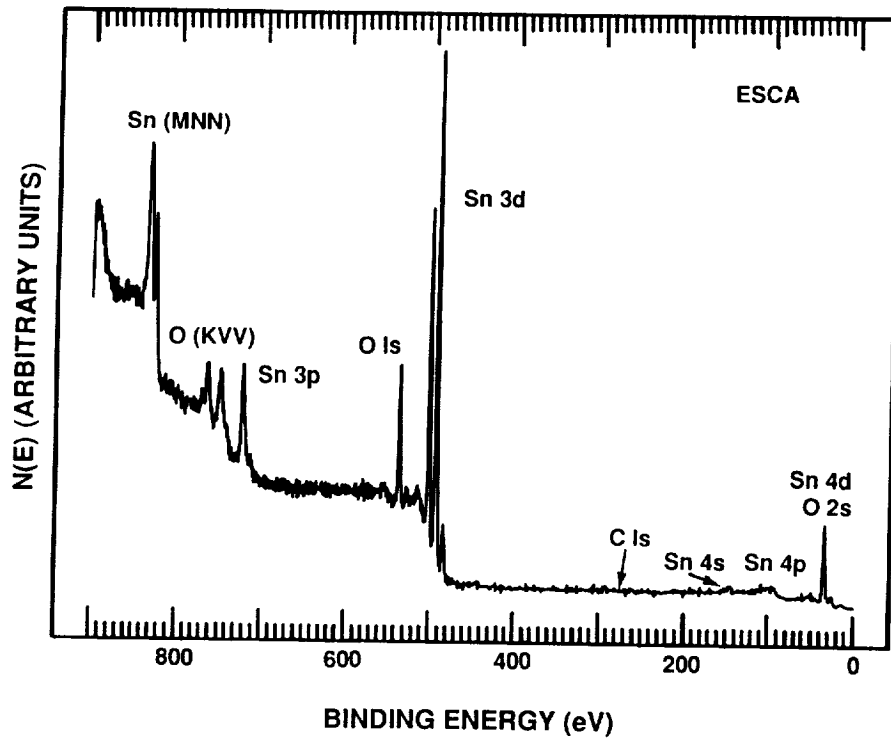48.   M.R. Davidson and G.B. Hoflund

49.   C.R. Corallo and G.B. Hoflund, Surface Inter. Anal. 12(1988)297.
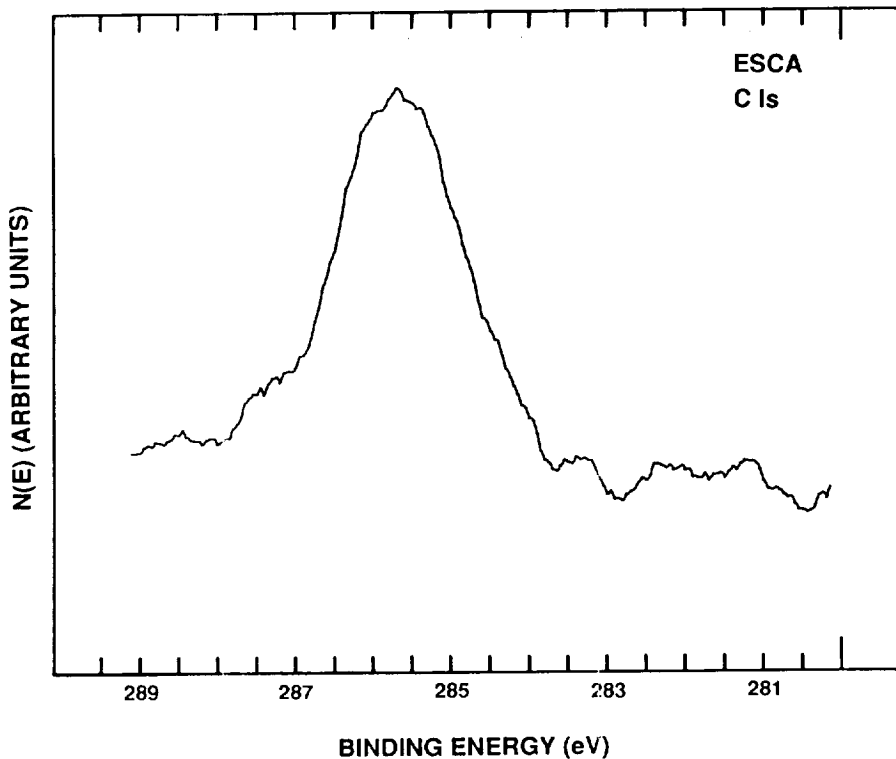
Figure 1.   Survey ESCA spectrum taken from the 100°C-reduced tin oxide sample.
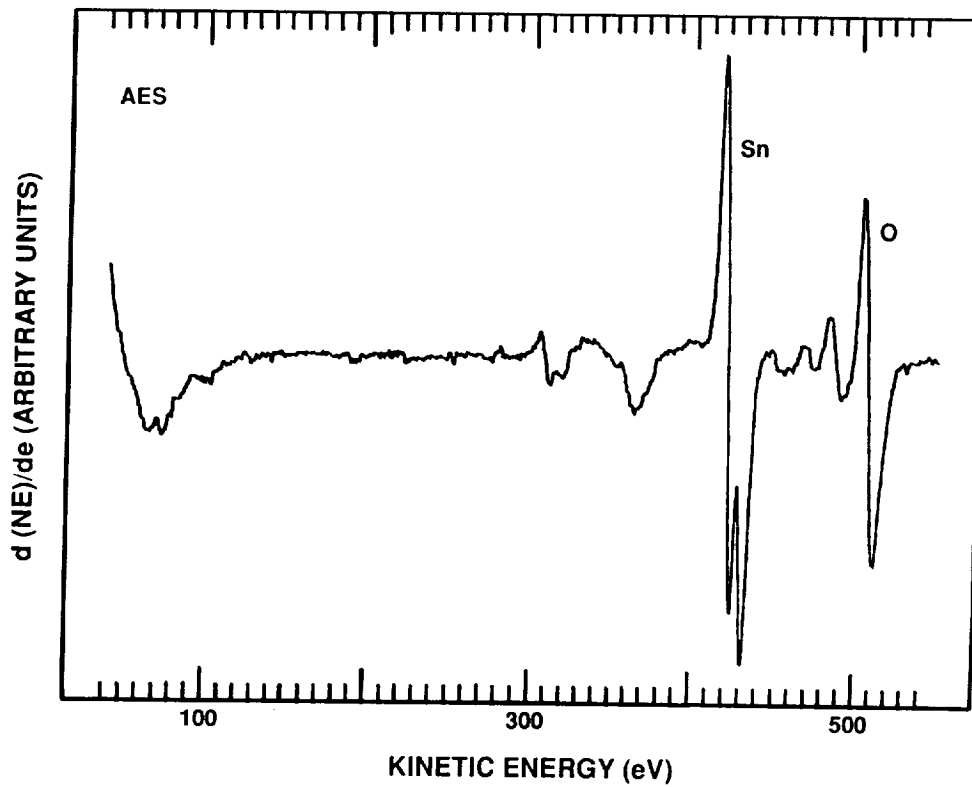
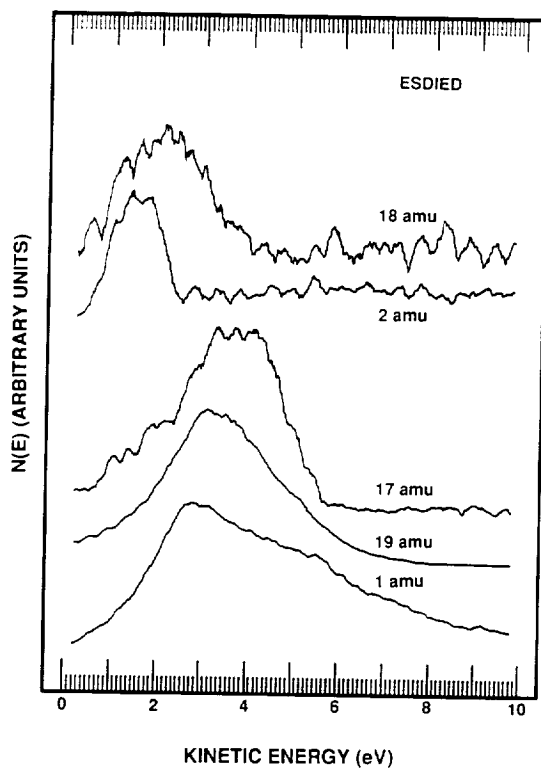

Figure 2.   Auger spectrum taken from the as-prepared tin oxide sample.
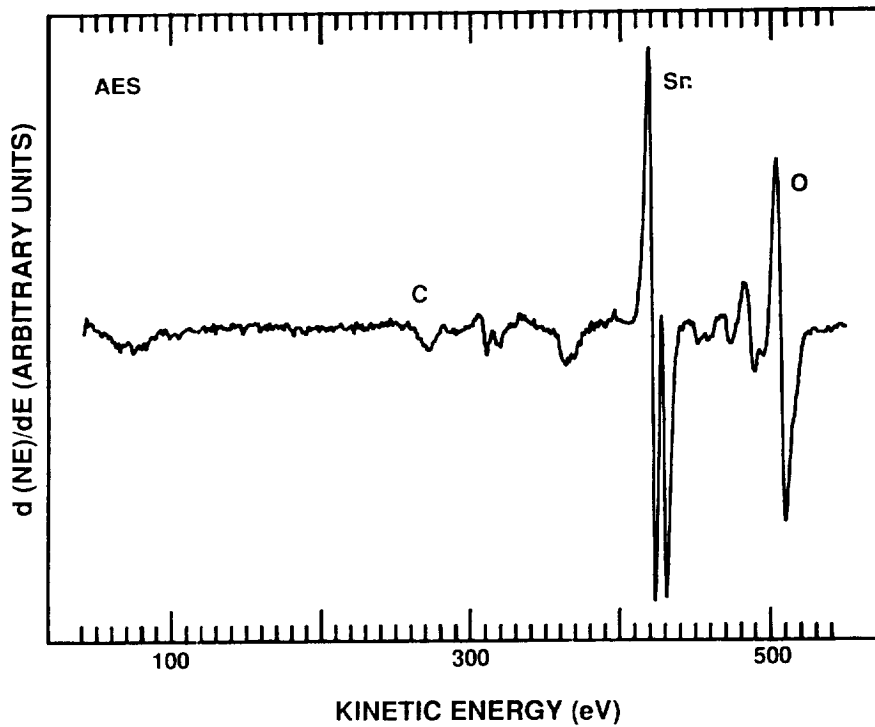
Figure 3.   Auger spectrum taken from the 100°C-reduced tin oxide sample.
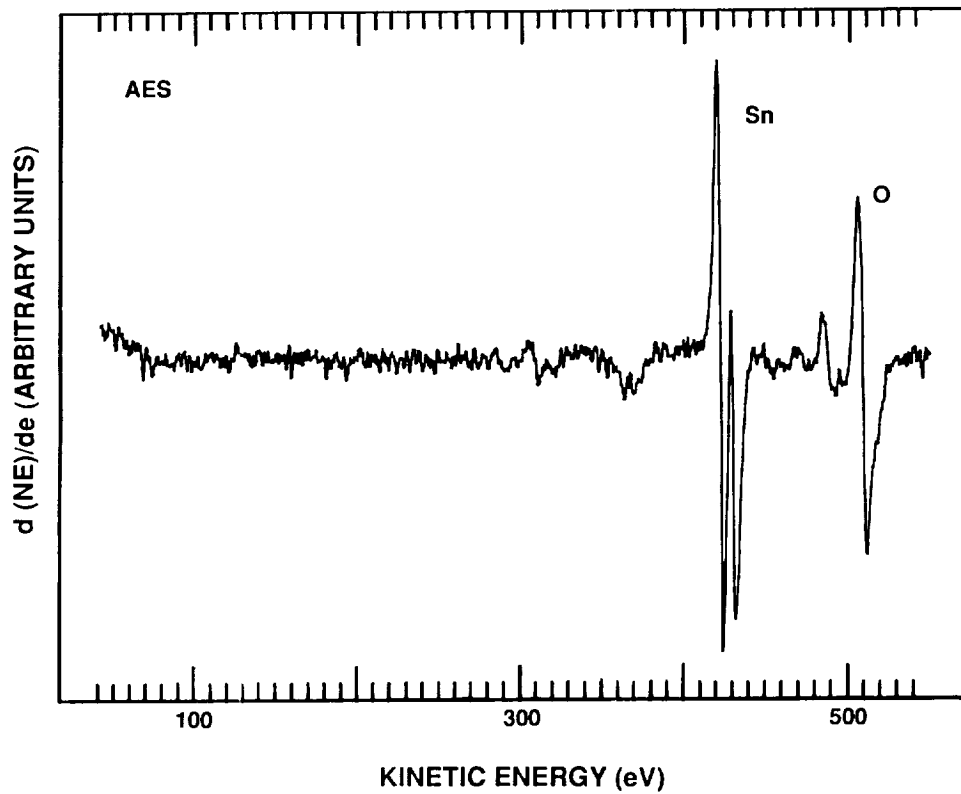
Figure 4.   Auger spectrum taken from the 175°C-reduced tin oxide sample.
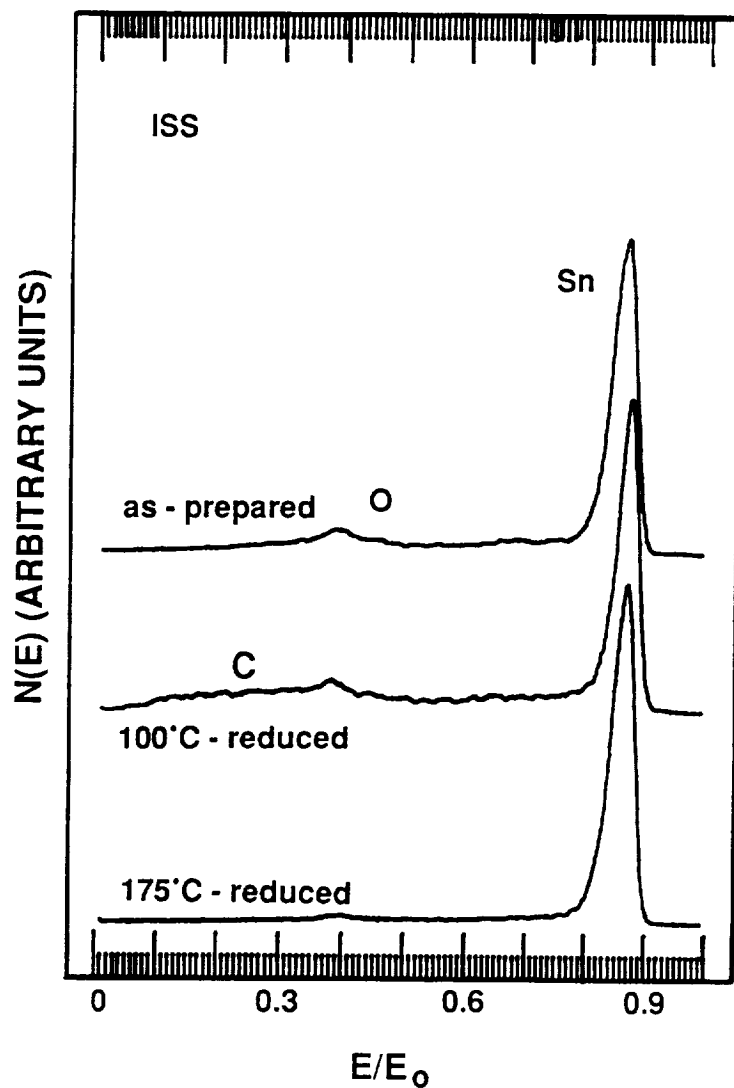
Figure 5.   ISS spectra obtained from (a) an as-prepared tin oxide surface, (b) a tin oxide reduced at 100°C in CO, and (c) a tin oxide surface reduced at 175°C in CO.
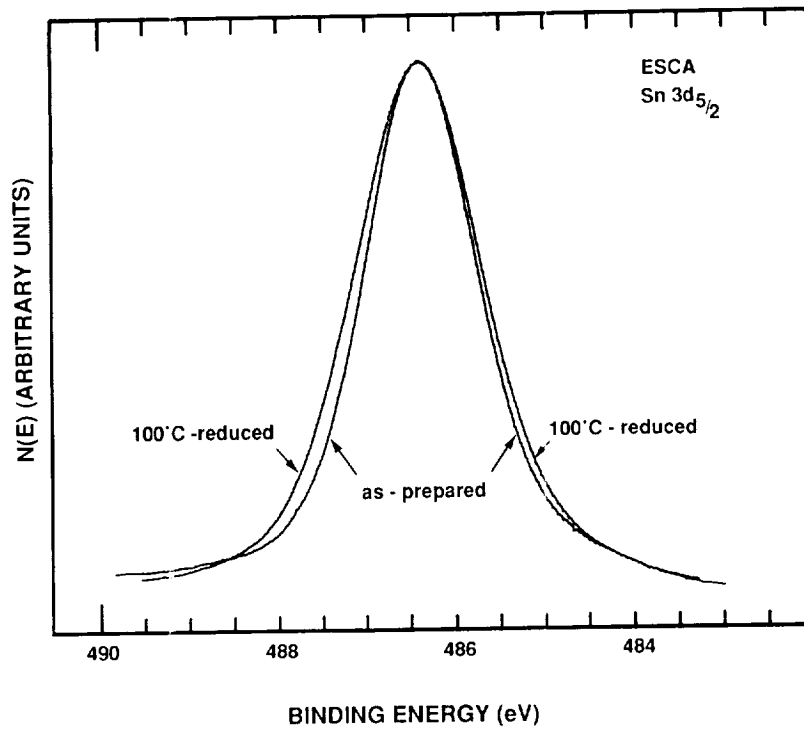
Figure 6. Sn $3d_{5/2}$ spectra taken from the as-prepared and 100°C-reduced tin oxide surfaces.
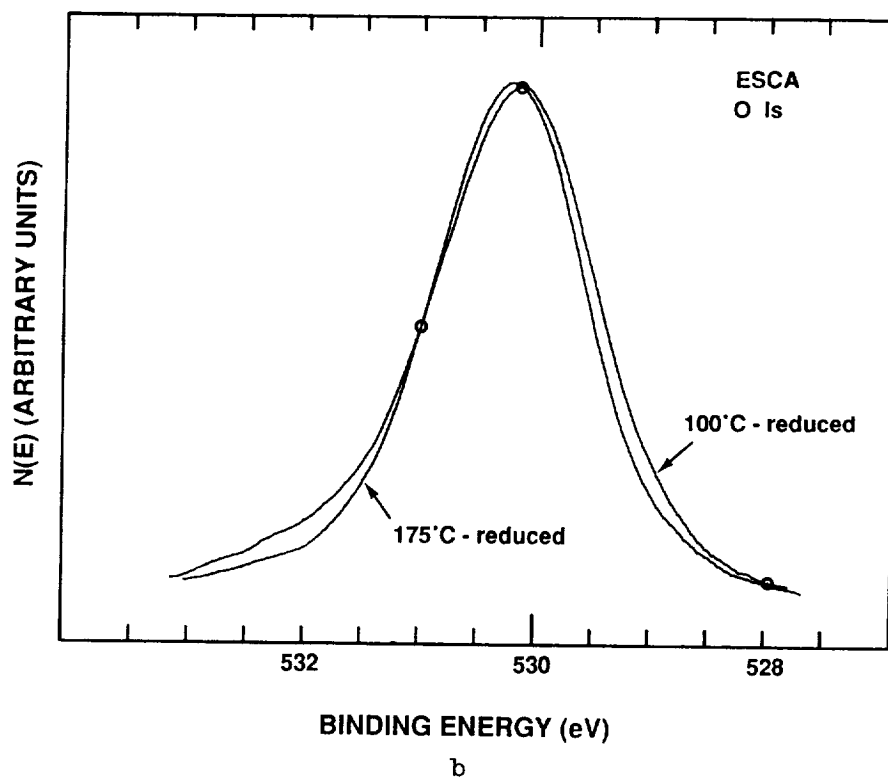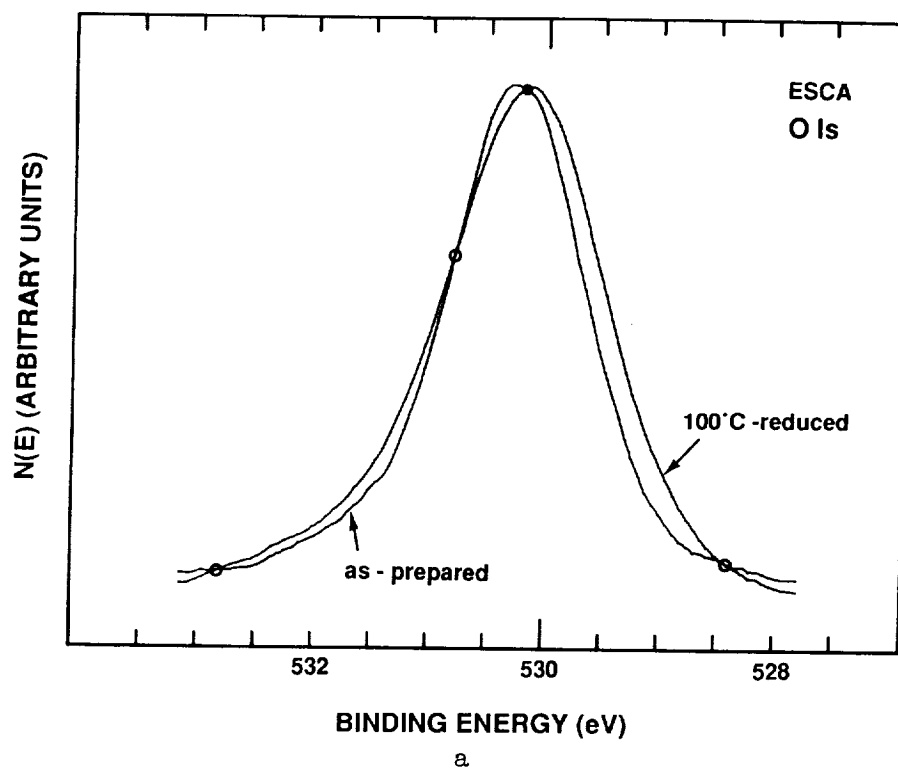
Figure 7. O 1s spectra taken from the as-prepared, 100°C-reduced and 175°C-reduced tin oxide surfaces.

Figure 8.   C 1s spectrum taken from the 100°C-reduced tin oxide surface.
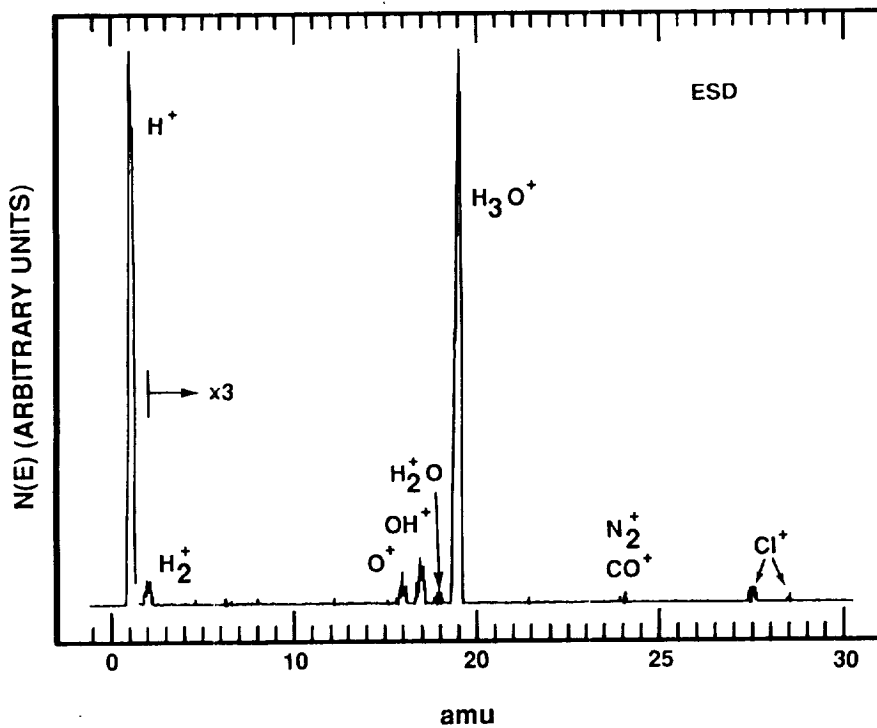
Figure 9.   m/e ESD spectrum taken from the as-prepared tin oxide surface.

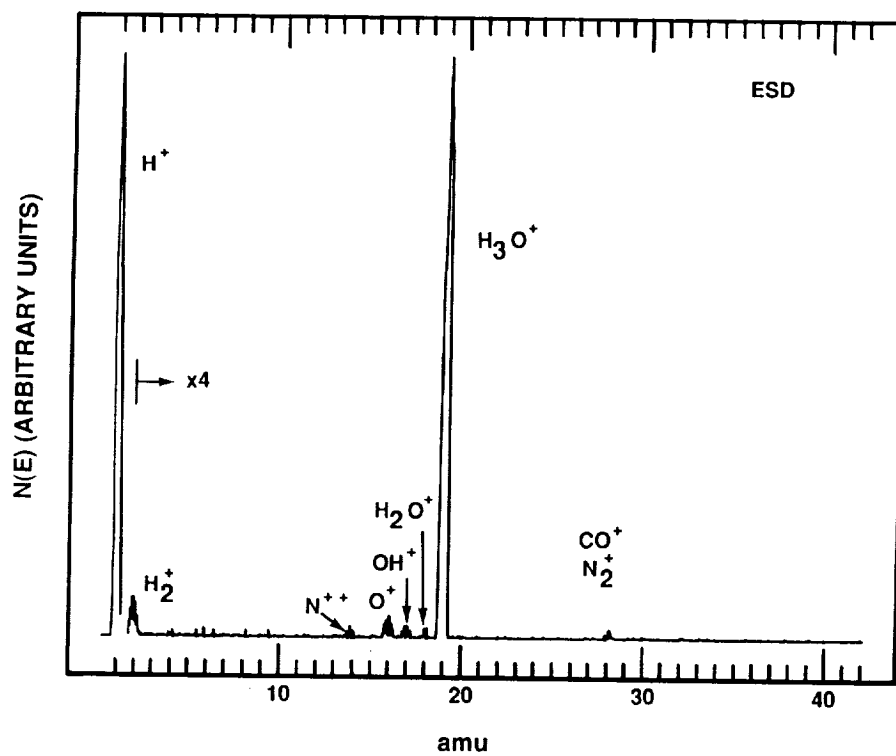Figure 10.   ESDIED spectra taken from the as-prepared tin oxide sample.

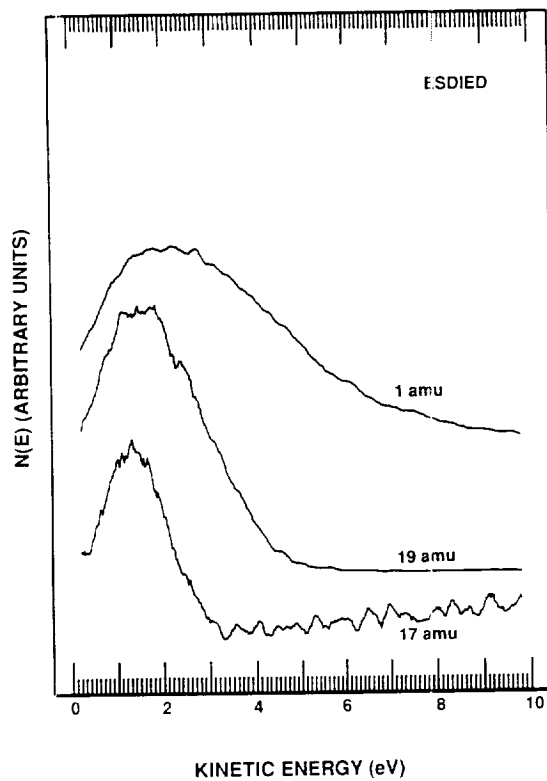Figure 11.   m/e ESD spectrum taken from the 100°C-reduced tin oxide surface.

Figure 12.   ESDIED spectra taken from the 100°C-reduced tin oxide surface.
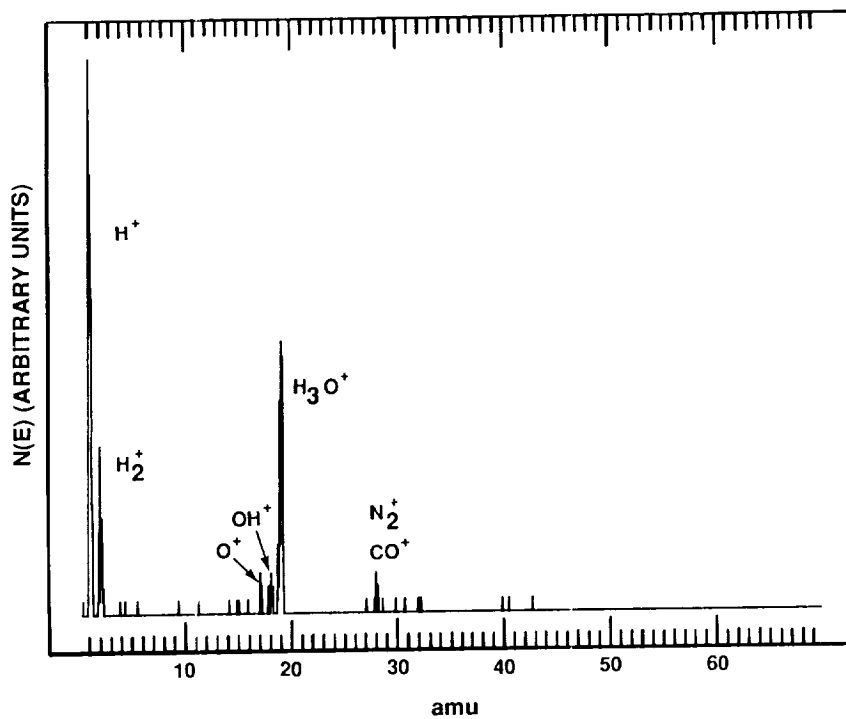

Figure 13.   m/e ESD spectrum taken from the 175°C-reduced tin oxide surface.
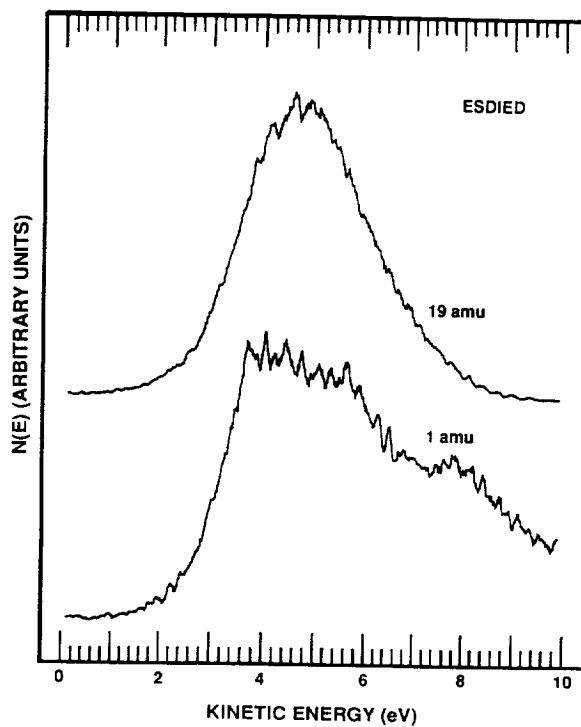
Figure 14.   ESDIED spectra taken from the 175°C-reduced tin oxide surface.

ISS AND TPD STUDY OF THE ADSORPTION AND INTERACTION OF CO AND H_2 ON POLYCRYSTALLINE Pt

Orlando Melendez and Gar B. Hoflund
Department of Chemical Engineering
University of Florida
Gainesville, Florida

David R. Schryer
NASA Langley Research Center
Hampton, VA

ABSTRACT

The adsorption and interaction of CO and H_2 on polycrystalline Pt has been studied using ion scattering spectroscopy (ISS) and temperature programmed desorption (TPD). The ISS results indicate that the initial CO adsorption on Pt takes place very rapidly and saturates the Pt surface with coverage close to a monolayer. ISS also shows that the CO molecules adsorb at an angular orientation from the surface normal and perhaps parallel to the surface. A TPD spectrum obtained after coadsorbing $^{12}C^{16}O$ and $^{13}C^{18}O$ on Pt shows no isotopic mixing, which is indicative of molecular CO adsorption. TPD spectra obtained after coadsorbing H_2 and CO on polycrystalline Pt provides evidence for the formation of a CO-H surface species.

INTRODUCTION

The adsorption characteristics of CO on polycrystalline Pt are of particular importance in understanding CO oxidation over Pt and Pt-containing catalysts such as Pt/SnO_x, which has been examined for use as a low-temperature CO oxidation catalyst in closed-cycle CO_2 lasers (1). Although many studies have been carried out on CO adsorption on Pt, contradictory conclusions have been reached so important questions remain unresolved.

Furthermore, hydrogen is present at most if not all surfaces, but it is often neglected in surface studies because commonly used surface techniques such as electron spectroscopy for chemical analysis (ESCA) and Auger electron spectroscopy (AES) are relatively insensitive to surface hydrogen. Nevertheless, it can have a large influence on the chemical behavior of a surface. This has been demonstrated in a study of a Pt/SnO_x catalyst by Schryer et al (2). For this catalyst the rate of CO oxidation depends strongly upon the surface hydroxyl group concentration. Using ESCA and electron stimulated desorption (ESD), Hoflund et al. (3) examined hydrogen at polycrystalline tin oxide surfaces and found that several different chemical states of hydrogen are present.

Hydrogen has also been shown to interact with CO during coadsorption on Pt to form a CO-H complex (4). In temperature programmed desorption (TPD) and ESD experiments by Craig (5,6), CO and H_2 were coadsorbed on a polycrystalline Pt. A mass 2 TPD spectrum shows the evolution of a new feature when CO is added to the hydrogen dosing gas and a corresponding feature is also observed

in the ESD O^+ ion energy distribution. These additional peaks are attributed to the formation of a CO-H complex at the Pt surface. Based on these results and those of Schryer et al. (2), it is quite possible that the CO-H complex plays an important role in CO oxidation over Pt/SnO_x surfaces.

Although the molecular adsorption of CO on low index PT crystals is well documented and generally accepted, much controversy still exists in the literature regarding the adsorption of CO on high index Pt planes. Both molecular and dissociative adsorption of CO on high index planes have been reported. Iwasawa et al. (7) reported dissociation of CO at step and kink sites of a Pt(s) - 6(111) × (710) surface. In their experiment the adsorption of CO was monitored by ESCA, and the data show that the initial adsorption is dissociative as evidenced by the appearance of a carbide peak. Park et al. (8) have also reported dissociation of CO on Pt(410). In their ESCA data obtained from a CO-saturated Pt(410) surface, they observed C 1s and O 1s peak shifts. These peak shifts are similar to those observed during dissociation of CO on W(110) (9) and NO on Pt(100) (10). The O 1s peak shift is also characteristic of dissociative adsorption of O_2 on Pt. Li and coworkers (11, 12) determined by work function measurements obtained using field emission microscopy (FEM) that the dissociation of CO occurs at surface regions containing kinked edges including {210}, {320}, {430}, {520}, {310}, {410}, {741}, {321} and {1195}. They concluded that the extent of dissociation is proportional to the surface kink density which can depend upon the areas and structure of the terraces ({111}, {100}, {110}) and to the concentration of Si contamination.

Several other studies (13-16), have concluded that CO does not dissociate on the stepped or kinked areas of Pt. Lang and Masel (16) reported that CO adsorbs molecularly on Pt(210) and desorbs without dissociation upon heating. Furthermore, they observed no shifts in the O 1s and C 1s ESCA peaks upon heating the Pt(210) surface, which is contrary to their observations on Pt(410) (8). Hayden et al. (13, 14) concluded that molecular CO adsorption occurs on Pt(533) initially in a linearly bonded configuration at sites associated with the steps and with subsequent adsorption on terrace sites with a reduced sticking coefficient. These controversial results seem to vary from one surface to another and may depend upon surface cleanliness.

EXPERIMENTAL

The AES, ion scattering spectroscopy (ISS) and TPD data were acquired in an UHV system described previously (17). AES and ISS data were taken using a Perkin Elmer PHI model 15-255GAR double pass cylindrical mirror analyzer containing an internal electron gun. AES was performed using a 3 keV primary beam and standard nonretarding mode parameters. ISS was also performed in the nonretarding mode using a 1 keV, 100 nA $^4He^+$ primary beam at a 151.3° scattering angle. Short scanning periods and a defocused primary ion beam were used to minimize sputter damage. This results in a low signal-to-noise ratio but no loss in spectral information. The TPD spectra were obtained using a quadrupole mass spectrometer controlled by a computer program which regulates the heating and data acquisition and allows for the rapid collection of a mass spectrum. $^{13}C^{18}O$ (99 at% ^{13}C and 96.6 at% ^{18}O) was obtained from Isotec, Inc., Miamisburg, Ohio. In order to ensure proper heating of the Pt sample during the TPD experiments, two pieces of tantalum foil were spotwelded to both ends of the Pt foil sample, and then the assembly was mounted in the

sample holder. The sample was heated resistively by passing a current through the heater leads attached to the sample holder, and the temperature was monitored using a 0.05 mm chromel-alumel thermocouple spotwelded to the back of the sample. The sample was cleaned using repeated cycles of sputtering with 2 keV Ar^+ and heating to 1100°C in 10^{-7} Torr of O_2. ISS and AES spectra taken from the cleaned sample are shown in figure 1. A small amount of background CO adsorbed on the surface during the collection of the Auger spectrum.

RESULTS AND DISCUSSION

A. ISS Results

The clean sample was exposed to 1×10^{-8} Torr of CO for several time periods, and the ISS spectra shown in figure 2 were collected after the various CO exposures. Peaks due to Pt, C and O appear in these spectra. The amount of adsorbed CO appears to saturate at an exposure period of 120 s (1.2 L), and no more CO adsorbs at larger exposures. The height of the Pt peak obtained from a CO-saturated surface is about one-fifth of that obtained from a clean surface using all of the same experimental settings and conditions. This implies that saturation coverage of the polycrystalline Pt surface by the CO is about 0.8 of a monolayer. Barteau et al. (18) reported an initial sticking coefficient close to 1 for CO on Pt(100) (5 × 20) up to coverages of approximately 15% of a monolayer after which a decline in the sticking coefficient is observed. McCabe and Schmidt (19) found a similar decline at approximately 20% of a monolayer. ISS can also be used to determine the sticking coefficient as a function of coverage, and such experiments are in progress.

Spectral features other than those due to elastic scattering are also observed in figure 2. The peak at about 25 eV is due to secondary ions. The SIMS cross section for Pt is quite small so the small SIMS peak observed in the ISS spectrum obtained from the cleaned Pt may be due mostly to contamination, such as hydrogen, which does not yield an elemental ISS peak at the scattering angle used in this study. The SIMS peak increases with CO exposure and, therefore, gives another measure of adsorbate surface concentration. The ISS background due to inelastically scattered primary ions gives a measure of the electron mobility of the near-surface region. The background is quite small for the metallic surface, which has a high electron mobility, and decreases with CO exposure as the adsorbate concentration increases resulting in a decrease in the electron mobility at the surface (20).

Structural information can also be deduced from the ISS data shown in figure 2. Several possible bonding structures for CO on Pt are depicted in figure 3 along with the expected ISS spectra which would be obtained from each structure assuming that ISS detects only the outermost atomic layer. If the CO bonds vertically and completely covers the Pt, then only an O peak should be observed in ISS. If the Pt is not completely covered, then both an O and a Pt peak would be observed. In the case that CO bonds dissociatively or molecularly at an angle (perhaps parallel) to the surface, then both C and O peaks would be observed, and the size of the Pt peak would depend upon coverage. Furthermore, the ISS cross section is a strong function of mass and scattering angle. Since C and O have similar masses, their cross sections are not very different, but Pt is much more massive and has an ISS cross section which is

at least 40 to 80 times that of C or O. Thus, even when the outermost atomic layer contains mostly C and O, the Pt peak may be predominant. The ISS spectra shown in figure 2 suggest that the CO bonds either molecularly at some angle parallel to the surface, or dissociatively, and that the Pt is not completely covered as stated above. The results of the isotopic TPD experiments described below indicate that CO bonds molecularly to polycrystalline Pt. This and the fact that the C and O peaks are nearly the same size suggest that the CO bonds molecularly and probably parallel to the polycrystalline Pt surface. Using electron stimulated desorption-ion angular distribution (ESDIAD), CO bonded nonvertically to several surfaces has been reported; Mo(100) (21), W(100) (22), W(111) (23, 24), Pd(210) (25), Ni(110) (26), Pt(111) (27) and Pt(110)-(1×2) (14).

Figure 4 shows ISS data which were taken from a CO-saturated Pt surface after exposure to 1×10^{-8} Torr of O_2 at room temperature for various times. It appears that very little change occurs with exposure of this surface to O_2 at room temperature. In fact, any reduction in the amount of adsorbed CO is probably due to loss by ion sputtering. This experiment is consistent with the well-known result that metallic Pt does not catalyze CO oxidation at room temperature because the CO essentially saturates the surface so that O_2 cannot adsorb and react with the adsorbed CO by a Langmuir-Hinshelwood mechanism. Attempts were also made to adsorb O_2 on a cleaned Pt surface at 20 to 300°C and up to 10 Torr, but adsorbed oxygen could not be detected with ISS.

B. TPD Results

The TPD spectra shown in figure 5 were obtained by dosing the cleaned polycrystalline Pt surface with CO at 1×10^{-8} Torr for various periods. The predominant desorption peak occurs at 276°C regardless of coverage. This is characteristic of a first-order desorption process. With a heating rate $\beta = 9.8$ degrees/sec and assuming a frequency factor $\nu = 10^{13}$ sec^{-1} (28), the desorption energy of CO is 33.2 kcal/mole. A second lower-temperature desorption peak emerges at exposures greater than 0.6 L, which is consistent with previous TPD studies of CO from polycrystalline Pt (4-6, 14, 18). Although the origin of this peak is unclear, Hayden and coworkers (14) have attributed it to a phase transition in the CO overlayer at overages $\theta > 0.5$ which involves the onset of strong lateral interactions and tilting of the CO molecules.

Figure 6 shows a 2 amu TPD spectrum obtained after dosing the cleaned polycrystalline Pt surface with 9 L of H_2 at room temperature. In this case only one desorption peak appears regardless of coverage, and the desorption process is first order with a desorption energy of 22.4 kcal/mole. As expected, a similar TPD spectrum is obtained using D_2 rather than H_2.

Two and 28 amu TPD spectra obtained after dosing the cleaned polycrystalline Pt surface with a 3.6 L exposure of a 1:1 mixture of H_2 and CO at room temperature are shown in figure 7. In addition to the predominant peaks seen in figures 5 and 6 from adsorbed CO and adsorbed H_2, new peaks appear in the 2 amu spectrum at about 280°C, the CO desorption temperature, and in the 28 amu spectrum at about 101°C, the H_2 desorption temperature. These two new features indicate the formation of a surface CO-H complex, which is consistent

with the findings of Kawasaki (4) and Craig (5, 6). This experiment was repeated by coadsorbing D_2 and CO, and similar results were obtained as shown in figure 8.

The ISS data indicate that the CO covers about 80% of the Pt surface and that it bonds at an angle and possibly parallel to the surface or dissociatively. An isotopic TPD experiment was carried out to determine if the adsorption is molecular or dissociative. Using two separate leak valves, $^{12}C^{16}O$ (28 amu) and $^{13}C^{18}O$ (31 amu) were admitted into the system each at a partial pressure of 1×10^{-8} Torr. During the TPD experiments, the 30 amu signal due to $^{12}C^{18}O$) and 29 amu signal (due to $^{13}C^{16}O$) were monitored, but no isotopic mixing was found. This result demonstrates that CO adsorption on polycrystalline Pt is molecular. Unfortunately, it was not possible to determine the various surfaces and step and kink concentrations at this polycrystalline Pt surface.

CONCLUSIONS

ISS and TPD have been used to examine the adsorption and coadsorption of CO and H_2 on a sputter-cleaned and annealed polycrystalline Pt surface. The data indicate that CO adsorbs molecularly and probably parallel to the surface with an average sticking coefficient $S \geq 0.8$ and a saturation coverage of about 80%. Exposure of a CO-saturated Pt surface to O_2 results in no loss of adsorbed CO. This finding is consistent with the fact that Pt does not catalyze CO oxidation at room temperature. The coadsorption experiments indicate that a CO-H surface complex forms on polycrystalline Pt.

ACKNOWLEDGMENTS

REFERENCES

1. Closed-Cycle, Frequency-Stable CO_2 Laser Technology, edited by C.E. Batten, I.M. Miller, G.M. Wood, Jr. and D.V. Willetts, NASA Conference Publication 2456.

2. D.R. Schryer, J.D. Van Norman, K.G. Brown and J. Schryer

3. G.B. Hoflund, A.L. Grogan, Jr., D.A. Ashbury and D.R. Schryer, Thin Solid Films 169(1989)69.

4. K. Kawasaki, T. Kodama, H. Miki and T. Kioka, Surface Sci. 64(1977)349.

5. J.H. Craig, Jr., Surface Sci. 111(1981)L695.

6. J.H. Craig, Jr., Surface Sci. 10(1982)315.

7. Y. Iwasawa, R. Mason, M. Textor and G.A. Somorjai, Chem. Phys. Lett. 44(1976)468.

8. Y.O. Park, W.F. Banholzer and R.I. Masel, Surface Sci. 155(1985)341.

9. E. Umback, J.C. Fuggel and D. Menzel, J. Electron Spectrosc. Rel. Phen. 10(1977)5.

10. H.P. Bonzel and G. Pirug, Surface Sci. 62(1977)45.

11. X.Q.D. Li and R. Vanselow, Surface Sci. 217(1989)L417.

12. X.Q.D. Li and R. Vanselow, Catal. Lett. 2(1989)113.

13. B.E. Hayden, K. Kretzschmar and A.M. Bradshaw, Surface Sci. 149(1985)394.

14. B.H. Hayden, A.W. Robinson and P.M. Tucker, Surface Sci. 192(1987)163.

15. M.R. McClellan, J.L. Gland and F.R. McFeeley, Surface Sci. 112(1981)63.

16. J.F. Lang and R.I. Masel, Surface Sci. 167(1986)261.

17. G.B. Hoflund, D.F. Cox, G.L. Woodson and H.A. Laitinen, Thin Solid Films 78(1981)357.

18. M.A. Barteau, E.I. Ko and R.J. Madix, Surface Sci. 102(1981)99.

19. R.W. McCabe and L.D. Schmidt, Surface Sci. 66(1977)101.

20. V.Y. Young and G.B. Hoflund, Anal. Chem. 60(1988)269.

21. H. Niehus, Surface Sci. 92(1980)88.

22. R. Jaeger and D. Menzel, Surface Sci. 93(1980)71.

23. H. Niehus, Surface Sci. 80(1979)245.

24. H. Niehus, Surface Sci. 87(1979)561.

25. T.E. Madey, J.T. Yates, Jr., A.M. Bradshaw and F.M. Hoffmann, Surface Sci. 89(1979)370.

26. W. Riedl and D. Menzel, Surface Sci. 163(1985)39.

27. M. Kiskinova, A. Szabo and J.T. Yates, Jr., Surface Sci. 205(1988)215.

28. R.P.H. Gasser, An Introduction to Chemisorption and Catalysis by Metals, Claredon Press, Oxford, 1985, p. 70.
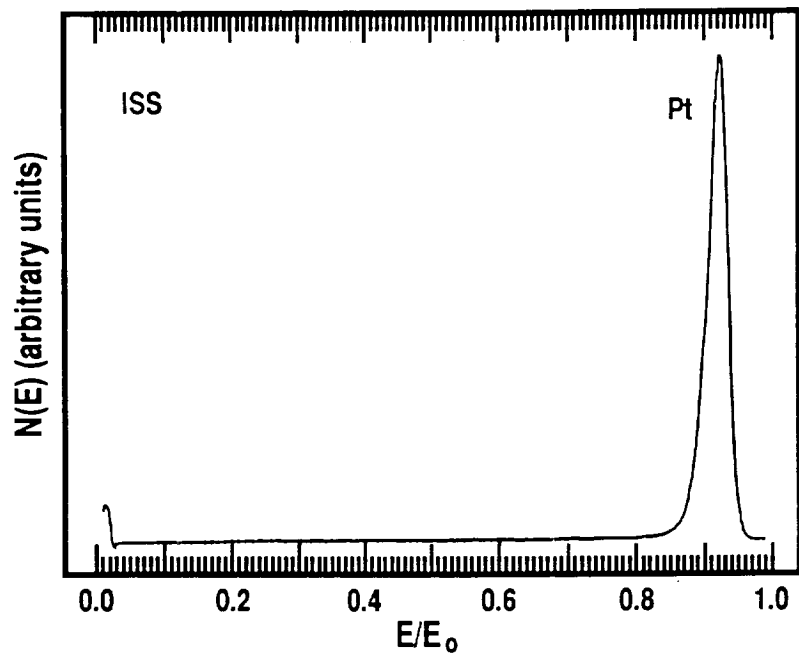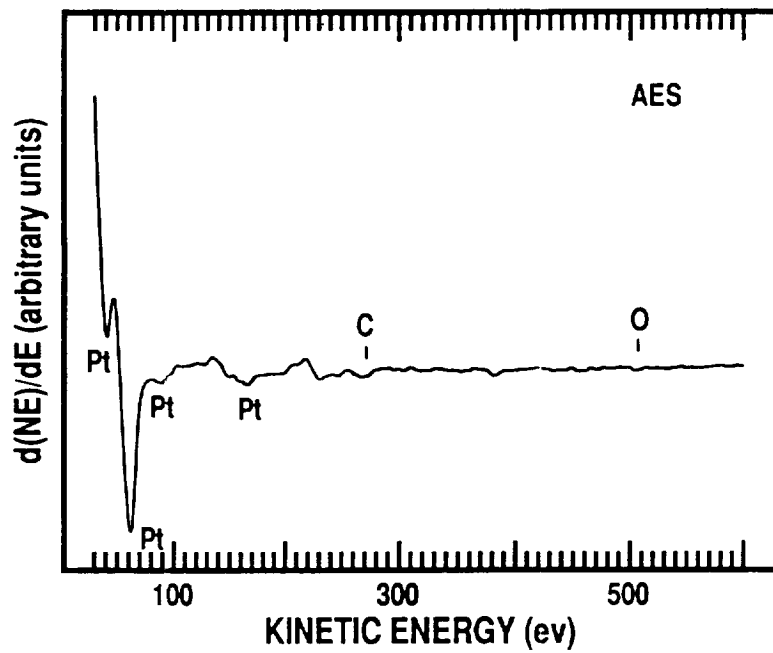
Figure 1. (A) ISS and (B) AES spectra taken from the cleaned polycrystalline
Pt surface.

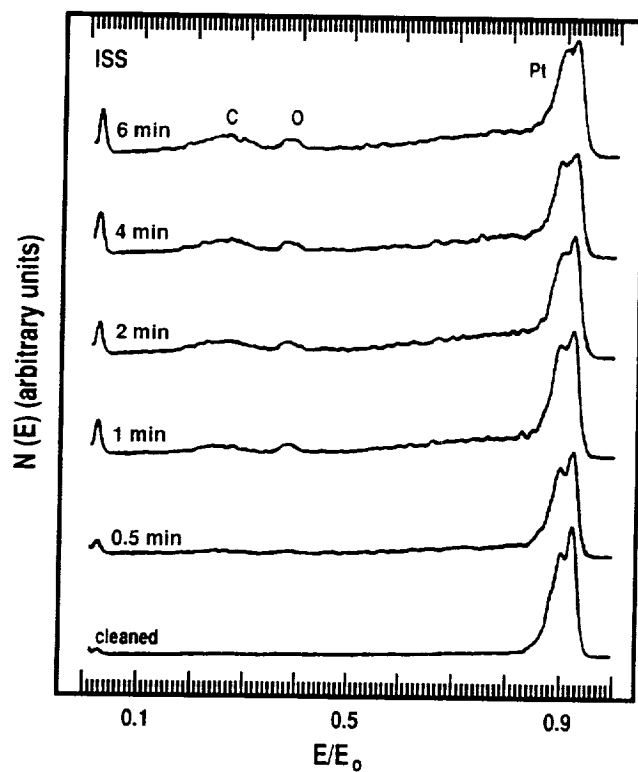Figure 2. ISS spectra taken from the polycrystalline Pt surface before and after exposure to 1 X 10⁻⁸ Torr CO at room temperature for 30 s (0.3 L), 60 s (0.6 L), 120 s (1.2 L), 240 s (2.4 L) and 360 s (3.6 L).
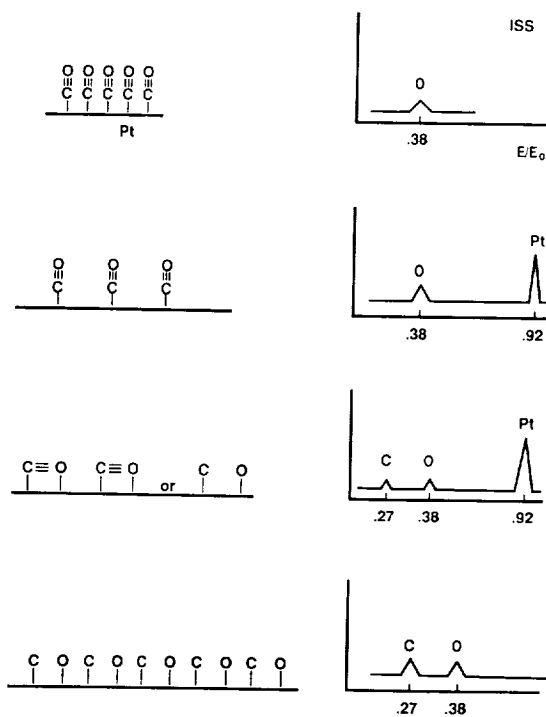

Figure 3. Various models for the adsorption of CO on a Pt surface and schematic ISS spectra which would be obtained from each bonding structure.
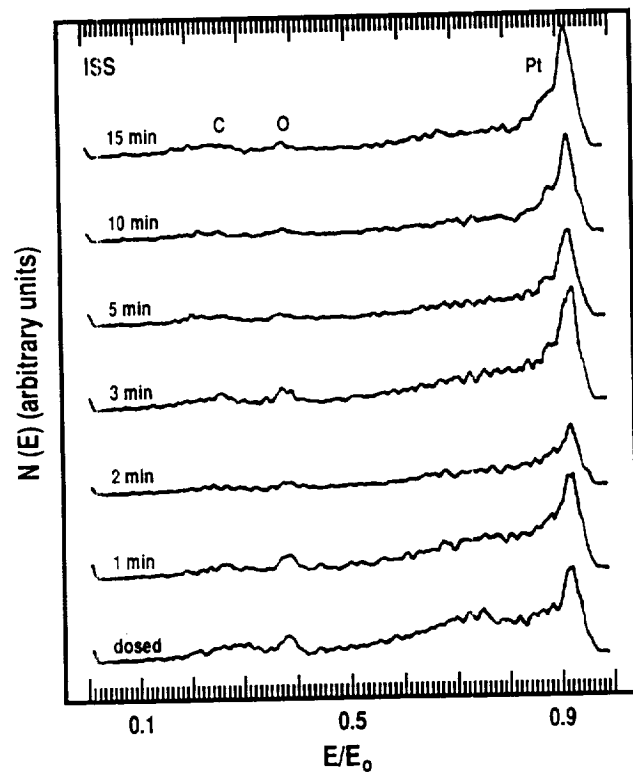
258

Figure 4. ISS spectra taken from a CO-saturated polycrystalline Pt after exposure to 1×10^{-8} Torr of O_2 for various periods.
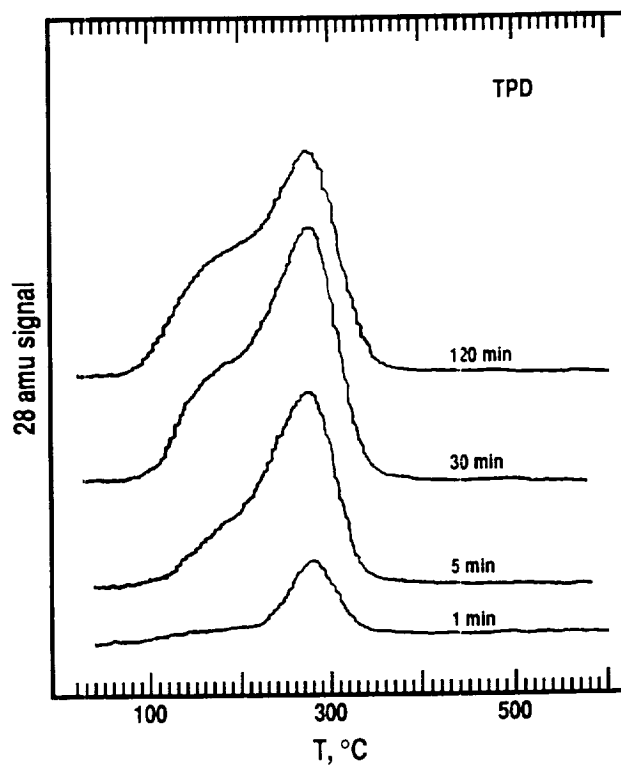

Figure 5. 28 amu TPD spectra obtained after exposing polycrystalline Pt to CO at 1×10^{-8} Torr and room temperature for various periods.
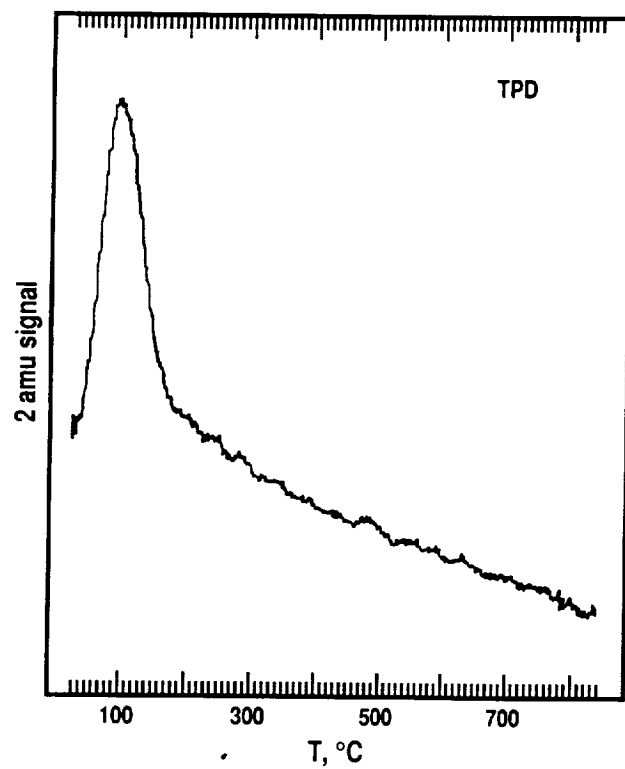
Figure 6. 2 amu TPD spectrum obtained after exposing polycrystalline Pt to 1 X 10^{-8} Torr of H$_2$ for 15 minutes at room temperature.
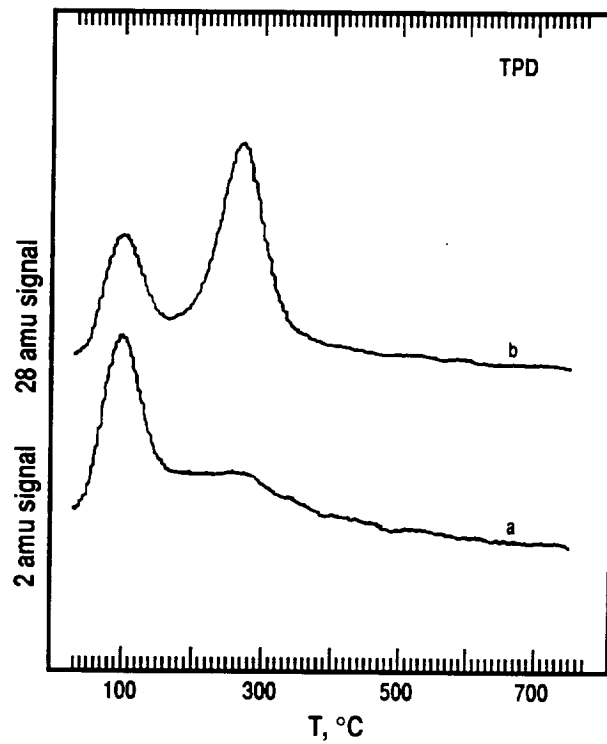

Figure 7. (a) 2 amu and (b) 28 amu TPD spectra obtained after exposing polycrystalline Pt to a 1:1 mixture of H$_2$ and CO for 3.6 L at room temperature.
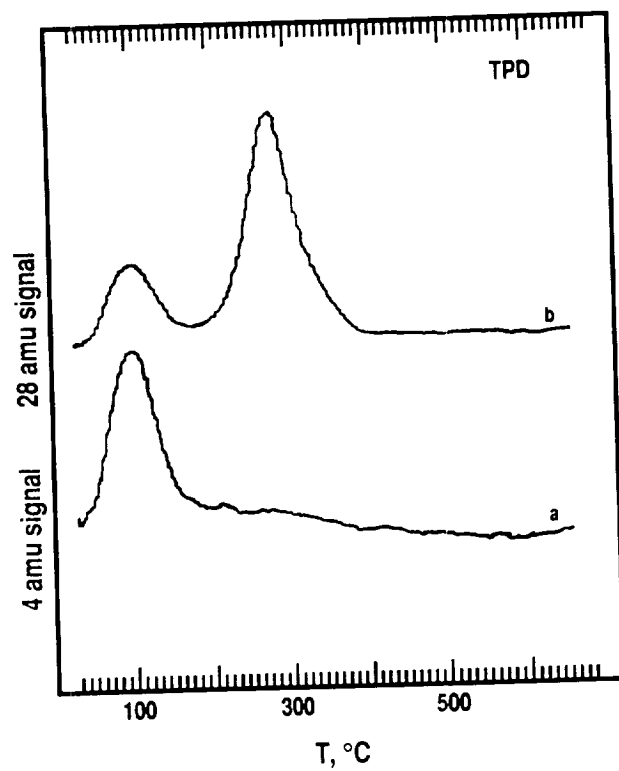
Figure 8. (a) 4 amu and (b) 28 amu TPD spectra obtained after exposing polycrystalline Pt to a 1:1 mixture of D_2 and CO for 3.6 L at room temperature.

SURFACE DEFECTS AND CHEMISTRY ON THE SnO$_2$(110) SURFACE

David F. Cox
Department of Chemical Engineering
Virginia Polytechnic Institute & State University
Blacksburg, Virginia

SUMMARY

A variety of ultrahigh vacuum (UHV) surface science techniques have been used to characterize the structural, electronic and chemical properties of SnO$_2$(110), a model catalytic surface. Two types of surface oxygen vacancies have been identified, each associated with different band gap (defect) electronic states. Adsorption experiments show that the interaction of simple gases with this surface occurs primarily through these oxygen vacancies and can show site-specificity to only one of the two types of vacancies.

INTRODUCTION

Tin oxide (SnO$_2$) is a useful catalytic material most often applied in multicomponent systems. In mixed-oxide systems, tin oxide has found application in catalysts for selective oxidation, ammoxidation, dehydrogenation and isomerization reactions [1-5]. Pure tin oxide typically forms combustion products [6-9], hence it has found an application as a support for Pt in the low-temperature CO oxidation catalyst for pulsed CO$_2$ lasers.

One of the primary difficulties in characterizing tin oxide surfaces (and hence Pt/SnO$_2$ catalysts) lies in determining the valence state of the surface tin species. It has been found that neither Auger electron spectroscopy (AES) [10-12] or x-ray photoelectron spectroscopy (XPS) [13] can distinguish between Sn^{+2} and Sn^{+4} because there is no significant change in the core-level binding energies. This distinction is important because it characterizes the redox condition of the tin oxide surface which in turn controls its interaction with gas-phase oxygen. In spite of these difficulties, progress has been made in distinguishing between Sn^{+2} and Sn^{+4} using electron loss spectroscopy (ELS) [13,14]. The ELS technique can clearly give a qualitative indication of the presence of Sn^{+2} species in an SnO$_2$ matrix. ELS is also sensitive to structural changes in the lattice, however, no clear interpretation other than an oxygen deficiency can be associated with the observed spectral changes [14]. In other words, it is impossible to distinguish between a true SnO surface layer and a partially reduced Sn^{+2} containing SnO$_2$ structures with oxygen vacancies.

These structural ambiguities in surface characterization can be removed by studying model SnO$_2$ single crystal surfaces. Surface characterization studies of SnO$_2$(110) are reviewed here as an example

263

of the types of information obtainable by studies of well-characterized, model, single-crystal surfaces which cannot be obtained from powders or polycrystalline materials. The (110) face was chosen for these studies because it is the most stable, predominant natural growth face for SnO_2. Extended high temperature treatments of tin oxide powders and films leads to a preferential growth of (110) faces [15], hence this particular crystal face is the most likely to be a successful model for realistic SnO_2(110) systems. Also, a perfect (110) crystallographic orientation gives the most "fully oxidized" or "stoichiometric" surface possible because it breaks the fewest number of cation-anion bonds at the surface [16].

BACKGROUND STRUCTURAL INFORMATION

SnO_2 is a wide-band-gap (E_g=3.6 eV), n-type semiconductor with the rutile (TiO_2) structure. When viewed along the (110) direction, the bulk crystal is seen to be composed of charge-neutral units containing three atomic planes [17]. The composition and arrangement of the planes in the unit are [(O^{-2})($2Sn^{+4}$ + $2O^{-2}$)(O^{-2})] per (110) unit cell. The charge on each plane is [(-2)(+4)(-2)], and the net charge per three-plane unit is zero. Because this unit has no net dipole moment in the (110) direction, the (110) surface is termed nonpolar. The lower surface energy of a nonpolar vs. a polar surface dictates that an ideal, stoichiometric (110) surface will be terminated by a charge-neutral unit. Terminating the (110) surface with a complete, nonpolar, charge-neutral unit corresponds to breaking the smallest number of cation-anion bonds relative to the bulk structure [16]. This termination results in equal numbers of five and six coordinate tin cations in the second atomic layer. The full bulk coordination per cation is six.

Figure 1 illustrates the structure, composition and charges of the individual atomic planes associated with the SnO_2(110) surface. From Fig. 1 it can be seen that the ideal (110) surface is terminated with an outermost plane of oxygen anions which appear as rows in the (001) direction and occupy bridging positions between the second-layer, six coordinate tin cations. Oxygen atoms may also be seen in Fig. 1 in the same plane as the observable tin atoms. For convenience, the two different types of oxygen anions are referred to as "bridging" oxygens and "in-plane" oxygens, respectively.

NEARLY STOICHIOMETRIC SURFACES

The preparation of clean, stoichiometric SnO_2 surfaces for study in UHV is nontrivial. The usual cleaning methods of ion bombardment and high temperature annealing in vacuum preferentially remove surface lattice oxygen, leaving the surface in a reduced condition. Attempts to quantify the surface composition following such treatments typically yields O/Sn ratios less than 2.0, indicative of a less than stoichiometric surface [14]. A clear indication of the electronic consequences of the deviation from stoichiometry is the appearance of defect electronic states in the band gap as seen with ultraviolet photoelectron spectroscopy (UPS).

Surface characterization studies [18] have shown that a nearly ideal $SnO_2(110)$ surface such as that illustrated in Fig. 1 may be reproducibly prepared by sputter cleaning, high temperature annealing in vacuum, and high temperature and pressure oxidation (700 K, 1.0 Torr O_2). The lack of band-gap emission in UPS following such a treatment is a sensitive indicator of a nearly-perfect, stoichiometric (110) surface. Figure 2 illustrates the variations observed in UPS for several surface preparations, including the in-situ oxidation treatment.

Heating the well-oxidized, nearly ideal, stoichiometric (110) surface in UHV removes large amounts of surface lattice oxygen. It has been shown with ion-scattering spectroscopy (ISS) [18] that vacuum annealing a nearly ideal $SnO_2(110)$ surface at 700 K causes a complete removal of the layer of bridging oxygen anions which terminate the surface, leaving a surface terminated by a tin and oxygen containing plane. In addition to the removal of bridging oxygens and the formation of four coordinate Sn^{+2} cations at 700 K, heating in vacuum above 700 K causes the further removal of some in-plane oxygen from the tin and oxygen containing plane of the $SnO_2(110)$ surface [18]. The formation of this second type of oxygen vacancy further lowers the coordination number of the neighboring tin cations from five and four coordination to four and three, respectively. Figure 3 is a ball-model illustration showing a nearly-perfect oxidized surface and a surface formed by removal of the top layer bridging oxygens and several in-plane oxygen anions. The figure illustrates the degree to which the composition changes in these treatments, and shows the variety of different coordination numbers of the tin cations.

The sequential fashion in which surface lattice oxygen can be removed from the oxidized $SnO_2(110)$ surface (bridging oxygen below 800 K, in-plane oxygen above 800 K) makes it possible to tailor this surface in a controlled fashion. The tin cation coordination can be varied from six to three by the proper choice of sample preparation conditions. Associated with these changes in cation coordination, only one surface periodicity is observed in low energy electron diffraction (LEED) when an oxidized surface is used as the starting condition: a (1x1) pattern characteristic of a simple termination of the bulk periodicity. The constancy of the LEED pattern indicates that there is no gross restructuring or reconstruction of the surface associated with the creation of the oxygen vacancies. While there is likely to be some degree of relaxation about the vacancies, the local geometry and coordination is similar to that expected from a simple removal of oxygen atoms from the surface. In essence, the vacancies are created without significantly altering the crystal structure at the surface except by substantial changes in coordination number of the tin cations.

While no changes are observed in the surface geometric structure for these treatments, the surface electronic structure in the band gap undergoes several interesting changes. Associated with the removal of the terminating layer of bridging oxygen anions and the requisite change in coordination of half the surface tin cations from sixfold to fourfold coordination, the appearance of defect electronic states low in the band gap is also observed with UPS. The appearance of these states low in the band gap has been interpreted as the

formation of Sn^{+2} centers associated with the fourfold-coordinated cations [17,18]. For temperatures above 800 K, the formation of threefold-coordinate cations at in-plane oxygen vacancies results in the appearance of a second set of defect electronic states in UPS high in the band gap extending up to the Fermi level. These changes in band-gap electronic structure are illustrated in Figure 4.

HIGHLY OXYGEN-DEFICIENT SURFACES

When ion is bombarded and annealed in vacuum, the SnO_2 (110) surface undergoes a number of reconstructions as characterized by low-energy electron diffractin (LEED) [19,20]. These reconstructions are driven by the high degree of oxygen deficiency associated with the ion-bombarded surface because of the preferential sputtering of oxygen. The most interesting of these reconstructions is the (4x1) surface which is formed by annealing the ion-bombarded surface near 900 K. This particular reconstruction corresponds to the formation of a reduced SnO(101) coincident overlayer [20] and the reduction of all surface cations to Sn^{+2} oxidation state. Therefore, by the choice of proper surface preparation conditions, a model SnO suboxide surface may also be reproducibly prepared from the SnO_2(110) surface. For annealing temperatures near 1000 K, the surface exhibits a (1x1) LEED pattern which has the same periodicity as the bulk, and hence approaches the same final condition regardless of whether the starting surface condition was ion bombarded or oxidized.

UPS photoemission studies of the various reconstructions of highly oxygen-deficient SnO_2(110) surfaces show similar band gap features to those observed for the well-defined (1x1) surface [20]. It has been shown that the conclusions regarding the origin of the band gap features on the well-defined (1x1) surfaces can be generalized for more structurally complex situations. Defect electronic states low in the band gap are associated with fourfold-coordinated Sn^{+2} cations. States higher in the gap are characteristic of oxygen vacancies with neighboring threefold-coordinated Sn cations [20].

SITE-SPECIFIC ADSORPTION OF SIMPLE MOLECULES

The interaction of adsorbates with the electronic states in the band gap provides information about the local geometric and electronic properties of the adsorption sites. The effects of O_2, H_2, and H_2O adsorption on the band gap density of states of an ion-sputtered surface are shown with UPS difference curves in Figure 5 [21]. An ion-sputtered surface was chosen for this illustration because it exhibits a large density of states in the band gap when clean. Oxygen adsorption causes a decrease in the photoemission intensity throughout the band gap. Hydrogen adsorption causes a decrease in the defect intensity primarily in states just above the valence band maximum (VBM). A positive change in intensity near the conduction band minimum (CBM) is also seen for hydrogen. This increase is associated with the movement of the Fermi level up in the gap (i.e., downward band bending) and comes from occupied states near the Fermi level for the hydrogen dosed surface. The difference curve

266

for water shows an increase in the density of states near the Fermi level (as with hydrogen), but a decrease in other states in the top half of the gap. Similar trends are observed for oxygen deficient (4x1) and (1x1) surfaces. The changes in the band-gap density of states caused by H_2, O_2, and H_2O indicate that defects associated with oxygen vacancies play an important role in chemisorption on the (110) surface. Additionally, the gases exhibit some specificity between the different electronic states associated with the defect sites.

The previously described assignments for the types of surface defects associated with the band gap electronic states demonstrate that hydrogen and water are site-specific in their interaction with tin oxide surfaces. The interaction of hydrogen with states low in the gap demonstrates that adsorption occurs at fourfold-coordinated cations similar to those found in the presence of bridging oxygen vacancies. The interaction of water with the states high in the band gap demonstrates the adsorption of water at threefold-coordinated cations similar to those associated with in-plane oxygen vacancies.

SITE-SPECIFIC ^{18}O ISOTOPIC LABELING OF THE LATTICE

As with the use of labeled compounds in thermal desorption spectroscopy (TDS), the use of ^{18}O-labeled lattice oxygen at the SnO_2(110) surface provides a means of investigating the interaction of lattice oxygen in surface reactions. The study of isotopic exchange of oxygen with metal oxide catalysts has been widely used, but isotopic exchange with the well-characterized SnO_2(110) surface provides the unusual possibility of labeling not just surface lattice oxygen in general, but the labeling of <u>only</u> <u>one</u> of two different forms of lattice oxygen at the (110) surface with ^{18}O .

Unlike TiO_2, the diffusion of lattice oxygen through the SnO_2 matrix is slow at temperatures as high as 1000 K, as evidenced by the inability to form a stoichiometric or near-stoichiometric SnO_2(110) surface by simply heating in vacuum after ion bombardment [20]. Therefore, at the 700 K temperatures required for the <u>in situ</u> oxidation treatment [18,20], interlayer mixing of oxygen atoms is expected to be small. Recent ISS results [22] have shown that it is possible to selectively label bridging oxygen positions with ^{18}O, since the two forms of surface lattice oxygen can be removed sequentially by heating to different temperatures in UHV. The labeling procedure will make it possible to distinguish between the participation of the two inequivalent forms of lattice oxygen in surface oxidation reactions using TDS.

COMPARISON BETWEEN EXISTING CATALYTIC DATA AND
THE SURFACE PROPERTIES OF SnO_2(110)

The previous work on CO oxidation and NO reduction [6-9,23,24] offers insight into the role of SnO_2 in catalyzing oxidation/reduction reactions. The studies using pure tin oxide show that a redox mechanism dominates the chemistry at the surface of SnO_2. CO is converted to CO_2 on oxidized SnO_2 by the removal of

lattice oxygen, a process which reduces and quickly deactivates the catalyst as surface oxygen is consumed. Conversely, NO is converted to N_2 on reduced SnO_2 surfaces through a process which reoxidizes the catalyst. Therefore, the formation and decomposition of oxygenates is dependent on the availability of lattice oxygen at the surface.

There is a close relationship between the $SnO_2(110)$ surface characterization and the existing catalytic data on the selective isomerization of 1-butene to cis-2-butene (cis-/trans-2-butene = 19) over tin oxide powder [5]. Itoh, et al. [5] found that the activity and selectivity for cis-2-butene increased dramatically when the catalyst was activated by heating _in vacuum_ to temperatures in the range of 400°C to 600°C (723 K to 823 K). Associated with this change was the appearance of electron-donating paramagnetic centers on the catalyst as seen by ESR. In the presence of 1-butene the ESR signal for this center decreased, indicating a direct interaction between 1-butene and the paramagnetic center. A direct correlation was found between the activity and selectivity of the catalyst and the concentration of paramagnetic centers.

Note that the temperature range and preparation conditions (i.e., heating in vacuum) associated with the catalyst activation is similar to that required to remove in-plane oxygen atoms and expose threefold-coordinated tin cations on the $SnO_2(110)$ surface. The electronic properties of the in-plane oxygen vacancies have been described previously in terms of surface color centers [18] which act as electron donors. In the ground state the anion vacancies bind two electrons by their Coulombic wells, and are thus doubly ionizable. The first ionization potential of the defect is small (25 meV [25]); therefore, the majority of these centers are singly ionized and contain one unpaired electron as seen in the ESR signal. These similarities suggest that the isomerization reaction over powders occurs in the presence of sites similar to the in-plane oxygen vacancies observed on the $SnO_2(110)$-1x1 surface.

Itoh, et al. also observed that the catalyst is poisoned by a number of compounds including H_2O. The UPS results described above for water adsorption on the $SnO_2(110)$ surface have shown that water preferentially adsorbs at in-plane oxygen vacancies on the $SnO_2(110)$ surface. Hence, both the isomerization activity of SnO_2 powders and the poisoning capacity of water can be explained in terms of the properties of the defective $SnO_2(110)$ surface.

REFERENCES

1. F.J. Berry, Adv. Catal. 30(1981)97.

2. D.J. Hucknall, Selective Oxidation of Hydrocarbons (Academic Press, New York, 1974).

3. S. Tan, Y. Moro-oka and A. Ozaki, J. Catal. 17(1970)125.

4. T. Sakamoto, M. Egashira and T. Seiyama, J. Catal. 16(1970)407.

5. M. Itoh, H. Hattori and K. Tanabe, J. Catal. 43(1976)192.

6. M.J. Fuller and M.E. Warwick, J. Catal. 29(1973)441.

7. G.C. Bond, L.R. Molloy and M.J. Fuller, J.C.S. Chem. Comm. (1975)796.

8. G.C. Bond, M.J. Fuller and L.R. Molloy, Proc. Int. Congr. Catal. 6th, 1(1977)356.

9. B. Hori, N. Takezawa and H. Kobayashi, J. Catal. 80(1983)437.

10. C.L. Lau and G.K. Wertheim, J. Vac. Sci. Technol. 15(1978)622.

11. T.W. Capehart and S.C. Chang, J. Vac. Sci. Technol. 18(1981)393.

12. W.E. Morgan and J.R. Van Wazer, J. Phys. Chem. 77(1973)964.

13. R.A. Powell, Appl. Surf. Sci., 2(1979)397.

14. D.F. Cox and G.B. Hoflund, Surf. Sci. 151(1985)202.

15. Z.M. Jarzebski and J.P. Marton, J. Electrochem. Soc. 123(1976)199,299,333.

16. V.E. Henrich, Rep. Prog. Phys. 48(1985)1481.

17. P.A. Cox, R.G. Egdell, C. Harding, W.R. Patterson and P.J. Tavener, Surf. Sci. 123(1982)179.

18. D.F. Cox, T.B. Fryberger and S. Semancik, Phys. Rev. B 38(1988)2072.

19. E. deFrésart, J. Darville and J.M. Gilles, Appl. Surf. Sci. 11/12(1982)637; Solid State Commun. 37(1980)13.

20. D.F. Cox, T.B. Fryberger and S. Semancik, Surf. Sci. 224(1989)121.

21. D.F. Cox, T.B. Fryberger, J.W. Erickson and S. Semancik, J. Vac. Sci. Technol. A 5(1987)1170.

22. D.F. Cox and T.B. Fryberger, Surf. Sci. Letters, 227(1990)L105.

23. M. Niwa, T. Minami, H. Kodama, T. Hattori and Y. Murakami, J. Catal. 53(1978)198.

24. F. Solymosi and J. Kiss, J. Catal. 41(1976)202.

25. J.W. Erickson and S. Semancik, Surf. Sci. 187(1987)L658.
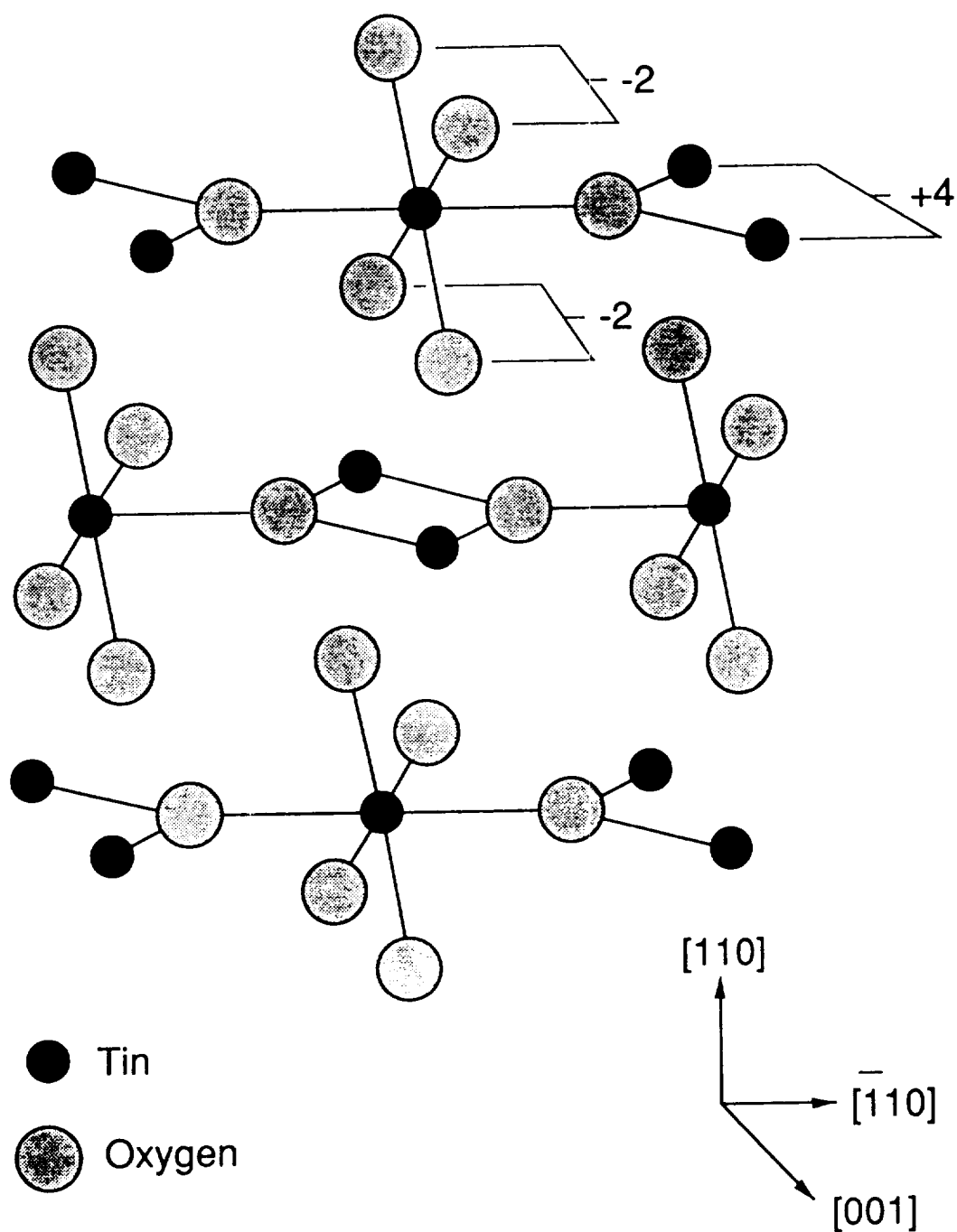
OUTER ATOMIC LAYERS OF SnO₂

Figure 1. Illustration of the atomic arrangement at the ideal SnO$_2$(110)-(1x1) surface. The net charge per surface unit cell is shown for each of the three atomic planes composing a charge neutral unit perpendicular to the (110) direction. (Reproduced from Ref. 20, permission to reproduce granted.)
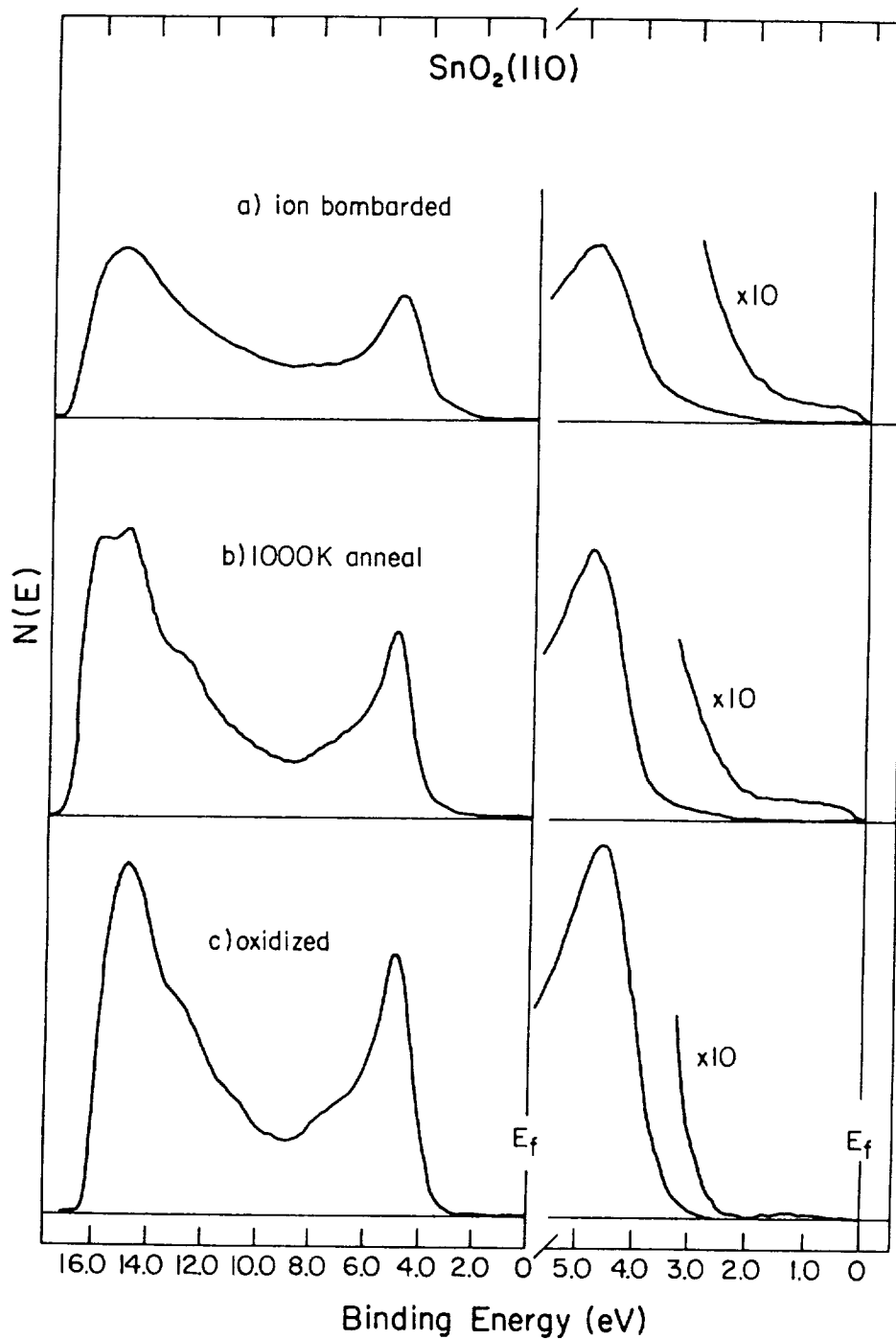
Figure 2. UPS spectra obtained following three different surface preparations: (a) 2-keV in bombardment, (b) ion bombarded and annealed in vacuum at 1000 K, and (c) oxidized in 1.0 Torr of O_2 at 700 K. The panels on the left are complete HeI spectra while the right-hand panels are enlarged views of the band-gap regions and the tops of the valence bands. All spectra are referenced to the Fermi level. (Reproduced from Ref. 18, permission to reproduce granted.)
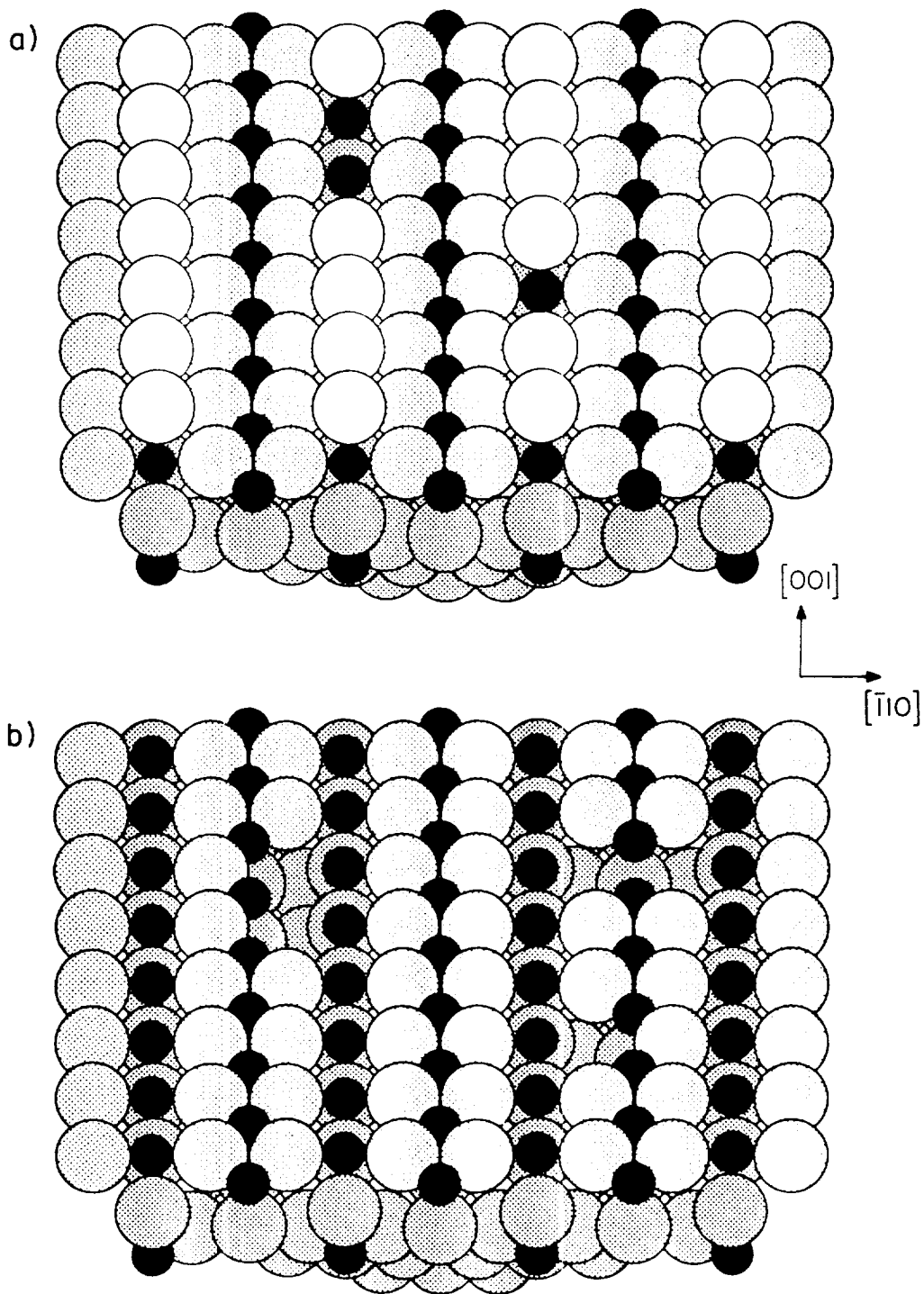
Figure 3. Ball model illustration of the surface viewed 50° off normal along the [001] azimuth. View (a) shows a nearly perfect (110) surface while (b) shows a bare surface following the removal of all top-layer bridging oxygen anions. A few in-plane oxygen vacancies are also shown in (b). (Reproduced from Ref. 18, permission to reproduce granted.)
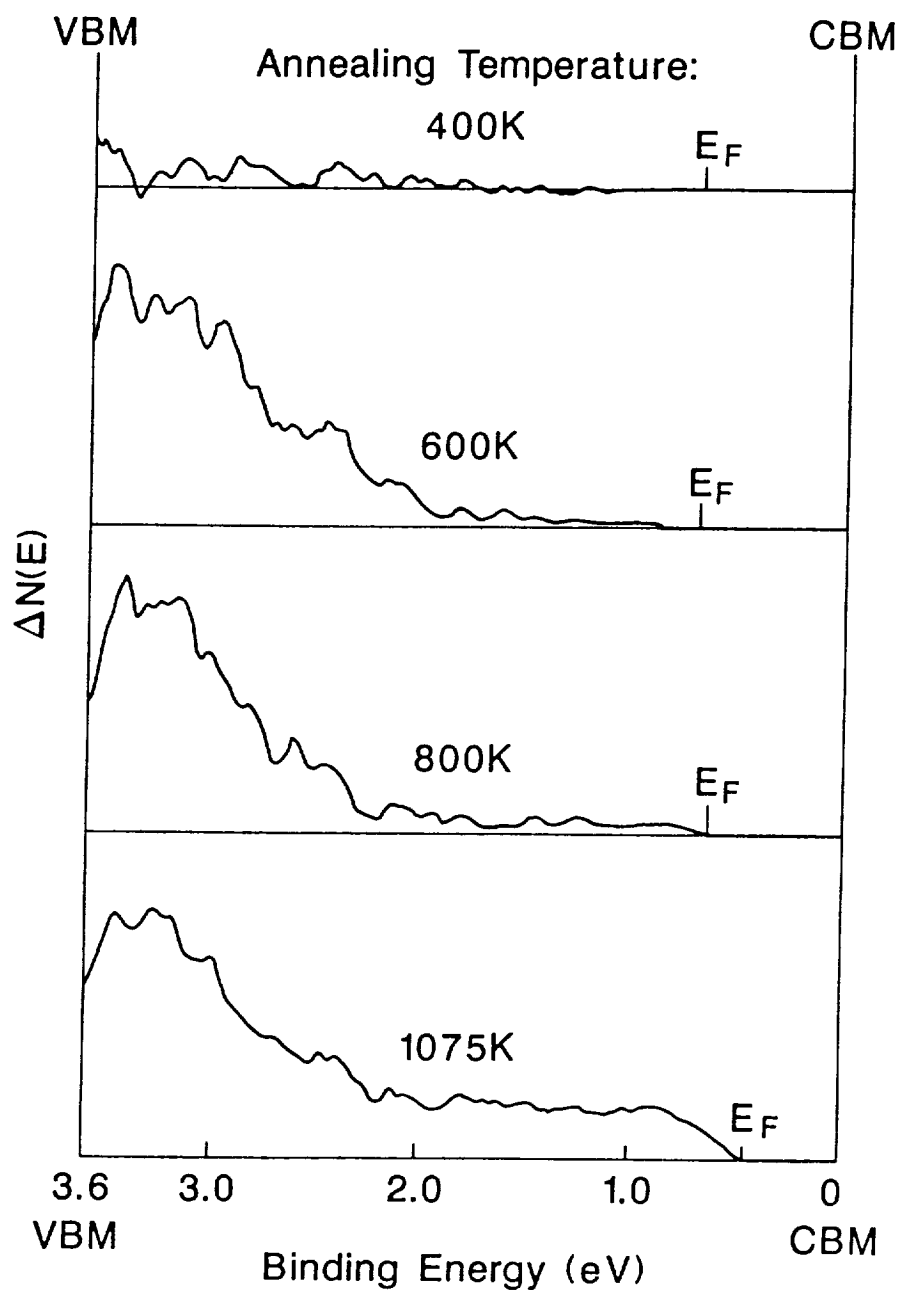
Figure 4. UPS difference curves showing the increase in band-gap (defect) electronic states caused by heating an oxidized surface in vacuum. The curves are referenced to the conduction band minimum (CBM). (Reproduced from Ref. 18, permission to reproduce granted.)
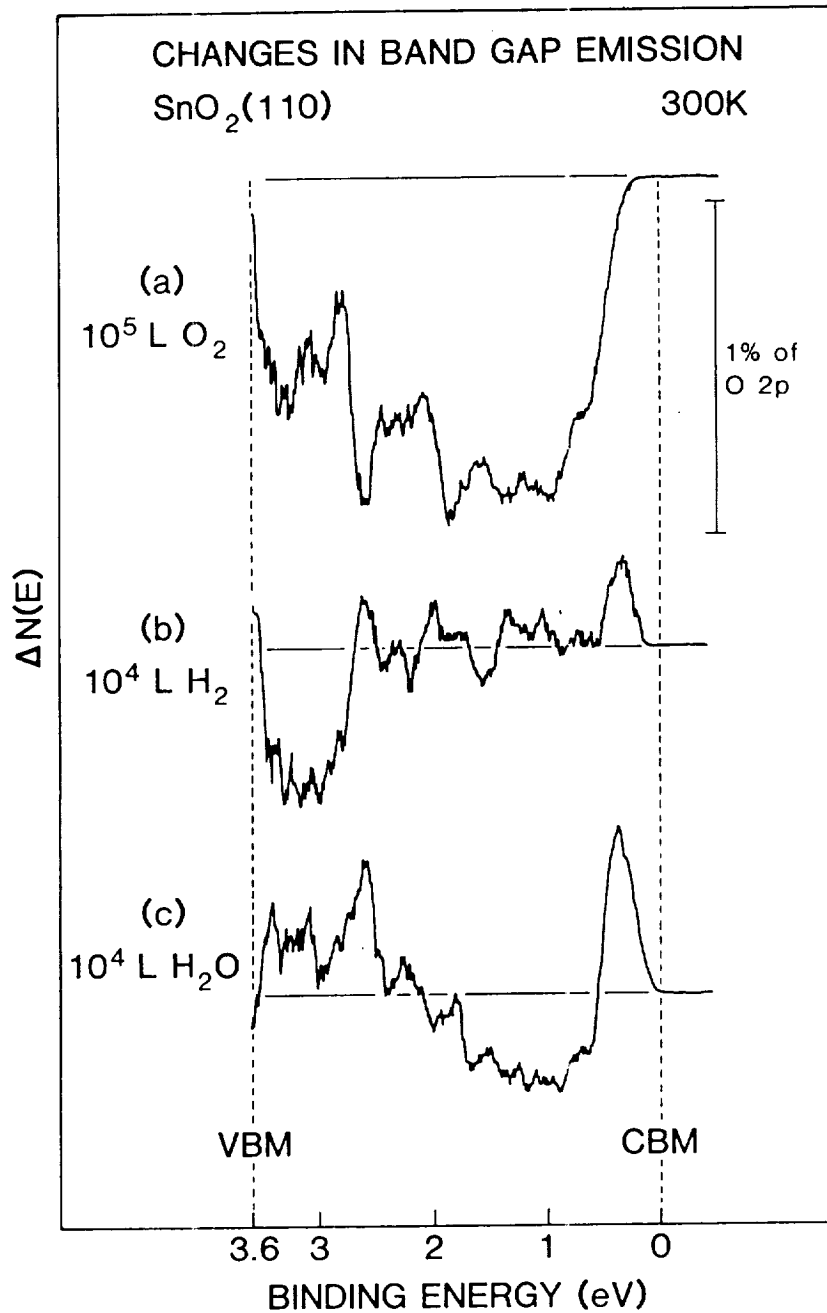
Figure 5. UPS difference curves indicating the changes in the band-gap density of states produced by adsorption of (a) 10^5L O_2, (b) 10^4L H_2, and (c) 10^4L H_2O on an ion sputtered surface. (Reproduced from Ref. 21, permission to reproduce granted.)

REVIEW OF MODEL SENSOR STUDIES ON Pd/SnO$_2$(110) SURFACES

Teresa B. Fryberger and Steve Semancik
Chemical Process Metrology Division
National Institute of Standards and Technology
Gaithersburg, Maryland

SUMMARY

In this paper, studies performed at the National Institute of Standards and Technology on the model gas sensor system, Pd/SnO$_2$(110), are reviewed. Adsorption and interfacial effects play a primary role in the gas sensing process, as they do in catalysis. For this reason, we have used a variety of surface sensitive techniques in our research, including x-ray and ultraviolet photoelectron spectroscopies (XPS and UPS), low energy electron diffraction (LEED), and ion scattering spectroscopy (ISS). By combining these complementary techniques with in situ gas response (conductance) measurements, we have been able to correlate directly sensor activity with the composition and structure of the Pd/SnO$_2$ interface. Although the intent of this work is develop an understanding of gas sensing mechanisms, its relevance to Pt/SnO$_2$ catalytic systems is obvious.

INTRODUCTION

The electrical conductivity of a semiconducting metal oxide like tin oxide (SnO$_2$) can be altered by adsorption of gases from the ambient. This phenomenon has been applied in gas sensing devices fabricated for detection of combustible and toxic gases such as hydrocarbons, alcohols, H$_2$, CO and NO$_x$ (ref. 1). Many commercial sensors use semiconducting SnO$_2$ sintered powders or films to which small amounts of a catalytic metal, such as Pd, have been added to increase sensitivity and selectivity towards specific gases. This type of sensor is essentially identical to a supported catalyst, such as the CO oxidation catalysts discussed in these proceedings. In gas sensing, however, one is interested in obtaining an electrical measure (conductivity change) of the extent that adsorption or reaction occurs, rather than a product yield.

In an attempt to understand the detailed mechanisms involved in gas sensing, and to improve sensing measurements, we have conducted step-wise studies on simplified, crystalline specimens of SnO$_2$ with and without surface-dispersed catalytic additives. In this paper, we first briefly summarize results on the surface properties of pure SnO$_2$(110). Second, the interaction between a catalytic additive, Pd, and the SnO$_2$(110) substrate is discussed. Both the growth mode of vapor-deposited Pd on the surface and the electronic interaction between the metal and the oxide are considered. Although we have investigated the role of substrate defect density on the Pd/SnO$_2$ interaction, results here are limited primarily to deposition on a nearly ideal, oxidized surface. Third, we report results for hydrogen and oxygen adsorption and coadsorption on the 3 ML Pd/SnO$_2$(110) model sensor surface. Hydrogen has obvious importance as a gas to be monitored and as a dissociation product of hydrocarbons and alcohols, and oxygen is nearly always abundant in the sensor ambient (often, air). These gases also provide the simplest

277

reducing and oxidizing environments for understanding mechanistic effects. It is worth noting, however, that the mechanistic effects studied in this work can, to a large extent, be generalized to other oxidizing and reducing gases, with kinetic details being dependent on the particular gas.

EXPERIMENTAL

Model Specimens

In order to isolate various chemical, structural, and additive effects and to more clearly evaluate their roles in gas sensing, we chose single crystal tin oxide samples for our model studies. The (110) face was chosen because it is the most stable, naturally occurring face (ref. 2) and can be expected to be predominant in polycrystalline sensing elements. Thus, studies on (110) crystals are particularly relevant to the local chemical and electronic effects occurring in real SnO_2 sensors. The SnO_2 sample used in this work was cut from a single crystal needle (ref. 3) and was oriented and polished to within 1° of the (110) face.

To investigate the role of a catalytic additive in sensing, we studied both the interaction of palladium with the SnO_2(110) surface and its effect on sensing response. The Pd was deposited under ultrahigh vacuum (UHV) conditions using a filament evaporator to coverages ranging from 0.1 to 30 monolayer equivalents (ML) as measured by a calibrated quartz crystal monitor. All Pd depositions were carried out with the substrate at room temperature.

Analytical Techniques

Since adsorption and interfacial effects play a primary role in gas sensing processes, we used surface-sensitive analytical techniques, all housed in a single vacuum system, in these studies. By using a variety of techniques we are able to monitor surface chemistry (oxide stoichiometry, chemical states of gas and additive adsorbates), atomic structure (crystallite orientation, surface reconstruction), and electronic structure (gap states, band bending, additive-induced density of state changes). In addition, in situ conductance measurements were carried out in order to correlate the model sensor electronic response to the specific changes in chemistry produced by adsorption.

The multi-technique facility used in this study is represented schematically in fig. 1, and is described in refs. 4-5. The system consists of two coupled vacuum chambers that can operate over pressures from 10^{-11} to 10^3 torr. A translation/rotation stage was used to move samples back and forth between the two chambers, permitting access to instrumentation and test ambients. The results presented here were obtained using XPS, UPS, ISS, LEED, and surface conductance change measurements.

XPS, UPS, and ISS spectra were collected in the analysis chamber of the vacuum system which is based on the VG ESCALAB MK II (ref. 6). Non-monochromatized Mg Kα radiation (1253.6 eV) was used for XPS and an RF discharge lamp was used as a He I (21.2 eV) source for UPS. All photoelectron binding energies were referenced to the Fermi level. For the ISS, a scattering angle of 130° was set by the fixed positions of the ion source and the analyzer. An He$^+$ or Ne$^+$ ion beam with a primary energy (E_o) of 1000 eV was used at an incident angle of 50° with respect to the surface normal along the (001) azimuth. All XPS, UPS, and ISS spectra were taken with the sample at room temperature. In situ conductance changes measurements were

made using a retractable, four-point probe similar to one described in detail in ref. 7.

Argon ion bombardment and heating were used to clean and order the surface of the SnO$_2$(110) crystal, and its condition was monitored by XPS and LEED. The sample mounting and heating arrangements are described in ref. 5. Sample temperatures could be controlled between 300 and 1000K, and were measured by a W5%Re/W26%Re thermocouple in direct contact with one end of the sample. Pure or mixed gases could be introduced at the desired partial pressures (up to 1 atmosphere) from a 12-port gas manifold. The base pressure was 1X10^{-10} mbar in both the preparation and the analysis chambers.

RESULTS AND DISCUSSION

In order to understand the detailed mechanisms involved in sensing (or catalysis) it was necessary to investigate model sensors (oxide-supported metals) in a step-wise fashion. That is, we studied 1) the properties of pure tin oxide surfaces; 2) the interaction of Pd with the SnO$_2$ surface; and 3) adsorption of H$_2$ and O$_2$ gases; and 4) coadsorption of these gases on the pure and Pd-dosed surfaces. In the following discussion, results are also presented, more or less, in this order.

Surface Properties of Clean SnO$_2$(110)

Tin oxide is an n-type semiconductor which, like TiO2, has a rutile crystal structure. The electrical conductivity of SnO$_2$ is due to the presence of oxygen vacancy defects, and the creation of oxygen vacancies and defect electronic states at the clean SnO$_2$(110) surface has therefore been studied in detail (refs. 5,8-10). It has been demonstrated that heating sputtered surfaces in UHV can result in the formation of well-ordered, oxygen deficient surfaces which exhibit (1x1), c(2x2),(4x1), and (1x2) LEED patterns depending upon the annealing temperature (refs. 8,10). In addition, the conductance of the disordered sputtered and ordered surfaces can vary by more than two orders of magnitude(ref. 8).

Cox et al (ref.5) have shown that surfaces with a nearly perfect termination of the rutile (110) plane can be formed by in situ oxidation of oxygen deficient SnO$_2$(110) at 700K in 1 Torr oxygen. Furthermore, by annealing the oxidized surface in vacuum, oxygen vacancies can be produced and their number density and type can be controlled by the choice of annealing temperature. In this paper, we discuss the effects of Pd when deposited on the nearly stoichiometric, oxidized surface formed by heating the sample at 700K in 1 torr of O$_2$ for 3 minutes as described in ref. 5. This surface should be most representative of a sensor surface since sensors generally operate under oxidizing conditions (i.e., in air at elevated temperatures).

Palladium Deposition on SnO$_2$(110)

The interaction of palladium with the nearly perfect, oxidized SnO$_2$(110) surface was studied by sequential Pd deposition at room temperature (ref. 11). XPS Pd 3d and Sn 3d core levels are plotted in figure 2 as a function of increasing palladium coverage. While the Sn 3d peaks (figure 2a) are increasingly attenuated as the Pd film grows, there are no large binding energy shifts or peak shape changes. This suggests that strong chemical interactions are not occurring between

Pd and surface Sn atoms. Note, however, that at coverages greater than ~8 monolayers (ML), a small shoulder appears on the low binding energy side of the Sn 3d peaks indicating the presence of a small amount of metallic Sn. We believe that this is due to the formation of a Pd-Sn alloy at higher Pd coverages*.
Unlike the Sn 3d spectra, the Pd 3d peaks (fig. 2b) show a substantial shift to lower binding energy as Pd coverage increases. The peaks get narrower with increasing Θ_{Pd} (the FWHM goes from 2.10 eV at 0.3 ML to 1.70 eV at >3.0 ML) and by 8.0 ML, both the lineshape and peak position are very similar to those of a palladium foil. This behavior suggests that the palladium film is metallic. A metallic overlayer is consistent with the lack of change in the Sn 3d peaks and the conclusion that most of the Pd does not strongly react with SnO_2. If a sizable amount of Pd reacted strongly with the surface, one would expect it to be at least partially oxidized. Oxidation would lead to core level broadening and/or higher binding energies that are not seen here (see also discussion below).

The weak chemical interaction between Pd and SnO_2 suggested by the XPS results is consistent with a clustering growth mode of the Pd overlayer*. To confirm that clustering of Pd occurs on SnO_2(110), Ne^+ ISS experiments, which probe the top surface layer, were performed at various coverages. The results are shown in figure 3. To avoid effects from surface damage due to the Ne^+ ion beam, ISS spectra were not taken after sequential Pd depositions. Instead, the surface was cleaned, reoxidized, and Pd was deposited to a given coverage before collecting each spectrum. Also, short scanning times were used to minimize beam damage. Since ISS provides qualitative information about the composition of the outermost layer, one would expect the Sn peak to completely disappear within the first few Pd monolayers if layer-by-layer growth occurs. Instead, it is seen in fig. 3, that the Sn signal at $E = 0.58 E_o$ is not completely attenuated until nearly 10 ML, suggesting that at least some bare substrate patches are present up to that coverage. This implies that initial clustering occurs with lateral growth to fill in the bare patches by <10 ML. Thus, both XPS and ISS results are consistent with growth by clustering.

To determine how the development of the Pd/SnO_2 interface affects the electronic and electrical properties of the composite surface, conductance and the photoelectron intensity at the Fermi level $N(E_F)$ were monitored as Pd was sequentially deposited. Results from these measurements are shown in figure 4. The photoelectron intensity at E_F, measured with UPS, correlates with the occupied density of states at E_F. It is, therefore, a measure of the metallic character of the overlayer. Figure 4 shows that the Fermi level intensity begins to rapidly increase between 1 and 2 monolayers. In contrast, the conductance does not begin to rise significantly until 7-8 ML, where it goes up sharply. The differing behavior between conductance and the $N(E_F)$, both measures of the metallic nature of the overlayer, can also be explained by the clustering growth mode of the Pd film. First, if Pd clusters are formed, one would expect to see the kind of rapid rise in $N(E_F)$ observed at low coverages, as each of the growing islands takes on metallic character. However, at these coverages (< 6 ML), the 4-point measurement is still responsive to the underlying substrate conductance since the Pd, although metallic, is in isolated clusters. As Θ_{Pd} increases and the clusters grow laterally to produce a connected adlayer, conductance should begin to increase; such behavior is observed at 7-8 monolayers. Note that this is in the same coverage range where the substrate Sn peak disappears in ISS (figure 3), indicating that a continuous film has formed.

*T. B. Fryberger and S. Semancik, Surface Science, work in progress.

Model Sensor Response

In general, the conductivity of SnO_2-based sensors increases when exposed to reducing gases (e.g. H_2, CO) and decreases when exposed to oxidizing gases (e.g. O_2). In order to better understand the mechanisms which control these conductivity changes, we have made in situ conductance measurements of the Pd/SnO_2(110) model sensor in both hydrogen and oxygen atmospheres. A Pd coverage of 3 ML was chosen since at this coverage, as discussed previously, the composite surface consists of metallic (catalytic) Pd clusters on the essentially unperturbed tin oxide substrate (previous work* has shown this to be the optimal configuration for electrical response to hydrogen). The 3 ML Pd/SnO_2(110) surface was subjected to a series of consecutive hydrogen and oxygen exposures while monitoring the conductance of the sample, which was held at 400K throughout the experiment (ref. 12). The results are shown in figure 5, where conductance versus time is plotted. The sequence of steps in this experiment was as follows:

1) The sample was held in UHV (<8 x 10^{-10} mbar) at 400K for several minutes to obtain an initial conductance value. It is seen in figure 1 that there is virtually no drift; the conductance remained constant at 58 x 10^{-6} A/V.

2) The sample was exposed to a constant pressure (10^{-5} mbar) of hydrogen for 6 minutes. This first hydrogen exposure provides a measure of the model sensor response in the absence of oxygen (both gaseous/ambient and chemisorbed). The conductance increased steadily during exposure to H_2; it increased by 47% after 6 minutes exposure at constant pressure. (Further exposure time results in a slow upward drift in conductance*.)

3) The chamber was evacuated to <8 x 10^{-10} mbar. Upon evacuation, the conductance decreased but did not return to its initial value, indicating that the interaction between hydrogen and the surface is not fully reversible.

4) The sample was exposed to 10^{-5} mbar of O_2 causing the conductance to decrease to 30% below the starting point (step 1).

5) The chamber was again evacuated to <8 x 10^{-10} mbar. Upon evacuation of O_2 the conductance did not increase, indicating that the O_2 interaction with the surface is even less reversible at 400K than the hydrogen interaction (step 3).

6) Steps 2-5 were repeated. The total response to H_2 following O_2 exposure and evacuation (step 6) was more than twice as large as the first H_2 response (step 2), where no previous oxygen exposure had occurred. In addition, the total conductance change occurred within a few seconds rather than over several minutes (as seen in the first H_2 exposure), and the response became reversible in the presence of oxygen.

As shown in figure 5 (step 2), exposure of the 3 ML Pd/SnO_2(110) surface to hydrogen results in a nearly 50% conductance increase. This can be compared to the small hydrogen response (3% increase) for the bare SnO_2(110) surface (not shown; see ref. 4). The enhancement by Pd is most likely due to a "spillover" mechanism wherein hydrogen molecules dissociate on the catalytic Pd clusters and then diffuse, probably across and/or through the clusters, to the substrate where the

*T. B. Fryberger and S. Semancik, Sensors and Actuators, work in progress.

hydrogen atoms can interact with the semiconducting SnO_2 to increase its conductance. The irreversibility of the response to H_2 at 400K is thought to be due to adsorbed hydrogen remaining on the surface at this temperature (ref. 12).

Figure 5 (steps 4 and 5) also shows that the conductance decreases to well below the starting point (step 1) upon exposure to O_2. It should be pointed out that, as in the case of H_2, the bare substrate shows no response to O_2 at 400K, indicating that the surface is activated toward oxygen by the Pd clusters (ref. 12). Since adsorbed hydrogen is most likely present on the surface (as discussed above), it is probable that chemisorbed oxygen reacts with the hydrogen atoms to form volatile water molecules (refs. 13,14). This would return the conductance only to its initial value (step 1), however. The fact that the conductance decreases an additional 30% suggests that oxygen must adsorb on the surface, in addition to reacting with adsorbed hydrogen (although a small amount of this additional decrease may be due to reaction of oxygen with residual hydrogen in the Pd clusters). It is well established that O_2 dissociates on, but does not oxidize, Pd surfaces in this temperature range (refs. 13-15). It is possible that the response of the Pd/SnO_2 surface toward O_2 is then produced by spillover of chemisorbed oxygen atoms, similar to that occurring for hydrogen. Note that the response to oxygen is even less reversible upon evacuation (step 5) than the response to hydrogen (step 3). This irreversibility is most likely due to the presence of chemisorbed oxygen, which desorbs only above 400K, as in the case of hydrogen.

The results in figure 5 suggest that the 400K response of Pd/SnO_2 to H_2 in the presence of oxygen is, to a large extent, due to reactions of chemisorbed species, both with the surface and with each other. To show that reactions between chemisorbed species are important, He^+ ISS experiments using isotopically labeled oxygen were performed (ref. 12). ISS is particularly useful here because of its top layer sensitivity, allowing qualitative determination of the atomic composition at a sample surface. The results are shown in figure 6 where the oxygen region of the ISS spectrum can be seen for a 3 ML Pd/SnO_2(110) surface (a) before exposure to any gases, (b) after exposure to 10^{-5} mbar of $^{18}O_2$ at 400K, and (c) after exposure of the surface in (b) to 10^{-5} mbar of H_2 at 400K. The spectrum in figure 6a represents the surface lattice oxygen signal since no gas exposures have been performed. It is seen in figure 6b that ^{18}O is clearly distinguishable from ^{16}O and that approximately 1/3 of the total signal is due to ^{18}O. When the surface is then exposed to hydrogen (figure 6c), essentially all of the ^{18}O signal is attenuated, indicating that hydrogen preferentially reacts with the ^{18}O. The most likely explanation for this is that ^{18}O is a chemisorbed, rather than a lattice oxygen species. These results provide strong evidence that the reaction

$$2H_{ads} + O_{ads} \longrightarrow H_2O_{gas}$$
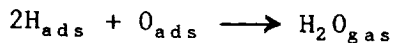
is a primary mechanism for the large conductance changes seen in figure 5 (steps 4 and 6). Whether this reaction takes place on the Pd particles, on the SnO_2 substrate, or on the boundaries between the two materials remains to be determined (ref. 12).

CONCLUSIONS

Multi-technique surface analytical studies of Pd-dosed SnO_2(110) samples have been performed in a step-wise manner to investigate the role of catalytic additives in gas sensing. It was found that metallic Pd clusters on a nearly unperturbed SnO_2 substrate can be formed by evaporating Pd onto the well-oxidized, nearly ideal SnO_2(110) surface at room temperature. By combining the surface techniques with

electrical gas response measurements, we showed that, at 400K, the response of the sensor to H_2, in the presence of O_2, is dominated by the water forming reaction between chemisorbed hydrogen and oxygen. Further work will focus on using gas mixtures to simulate more realistic sensing environments. These studies demonstrate the utility of combining basic research tools (e.g. surface science) with simulations of actual operating conditions for understanding the mechanistic aspects of device (e.g. sensor, catalyst) operation.

REFERENCES

1. See, for example, P. K. Clifford, and D. T. Tuma: Characteristics of Semiconductor Gas Sensors II. Transient Response to Temperature Change. Sensors and Actuators, vol. 3, 1982/3, pp. 255-281; J. N. Zemel: Theoretical Description of Gas-Film Interaction on SnO_x. Thin Solid Films, vol. 163, 1988, pp. 139-202; D. Kohl, Surface Processes in the Detection of Reducing Gases with SnO_2-based Devices. Sensors and Actuators, vol. 18, 1989, pp. 71-113.

2. Z. M. Jarzebski and J. P. Morton: Physical Properties of SnO_2 Materials. J. Electrochem. Soc., vol. 123, 1976, pp. 199c-205c.

3. B. Thiel and R. Helbig: Growth of SnO_2 Single Crystals by a Vapour Phase Reaction Method. J. Cryst. Growth, vol. 32, 1976, pp. 259-264. (We thank Professor Helbig for supplying the crystal used in this study.)

4. S. Semancik and T. Fryberger: Model Studies of SnO_2-Based Gas Sensors: Vacancy Defects and Pd Additive Effects. Sensors and Actuators, vol. B1, pp. 97-102, 1990.

5. D. F. Cox, T. B. Fryberger, and S. Semancik: Oxygen Vacancies and Defect Electronic States on the SnO_2(110)-1 x 1 Surface. Phys. Rev., vol. B33, pp. 2072-2083, 1989.

6. Certain commercial instruments are identified in order to adequately specify the experimental procedure. In no case does such identification imply endorsement by the National Institute of Standards and Technology.

7. J. W. Erickson and S. Semancik: An Economical Ultrahigh Vacuum Four-Point Resistivity Probe. J. Vac. Sci. Technol., vol. A5, 1987, pp. 115-117.

8. E. deFresart, J. Darville and J.M. Gilles: Influence of the Surface Reconstruction on the Work Function and Surface Conductance of (110) SnO_2. Appl. Surf. Sci., vol. 11/12, 1982, pp. 637-651.

9. S. Munnix and M. Schmeits: Electronic Structure of Tin Dioxide Surfaces. Phys. Rev., vol. B27, 1983, pp. 7624-7635; Electronic Structure of Point Defects on Oxide Surfaces. Phys. Rev., vol. B33, 1986, pp. 4136-4144.

10. D. F. Cox, T. B. Fryberger, and S. Semancik: Surface Reconstructions of Oxygen-Deficient SnO_2(110). Surf. Sci., vol. 224, pp. 121-142, 1989.

11. T. B. Fryberger, J. W. Erickson, and S. Semancik: Chemical and Electronic Properties of Pd/SnO_2(110) Model Gas Sensors. Surface and Interface Analysis, vol. 14, 1989, pp. 83-89.

12. T. B. Fryberger and S. Semancik: Conductance Response of Pd/SnO_2 (110) Model Gas Sensors to H_2 and O_2. Sensors and Actuators, 1990.

13. L.-G. Petersson, H. M. Dannetun, and I. Lundstrom: Water Production on Palladium in Hydrogen-Oxygen Atmospheres. Surface Science, vol. 163, 1985, pp. 273-284; and references therein.

14. T. Engel and H. Kuipers: A Molecular-Beam Investigation of the Reaction $H_2 + 1/2\ O_2 \rightarrow H_2O$ on Pd(111). Surface Science, vol. 90, 1979, pp. 181-196.

15. M. Milun, et al.: Thermal Desorption Spectroscopy of the O_2/Pd(110) System. Surface Science, vol. 211/212, 1989, pp. 887-895.

MULTI-TECHNIQUE CHARACTERIZATION SYSTEM
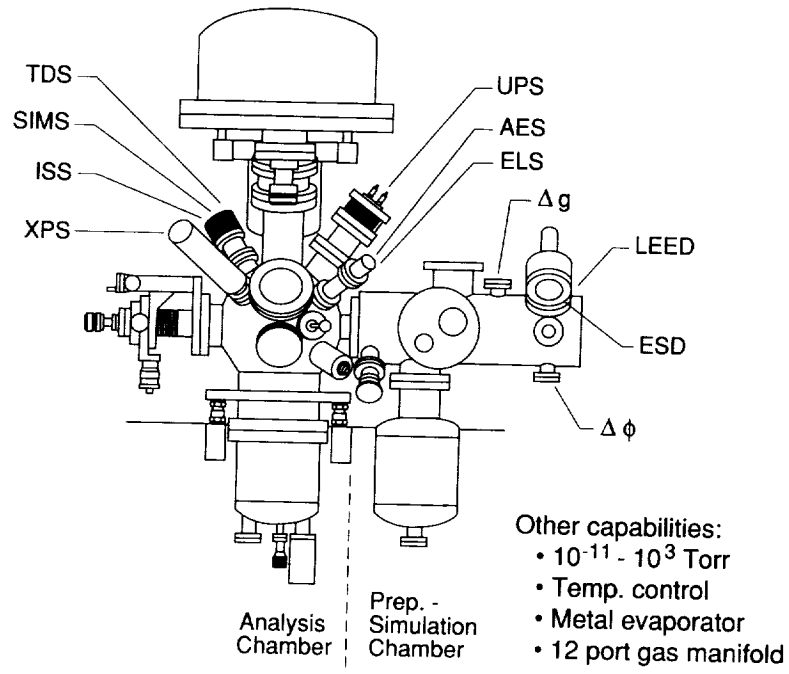
Figure 1.   Schematic of the multi-technique surface analytical facility used to characterize sensor materials and processes.
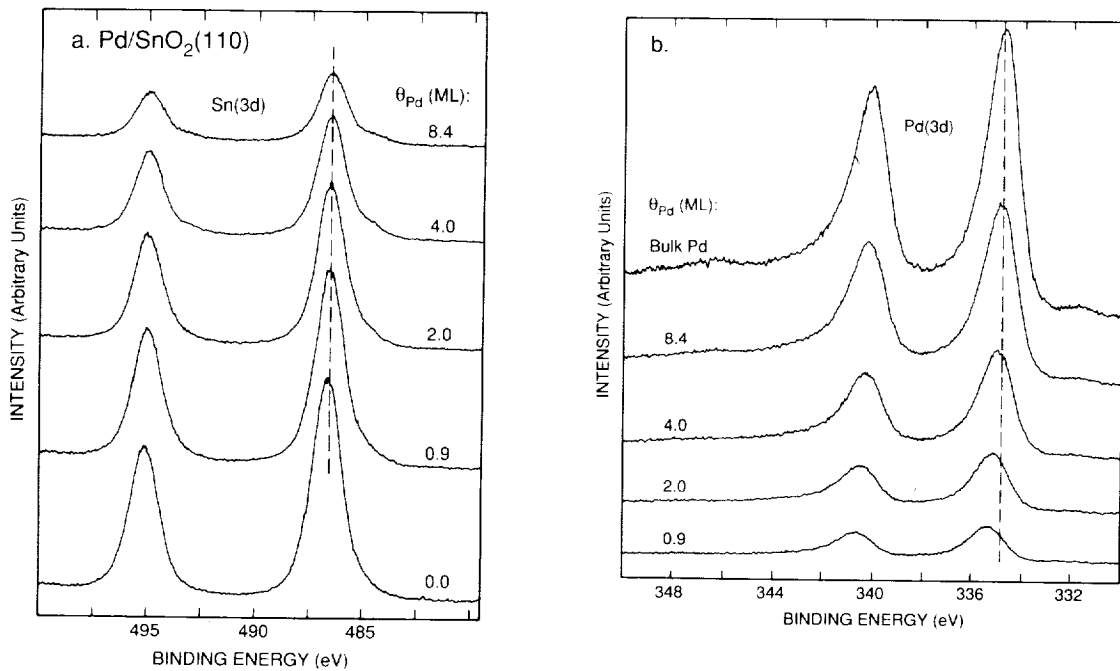
Figure 2.   XPS core level (a) Sn 3d and (b) Pd 3d spectra for various Pd coverages on oxidized $SnO_2(110)$.

286
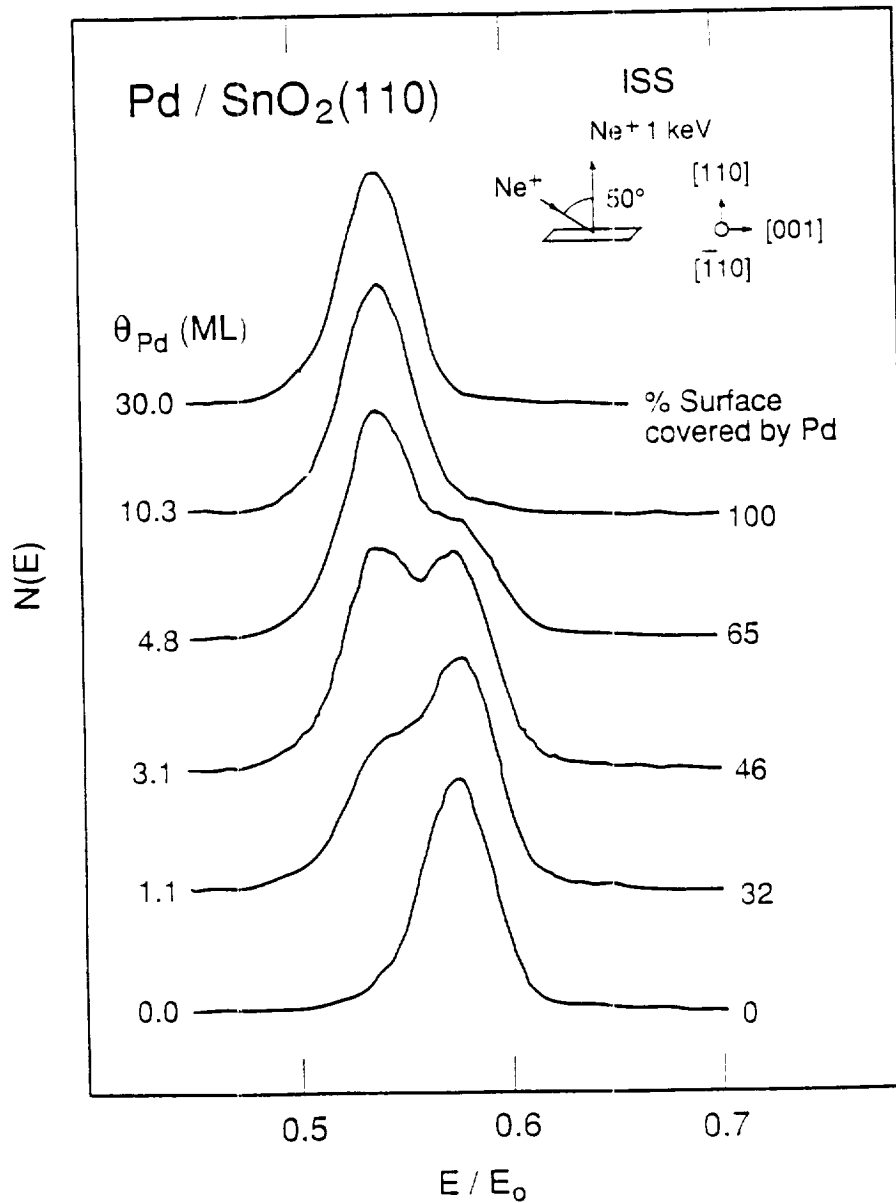
Figure 3. Ne⁺ ISS spectra for various coverages of Pd on oxidized SnO_2(110). E_0 = 1000 eV. Spectra are not drawn to scale.
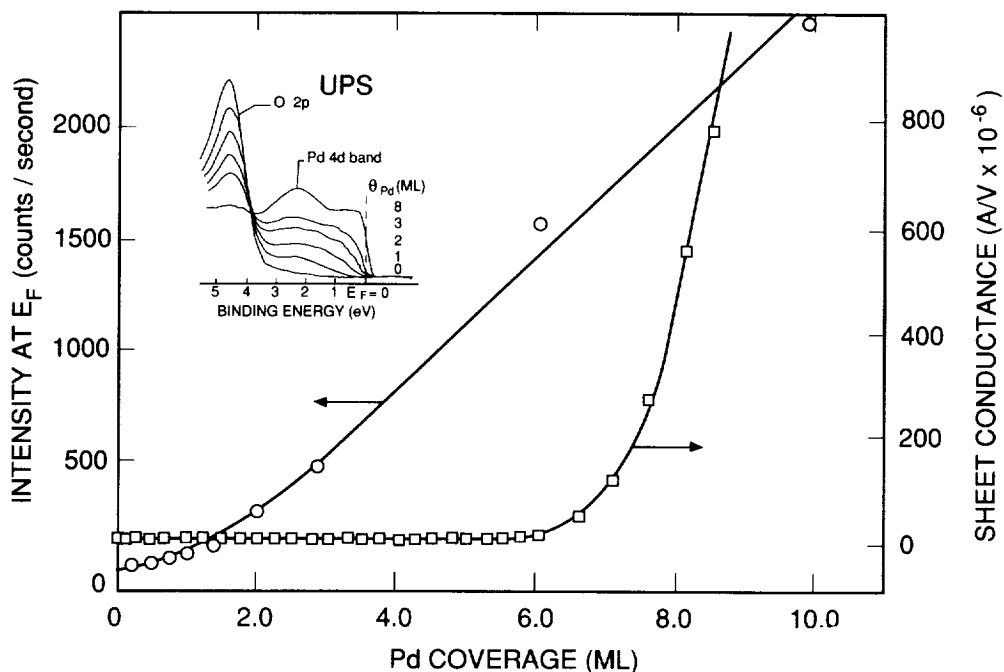
METALLIC NATURE OF OVERLAYER

Figure 4. UPS photoelectron intensity at the Fermi level, $N(E_F)$, and 4-point conductance as a function of Pd coverage for deposition on oxidized SnO_2 (110).
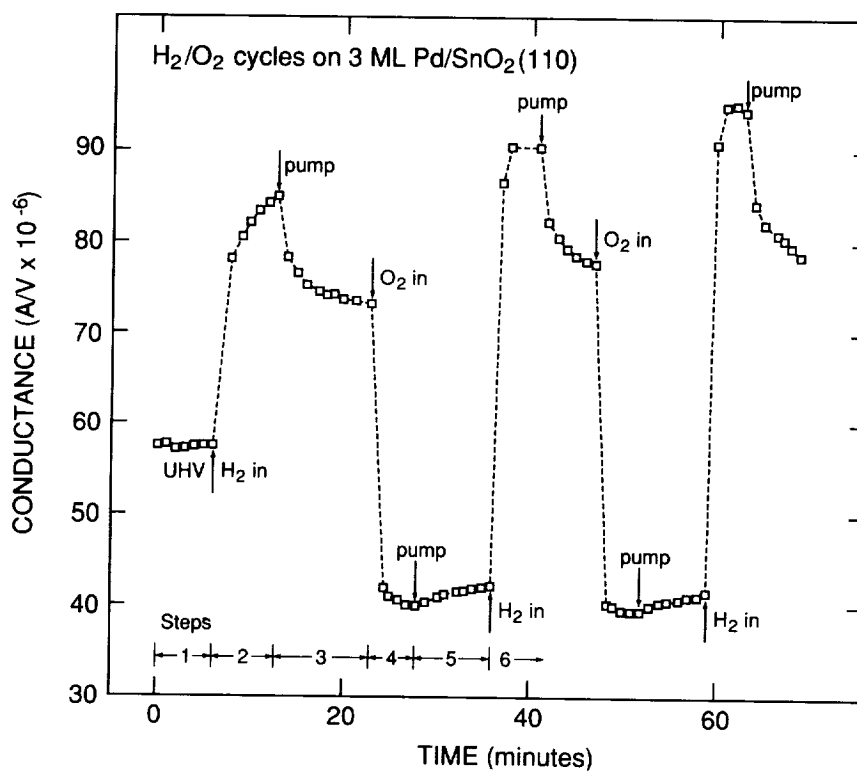
Figure 5. Conductance versus time for sequential hydrogen and oxygen exposures of the 3 ML Pd/SnO_2(110) surface at 400K. All gas exposures were performed at a constant pressure of 10^{-5} mbar. Refer to text for further details.
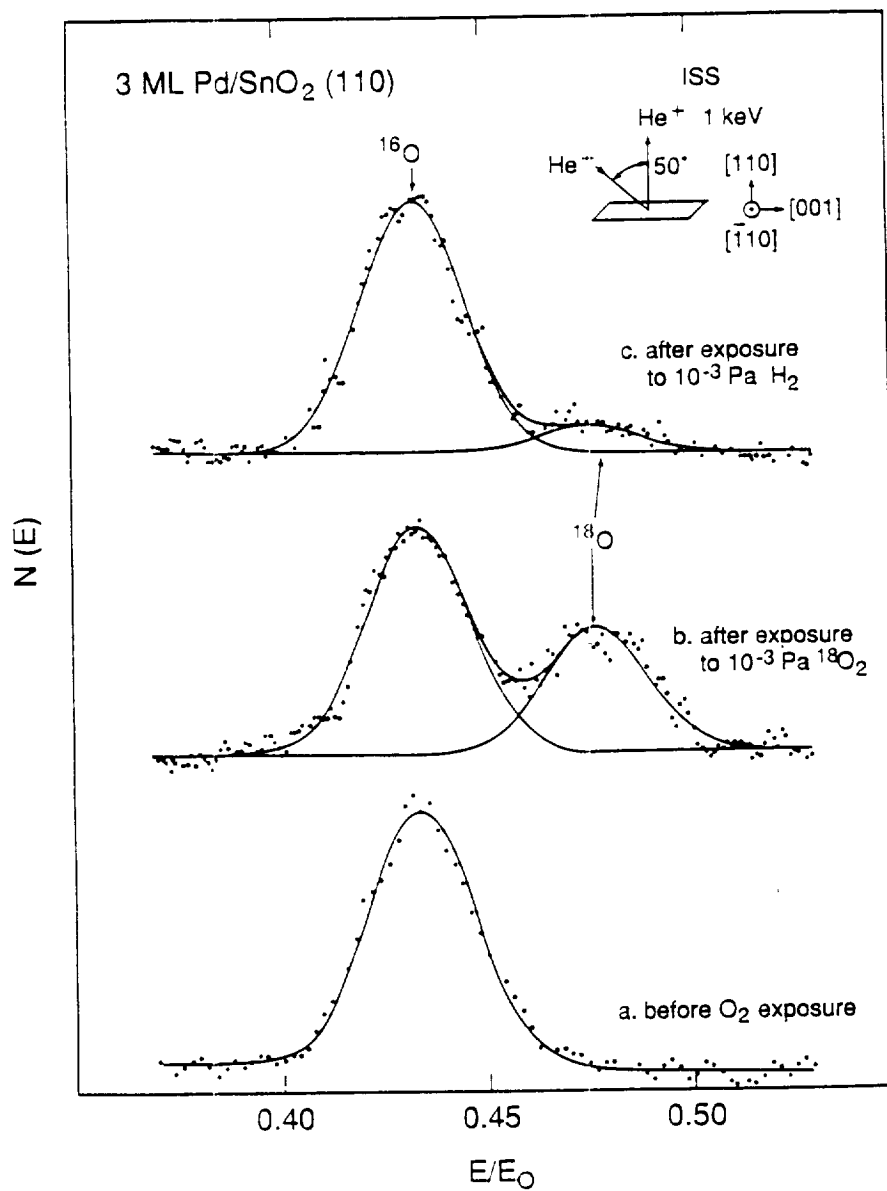
Figure 6. Ion scattering spectroscopy for 3 ML Pd/SnO$_2$(110) surface after a) 500K anneal for 3 minutes in UHV; b) exposure of the surface in a) to 10^{-5} mbar ^{18}O$_2$ at 400K for 5 minutes; and c) exposure of the surface in b) to 10^{-5} mbar H$_2$ at 400K for 5 minutes.

IN SITU ANALYSIS OF CO DURING CHEMISORPTION AND OXIDATION ON GRAPHITE-SUPPORTED Pt BY FTIR-MICROSPECTROMETRY

Valerie A. Self and Paul A. Sermon
Department of Chemistry, Brunel University, Uxbridge UB8 3PH, UK

SUMMARY

For chemisorption and oxidation on Pt/HOPG (highly-orientated pyrolytic) graphite, reflectance Fourier Transform Infrared (FTIR)-microspectrometry reveals a variable state and reactivity for $\underline{CO}$.

INTRODUCTION

Even for model surface science systems, where surface heterogeneity (ref. 1) is minimal, surface diffusion may be too slow relative to the reaction rate to avoid segregation of reactants into surface islands (ref. 2) under steady-state conditions. Thus in CO oxidation on Pt (where the relevant surface diffusion coefficients are such that $D_O < D_{CO}$ (ref. 3)) then reactant $\underline{CO}$ islands exists (refs. 4,5) at the perimeters of which the surface reaction is thought to occur (ref. 6). Furthermore CO can chemisorb on metals in linear (atop) and bridge forms to extents which vary with the precise faces predominantly exposed (ref. 7), coverage, etc.

Infrared has long been used to probe the nature of adsorbed CO (ref. 8) on model film and heterogeneous surfaces, but it may now be that FTIR-microspectrometry will allow the state of this adsorbate and reactant to be investigated with a spatial resolution of 4.4 μm on model (and real) catalytic surfaces.

EXPERIMENTAL

Because of its high degree of perfection at an atomic level, highly orientated pyrolytic graphite (HOPG) has been used as a standard for scanning tunnelling microscopy (ref. 9). Here it has been coated with Pt by vacuum deposition to form a sample of polycrystalline Pt/C, which is well defined. Specifically the HOPG sample was sputter-coated with Pt for 30 min to give a Pt layer 60 nm in thickness. No other metallic impurities were detected.

The sample was placed in the FTIR cell within the IRPLAN (Spectra-Physics) IR microscope linked to a Perkin Elmer 1710 FTIR, through which the reactant gases could flow as follows:

(i) in chemisorption 6% CO/N_2 flowed at 23 ml/min while heating to 425K at 5K/min and holding at 425K for 45 min before cooling to room temperature;

(ii) in CO oxidation where 6% CO/N_2 (21.4 ml/min) and 6% O_2/N_2 (21.1 ml/min) flowed while heating to 425K at 5K/min and holding isothermally for 2h before cooling to room temperature.

Using this IR microscope it was possible to measure reflectance FTIR spectra for selected areas of the surface of the catalyst. All spectra were measured using 50 scans with no subsequent smoothing and with a resolution of 8 cm^{-1}.

In CO chemisorption and oxidation it is thus possible to differentiate linearly-bound and bridge-bound CO by IR (ref. 10).

RESULTS

Reflectance spectra for the surface CO and CO_2 species on Pt/HOPG catalyst in CO chemisorption and CO oxidation are shown in Figure 1, where the area being sampled is 440 μm^2. No significant gas phase bands were noted in this region.

Consistent with analysis of CO on low index crystallographic planes of Pt (ref. 11) the

(i) α peak at 1890 ± 9 cm^{-1} is bridge-bound CO;

(ii)   weaker bands at 1933, 1953 and 1982 ± 2.4 cm^{-1} are γ bands;

(iii) β peak at 2082 ± 1 cm^{-1} is linearly-bound CO.

In CO chemisorption it is clear that the ratio of $\alpha : \beta$ peaks varies with analytical position across the Pt/HOPG crystal; so does the extent of observation of γ bands. In other words the surface is not entirely homogeneous with respect to CO adsorbate. The intensity of the bridge-bound CO band is greater than was expected on Pt. In CO oxidation CO_2 is observed at 2360 cm^{-1} when the smaller γ peaks are not observed and the α peak is severely reduced relative to the intensity observed in chemisorption of CO alone. This suggests that the α and γ peaks are associated with the most active species in CO oxidation on this Pt, either because they are at the edge of CO islands or because their vibrational characteristics make the transformation CO_2 easier. In addition, the α peak is shifted to 1887 ± 1 cm^{-1} while the β peak remains at about its earlier position in CO chemisorption: therefore linearly-bound CO may be quite unreactive on this surface and unaffected by the presence of O. On Pt/HOPG the apparently more reactive bridge-bound state decreased in intensity on CO oxidation, but the evidence of CO_2 formation and α/γ peak decrease is not uniformly exhibited by the whole surface.

DISCUSSION

The surface diffusion coefficient D_0 of oxygen is thought to be smaller on Pt (ref. 4) than that for CO, although both coefficients may be decreased substantially as the surface becomes less energetically homogeneous since the periodic nature of the potential energy surface governs (ref. 12) the whole question of surface mobility (ref. 4). This may then be the cause of the spatial difference of CO on the Pt/HOPG seen here in adsorption and catalysis. It may be that reactant islands are

important in defining catalysis since the perimeters of these might have highest densities of bridge-bound CO, but alternatively bridge-bound CO may from a vibrational point be more readily converted to CO_2. Nevertheless, the relationship of these results to those obtained* for Pt foil in CO oxidation, where active surface grains were seen, may be interesting.

Although since the mid 1950's infrared has been used to identify adsorbed species on the surfaces of solids and catalysts, it often remains uncertain whether the species detected are the important participants in surface reactions rather than mere spectators, which may numerically exceed the more reactive metastable short-lived participants which are responsible for catalysis.

The present microspectroscopy may be useful in understanding the microchemistry of catalytic surfaces in the sense that here in CO oxidation it suggests that the surface is not uniformly reactive (which is consistent with the presence of reactant islands). Ultimately, this may allow us to understand and control activity-selectivity of such surfaces via fractality-diffusional modes. This new analytical approach could lead to heterogeneous reactions being more effectively and selectively catalysed by surfaces which are even better understood and properly optimised.

CONCLUSIONS

It may be that the present analytical approach provides a method of relating surface chemistry of catalysts relevant to surface science and practical catalysis.

ACKNOWLEDGEMENTS

REFERENCES

1. Taylor, H.S., Proc. Roy. Soc., 108, 1925, 105.

2. Anacker, L.W.; and Kopelman, R., Phys. Rev. Lett., 58, 1987, 289.

3. Saltsburg, H.; Smith, J.N.; and Rogers, M., 'Fundamentals of Gas-Surface Interactions', Acad. Press, 1967; Dacey, J.R., Ind. Eng. Chem., 57(6), 1965, 26; Somorjai, G.A., Catal. Rev., 18, 1982, 173; Gasser, R.P.H., 'An Introduction to Chemisorption and Catalysis by Metals', OUP, 1985.

4. Bernasek, S.L.; Lenz, K.; Poelsema, B.; and Comsa, G., Surf. Sci., 183, 1987, L319.

5. Engel, T.; and Ertl, G., Adv. Catal., 28, 1979, 1.

6. Araya, P.; Porod, W.; Sant, R.; and Wolf, E.E., Surf. Sci. Lett., 208, 1989, L80.

7. de Koster, A.; Jansen, A.P.J.: van Santen, R.A.; and Geerling, J.J.C., Far. Disc. Chem. Soc., 87, 1989, 221.

*Kordersch, M. E.; Engel, W.; Zeitler, E. R.; and Bradshaw, A. M., 8ISSC, Paper A.2.

8. Hollins, P., Adsn. Sci. Tech., 2, 1985, 177; Sheppard, N.; and Nguyen, T.T., Adv. Infrared Raman Spec., 5, 1978, 67; Queau, R.; and Poilblanc, R., J. Catal., 27, 1972, 200; Blyholder, G., J. Phys. Chem., 68, 1974, 277.

9. Binnig, G.; and Rohrer, H., Angew Chem., 26, 1987, 606; J. Vac. Sci. Tech., 6A(2), 1987, 257; Proc. Roy. Micro. Soc., 23(3), 1988; Marti, O.; Binnig, G.; Rohrer, H.; and Salemink, H., Surf. Sci., 181(1-2), 1987, 230; West, P.; Kramar, J.; Baxter, D.V.; Cave, R.J.; and Baldeschwieler, J.D., IBM J. Res. Dev., 30, 1986, 484; Gauthier, S.; Rousset, S.; Klein, J.; Sacks, W.; and Belin, M., J. Vac. Sci. Tech., 6A, 1988, 360; Morita, S.; Tsukada, S.; and Mikoshita, N., J. Vac. Sci. Tech., 6A, 1988, 354; Bando, H., J. Vac. Sci. Tech., 6A, 1988, 344; Colton, R.J.; Baker, S.M.; Driscoll, R.J.; Youngquist, M.G.; Baldeschwieler, J.D.; and Kaiser, W.J., J. Vac. Sci. Tech., 6A, 1988, 349.

10. Yates, J.T.; and Garland, C.W., J. Phys. Chem., 65, 1961, 617; Eischens, R.P.; Francis, S.A.; and Pliskin, W.A., J. Phys. Chem., 60, 1956, 194.

11. Crossley, A.; and King, D.A., Surf. Sci., 68, 1977, 528; Surf. Sci., 95, 1980, 131; Bare, S.R.; Hofman, P.; and King, D.A., Surf. Sci., 144, 1984, 347; Eischens, R.P.; and Pliskin, W.A., Adv. Catal., 10, 1958, 1; Blyholder, G., J. Phys. Chem., 68, 1964, 2772.
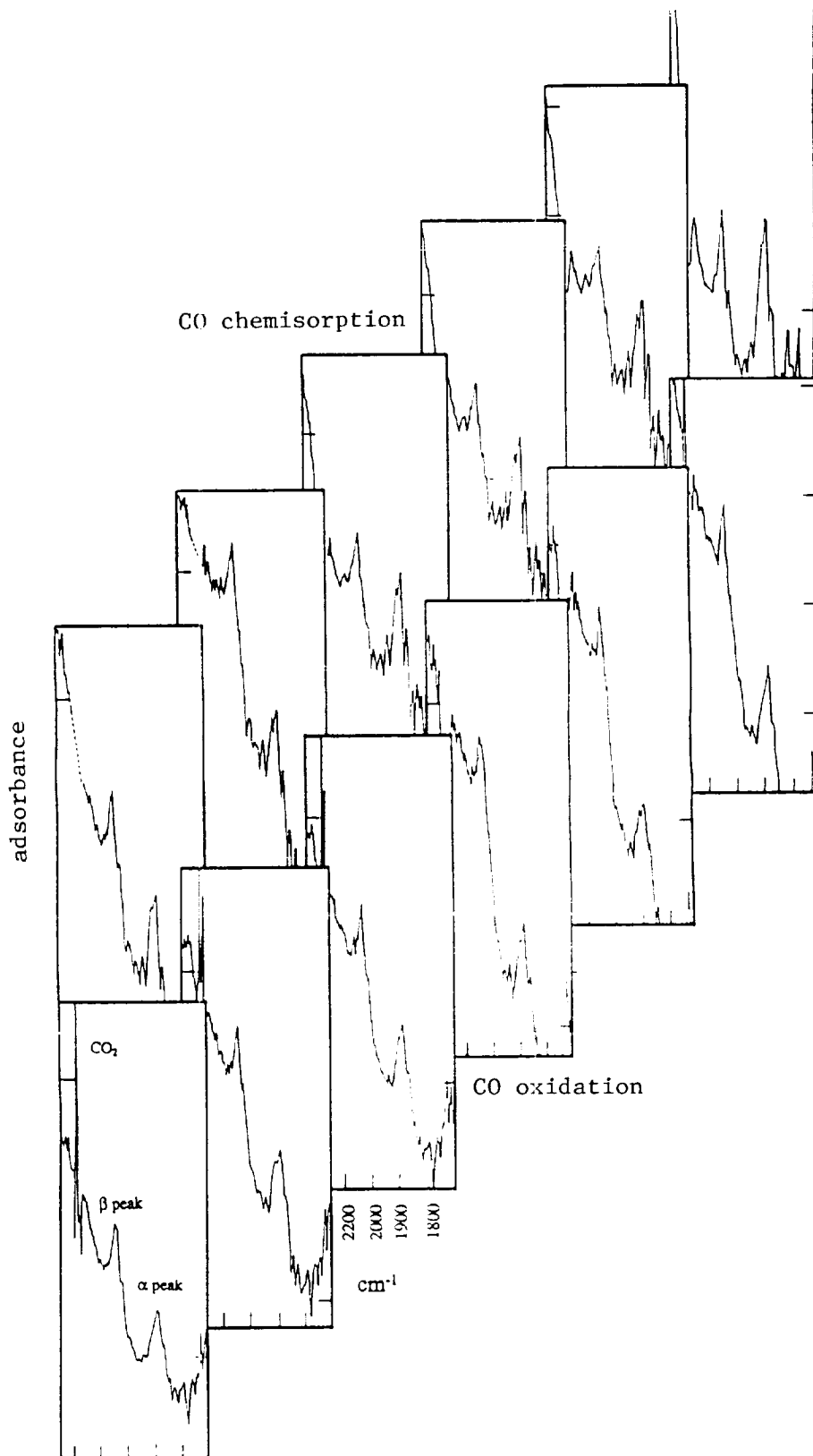
12. Kemball, C., Proc. Roy. Soc., 187A, 1946, 73.

Figure 1. Reflectance FTIR-microspectrometry during CO chemisorbed an oxidation on PT/HOPG.

CALORIMETRY, ACTIVITY AND MICRO-FTIR ANALYSIS OF CO CHEMISORPTION, TITRATION AND OXIDATION ON SUPPORTED Pt

Paul A. Sermon, Valerie A. Self, Mariana S.W. Vong, Alpha T. Wurie, and Nigel D. Hoyle

Department of Chemistry, Brunel University, Uxbridge UB8 3PH, UK

SUMMARY

The value of in-situ analysis on CO chemisorption, titration and oxidation over supported Pt catalysts using calorimetry, catalytic and micro-FTIR methods is illustrated using silica- and titania-supported samples.

INTRODUCTION

Catalysis of CO oxidation has been extensively studied (ref. 1). The catalysed reaction is important in the clean-up of car-exhaust gases, but a far more demanding situation is to be found within the laser field.

CO_2 TEA lasers, which emit ultra-short pulses of ir radiation in essentially parallel beams, contain a high partial pressure of CO_2 (i.e. 1 atmosphere) some of which during laser operation dissociates

$$2CO_2 \rightleftharpoons 2CO + O_2$$
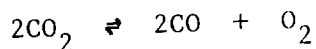
with the result that there is localised arcing. The percentage dissociation of 1 atmosphere CO_2 was shown by Pourbaix in 1948 (ref. 2) to increase with increasing temperature in the manner below.

% decomposition	T(K)
10	2474
1	1841
0.1	1635
0.01	1400
0.001	1225

Originally Pt wire at 1373K was used to catalyse the re-oxidation of the CO produced. On such surfaces not only are oscillations in the rate seen as a result of microfaceting (ref. 3), but also moderate temperatures are required. In other words, the Pt wire was not a particularly good catalyst. More recently Pt/stannic oxide and Pt/Fercalloy have been reported to be more effective in catalysing the recombination of CO and O_2 in sealed CO_2 lasers (ref. 4).

Previously, the oxidation of CO on Pt surfaces has been followed by molecular beam (ref. 5), transient (ref. 6) and theoretical (ref. 7) methods, showing that CO reacts with pre-adsorbed $\underline{O}$ at 600K rapidly with a first-order collision frequency.

The reverse reaction is very slow and formation of unreactive surface oxygen may be involved. Attention here is given to methods of studying and analysing the activity of Pt-based catalysts in this reaction and to probes which allow rationalisation and interpretation of their surface properties.

EXPERIMENTAL CATALYSTS

Two silica-supported Pt samples were used. (i) 3% Pt/SiO_2 on non-porous Degussa Aerosil 200 was prepared by impregnation to the point of incipient wetness using an aqueous solution of hexachloroplatinic acid (H_2PtCl_6; Johnson Matthey). This was then dried in air at 393K for 16h and reduced in H_2 at 570K. Chemisorption of oxygen suggested that this had a Pt surface area of 31.7m^2/g Pt. (ii) 6.3% Pt/SiO_2 EURO-Pt was used as supplied; its metal area estimated by oxygen chemisorption was 187.7 m^2/g Pt and the support exhibited porosity. These catalysts are denoted S3 and S6.

Titania-supported Pt (metal loading 3%) was prepared by impregnation of non-porous Degussa P25 titania, drying and reducing. This is denoted T3.

METHODS

Calorimetry of CO-O Titrations (ref. 8)

A sapphire-calibrated Dupont 990 differential scanning calorimeter (DSC) was used to follow titrations of preadsorbed $\underline{O}$ by $CO_{(g)}$ and preadsorbed $\underline{CO}$ by $O_{2(g)}$ at constant temperatures on samples (10-25 mg) of the above catalysts. Thermokinetic profiles of heat flow versus titration time were obtained. Reactant gases were 6% CO/N_2 (BOC: 99.995% purity from which traces of oxygen and water had been removed via passage through Pd/alumina and molecular sieve beds) and 12% O_2/N_2 (BOC: 99.995% purity).

Calorimetry of Catalysed CO Oxidation

Previously calorimetry has shown that the rate of heat generation in exothermic reactions is proportional to the rate of catalysed reaction (ref. 9). DSC was used here in CO oxidation with 6% CO/N_2 and 6% O_2/N_2 reactant gases over catalyst samples (20-30 mg) during temperature programming at 10K/min in the range 293-848-293K. Silica was used in the reference pan. A septum was placed at the DSC outlet and from this samples were taken and injected onto a Pye 104 gas chromatograph with a HWD and a silica-gel column at 373K. This separated CO_2 and gave a response which was linear with CO_2 concentration in the relevant range.

Catalysis of CO Oxidation

Studies of the rates of CO oxidation over samples (0.1g) of the catalysts were followed in a micro-reactor with gc-ir analysis of products. Reactant streams of $CO/O_2/N_2$ were passed at 40 cm^3/min through catalyst samples (preheated in flowing N_2 (40 cm^3/min) for 30 min at 393K) as these were heated and cooled at 2K/min.

FTIR Microspectroscopy (ref. 10)

Infrared has long been used to probe the nature of CO adsorbed on metal surfaces (ref. 11). The samples were placed in an FTIR cell within an IRPLAN (Spectra-Physics) IR microscope linked to a Perkin Elmer 1710 FTIR through which reactant gases could flow as follows:

(i) in chemisorption 6% CO/N_2 flowed at 23 cm^3/min while heating to 425K at 5K/min before cooling to room temperature

(ii) in CO oxidation where 6% CO/N_2 (21.4 cm^3/min) and 6% O_2/N_2 (21.1 cm^3/min) flowed while heating at 425K at 5K/min and holding isothermally for 2h before cooling to room temperature.

RESULTS

Pt/SiO$_2$

Titrations of CO-oxygen at 373K over S6 were entirely repeatable in sustained titration cycles and thermokinetic profiles were identical to those shown in Figure 1, suggesting that the titrations were entirely reversible at this temperature. Interestingly the shapes of the two titrations are different, but it is not yet possible to suggest that the titration with the induction period and lower symmetry is not involving a Langmuir-Hinshelwood mechanism. However, it is tempting to associate the induction period of low heat flux with chemisorption of the gaseous titrant on the preadsorbed monolayer. Interestingly, the induction period on S6 when $O_{2(g)}$ is titrating the CO-covered surface decreases as the temperature of titration rises:

T(K):	293	323	373	423	473	523	573
t(s)	330	168	80	48	0	0	0

At 373K the heat liberated in the two titration steps on S6 is not identical (i.e. 2270J were liberated per g Pt in CO titration of preadsorbed O and 1260J per g Pt were liberated in O_2 titration of preadsorbed CO).

Now consider what calorimetry can reveal about the catalysed CO oxidation reaction. Figure 2 shows that as the temperature of S3 increases, DSC shows a light-off at 473K with a maximum heat flow at 573K of about 75 mJ/s. Bearing in mind the relationship of heat flow and rates of reaction (ref. 9) it might be expected that the catalysed rate would also follow a similar profile. However, this would suggest that the rate of reaction would decrease to a low value at about 773K. This low rate of heat flow is interesting at high temperature and requires further investigation. On decreasing temperature the same type of profile was noted but displaced to a lower temperature than that seen with increasing temperature (i.e. hysteresis is shown). On decreasing temperature oscillations appear close to the point where extinction of the reaction might occur.

Comparison in Figure 3 of DSC-thermokinetic profiles with measured rates during CO oxidation over S3 during temperature programmed analysis confirms the difference between DSC and catalytic analysis especially at highest temperatures of analysis.

There is the suggestion that at these higher temperatures after light-off the reaction does not proceed entirely on the catalyst surface.

Sustained analysis of the catalysis of CO oxidation on S6 (see figure 4) revealed substantial activity-temperature hysteresis loops where activity was stable with reaction time. The hysteresis may in part be aggravated by support porosity (not seen in S3). At high P_{O_2} rates of oxidation are higher than in Figure 3.

Turning now to the micro-FTIR-spectrometry it is seen in Figure 5 that different parts of the top surface of a bed of S6 during CO chemisorption and CO oxidation under isothermal conditions show different spectral characteristics. It is known that average metal surface atom coordination affects the nature of adsorbed CO (ref. 12) and results are consistent with CO on low index crystallographic planes (ref. 13):

(i) 1890 ± 9 cm^{-1} bridge-bound CO

(ii) 2082 ± 1 cm^{-1} linearly-bound CO.

Thus the two areas show little bridge-bound CO in chemisorption, when CO coverage should be almost complete, but a greater proportion of this species during CO oxidation when the CO coverage is lower.

Pt/TiO$_2$

Results over T3 in Figures 6 and 7 should be compared with those in Figures 1 and 4 for Pt/silica. First, the thermokinetic profiles are different, with much enhanced induction periods and diminished total heat flows. Second, the activity-temperature hysteresis is absent and as expected closer to non-porous S3 than S6. DSC of CO oxidation on 3% Pt/TiO$_2$ under the same conditions as in Figure 2 showed a light-off at 498K.

DISCUSSION

Isothermal CO-$\underline{O}$ and O_2-$\underline{CO}$ titrations have not been widely used on metal surfaces (ref. 14) and may be complicated if some oxide supports are reduced by CO titrant (ref. 15). However, they can illuminate the kinetics of CO oxidation on metal/oxide catalysts (ref. 16) since during such titrations all $\underline{O}$ and $\underline{CO}$ coverages are scanned as a function of time. There are clear advantages in following the rates of the catalysed CO oxidation via calorimetry and gc-ms simultaneously. At lower temperatures the evidence they provide is complementary. CO oxidation and its catalysis of CO oxidation have been extensively studied (ref. 1), with hysteresis (ref. 17) and oscillations apparent, and the present results suggest the benefits of a combined approach. Silica support porosity may be important in defining activity-temperature hysteresis.

FTIR microspectroscopy reveals the chemical heterogeneity of the catalytic surfaces used; it is interesting that the evidence with regard to the dominant CO surface species and their reactivities with regard to surface oxygen for present oxide-supported Pt are different from those seen on graphite-supported Pt (ref. 9).

It is clear using these techniques that Pt supported upon reducible oxides behaves differently in this reaction to Pt upon a more unreactive support.

CONCLUSIONS

It is expected that the application of these analytical approaches to this ancient yet intriguing catalytic reaction will lead to a new understanding of the catalytic process and more effective catalysts.

ACKNOWLEDGMENTS

REFERENCES

1. Engel, T.; and Ertl, G., Adv. Catal., 28, 1979, 1; Gasser, R.P.H., 'Introduction to Chemisorption and Catalysis by Metals', Oxford Univ. Press, 1985.

2. Pourbaix, M.J.N.; and Rorive-Boute, C.M., Disc. Far. Soc., 4, 1948, 141.

3. Schuth, F.; and Wicke, E., Ber. Bunsen. Phys. Chem., 93, 1989, 191; Eiswirth, M.; Moller, P.; and Ertl, G., Surf. Sci., 208, 1989, 13; Tsai, P.K.; Maple, B.M.; and Herz, R.K., J. Catal., 113, 1988, 453; Plath, P.J.; Moller, K.; and Jaeger, N.I., J. Chem. Soc. Far. Trans. I, 84, 1988, 1751.

4. Stark, D.S., Plat. Met. Rev., 28, 1984, 166; Stark, D.S.; and Harris, M.R., J. Phys., 21E, 1988, 715.

5. Alnot, M.; Fusy, J.; and Cassuto, A., Surf. Sci., 57, 1976, 651; Pacia, N.; Cassuto, A.; Penetenero, A,; and Weber, B., J. Catal., 41, 1976, 455.

6. Hori, G.K.; and Schmidt, L.D., J. Catal., 38, 1975, 335; White, J.M., J. Chem. Phys., 66, 1977, 5744.

7. Weinberg, W.H.; and Merrill, R.P., J. Catal., 40, 1975, 268.

8. Martin Luengo, M.A.; Sermon, P.A.; and Wurie, A.T., J. Chem. Soc. Far. Trans. I, 83, 1987, 1651.

9. Beecroft, T.; Miller, A.W.; and Ross, J.R.H., J. Catal., 40, 1975, 281.

10. Self, V.A.; and Sermon, P.A., J. Phys. C, Matter 1, 1989, SB221-SB224.

11. Hollins, P., Ads. Sci. Tech., 2, 1985, 177; Sheppard, N.; and Nguyen, T.T., Ad. Infrared Raman Spec., 5, 1978, 67; Queau, R.; and Poilblanc, R., J. Catal., 27, 1972, 200: Blyholder, G., J. Phys. Chem., 68, 1964, 277.

12. de Koster, A.; Jansen, A.P.J.; van Santen, R.A.; and Geerling, J.J.C., Far. Disc. Chem. Soc., 87, 1989, 221.

13. Crossley, A.; and King, D.A., Surf. Sci., 68, 1977, 528; Surf. Sci., 95, 1980, 131; Bare, S.R.; Hofman, P.; and King, D.A., Surf. Sci., 144, 1984, 347; Eischens, R.P.; and Pliskin. W.A., Adv. Catal., 10, 1958, 1; Blyholder, G., J. Phys. Chem., 68, 1964, 2772.

14. Wentrcek, P.; Kimoto, K,; and Wise, H., J. Catal., 33, 1973, 279; Langmuir, I., J. Amer. Chem. Soc., 40, 1918, 1361; Akhtar, M; and Tompkins, F.C., Trans. Far. Soc., 67, 1971, 2461; Linares-Solano, A.; Rodriguez-Reinoso, F., and Salinas-Martinez de Lecea, C.; Carbon, 20, 1982, 177; Falconer, J.L.; Wentrcek, P.R.; and Wise, H., J. Catal., 45, 1976, 248.

15. Pajares, J.A.; Gonzalez de Prado, J.E.; Garcia Fierro, J.L.; Tejuca, L.G.; and Weller, S.W., J. Catal., 44, 1976, 421.

16. Cox, M.P.; Ertl, G., Imbihl, R; and Rustig, J., Surf. Sci., 134, 1983, L517.

17. Hlavacek, V.; and Votruba, J., Adv. Catal., 27, 1978, 59.
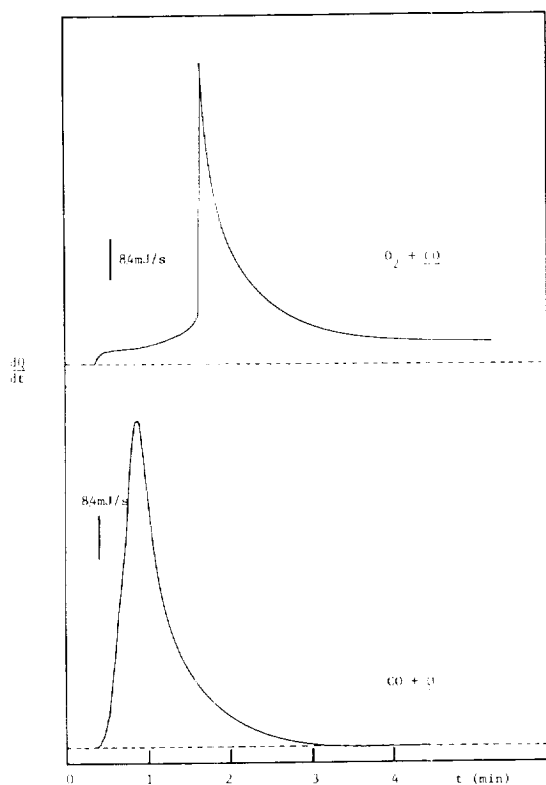
Figure 1   Thermokinetic profiles during titration of pre-adsorbed $\underline{O}$ by $CO_{(g)}$
and preadsorbed $\underline{CO}$ by $O_{2(g)}$ on Pt/SiO_2 (S6).
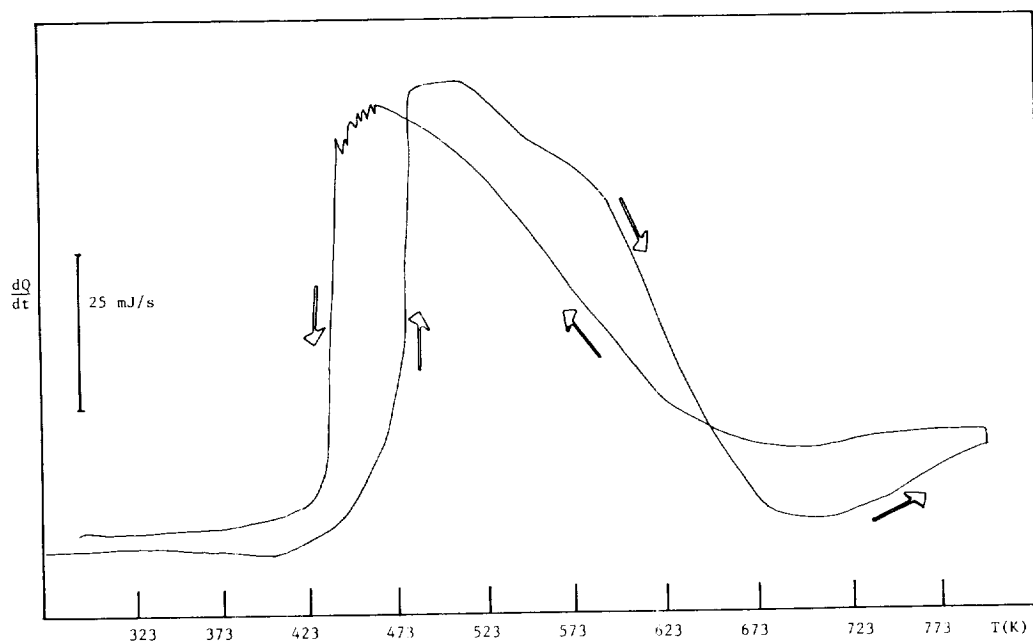
Figure 2 Thermokinetic profiles for CO oxidation ($P_{CO}:P_{O_2}:P_{N_2}$ = 23:23:714; P_{total} = 101 kPa) over
44 mg Pt/SiO_2 during temperature programming at 10K/min in the range 328-848-323K.
Oscillations set in at the point at which exctinction of the reaction was imminent.

303
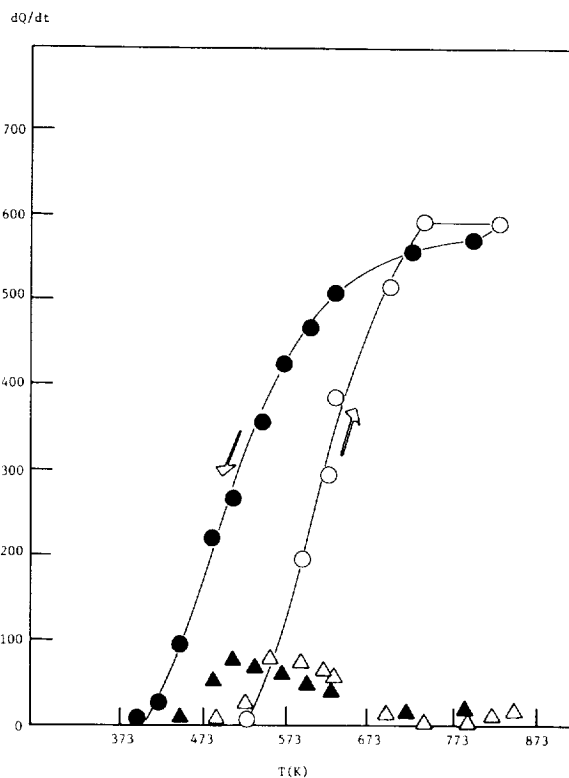
Figure 3 Comparison of thermokinetic ($\triangle$,$\blacktriangle$) and catalytic ($\bigcirc$,$\bullet$) results for CO oxidation over Pt/SiO_2 during temperature programmed investigation. Conditions as in Figure 3. $\bigcirc$,$\triangle$ denote increasing temperature and $\bullet$,$\blacktriangle$ decreasing temperature.
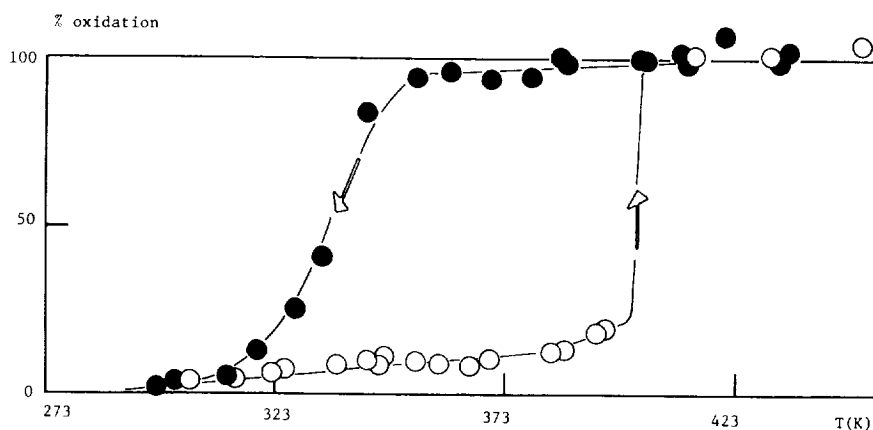
Figure 4 % oxidation of CO (when $P_{CO}:P_{O_2}:P_{N_2}$ = 15:120:520; P_{total} is 101 kPa; flow rate 40 cm^3/min) during programming 273-433-273K at 1K/min with increasing ($\bigcirc$) and decreasing ($\bullet$) temperature over Pt/SiO_2. At high temperature there is additional desorption of adsorbed CO_2. The temperature width of the hysteresis loop at 50% conversion is 60K.

304
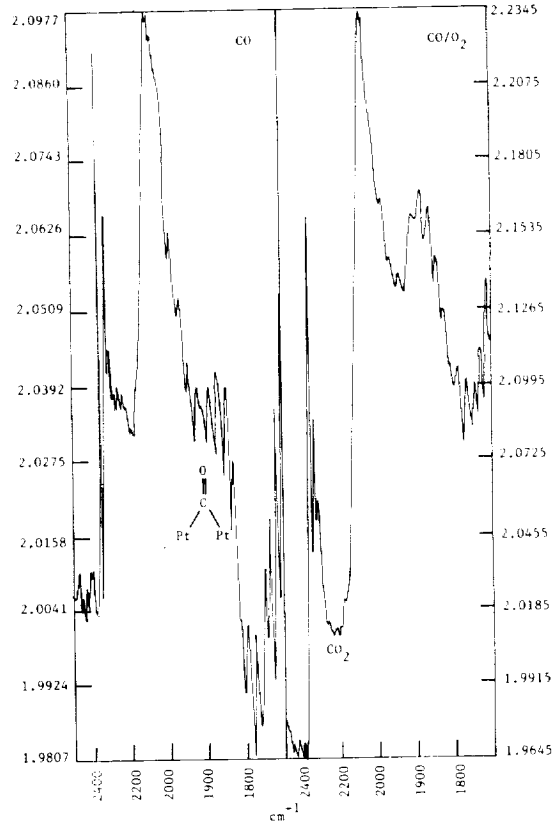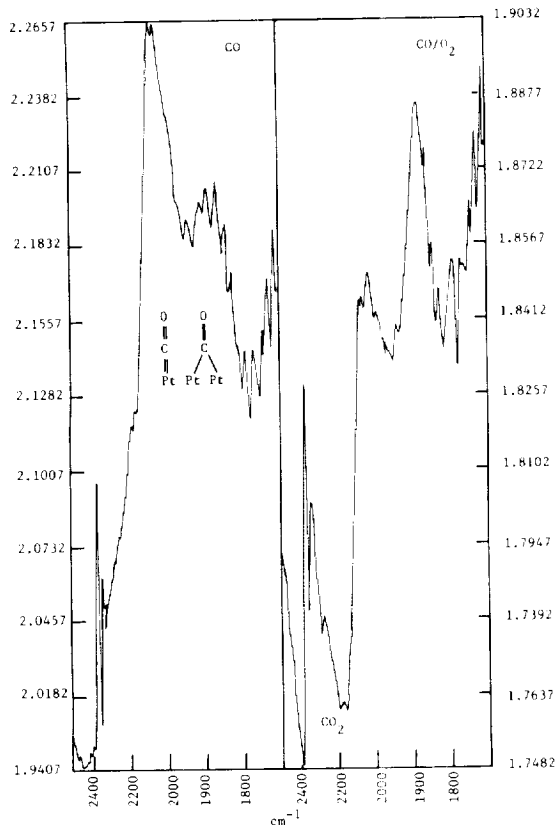
Figure 5

Figure 5 (continued)

Reflectance FTIR of two areas of the surface of a bed of Pt/SiO_2 during CO chemisorption and CO oxidation.
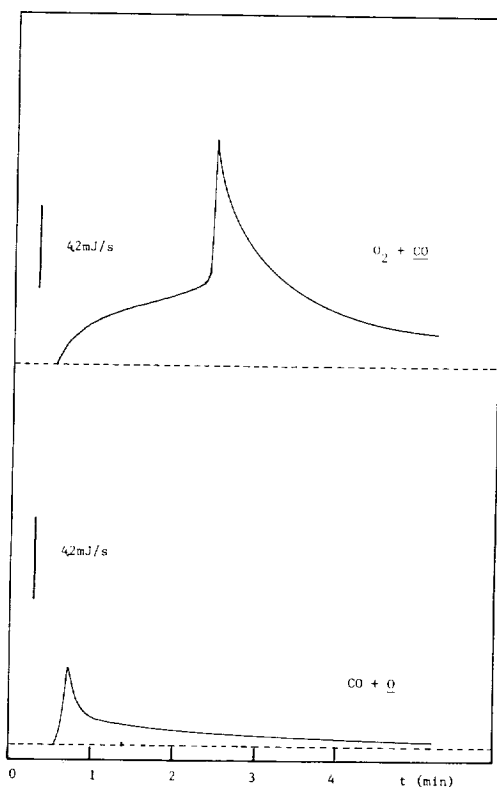
Figure 6   Thermokinetic profiles during titrations of preadsorbed $\underline{O}$ by $CO_{(g)}$ and preadsorbed $\underline{CO}$ by $O_{2(g)}$ on Pt/TiO_2. The former shows a greater contribution from the precursor step to that for Pt/SiO_2 (seen in Figure 1).
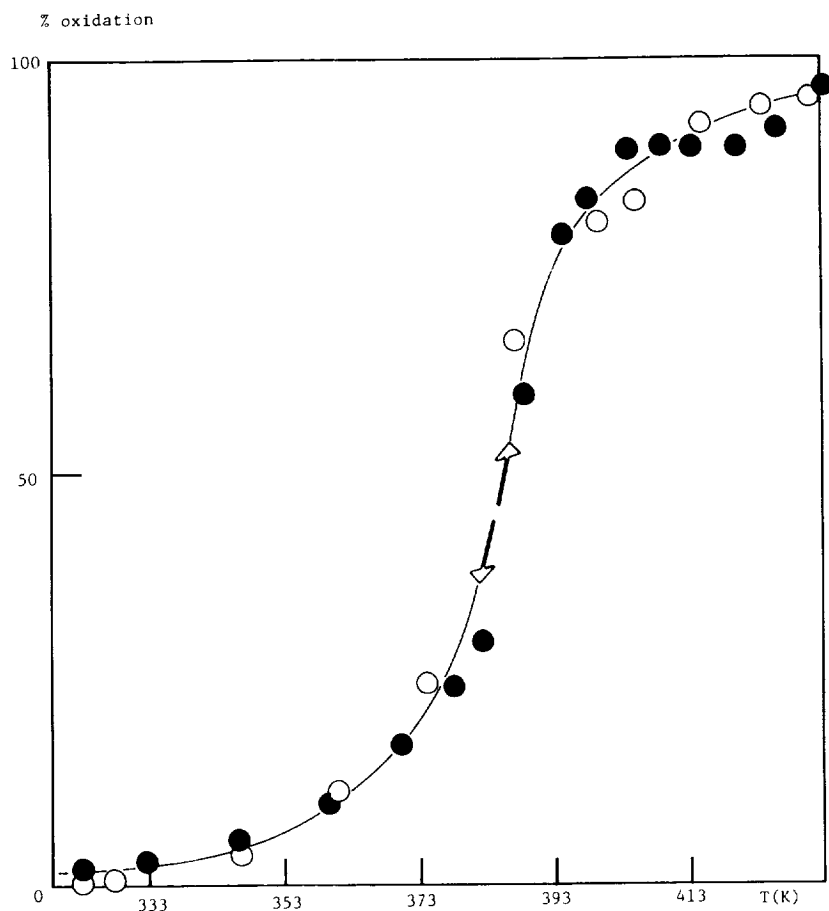
% oxidation

Figure 7   % oxidation of CO under the conditions in Figure 4 over Pt/TiO_2.
○ and ● denote data with increasing and decreasing temperature.
The catalysed reaction occurs at a faster rate at lower temperatures
over this catalyst than Pt/SiO_2 (see Figure 4) and without activity-T
hysteresis seen when temperatures decreased.

Analysis of Pt/SnOx During Catalysis of CO Oxidation

Paul A.Sermon, Valerie A.Self and E.P.S.Barrett
Department of Chemistry, Brunel University, Uxbridge, Middx., UB8 3PH, UK

SUMMARY

Temperature-programmed reduction using 6kPa H_2 suggests that a sample consisting of 3%Pt supported directly on SnO_2 is, under conditions of catalysis of CO oxidation used here, best represented as 3%Pt/SnO$_x$ since the support is likely to partially reduced, probably in the vicinity of the metal/oxide interface. Catalytic measurements at 421-424K show that this 3%Pt/SnO$_x$ is significantly more active per unit area of Pt than 6%Pt/SiO$_2$ in catalysing the oxidation of CO. In-situ micro-FTIR reveals that while the latter has predominantly linearly bound CO on the surface under reaction conditions, the Pt/SnO$_x$ also has a species absorbing at 2168cm^{-1} which may be CO upon Pt in a positive oxidation state or weakly chemisorbed CO on zero-valent Pt. This may be directly involved in the low temperature oxidation of CO on the Pt/SnO$_x$ since being weakly held the activation energy for its surface diffusion to the metal/oxide interface will be low; such mobile species could allow the high rates of surface transport and an increase in the fraction of the surface over which the CO oxidation occurs. FTIR also reveals carbonate-type species on the P/SnO$_x$ surface.

INTRODUCTION

Earlier papers by the present authors (ref.1,2) have illustrated the use of calorimetric, catalytic-activity and micro-FTIR measurements during CO oxidation on oxide-supported Pt catalysts. Here some of these analyses are applied to Pt/SnO$_x$ which are relevant to catalysts for the recombination of CO and O_2 in CO_2 lasers. It was a number of years ago that studies at Brunel (ref.3) showed that 2%Pd/SnO$_2$ was more active than 2%Pd/SiO$_2$ in that it achieved a given rate of CO oxidation at a temperature some 60K below that required on the silica-supported catalyst.

CATALYSTS

EuroPt-1 Pt/SiO$_2$ has been described elsewhere (ref4). 3%Pt/SnO$_x$ was prepared by impregnation of the support with H_2PtCl_6 (Johnson Matthey); after equilibration for 24h at room temperature, the catalyst was dried at 393K for 18h and then calcined at 773K for 6h.

While 1g of the reduced Pt/SiO$_2$ sample chemisorbed 168-188μmol H_2, only 14.2μmol H_2 were chemisorbed on the same weight of Pt/SnO$_x$, and furthermore this was very dependent upon the temperature of reductive pretreatment. This means that the Pt dispersion and surface area (58.2 m^2/g) was rather modest for Pt/SnO$_x$ and may in future be greatly increased. Temperature-programmed reduction showed that the Pt in this catalyst promoted the reduction of the support at temperatures below those where the support alone would have reduced to give Pt/SnO$_x$ with x<2; it is likely that this reduction is predominantly at the metal-oxide interface.

METHODS

The CO oxidation reaction was followed at 421-4K over 0.06-0.01g catalyst in a microflow reactor with a stream consisting of 1.64kPa CO and 1.78kPa O_2 with a N_2 balance to 101kPa which flowed at 21.1cm^3/min; in in-situ micro-FTIR analysis the reactant partial pressures and flow rates were within 1.67kPa CO and 1.86kPa O_2. Rates of CO oxidation were measured after reduction in H_2 at 423K for 30min and flushing in N_2 at the same temperature for 10min. Gas chromtography was used to determine product [CO_2] concentrations at 10min intervals.

A spectra-Tech FTIR-PLAN microscope was used in conjunction with a Perkin Elmer 1710 FTIR spectrometer. Reflectance IR spectra were measured with a resolution of 8cm^{-1} within a field of view of 795µm and those for the surface before reaction subtracted.

RESULTS

From Table 1 it is clear that per surface Pt atom detected by hydrogen chemisorption Pt/SnO$_x$ is significantly more active than Pt/SiO$_2$ at 423K.

Table 1 Activities in CO oxidation (under conditions indicated in text)

| T(K)	t(min)	%conversion CO	molCO/gPt/min	molec/Pt$_s$/min	
424.1	20	8.72	1.31	0.26	
423.6	30	11.52	1.74	0.34	Pt/SiO$_2$
423.2	40	17.80	2.67	0.52	
424.4	10	19.47	1.12	1.19	
421.5	20	29.23	1.69	1.79	
420.5	30	38.27	2.22	2.35	Pt/SnO$_x$
420.5	40	30.97	1.79	1.90	
424.4	50	43.15	2.48	2.62	

CO catalysis and chemisorption on Europt-1 Pt/SiO$_2$ revealed a peak at 2080 cm-1 corresponding to linearly-bound CO on the platinum surface (black band in Figure 1). However, in addition to this CO on Pt/SnO$_x$ also showed a band at 2168cm-1 (see hatched band Figure 1); in no case was there strong evidence of bridge-bound CO. This band at 2168cm-1 on tin-oxide supported Pt is quite significant and further consideration will be given to this.

In addition during CO oxidation on Pt/SnO$_x$ bicarbonate sbands (1775, 1726, 1676, 1595, 1580, 1440-1490, 1320-1300 and 1275cm-1),were seen and these may correspond to bicarbonate species (ref.5) arising from adsorption of product CO$_2$ on the hydroxylated SnO$_x$:
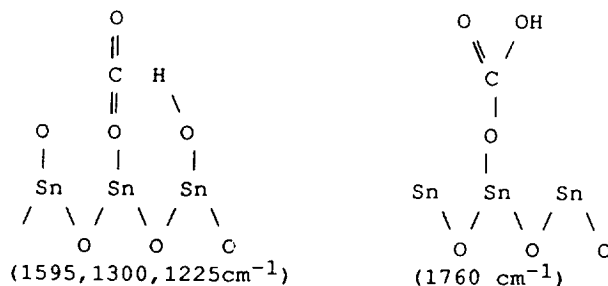
DISCUSSION & CONCLUSIONS

It has been proposed (ref.3) that the mechanism of CO oxidation on Pd/SnO$_x$ involves a synergy between the metal and the support with area around the interfacial contacts being active. CO may migrate from the metal to the oxide where additional oxidation occurs:

$$CO + O^{2-}\text{-}Sn^{4+}\text{-}O^{2-} = CO_2 + \square\text{-}Sn^{x+}\text{-}O2$$
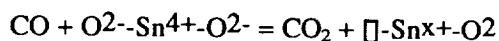
where oxygen vacancies in the SnO$_x$ are then removed on direct O$_2$ adsorption. The present Pt/SnO$_x$ results are consitent with this picture and as a result per unit area of Pt,

Pt/SnO$_x$ is more active in the CO oxidation reaction than Pt/SiO$_2$ alone. Hydrogen chemisorption reveals the close interaction between the Pt and the SnO$_x$ with even mild reduction causing a loss of adsorption capacity as a result of SnO$_x$ decoration of the Pt in essentially a low temperature SMSI type process. In this context it is interesting that the binding energy for Pt upon silica (i.e.Pt 4f(7/2)=71.4eV) is lower than on SnO$_x$ (75eV), suggesting that the tin-oxide sustains the Pt thereon in a positive oxidation state. Equally, conductivity measurements show that Pt modifies the solid-state properties of the tin oxide.

Clearly from Figure 1 in various parts of the Pt/SnO$_x$ surface the weakly-held CO has a concentration which is variable in comparison with the strongly-held CO, and so as one would expect there is surface heterogeneity. Consider now the mode of increase in CO oxidation activity and the surface species involved. FTIR reveals (in addition to linearly-bound CO (ref.6) an additional band at 2168cm^{-1} which is close to that attributed to stretches for physically-held CO on Rh$^+$ (ref.7) or indeed even gaseous CO (2143cm^{-1}); here we assume that this is weakly-held CO. It would be this CO which would *spillover* onto the supporting SnO$_x$ most easily and with the smallest activation energy barrier. Thus a weakly bound surface species may be directly involved in the accelerated oxidation on Pt/SnO$_x$ in line with earlier postulates (ref.8).

ACKNOWLEDGMENTS

REFERENCES

1. P.A. Sermon, V.A. Self, M.S.W. Vong, A.T. Wurie and N.D. Hoyle, (1st NASA paper at 1989 meeting).

2. V.A. Self and P.A. Sermon, (2nd NASA paper at 1989 meeting).

3. G.C. Bond, L.R. Molloy and M.J. Fuller, J. Chem. Soc. Chem. Commun., 796, (1975).

4. A. Frennet and P.B. Wells, Appl. Catal., 18, 243, (1985).

5. E.W. Thornton and P.G. Harrison, Trans. Far. Soc., year, vol, 461.

6. A. Crossley and D.A. King, Surf. Sci., (1977), 68, 528; Surf. Sci., (1980), 95, 131; S.R. Bare, P. Hofman and D.A. King, Surf. Sci., (1984), 144, 347; R.P. Eischens and W.A. Pliskins, Adv. Catal., (1958), 10, 1; G. Blyholder, J. Phys. Chem., (1964), 68, 2772.

7. J.T. Yates and G.L. Haller, J. Phys. Chem., (1984), 88, 4660.

8. D.A. Dowden, Annual Reports on Progress of Chemistry C in, 1979, (1980), 76, 3, (RSC).
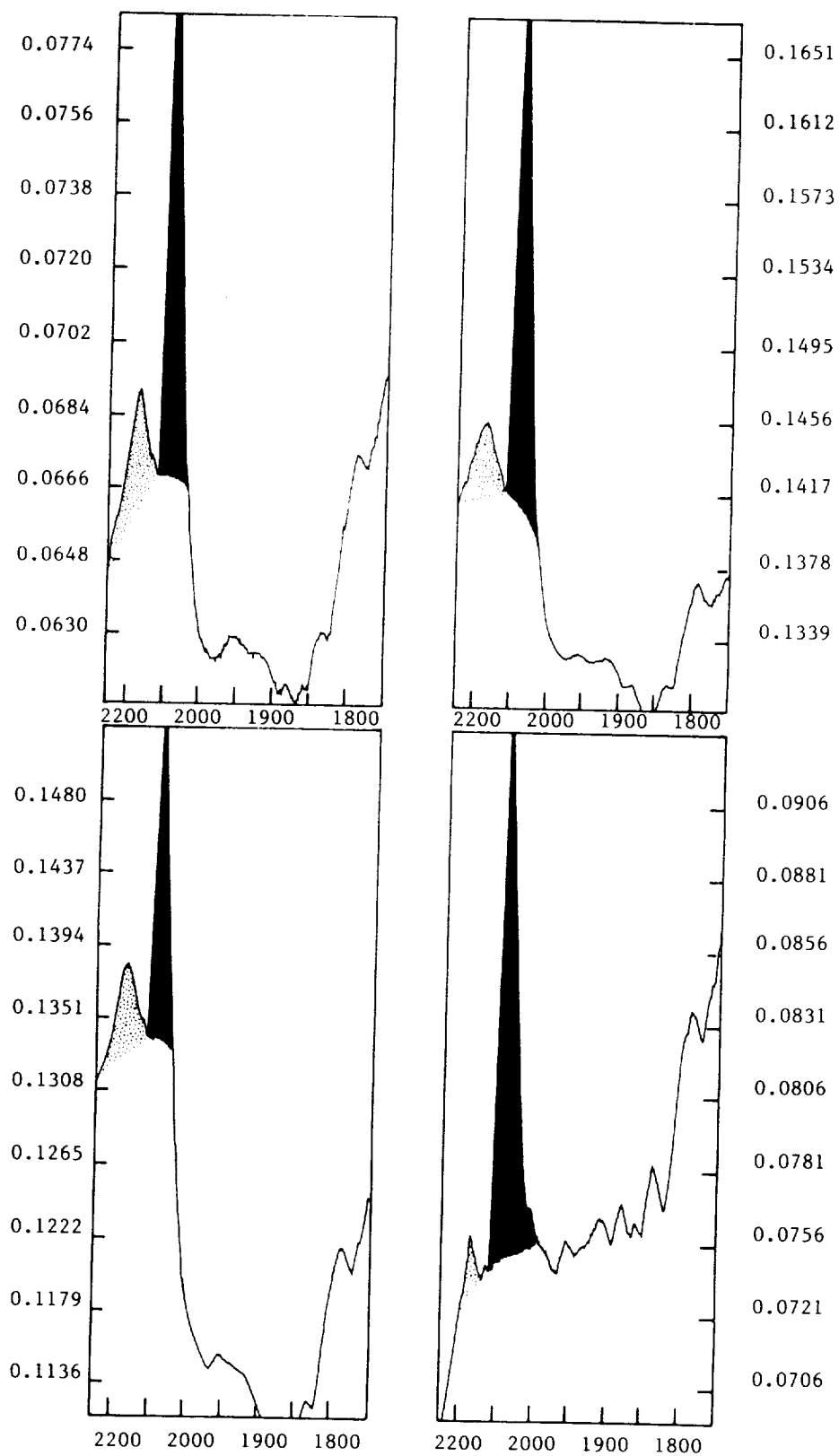
Figure 1 Reflectance FTIR for weakly-held (hatched) and linearly-bonded (black) surface-CO species during CO oxidation on Pt/SnO_x at measured in different segments of its surface

CHARACTERIZATION OF THE SURFACES OF PLATINUM/TIN OXIDE BASED CATALYSTS BY FOURIER TRANSFORM INFRARED SPECTROSCOPY (FTIR)

Joseph T. Keiser[*] and Billy T. Upchurch
NASA Langley Research Center
Hampton, VA 23665

INTRODUCTION

A Pt/SnO_2 catalyst has been developed at NASA Langley that is effective for the oxidation of CO at room temperature (1). A mechanism has been proposed to explain the effectiveness of this catalyst (2), but most of the species involved in this mechanism have not been observed under actual catalytic conditions. A number of these species are potentially detectable by Fourier Transform Infrared Spectroscopy (FTIR), e.g., $HOSnO_x$, $(HO)_yPtO_z$, $Pt \cdot CO$, and $SnHCO_3$. Therefore a preliminary investigation was conducted to determine what might be learned about this particular catalyst by transmission FTIR.

The main advantage of FTIR for this work is that the catalyst can be examined under conditions similar to the actual catalytic conditions. This can be of critical importance since some surface species may exist only when the reaction gases are present. Another advantage of the infrared approach is that since surface vibrations are probed, subtle chemical details may be obtained.

The main disadvantage of this approach is that FTIR is not nearly as sensitive as the Ultra High Vacuum (UHV) surface analytical techniques such as Auger, Electron Spectroscopy for Chemical Analysis (ESCA), Electron Energy Loss Spectroscopy (EELS), etc. Another problem is that the assignment of the observed infrared bands may be difficult.

* NASA/ASEE Faculty Fellow, Summer 1989. Current Address:
Department of Chemistry, Virginia Commonwealth University, Richmond, VA 23284

EXPERIMENTAL

The "NASA 12C" catalyst (6.43% Pt, 44.35% SnO_2, 49.22% SiO_2 (dry wt.); 4% water by ignition, 80 m^2/g B.E.T. surface area), and some of its components, Davidson Silica gel (Grade 11, Mesh 28-200), SnO_2 (made in house by the dissolution of tin with nitric acid) were pressed into neat half inch diameter pellets weighing around 20-30 milligrams each. A pellet was held between 2 stainless steel washers in the middle of a specially designed infrared cell. (A detailed description has been given previously (3)). This cell was connected by a stainless steel tube to a vacuum system which enabled gases to be exchanged with the cell while it was in the sample compartment of the FTIR. The cell could also be heated and cooled without being removed from the FTIR.

The vacuum system used was an all welded bakeable stainless system which was pumped by a turbomolecular pump backed by a mechanical pump. The base pressure of the system was around 1×10^{-7} Torr. The surface was probed by transmission FTIR using a Nicolet 5PC system with 4 wavenumber resolution. All gases used were of research grade.

RESULTS AND DISCUSSION

Reference Spectra

Initially, reference spectra of "neat" pellets of the NASA 12C catalysts, SiO_2, and SnO_2 were recorded. The SiO_2 spectrum contained a broad OH stretching band between 3750 and 2800 cm^{-1}, two unknown bands at approximately 1950 cm^{-1} and 1868 cm^{-1}, the water scissor mode at 1635 cm^{-1}, and a band at 1264 cm^{-1}. Below 1264 cm^{-1} the sample was highly absorbing, probably due to various Si-O-Si modes. The unknown bands at 1950 and 1868 cm^{-1} were present in the as received material, and these are assumed to be due to some sort of contaminant picked up in the

manufacturing process. The 1635 cm^{-1} band was observed to significantly decrease as the sample was exposed to dry air. However, this band could not be completely removed at room temperature, even after being purged with dry air for two and a half days. In fact, even after baking the catalyst at 125°C for one hour this band was still observed. Obviously some water is strongly held by the silica gel.

The spectrum of a neat pellet of SnO_2 was also recorded. SnO_2 fundamental and combination bands have been reported at various wavelengths between 1560 and 300 cm^{-1}(4). We also observed many absorption bands in this region. However, many bands were observed that could not be attributed to SnO_2. For example, a strong band in the OH stretching region (around 3500 cm^{-1}) was observed. Also observed was a band in the CH stretching region (around 2900 cm^{-1}, and a band in the carbonyl region at 1731 cm^{-1}).

Since the SnO_2 was produced by the reaction of tin with nitric acid, it was expected that some nitrates might be detected. Indeed, strong bands were observed at 1600, 1506, and 1240 cm^{-1}, which could possibly be due to the presence of nitrates. In the preparation of this material the final product is baked only to several hundred degrees Centigrade to avoid sintering and loss of surface area. However, it is apparent that some contaminants are not removed under these conditions. It is not known at this time what role, if any, these contaminants play in the catalytic mechanism.

The transmission spectrum of a neat pellet of the NASA 12C catalyst was also analyzed. The platinum was added to this catalyst by way of a platinum ammonia complex which was then reduced with formic acid. Therefore, we were concerned that some additional contamination might be present from this procedure. However, the bands observed were essentially identical to those observed in the silica gel and/or the SnO_2. i.e., no bands due to the platinum incorporation procedure were observed.

Effect of Pretreatment

The effect of the pretreatment on the NASA 12C catalyst was investigated as follows. First, the catalyst was heated under vacuum. The

315

temperature was slowly brought up to 125°C and then held at that temperature for 1 hour. No significant changes in the infrared spectrum were observed as a result of this treatment. At this point 50 Torr of CO was allowed into the cell. Spectra were recorded after 10 minutes and 35 minutes. The new features observed were due to gas phase CO_2 (doublet between 2300 and 2400 cm^{-1}), gas phase CO (doublet between 2100 and 2230 cm^{-1}) and chemisorbed CO (2070 cm^{-1}). The location of the chemisorbed CO peak is consistent with the linear or "atop" Pt-CO species. The bridge bonded Pt$_2$CO species which normally absorbs in the vicinity of 1840 cm^{-1} was not observed. It is interesting to note that the intensity of the Pt·CO peak observed was only 0.01 Absorbance units. This value is dramatically smaller than the intensity that is normally observed for CO chemisorption on supported platinum. Bastein et. al. observed that a 50/50 Pt/Sn alloy supported on alumina had a 5 fold reduction in the intensity of the chemisorbed CO peak compared to unalloyed platinum (5). Given this size of pellet and platinum loading in our experiments the reduction of the chemisorbed CO peak is somewhere between a factor of 20 and 100! In other words, the presence of the tin oxide has significantly altered the nature of the platinum, probably due to the formation of some kind of alloy.

Compared to the spectrum taken after 10 minutes the 35 minute exposure produced more CO_2 but there was no significant change in the chemisorbed CO peak. This indicates that the steady state concentration of chemisorbed CO was reached in 10 minutes or less. The cell was then cooled to 38°C and evacuated for 10 minutes. This resulted in the removal of gas phase CO and CO_2 but caused no significant change in the chemisorbed CO peak; however, after an overnight evacuation virtually all of the chemisorbed CO was removed.

Room Temperature Absorption of CO

The room temperature uptake of CO on NASA 12C was also investigated. Following the reductive pretreatment described above the catalyst was exposed to various concentrations of CO gas in a static cell at room temperature. Exposures of 1, 4, 9, and 50 Torr of CO were used. A graph of the chemisorbed peak height as a function of the CO gas pressure is given on the next page.
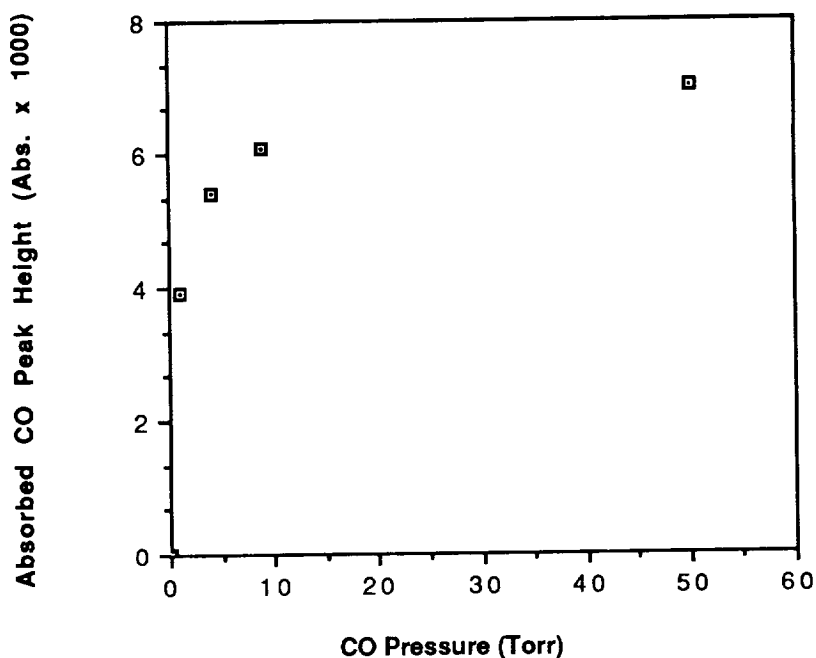
The shape of the above graph is apparently logarithmic. This is not surprising since there are a finite number of sites which become filled as the CO pressure is increased and then regardless of further increases in the pressure no more CO will chemisorb. This would mean that full coverage for this particular sample (19 mgs) is around 7 milliabsorbance units. When the sample was heated to 125°C and exposed to 50 Torr CO then the peak height was 10 milliabsorbance units. The fact that this is higher than the room temperature exposure could be due to the precision of the measurement or it could mean that some sites have a higher activation energy barrier than others. This latter view is supported by the fact that the CO which chemisorbed at room temperature was more easily pumped off than the CO chemisorbed at 125°C. In fact approximately 4 times as much CO was present after 10 minutes of evacuation for the case in which CO was absorbed at 125°C, versus CO absorption at room temperature.

It is interesting to note that as the CO coverage was increased, the CO absorption maximum decreased. For example, when the CO pressure was 1 Torr the absorption maximum was 2088 cm^{-1}, but when the CO pressure was 50 Torr it had shifted to 2070 cm^{-1}. These kinds of shifts are

generally attributed to dipole-dipole coupling of neighboring CO's and normally the absorption maximum increases with CO coverage (5).

Effect of Catalyst Reduction in Hydrogen

The catalyst was exposed to 400 Torr of H_2 and heated. Spectra were taken at the following invervals: a) 15 minutes at 35°C; b) 30 minutes at 50°C; c) 35 minutes at 100°C; d) 30 minutes at 150°C; e) cooled to room temp and evacuated for 2 and 1/2 days. In the initial spectrum (a), two strong and sharp bands were observed at 1159 and 1100 cm^{-1}. These bands were gone when spectrum (b) was recorded. Most likely these are OH bending modes due to the presence of SnOH and/or SiOH. This treatment also caused a steady decrease in most of the "impurity bands" described earlier in the section entitled Reference Spectra.

After the above treatment was completed the catalyst suprisingly would not chemisorb CO at either room temperature or elevated temperatures (140°C). All attempts to restore the catalyst's ability to chemisorb CO were unsuccessful. These included baking the catalyst in oxygen and water vapor (to 200°C). Ultra High Vacuum studies on this catalyst have shown that a high temperature reduction in hydrogen causes an irreversible migration of impurities such as silicon to the surface[*]. These impurities are apparently responsible for the supressed CO chemisorption we have observed.

Presence of Bicarbonates

Surface hydroxyl groups have sometimes been observed to react with CO_2 to form bicarbonates. The proposed mechanism for the degradation of this catalyst involves a tin bicarbonate species. Since FTIR has been used to observe surface bicarbonates in other systems (3) it was hoped that a bicarbonate species might be observed in these experiments. Yet, no bicarbonates or carbonates were observed under any of the conditions tested, including an experiment in which the catalyst was exposed to 10

[*] Hoflund, Gar B., University of Florida, private communication.

Torr of CO_2 and heated 2 hours at 50°C. However, the degradation of the catalyst occurs very slowly over a period of months under conditions in which the catalyst is constantly exposed to CO and O_2. The FTIR experiments conducted to date do not even remotely approach these conditions.

CONCLUSIONS

This preliminary FTIR study of the NASA Pt/SnO_2 CO oxidation catalyst has shown the following:

1. The catalyst contains suprisingly high levels of impurities which are detectable by FTIR.
2. The chemisorption of CO on platinum is dramatically reduced by the presence of the tin oxide, probably due to alloy formation.
3. The reduction of this catalyst in hydrogen at 150°C causes total and irreversible loss of CO chemisorption.
4. No carbonate or bicarbonate species were observed under the conditions tested.

REFERENCES

1. Upchurch, Billy T.; Schryer, David R.; Wood, George M.; and Hess, Robert V.: Development of CO Oxidation Catalysts for the Laser Atmospheric Wind Sounder (LAWS). SPIE Proc., Vol. 1062, 1989.

2. Schryer, David R.; Upchurch, Billy T.; Hess, Robert V.; Wood, George M.; Sidney, Barry D.; Van Norman, John D.; Miller, Irvin M.; Brown, Kenneth G.; Schryer, Jacqueline; and Brown, David R.: CO-Oxidation Catalysts for Long-Life Closed-Cycle CO_2 Lasers. CO Oxidation Catalysts for Long-Life CO_2 Lasers, David R. Schryer, Ed., NASA CP-10037, pp. 7-17, 1989.

3. Booker, Carolyn P.; and Keiser, Joseph T.: Reduction of Rh^{3+} on Supported Rhodium Surfaces by CO. J. Phys. Chem., Vol. 93, No. 4, pp. 1532-1536, 1989.

4. Summitt, Robert; and Borrelli, N. F.: Infrared Absorption in Single Crystal Stannic Oxide. J. Phys. Chem. Solids, Vol. 26, pp. 921-925, 1965.

5. Bastein, A. G. T. M.; Toolenaar, F. J. C. M.; and Ponec, V.: Adsorption of Carbon Monoxide on Platinum Alloys: An Infrared Investigation. J. of Catalysis, Vol. 90, pp.88-95, 1984.

CHEMISORPTION STUDIES OF Pt/SnO$_2$ CATALYSTS

Kenneth G. Brown, Susan K. Ohorodnik, John D. Van Norman
and Jacqueline Schryer, Department of Chemistry,
Old Dominion University, Norfolk, Va

Billy T. Upchurch and David R. Schryer
NASA-Langley Research Center
Hampton, Va

INTRODUCTION

The low temperature CO oxidation catalysts that are being developed and tested at NASA-Langley are fairly unique in their ability to efficiently oxidize CO at low temperatures (~303K). The bulk of the reaction data that has been collected in our laboratory has been determined using plug flow reactors with a low mass of Pt/SnO$_2$/SiO$_2$ catalyst (~0.1g) and a modest flow rate (5 - 10 sccm). We have previously characterized the surface solely in terms of N$_2$ BET surface areas. These surface areas have not been that indicative of reaction rate. Indeed, some of our formulations with high BET surface area have yielded lower reaction rates than those with lower BET surface areas. As a result we have begun a program, initially described at the previous NASA/RSRE conference(1), of determining the chemisorption of the various species involved in the reaction; CO, O$_2$ and CO$_2$. Such a determination will lead to a better understanding of the mechanism and overall kinetics of the reaction.

The pulsed-reactor technique, initially described by Freel (2,3), is used to determine the amount of a particular molecule that is adsorbed on the catalyst. Since there is some reaction of CO with the surface to produce CO$_2$ the pulsed reactor had to be coupled with a gas chromatograph in order to distinguish between the loss of CO that is due to adsorption by the surface and the loss that is due to reaction with the surface. The experimental apparatus and the technique used to determine the number of moles adsorbed is described in the next section.

METHODS

The experimental system consists of an Shimadzu Gas Chromatograph (GC) which is equipped with a Thermal Conductivity Detector (TCD). The GC column acquired from ALLTECH® is two concentric tubes, the inner tube being filled with molecular sieve while the outer column is filled with a porapak mixture. The output from the detector is recorded on a Shimadzu CR5A integrating recorder.

The catalyst sample is contained in a stainless steel tube of 1/8" O.D. The catalyst is held between two stainless steel frits, as shown in figure 1. This tube, which is located immediately upstream of the column, is placed in a small oven which is mounted on the front of the GC. The temperature of the

catalyst can be controlled to within 0.5 C. The flow rate through the catalyst and column is 20 sccm and is monitored by a Hastings mass flow controller. All gases were High Purity. The gas mixtures all contained 2% Ne as an internal standard. These mixtures were prepared gravimetrically by Scott. The carrier gas, high purity Helium, was obtained from Union Carbide, Linde Division.

A flow schematic of the entire system is shown in figure 2. An empty tube is located in the reactor oven in addition to the tube containing the catalyst. We can switch between this tube and the reactor tube to provide an initial calibration of the system and to monitor system conditions as the reaction progresses. With this system we are able to expose the catalyst to all of the reaction conditions that have been previously used to study the reaction. We can pretreat the catalyst using our accepted procedure of 5% CO in He at 125 C for one hour. At the end of the pretreatment we can allow the catalyst to cool under Helium flow to the desired temperature. At that time we can begin introducing 1 cc pulses of the desired gas mixture onto the catalyst surface. Since it takes approximately 8 minutes to take the complete chromatogram the pulses are separated by 8 minutes. The sample is pulsed with the gas of interest until the area of the observed peak is identical to that obtained from the bypass measurements, as shown in figure 3 or until there is no discernible change in the CO concentration.

The catalyst samples were prepared at NASA-Langley using the synthetic technique described elsewhere in this issue. The particular catalysts used in this study have the following compositions by weight per cent: 1.) 5.8% Pt, 39.96% SnO_2, 54.24% SiO_2 (5%Pt/SnO_2/SiO_2); 2.) 19.5% Pt, 80.5% SnO_2(19%Pt/SnO_2); 3.) 8.55% Pt, 8.60% Pd, 35.1% SnO_2, 47.6% SiO_2(9%Pt,9%Pd/SnO_2/SiO_2). A 2%Pt/SnO_2 sample was obtained from Englehard Industries. In this paper these catalysts will also be referred to as 5% Pt, 19% Pt, 9% Pt/Pd, and 2% Pt respectively.

The BET surface areas reported herein were obtained at NASA-Langley with a Quantasorb[®] apparatus using N_2 as the adsorbate.

<div align="center">RESULTS</div>

CO ADSORPTION

The fraction of CO remaining in the gas mixture as a typical experiment progresses for both a non-pretreated and a pretreated catalyst is shown in figures 4 and 5. The changes in CO are the result of both CO adsorption and the reaction of CO with the surface to produce CO_2. In both the non-pretreated and pretreated cases the initial pulses result in a significant amount of CO_2 production, as shown in figure 6. After 400 min. (approximately 50 pulses) for the non-pretreated catalyst and 100 min. (approximately 12 pulses) for the pretreated catalyst most of the processes affecting the freestream composition have ceased and the CO concentration approaches the bypass level. The fraction of CO in the freestream does not attain the original concentration but remains below that value for times of exposure that have been

as long as 1000 min. in the case of the non-pretreated sample. CO_2 production is essentially finished in the pretreated sample after approximately 50 min. (approximately 6 pulses).

Figures 7 and 8 summarize the CO_2 production observed for all of the catalysts employed in this study. The most persistent CO_2 production occurred with the 19% Pt catalyst which also exhibits a sharp reduction in CO_2 production at 400 min. (50 pulses). After pretreatment this particular catalyst exhibited no CO_2 production. The other non-SiO_2 supported catalyst, 2% Pt, did not behave in the same manner. It continued to produce CO_2 after 400 min. in the non-pretreated case and it has the highest initial CO_2 production after pretreatment. With or without pretreating the 9%Pt/Pd catalyst is the most persistent producer of CO_2.

Correcting for the amount of CO_2 produced we can determine the amount of CO that remains chemisorbed on the surface. The total amount chemisorbed is then determined by adding the amount adsorbed per pulse until the adsorption process ceases. The point at which chemisorption ceases is taken to be when the CO freestream concentration attains a constant value. This point is determined graphically as the intersection between the curved portion of the chemisorption curve with the line extended from the level portion of the graph.

The number of moles of CO that are chemisorbed can then be used to determine the number of Pt atoms exposed on the surface assuming a particular geometry for the Pt-CO complex. The surface area occupied by these Pt atoms can then be determined using a Pt cross-sectional area of .0841 nm^2 (4). The dispersion, defined as the ratio of the number of moles of CO adsorbed to the total number of moles of metal present in the catalyst, is then calculated. The results of these calculations are summarized in Table I. The catalyst with the highest CO chemisorption surface area is the 19% Pt/SnO_2. Such a result is contrary to that obtained from N_2 BET measurements as summarized in table II.

The effect of temperature upon the surface area and the dispersion is summarized for two of the catalysts in table III. Both catalysts seem to be relatively unaffected by temperature over this temperature range. There does seem to be a slight decrease in the surface area for the 2% catalyst, although the number of experiments are too limited for the results to have much significance.

O_2 Adsorption

O_2 adsorption is not observed to occur on the non-pretreated catalysts. When the catalyst is pretreated we obtain the adsorption curve shown in figure 9. This curve is identical in shape to that observed for the CO experiment except that the freestream composition does reach its original value. In addition, CO_2 was not observed even though the catalyst had been exposed to CO during the pretreatment process. The O_2 surface area and the resultant dispersion can then be calculated and are summarized for the two catalysts studied thus far in table IV. The results in table IV are calculated with the assumption that

the following reaction occurs

$$O_2(gas) \rightarrow 2O(surface)$$

As a result each O_2 molecule occupies two sites on the surface.
The sample that had been given the normal pretreatment and
then exposed to O_2 as discussed in the preceding paragraph was
then used for a CO chemisorption experiment. Figure 10 shows the
CO_2 production with this extensive history compared to the CO
chemisorption studies of the same catalyst with no pretreatment.
The CO_2 evolution is virtually the same in both cases. The
chemisorption curve for both cases is shown in figure 11. The
chemisorption/reaction process reaches a plateau after
approximately the same number of pulses in each case. The
pretreated-oxygen exposed catalyst does seem to have a higher
initial activity than the sample with no pretreatment.

CO_2 Adsorption

Exposing the 1% CO_2 mixture to the 5% Pt non-pretreated
catalyst results in apparent chemisorption as shown in figure 12.
The apparent chemisorption is observed to be much larger when the
catalyst is pretreated but does not exist for the 2% Pt catalyst
as is also shown in figure 12. Closer examination of the
chromatograms showed that, for the 5% mixture (an SiO_2 based
catalyst), the CO_2 peaks had broadened, interfering with the Ne
peaks used as an internal standard. As a result the amount of
error in the CO_2 concentration calculation increased
significantly. When the total mass of the catalyst is reduced
this apparent chemisorption is seen to decrease significantly.
The apparent chemisorption that we have observed is therefore a
chromatographic effect due to the SiO_2 present in the catalyst.
We conclude, therefore, that the catalyst samples do not
chemisorb CO_2 from the freestream gas mixture.

DISCUSSION

Up to this point the numerical comparisons have been made
with reference to the total mass of the catalyst. The actual
catalytic material is the metal(Pt,Pd)/SnO_2 with the SiO_2 present
as a source of water to enhance catalyst longevity. To more
accurately compare catalysts with and without SiO_2 the surface
area has been calculated with respect to the amount of Pt/SnO_2
present in the material. These calculations are summarized in
table V. The surface areas of the two high metal load catalysts
are now similar, indicating that the SiO_2 is serving primarily as
a diluent and not interacting directly with the metal or the
SnO_2. However, the ratio of the CO surface area to the BET
surface area for both SiO_2 containing catalysts is still quite
low compared to the 2% Pt catalyst. This latter result is due,
most likely, to differences in synthetic technique which would
appear to allow more CO to bind to the surface of the 2% Pt
catalyst than to any of the other catalysts in this study.
It is apparent that there can be experimental difficulties

due to the design of the system which places the catalyst immediately upstream of the GC column. Should the catalyst contain material which is also an effective chromatographic material, such as SiO_2, peak resolution may be severely affected resulting in errors in the determination of concentration. We did not observe such an effect for either O_2 or CO but with CO_2, band broadening became readily apparent. Indeed the CO_2 peak was observed to not return to baseline, overlapping severely with the Neon peak. The extent of the broadening could be affected by reducing the amount of material that is used and by the physical nature of the catalyst. The effect was not observed in the catalyst that did not contain SiO_2. In the other non-pretreated catalyst the chromatographic effect was observed to disappear when the mass of the catalyst material was reduced. However, significant error still occurred when the SiO_2 containing catalyst underwent our standard pretreatment. The retention of CO_2 by the catalyst seems to be altered in some manner. What effect this has on catalyst activity and/or catalyst longevity is unknown at this time.

Another problem with the technique is the inability, in some of the samples, to attain the bypass value of the freestream composition after long exposure of the catalyst to the gas of interest. Since attaining the bypass value was not a problem when O_2 was the gas of interest or when CO was passed over a passive material such as SnO, it is thought that the non-attainment of the bypass value is due to some equilibrium process between the gas phase and the surface. A possibility would be the presence of physisorbed CO which, upon leaving the surface, creates a vacant site for gas phase adsorption. The time scale of this process could be such that the released CO is not observed on the chromatogram, possibly appearing on the wings of bands or as part of a weak broad background. Such an explanation would require that, for these sites, the adsorption process is much faster than the desorption process although desorption should be essentially finished in approximately 8 minutes, the time between pulses. Experiments are currently underway where the time between pulses is varied to evaluate whether or not such an equilibrium is of importance.

CO can chemisorb upon a surface in at least two different configurations, either linear or bridged(5). The surface area will then depend upon the geometry chosen for the chemisorbed species with the bridged configuration essentially occupying two sites with twice the coverage of the linear configuration. O_2 is assumed to dissociate upon contact with the surface resulting in two surface sites for each molecule of O_2. If we assume that dissociation is occurring then the results of the O_2 experiments count the fraction of metal atoms exposed to the surface. If it is further assumed that these same atoms provide sites for CO adsorption then a comparison of O_2 chemisorption with CO chemisorption should provide an indication of the geometry of the CO chemisorbed species. The dispersion determined for 2% Pt/SnO_2 using oxygen, 0.076, compares quite favorably to that determined using CO if the linear geometry for the metal-CO complex is assumed. In contrast, the O_2 dispersion for the 5.8% $Pt/SnO_2/SiO_2$

catalyst, 0.044, is in good agreement with the CO dispersion if the bridged structure is assumed. Further work on these catalysts is in progress to determine if these apparent geometric differences depend on the presence of SiO_2 or upon the overall method of synthesizing the catalyst.

The difference for all the catalyst samples in the amount of CO chemisorbed for the pretreated and non-pretreated cases is quite large. This difference may be due in part to the presence of CO on the surface following pretreatment which would then block sites for further CO adsorption. We have not been able to observe the surface adsorbed CO spectrophotometrically with infrared spectra taken a few minutes after the pulsing of the sample is finished. Our preliminary interpretation is that the adsorbed CO will desorb particularly in the amount of time that it takes for the sample to cool from the 398 K pretreatment temperature. In addition we have already discussed the possibility that CO desorption is responsible for the concentration not reaching the bypass value for CO after a significant number of pulses. If CO is not present and blocking sites then there must be fewer sites available for adsorption after pretreatment than before pretreatment. An obvious conclusion is that there are fewer Pt atoms exposed to the surface, and that they have been covered by other atoms present in the sample. Hoflund et al (6) have observed this phenomenon in high vacuum work where they see the Sn atom becoming more dominant on the surface, effectively covering most of the Pt.

The interpretations discussed above are, of course, preliminary, with several experiments yet to be done. These include further O_2 adsorption work, and varying the time between the pulses to attempt to quantify whether or not desorption is affecting our surface area measurements. In addition, H_2 adsorption measurements must be performed to determine whether or not our conclusions about the geometry of the CO metal complex are correct.

REFERENCES

1. K. G. Brown et. al., in "Closed-Cycle, Frequency-Stable CO_2 Laser Technology" (C. E. Batten et. al. eds) NASA Conference Publication 2456, 1986 p. 219-226.

2. J. Freel, J. Catalysis, **25** 139-148 (1972).

3. J. Freel, J. Catalysis, **25** 149-160 (1972).

4. J. L. Lemaitre, P. G. Menon, and F. Delannay, in "Characterization of Heterogeneous Catalysts" (F. Delannay, ed.), Marcel Dekker, New York, U.S.A., 1984, p. 318.

5. N. V. Richardson and A. M. Bradshaw, Surface Sci. **88**, 255 (1979).

6. G. B. Hoflund, J. E. Drawdy, S. D. Gardner, M. R. Davidson, D. R. Schryer and B. T. Upchurch, This volume 1990.

TABLE I: Surface areas and dispersions determined by CO chemisorption at 303K. All calculated values refer to the linear form for the CO-metal complex.

Catalyst	Pretreated?	Surface area (m^2/g)	Dispersion
5.8%Pt/SnO$_2$/SiO$_2$	No	0.66 ± 0.18*	0.044 ± 0.010
	Yes	0.33 ± 0.05**	0.022 ± 0.0035
2%Pt/SnO$_2$	No	0.53	0.101
	Yes	0.36	0.069
19.5%Pt/SiO$_2$	No	4.91 ± 1.04**	0.097 ± 0.021
	Yes	3.37	0.0067
8.6%Pt,Pd/SnO$_2$/SiO$_2$	No	2.08 ± 0.132#	0.033 ± 0.002
	Yes	1.34	0.024

* Average of three measurements
** Average of four measurements
# Average of two measurements

Table II: A comparison of BET and CO surface areas for non-pretreated catalysts. All surface areas in m^2/g.

CATALYST	BET	CO	CO/BET
2% Pt/SnO$_2$	6.8	0.53	0.078
5.8% Pt/SnO$_2$/SiO2	80.18	0.66	0.008
19.5% Pt/SnO$_2$	100.0	4.91	0.049
8.6% Pt,Pd/SnO$_2$/SiO$_2$	118.6	2.08	0.018

Table III: Temperature dependence of the surface area and dispersion for two of the catalysts.

Temperature (K)	2%Pt/SnO$_2$		5.8%Pt/SnO$_2$/SiO$_2$	
	Area (m^2/g)	Dispersion	Area (m^2/g)	Dispersion
303	0.36	0.069	0.33	0.02
323	0.31	0.059	0.24	0.016
348	0.30	0.057	0.33	0.022

Table IV: Surface area and dispersions for O_2 chemisorption measurements at 303K.

Pretreatment?	2% Pt/SnO$_2$ Area (m^2/g)	Dispersion	5.8% Pt/SnO$_2$/SiO$_2$ Area (m^2/g)	Dispersion
No	0.0	0.0	0.0	0.0
Yes	0.39	0.076	0.66	0.044

TABLE V: Surface areas and the ratio of surface areas based on the amount of Pt/SnO$_2$ present in the total sample.

Catalyst	Pretreated?	Surface area (m^2/g)	CO/BET
5.8%Pt/SnO$_2$/SiO$_2$	No	1.44	0.018
	Yes	0.72	
2%Pt/SnO$_2$	No	0.53	0.078
	Yes	0.36	
19.5%Pt/SiO$_2$	No	4.91	0.049
	Yes	3.37	
8.6%Pt,Pd/SnO$_2$/SiO$_2$	No	4.98	0.034
	Yes	2.57	
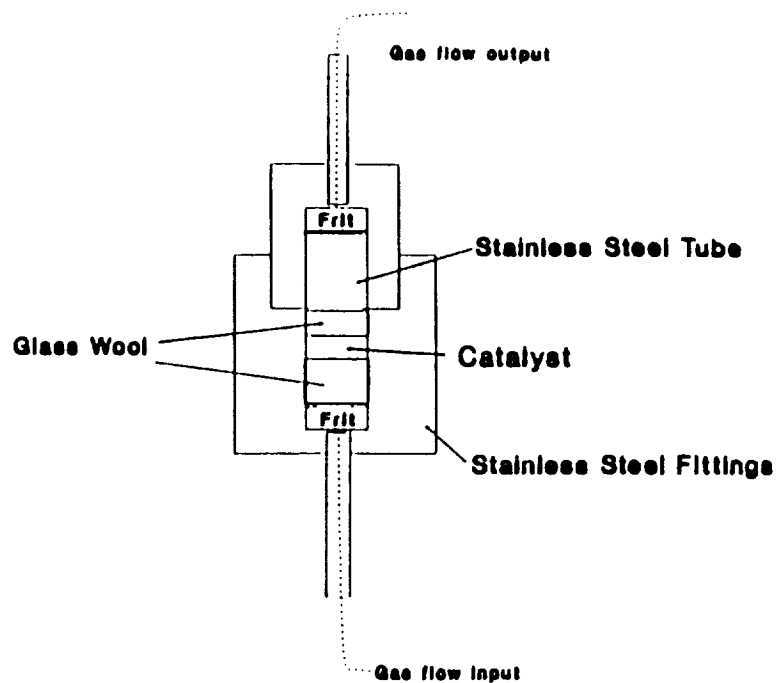
Figure 1: The sample holder for the catalyst.
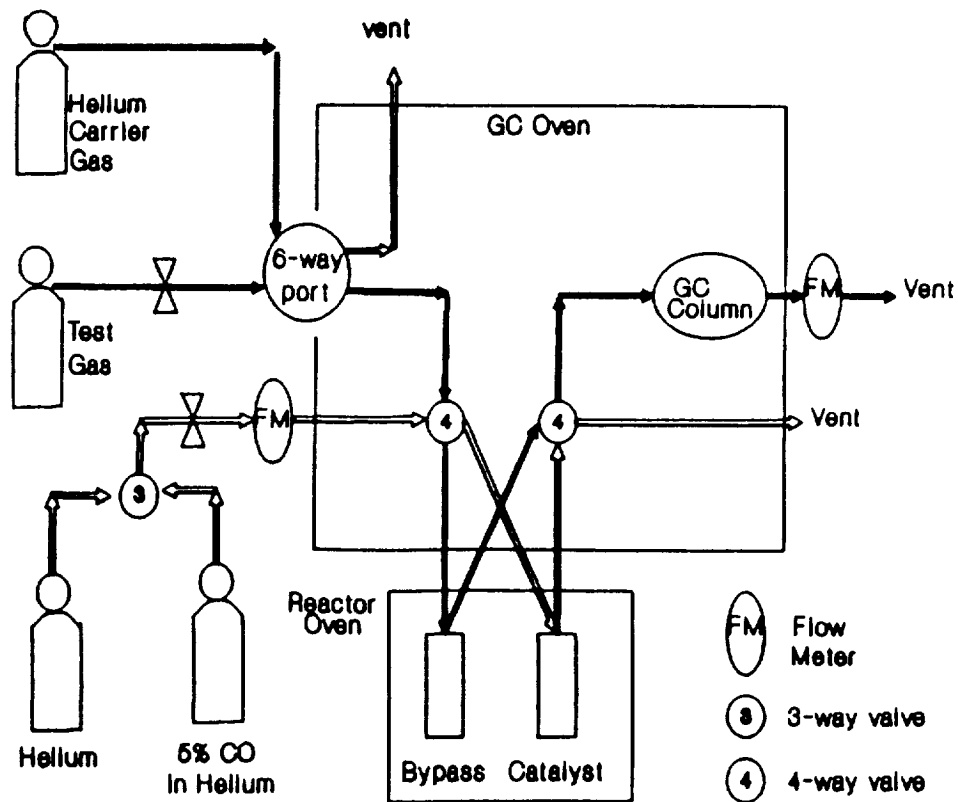
Figure 2: The flow diagram for the pulse reactor.

Time
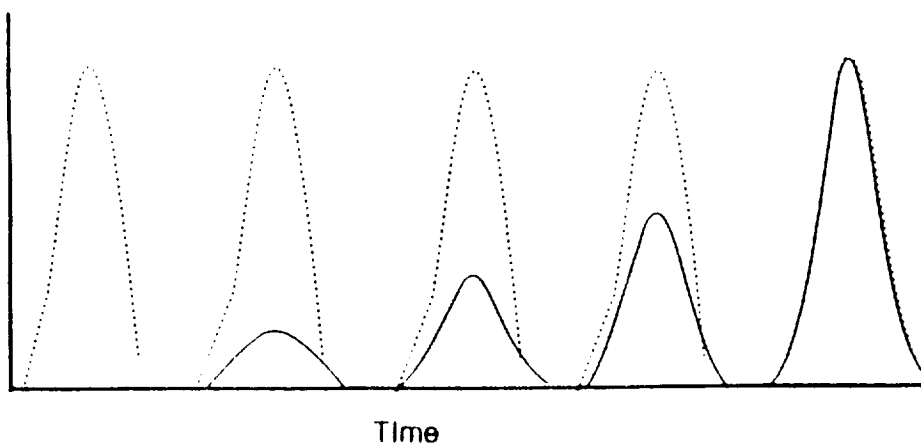
Figure 3: The dashed curves represent an observed GC peak with no catalyst present. The solid curves represent a model experiment with catalyst present. At the left complete adsorption of the gaseous material occurs while at the right the area again matches the original (bypass) area.
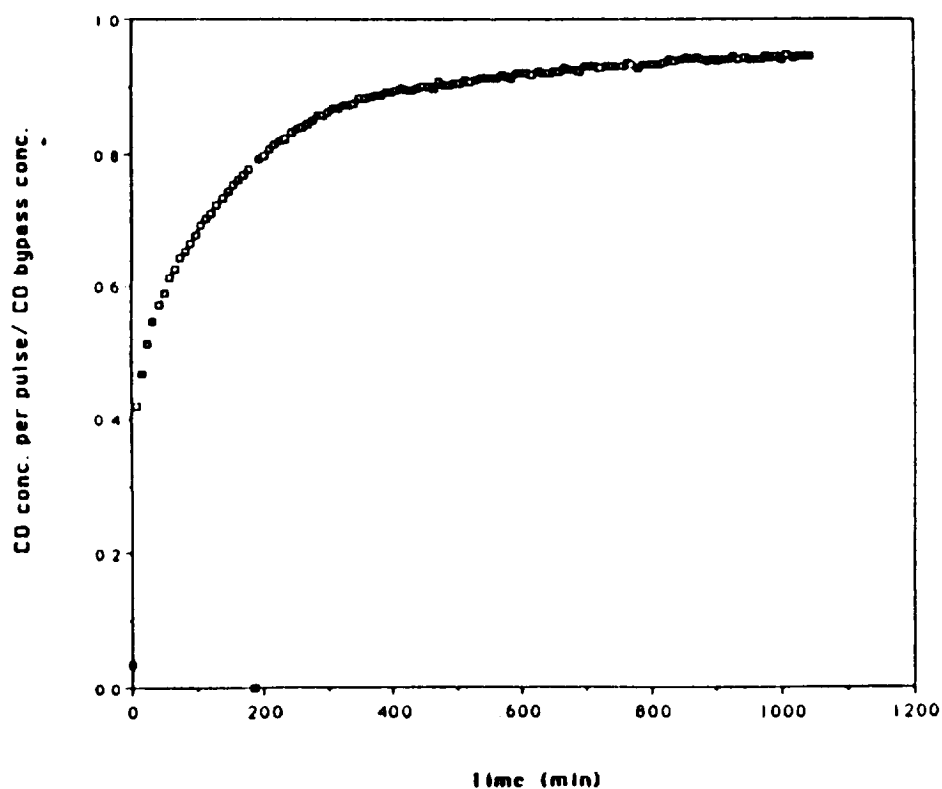
Figure 4: CO concentration as a function of time (number of pulses) for a non-pretreated 5.8% Pt/SnO_2SiO_2 catalyst at 303 K using 1% CO, 2% Ne, balance He as the pulsing gas.
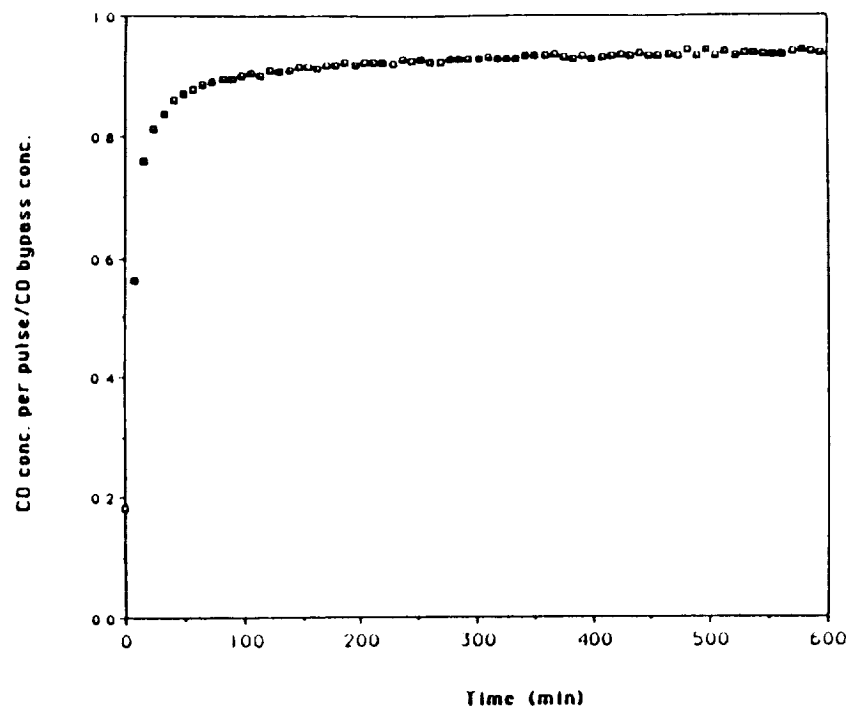
Figure 5: Same as figure 4 except the catalyst has been pretreated.
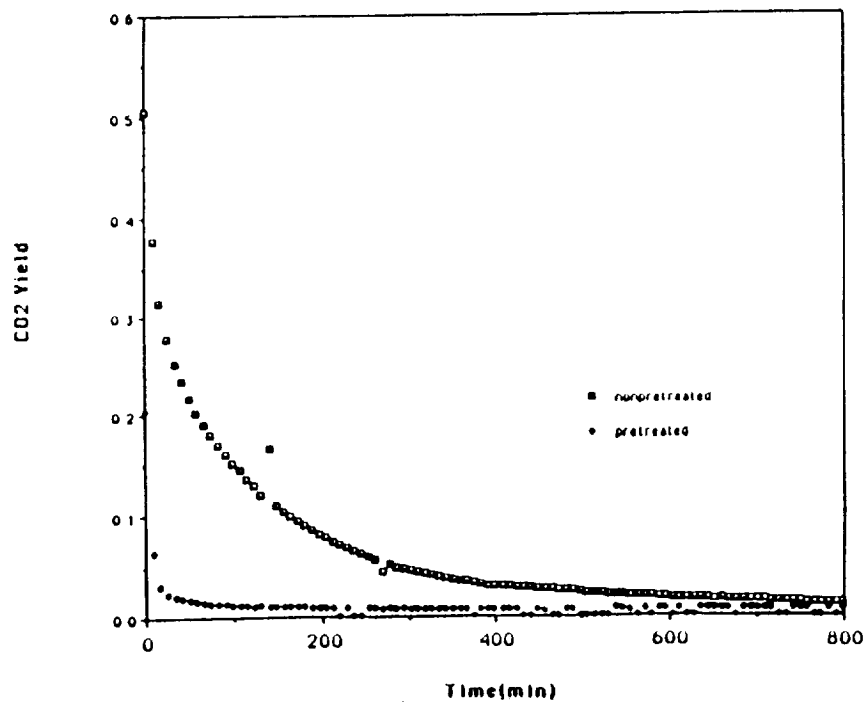
Figure 6: Carbon dioxide yield for the nonpretreated, □ , pretreated, ♦. The sample is the same as that in figure 4 and 5.
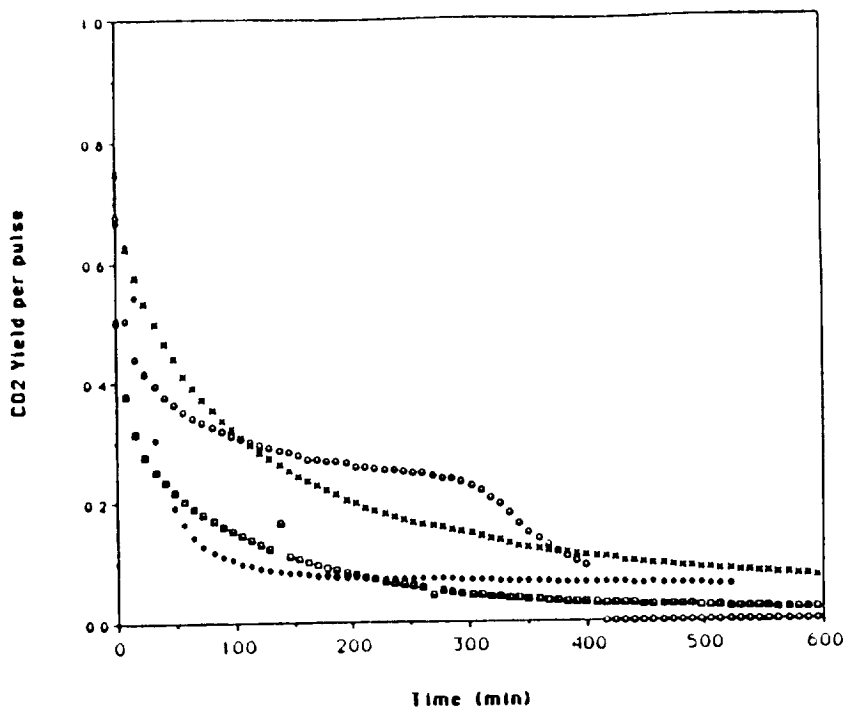
Figure 7: A summary of the CO_2 yields for the four non-pretreated catalysts at 303 K; ○ 19.5% Pt/SnO_2, x 8.6% Pt/8.6% pd/SnO_2/SiO_2, □ 5.8%Pt/SnO_2/SiO_2, ◆ 2% Pt/SnO_2.
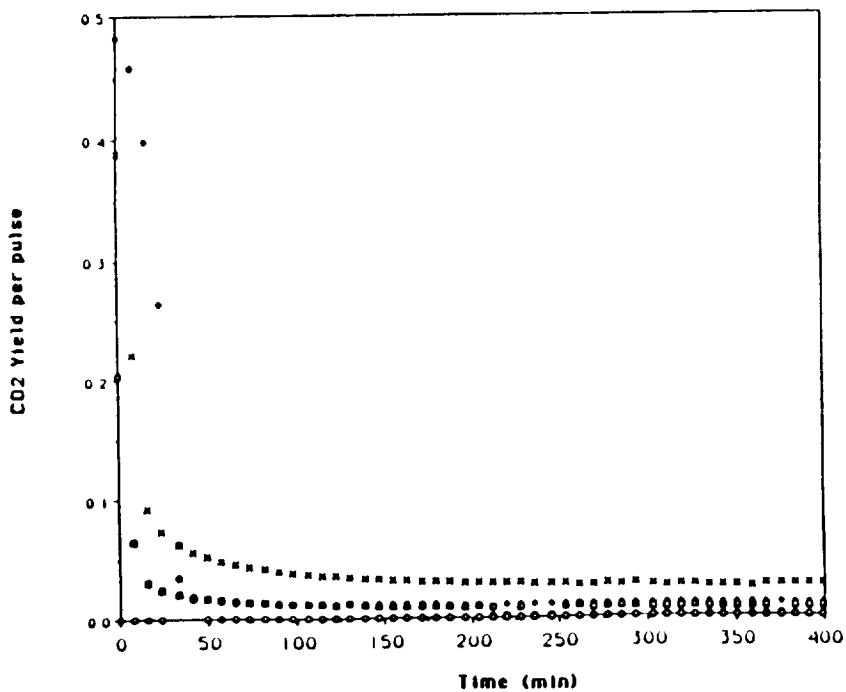
Figure 8: A summary of CO_2 yields for the four pretreated catalysts at 303 K. The symbols have the same meaning as in figure 7.
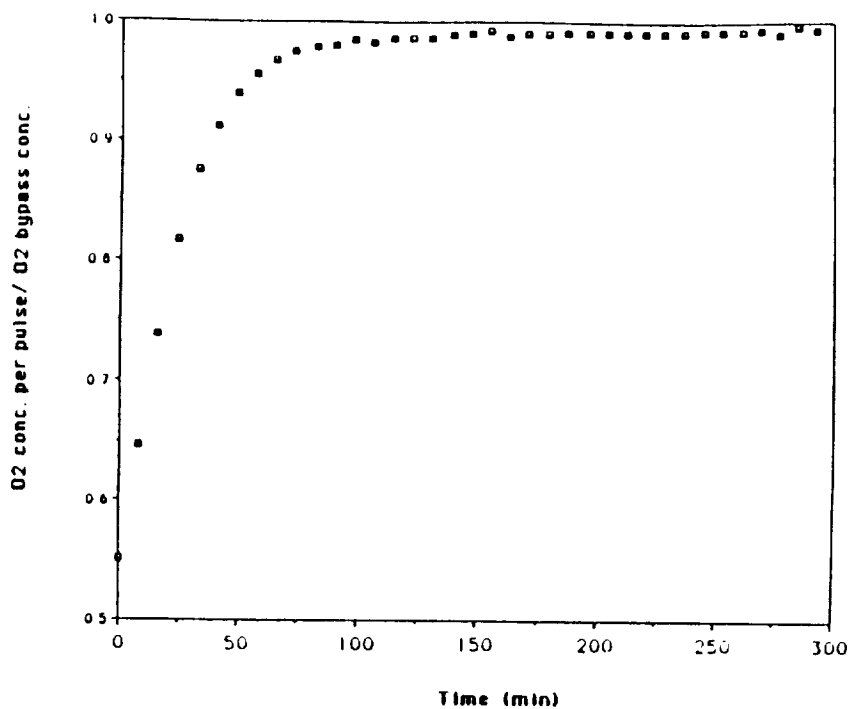
Figure 9: O_2 concentration as a function of time for the pretreated 5.8% $Pt/SnO_2/SiO_2$ catalyst at 303 K using 1% O_2, 2% Ne, balance He as the pulsing gas.
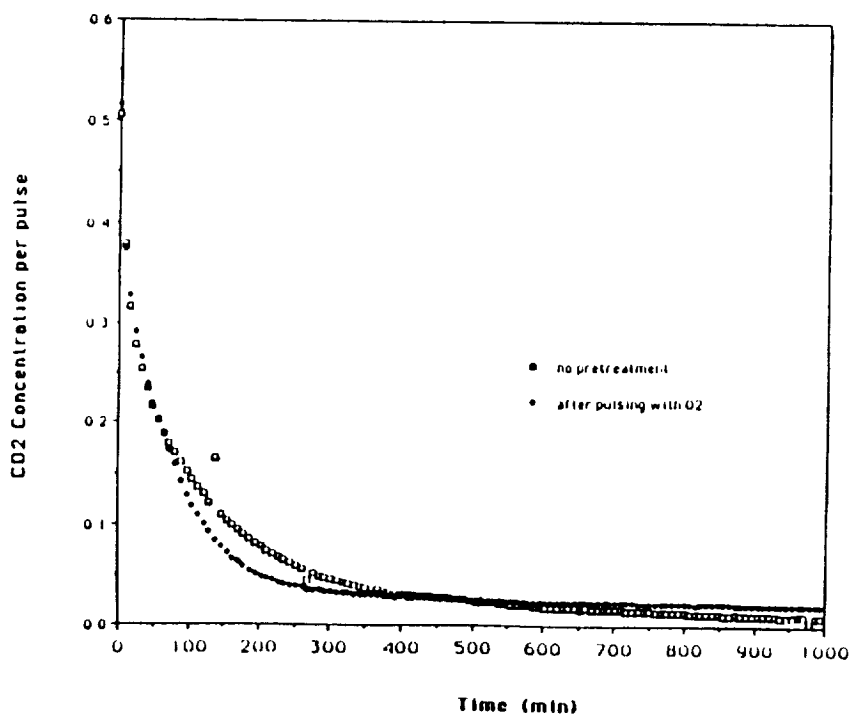
Figure 10: A comparison of CO_2 yields for the 5.8% $Pt/SnO_2/SiO_2$ catalyst with no pretreatment □ , and after the pretreated catalyst had been exposed to O_2 ◆.
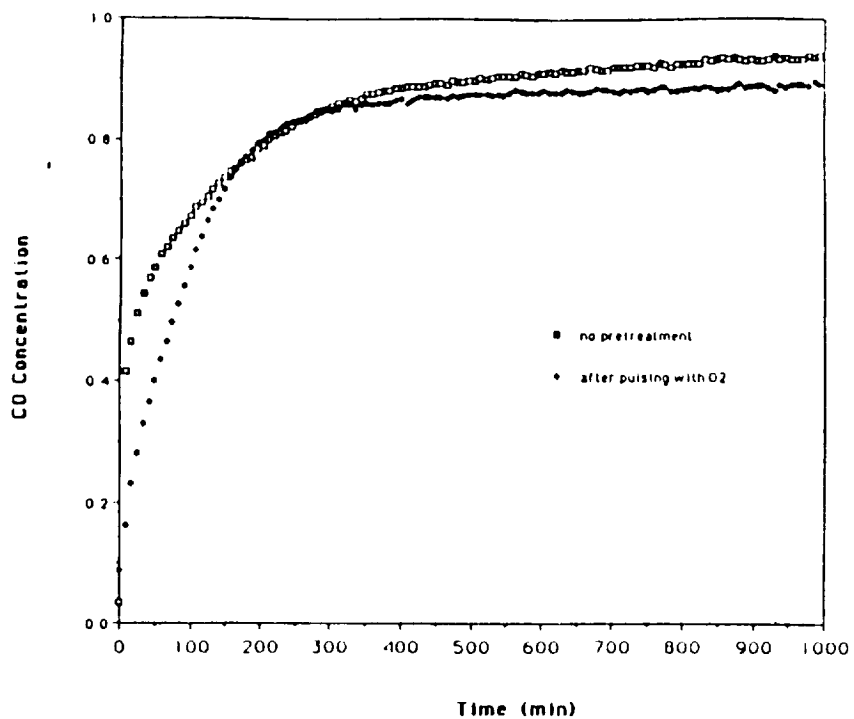
334

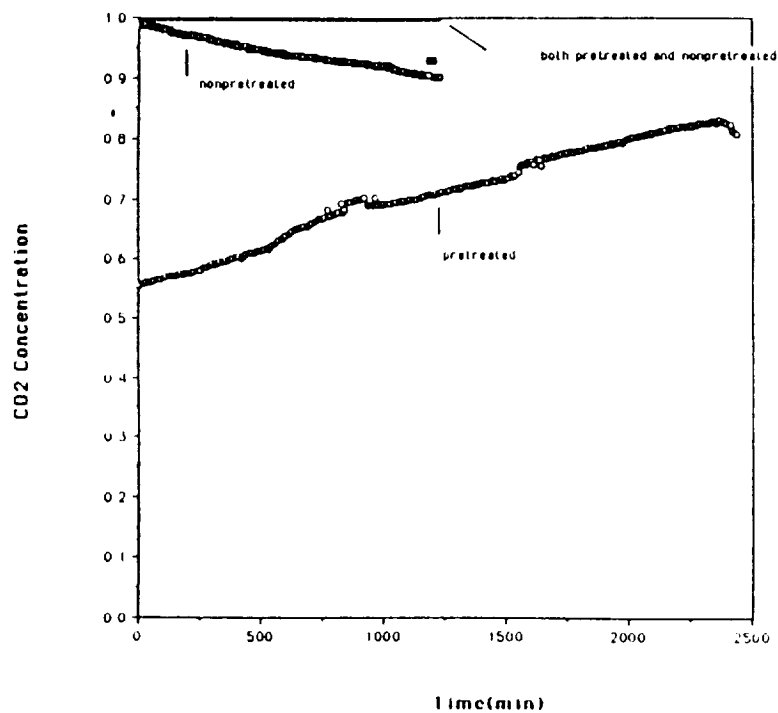Figure 11: Change in CO concentration for the conditions described in figure 10.

Figure 12: The effect of exposure of the catalyst to CO2 with the indicated conditions. ♦ 2% Pt/SnO₂, ▫ and ○ 5.8% Pt/SnO₂/SiO₂.

SECTION IV

LASER STUDIES AND OTHER APPLICATIONS

DISSOCIATION PHENOMENA IN ELECTRON-BEAM SUSTAINED

CARBON DIOXIDE LASERS

Michael R. Harris and David V. Willetts
Royal Signals and Radar Establishment
Great Malvern, Worcestershire   WR14 3PS, UK

INTRODUCTION

A number of applications are emerging requiring efficient, long pulse, long-life sealed CO_2 lasers. Examples include the proposed NASA and ESA wind lidars. Electron-beam sustained discharge devices are strong contenders. Unlike self-sustained discharges e-beam sustenance readily provides efficient performance from large volume discharges and offers pulse lengths well in excess of the microsecond or so generally associated with self-sustained devices.

In the case of the e-beam sustained laser, since the plasma is externally maintained and operated at electric field strengths less than that associated with the glow to arc transition, the discharges can be run even in the presence of strongly attacking species such as O_2. Build up of large levels of attacking contaminants is nevertheless undesirable as their presence reduces the current drawn by the plasma and thus the pumping rate to the upper laser level. The impedance rise leads to a mismatch to the pulse forming network with a consequent loss of control over energy deposition, operating E/N, and gain.

Clearly CO_2 dissociation rates, the influence of dissociation products on the discharge and gain, and tolerance of the discharge to these products need to be determined. This information can then be used to assess co-oxidation catalyst requirements for sealed operation.

CARBON DIOXIDE DISSOCIATION

Experimental Apparatus

The equipment used for the oxygen tolerance determination is shown schematically in Figure 1. The electron gun was a cold cathode plasma device run at a pressure of a few tens of microns of helium which was continuously bled in and pumped out by a Roots blower/backing pump combination. This type of gun has been described elsewhere (ref 1); briefly an auxiliary glow discharge is maintained in the drift region and provides ions for acceleration by the pulsed electric field. Secondary electrons emitted from the cathode are accelerated through a capacitative voltage dividing structure to provide an internal gun current of about an amp. The 150kV voltage pulse is delivered by a 6 mesh PFN of total capacitance $0.3\mu F$ and total inductance $918\mu H$, switched by a thyratron through the primary of a 10:1 turns ratio pulse transformer. Gun current and voltage could be monitored by inductive loop and resistive division probes and recorded on a storage oscilloscope. The area of the foil separating the main discharge chamber and the gun was 30 x $2cm^2$.

The main discharge chamber was constructed almost entirely of Monel, except that Viton O-rings were used for the demountable seals, the foil separating the gun from the main discharge was $25\mu m$ aluminium, and insulating lead throughs were made of PTFE. The removable discharge limiters were constructed of alumina. For the majority of the experiments the Monel grid protecting the foil was operated as the anode so that the cathode material could readily be changed. The

main discharge PFN was a 6 mesh configuration of total capacitance $0.6\mu F$ and total inductance $322\mu H$. Voltage and current monitors were provided for the main discharge as for the gun. Figure 2 illustrates the primary current transmitted through the foil; the current could be altered by adjustment of gas pressure in the gun and by control of gun voltage. Figure 3 shows typical main discharge current and voltage waveforms. Note that the current trace is inverted and that the current monitor baseline falls during the pulse.

Continuous analysis of oxygen and carbon monoxide was available using a paramagnetic oxygen analyser and an infrared CO analyser in a flow loop as shown in Figure 1. The oxygen analyser incorporated a pump which resulted in a residence time within the main discharge chamber of about one minute. The device was normally filled by pumping and flushing with the 3:2:1 $He:N_2:CO_2$ gas mixture introduced from a gas manifold before final tap–off. The gas manifold incorporated a range of flow meters for appropriate gases calibrated by a direct water displacement and timing method. Mixtures prepared using these flowmeters were used to check the calibration of the two gas analysers. Main discharge and analyser volume was measured to be 2.28 1 by a pressure change method.

Dissociation by Main Discharge

The basic method used to measure this parameter is described below. The main discharge chamber was filled with gas mixture and the gun run at a prf of about 1Hz. The voltage on the main discharge PFN was set to give a value of 4kV/cm atm (1.5×10^{-16} V cm^2) for the operating E/N. As dissociation took place, attaching products were formed which raised the discharge impedance. This caused a mismatch to the PFN so the PFN charging voltage was altered to maintain the E/N at the desired value. Thus the charge passed per shot gradually fell as a consequence of the discharge voltage and duration being held constant and the rise of the main discharge impedance. The result is the nonlinear variation of discharge impedance and oxygen (and CO) concentration with number of pulses shown in Fig 4. A more useful measure of dissociation is as a function of total charge passed and Figure 5 shows such a plot, as crosses, abstracted from the data of Figure 4. It is to be expected that the dissociation rate should depend linearly on CO_2 partial pressure, and thus as oxygen is formed, CO_2 is lost and the dissociation rate falls. Correcting for this loss we obtain the circles as data points in Figure 5 which is thus essentially a dissociation rate at constant CO_2 partial pressure of 0.167 atm. The linear dependence on total charge passed is exactly what would be naively expected, and corresponds to 26.1 μmoles of oxygen formed per Coulomb of charge passed by the main discharge, which is equivalent to 2.15 molecules of oxygen produced by each secondary electron crossing the main discharge gap. The CO:O_2 stoichiometry was found to about 2.5:1 in all our experiments, similar to results for self–sustained devices. The validity of the assumption that the dissociation rate depends on the CO_2 partial pressure was verified by studying a range of CO_2 concentrations up to 30%. The resultant O_2 generation rates are plotted in figure 6.

Calculations were performed of the **bulk** dissociation by thermalised secondary electrons. The dissociation in moles per coulomb F is given approximately by (ref 2)

$$F = \frac{G_{PCO_2}}{e\bar{v}V_o} Q_{oj} \left[\frac{kT}{e}\right]^{\frac{1}{2}} \left[1 + \frac{\epsilon_j}{kT_e}\right] \exp - \left[\frac{\epsilon_j}{kT_e}\right] \times 6.7 \times 10^7 \qquad (1)$$

where e and m are the charge and mass of the electron, T_e is the glow electron temperature, ϵ_j is the onset energy of the dissociation process of peak cross–section Q_{oj}, $\bar{v}$ is the electron drift velocity at the appropriate value of E/N, PCO_2 is the partial pressure of CO_2 in the gas mixture and V_o is the volume containing one mole at the working pressure of one atmosphere. Relevant data on T_e and $\bar{v}$ for the 3/2/1 mixture at the appropriate E/N was taken from References (3) and (4) but it

should be noted that Judd's value of T_e of 0.37eV is hardly more than half of Lowke Phelps and Irwin's value of 0.7eV. For all the subsequent calculations we quote both values with the parenthetic note (J) for the 0.37eV and (LPI) for the 0.70eV case. Using values of ϵ_j and Q_{oj} applicable to dissocation (6.2eV and 3.5 x 10^{-17} cm^2; reference 5) and dissociative attachment (3.9eV and 1.5 x 10^{-19} cm^2; reference 6), we found similar rates for both processes, but these were in excess of three orders of magnitude lower than experimental findings. This suggests that dissociation is not a bulk process but may be confined to the (cathode) sheath region. This lead us to repeat the dissociation measurement with the gap reduced from 2cm to 1cm and in support of this conjecture it was found that the dissociation rate was unaltered within experimental error. Further measuremets were carried out at halved E/N, and also with the cathode changed from Monel to Dural (a hardened Al alloy), and to 60/40 brass. Also explored was the effect of altering the electrode polarity so that dissociation takes place on the grid rather than on the smoothly profiled electrode. These changes did not significantly alter the dissocation rate either; addition of alumina discharge limiters increased the dissociation rate by about 10%, which we suspect to be due to field distortions caused by the presence of the thick high permittivity limiters. All this evidence is shown in Figures 7 and 8 and points toward dissociation in the sheath region; we have made initial attempts to estimate the magnitude of this process.

It is probably fair to say that the detail of the cathode fall mechanism is not well understood. J J Thomson (ref 7) derived the form of potential fall in a gap which is externally sustained and in which the electron loss process is by recombination. This theory is readily altered to encompass the attachment loss mechanism operative in our device (see below) but unfortunately the assumption that the loss mechanism can be neglected in the sheath leads to preposterous values of cathode fall Φ and sheath thickness L. A much better model has been provided by N G Basov (ref 8) who has adapted the von Engel and Steenbeck treatment of self-sustained discharges for the nonself-sustained case. The assumptions are

1. Electron emission from the cathode occurs solely by positive ion bombardment, so that

$$j_e = \gamma j_+$$

2. The field varies linearly in the sheath,

$$E(X) = E_0(1-X/L)$$

where X is the distance from the cathode.

Hence from Poisson's equation, ρ is a constant and since

$$\frac{n_+}{n_e} = \frac{j_+ v_e}{j_e v_+} = \gamma^{-1} \frac{v_e}{v_+} \gg 1,$$

$$\rho = \rho_+ = \frac{1}{4\pi}\left[\frac{E_0}{L}\right]$$

3. The positive ion velocity v_+ is constant in the sheath, implying that j_+ is constant and

$$v_+ = \frac{4\pi j_+}{(E_0/L)} = \frac{4\pi j_{tot}}{(E_0/L)} \quad \text{since } \gamma \ll 1.$$

341

4. The total current density j_{tot} is equated to the value outside the sheath

$$j_{tot} = N_e e \mu_e \left[\frac{E}{p}\right]$$

5. The Holst and Oosterhuis–Seeliger condition holds for balance of electron loss and gain in the cathode fall:

$$\ln\left[1 + \frac{1}{\gamma}\right] = \int_0^L \alpha(X)\,dX$$

6. The ionisation coefficient α may be written as

$$\alpha/p = A\left[\frac{E}{p} - B\right]^2$$

The results Basov finds are

$$\Phi = \left[\frac{E_o}{p}\right]^2 \frac{Dp^2}{N_e(E/p)}$$

and

$$\frac{E_o}{p} = C\left[\frac{N_e E/p}{p^2}\right]^{1/3} + B$$

and

$$L = \frac{2\Phi}{E_o}$$

Here $D = v_+/8\pi\mu_e$ and $C^3 = 3/2DA \ln 1/\gamma$.

We have attempted to use this approximate analysis to examine dissociation in the sheath. Lowke et al (ref 3) give α/p for the 3/2/1 mixture which best fits the Basov formulation near 100V/cm torr for $A = 1.32 \times 10^{-4}$, $B = 0$. γ was set equal to 0.011 and v_+ was taken to be 1.3×10^5cm/sec, with μ_e equal to 8×10^5cm^2 torr/sec V. D was thus found to be 4.5×10^4 and C to be 1.045. Φ varied between 200 and 330 V with L varying between 22 and 55μ as N_e was varied over a range 3.5×10^{11}cm^{-3} to 1.4×10^{12}cm^{-3}. Next the gap was divided into ten equal slices and the electron current and thus dissociation evaluated in each slice. It was found that the dissociation increased as E/N fell and electron energy better matched that required for dissociation; the rate maximised at about 70–80% of the distance from the electrode to the negative glow. Agreement with the measurement was not good – calculation was about 50 times less, but is nevertheless much better than that of the bulk process, especially considering the large number of approximations in the analysis. The most disturbing feature of this analysis is the prediction of a

changing dissociation rate as N_e changes as a consequence of oxygen buildup, ie significant curvature should be expected in Figures 5, 7 and 8. It may well be that dissociation is taking place in the negative glow region rather than the cathode fall. It is important to note that the lack of volume scaling indicates that the result should be applicable to any e-beam sustained laser device.

Dissociation by Primary Beam Alone

The results quoted above obviously indicate dissociation by both main discharge and primary electron beam. The latter has a very high energy of about one hundred keV at which dissociative cross sections are very small. Thus bulk dissociation due to primaries is not expected to be an important process. Exactly the same method was used to assess the effect of the primary beam alone as already described, except that the collector electrode was 'earthed' through a 50ohm resistive current probe. Figure 9 illustrates the findings with a linear buildup of oxygen with number of pulses at a rate dependent on current within the pulse. Figure 10 shows that the dependence on current is linear and so the dissociation scales linearly with charge passed. Much more surprising is the independence on the volume exposed to primaries, very similar to the observations on the main discharge. It would thus appear that a surface mediated effect is being observed which was quite unexpected. A further experiment was performed of varying widely the carbon dioxide partial pressure in the gas mixture, starting with a system cleaned by evacuation and repetitive pulsing of the gun and gradually increasing pCO_2. Figure 11 records the results which are absorption isothermal in form, suggestive of a true surface dissociation. However, the rate is amazingly high, at 15mmole/coulomb for the 3/2/1 mixture. This corresponds to 3000 CO_2 molecules being broken up for each primary electron passed which corresponds to a few monolayers/pulse and an overall efficiency of about 20% of total primary beam energy going into dissociation. The primary process appears to be contributing 10–15% of the total cracking observed in the main discharge.

A number of possible mechanisms have been investigated theoretically to account for the large dissociation by the primary beam. These include:

1. Cracking by the fast initial secondaries which have an energy of 30–40eV and thermalise in about 1ns. A bulk effect of 2.4 molecules/electron for a one centimetre gap.

2. Dissociation by thermalised secondaries. At equilibrium, rate of loss by dissociative attachment equals rate of ionisation, so the ionisation and dissociation rates become equal. This is also a bulk process with 13 molecules dissociated/electron crossing a one centimetre gap.

3. Effect of secondary electrons emitted from the electrode surface by the impact of the primary beam or of the fast nonthermalised bulk secondary electrons near the surface. The latter are found to predominate, but the emitted secondaries peak at only 2–3eV energy so the dissociation they give rise to is very small, about 0.1 molecule/primary electron. Although this is a surface mediated effect which is expected to be volume independent, it is of insignificant magnitude.

4. Thermal effects. Thermodynamic data (ref 9) gives

$$\Delta G^{\bullet} = -135100 + 41.5T$$

for the process

$$2CO_2 \rightarrow 2CO + O_2$$
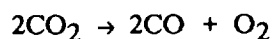
Thus $\ln K_p \equiv 6.82 \times 10^4/T - 20.96$

where

$$K_p = \frac{P_{CO_2}^2}{P_{CO}^2 P_{O_2}}$$

Substantial thermal dissociation occurs at $K_p = 1\text{atm}^{-1}$ which corresponds to 3000°C. In the absence of surface conduction and assuming all the primary energy to be deposited in an infinitely thin surface layer, radiative loss limits the surface temperature to 2300°C. In practice, the primary energy is deposited in a thickness of tens of microns and the instantaneous surface temperature rise is limited to a few tens of centigrade degrees. Thus it would appear that this true surface effect is untenable.

We have no explanation at this stage for the large cross section observed. The process might be akin to electron stimulated desorption but the cross sections for ESD are normally quite small. Like the main discharge effect the result we have found should be general for any size of e-beam sustained laser.

DEPENDENCE OF MAIN DISCHARGE CURRENT ON TRANSMITTED PRIMARY CURRENT

A study of the ratio of secondary to primary currents I_s/I_p is of importance for the following reasons. The design process for the main discharge normally sets the operating E/N on efficiency/gain considerations to be about 1.5×10^{16} V cm²; the current density is then set by specific energy deposition requirements. The transmitted gun current then follows from I_s/I_p which is a powerful influence on gun design.

Figure 12 shows, plotted as circles, the results of measuring this parameter for the 3:2:1 gas mixture. Gun current was altered by varying the helium pressure within the gun and hence its impedance. Gun voltage and hence primary beam energy were maintained constant. The main discharge E/N was also kept invariant. A linear plot results, implying an attachment dominated loss process. In the steady state, the differential equation

$$\frac{dn_e}{dt} = S_o - \beta n_e$$

governing the electron density reduces to $n_e = S_o/\beta$.

Since S_o, the ionisation rate, is proportional to primary current density H_p through the relation (10)

$$S_o = \frac{J_p}{e} \sum_i \sigma_i N_i$$

where σ_i and N_i are the cross section and number density of the ith species present in the discharge, and

$$J_s = n_e e \bar{v},$$

we find

344

$$\frac{I_s}{I_p} = \frac{J_s}{J_p} = \frac{n_e \overline{ev}}{S_o e} \sum_i \sigma_i N_i$$

$$\therefore \frac{I_s}{I_p} = \frac{\overline{v}}{\beta} \sum_i \sigma_i N_i \tag{2}$$

Taking σ_{N2} to be $1.5 \times 10^{-18} cm^2$ and $\sigma_{He} = 0.3 \times 10^{-18} cm^2$,

$$\sum_i \sigma_i N_i$$

is $17.4 cm^{-1}$ for a 1 atm 3/2/1 mixture. $\overline{v}$ is known to be 4.4×10^6 cm sec^{-1} for this mixture and E/N (refs 3, 4). β was evaluated from an overlap integral of the form of equation (1) with the values of Q_{oi} and ϵ_i enjoyed by dissociative attachment to carbon dioxide; a value of 7.7×10^3 (J) and 9.4×10^5 (LP&I) sec^{-1} were found. Thus the predicted value of 3660 (J) is in remarkable agreement, considering the approximations, with the slope of Figure 12 namely 3750. The LPI prediction is for $I_s/I_p = 30$. Inclusion of alumina discharge limiters alters the ratio to 2700, which we presume to result from field distortions arising from inclusion of a substantial thickness of high dielectric constant material.

Composition Dependence of Secondary to Primary Current Ratio

The ratio of secondary to primary currents was measured for a variety of gas compositions. Figure 12 compares the results of experiments on 3:2:1 and 13:2:1 gas mixtures, these results and a number of others are listed in Table 1. The results can be understood from formula (2) above.

The drift velocity $\overline{v}$ varies weakly with composition, but the attachment coefficient β varies strongly and like the ionisation cross section, may be written as

$$\beta = \sum_i \beta_i N_i$$

Since the attachment coefficients of nitrogen and helium are much less than that of CO_2, and σ_{He} is very small

$$\frac{I_s}{I_p} \simeq \frac{\overline{v}\sigma_{N_2}}{\beta_{CO_2}} \left[\frac{y}{z} + \frac{\sigma_{CO_2}}{\sigma_{N_2}} \right]$$

for a x:y:z $He:N_2:CO_2$ gas mixture. It is immediately apparent that M should be constant for a fixed ratio of N_2 to CO_2, independent of the helium content of the mixture. This prediction is well borne out for y = 2, z = 1, and x = 13, 3 and 0. Examining the pure CO_2 ratio, and taking $\beta(CO_2)\overline{v}$ to be about $10^{-21} cm^2$ for CO_2 at 4kV/cm atm, we find $\sigma(CO_2)$ to be roughly $3 \times 10^{-17} cm^2$, considerably less than $\sigma(N_2)$. Thus to a good approximation,

$$\frac{I_s}{I_p} \simeq \frac{\overline{\nu \sigma} N_2}{\beta CO_2} \left[\frac{y}{z}\right]$$

Taking $\sigma(N_2)$ to be $1.5 \times 10^{-18} cm^2$, we predict I_s/P_p to be about $1500(y/z)$. For $y/z = 2$, the prediction of $I_s/I_p = 3000$ compared with a measurement of 3500 is quite satisfactory. It is clear that the ratio can be tailored by control of the nitrogen to carbon dioxide ratio.

Attachment dominated discharges have been found for all the e-beam sustained lasers operated at RSRE. These observations are at variance with the usual assumption of a recombination dominated plasma.

EFFECT OF OXYGEN ON DISCHARGE IMPEDANCE

Having explored the oxygen generation rate, we investigated the effect of oxygen both produced by the discharge, and added directly, on the plasma impedance. It will transpire that the impedance change completely specifies the effects of dissociation products. The data on oxygen added in small amounts in a flowing gas method are shown in Figure 13. The linearity of the impedance – oxygen percentage plot implies that the oxygen also removes electrons by attachment, thus

$$z = \frac{V_s}{I_s} = \frac{V_s}{I_p \sum_i \sigma_i N_i \overline{\nu}} (\beta + N_{o_2} \beta_{o_2})$$

Thus

$$\frac{\partial Z}{\partial N_{o_2}} = \frac{V_s \beta_{o_2}}{I_p \sum_i \sigma_i N_i} \tag{3}$$

where N_{o2} and β_{o2} are the number density and attachment coefficient of oxygen respectively. The measured value of this parameter obtained from the slope of Figure 13 is 1.72×10^{-16} Ω cm^3. Taking the dissociative attachment data of Rapp and Briglia on oxygen (ref 6), we calculate a value of β_{o2} of $1.0 \times 10^{-15} cm^3 sec^{-1}$ (J) which is about 400 times smaller than demanded by equation (3) and our data in Figure 13. The LPI calculation yields $5 \times 10^{-13} cm^3 sec^{-1}$ which fits our data exactly.

However it is important to recognise that at low electron energies a 3-body process can occur leading to the formation of O_2^- with quite significant cross section

$$O_2 + M + e \rightarrow O_2^- + M$$
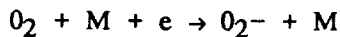
Then the attachment coefficient β_{o2} is given by

$$\beta_{o_2} = \sum_i k_i N_i$$

where the k_i's are the electron and gas temperature dependent three body coefficients for each of the neutral species i present in the gas mixture, which have been measured by Chanin et al (ref 11). The values at T_e = 0.36eV are 2×10^{-32}, 2×10^{-30} and $\sim 10^{-33} \text{cm}^6 \text{sec}^{-1}$ for N_2, O_2 and He respectively falling to $\leqslant 1 \times 10^{-32}$, 1×10^{-30} and $\approx 10^{-34}$ at T_e = 0.7eV. The values for H_2O and CO_2 are tabulated at a mean electron energy of 0.03eV only, where they are 2×10^{-29} and $3 \times 10^{-30} \text{cm}^6 \text{sec}^{-1}$ respectively. Thus

$$\frac{\partial Z}{\partial N_{O_2}} = \frac{V_s \sum_i k_i N_i}{I_p^{\bar{\nu}} \sum_i \sigma_i N_i}$$

The k_i and σ_i for i = He may be neglected; if these coefficients are also neglected for CO_2, oxygen and water, we find

$$\frac{\partial Z}{\partial N_{O_2}} = \frac{V_s k_{N_2}}{I_p^{\bar{\nu}} \sigma_{N_2}} = 2.7 \times 10^{-16} \ \Omega \ \text{cm}^3 \ (0.36\text{eV})$$

$$\leqslant 1.3 \times 10^{-16} \ \Omega \ \text{cm}^3 \ (0.7\text{eV})$$

in good agreement with the experimental determination. It is difficult to justify the neglect of the k_i's for O_2, H_2O and CO_2 except for the fact that the latter pair are ill-determined; at face value the oxygen k_i should introduce significant curvature into the graph of Figure 13. The influence of discharge-produced oxygen is shown in Figure 14. Here we have plotted the discharge resistivity rather than impedance with allows ready scaling to other discharge dimensions or for the presence of discharge limiters. It is apparent that the dissociation products influence the discharge in the same way as deliberately added oxygen, the impedance doubling at an oxygen concentration of about one per cent. This fact is consistent with the observation that carbon monoxide has no influence on the discharge impedance.

GAIN MEASUREMENTS

Methodology

The optical arrangement used to measure the gain in the amplifier is shown in Figure 15; it relies on the usual method of probing with a low power cw laser. The output from this cw laser was transmitted by variable attenuators of CaF_2 and then double passed through the gain medium. The probe beam was focussed onto the surface of a room-temperature CMT photoconductive detector whose output voltage was amplified and displayed by a storage oscilloscope. Although the oscilloscope was restricted to a maximum bandwidth of 1MHz it was confirmed that this response was more than adequate for the long pulse observations of interest. A removable mirror allowed the operating transition of the cw laser to be examined using a wavelength monitor; the probe laser was set on the 1OP(20) line for all measurements by adjustment of its cavity length, by control of the voltage on the piezoelectric transducer to which one vacity mirror was attached. Two periscopes, omitted from the diagram for clarity, changed the height of the probe beam out of the plane of the diagram in passing through the lead X-ray shield around the gain cell. The polarisation of the cw probe was roughly parallel with the main discharge electric field.

A typical example of a gain measurement is shown in Figure 16. The chopped signal shows the probe power and zero power baseline in the absence of gain. The continuous trace shows the time variation of the amplified probe laser power in the presence of pulsed gain; since the amplifier could not be DC coupled the <u>change</u> in probe power is observed, ie the baselines of the chopped and cw signals are different and this was borne in mind when calculating the gain. Addition of optical attenuation did not alter the gain, confirming that a small–signal measurement had been successfully achieved. The small–signal gain was measured for the 3/2/1 gas mixture as a function of main discharge current at various values of E/N and the influence of oxygen on the gain was also examined. Figure 17 illustrates a graph of the peak small signal gain against main discharge current, in which the gun conditions were held constant and the secondary current was varied by changing the impedance by the deliberate addition of oxygen. The behaviour observed, in which the gain levels off with increasing curent, is quite typical of such systems (ref 12). In Figure 18 similar data on single pass gain is presented for three different values of E/N in a flowing gas 3/2/1 mixture wherein the main discharge current was altered by variation of the primary beam current. Note that all the quoted values of E/N are nominal since they do not allow for voltage drops in electrode sheaths. Figure 19 shows how the gain varies with main discharge current at a constant E/N of 1.5×10^{-16} V cm^2. The main discharge current was altered by three different means: (i) variation of primary current, (ii) deliberate addition of oxygen in a flow gas configuration, (iii) sealed operation in which dissociation products were allowed to accumulate. It can be seen that there is no significant difference between these cases which proves that dissociation products influence the gain only through the impedance change caused by the presence of oxygen. This result is unsurprising since it is known that neither oxygen nor carbon monoxide absorb at $10.59\,\mu m$.

SIGNIFICANCE OF RESULTS TO AMPLIFIER DESIGN PHILOSOPHY

Discharge Impedance

Since the effects of discharge impedance mismatch to the PFN are of overriding significance in understanding the device operation, we will briefly explore these here. We assume a PFN imepdance of Z with a discharge impedance MZ, where M can be greater or less than unity and equals one at match. Then the discharge current I and voltage V during the conduction stage are given by

$$I = \frac{V_o}{Z(1+M)}$$

$$V = \frac{V_o}{1 + \dfrac{1}{M}} = \frac{MV_o}{1+M}$$

The total capacitance C_o of the PFN is related to the pulse length τ by $C_o = \tau/2Z$ which ensures that at match, (M=1) the PFN is completely discharged. In the general mismatched case the charge lost $I\tau$ is obviously

$$I\tau = Q_{lost} = \frac{V_o \tau}{2(1+M)} = \frac{2ZC_o V_o}{Z(1+M)} = \frac{2Q_o}{1+M}$$

348

Thus Q_r, the charge remaining on the PFN at the end of the pulse is

$$Q_r = Q_o - Q_{lost} = \left[\frac{M-1}{M+1}\right] Q_o$$

and so V_r, the voltage remaining on the device at the end of the pulse is

$$V_r = \frac{Q_r}{C_o} = \frac{Q_o}{C_o}\left[\frac{M-1}{M+1}\right] = V_o\left[\frac{M-1}{M+1}\right]$$

Similarly, the energy E deposited by the discharge is

$$E = IV\tau = \frac{2C_o MV_o^2}{(1+M)^2}$$

which at match equals $\frac{1}{2}C_o V_o^2$; thus the fraction F of energy deposited compared with the matched case is given by

$$F = \frac{4M}{(1+M)^2}$$

In Figure 20 the voltage multiplication factor 2M/1+M, fractional voltage remaining V_r/V_o = M-1/M+1, and F are plotted vs the impedance multiplication factor M, which is a function of oxygen present in the discharge. Clearly for M = 1.5 which corresponds to $\frac{1}{2}$% oxygen, V/V_m = 1.2, V_r/V_o = 0.20 and F = 0.96. This means that the operating E/N would exceed the design value for 0% oxygen by 20%, a residual E/N of 40% (E/N)$_{design}$ would remain after the pulse, and 96% of design energy would be delivered to the plasma. Although we have yet to elaborate on the residual voltage, these figures suggest that even without any measures being taken to counteract the oxygen produced, a level of $\frac{1}{2}$% should be tolerable.

It is instructive to compare the energy deposited in Figure 20 with the small signal gain of Figure 18. For a matched design E/P of 4kV/cm atm, at 170 A secondary current the gain equals 1.92% cm^{-1}; for M = 1.86, we find an actual E/P of 5.2kV/cm atm, F = 0.91, and I = 119A so that the gain becomes 2.35% cm^{-1}. As the discharge moves out of match the gain changes along the broken line in Figure 18. Thus as the energy deposition falls the small signal gain g_o rises. This happens because the output energy $g_o E_s L$ depends also on the saturation parameter E_s which we have not investigated.

Discharge Stability

The design E/N is well below the region of the attachment instability, so an arc will develop in the main discharge only if the instantaneous value of E/N gets too high. The previous section deals with the effect of impedance matching on the field E during and after the conduction phase; thus information is also required on the gas density N. The latter changes during the period of energy deposition due to gas heating and consequent expansion, which lowers N and raises E/N. Clearly such a rapid expansion must be adiabatic, and with the assumption of reversibility has been treated by Baranov and Breev (ref 13) who find for the ratio of densities before and after expansion

$$\frac{N'}{N} = \left\{ 1 + (\gamma - 1) \frac{\epsilon}{P_o V} \right\}^{-\frac{1}{\gamma}}$$

where ϵ/V is the energy density imparted to the gas at initial pressure p_o and γ is C_p/C_v. The assumption of reversibility is obviously very questionable for an explosive expansion, and we find (14) for the irreversible abiabatic expansion that

$$\frac{N'}{N} = \left\{ 1 + \frac{\gamma-1}{\gamma} \cdot \frac{\epsilon}{P_o V} \right\}^{-1}$$

For our constant current and voltage discharge, ϵ increases linearly with time during the conduction phase and is essentially constant thereafter. For typical energy loadings of 150J/1, N falls near the end of the pulse by a factor of 1.5 times its initial value. With this preamble we are now in a position to consider in more detail the conditions under which an arc can form.

1. Arcs near end of conduction phase

During the main discharge the voltage and thus field remain constant but the density progressively falls. Thus arcs are most likely to form near the end of the discharge by an avalanching process called the glow to arc transition. The value of E/p necessary for this process to occur is much less than that in an unionised gas, ie the static breakdown field. Near the end of the conduction phase the initial value of E/N will have risen by $(1+(\gamma-1)\epsilon/\gamma p_o V)$ which is thus a function of the energy loading and particularly nonuniformities in the latter. In our device, assuming the nonuniformity to be zero, the glow-arc transition sets in at about 10kV/cm atm, ie at $\epsilon/V = 200$ J/1 atm and initial E/N = 6 kV/cm atm. Note that E/N dependence on gas composition through the $(1-\gamma^{-1})$ term.

2. Arcs due to gun failure

Should the gun current cease before the PFN has discharged the impedance matching analysis has to be modified. The worst case applies for early gun failure, when the gas will have hardly expanded and the charge on the PFN has insignificantly, so the value of E/N immediately after cessation of gun current might be almost as high as that applicable before the gun was switched on, namely twice the design E/N for the matched case. However, this field is now present in the conducting medium, which can undergo the glow-arc transition as previously explained. We have not observed this failure mode working at E/p of 4 kV/cm atm but obviously it could set in for mismatches or design E/p's of 5 kV/cm atm or above. It could be beneficial to deliberately mismatch with M > 1 to guard against main discharge arcs arising from gun failure.

3. Post conduction phase arcs

For a matched case, no voltage remains on the PFN at the end of the conduction phase and obviously further discharges cannot occur. For mismatched cases, voltages do remain which are most noticeable for M < 1, and furthermore gas expansion has taken place. For example, for M = ½, a voltage reversal takes place at the end of the conduction phase so that there is set up a field equal in magnitude but opposite in sign to that prevailing during the main discharge. Gas expansion has occurred so that E/N at the end of the pulse is the same as that in the post conduction phase or afterglow. Since electron density decays in the afterglow, the situation here is more akin to static breakdown than the glow-arc transition. Hence since a type I arc has not occurred for M ⩾ ½ the post conduction phase should be stable. For M < ½ the residual voltage is greater than that during

350

conduction and could lead to breakdown, depending on the PFN risetime. Such mismatches should not be encountered since they require inordinately high PFN charging voltages and dissociation products increase the value of M. For these reasons we have not encountered post conduction phase arcs.

Discharge stability is thus governed by the design E/N and energy loading, but especially by matching criteria for the PFN and discharge impedance.

SUMMARY

1. The oxygen concentration was found to rise linearly with charge passed, at a rate of 30 μmole/Coulomb. This dissociation rate was independent of volume, implying effects in the cathode fall or negative glow regions. The result should therefore be applicable to any size of device, and is roughly one hundred times less than for self-sustained devices.

2. Discharge limiters altered the above figure by about 50%, probably due to field distortions.

3. The $CO:O_2$ ratio departed from 2:1 stoichiometry, as is typical of self-sustained devices, to a value of about 2.5:1.

4. CO does not attach and was found to have negligible effect on the discharge impedance.

5. The discharge impedance was found to rise linearly with oxygen partial pressure, doubling at 1% added oxygen. This arises from electron attachment.

6. The secondary current was found to depend linearly on the primary current, implying electron loss by attachment rather than recombination. $I_s:I_p$ was found to depend mainly on the ratio of readily ionised N_2 to electro-negative CO_2 in the gas mixture. For X:2:1 $He:N_2:CO_2$ mixtures $I_s:I_p$ was found to be about 3500.

7. Dissociation by the primary beam alone contributes about 10% of the total dissociation observed. It scales linearly with charge passed, the oxygen concentration rising at 15 millimoles/coulomb of primary current.

8. Like the main discharge effect, this rate did not change with volume, implying some kind of surface mediated phenomenon. The result should therefore be applicable to any size of laser.

9. Dissociation by primaries was measured as a function of CO_2 partial pressure to further investigate the process. The dependence was nonlinear, with an absorption isothermal shape suggesting a true dissociation process, perhaps akin to electron stimulated desorption.

10. The primaries appear to dissociate CO_2 with amazing efficiency, around 10%. 3000 CO_2 molecules are cracked by each primary electron. The process is not understood.

11. Gain measurements have been carried out on the P(20) line. Small signal gain was a sublinear function of E/N and main discharge current. Oxygen, produced by the discharge or deliberately added, influenced the gain only through changes in secondary current brought about by impedance alteration.

12. Dissociation has been shown to influence discharge stability only through impedance changes caused by oxygen formation.

REFERENCES

1. A Crocker et al, Electron Lett $\underline{8}$, 460 (1972).

2. C Webb in Inst Phys Conf Ser No 29 (1976).

3. J J Lowke et al, J Appl Phys $\underline{44}$ (10) 4669 (1973) and O P Judd, J Appl Phys $\underline{45}$ (10) 4572 (1974).

4. M C Cornell et al, J Appl Phys $\underline{54}$ (4) 1723 (1983).

5. K K Corvin and S J B Corrigan, J Chem Phys $\underline{50}$ 2570 (1969).

6. D Rapp and D D Briglia, J Chem Phys $\underline{43}$ (5) 1480 (1965).

7. J J Thomson, "Conduction of Electricity through gases" (Cambridge 1933).

8. N G Basov et al, Sov Phys Tech Phys $\underline{17}$ (12) 1976 (1973).

9. J D Gilchrist, "Extraction Metallurgy", Pergamon (1967).

10. O P Judd in Inst Phys Conf Ser No 29 (1976).

11. L M Chanin et al Phys Rev Lett $\underline{2}$ 344 (1959); Phys Rev $\underline{128}$ 219 (1962).

12. J C Comly et al, IEEE J Quant Electron $\underline{QE17}$ 1786 (1981).

13. V Yu Baranov et al, Sov J Quant Electron $\underline{7}$ 1059 (1977).

TABLE 1

CATALYSTS FOR CO_2 LASERS

SECONDARY TO PRIMARY CURRENT RATIO

He : N_2 : CO_2	M
13 : 2 : 1	3500
3 : 2 : 1	3500
0 : 2 : 1	2500
3 : 2 : 0	6500
1 : 0 : 0	> 6000 (G → A)
0 : 1 : 0	4500
0 : 0 : 1	300

@ 4 kV cm^{-1} Atm^{-1}

$$M = \frac{\text{Secondary current}}{\text{Transmitted primary current}}$$
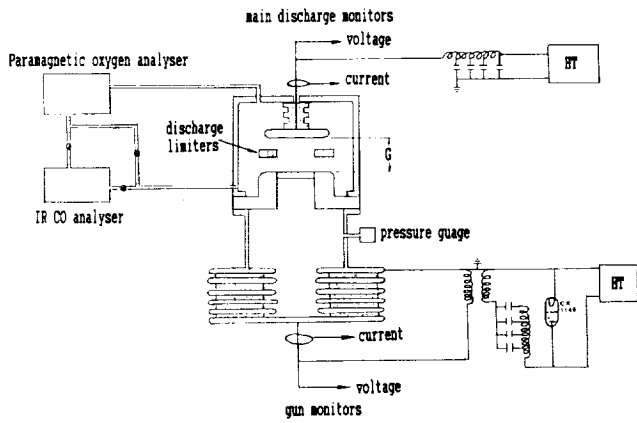
Fig. 1 Schematic diagram of experimental apparatus.
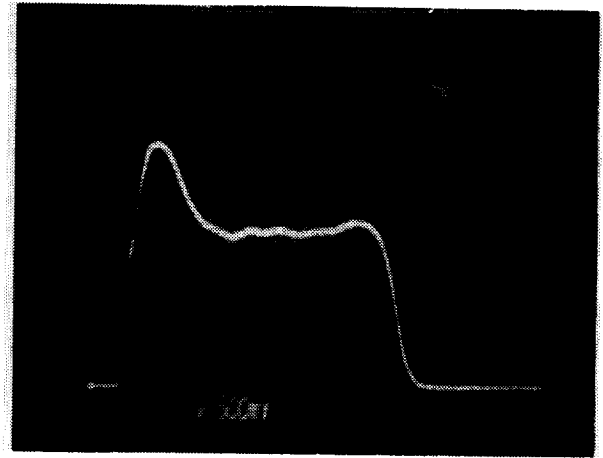
Fig. 2 Transmitted primary current collected at cathode.
10 mA/div. 5 μS/div
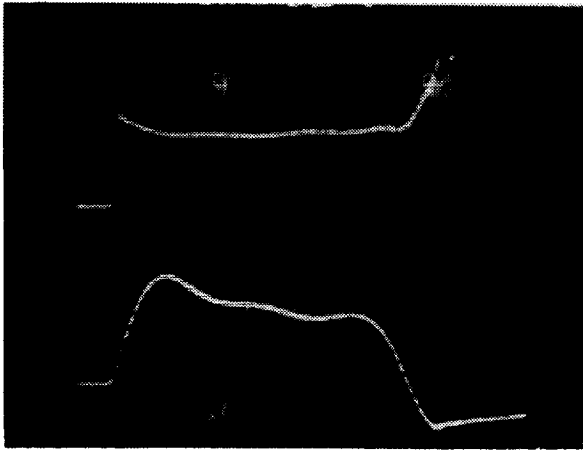
Fig. 3. Main discharge voltage and current waveforms.
5 KV/div, 45 A/div, 5μS/div
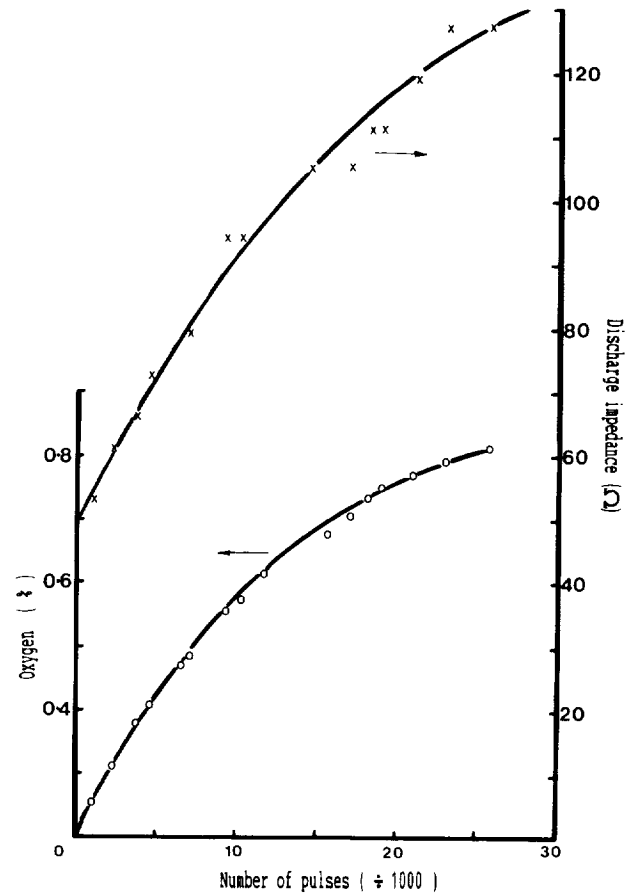
Fig. 4 Oxygen level and Discharge impedance vs Pulse number.

354
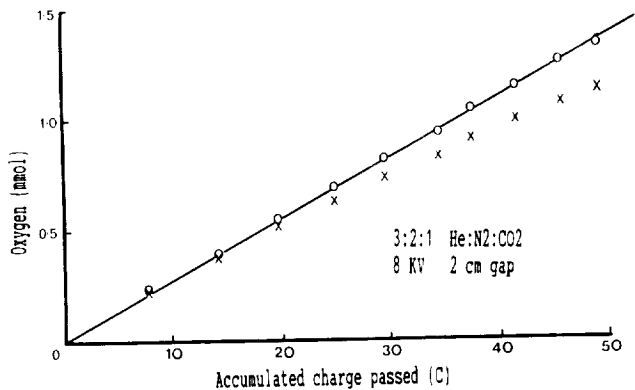
Fig. 5 Oxygen generation vs accumulated charge passed.
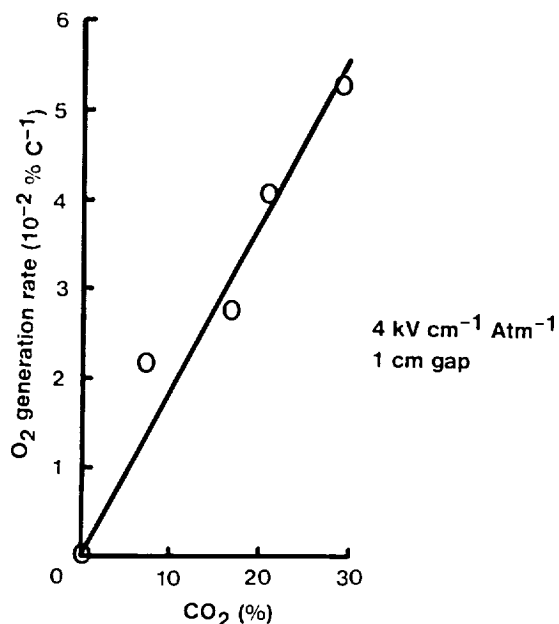
Fig. 6 Dependence of oxygen generation rate on carbon dioxide concentration.
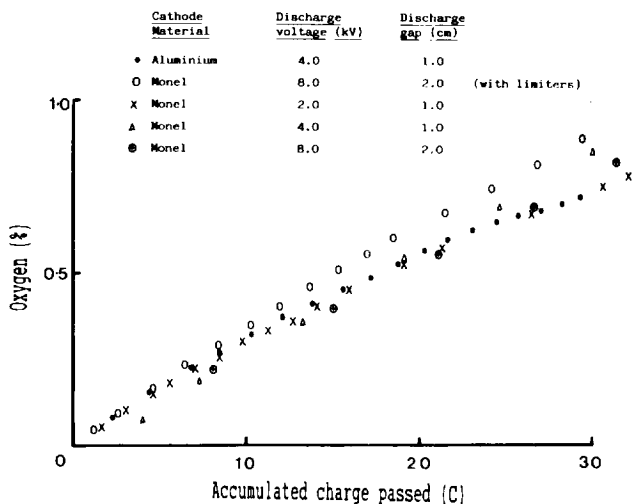
Fig. 7 Production of oxygen in discharge
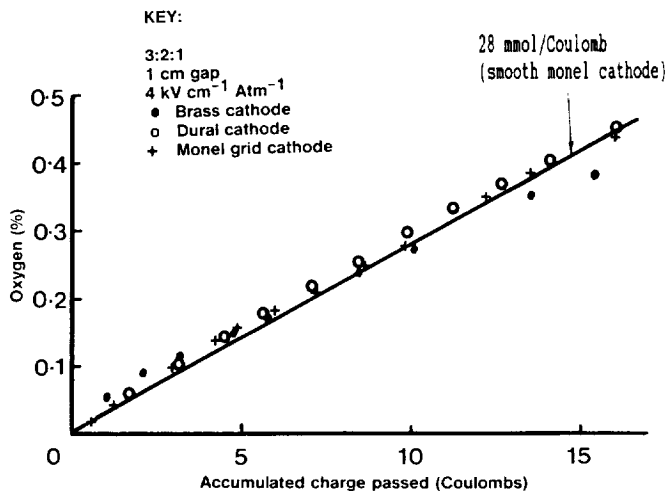
Fig. 8 Dependence of oxygen generation rate on cathode material and form.

355
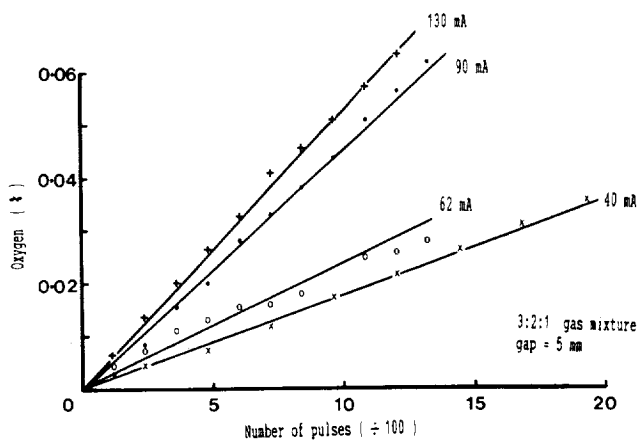
Fig. 9   Oxygen generation by transmitted
          primaries.
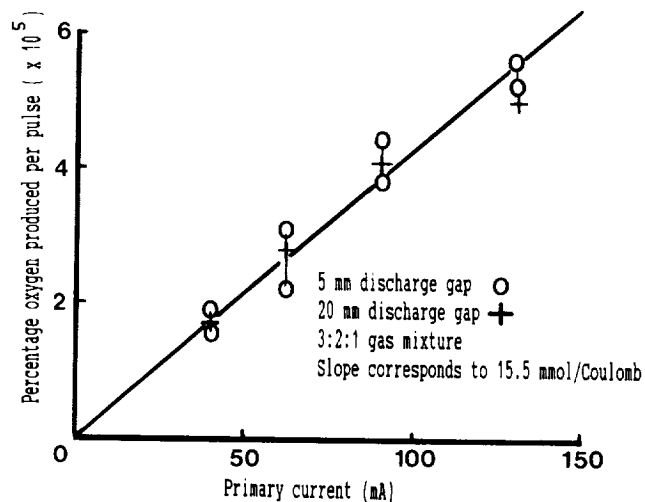
Fig. 10   Oxygen generation rate vs Transmitted
           primary current.
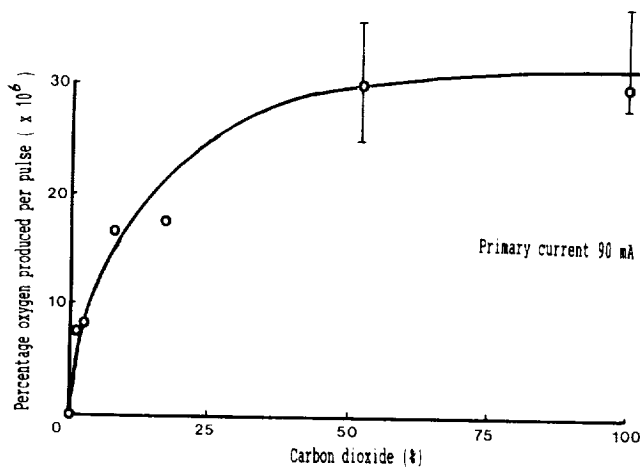
Fig. 11   Dependence of primary beam oxygen
           generation rate on carbon dioxide
           concentration.
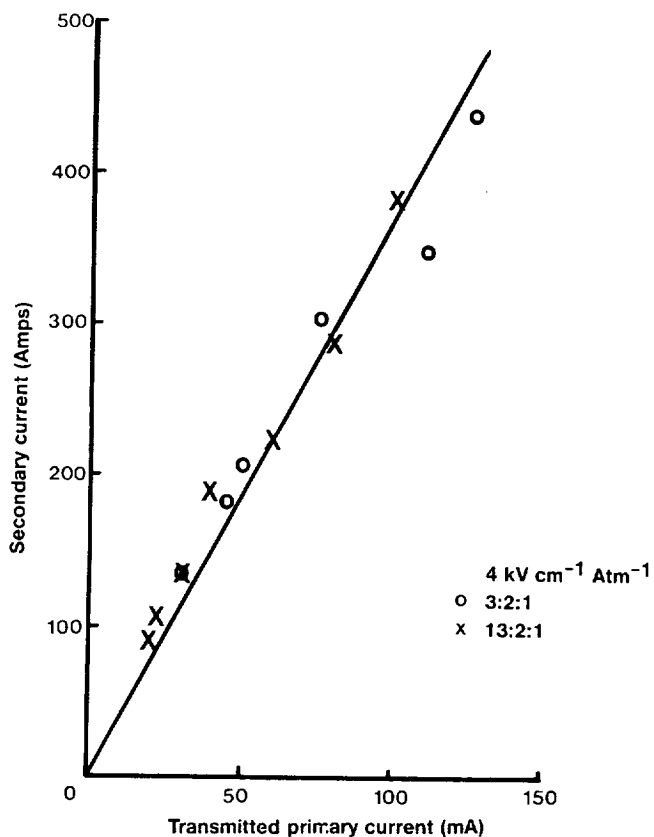
Fig. 12   Dependence of secondary current on
           transmitted primary current.

356

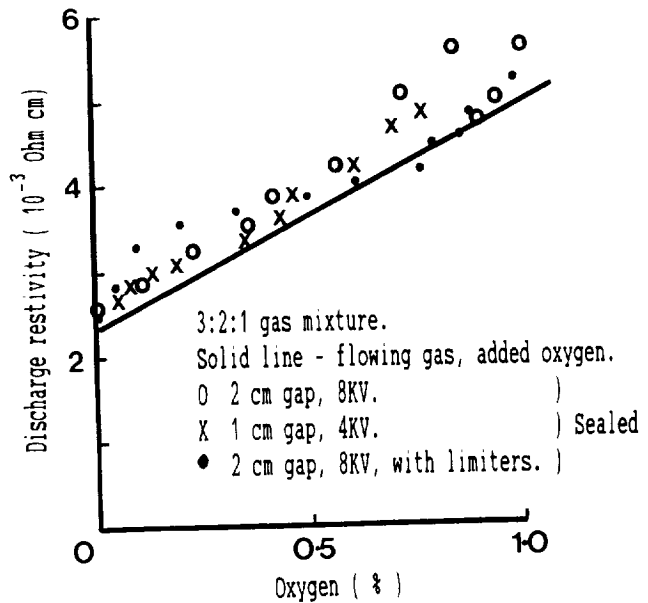**Fig. 13 Influence of oxygen on discharge impedance.**

3:2:1 flowing gas mixture, oxygen added.
gap = 2 cm, E/p = 4KV/cm atm.

3:2:1 gas mixture.
Solid line – flowing gas, added oxygen.
O 2 cm gap, 8KV.   )
X 1 cm gap, 4KV.   ) Sealed
● 2 cm gap, 8KV, with limiters.)
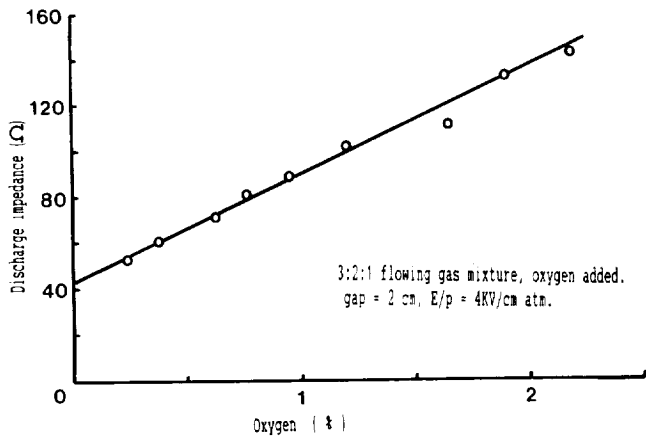
Fig. 14 Influence of oxygen on discharge restivity.
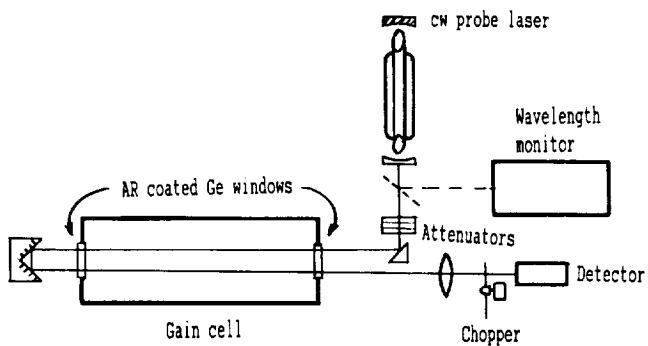
Fig. 15 Experimental arrangement for gain measurement.
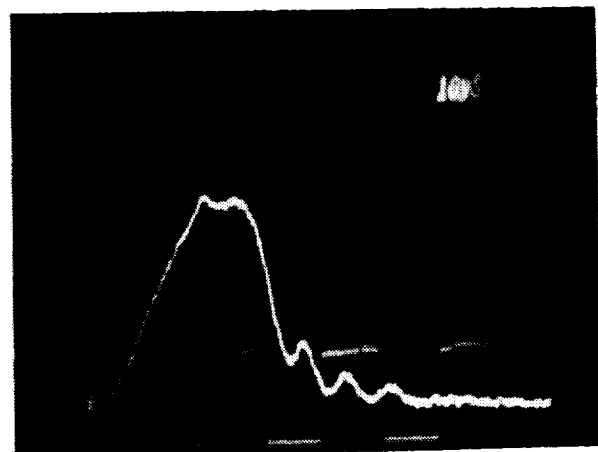
Fig. 16 Measurement of small signal gain.
Chopped signal 2mS/div
Gain signal 10 μS/div
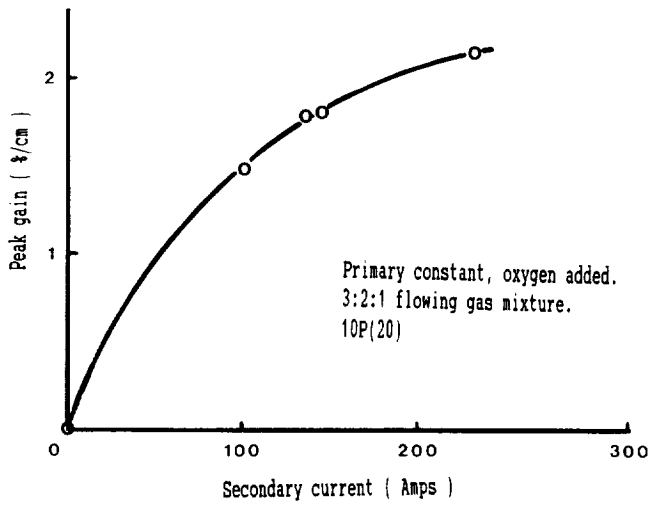3:2:1 He:N$_2$:CO$_2$ + 1% O$_2$
10P(20)

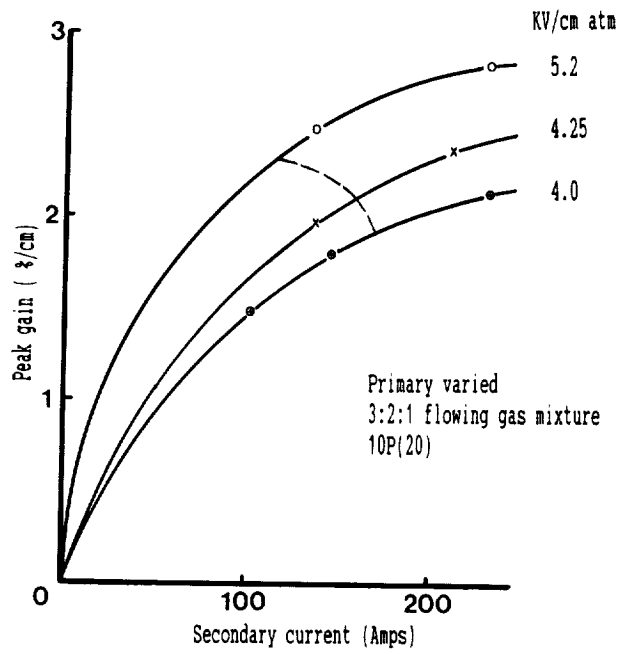**Fig. 17** Dependence of small signal gain on secondary current.

Fig. 18 Dependence of small signal gain on secondary current and electric field.
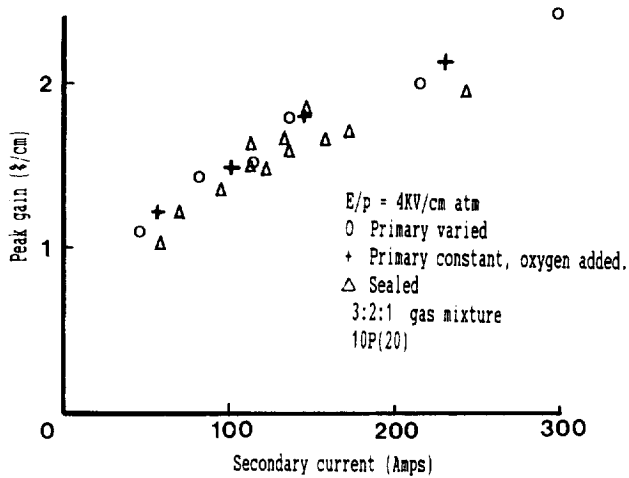

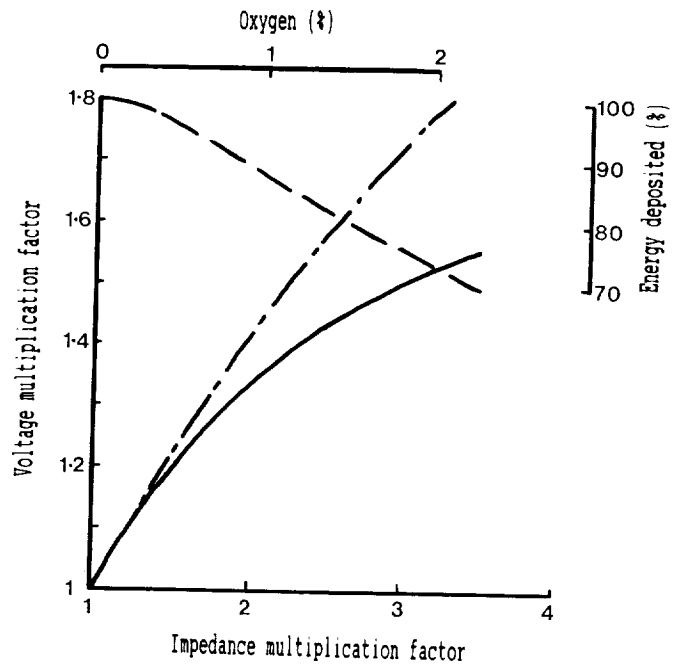**Fig. 19** Dependence of small signal gain on secondary current.

Fig. 20 Effect of increasing discharge impedance on input energy deposition.

e-BEAM SUSTAINED CO$_2$ LASER AMPLIFIER

M.J. Brown, S.R. Shaw, M.H. Evans, I.M. Smith, W. Holman
Applied Physics Division, GEC Avionics Limited, Borehamwood,
Hertfordshire, WD6 1RX, United Kingdom.

SUMMARY

The design features of an e-beam sustained CO$_2$ amplifier are described. The amplifier is designed specifically as a catalyst test-bed to study the performance of room temperature precious metal CO-oxidation catalysts under e-beam sustained operation.

The amplifier has been designed to provide pulse durations of 30 microseconds in a discharge volume of 2 litres. With a gas flow velocity of 2 metres per second, operation at repetition rates of 10Hz is accommodated. The system is designed for sealed-off operation and a catalyst bed is housed in the gas circulation system downstream from the discharge region. CO and oxygen monitors are used for diagnosis of gas composition in the amplifier so that catalyst performance can be monitored in-situ during sealed lifetests.

INTRODUCTION

Over the past two years, a joint RSRE/UK industry programme of work has been underway addressing the design of CO-oxidation catalysts to be used in sealed e-beam sustained CO$_2$ laser systems.

In order to test catalysts prepared under this contract, GEC Avionics has designed and built a dedicated catalyst test bed consisting of an e-beam sustained CO$_2$ gain cell, gas re-circulation system and ancillary diagnostic equipment. The specified operating parameters of the test are

Pulse duration	30 microseconds
Discharge volume	2 litres
Repetition frequency	10 Hz
Injected e-beam density	2mA/cm^2
Secondary current density	1.5 Ampere/cm^2
Gas flow velocity	2 metres per second
Operating pressure	1 Atmosphere
Gas mixture	1 CO$_2$:2N$_2$:3He

For a typical operating voltage of 4 kilovolts per centimetre, this results in the following gain cell design requirements:

Discharge area	50 cm x 8 cm
Discharge gap	5 cm
Total current	600 Amperes
Specific energy loading	180 Joules/litre
Volumetric gas flow rate	50 litres per second

This paper will describe the design of this system, and briefly discuss initial test results.

SYSTEM DESIGN

The e-beam sustained test system is shown schematically in figure 1. The design is based largely around an existing RSRE system (HRREBL 2), with modifications being made to allow sealed operation of the system over prolonged periods.

The electron gun is a low pressure helium, cold cathode device with the correct helium pressure being maintained using a gas bleed and Roots Blower system. A 30 microsecond, 150 kilovolt pulse is applied to the cathode via a thyratron controlled pulse forming network (PFN) and a 10:1 pulse transformer. Electrons emitted by the cathode are accelerated down the gun stack by capacitively coupled electrodes. Beam uniformity is maintained by a d.c. discharge generated in the drift tube and by beam shaping slats.

A more detailed view of the gun mechanical design is shown in figure 2. The gun stack is constructed from aluminium and tufnol components and mounts on the underside of the welded stainless steel drift tube which also contains the beam shaping slat and auxiliary electrode. Ports are provided for connection to the Roots Blower, Baratron pressure gauge and helium inlet. The entire electron gun assembly mounts directly to the underside of the discharge cell.

The gun is driven by a six stage pulse forming network with 4mH total inductance and 60nF total capacitance. Each stage consists of a 680μH wire wound inductor and a 10nF Custom capacitor with the input stage having a slightly higher inductance to match the higher mutual inductance of the other stages. A diode clamp consisting of diodes and a matching resistor is connected to one end of the network to prevent a negative voltage appearing across the thyratron.

The operational characteristics of the gun using a GEC Avionics Ltd. designed pulse transformer, are shown in figure 3. The results were obtained by maintaining a PFN charge voltage of 30 kilovolts and varying the gun helium pressure. Typical voltage and current pulse shapes are shown in figure 4, with a Full Width Half Maximum (FWHM) pulse length of 35 microseconds.

The gain cell mechanical design is shown in figure 5. The entire construction sits on a central stainless steel plate to which the electron gun is also attached. Channels are provided in this plate to provide coolant to the foil support. Chrome copper was chosen as the foil support material due to its high thermal conductivity combined with good machining properties. The 0.001 inches thick aluminium foil is then trapped between grids machined in the foil support and cathode.

The remainder of the cell is constructed from stainless steel and alumina ceramic (Al_2O_3). A large gas volume is provided to damp out pressure pulses from the main discharge. The ceramic discharge limiters act as flow guides as well as containing the main discharge. Six ceramic assemblies are used - three on each side of the active volume with each assembly being constructed from several piece parts bonded together.

The gain cell PFN consists of nine stages with each stage consisting of a 69μH wire wound inductor and a 50nF Hivolt capacitor. Again, the end stages have a higher inductance to balance mutual inductance effects. At a 40kV charging voltage this gives a total stored energy of 360 Joules. Typical voltage/current characteristics for the gain cell operating with one atmosphere of 3:2:1 $He:N_2:CO_2$ are shown in figure 6. Comparison of the gain cell current with the transmitted primary measurements indicates a current magnification ratio of approximately 3000, in good agreement with measurements reported by RSRE.

As illustrated in figure 1, the gas re-circulation system consists of a motor driven fan, catalyst holder, heat exchanger and connecting ductwork. The fan is a 180mm diameter, 74mm wide centrifugal impeller capable of maintaining a pressure drop of up to 100mm of water at 60 litres per second flow rate.

The fan may be coupled to the drive motor by either a magnetic or ferrofluidic coupling.

The catalyst holder comprises a section of ductwork with a 5½ inch internal bore fluted at either end to match the rest of the ductwork, this diameter being dictated by the maximum size of commercially available ceramic monoliths. The catalyst sample is held in place using spring loaded retainers with a maximum sample length of 12 inches being accommodated. Sections of ductwork either side of the catalyst holder contain diagnostic ports to allow gas temperature and flow rate measurements to be made as well as being CO and oxygen monitoring points.

The heat exchanger is a chlorodifluoromethane cooled unit with a capacity of 4kW. As the response time of this type of cooler is long, temperature control is achieved by heaters placed in the ductwork before the heat exchanger. The temperature control circuit then maintains the gas temperature by altering the heating rate rather than the cooling rate.

All interconnecting ductwork pieces are welded stainless steel assemblies with an 8 inch internal diameter. All changes of cross-sectional shape are achieved using fluted sections in order that the same cross-sectional area is maintained throughout most of the recirculation system.

The complete re-circulation system can be evacuated to less than 10^{-4} Torr with all vacuum seals having been leak tested to better than 10^{-8} millibar litres per second.

TEST RESULTS

Baseline oxygen and carbon monoxide generation rates were measured for the gain cell running at 500 Amperes (figure 7). The oxygen generation rate of 32.9 μmoles/coulomb agrees well with previously reported results, however, the $CO:O_2$ ratio of 3:1 was higher than expected. This may well decrease as clean internal surfaces are oxidised during initial operation of the system.

Testing of a coated ceramic monolith has proceeded utilising a 5½ inch diameter by 6 inch long, 200 cell per inch, cordierite monolith coated with 10% by weight tin oxide based catalyst.

The amplifier was operated at a PRF of 6Hz for 6 to 8 hours per day with CO, O_2 and gain cell current being monitored continuously. Throughout the 2×10^6 pulse lifetest, the catalyst maintained the oxygen concentration below 0.001%, the limit of detectability of the analyser. Small accumulations of CO were detected during the first two day's operation (typical levels being 0.02%) but not thereafter.

Gain cell current remained constant throughout the lifetest at 580 Amperes denoting the success of the catalyst in maintaining the gas properties. Figure 8 shows waveforms taken at the beginning of the test and after 10^6 pulses while figure 9 summarises the operating conditions and results from this very significant test.

CONCLUSION

A sealed, high repetition mode, e-beam sustained amplifier has been constructed and tests have been performed on large scale catalyst artefacts developed specifically by the UK industry consortium for this type of system. Prolonged sealed-off operation of an e-beam sustained system has been successfully demonstrated.
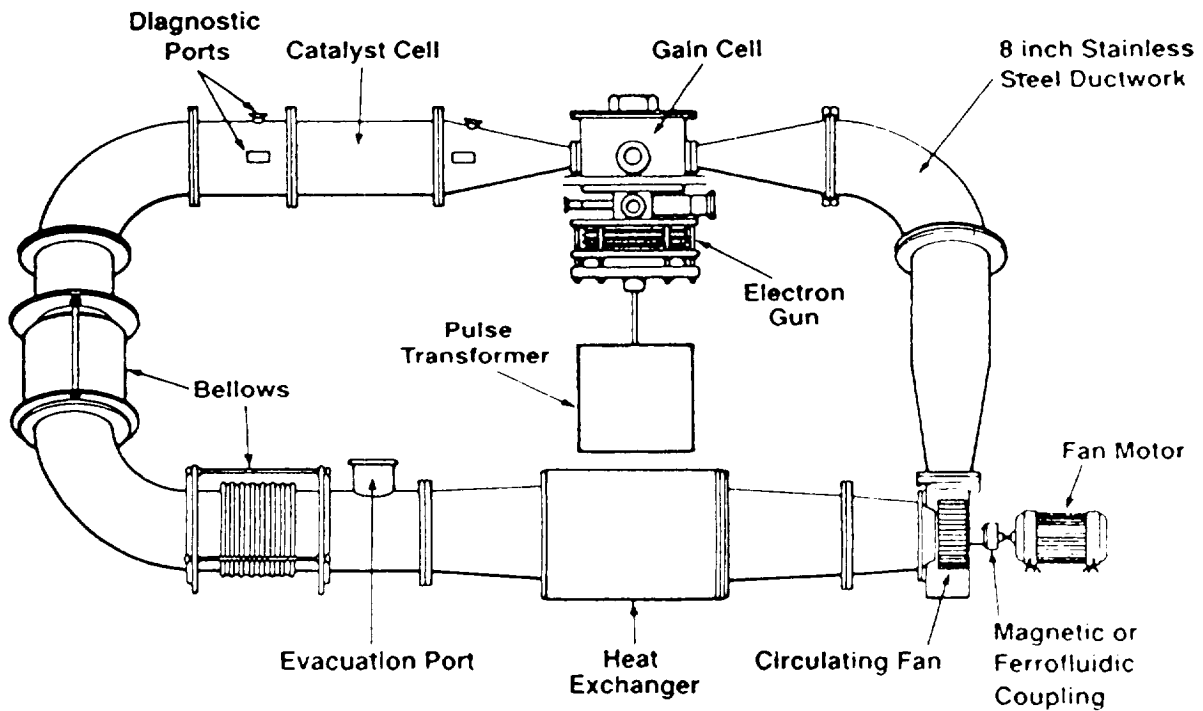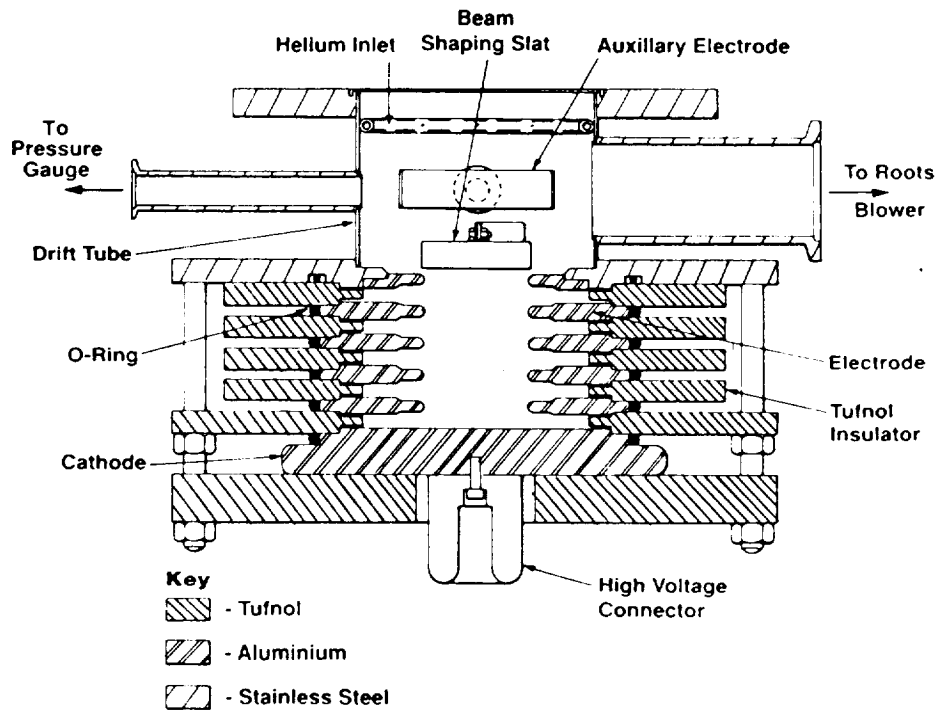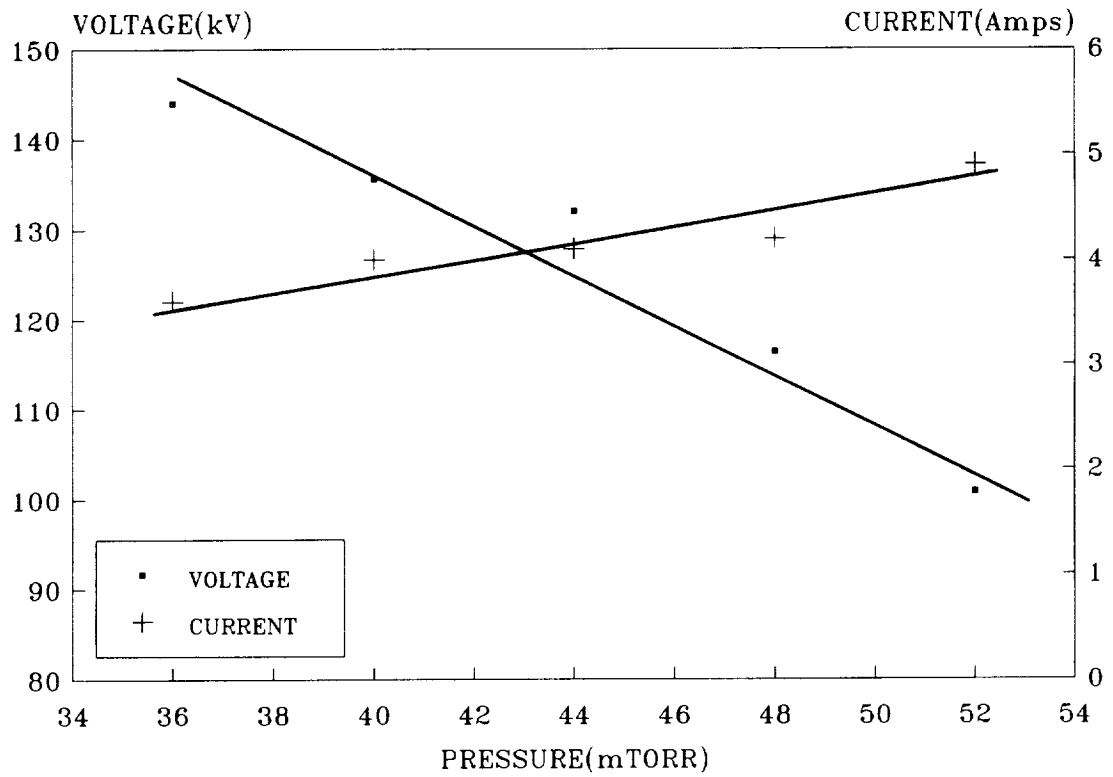
Diagnostic Ports | **Catalyst Cell** | **Gain Cell** | **8 inch Stainless Steel Ductwork**

Electron Gun

Pulse Transformer

Bellows

Fan Motor

Evacuation Port | Heat Exchanger | Circulating Fan | Magnetic or Ferrofluidic Coupling

Helium Inlet | **Beam Shaping Slat** | **Auxillary Electrode**

To Pressure Gauge

To Roots Blower

Drift Tube

O-Ring

Electrode

Tufnol Insulator

Cathode

Key

⬚ - Tufnol

⬚ - Aluminium

⬚ - Stainless Steel

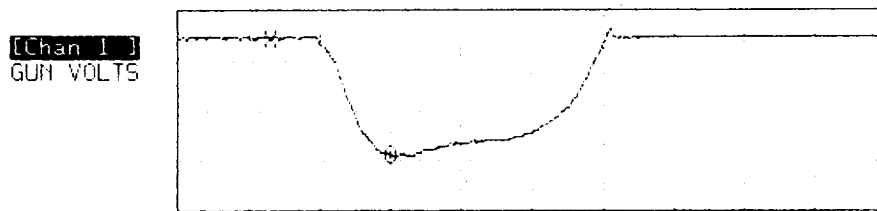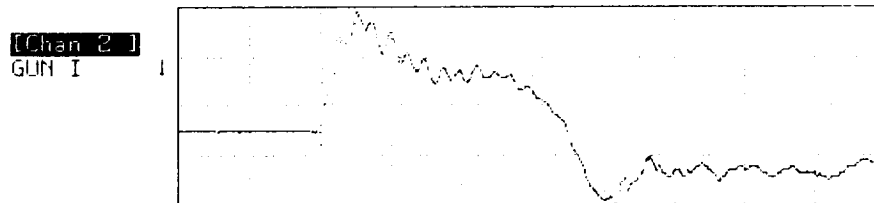High Voltage Connector

FIGURE 3: GUN OPERATIONAL CHARACTERISTICS

VOLTAGE WAVEFORM

(60 kV per div)

CURRENT WAVEFORM

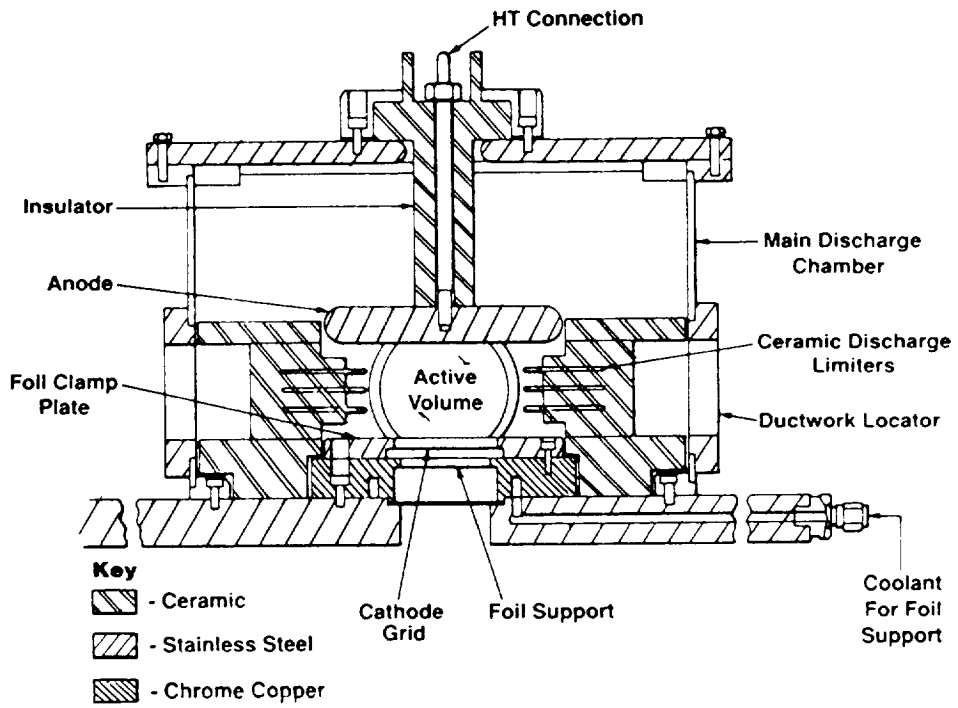(2.5 Amps per div)

FIGURE 4: ELECTRON GUN WAVEFORMS

364

Key
- Ceramic
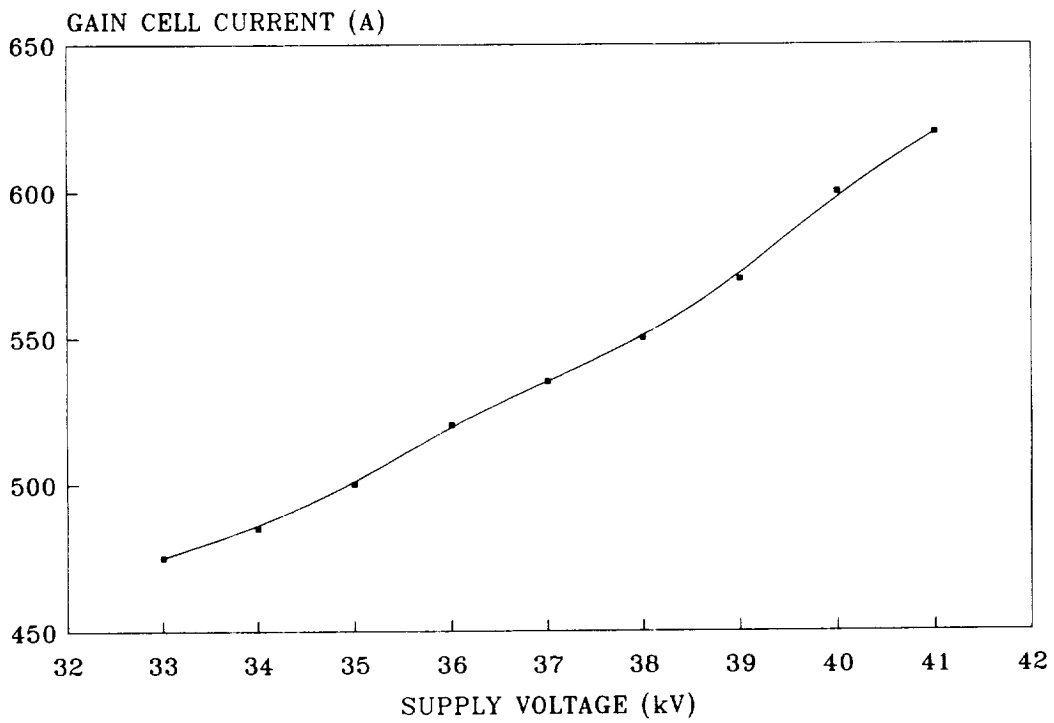- Stainless Steel
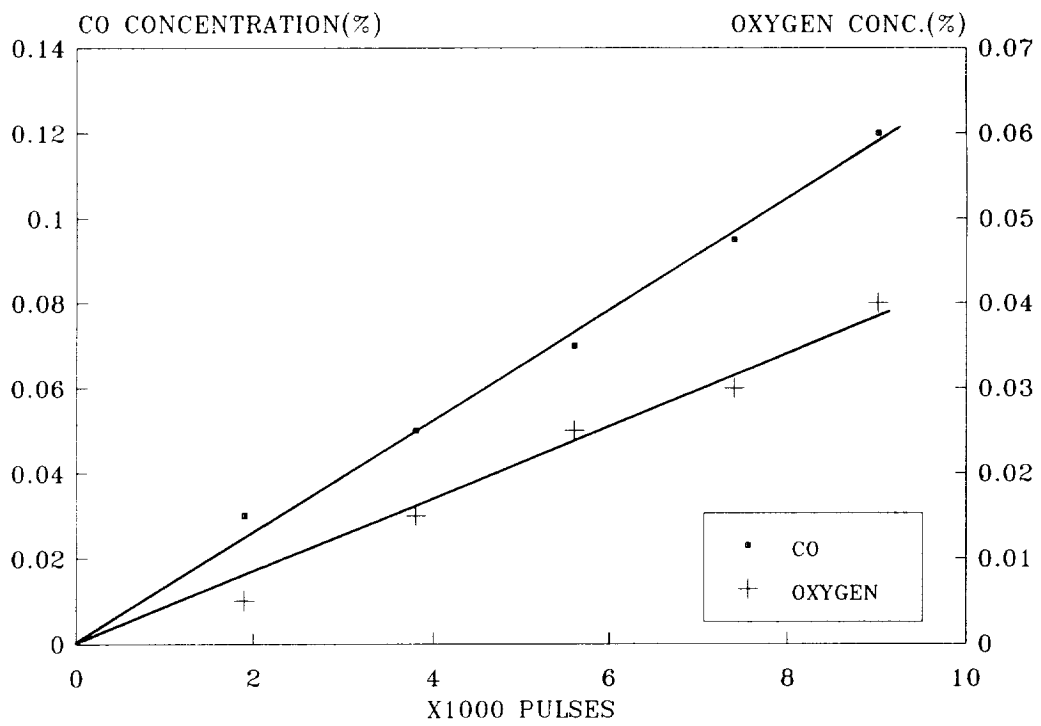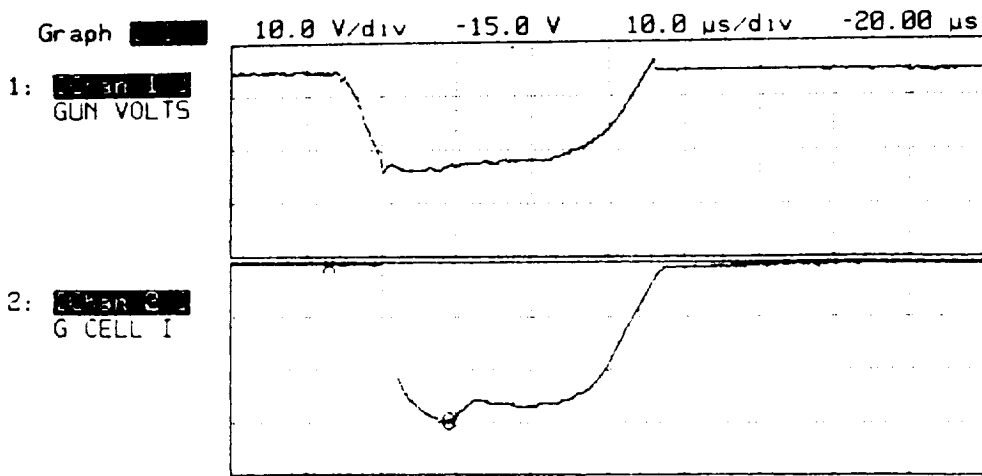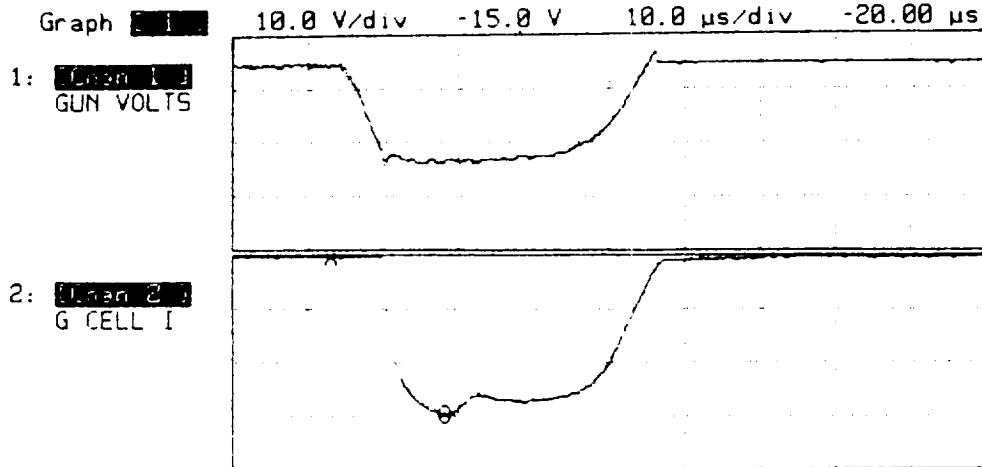- Chrome Copper

FIGURE 5: GAIN CELL DESIGN

FIGURE 6: GAIN CELL CHARACTERISTICS

FIGURE 7:   UNCATALYSED OXYGEN BUILD-UP

WAVEFORMS AT BEGINNING OF LIFETEST

WAVEFORMS AFTER 2 MILLION PULSES

FIGURE 8

GUN VOLTAGE : 125 kV   GAIN CELL CURRENT : 580 AMPERES

GUN PRESSURE : 40 mTORR   PFN VOLTAGE : 36.5 kV

CATALYST : Pt/Pd/Mn MONOLITH

TEMPERATURE : 30 C

STARTING DATE : 20/9/89

DUTY CYCLE : 6-8 HOURS CONTINUOUS OPERATION / DAY

PRF : 6-7 Hz

TOTAL PULSES : 2,000,000

TOTAL PULSES ON FOIL : 2,264,000

FIGURE 9:   CATALYST LIFETEST DATA

A COMPACT, RUGGED, HIGH REPETITION RATE
CO$_2$ LASER INCORPORATING CATALYST

P M Schwarzenberger and X Matzangou
Applied Physics Division, GEC Avionics Limited
Borehamwood, Hertfordshire
United Kingdom

SUMMARY

The principal design features and operating characteristics of a high repetition rate CO$_2$ laser are outlined. The laser is a compact, rugged unit, completely sealed and incorporating unheated solid catalyst. Stable operation has been successfully demonstrated over a temperature range of -35°C to 65°C.

INTRODUCTION

There is currently a high level of interest in the use of CO$_2$ lasers for military and space applications. This has led to the development and testing of catalysts to provide long sealed pulse lifetimes without the need for gas replenishment.

At the 1986 NASA conference on Closed-Cycle, Frequency-Stable CO$_2$ Laser Technology, GEC Avionics reported the development of a sealed high repetition rate TEA CO$_2$ laser with a pulse lifetime of 20 million pulses using a solid catalyst (Reference 1). This paper provides an update on some of the work carried out by GEC Avionics since then, on high repetition rate lasers incorporating catalyst.

Having established a stable laser/catalyst system and demonstrated long-term sealed operation, the objectives of the work which followed were to produce a compact, rugged version of the laser suitable for tactical military use, and then qualify the unit against environmental requirements of which the most important are vibration and shock, and operation over a wide range of temperatures. Many of these stringent operating specifications also apply to space-based systems, such as the Laser Atmospheric Wind Sounder (LAWS).

One particular area of concern is low temperature stability, as all catalysts, depending as they do on chemical reactions, suffer a drop in activity as the ambient temperature is reduced.

LASER DESIGN

A schematic diagram of the laser is shown in Figure 1. The laser is a completely sealed unit, the gas seal being formed by a metal enclosure which also provides electromagnetic screening of the device. There is an output window incorporated to allow the laser beam to

C5

exit, and a military standard high voltage connector to provide connections to the discharge circuit. The laser discharge is formed between two modified Rogowski profile electrodes with a discharge volume of 11cm^3. A tangential fan, powered by a military standard motor, circulates the gas within the enclosure at a high speed. Catalyst is mounted in the region of the fan intake. A rugged mounting scheme has been introduced for the resonator optics, and parallelism between the cavity optics is retained over a wide temperature range. The size of the laser head is 300mm x 100mm x 90mm, and the weight is 3.9kg. A photograph of the laser is shown in Figure 2.

LASER PERFORMANCE

Typical laser performance parameters are summarised below:-

Power	870kW
Pulse Width	31 nanoseconds
Energy	64mJ
Beam Divergence	3.8 mRad
Beam Wander	0.18 mRad
Mode Purity	95% TEM_{00}
Polarisation	>100:1
Pulse Repetition Rate	50Hz maximum

CATALYST CHARACTERISATION

GEC Avionics are currently evaluating a variety of catalysts from both UK and US sources. In all cases, the precious metal catalysts are solid particles mounted to the inside of the laser gas envelope by a clamp arrangement without the use of any adhesives.

The oxygen generation rate of the laser is typically 0.12 μmoles/pulse, catalyst activities had an average value of around 0.25 μmoles/second/gram, and 70g - 100g of catalyst is used.

The laser was operated at a high repetition rate and various parameters monitored, initially at room temperature. One good indicator of the catalyst activity is the laser discharge stability; in a self-sustained laser, arcing, as opposed to the correct glow discharge, can occur due to electron attachment if oxygen levels in the laser gas mix rise above approximately 0.5%. For much of the initial characterisation, the discharge stability only was monitored during some more recent testing; laser output power measurements were also recorded. Following successful operation at room temperature, the laser system was installed in a temperature chamber with a suitable aperture to allow the laser beam to exit, and diagnostic equipment was placed outside the chamber.

CATALYST A

Using catalyst A, the laser was operated in a temperature chamber at 10Hz for periods of one hour at each temperature.

The results obtained are shown in figure 3, and indicate excellent stability at room temperature, with 100% discharge stability observed throughout the 10Hz, one hour run, and very good results from 0°C to 65°C. At -15°C, however, the discharge stability drops to less than 99%, an unacceptably low level, which is thought to be due to the drop in activity of the catalyst at these low temperatures. The laser was also operated for 50Hz, one second bursts at each temperature with 100% discharge stability, even at -15°C, presumably because the run time was too short for significant oxygen build-up. While this catalyst therefore may not meet the requirements for military use, where a low operating temperature of around -30°C is normally required, it may be suitable for space applications such as LAWS, where it is anticipated that the satellite temperature can be controlled to between 0°C and 100°C.

CATALYST B

With catalyst B installed to the unit, a number of measurements were taken. Power readings were taken with the laser at a variety of temperatures. These results are shown in figure 4, and indicate a high output power level over the tested range of 0°C to 60°C.

As before, discharge stability measurements were also recorded for a 10Hz, one hour run at each temperature and the results are shown in figure 5. These results are very encouraging as they demonstrate a good discharge stability at the low end of the military temperature range, for an extended period of laser operation.

The laser was then subjected to 10 minutes random vibration in each of three axes, at a level of 6g RMS from 5Hz to 2000Hz, with no cracking or dusting of the catalyst particles.

CATALYST C

With catalyst C installed to the laser, discharge stability results were obtained over the range -35°C to 65°C and are shown in figures 6, 7, and 8, for 10Hz, 30Hz and 50Hz operation respectively. Again these results are very promising, in that they demonstrate good discharge stability over the entire temperature range required for military applications for various laser repetition rates and operating times.

They were followed by peak power and pulse width measurements taken at a range of temperatures. Figure 9 shows the output power and pulse width, at 30Hz, and figure 10 shows similar results at 50Hz. In both cases the output power remains high, even at the lowest extreme tested, -35°C, and the pulse width remains essentially constant indicating a consistent gas mix at all temperatures.

Figure 11 shows measurements at the start and end of a 10Hz, one hour run, at different temperatures. They show a drop in laser output of typically 15% over the one hour run, and a slight rise in the pulse

width. The parameters even at the end of the run are well above the laser output requirements, and a short rest period is found to restore the power to its original level.

Taken together, these results demonstrate good stability and a high laser output power over a wide temperature range. It should also be noted that, throughout the series of tests, the transverse mode quality of the laser output remained constant, with no evidence of detuning at temperature extremes. This is a particularly notable engineering achievement, as it implies the resonator optics remained parallel to within approximately five arc-seconds, over the entire temperature range tested.

In initial proving tests, the catalyst was tested for a total of 90 minutes random vibration and six 30g, 11ms shock pulses, with no adverse effects.

A laser incorporating Catalyst C was exposed to 10 minutes 6g RMS random vibration in each of three axes. The laser output was consistent before and after the test, there was no evidence of damage to any laser components, and no cracking or dusting of the catalyst.

CONCLUSION

Over the past three years, GEC Avionics' pioneering work in long life, high repetition rate CO_2 lasers has continued with the development of a compact, rugged version of the laser.

The unit has been shown to survive severe levels of environmental testing, and stable operation with high output powers has been demonstrated over a temperature range suitable for both military and space applications. This is indicative not only of the recent advances in laser catalyst technology, but also of the high engineering standards of laser design and construction.

REFERENCES

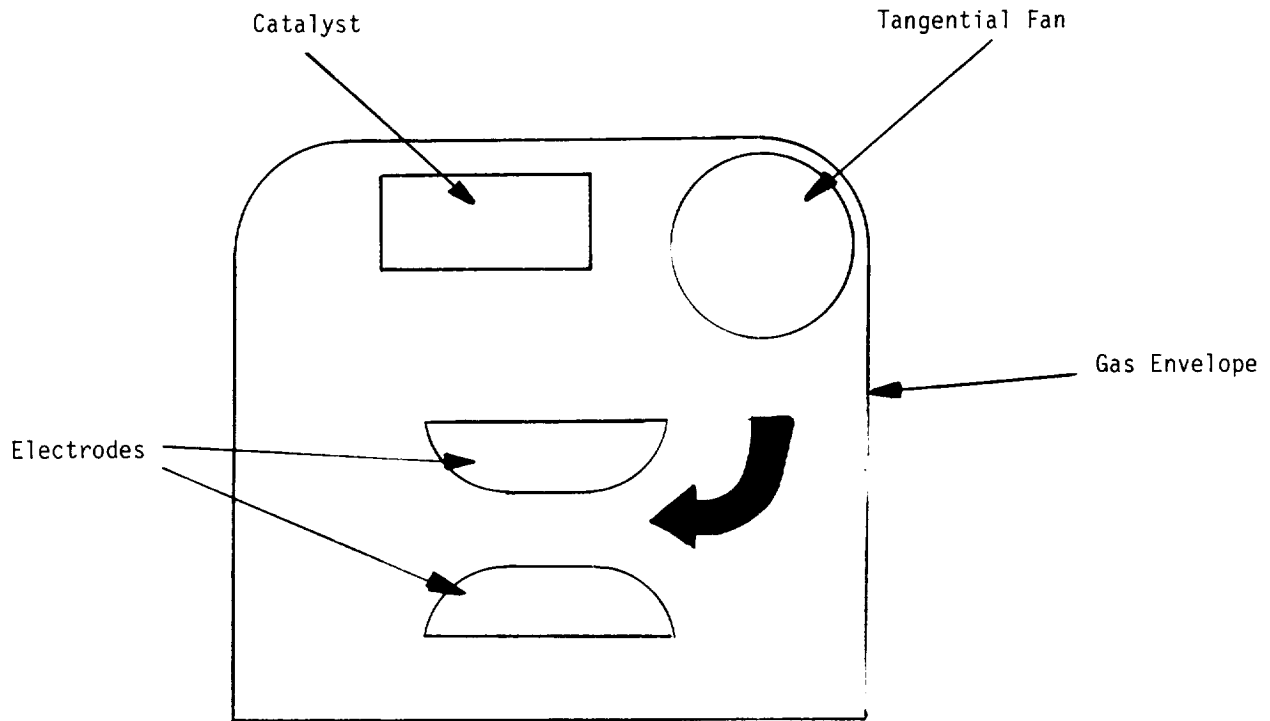1. H T Price, S R Shaw: NASA Conference Publication 2456, pages 77-84, 1986.

Figure 1:   High Repetition Rate Laser Schematic
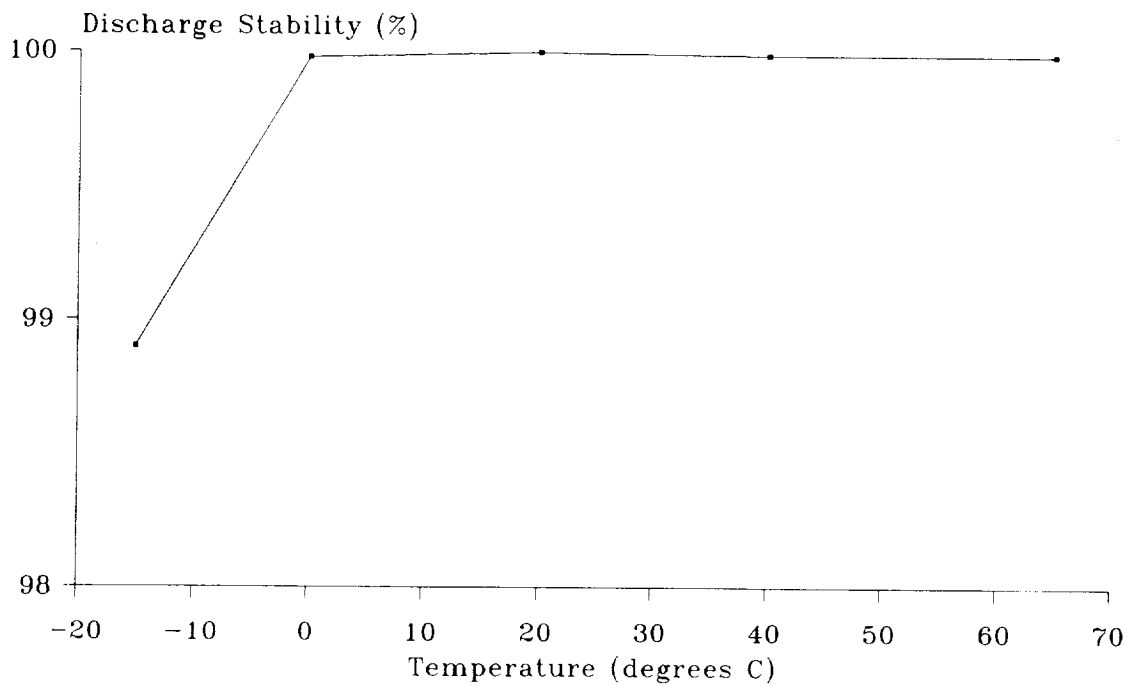

Figure 2

Catalyst A   10 Hz, 1 hour run

Figure 3

Catalyst B   30 Hz, 2 minutes run

Figure 4
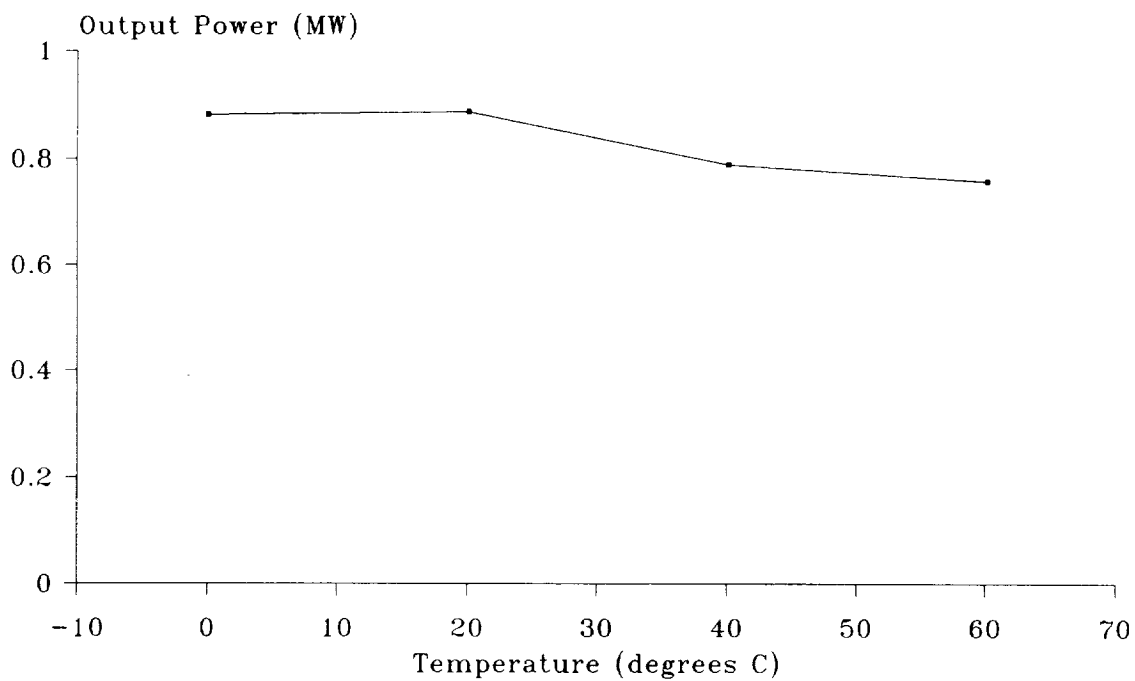
374

Catalyst B   10 Hz, 1 hour run

Discharge Stability (%)

Temperature (degrees C)
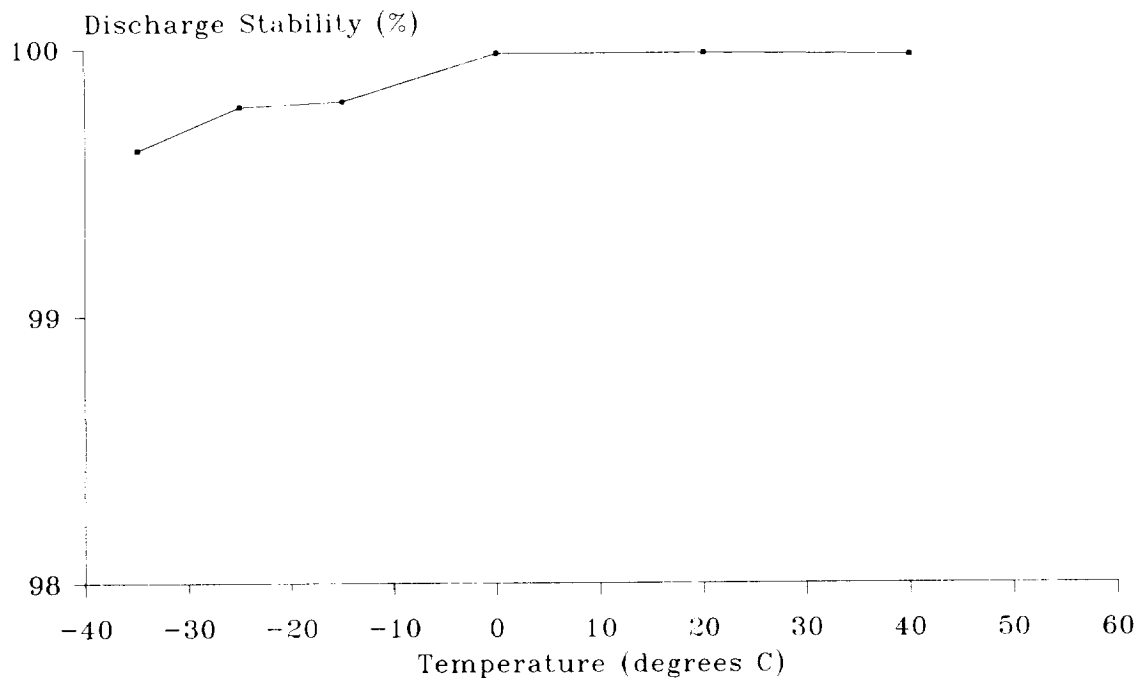
Figure 5

Catalyst C   10 Hz, 1 hour run

Discharge Stability (%)

Temperature (degrees C)
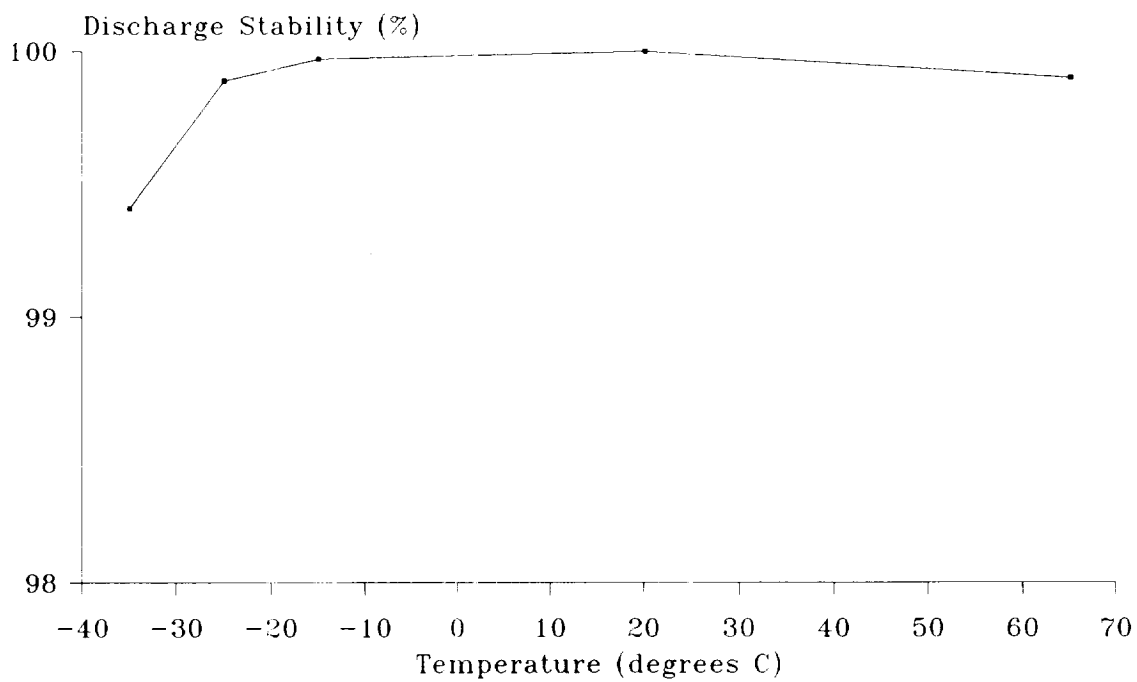
Figure 6

Catalyst C   30 Hz, 2 minutes

Discharge Stability (%)
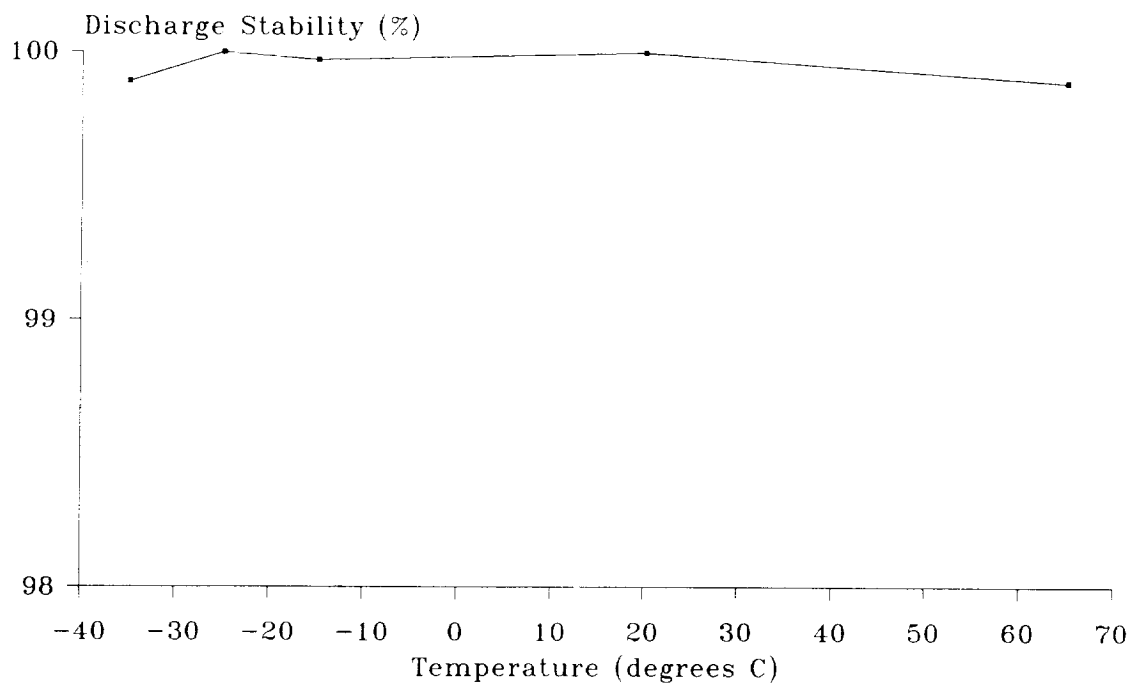
Figure 7

Catalyst C   50 Hz, 1 second

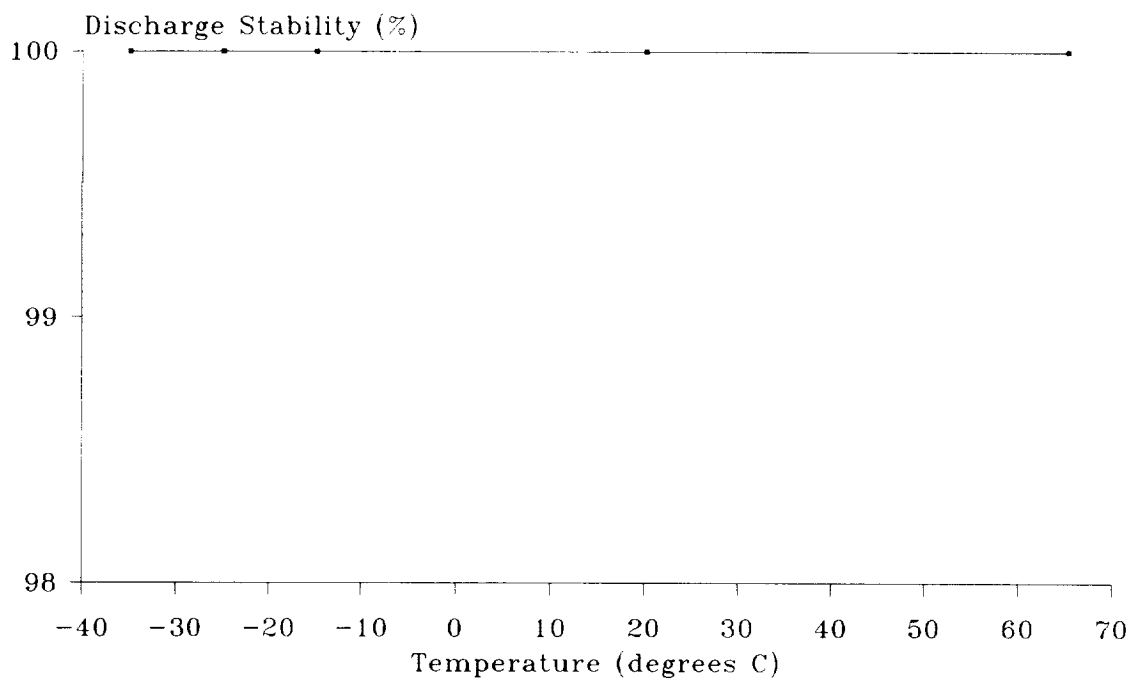Discharge Stability (%)

Figure 8

Catalyst C   30 Hz, 2 minutes run
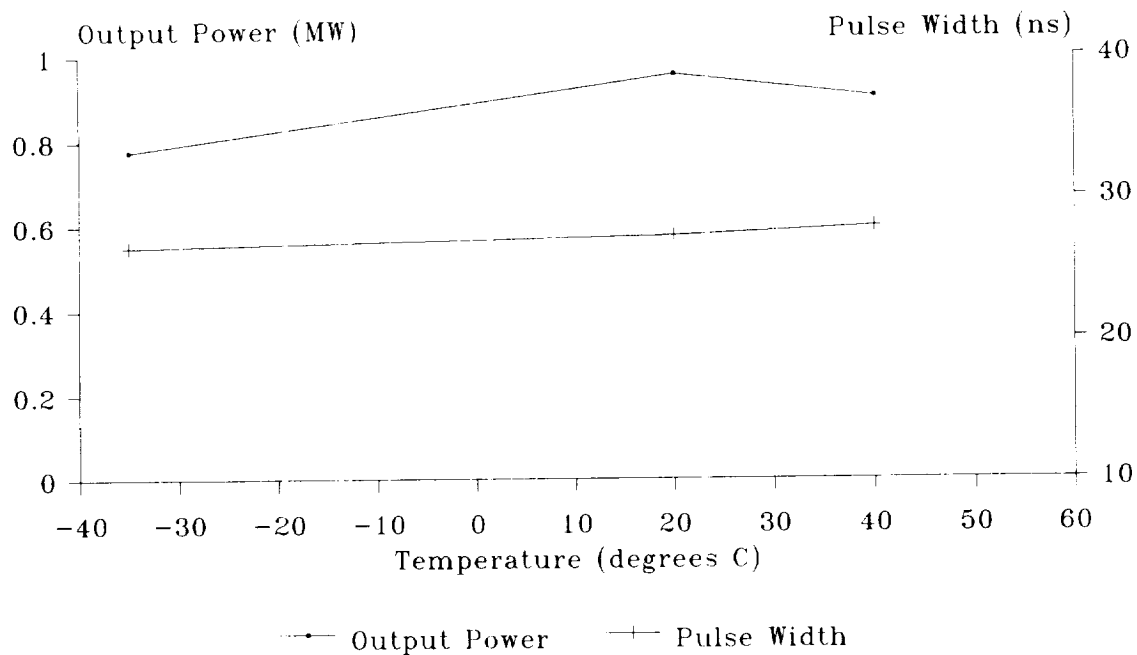

Figure 9

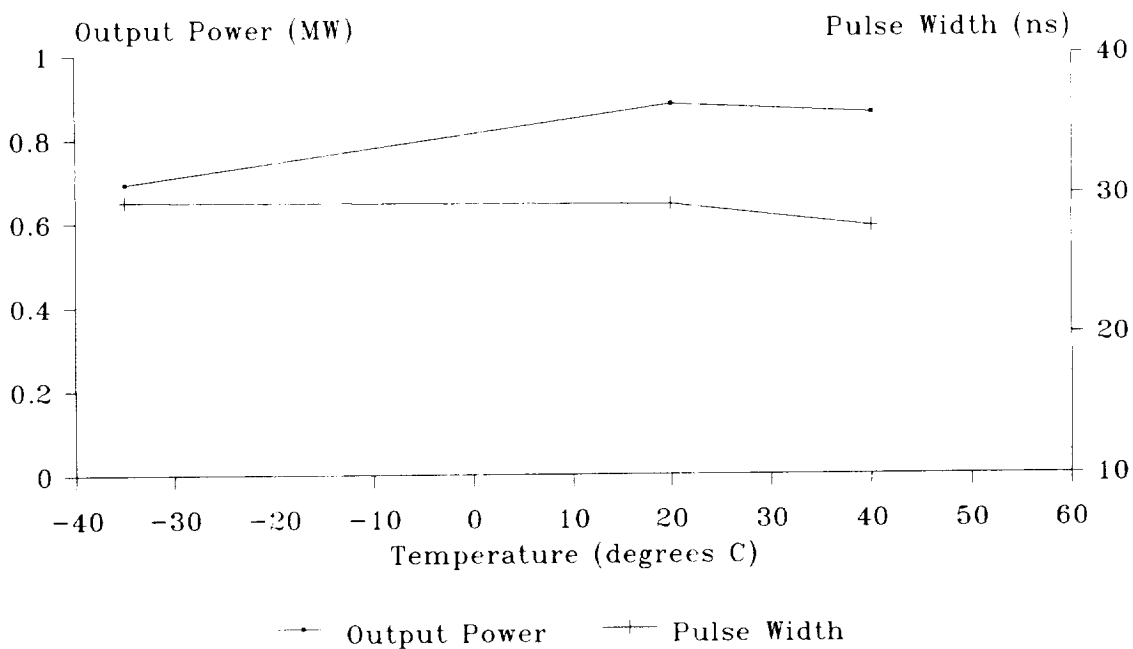## Catalyst C   50 Hz, 1 second run

Figure 10

377

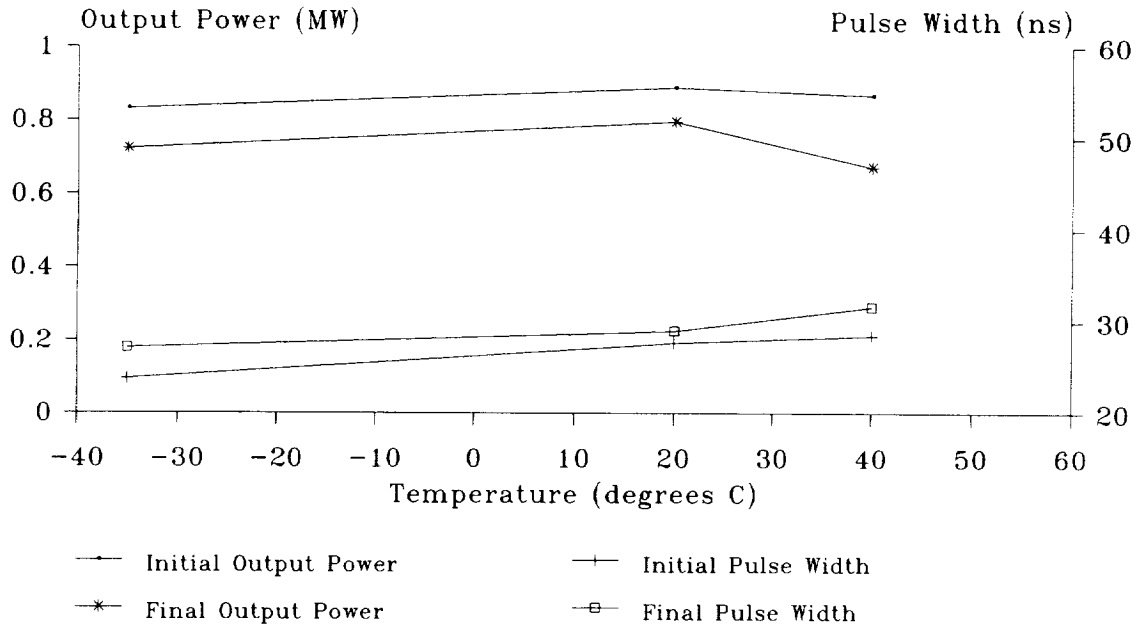## Catalyst C   10 Hz, 1 hour run

Figure 11

PERFORMANCE OF ALUMINA-SUPPORTED Pt CATALYSTS IN AN ELECTRON-BEAM-SUSTAINED CO_2 LASER AMPLIFIER

D.L. Cunningham, P.L. Jones, C.I. Miyake, and S.E. Moody
Spectra Technology, Inc.

SUMMARY

The performance of an alumina-supported Pt catalyst system used to maintain the gas purity in an electron-beam-sustained (636) isotope CO_2 laser amplifier has been tested. The system characteristics using the two-zone, parallel flow reactor were determined for both continuous- and end-of-day reactor operation using on-line mass spectrometric sampling. The laser amplifier was run with an energy loading of typically 110 J-ℓ/atm and an electron-beam current of 4 mA/cm^2. With these conditions and a pulse repetition frequency of 10 Hz for up to 10,000 shots, increases on the order of 100 ppm O_2 were observed with the purifier on and 150 ppm with it off. The 1/e time recovery time was found to be approximately 75 minutes.

INTRODUCTION

Purification of gas mixes used in isotopic or long-life carbon dioxide lasers has become an increasingly active area of investigation. For ground-based applications where power and size requirements are not limiting factors, traditional catalyst technology may be employed, such as the well-developed alumina-supported platinum catalysts. In the present work, we have used an alumina-supported Pt catalyst to provide either on-line continuous or "end-of-day" purification of 13:2:1 He:N_2:$^{13}CO_2$ laser gas mixtures used in a large-scale laser amplifier.

The laser amplifier system (CORA) is an atmospheric pressure, electron-beam-sustained, pulsed discharge device with the parameters of Table I. The design emphasizes the use of clean and stable materials for maintaining the purity of the isotopic CO_2 used in the 6200-ℓ device. The catalyst system is incorporated into the amplifier by attaching it to an ancillary system that provides purging of the anode triple point and the electron-beam drift regions of the gain module assembly. Approximately 9 ℓ/sec are removed from the gain module, of which 3 ℓ/sec are sent through the catalyst bed housed in a separate unit.

The catalyst system was built to our specifications by Applied Photonics, Inc. It consists of a two 30" Iconel retort tubes each containing 4 to 5 mesh-size platinized

pellets layered between stainless steel strainer elements. The tubes each have a surface area of approximately 7500 cm^2, are separately heated, and are arranged in a parallel flow configuration. Based upon vessel size and flow rates the time required to pass a module volume through the purifier is approximately 34 minutes. Typically the catalyst zones are held at 600 ± 5 °C during operation with the gas entering and leaving the purifier at room temperature.

Initial treatment of the catalyst after receipt from Applied Photonics was to heat the catalyst to 800 °C in steps which maintained a 100 mTorr or better vacuum above the catalyst. The catalyst was then held at 800 °C for one hour after outgassing was complete and allowed to cool. The system was flushed with a laser mix using $^{12}CO_2$, evacuated, and the heating process repeated to 300 °C. At this point the purifier was again flushed with laser gas, evacuated again, and the catalyst heated to 800 °C under a continuous flow of laser gas. The laser gas was discarded, the complete system pumped to 5 x 10^{-5} Torr and refilled with a clean gas mix. Initial experiments were performed with carbon-12 carbon dioxide. The quality of the laser gas in the module was monitored using a quadrupole mass spectrometer and the discharge behavior of the gas. Since the discharge diagnostics included color video as well as current and voltage monitors, it was very easy to spot changes in the gas composition either by changes in the discharge color or the presence of bright spots in enhanced field regions of the discharge, as well as by changes in the discharge impedence.

The quadrupole mass spectrometer was a Dycor 200M, 0-200 amu gas analyzer with computer control and data acquisition. The position available for sampling from the gain module was not directly on the flow loop, so the mixing time of the flow loop with other regions needed to be considered in measurements involving real-time monitoring of the gas composition. The mixing time was observed to be the order of 30 minutes. The pressure at the QMS was maintained at a tolerable level by providing a differentially pumped sample volume. The first aperture was a small-diameter, thin-walled hole in a copper disk while the second was provided by a sampling valve provided by Dycor. A mechanical forepump was used as the differential pump. Calibration of the spectral intensities was made using the known composition of the commercial laser gas mixes and assuming constant ionization efficiencies. Examples of the data are shown in Figure 1.

RESULTS AND DISCUSSION

The first round of experiments involved running the system with the catalyst cold. The gas was sampled before and after the accumulation of 14,000 shots at 3-kJ energy loading per shot. The O_2 concentration rose 208 ppm from 135 ppm to 343 ppm; an oxygen generation rate of 30 ppm - L/kJ for the device. This was lower than expected based upon DVT studies in a single-shot device using similar materials. The reason is due the the ability to effectively electron-beam scrub the insulator surfaces of the discharge volume in the CORA device. We found that electron-stimulated desorption from the insulator surfaces produced large quantities of oxygen and water and that 15,000 shots of the electron beam (order 2 mA/cm^2 and 150 keV

at the insulator) and simultaneous flushing of the gas were required to produce a clean discharge and stable gas composition.

The catalytic purifier was then heated and the laser gas cycled for several hours. The plotted data in Figure 2 show that the oxygen concentration decayed with a 1/e time of 75 minutes.

For our application, use of the purifier at all times is desired. A typical run of the system is several short bursts of a few thousand shots within an hour of a 10,000 shot run at 10 pps and full energy loading and a run time of just over 17 minutes. The amplifier then requires a two-hour cool-down period. Under these conditions continuous on-line purification maintains a stable initial gas composition. For example, running the purifier at 600 °C while operating through the accumulation of 32,000 shots in one day resulted in a change in O_2 concentration, as measured within a half hour of the final firing, of 20 ppm over that at the beginning of the day. The gas composition recovered completely by leaving the purifier on a longer time. An estimated "dynamic" production rate, which ignores the issues of gas mixing times, is 20 ppm - L/kJ. This is two thirds of the rate of oxygen production during a run without the purifier operating.

Table I

CORA WIDEBAND AMPLIFER - GENERAL INFORMATION

- Electron-Beam-Sustained Pulsed Discharge

- Gas Mix: 13:2:1 $He:N_2:CO_2$

- Clean System, Designed for $^{13}CO_2$ Isotope

- Parameters

  - 10-pps burst-mode operation of 10,000 shots

  - ~110-J/ℓ-atm energy loading

  - ~5-mA/cm^2 electron beam

  - 25-kV, 3.5-kA discharge

  - ~2.5-m active length

  - 2.5 ms^{-1} transverse flow through cavity

  - 2400 ℓ flow loop volume
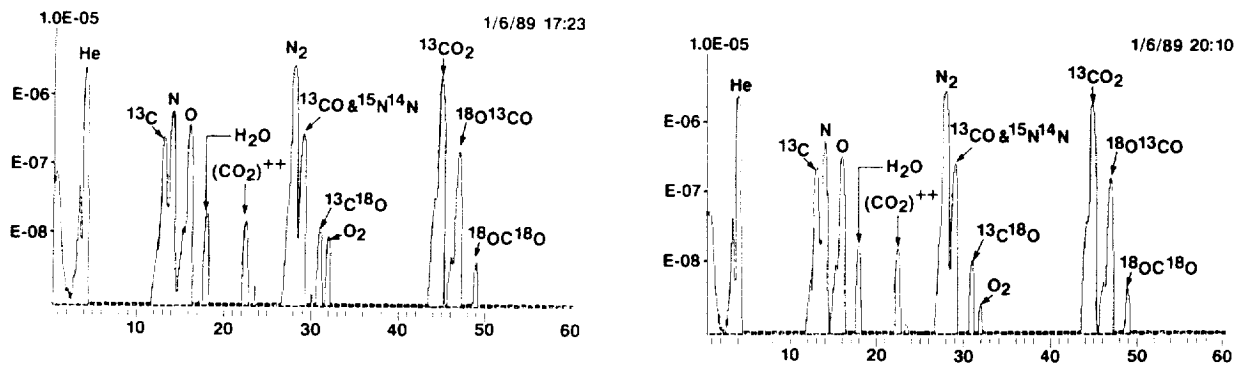   6200 ℓ total volume

Figure 1. Mass Spectra for ^{13}C Isotope Showing Reduction in O_2 by Catalyst
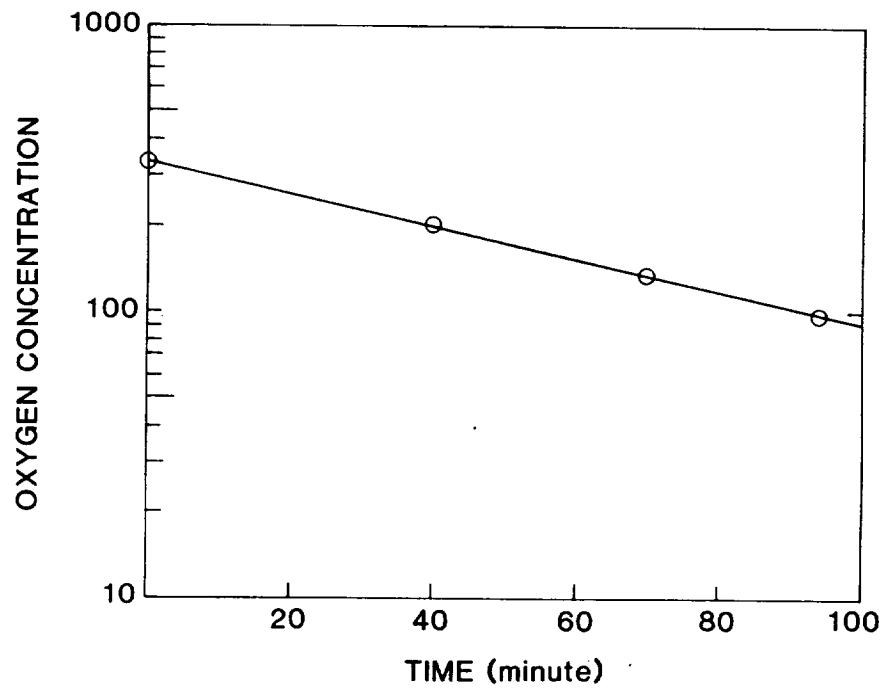

Figure 2. Purifier Performance: Gas Cleanup After 14,000 Shots

MONITORING OF CATALYST PERFORMANCE IN CO_2 LASERS
USING FREQUENCY MODULATION SPECTROSCOPY WITH DIODE LASERS

Liang-guo Wang
Department of Physics, College of William and Mary
Williamsburg, Va

Glen Sachse
NASA Langley Research Center
Hampton, Va

Closed-cycle CO_2 laser operation with removal of O_2 and regeneration of CO_2 can be achieved by catalytic $CO-O_2$ recombination. Both parametric studies of the optimum catalyst formulation and long-term performance tests require on line monitoring of CO, O_2 and CO_2 concentrations.

There are several existing methods for molecular oxygen detection. These methods are either intrusive (such as electrochemical method or mass spectrometry[1]) or very expensive (such as CARS, UV laser absorption[2,3]).

We present here a high-sensitivity spectroscopic measurement of O_2 using two-tone frequency modulation spectroscopy (FMS) with a GaAlAs diode laser. Recently frequency modulation spectroscopy has been developed as a powerful method of doing highly sensitive, real-time spectroscopic measurements[4-8]. The theory of single-tone FMS and two-tone FMS have been studied and discussed in detail[4-6]. Since frequency modulation of diode lasers can be achieved by direct injection current modulation, FMS with near infrared diode lasers becomes a very attractive technique to make inexpensive, room-temperature spectroscopic probes for a variety of gases. It has been successfully used for water vapor absorption measurements at wavelengths near 815 nm[9] and methane absorption at wavelengths near 840 nm[*]. With careful selection, an inexpensive commercial laser diode can be obtained that is wavelength tunable from 760-770 nm, where the oxygen A band absorption occurs. This is the $v'=0$ $\leftarrow$ $v''=0$ band of the magnetic dipole transition from the $x\,^3\Sigma_g^-$ ground electronic state to the excited $b\,^1\Sigma_g^+$ state. This band is known as the O_2 atmosphere band and has been well studied for line strengths, line widths and other spectroscopic parameters[10-13].

We have used a frequency modulation spectrometer, which was built at the University of Virginia, to make the O_2 spectroscopic measurement. Fig. 1 shows the schematic diagram of the frequency modulation spectrometer. A GaAlAs laser (Sharp LT030MF) operating at near 760 nm was mounted on a thermoelectrically cooled/heated block. The laser frequency is varied either by sweeping the injection current of the diode laser or by scanning its temperature with a tunability of 0.12 cm^{-1}/mA (3.6 GHz/mA) or 1.1 cm^{-1}/°C (33 GHz/°C), respectively. In the first case the injection current of the diode laser is swept by an internal function generator to provide straightforward injection-current tuning of the laser frequency. Injection-current tuning gives relatively fast scans ($\approx$120 Hz) which permits us to monitor the FM signal directly on an

---

[*]L. G. Wang, unpublished data.

oscilloscope. This frequency modulation spectrometer also includes a computer-interfaced temperature controller to provide a slow scan of temperature and hence a slow scan of the frequency of the laser. The temperature controller provides a temperature stability of better than 0.01°C over several hours. A built-in automatic power controller stabilizes the laser output power within 2% when the laser temperature is varied from 10°C to 60°C. The GaAlAs diode laser is injection current modulated at two closely spaced frequencies (1 GHz ± 12 MHz) using capacitive coupling. The two-tone frequency modulated light from the laser is collimated by a 7-mm focal-length lens and passes through a 20-cm-long O_2 sample cell at approximately one atmosphere pressure. The 24 MHz rf beat signal of the two laser modulation frequencies is detected and amplified by using a photodetector (EG & G FND-100) and low-noise rf amplifiers. The signal is then phase detected by a mixer. Finally the signal is directed either through a 100-kHz low-pass filter to be displayed on an oscilloscope (i.e. for injection current tuning) or through a 0.8-Hz low-pass filter to be plotted on a plotter or to be stored into a computer (i.e. for temperature tuning).

Fig. 2 shows two-tone FMS signals of five Oxygen A band absorption lines. The absorption for these lines ranged from 0.8% to 1.2%. The O_2 A band consists of P and R branches. Due to the splitting of the ground electronic state rotational levels, each of these branches is composed of pairs of lines (PP and PQ for P branch; RR and RQ for R branch). The five absorption lines in Fig. 2 belong to the R branch of oxygen A band near 760 nm.

FMS[*] with diode lasers provides high detection sensitivity. Near quantum limit absorption sensitivity of 3×10^{-7} in a 0.8 Hz bandwidth for water vapor absorption lines has been reported[9]. A sensitivity of 10^{-6} can be easily obtained with a little care on eliminating the interference fringes. With a reference cell of O_2, the GaAlAs diode laser can be locked at a particular oxygen absorption line using an electronic feedback circuit. In this way the continuous monitoring of oxygen concentration in an on-line sample cell can be achieved. The minimum detectable (i.e. with S/N of 1) optical depth is estimated to be 5 ppm·meters with a 1-Hz bandwidth.

In conclusion, we have demonstrated a high-sensitivity spectroscopic measurement of O_2 using the two-tone FMS technique with a near infrared GaAlAs diode laser. Besides its inexpensive cost, fast response time, nonintrusive measurements and high sensitivity, this technique may also be used to differentiate between isotopes due to its high spectroscopic resolution.

This frequency modulation spectroscopy technique could also be applied for the on-line monitoring of CO and CO_2 using InGaAsP diode lasers operating in the 1.55 μm region and H_2O in the 1.3 μm region. The existence of single mode optical fibers at these near infrared region makes it possible to combine FMS with optical fiber technology. Optical fiber FMS is particularly suitable for making

---

[*]FMS is frequency modulation spectroscopy.

point-measurements at one or more locations in the CO_2 laser/catalyst system.

REFERENCES

1. J. J. Singh, W. T. Davis and R. L. Puster: Proposed Fast-Response Oxygen Monitoring and Control System for the Langley 8-Foot High-Temperature Tunnel. NASA TP-2218(1983).

2. M. P. Lee, P. H. Paul and R. K. Hanson, Opt. Lett. 11, 7(1986).

3. J. E. M. Goldsmith and R. J. M. Anderson, Opt. Lett. 11, 67(1986).

4. G. C. Bjorklund, M. D. Levenson, W. Lenth, and C. Ortiz: Frequency Modulation (FM) Spectroscopy: Theory of Line Shapes and Signal-to-noise Analysis. Appl. Phys. B32, 145(1983).

5. G. R. Janik, C. B. Carlisle, and T. F. Gallagher: Two-Tone Frequency Modulation Spectroscopy. J. Opt. Soc. Am. B 3, 1070 (1986).

6. D. E. Cooper and R. E. Warren: Two-Tone Optical Heterodyne Spectroscopy with Diode Laser: Theory of Lineshapes and Experimental Results. J. Opt. Soc. Am. B4, 470 (1987).

7. N. -Y. Chou and G. W. Sachse: Single-Tone and Two-Tone AM-FM Spectral Calculations for Tunable Diode Laser Absorption Spectroscopy. Appl. Opt. 26, 3584(1987)

8. L. G. Wang, H. Riris, C. B. Carlisle and T. F. Gallagher: Comparison of Approaches to Modulation Spectroscopy with GaAlAs Semiconductor Lasers: Application to Water Vapor. Appl. Opt. 27, 2071(1988).

9. L. G. Wang, D. A. Tate, H. Riris and T. F. Gallagher: High-Sensitivity Frequency Modulation Spectroscopy With A GaAlAs Diode Laser. J. Opt. Soc. Am.B, 6, 871(1989).

10. D. E. Burch and D. A. Gryvnak: Appl. Opt. 8, 1493(1969).

11. J. H. Miller, R. W. Boese and L. P. Giver: J. Quant. Spectrosc. Radiat. Transfer 9, 1507(1969).

12. L. S. Rothman et al.: The HITRAN database (1986 edition). Appl. Opt. 26, 4058(1987).

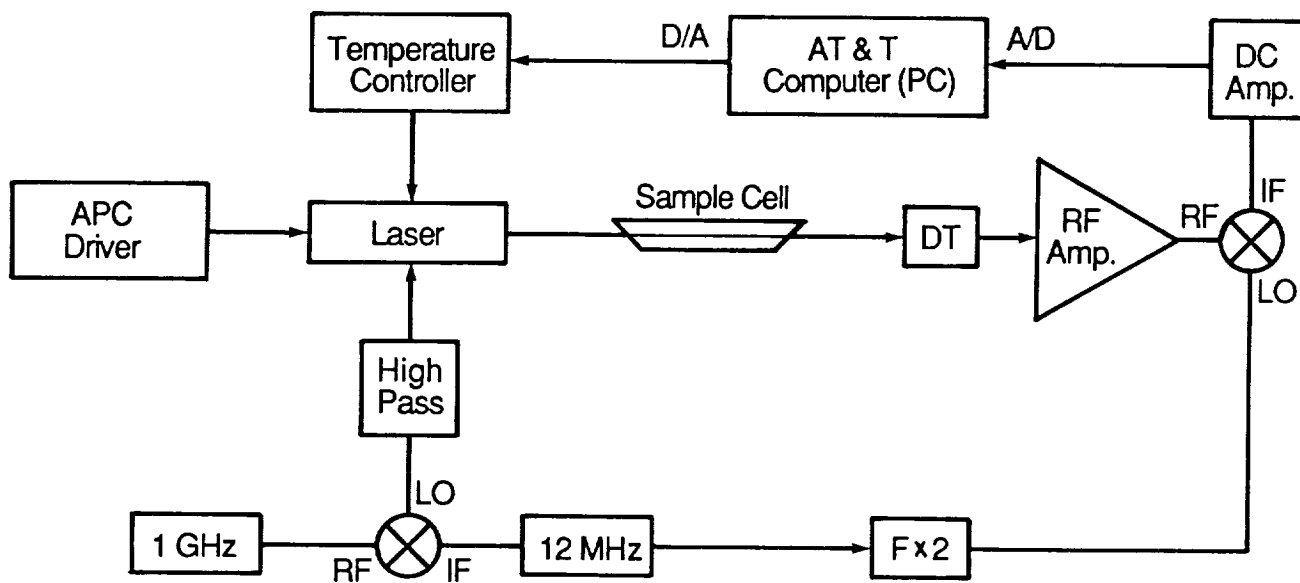13. K. J. Ritter and T. D. Wilkerson: J. Mol. Spectrosc. 121, 1(1987).

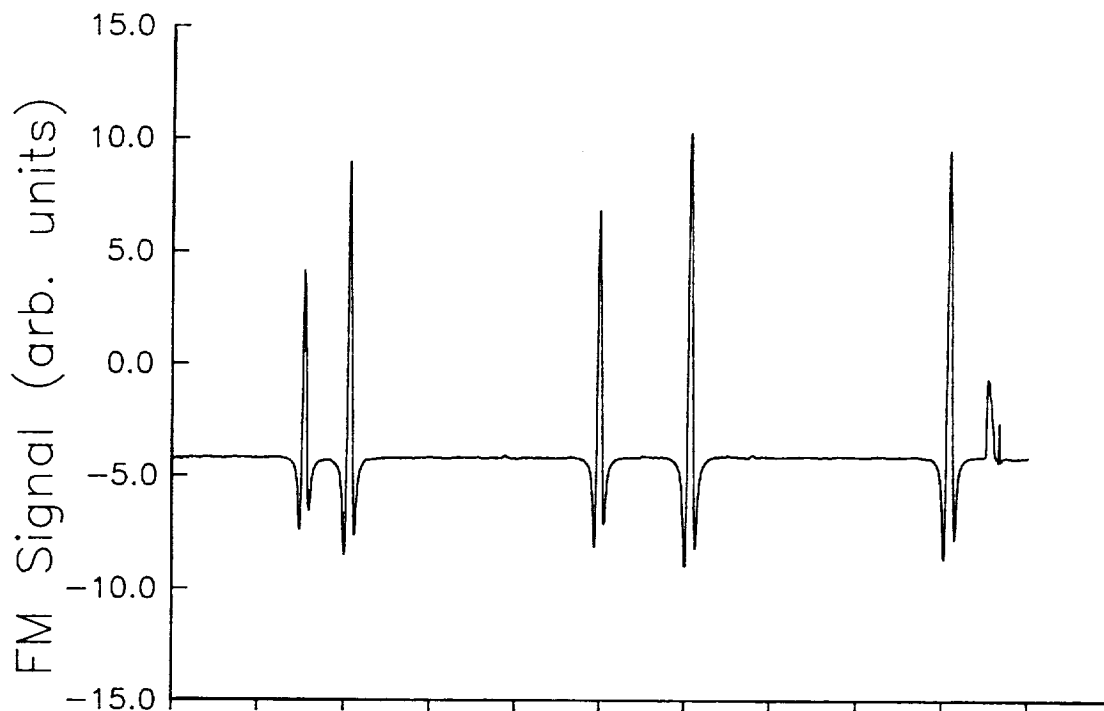Figure 1. Experimental setup for two-tone frequency modulation spectroscopy.

Figure 2. Two-tone FMS signal of five O_2 absorption lines.

APPLICATIONS OF LOW TEMPERATURE CO-OXIDATION CATALYSTS

TO BREATHABLE GASES

Ehsan Noordally, and John R Richmond
UOP Limited, Enfield, Middlesex, EN3 7PN, England

SUMMARY

Modifications of tin oxide/precious metal catalysts described for use in CO_2 lasers have also been developed by UOP for use in other applications; namely, as low temperature CO oxidation components in fire escape hoods/masks for mines, aircrafts, hotels, and offices and in sealed environments, such as hyperbaric chambers and submarines. Tin oxide/precious metal catalysts have been prepared on a variety of high surface area cloth substrates for application in fire escape hoods. These show high and stable CO oxidation capability (10^4 ppm CO reduced to 10^1 ppm CO) at GHSV of 37,000 h^{-1} with water saturated inlet gas at body heat ($37^{\circ}C$) and below.

Water vapour plays an important role in the surface state/performance of tin oxide catalyst. Water-resistant formulations have been produced by the introduction of transition metal promoters.

Tin oxide/precious metal catalysts have also been developed for CO oxidation in the North Sea diving environment. These are currently in use in a variety of hyperbaric chambers and diving vehicles. Ambient temperature operation and resistance to atmospheric water vapour have been demonstrated, and as a result, they offer a viable alternative to hopcalite or heated catalyst systems.

A new range of non-tin oxide based low temperature CO oxidation catalysts is described. They are based on reducible metal oxides promoted with precious metals. Preliminary data on selected materials in the form of both cloth artefacts and shaped pellets are presented. They are expected to be applicable both to the breathable gas application area and to CO_2 lasers.

INTRODUCTION

The study of the heterogeneous oxidation of CO has been fruitfully researched by many investigators in heterogeneous catalysis and is still ongoing, as is evident at this workshop. Active catalysts have been prepared from simple oxides and

multicomponent oxides, largely from transition metals, groups III and IV of the periodic table. Many of these oxides contain small amounts of precious metals in order to achieve low temperature catalytic oxidation. Several catalysts have thus far been commercially developed, and although these are of considerable theoretical and practical significance, they do not all possess sufficient activity to warrant their use in, for example gas masks for effective removal of CO from air. For this purpose only the most powerful, highly reactive, oxidising catalysts can be utilized.

Catalysts used in breathable gas systems must initiate the oxidation of CO without an appreciable induction period. The reaction must proceed at the high space velocity required for breathing purposes and under all environmental conditions likely to be encountered in use. The catalyst must have a sufficiently long life and in static systems preferably be regenerable. The catalyst artefact must be sufficiently porous to offer very little resistance to air flow, i.e., low pressure drop across the catalyst bed, and have sufficient chemical stability to withstand prolonged storage at temperature up to 60°C. The ideal catalyst would be one that would be capable of reacting completely with CO in low as well as high gas/air concentration within the temperature range of 0-40°C and not be poisoned by water vapour or small amounts of impurity likely to be encountered in contaminated air.

APPLICATIONS

A major use of low temperature CO oxidation catalyst is in respiratory protection. The latter is necessary where the prevailing breathable environment is not capable of supporting life because of contamination with CO. The most usual circumstances are those involving fires and toxic gases encountered both by the public and fire rescue services. Low temperature CO oxidation catalysts reported here have been developed for this specific purpose, where CO removal down to ppm level is required for air purification and where the catalyst is

1. In granular form and is fitted as part of a life-support system either with or without supplemental oxygen.

2. Deposited on high surface area cloth and incorporated in a smokehood filter device.

These commercial low temperature tin oxide catalysts have found actual and potential use in

1. Diving industry
2. Underground shelters as static systems
3. Smokehoods or portable self-rescue breathing sets
4. Process applications

Diving Industry

Oil explorations in offshore locations have given rise to the need and development of extended duration diving techniques. Using a helium/oxygen mixture as the breathable gas, divers can work for several weeks at depths of up to 300 m. During this time the breathing gas is scrubbed clean of contaminants, such as CO_2, CO and NO_x, that are produced during respiration and welding operations. Removal of these toxic compounds together with close monitoring of the oxygen levels ensures a high level of diver safety. Precious metals on tin oxide with trace quantities of a promoter provide the CO scrubbing capability.

Typically hydrocarbon and sulphur compounds are removed by appropriate adsorbents upstream of the CO oxidation catalyst.

Underground Shelters

The provision by civil authorities of the safe shelters for the majority of the population in the event of a catastrophe or war is becoming a more acceptable practice. A major consideration in the design of such structures is environmental control equipment to prevent the buildup of toxic gases such as CO produced from smoking and fires and CO_2 from respiration. The precious metals on tin oxide are an appropriate catalyst for this application; it has high tolerance to water vapour and is regenerable.

Smokehoods

Fire in a confined area such as a mine, aircraft or a hotel room, frequently incapacitates and kills more from the smoke, poison gases and choking particles emitted than from the heat generated.

Oxygen levels often remain as high as 15-16% until just before the flashover point when the fireball moves through the whole of the confined area. Emergency self-rescue devices or smokehoods can therefore utilise catalytic oxidation of the CO to deal with that particular toxic component.

389

Filter self-rescue systems generally consist of adsorptive sections to remove toxic components, such as HCN, other acid gases and hydrocarbons, together with a catalytic system for the oxidation of carbon monoxide.

Rebreather systems typically provide supplemental oxygen by chemical means or pressure bottles. The CO_2 and H_2O are removed by appropriate adsorbents in the recirculating gas.

The filter systems need to cope with potentially high ambient CO levels and current draft standards are based on challenge gases containing 1% CO. Rebreather systems also have to deal with CO arising from potential leakage into the mask from the face and neck seal and from exhalation, but these levels will be lower.

Process Applications

Air fed to air-separation plants and compressors producing pressurised air for breathing purposes requires incoming air to be free of CO (and usually CO_2). Carbon dioxide, water and other contaminants can usually be adequately removed by the appropriate regenerable adsorbents, but carbon monoxide is not normally adsorbed sufficiently well.

Oxidation of trace CO can be achieved with catalysts described in this paper at typical compressor exit temperatures of 50-100°C, thus eliminating the need for additional preheat. Their ability to work at high relative humidity also eliminates the need for water vapour removal from the feed gas.

CATALYST DESIGN AND MANUFACTURE

The composition of almost any catalyst is dictated by the requirement for activity, stability and regenerability. In the case of a commercial precious metal catalyst, the economics of the process is an important consideration as well. The method of preparation, the precious metal precursors, the metal oxide/substrate, all have an important effect on the performance of the catalyst.

In certain applications, such as escape hoods where there may be no assisted gas circulation by fans, pumps or pressurised gas, the pressure drop across the catalyst is of particular importance.

Catalysts have therefore been produced in the form of impregnated cloth as well as granules of various configurations and the performance characteristics are discussed further on.

1. Precious metals/SnO_2 in extrudate form.

2. Precious metals/SnO_2 on highly adsorptive cloth fabric.

3. Precious metals/reducible metal oxide as an alternative non-tin oxide, low temperature CO oxidation catalysts, both on cloth fabric and in pellet form.

CATALYST TESTING AND EVALUATION

Three basic catalyst-activity testing methods have been adopted, depending upon the catalyst format and its final application. In all these tests, it is assumed that the only function of the catalyst being considered is the oxidation of CO in the presence of H_2O and CO_2. Tests of complete devices always include the full range of poisons.

Filter Self-Rescuers or Smokehoods

Several draft test protocols are in existence for this type of device, including those issued by the United Kingdom Civil Aviation Authority, the Japanese and British Coal industry and others. There are differences, but in respect to CO removal, a typical challenge conditions would be:

1% CO
3.5% CO_2
balance air at > 80% R.H.
inlet temperature, 20°C or 37°C
gas flow – 30 l/min sinusoidal
        – 90 l/min constant

Performance requirements also vary but again typically would be:

exit CO, below 100 ppm
test duration, 20 minutes
total exit CO volume, < 200 cm^3
pressure drop, < 8.1 cm H_2O

Both sinusoidal flow and constant flow, once-through testing has been applied to these low temperature CO oxidation catalysts. The testing conditions are given in the Appendix.

Recirculating Units (Both Static and Portable)

CO oxidation can of course be achieved by means of forced recirculation over the catalyst in a multipass mode. This is typical of either a rebreathing escape device or static environmental system, such as a submarine or diving chamber.

Typically, granular catalyst or monolith is used in these applications and the test protocol made specific to the duty required. The test itself can be run as once-through conversion or in recirculation mode. One specific test protocol used by UOP in once-through mode is

Test gas	:	1% CO in air
Flow rate	:	2.5 $lmin^{-1}$
Pressure	:	atmospheric
Temperature	:	20-25 ^oC
Gas humidity	:	50-60%
Test duration	:	60 mins

$$\text{Catalyst efficiency} = \frac{\text{CO reacted over 60 mins}}{\text{Total CO passed}} \times 100$$

Volume of CO reacted per gram of catalyst in cm^3 $gram^{-1}$ is given by

$$\frac{\text{Flow rate } (cm^3min^{-1}) \times \text{ time (mins) } \times \text{ gas conc(\%)} \times \text{ efficiency(\%)}}{\text{Weight of catalyst (grams)}}$$

Under these test conditions, the specified catalyst must convert 58 cm^3 of CO or more per gram to be acceptable.

CATALYST PERFORMANCE

Tin Oxide Based Granular Catalyst

Precious metals on tin oxide is one of a range of fully commercial low temperature CO oxidation catalysts. It is made in extrudate form, it has an average bulk density of 1.5 gcm^{-3} and it is regenerable. This catalyst exhibits long-term stability

392

during the reaction and is not only tolerant to water vapour, it actually performs better in the presence of wet gas, as is evident in figure 1, which is a typical set of results. It has long shelf life when kept in a closed container. It tends to deactivate when left in the open (figure 2), but total reactivation is achieved by hydrogen reduction and slow passivation, as illustrated in figure 1. This catalyst outperforms hopcalite in 2 major respects.

1. It oxidises CO at room temperature and below.

2. It is tolerant to high relative humidity.

Figure 3 illustrates the activity results of 3 commercial catalysts, namely precious metals/SnO_2, precious metal/Al_2O_3 and hopcalite, using test gas 1.5% CO in air. These results confirm the superiority of SnO_2-based catalyst.

Tin Oxide Based Catalyst Cloth

Catalyst cloths for filter-type smokehoods have been prepared based on tin oxide with precious metals. Cloth was supplied by a variety of manufacturers, including Siebe Gorman, with surface areas of 1000 m^2g^{-1} to 1200 m^2g^{-1} and have all been used successfully to make active catalysts. The activity results of the 3 types of cloth are illustrated in figure 4.

As a result of the temperature sensitivity of the CO oxidation reaction, the performance of the catalyst at low temperature is dependent on the metal loading and dispersion. For instance a 30% drop in the tin loading, whilst keeping the precious metals level constant resulted in a failure at 25°C as per the prescribed test, but the catalyst passed the test at 37°C, as illustrated in figure 5. This is probably due to the surface kinetics manifesting itself at higher temperatures to help some species readily desorb or undergo rearrangement at the tin oxide sites. The temperature trend is further confirmed in figure 6, which shows the effect of initial test-bed temperature on activity. Consequently, for catalyst that is required to operate at an initial temperature of 37°C, the precious metal loading has been reduced to an optimum level.

STEM And ESCA Analysis Of Carbon Cloth Catalysts

The cloth specimens were ground to a fine powder, and a prewet carbon-coated nylon grid was dipped into the powder, allowed to dry and placed into the STEM for analysis. The metal particles

existed as highly dispersed clusters of precious metals/Sn. The clusters generally range in size from 2-6 nm. Particle-to-particle analysis showed good heterogeneous distribution of the metals on the fibres. Low quantities of Al and Zn were found to be associated with the fibres. It does not appear that these impurities have any significant effect on activity. ESCA results suggest that the calcination, reduction steps of this catalyst were effective at generating low oxidation states of the precious metals. The precious metals readily chemisorb oxygen on exposure to air, but the latter does not totally oxidise the precious metals from (0) to (II) oxidation state and is readily reactive with CO to form CO_2.

Alternative Non Tin Oxide Low Temperature CO Oxidation Catalysts.

Precious metal on reducible metal oxide deposited on high surface area cloth fabric (Ref. 1) have exhibited low temperature activity towards CO oxidation. The metal loadings used are broadly similar to those of SnO_2 type. The results are shown in figure 7. The tendency for the cloth to ignite fairly readily during processing, in particular, at the calcination step limits the temperature range and atmosphere that can be used to obtain the base oxide by thermal decomposition of nitrate precursors. In the case of precious metals/transition metal oxide catalyst supported on 2-3 mm diameter SiO_2 spheres, preliminary results indicate good low temperature CO oxidation activity. Figure 8 shows the effect on catalyst activity at room temperature. In the absence of the transition metal oxide, the initial activity is steadily lost, whereas when the catalyst contained the transition metal oxide, its activity is maintained over an extended period. The unsupported reducible metal oxides containing precious metals show equally good activity towards CO oxidation, as depicted in figure 9. These novel catalysts have potential application in breathable gases purification, in CO_2 lasers and in CO oxidation generally.

APPENDIX

Once Flow-Through Test

In the self-rescue filter device, the minimum performance requirement as laid down by UK Civil Aviation Authority is that the device shall provide the wearer a minimum duration of respiratory protection of 20 minutes against the challenge atmosphere, which contains, among other toxic gases, 3.5% CO_2 and 1% CO at 85% relative humidity. The specified CO inhalation limit of 100 ppm or 200 cm^3 integrated volume shall not be exceeded at anytime.

The laboratory test that has been devised to meet the above specification has the catalyst operating in 2 regimes: initially at a lower workload representing the in-flight sedentary phase in an on-board emergency (taking into account anxiety during this phase which will increase respiratory rate) for a period of 10 minutes, rising to a higher workload for a further 10 minutes corresponding to an evacuation exercise, whilst keeping the CO level down to below 100 ppm over the whole 20-minute period.

Test Conditions

Test gas : 1% CO, 3.5% CO_2 in air

Catalyst temperature : $20^{\circ}C$ or $37^{\circ}C$

Relative humidity : 85%

Pressure drop : < 8.1 cm H_2O

Test duration : 20 mins

Space velocity : 12600 h^{-1} for 10 mins and 37000 h^{-1} for a further 10 mins

Performance requirement : exit CO < 100 ppm or integrated CO volume slipped < 200 cm^3 over 20-min period.

Sinusoidal Flow Test

This test makes use of a breathing machine, which is basically a lung simulator, to provide a sinusoidal flow. It produces a mean flow of $30 lmin^{-1}$ of filtered air saturated with water at body temperature ($37^{\circ}C$). The peak rate of flow is approximately π times the mean flow rate and the breathing frequency is 20 inspirations per minute. The test gases are 0.25% CO in air or 1.5% CO in air by volume at 95% relative humidity. The inhalation resistance must be less than 14 mbar.

Test Conditions

Test gas : 0.25% CO or 1.5% CO in air

Lung capacity : 1.5 l

Average flow rate : 30 lmin^{-1}

Peak flow rate : 94 lmin^{-1}

No of inspiration per min : 20

Relative humidity : 95%

Catalyst temperature : 25°C or 37°C

Inhalation resistance : < 14 mbar

Test duration : time for 400 cm^3 of CO to slip, define as test life of catalyst.

Performance requirement : Integrated CO slipped < 400 cm^3

Once Flow-Through Test (For Recirculating Units)

This test has been devised to meet the requirement of deep sea working habitats breathing atmosphere (Heliox = 80% He and 20% O_2), where the catalyst is used for scrubbing CO by recycling via a purification unit either on the sea bed or through an umbilical cord to the diving support vessel. In welding environment the CO level can rise in excess of 60 ppm. The TLV value for CO at atmospheric pressure is 50 ppm. In hyperbaric conditions (200 m depth, equivalent to 20 bar pressure), this figure is 2.5 ppm. Consequently, in a welding chamber habitat, the divers can be exposed to environmentally unacceptable level of CO, hence the need for CO scrubbing.

Test Conditions

Test gas : 1% CO in air

Flow rate : 2.5 lmin^{-1}

Catalyst temperature : 25°C

Relative Humidity : 60%

Test duration : 60 mins

Performance requirement : to convert 58 cm^3 CO per minute per gram of catalyst.

REFERENCES

1. British Patent Application 89/6984.1
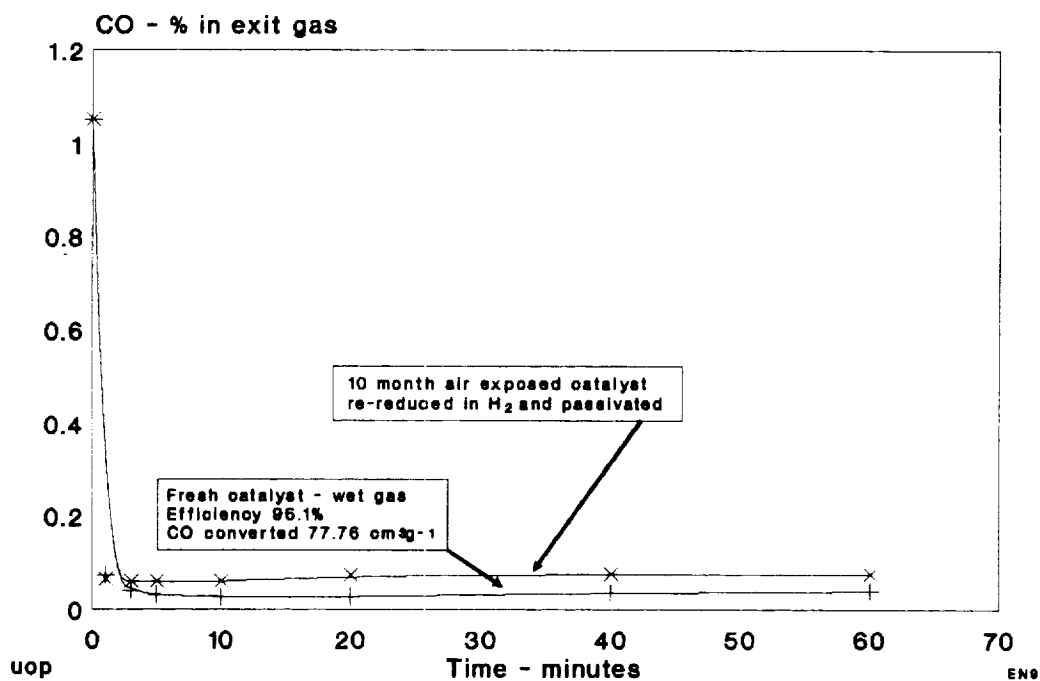
Fig.1 - Activity results of CO oxidation on precious metals/ SnO_2/ promoter using 1% CO in air (wet) at room temperature
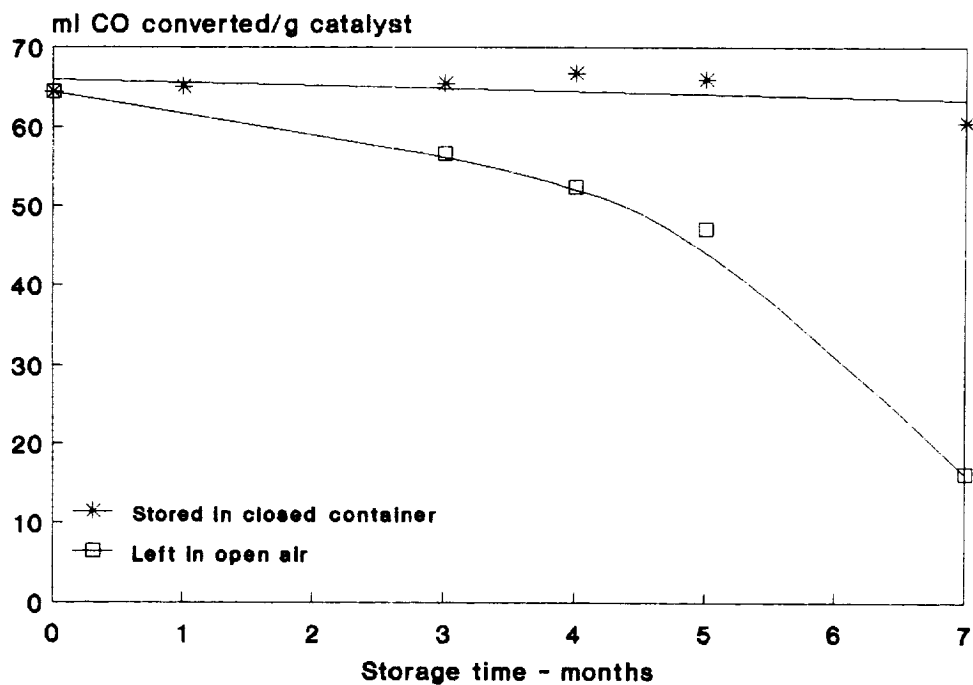

Fig.2 - Precious metals/SnO_2 catalyst
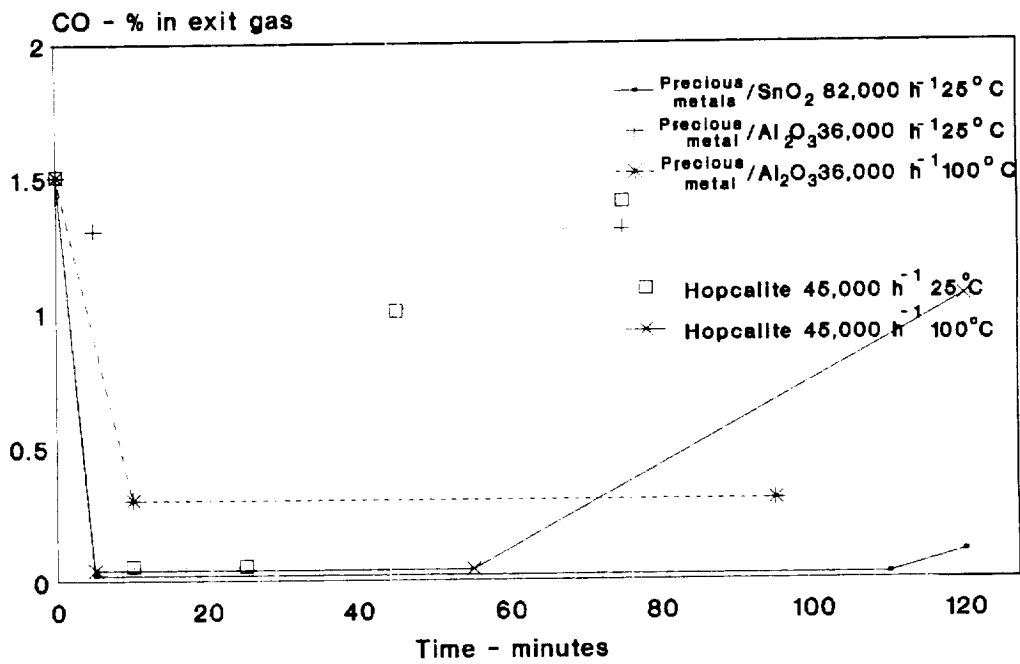Storage time vs. Activity test

Fig.3 - Activity results of different CO
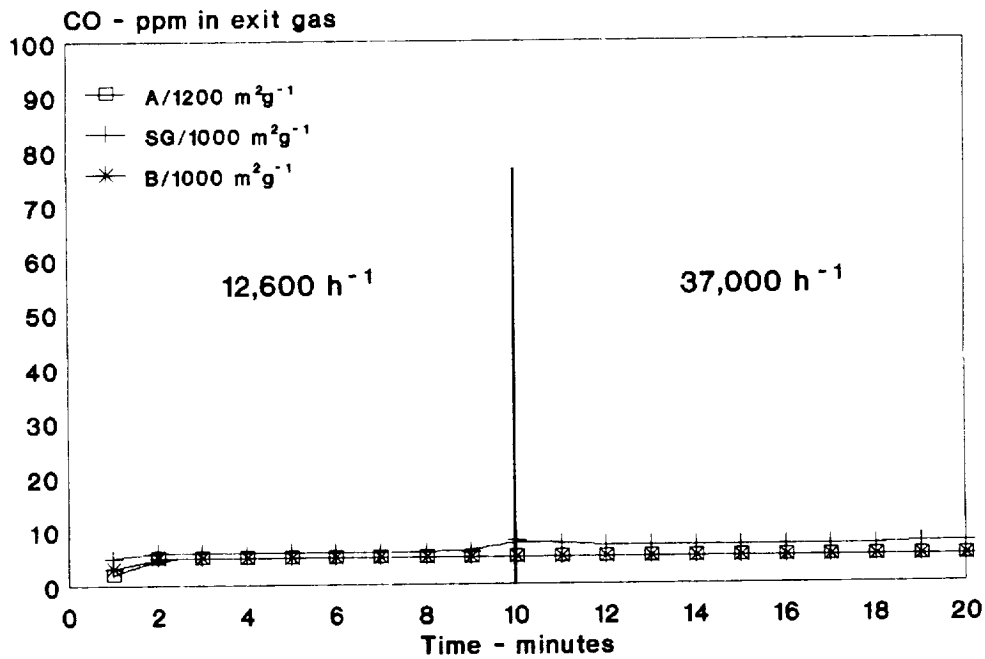oxidation catalysts - 1.5% CO in air

Fig.4 - Activity of various catalyst cloths at 25 °C
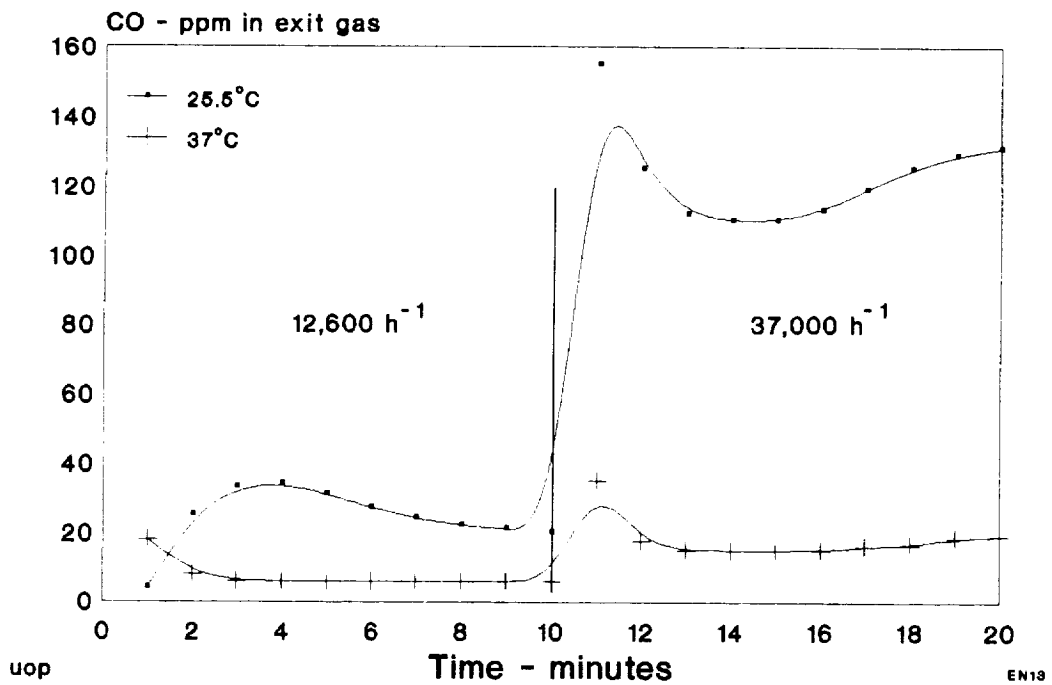Test gas 1% CO, 3.5% CO_2 in air, (wet)

Fig.5 - Activity of cloth with 30% less Sn at 25.5°C & 37°C
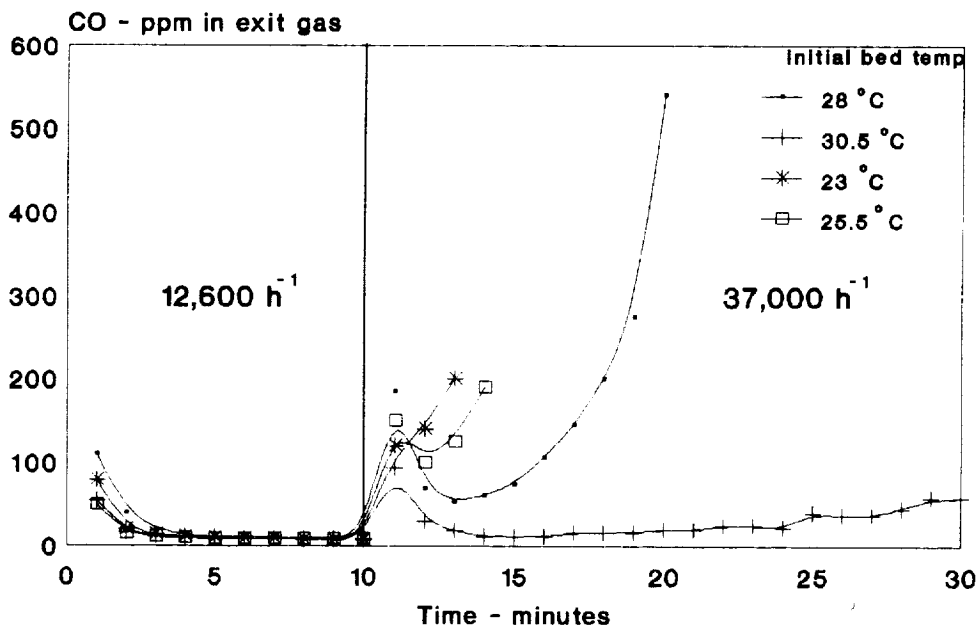Test gas 1% CO, 3.5% CO_2 in air (wet)

Fig.6 - CO oxidation of catalyst cloth A/1200 m^2g^{-1}
at various temperatures.
Test gas 1% CO, 3.5% CO_2 in air, (wet)

400
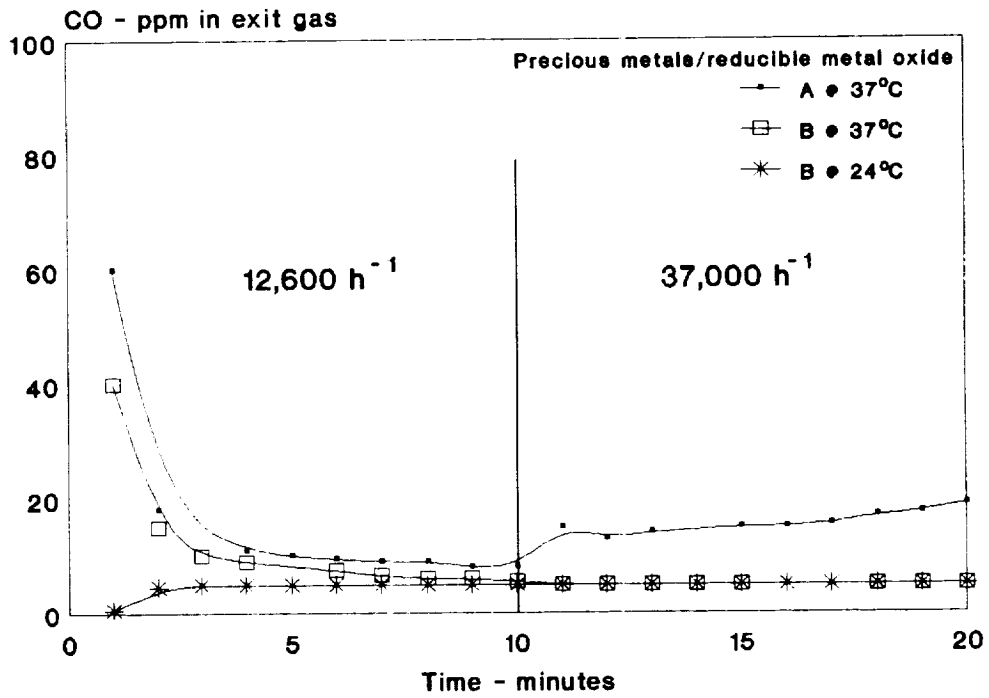
Fig.7 - Alternative low temperature CO oxidation on cloth fabric
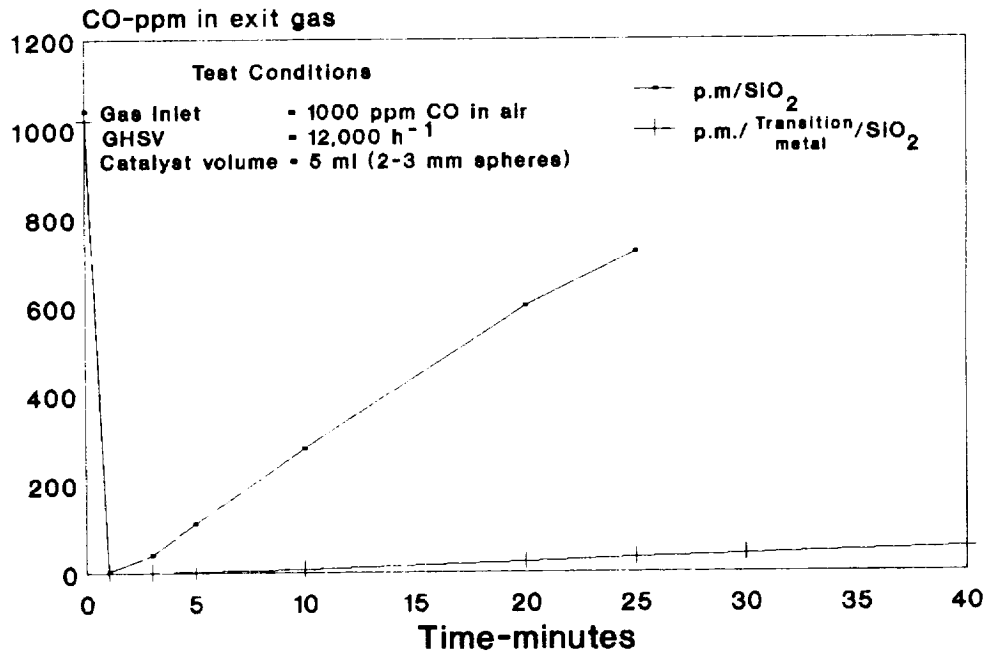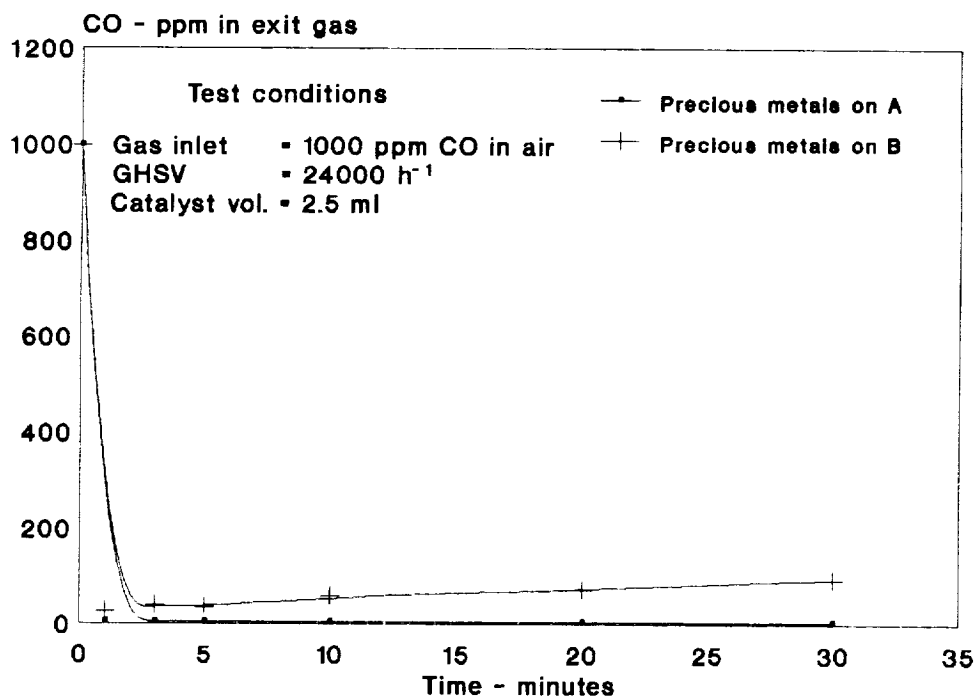Test gas 1% CO, 3.5% CO₂ in air, (wet)

Fig.8 - Activity results of precious metals on
SiO₂ and on Transition metal/SiO₂ at room temperature

Fig.9 - Activity results of precious metals on reducible
metal oxides A and B at room temperature

POTENTIAL TECHNOLOGY TRANSFERS OF RESEARCH ON LOW-TEMPERATURE

CARBON MONOXIDE - OXYGEN RECOMBINATION CATALYSTS

Edward J. Poziomek
Artech Associates
80-4 Cosey Beach Avenue, East Haven, CT

SUMMARY

Results from research on catalytic recombination of CO-O_2 for stable closed-cycle operation of CO_2 lasers hold much promise for a variety of technology transfers. Expansion of CO_2 laser remote sensing applications toward chemical detection and pollution monitoring would certainly be expected. However, the catalysts themselves may be especially effective in low-temperature oxidation of a number of chemicals in addition to CO. It is therefore of interest to compare the CO-O_2 catalysts with chemical systems designed for chemical sensing, air purification and process catalysis. Success in understanding the catalytic mechanisms in the recombination of CO-O_2 could help to shed light on how catalyst systems operate. New directions in low-temperature oxidation catalysts, coatings for chemical sensors and sorbents for air purification could well emerge.

INTRODUCTION

There are a number of applications for CO-O_2 recombination catalysts. An important one is the achievement of long-term, closed-cycle operation of CO_2 lasers. The lasers are used for remote-sensing applications such as observing and predicting atmospheric behavior. The ability to understand catalyst performance and to control frequency stability is critical. CO_2 can dissociate in the laser discharge to CO and O_2. The loss of CO_2 results in a corresponding loss of laser power. The buildup of O_2 can cause discharge instabilities. A catalyst is needed to facilitate recombination of the CO-O_2. It is critical that the mechanisms involved in the catalytic recombination be understood. The challenges are multifold and include the need for studies of the catalytic process as well as the physical and chemical properties of the catalyst. An excellent review of approaches toward efficient recombination catalysts appeared in the proceedings of a workshop held at the NASA Langley Research Center in 1986 (ref. 1). A review of recent advances was presented in 1988 (ref. 2).

Pt/SnO_2 appears to be the most promising catalyst system for the recombination of CO and O_2 in CO_2 lasers (ref. 3). A systematic study of Pt, Pd/SnO_2 catalysis has been underway for several years. There are many parameters including catalyst preparation, catalyst surface area, effect of CO_2 concentration, catalyst pretreatments, catalyst distribution and quality control of test procedures, to mention several. Considerable progress has been made toward high activity systems for combining CO and O_2 to form CO_2 in high powered lasers. This will be discussed at the International Conference on CO Oxidation Catalysts for Long-Life CO_2 Lasers in October 1989 at the NASA Langley Research Center, Hampton, VA.

As pointed out during the international conference in 1986, the immediate United States interest in the development of pulsed CO_2 lasers is for the NASA Marshall Space Flight Center Windstat program (involving the measurement of wind) (ref. 4). However, it was mentioned that the potential for technology transfer to industrial, medical, defense and other research applications is significant. Industrial process control, laser ranging, communication, frequency stability and reliable long-term unattended operation were mentioned as being most important. United Kingdom

interests relate heavily to military applications; however, there is also a policy of technology transfer to industry (ref. 5).

The purpose of the present paper is to more specifically outline the potential technology transfers from the research on low-temperature $CO-O_2$ recombination catalysts. Major areas discussed include:

- Remote sensing
- Chemical sensors
- Air purification
- Process catalysis.

REMOTE SENSING

An appreciation of the utility of lasers in meteorology, and earth and atmospheric remote sensing can be obtained by reviewing the proceedings of a recent conference on the subject (ref. 6). The titles of the sessions reflect the scope:

- Advances in laser technology for remote sensing
- Laser remote sensing for meteorology applications
- Laser remote sensing for surface applications
- Laser remote sensing of trace species
- Laser remote sensing of velocity fields.

Titles in the session on trace-species sensing follow:

- Remote active spectrometer
- Measurement of atmospheric trace species and rocket fuels using CO_2 lidars
- Development of an active imaging system and its application to the visualization of gas clouds
- Multiwavelength and tripled CO_2 lidars for trace gas detection
- Analysis of laser diagnostics in plumes
- CO_2 laser photoacoustic detection of trace toxic compounds in the ambient air
- Stratospheric ozone measurements with a ground-based, high power lidar
- CO_2 DIAL measurements of toxic gases.

Chemical analysis at a distance is of special interest for many reasons. Recent progress in the possibility of a chemical warfare treaty highlights the need for chemical monitoring and verification procedures. The war on drugs could benefit from stand-off sensors to locate and identify organic vapors from suspected drug-processing facilities. Also, many environmental situations require a variety of chemical sensors including stand-off systems. Use of differential absorption lidar for pollution mapping is a good example. Table I lists molecules of interest in air pollution and their absorption wavelengths corresponding to wavelegths of line-tunable CO_2 lasers.

Achievement of long-term, closed cycle operation of CO_2 lasers should significantly expand the use of remote sensing especially in the detection, identification and monitoring of pollutants.

404

CHEMICAL SENSORS

The first SnO_2 semiconducting gas sensor was marketed over two decades ago for the detection of combustible gases. Applications have been extended to the sensing of ammonia, hydrogen sulfide, thiols, ethanol, hydrogen, CO, arsine, acetic acid and other compounds. A recent review on the development of SnO_2 sensors is available (ref. 8), as well as an outline of what was published on conductometric sensors during the 1985-1987 period (ref. 9). The mechanism of detection in air is usually a catalytic oxidation at the surface of the oxide inducing an increase in conductance. The operating temperature for a particular sensor would most likely be found in the range of 200-400°C. Recent advances relate to selectivity and include a combustible gas detector having insensitivity to reductive gases (ref. 10). Several patents (mostly to Japanese companies) have appeared for CO detection using semiconducting oxides.

SnO_2 is the most frequently used material for semiconducting gas sensors. Few other materials have been put into practical use. The sensitivity of the sensor for CO can be improved significantly by adding Pt or Pd; silanization with trichlorosilane enhances the selectivity for H_2S (ref. 9). There appears to be more interest at the presnt time in studying SnO_2 to increase its performance rather thna to search for new materials. Increasing selectivity, sensitivity, reliability and long-term stability are the goals.

Applications of SnO_2 gas sensors include:

- Toxic gas detection (CO, NH_3, H_2S, etc.)
- Combustion monitoring
- Gas-leak detection
- Air quality monitoring
- Fermentation control
- Ventilation control
- Fire detection (CO)
- Breath analyzer (alcohol).

These and some new applications such as detection of odors (e.g., in testing for freshness of foods) are discussed briefly in reference 8.

The SnO_2 and other catalysts emerging in the research on $CO-O_2$ recombination for the CO_2 laser application should be considered candidates for semiconducting oxide sensors and vice versa. A low-temperature SnO_2 system developed in the laser work could dramatically expand the utility of semiconducting oxides in chemical sensing.

AIR PURIFICATION

Catalysts for removal of CO from air at room temperature are commercially available. Hopcalite, a co-precipitate of oxides of manganese and copper, is a classic example. As pointed out by Sampson and Gudde (ref. 11), the main difference between CO oxidation for air purification and for laser control lies in the gas composition. The CO and O_2 concentrations are much higher and the CO_2 concentrations much lower in the air purification application than in the laser recombination one. However, the operating requirements are very similar.

It is of interest to compare the CO-O_2 recombination catalysts with other systems known to react with CO. For example, the current U.S. Department of Defense sorbent for air filters in chemical defense is whetlerite. This is an activated charcoal which has been impregnated with a mixture of copper, silver and chromium. It functions through a combination of physical adsorption and chemisorption. Descriptions of some of the chemistry and characteristics of whetlerite are available (ref. 12, 13). It is known that CO is oxidized at room temperature in air using whetlerite (ref. 14, 15). The activation energy for the oxidation was estimated to be 14.6 kJ mol^{-1} (ref. 16). The oxidation of CO has also been proposed as a nondestructive test for predicting the residual chemical life of whetlerite (ref. 17, 18). The chemical reactivity of whetlerite involves both hydrolysis and oxidation. However, the mechanisms are complicated; complete details have not been worked out. Several analogies can be drawn between the Pt/SnO$_2$ oxidation of CO in the laser application and the chemisorption processes in air purification using whetlerite. It is pertinent to compare the proposed reaction mechanisms for the respective systems. Success in understanding the catalytic process in the recombination of CO-O_2 could help to shed light on how other oxidation catalysts work including whetlerite.

New or modified sorbents for air purification could emerge as a result of the research on CO-O_2 recombination catalysts. Low temperature oxidation catalysts for CO have been investigated with other toxics for air purification. (ref. 19).

PROCESS CATALYSIS

A product review on process catalysts showed that nearly every segment of the catalyst business is growing (20). The value of catalysts consumed in pollution abatement uses this year is expected to exceed the value of catalysts consumed in petroleum processing. However, the physical volume of catalysts used in pollution control is actually quite small because of the high activity and cost of Pt and other metals of the Pt group used as catalysts. Automotive catalysts accounted for 43% of all U.S. consumption of platinum group metals in 1987. A major problem is still the stability of the noble-metal catalysts and the catalyst supports (21). Environmental catalysts should lead value growth among other catalysts into the next century, however, research is underway to find catalysts that are less expensive than the noble metal ones.

It has been estimated that almost 25% of the total production volume of the top 20 chemicals worldwide depends upon selective oxidation catalyzed by solid metal oxides (22). The most selective catalysts contain a cation with an empty or full outermost d orbital. This includes Sn(IV) which has a $4d^{10}$ orbital.

The work on Pt/SnO$_2$ for CO-O_2 recombination should lead to new insights on catalytic oxidation mechanisms as well as materials which may be relvant to various aspects of process catalysis.

REFERENCES

1. Batten, C. E.; Miller, I. M.; Wood, G. M., Jr.; Editors,: Closed-Cycle, Frequency-Stable CO$_2$ Laser Technology, NASA Conference Publication 2456 (Proceedings of a workshop sponsored by the National Aeronautics and Space Administration and held at the Langley Research Center, Hampton, Virginia, 10-12 June 1986). Published 1987.

2. Hess, R. V.; Buoncristiani, A. M.; Brockman, P.; Bair, C. H.; Schryer, D. R.; Upchurch, B. T.; and Wood, G. M.: Recent Advances in Efficient Long-Life, Eye-Safe Solid-State and CO$_2$ Lasers for Laser Radar Applications. Proceedings of SPIE Symposium on Fiber Optics. Optometrics and Other Laser Applications. Boston, MA. September 1988.

3. Rogowski, R. S.; Miller, I. M.; Wood, G.; Schryer, D. R.; Hess, R. V.; and Upchurch, B. T.: Evaluation of Catalysts for Closed-Cycle Operation of High Energy Pulsed CO$_2$ Lasers. SPIE Proceedings, vol. 415, 1983, p. 112.

4. Wood, G. M., Jr.: Reference 1. pp. 1-2.

5. Willetts, D. V.: Reference 1. pp. 7-8.

6. Sokolowski, M. M., Chair: Conference on Laser Applications in Meteorology, and Earth and Atmospheric Remote Sensing. Los Angeles, CA. SPIE Proceedings, vol. 1062; January 1989.

7. Fredriksson, K. A.: Differential Absorption LIDAR for Pollution Mapping. In: Laser Remote Chemical Analysis. Measures, R. M., ed. John Wiley & Sons. New York. 1988. pp.273-332.

8. Takahata, K.: Tin Dioxide Sensors - Development and Applications. In: Chemical Sensor Technology, Vol. 1. Seiyama, T., ed. Elsevier. New York. 1988. pp. 39-55.

9. Janata, J; and Bezegh, A; Chemical Sensors. Anal. Chem., vol. 60, no. 3, 15 June 1988, pp.62R-74R.

10. Otani, H.: Combustible Gas Detector Having Insensitivity to Reductive Gases. Japanese Patent JP 86195339 A2. 29 August 1986. (Chem. Abstr., vol. 106, no. 2, p. 6835e.)

11. Sampson, C. F.; and Gudde, N. J.: The Oxidation of Carbon Monoxide Using a Tin Oxide Catalyst. Reference 1. pp. 65-69.

12. Poziomek, E. J.; Mackay, R. A.; and Barrett, R. P.: Electron Spin Resonance Studies with Copper/Silver/Chromium Impregnated Charcoals. Carbon, vol. 13, 1975, p. 259.

13. Deitz, V. R.; Robinson, J. N.; and Poziomek, E. J.: Electron Transmission Microscopy of Charcoals Impregnated with Ammonium Salts of CuII and CrVI. Carbon, vol. 13, 1975, p. 181.

14. Meier, E. P.; Luckan, S. K.; and Poziomek, E. J.: Reaction of Carbon Monoxide with Impregnated Carbons. Carbon, vol. 11, 1973, p. 417.

15. Lutchko, J. R; and Stoneburner, G. R.: U.S. Patent 3,545,915, 8 December 1970.

TABLE I. - ABSORPTION WAVELENGTHS FOR MOLECULES OF INTEREST IN AIR POLLUTION STUDIES (REF. 7)

Compound	Wavelength
Carbon Monoxide	4.709
	4.776
Nitric Oxide	5.263
Sulfur dioxide	8.881
	9.024
Ammonia	9.220
Freon-11	9.261
Ozone	9.505
	9.508
Freon-113	9.604
Benzene	9.621
Methyl hydrazine	10.182
Ethyl mercaptan	10.208
Ethyl chloride	10.275
Ammonia	10.333
Ethylene	10.533
Sulfur hexafluoride	10.551
Trichloroethylene	10.591
1,2,-Dichloroethane	10.591
Hydrazine	10.612
Vinyl chloride	10.612
1,1-Dimethylhydrazine	10.696
Freon-12	10.719
Perchloroethylene	10.742
1-Butene	10.787
Perchloroethylene	10.834

408

16. Deitz, V. R.; and Poziomek, E. J.: Temperature-Reversible Oxidation of Carbon Monoxide by New and Weathered Whetlerite. Carbon, vol. 24, no.4, 1986, pp. 463-468.

17. Deitz, V. R.; Poziomek, E. J.; and Baker, J. A.: Nondestructive Analysis of the Chemical Reactivity of Copper/Chromium/Silver Impregnated Charcoals. Anal. Letters, vol. 16, no. A8, 1983, pp. 643-653.

18. Hui-ping, Z.; Dai-yun, C.; and Fang, G.: The Non-Destructive Test Method of Chemical Reactivity of Impregnated Carbon Bed. Proceedings of the 3rd International Symposium on Protection Against Chemical Warfare Agents. Umea, Sweden. 11-16 June 1989, pp. 257-262.

19. Collins, M. F.: Characterization of the LTC Catalyst: Performance Against Common Air Pollutants. Reference 1. pp. 153-163.

20. Greek, B. F.: Process Catalysts Enjoy Surging Market. Chem. Engr. News, 29 May 1989, pp. 29-56.

21. Haggin, J.: Catalysis Gains from Auto Emission Work. Chem. Engr. News, 15 May 1989, p.23.

22. Campbell, I. M.; Catalysis at Surfaces. Chapman and Hall. New York. 2nd Edition. 1988. p.169.

ACKNOWLEDGMENT

1. Report No. NASA CP-3076	2. Government Accession No.	3. Recipient's Catalog No.
4. Title and Subtitle Low-Temperature CO-Oxidation Catalysts for Long-Life CO_2 Lasers		5. Report Date June 1990
		6. Performing Organization Code
7. Author(s) David R. Schryer and Gar B. Hoflund, Editors		8. Performing Organization Report No. L-16797
		10. Work Unit No. 584-01-31-50
9. Performing Organization Name and Address NASA Langley Research Center Hampton, Virginia 23665-5225		11. Contract or Grant No.
12. Sponsoring Agency Name and Address National Aeronautics and Space Administration Washington, DC 20546 Royal Signals and Radar Establishment Malvern, United Kingdom WR14 3PS		13. Type of Report and Period Covered Conference Publication
		14. Sponsoring Agency Code

15. Supplementary Notes

David R. Schryer, NASA Langley Research Center, Mail Stop 468, Hampton, Virginia

Gar B. Hoflund, University of Florida, Gainesville, Florida

16. Abstract

Low-temperature CO-oxidation catalysts are necessary for closed-cycle pulsed CO_2 lasers as well as for other applications, including air purification. The papers presented in this volume discuss several such catalysts, including information on catalyst preparation, techniques for enhancing catalyst performance, laboratory and laser test results, and mechanistic considerations.

17. Key Words (Suggested by Author(s)) CO Oxidation Catalysts CO_2 Lasers	18. Distribution Statement Unclassified - Unlimited Subject Category 36

19. Security Classif. (of this report) Unclassified	20. Security Classif. (of this page) Unclassified	21. No. of pages 424	22. Price A18